RECENT ADVANCES IN THE EVOLUTION OF EUARCHONTOGLIRES

EDITED BY: Lucja A. Fostowicz-Frelik, Deyan Ge and Irina Ruf
PUBLISHED IN: Frontiers in Ecology and Evolution and Frontiers in Genetics

frontiers Research Topics

frontiers

ISSN 1664-8714
ISBN 978-2-88974-180-9
DOI 10.3389/978-2-88974-180-9

About Frontiers

Frontiers is more than just an open-access publisher of scholarly articles: it is a pioneering approach to the world of academia, radically improving the way scholarly research is managed. The grand vision of Frontiers is a world where all people have an equal opportunity to seek, share and generate knowledge. Frontiers provides immediate and permanent online open access to all its publications, but this alone is not enough to realize our grand goals.

Frontiers Journal Series

The Frontiers Journal Series is a multi-tier and interdisciplinary set of open-access, online journals, promising a paradigm shift from the current review, selection and dissemination processes in academic publishing. All Frontiers journals are driven by researchers for researchers; therefore, they constitute a service to the scholarly community. At the same time, the Frontiers Journal Series operates on a revolutionary invention, the tiered publishing system, initially addressing specific communities of scholars, and gradually climbing up to broader public understanding, thus serving the interests of the lay society, too.

Dedication to Quality

Each Frontiers article is a landmark of the highest quality, thanks to genuinely collaborative interactions between authors and review editors, who include some of the world's best academicians. Research must be certified by peers before entering a stream of knowledge that may eventually reach the public - and shape society; therefore, Frontiers only applies the most rigorous and unbiased reviews.
Frontiers revolutionizes research publishing by freely delivering the most outstanding research, evaluated with no bias from both the academic and social point of view. By applying the most advanced information technologies, Frontiers is catapulting scholarly publishing into a new generation.

What are Frontiers Research Topics?

Frontiers Research Topics are very popular trademarks of the Frontiers Journals Series: they are collections of at least ten articles, all centered on a particular subject. With their unique mix of varied contributions from Original Research to Review Articles, Frontiers Research Topics unify the most influential researchers, the latest key findings and historical advances in a hot research area! Find out more on how to host your own Frontiers Research Topic or contribute to one as an author by contacting the Frontiers Editorial Office: frontiersin.org/about/contact

RECENT ADVANCES IN THE EVOLUTION OF EUARCHONTOGLIRES

Topic Editors:
Lucja A. Fostowicz-Frelik, Institute of Paleobiology (PAN), Poland
Deyan Ge, Chinese Academy of Sciences (CAS), China
Irina Ruf, Senckenberg Research Institute and Natural History Museum Frankfurt, Germany

Image: Martin Pelanek/Shutterstock.com

Citation: Fostowicz-Frelik, L. A., Ge, D., Ruf, I., eds. (2022). Recent Advances in the Evolution of Euarchontoglires. Lausanne: Frontiers Media SA.
doi: 10.3389/978-2-88974-180-9

Table of Contents

frontiers in Genetics

EDITORIAL
published: 11 October 2021
doi: 10.3389/fgene.2021.773789

Editorial: Recent Advances in the Evolution of Euarchontoglires

Łucja Fostowicz-Frelik[1,2,3]*, *Deyan Ge*[4]* and *Irina Ruf*[5]*

[1]Department of Evolutionary Paleobiology, Institute of Paleobiology, Polish Academy of Sciences, Warsaw, Poland, [2]Key Laboratory of Vertebrate Evolution and Human Origins, Institute of Vertebrate Paleontology and Paleoanthropology, Chinese Academy of Sciences, Beijing, China, [3]Center for Excellence in Life and Paleoenvironment, Chinese Academy of Sciences, Beijing, China, [4]Key Laboratory of Zoological Systematics and Evolution, Institute of Zoology, Chinese Academy of Sciences, Beijing, China, [5]Abteilung Messelforschung und Mammalogie, Senckenberg Forschungsinstitut und Naturmuseum Frankfurt, Frankfurt am Main, Germany

Keywords: lagomorphs, primates, rodents, behavior, evolution, genetics, morphology

Editorial on the Research Topic

Recent Advances in the Evolution of Euarchontoglires

INTRODUCTION

Euarchontoglires, recognized two decades ago in molecular studies (Murphy et al., 2001), is the most numerous and arguably, one of most important clades of placental mammals. First, Euarchontoglires include extremely variable and numerous rodents, the most speciose extant mammalian clade on Earth. Rodent diversity and array of adaptations found in this clade allow us to study genetics and diversification, mechanisms and the evolutionary patterns of speciation. Second, Euarchontoglires include primates (among them humans), which are characterized by notably increased encephalization. This major adaptive transformation alone warrants our attention. Third, the considerable antiquity of Euarchontoglires with over 63 million years of evolutionary history documented in the fossil record also makes this clade important for understanding mammalian evolution.

Apart from rodents (~2,500 living species) and primates (~300 species), representing approximately half of extant mammalian species nowadays (Wilson et al., 2016) and supplying us with excellent models to study extremely successful mammalian radiations, Euarchontoglires include also a few less numerous groups such as lagomorphs (rabbits, hares, and pikas), scandentians (tree-shrews), and dermopterans, otherwise known as colugos or flying lemurs. These understudied clades certainly contribute to our understanding of the Euarchontoglires evolution and early divergence of major lineages.

That said, the exceptional diversity of both fossil and living taxa of Euarchontoglires can be seen as a challenge, because the multitude of forms and adaptations found in these placentals makes their origins and evolution sometimes hard to decipher. Particularly characteristic of the Glires clade (lagomorphs + rodents) is their frequently convergent morphological evolution, which we now start testing quantitatively (e.g., Morris et al., 2018).

For this Research Topic, we collected 14 original research papers and reviews concerning evolution of Euarchontoglires at molecular, morphological, and behavioral levels, and conservation issues in this clade.

EUARCHONTOGLIRES IN GENERAL

Two papers in this volume address the broader context of Euarchontoglires evolution. Among several important issues which remain poorly studied, unresolved or debatable for this clade are convergence, reconstruction of ancestral morphotype and comparative genome-wide studies. Geng et al. investigate

OPEN ACCESS

Edited and reviewed by:
Alison G. Nazareno,
Federal University of Minas Gerais, Brazil

***Correspondence:**
Łucja Fostowicz-Frelik
lfost@twarda.pan.pl
Deyan Ge
gedy@ioz.ac.cn
Irina Ruf
irina.ruf@senckenberg.de

Specialty section:
This article was submitted to Evolutionary and Population Genetics, a section of the journal Frontiers in Genetics

Received: *10 September 2021*
Accepted: *27 September 2021*
Published: *11 October 2021*

Citation:
Fostowicz-Frelik Ł, Ge D and Ruf I (2021) Editorial: Recent Advances in the Evolution of Euarchontoglires. Front. Genet. 12:773789. doi: 10.3389/fgene.2021.773789

phenotypic convergence of locomotor modes across Euarchontoglires (122 species excluding Lagomorpha) on the basis of some forelimb skeleton indices. Song et al. present a survey of microsatellite DNA composition and its diversity within all major clades of Euarchontoglires including Scandentia and Dermoptera.

PRIMATES

Since the last two decades it has become evident that evolutionary biology and conservation issues are greatly interconnected. Thus, a sizeable portion of this volume is dedicated to primate research at the interface of molecular research and species at-risk. Guo et al. investigated the genetic structure of critically endangered Hainan gibbon (*Nomascus hainanus*), the rarest primate in the world. Endangered or critically-endangered snub-nosed monkeys (*Rhinopithecus*) were the subject of three studies. Zhang et al. investigate the role of major histocompatibility complex (MHC) genes in mate choice in the golden snub-nosed monkey (*R. roxellana*). Li et al. tackle the genetic structure of the Qinling Mountains population of the same species. Kuang et al. present a comprehensive study concerning the genomic impact of population dwindling of these monkeys across the entire genus, and find deleterious mutations that are affecting immunity especially in smaller populations. Finally, Yousaf et al. in their mini-review share the current state of the art in the field of great apes genome analysis, showing variety of approaches, recent views at the species relationships and the evolutionary history of the closest human relatives from the standpoint of molecular studies, as well as the emergence of modern human genome.

Behavior has been frequently studied in primates, due to size and structure of their brain resulting in social organization. Xia et al. investigate social status in female Tibetan macaques (*Macaca thibetana*) as expressed by grooming relationships within the group.

RODENTIA

Wölfer et al. investigate locomotion in Swinhoe's striped squirrel (*Tamiops swinhoei*). They hypothesize that asymmetrical gait may have been characteristic of earliest representatives of Euarchontoglires.

Traditionally, the fossil record has been established as a tool for understanding macroevolutionary changes. Due to very dense sampling, Kimura et al. in their paleobiological study of murine rodents were able to document morphological evolution in a rodent species with a resolution of hundreds of thousands of years.

A complex social organization is also characteristic of some rodents. Caspar et al. explore how and to what degree sex and breeding status influence skull characters in a eusocial mole-rat (*Fukomys*). Their study contributes to a deeper understanding of morphofunction and sexual dimorphism in Bathyergidae.

LAGOMORPHA

Although usually overshadowed by rodents, their sister clade, lagomorphs are important for our understanding of non-primate Euarchontoglires evolution. Two papers focus on the cranial anatomy of one of the most common and widespread North American Paleogene lagomorph *Palaeolagus*. This early "rabbit" waited, perhaps too long, for a new appraisal since Wood's (1940) classic study. Using modern digital imaging techniques, Wolniewicz and Fostowicz-Frelik present the general anatomy of the *Palaeolagus* skull, complemented by Ruf et al. on the nasal and auditory regions in detail. In their review, Kraatz et al. describe lagomorphs as a good model system to study multiple evolutionary patterns of morphological change. This truly collaborative effort shows not only how much has been learned on lagomorphs recently, but may suggest new prospects for future research.

PERSPECTIVES

The above contributions give us only a snapshot of recent developments in Euarchontoglires studies. Here we offer a handful of predictions as to future research directions in the field (Although we refrain from mentioning in detail recent developments in molecular biology). First, it is evident from anatomical studies on the skeleton that it is important to investigate more closely soft tissues (muscles, blood vessels and brain in particular). Second, methods should be used not only to generate image data but also to simulate and model function of various systems. Even established methods, e.g., finite element analyses (FEA) have been employed only rarely to understand the biomechanics in non-primate Euarchontoglires. Third, there is a whole evo-devo modern approach that links ontogeny with morphological change. Moreover, new sequencing methods have resulted in generation of large genomic datasets, which not only helps reconstruct more robust phylogenies of Euarchontoglires, but also facilitates studies on adaptive evolution and demographic histories, and the mechanisms underlying speciation and key traits evolution.

However, there is a lack of balance in the coverage of existing diversity of Euarchontoglires; the primates (especially) and rodents are quite well explored, whereas other clades, such as lagomorphs, scandentians and dermopterans are rather neglected. Thus, one of immediate goals should be to focus on the understudied groups of Euarchontoglires in order to bring research on these clades to the standards now available only for primates.

Last but not least, we are very grateful to all the authors and reviewers who generously contributed their work and time to this volume. Hopefully, our collection will stir further interest in these fascinating placental mammals and will provide a starting point for new research or even revisiting old questions.

AUTHOR CONTRIBUTIONS

All authors listed have made a substantial, direct, and intellectual contribution to the work and approved it for publication.

REFERENCES

D. E. Wilson, T. E. Lacher, and R. A. Mittermeier (Editors) (2016). *Handbook of the Mammals of the World: Lagomorphs and Rodents I* (Barcelona: Lynx Edicions).

Morris, P. J. R., Cobb, S. N. F., and Cox, P. G. (2018). Convergent evolution in the Euarchontoglires. *Biol. Lett.* 14, 20180366. doi:10.1098/rsbl.2018.0366

Murphy, W. J., Eizirik, E., O'Brien, S. J., Madsen, O., Scally, M., Douady, C. J., et al. (2001). Resolution of the early placental mammal radiation using Bayesian phylogenetics. *Science* 294, 2348–2351. doi:10.1126/science.1067179

Scott, W. B., Jepsen, G. L., and Wood, A. E. (1940). The Mammalian Fauna of the White River Oligocene: Part III. Lagomorpha. *Trans. Am. Phil. Soc.* 28, 271–362. doi:10.2307/1005524

Conflict of Interest: The authors declare that the research was conducted in the absence of any commercial or financial relationships that could be construed as a potential conflict of interest.

frontiers in Genetics

ORIGINAL RESEARCH
published: 04 December 2020
doi: 10.3389/fgene.2020.608633

The Genetic Status of the Critically Endangered Hainan Gibbon (*Nomascus hainanus*): A Species Moving Toward Extinction

Yanqing Guo[1,2†], Jiang Chang[3†], Ling Han[1], Tao Liu[1], Gang Li[1], Paul A. Garber[1,4], Ning Xiao[5] and Jiang Zhou[1]*

[1] School of Karst Science, Guizhou Normal University, Guiyang, China, [2] College of Life Sciences, Northwest University, Xi'an, China, [3] State Key Laboratory of Environment Criteria and Risk Assessment, Chinese Research Academy Environmental Sciences, Beijing, China, [4] Department of Anthropology, Program in Ecology, Evolution, and Conservation Biology, The University of Illinois at Chicago, Urbana, IL, United States, [5] Guiyang Nursing Vacational College, Guiyang, China

OPEN ACCESS

Edited by:
Deyan Ge,
Institute of Zoology, Chinese Academy of Sciences (CAS), China

Reviewed by:
John Lau,
Key Laboratory of Animal Ecology and Conservation Biology, Institute of Zoology (CAS), China
Shingo Kaneko,
Fukushima University, Japan

***Correspondence:**
Jiang Zhou
zhoujiang@ioz.ac.cn

[†]These authors share first authorship

Specialty section:
This article was submitted to Evolutionary and Population Genetics, a section of the journal Frontiers in Genetics

Received: 21 September 2020
Accepted: 30 October 2020
Published: 04 December 2020

Citation:
Guo Y, Chang J, Han L, Liu T, Li G, Garber PA, Xiao N and Zhou J (2020) The Genetic Status of the Critically Endangered Hainan Gibbon (Nomascus hainanus): A Species Moving Toward Extinction. Front. Genet. 11:608633. doi: 10.3389/fgene.2020.608633

The Hainan gibbon (*Nomascus hainanus*), once widespread across Hainan, China, is now found only in the Bawangling National Nature Reserve. With a remaining population size of 33 individuals, it is the world's rarest primate. Habitat loss and fragmentation are the primary drivers of Hainan gibbon population decline. In this study, we integrated data based on field investigations and genotype analyses of 10 microsatellite loci (from fecal samples) to assess genetic diversity in this Critically Endangered primate species. We found that the genetic diversity of the Hainan gibbon is extremely low, with 7 of 8 microsatellite loci exhibiting decreased diversity. Additional molecular analyses are consistent with field observations indicating that individuals in groups A, B, and C are closely related, the female–male sex ratios of the offspring deviates significantly from 1:1, and the world's remaining Hainan gibbon population is expected to experience continued high levels of inbreeding in the future. Given extensive habitat loss (99.9% of its natural range has been deforested) and fragmentation, this rarest ape species faces impending extinction unless corrective measures are implemented immediately.

Keywords: critically endangered, genetic status, population size, Hainan gibbon, conservation

INTRODUCTION

Species classified by the IUCN as Endangered (EN) or Critically Endangered (CR) face an impending extinction crisis and require immediate protection. In the case of nonhuman primates, which represent the 3rd most speciose mammalian order (some 512 species, Estrada et al., 2017), 17% of species are currently listed as CR and 28% as EN (Iucn, 2020). In the case of gibbons and siamangs (Hylobatidae, Primates) or small bodied Asian apes (genera *Hylobates*, *Hoolock*, *Nomascus*, and *Sympalangus*), the threat of extinction is extremely severe. Ninety-five percent (18 of 19 species) of gibbon and siamang species are EN or CR. This includes the world's most threatened primate species, the Hainan gibbon (*Nomascus hainanus*). Only 33 Hainan gibbons remain in the wild. In the current study, we examine the genetic status of the critically endangered primate species.

There are several evaluation criteria used to assess a species viability and conservation status for it to be assessed as CR. These include the remaining population is small, declining, and geographically restricted; the species geographic range is highly fragmentated and decreasing; and quantitative assessments indicate that the extinction risk is high (Iucn, 2004). Given the difficulty of obtaining DNA samples of highly threatened and rare primate species, population genetics have seldom been used to assess their population viability. However, population genetic assessments are essential for effective programs of species management and conservation. For example, in 1958 China established the Xishuangbanna National Nature Reserve in Yunnan Province in an attempt to protect the Critically Endangered northern white-cheeked gibbon (*Nomascus leucogenys*). In 1980, China established the Nangunhe National Nature Reserve, also in Yunnan Province, to protect the Endangered lar gibbon (*Hylobates lar*). Although both gibbon species were censused and demographic information collected, studies by Fan et al. (2013) indicate that both gibbon species have been extirpated from China. Thus, although the creation of protected areas and periodic population re-censusing are important components of a species survivorship plan, population genetics research that includes estimates of genetic diversity, effective population size, inbreeding potential, and strategies for increasing gene flow also are essential.

Many species are facing a significant threat due to anthropogenically induced habitat fragmentation and habitat loss that has resulted in previously continuous populations becoming isolated (David and Richard, 2003; Frankham, 2005; Wei et al., 2012; Estrada et al., 2017; Li et al., 2018). As subpopulations decrease in size, they also are expected to decline in genetic diversity. In general, populations with higher genetic diversity have a greater ability to adapt and respond to changing environmental conditions (Lindsey et al., 2013) and are more disease resistant (Siddle et al., 2007), then populations characterized by limited genetic diversity (Swinnerton et al., 2004; Hemmings et al., 2012). At the same time, small populations are at greater risk for inbreeding, which will increase the degree of genetic drift and allelic loss, leading to reduced genetic diversity (Frankham et al., 2009; Frankham et al., 2014).

Research in conservation genetics has found that many small and isolated populations exhibit low genetic diversity. For example, the population of northern elephant seals (*Mirounga angustirostris*) inhabiting Guadalupe Island was reduced to a relic population of only 10–30 individuals in the 19th century. By 1991, the population had increased to 127,000. Despite this rapid population increase, genetic research indicates that the genetic variation of northern elephant seals remains extremely low and has been severely affected by inbreeding and genetic drift. The genetic diversity of the population is only 45% of the original population (Hoelzel, 1997). Similarly, recent habitat fragmentation has resulted in several primate species in China (e.g., *Rhinopithecus roxellana*, *Rhinopithecus bieti*, *Rhinopithecus brelichi*, *Trachypithecus francoisi*, and *Trachypithecus leucocephalus*) distributed into small isolated subpopulations. Genetic differentiation across subpopulations is high (0.109–0.177), and in at least three of these five species, genetic drift has occurred (Liu et al., 2015). In the black snub-nosed monkey (*Rhinopithecus strykeri*), which has a remaining population of approximately 400 individuals (200 individuals in China and 200 individuals in Myanmar; Yang et al., 2019), genetic diversity in the mitochondrial control region indicates no variability (Andie et al., 2016). A greater understanding of the genetic diversity of threatened species is critical for developing effective management and conservation plans.

The Hainan gibbon (*Nomascus hainanus*) (Thomas, 1892) is endemic to China, and although it was once widespread across Hainan Province, it is now considered the world's rarest ape, with a remaining population of only 33 individuals. These 33 Hainan gibbons are distributed in five groups (A, B, C, D, and E) that inhabit the Bawangling National Nature Reserve, which is a protected area of some 16 km^2 (Deng et al., 2015). In the past 70 years, the Hainan gibbon population has declined by 99.4%and its habitat has declined by 99.9% (Liu et al., 1989; Zhou et al., 2005; Deng et al., 2015). Systematic field observations have been conducted in the reserve since 2001, and over the past 17 years, only two new breeding groups have been established. The genetic relationships among breeding individuals as well the sex of the offspring recently born into each family group remain unknown.

Previous genetic studies of the Hainan gibbon have focused either on broad phylogenetic analyses (Su et al., 1995; Zhang, 1995; Thinh et al., 2010a,b), or attempts to identify microsatellite diversity of the mitochondrial DNA (mtDNA) control region (Li et al., 2010; Bryant et al., 2016b). Unfortunately, sampling limitations have made it difficult to conduct a comprehensive genetic analysis, and therefore our understanding of genetic variation in this last remaining Hainan gibbon population is extremely limited.

In the current study, over the course of one year, we collected fresh fecal samples from Hainan gibbons inhabiting three groups and combined field surveys and DNA analysis to identify patterns of gene flow, genetic drift, inbreeding depression, and genetic variability in this Critically Endangered primate species. Based on the research of Bryant et al. (2016b), we selected 10 microsatellite markers to obtain detailed information on Hainan gibbon genetic diversity. Our goal was to use these data to develop an effective management strategy to protect the last remaining Hainan gibbon population.

MATERIALS AND METHODS

Sampling and DNA Extraction

We studied Hainan gibbons inhabiting the Bawangling National Nature Reserve (19N 02′–19N 08′, 109 E 02′–09 E 13′), Hainan, China (**Figure 1**). Male and female Hainan gibbons display each morning by producing a set of highly stereotypic vocalizations. From September 2017 to December 2018, we monitored these vocalizations to identify group location (for groups A, B, C, and D; we did not monitor group E) and at these locations we collected fecal samples noninvasively and immediately after defecation (for groups A, B, and C). High-temperature sterilized

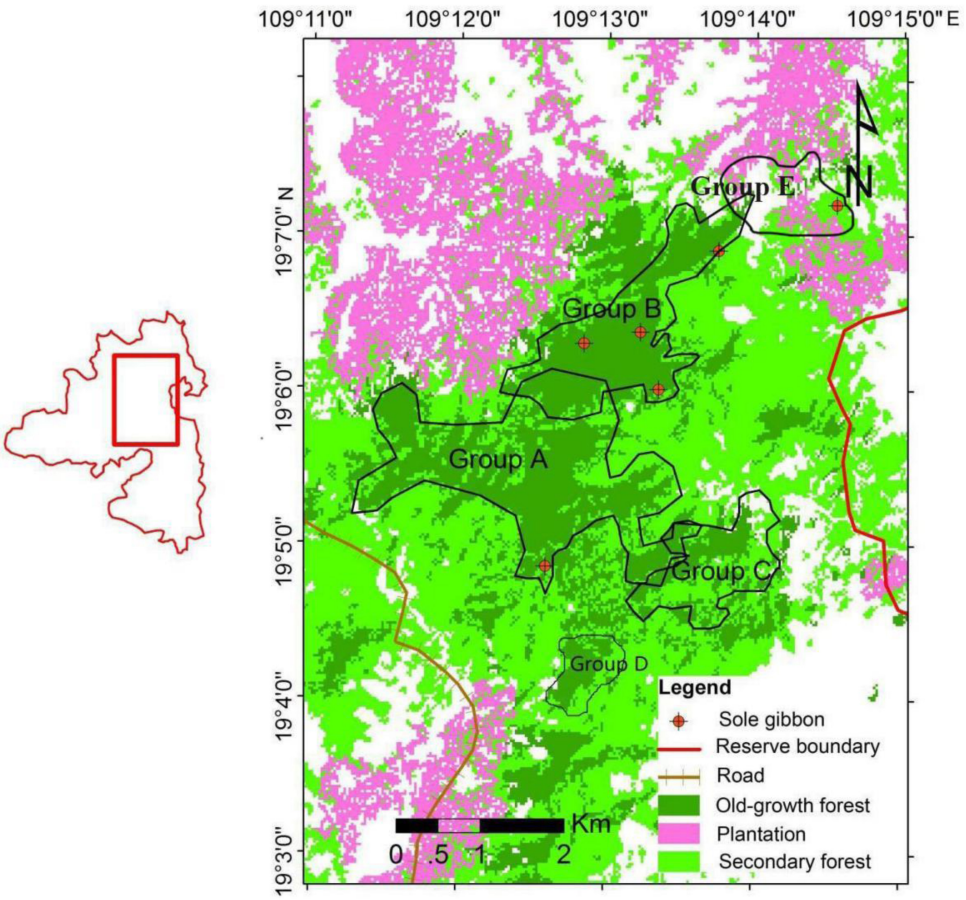

FIGURE 1 | Distribution of the five remaining groups of Hainan gibbons (Group E was discovered in June 2020; the survey of this study does not include Group E).

tweezers and petri dishes were used to collect fecal samples, which were stored in liquid nitrogen, and then kept cold using dry ice to transport the samples back to our laboratory for cryogenic storage. We also collected blood samples from two yellow-cheeked gibbons (*Hylobates gabriellae*) housed at the Nanning Zoo, Guangxi, China, and used these for comparative analyses.

We extracted DNA from 100 to 150 mg of feces using a QIAamp Fast DNA Stool Mini Kit and from 1 ml of blood using a QIAamp Blood & Cell Culture DNA Kit, following the manufacturer's instructions. The extracted DNA was subjected to 0.8% agarose gel electrophoresis, GreenView nucleic acid dye staining, and the estimated concentration and purity (260/280, 260/230 value) were recorded using a UV transilluminator. At the same time, we employed a Qubit 3.0 fluorescence quantifier to accurately quantify the concentration of DNA.

Identification of Polymorphic Markers and Genotyping

Microsatellite Loci

We tested 10 microsatellite loci previously described to be polymorphic in Hainan gibbons (Bryant et al., 2016b). Using the method of searching for microsatellite loci in the whole genome (Hou et al., 2018), and based on the reference genome of the northern white-cheeked gibbon (*Hylobates leucogenys*), 20 microsatellite loci were screened. To guarantee high-amplification success, particularly for DNA sourced from noninvasive samples, we selected microsatellites with >20 repeats and a product length of 100–300 bp. From the library of microsatellites that met our requirements, we randomly selected loci comprising different motifs for further optimization.

DNA extracts from two blood samples obtained from captive yellow-cheeked gibbons were used to amplify the 30 loci (**Supplementary File 1**). Polymerase chain reaction (PCR) amplification was performed in a 10-μl reaction volume, containing 1 μl of template DNA, 1 μl of forward and reverse primers, respectively, 5 μl of QIAGEN Multiplex PCR Master Mix (Qiagen), and 2 μg/μl of bovine serum albumin (BSA). The amplification conditions were 94°C for 15 min, 35 cycles at 94°C for 30 s, 43–65°C for 45 s, 72°C for 45 s, and final extension at 72°C for 5 min. Polymerase chain reaction products were separated on 3% agarose gels by electrophoresis to visually assess the amplification efficiency.

Next, we filtered the reliably sites from the *Hylobates gabriellae* blood sample amplifications and used the fecal samples of the Hainan gibbons to select appropriate microsatellite loci. Human blood was used for comparison to ensure that there was no contamination during the DNA extraction process.

PCR products were visualized on an ABI3730 XL Genetic Analyzer. Alleles were scored using GENEMARKER version 2.2.0. Readable peak: peak reading at ≤100 and lower intensity peak ≤50% of the higher intensity peak (the peak reads 50), otherwise the reading was abandoned and set to 0. According to genotyping criteria for the number of repeated experiments outlined by Taberlet and Luikart (1999), the length of allele fragments and the data were counted according to the integer multiples of 2, 3, and 4 bp in the length of different alleles. These data were transposed into an Excel table for subsequent population genetic testing.

Sex Markers

Three primers from Palle and Tina (2006), Valiere (2002), and Bolechova et al. (2016) were tested. We used known females and males to test the reliability of these primers for determining sex identification.

Individual Identification

We used the MICROSATELLITE TOOLKIT to obtain individual genotype data from each fecal sample (Park, 2001; Zhan et al., 2007; Hou et al., 2018), and combined sex identification (see above) and field survey data to obtain individual identities.

Data Assess

Genotyping

The presence of null alleles and scoring errors for each locus was estimated using MICRO-CHECKER v 2.2.3. Next, we used three indices to assess the reliability of genotyping. (1) Genotyping errors that resulted in allelic dropout (ADO), false alleles (FA), ADO, and FA were calculated using GIMLET v 1.1.3. (2). PCR success rates were estimated by calculating the percentage of successful PCRs that matched the consensus genotype (Wulstch et al. 2014). (3) For a specific locus i, we calculated the mean quality index (QI) of n samples for that locus using the following equation (Miquel et al., 2006).

$$\mathrm{QI}_{i,} = \sum_{j=1}^{n} \mathrm{QI}_{i,j} \tag{1}$$

Where n is the number of samples and QI_i, j the quality index of the ith locus for the jth sample. $\mathrm{QI}_{i,j}$ is estimated by the proportion of correct genotypes in three PCR replicates.

$$\mathrm{QI}_{,j} = \sum_{i=1}^{m} \mathrm{QI}_{i,j} \tag{2}$$

$$\mathrm{QI} = \frac{\sum_{i=1}^{m} \sum_{j=1}^{n} \mathrm{QI}_{i,j}}{n \times m} \tag{3}$$

We further calculated the quality index of each sample using Eq. 2 (e.g., jth sample) and we calculated the global quality index using Eq. 3: In Eq. 3, n and m represent the numbers of loci and samples, respectively.

Polymorphic Information Content and Hardy–Weinberg Equilibrium

To investigate the suitability of our markers, we calculated the polymorphic information content (PIC), which is an estimate of the discriminating power of markers (ranging from 0 to 1, from no allelic variation to only new alleles) (Botstein et al., 1980). We also tested markers for deviation from Hardy–Weinberg equilibrium (HWE). We assumed that deviation from HWE would indicate genotyping problems, such as segregating null alleles or incorrectly distinguished alleles.

Individual Recognition Ability

The individual identification ability of each loci can be determined by calculating the PID (probability of identity) value (Valiere, 2002; Zhan et al., 2007). We used the software Gimlet v1.1.3 to calculate the values of PID and PIDsib. Judgment criteria: PID < 0.001 and PIDsib < 0.01 (Waits et al., 2001; Hou et al., 2018). According to the curve produced by plotting the PID value of each locus, the closer the curve is to the X axis, the stronger the individual recognition ability.

Assessing Genetic Variation and Inbreeding

For each of the selected markers, we computed standard population genetic parameters of genetic variation. First, we calculated the expected heterozygosity (He), the observed heterozygosity (Ho), allelic frequencies, and the effective number of alleles. If the observed heterozygosity is lower than expected, this indicates inbreeding, while a higher than expected heterozygosity suggests the admixture of two previously isolated populations (Hartl and Clark, 1997). Furthermore, we determined inbreeding coefficients (FIS), with negative values indicating an excess of heterozygosity (Hedrick, 2000). We conducted all calculations in GeneALEx V.6.51 except the Wright F statistic (FIS), which we computed using FSTAT (version 2.9.3.) (Goudet, 2001).

Parentage Analysis

We used COLONY V.2.0.6.4 to conduct kinship analyses in order to infer the theoretical parental pair (Jones and Wang, 2010). We used the criterion probability of ≤95% to determine kinship (parent–child, mother–child, parental pair) (Wang and Santure, 2009; Bryant et al., 2016b; Wang, 2017).

Population Size Estimation

Based on linkage disequilibrium, we used NeEstimator V2.1 to calculate the effective population size.

Allele Loss

To detect allelic loss in our study population, we used genotype data from the microsatellite loci and compared those results

with the historical population of Hainan gibbons presented in Bryant et al. (2016b).

RESULTS

Study Population

We investigated the size and composition of four of the five remaining family groups of Hainan gibbons. The total population size of these four groups is 25 individuals (**Figure 2**). A total of 36 fecal samples were collected from three of these four groups, of which 6 samples were collected from Group A, 11 samples were collected from Group B, and 19 samples were collected from Group C. No genetic data were collected for Group D (**Supplementary File 2**).

Characterization of Markers

Microsatellite Markers

Overall, 33% (10/30) of the microsatellite markers tested suitable for investigating genetic diversity in the Hainan gibbon population. These included 6 tetranucleotide and 4 dinucleotide loci with 4–9 alleles per locus (**Table 1** and **Supplementary File 3**).

Sex Markers

Comparing the electropherograms of the sex-marked PCR products, we found that PCR products numbered 1 to 8 had no bands in the blank control group, and the target bands were bright and the background was clean. Select A-UTXTUY_F1, A-UTXR1, A-UTYR1, A-SRY_F1, and A-SRY_R1 (Valiere, 2002) were found to be reliable as sex identification markers (**Figure 3**).

Individual Identification

Combined with the results of sex identification, a total of 12 different individuals (4 females and 8 males) were identified. These 12 individuals included three residents of Group A (1 female and 2 males, accounting for 60% of this group), four residents of Group B (1 female and 3 males, accounting for 57% of this group), and five residents of Group C (2 females and

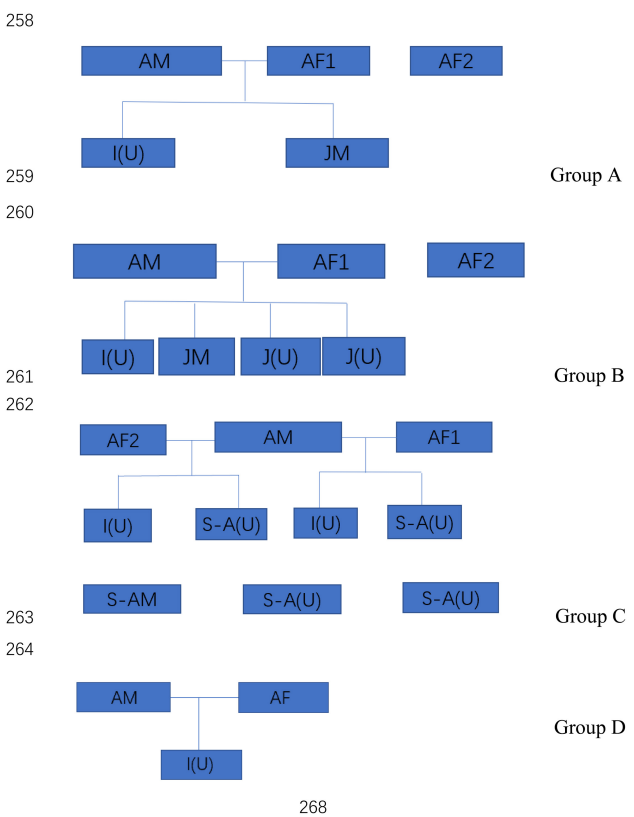

FIGURE 2 | The size and composition four wild Hainan gibbon groups. AM represents an adult male, AF represents an adult female, S-A represents a subadult, JM represents a juvenile, I represents an infant, and (U) represents an adult, subadult, juvenile, or infant of unknown sex. Infants are 0–24 months of age, juveniles are >2–7 years of age, subadults are >7–9 years of age, and adults are >9 years of age.

TABLE 1 | Ten pairs of microsatellite loci and their primers.

Locus	5′ modification	Duplication	Alleles	PCR product size/bp
SSR15	HEX	AAT	3	232
SSR17	FAM	TATT	3	208
D2S367	FAM	CA	5	138–156
D5S1457	HEX	GATA	3	110–118
D7S817	TAM	GATA	6	130–148
D1S548	FAM	TATC	3	161–173
D5S1470	HEX	GATA	4	192–204
D6S265	TAM	CA	5	118–134
D20S206	TAM	GATA	2	132–144
DQcar	HEX	CT	4	86–104

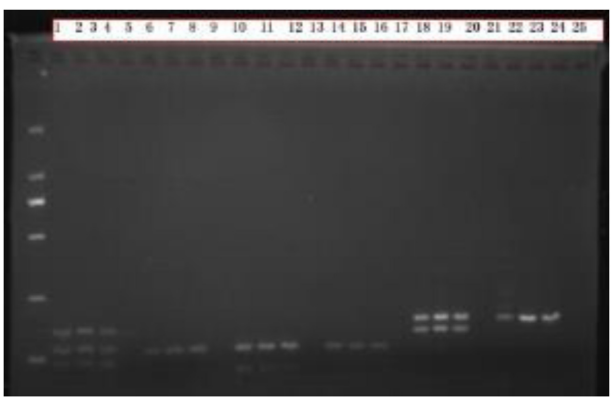

FIGURE 3 | Sex identification electrophoresis test results. Males have 2–3 bands, females have only 1 band, and numbers 1–8 are the PCR products of Scheme A. The blank control group does not have any bands, the target band is bright, and the background is clean; Numbers 9–16 are the PCR products of Scheme B. The blank control group has no bands, the target bands have a clean background, and the bands are fuzzy; Numbers 17–25 are the PCR products of Scheme C. The blank control group has no bands, the target bands are bright, and the background is clean, but some samples have nonspecific amplification.

3 males, accounting for 50% of this group). Fecal samples of infants (wet and scattered after voided) could not be collected. Overall, the 12 genetically identified Hainan gibbons accounted for approximately 67% of the total number of individuals present in the A, B, and C Groups (**Table 2**).

Performance of the Microsatellite System in Hainan Gibbons

None of 10 loci showed allelic loss, null alleles, or reading errors caused by stuttering (shadow peak). The amplification success rate was 74.09–100%, and the average amplification success rate was 93.40%. The quality index was 0.766–1, and the average quality index was 0.891.

The PIC results ranged from 0.1948 to 0.6682, suggesting that our markers had high discriminating power. The 10 loci all conformed to a Harvin equilibrium, indicating that the selected 10 microsatellite loci were all neutrally inherited (**Table 3**).

Individual Recognition Ability P(ID)DQcar was <0.001, indicating that only five sites were useful in recognizing two unrelated individuals. Similarly, P(ID)sib D5S1457 was <0.01, and thus using data from 9 sites allowed us to recognize two related individuals (**Figure 4**). Therefore, the individual identification system of 10 sites in this study was sufficient for individual recognition of Hainan Gibbon.

Sex Ratio

We found that across all three of our main study groups, there was a greater number of male Hainan gibbons than female Hainan gibbons. Of the 12 genetically identified individuals, 8 were males and four were females. In addition, of the 7 individuals for which parentage was determined, 6 were males and one was female. Based on the results of individual DNA identification, although this population contains many more males than females, the observed sex ratios of the offspring in Groups A, B, and C deviate from an expected 1:1 (**Table 4**).

TABLE 2 | Individual identification of residents in the A, B, and C Hainan gibbon social groups.

Group	No.	Sex	The same individual	Individual identification (combined with field investigation)
A	A01	female	A03, A05	Female adult without infant
	A02	male		Male juvenile
	A04	male	A06	Male
B	B01	female	B01	Female adult with infant
	B02	male	B02	Male subadult "Anan"
	B06	male	B06	Male
	B07	male		Male juvenile
C	C07	male	C07	Male subadult
	C19	male	C19	Male subadult
	C06	male	C06	Male subadult
	C10	female	C10	Female adult with infant
	C08	female	C09, C11, C12, C16, C18	Female subadult

Genetic Variation and Inbreeding

The observed heterozygosity (Ho) ranged from 0.250 to 0.917 and expected heterozygosity (He) from 0.219 to 0.719 (**Table 3**). The mean observed heterozygosity (mean ± SD = 0.608 ± 0.074) was greater than the mean expected heterozygosity (mean ± SD = 0.460 ± 0.049) (**Table 3**), In other words, although we expected approximately 46% of individuals to be heterozygous at a given locus under random mating conditions, on average 60% of individuals were heterozygous. Similarly, the mean FIS was −0.283 (mean), with FIS consistently <0 for all 12 polymorphic loci, indicating an excess of observed heterozygosity (see Hedrick, 2000, for comparison). Thus, individuals in our three study groups were less closely related than expected under random mating.

Parentage Analysis

We constructed a genetic pedigree (**Figure 5**) based on the results of kinship analysis (**Table 5**), Six individuals in Groups A, B, and C were identified as parent–child or full-sibs.

Population Size

The effective population size of the Hainan Gibbon is 5 (**Table 6**). The actual population is 33 individuals, and the ratio of effective population to actual population is 1:6.

Allele Loss

We compared the published microsatellite genotyping data of the historical population of Hainan gibbons with our results (Bryant et al., 2016b). Among the 8 microsatellite loci we examined, the number of alleles at 7 microsatellite loci in the present Hainan gibbon population has decreased, allelic loss has occurred, and allelic frequency has changed (**Supplementary File 4** and **Table 7**). Alleles fall into frequency classes (1–10). The current population showed fewer alleles in low-frequency classes and more in higher-frequency classes. This suggests that some alleles with low frequency recently have been lost in this population (**Figure 6**). This is consistent with the profile of a population characterized by a marked decline in genetic diversity.

DISCUSSION

Sample Collection and Suitability of Selected Markers

This study represents the first integrated investigation of the population demography and genetic diversity of the critically endangered Hainan gibbon. We have conducted long-term field observations of this species, and in the present study we also collected and analyzed DNA (from feces) from 50 to 60% of all residents in three of the five remaining wild groups. Our DNA sampling coverage was greater than in any previous study of this species (Li et al., 2010; Bryant et al., 2016b). In this regard, as pointed out by Tajima (1982), a DNA sequencing sample size of >10 is expected to result in limited variance and a representative genetic profile.

Prior to 2007, field surveys reported the existence of only two wild groups of Hainan gibbons, Group A and Group B

(Zhou et al., 2008). Subsequently, Group C was discovered in 2011. Group C was formed by the reorganization of individuals from groups A and B (Deng et al., 2015). In 2015, Bryant et al. (2016a) used the method of acoustic playback to identify a newly formed group of Hainan gibbons (Group D). In 2020, we located a fifth group of Hainan gibbons (Group E). Although our study did not collect genetic samples from residents of Group D or Group E, we assume that these groups were founded by members of Groups A, B, and/or C, and therefore from the perspective of population structure, the samples we collected are likely to reflect the genetic information present in Hainan gibbons.

The microsatellite markers used in this study fulfill important genetic and technical criteria that allow for high levels of precision and efficacy using high-throughput genotyping, which greatly improves the reliability of the genetic information (Butler et al., 2001). Twenty microsatellite loci were screened from the reference genome of *Hylobates leucogenys*, a close relative of the Hainan gibbon. The availability of several reference genomes provides valuable resources for genetic marker identification, and this resulted in simpler procedures for sample preparation and provided a larger amount of genetic information than other types of sequencing data (e.g., transcriptome). Compared with other types of genetic markers (SNPs), microsatellites have relatively high amplification success rates, especially for noninvasive samples, and have been used widely for individual identification in avian populations (Hou et al., 2018). Our results show that the 10 microsatellites used in this study provided reliable information on the sex and genotype of individual Hainan gibbons, provided high confidence paternity assignment, presented a relatively high level of polymorphic information and genetic variation, and resulted in a high accuracy of allelic characterization and a low occurrence or absence of mutations.

Declining Genetic Diversity

At the microsatellite level, the genetic diversity of the Hainan gibbon population is significantly lower than that reported in other gibbon species. For example, the number of alleles (Na) of the lar gibbon (*Hylobates lar*) is 7 and the expected heterozygosity (He) is 0.725 (Chambers et al., 2004); the number of alleles (Na) in Müller's gibbon (*Hylobates muelleri*) is 14.8 (Oka and Takenaka, 2001). Similarly, the Endangered Borneo elephant (*Elephas maximus*), which today is only distributed in the northeastern part of Sabah, Malaysia, and has a remaining population of only 2,000 individuals, also is characterized by low genetic diversity (Ho = 0.14–0.41) and significant inbreeding (Fis = 0.14–0.38) (Benoit et al., 2016). In the case of the Mexican howler monkey (*Alouatta palliata mexicana*), a Critically Endangered subspecies endemic to Mexico, extensive habitat loss and fragmentation over the past 30 years have resulted in a major population decline. Presently, this primate taxon is distributed in four forest fragments in the state of Veracruz, Mexico. Genetic testing revealed that haplotype diversity and nucleotide diversity (h = 0.486; π = 0.0007) are extremely low compared with other Neotropical primates (Jacob et al., 2014).

The low genetic diversity of the remaining Hainan gibbon population is consistent with their severe population decline (99.4%), which has occurred over the past 70 years (Zhou et al., 2008). Their current population size of only 33 individuals is the result of extreme deforestation and forest fragmentation that has decreased their remaining area of suitable habitat from 27,784 km^2 (Zhou et al., 2005) to approximately 16 km^2 (Zhou et al., 2008). The number of alleles in the existing population, and therefore its genetic diversity, is far less than historically reported (Bryant et al., 2016b) and extremely low compared to other primate populations.

Probability of Inbreeding in the Future

The social and breeding system of Hainan gibbons is described as monogamous (Liu et al., 1989; Zhou et al., 2008). When the number of reproducing males in a population is small, binomial sampling error occurs, and the frequency of alleles contributed by paternal and maternal lines is unequal (Storz et al., 2001). Our analysis indicated no evidence of inbreeding in the existing population of Hainan gibbons. The excessive heterozygotes (FIS $<$0) reveal that mating in the current population is biased toward individuals with relatively distant relationships. Combining kinship analysis with behavioral field observation, the genetic pedigrees of the 12 identified Hainan gibbons indicate high

TABLE 3 | Number of alleles (Na), observed and expected heterozygosity (Ho, He), polymorphic information content (PIC), inbreeding coefficient (FIS), and Hardy–Weinberg deviation (P_{HWE}) for 10 selected markers with the mean and standard deviation (SD) across all markers.

Loci	Na	Ho	He	*FIS*	P_{HWE}	PIC values
SSR12	2	0.417	0.497	0.203	0.5939	0.3733
SSR17	3	0.750	0.517	−0.414	0.2839	0.4443
D1S548	3	0.750	0.642	−0.125	1.0000	0.5697
D5S1470	2	0.417	0.330	−0.222	1.0000	0.2755
D6S265	4	0.917	0.719	−0.235	0.9132	0.6682
D2S367	2	0.667	0.444	−0.467	0.2160	0.3457
D5S1457	2	0.333	0.278	−0.158	1.0000	0.2392
D7S817	2	0.750	0.469	−0.571	0.0922	0.3589
D20S206	2	0.250	0.219	−0.100	1.0000	0.1948
DQcar	2	0.833	0.486	−0.692	0.0631	0.368
Mean	2.400	0.608	0.460	−0.283		0.3838
S.D.	0.221	0.074	0.049	*n/a*		–

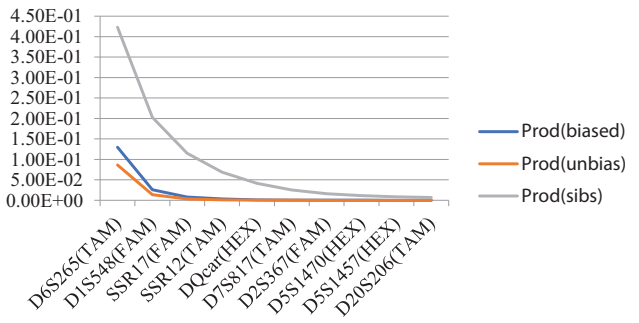

FIGURE 4 | Individual identification system ability curve.

TABLE 4 | Sex ratio of the Hainan gibbon study population.

Sample	Female	Male	Sex ratio	Yates-corrected chi-square test against 1:1 $P < 0.1$
All	4	8	1:2	$\chi^2 = 1.333$, $P = 0.248$
Group A	1	2	1:2	$\chi^2 = 0.333$, $P = 0.564$
Group B	1	3	1:3	$\chi^2 = 1$, $P = 0.317$
Group C	2	3	2:3	$\chi^2 = 2$, $P = 0.655$
All offspring	1	6	1:6	$\chi^2 = 3.571$, $P = 0.059$

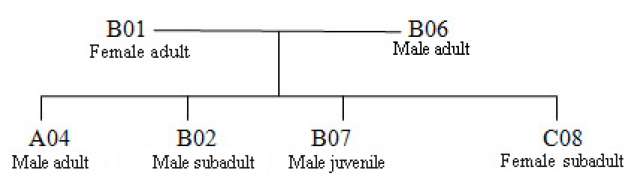

FIGURE 5 | Genetic maps of 3 Hainan gibbon groups.

TABLE 5 | Parent–offspring pair inferred using the software COLONY.

Offspring ID	Inferred father	Inferred mother	Probability
A04	B06	B01	1.000
B02	B06	B01	0.9744
B07	B06	B01	0.9892
C08	B06	B01	0.9945

The letters A, B, and C refer to the groups in which these individuals currently reside.

levels of relatedness among individuals in Groups A, B, and C (**Figure 7**). Also, the offspring sex ratio deviates significantly from 1:1; given the large number of males in the population, we anticipate high levels of inbreeding in the future. Inbreeding may build up over a much longer time frame than relatedness. Next, we will use genome technology to deeply analyze the mechanism of inbreeding.

Long-Term Survival Goals

The remaining area of suitable habitat for Hainan Gibbons is extremely small and highly fragmented.

TABLE 6 | Effective population size estimates of Hainan gibbon.

	Estimated Ne (P_{crit}=0.010)	
	Ne	95% confidence interval
Hainan gibbon	5.3	5.3

TABLE 7 | The difference in the number of alleles at 8 microsatellite loci between the existing population and the historical population.

	Current population	Historical population
Locus	Number of alleles	Number of alleles
D1S548	3	3
D5S1470	2	3
D6S265	4	5
D2S367	2	4
D5S1457	2	3
D7S817	2	5
D20S206	2	1
DQcar	2	4

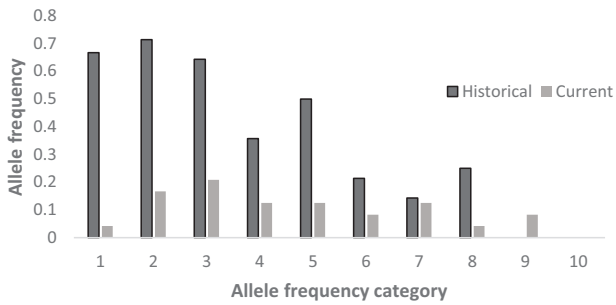

FIGURE 6 | Distribution of allele frequencies for the historical and current populations across 8 loci.

Low genetic diversity of the population is likely the result of founder effect and a sharp decline in effective population size (Frankham, 1997; Groombridge et al., 2009). Compared with the effective population size of the historical population (Ne = 1162.96), the effective population size of the existing population (Ne=5.3) has been significantly reduced. When the effective population size (Ne) is <50, population viability decreases significantly (Madsen et al., 1999). The long-term evolutionary survival of any population is expected to require an Ne ≥1000 (Frankham et al., 2014).

In the 1970s, the total Hainan gibbon population in the Bawangling National Nature Reserve was 7–8 individuals (Zhou et al., 2005). It has taken more than 40 years for this population to reach its current size of 33 individuals (rate of 0.625 individuals added to the population per year). Given their relatively slow life history (individuals do not reach adulthood until >9 years of age and females give birth every 2–4 years), the long-term viability of the current Hainan

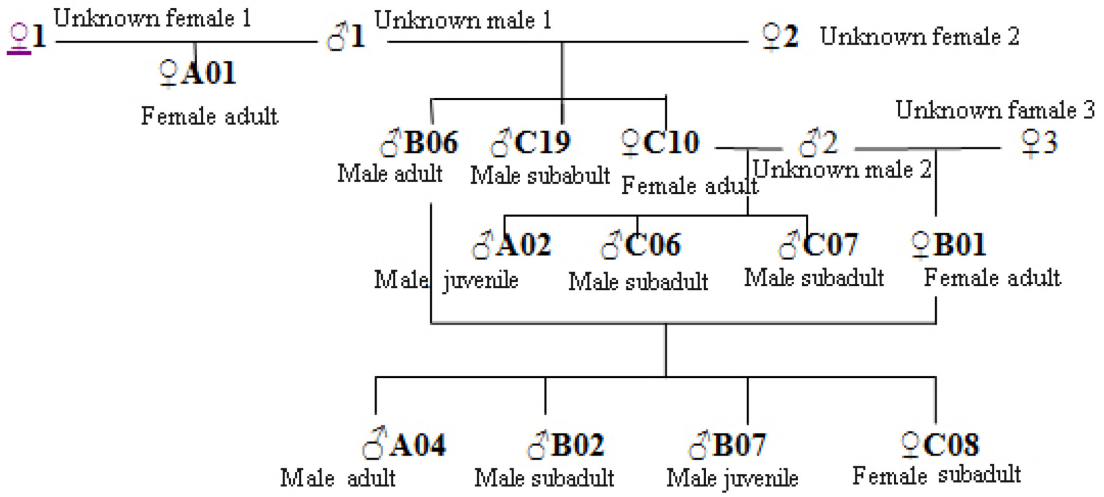

FIGURE 7 | Kinship diagram of individuals in Groups A, B, and C. Based on these results, both males and females transfer between established groups, and given the existence of new groups (D and E), individuals periodically form new groups.

gibbon population remains doubtful unless there is an immediate and significant reforestation effort and targeted programs to protect the remaining Hainan gibbon population.

Conservation and Management

Given their limited remaining habitat, low genetic diversity, extremely small effective population size, and high potential inbreeding for inbreeding, we plan to establish a genetic profile for each of the remaining 33 Hainan gibbons. This will allow us to monitor both behaviorally and genetically the degree of population inbreeding and potential for disease transmission and, if necessary, intervene to promote increased genetic variability and population health. We also propose that the Bawangling National Nature Reserve immediately initiates a program to professionally train reserve staff so that they can continuously monitor the behavior, diet, and demography of individuals in all five gibbon groups and reforest and restore the current fragmented habitat in ways to minimize the negative impact of human disturbance on gibbon survivorship. Finally, efforts must be made to strengthen communication and cooperation among all stakeholders and reach a scientifically based consensus on measures that must be taken to ensure the long-term survival of the last remaining Hainan gibbon population.

DATA AVAILABILITY STATEMENT

The datasets presented in this study can be found in online repositories. The names of the repository/repositories and accession number(s) can be found in the article/**Supplementary Material**.

ETHICS STATEMENT

Ethical review and approval was not required for the animal study because Noninvasive sampling method.

AUTHOR CONTRIBUTIONS

JZ, JC, and NX designed the study. YG wrote the manuscript and analyzed the data. LH completed the experiments and analyzed the data. PG wrote the manuscript. TL and GL conducted the field investigations. All authors contributed to the article and approved the submitted version.

FUNDING

This work was supported by the project of the National Natural Science Foundation Project of Research on Conservation Genetics of Hainan Gibbon (31770456); Ministry of Science and Technology of the People's Republic of China major project (2016YFC0503200); Science and Technology Program of Guizhou Province: the Key Project of Science and Technology Program of Guizhou Province (20182780); Science and Technology Program of Guizhou Province: Ecological Study on Viruses Carried by Bats in Guizhou Province (20161004); Strategic Priority Research Program of the Chinese Academy of Sciences (XDA23080201); Biodiversity Survey, Monitoring and Assessment Project of Ministry of Ecology and Environment, China (2019HB2096001006); The Project for National Top Discipline Construction of Guizhou Province: Geography in Guizhou Normal University (201785-01); and Reproductive Biology of Hainan Gibbon of Hainan National Park Research Institute.

ACKNOWLEDGMENTS

We thank Chrissie, Sara, Jenni, and Dax for their continued support and insights into the importance of kinship in understanding primate evolution.

SUPPLEMENTARY MATERIAL

The Supplementary Material for this article can be found online at: https://www.frontiersin.org/articles/10.3389/fgene.2020.608633/full#supplementary-material

REFERENCES

Andie, A., Amrita, S., Rudolf, M., Tuong, B. L., Quyet, K. L., and Herbert, C. (2016). No evidence for mitochondrial genetic variability in the largest population of critically endangered tonkin snub-nosed monkeys in vietnam. *Primates.* 57, 449–453. doi: 10.1007/s10329-016-0571-x

Benoit, G., Reeta, S., Nurzhafarina, O., Célia, K. R., Rosdi, S. M. A., Laurentius, N. A., et al. (2016). Habitat fragmentation and genetic diversity in natural populations of the bornean elephant: implications for conservation. *Biol. Conserv.* 196, 80–92. doi: 10.1016/j.biocon.2016.02.008

Bolechova, P., Jecminkova, K., and Hradec, M. (2016). Sex determination in gibbons of genus *Nomascus* using non-invasive method. *Act. vet. Brno.* 85, 363–366. doi: 10.2754/avb201685040363

Botstein, D., White, R. L., Skolnick, M., and Davis, R. W. (1980). Construction of a genetic linkage map in man using restriction fragment length polymorphisms. *Am. J. Hum. Genet.* 32, 314–331.

Bryant, J. V., Gottelli, D., Zeng, X., Hong, X., Chan, B. P., Fellowes, J. R., et al. (2016a). Assessing current genetic status of the hainan gibbon using historical and demographic baselines: implications for conservation management of species of extreme rarity. *Mol. Ecol.* 25, 3540–3556. doi: 10.1111/mec.13716

Bryant, J. V., Brule, A., and Wong, M. H. G. (2016b). Detection of a new Hainan gibbon (*Nomascus hainanus*) group using acoustic call playback. *Int J Primatol.* 37, 534–547. doi: 10.1007/s10764-016-9919-8

Butler, J. M., Ruitberg, C. M., and Vallone, P. M. (2001). Capillary electrophoresis as a tool for optimization of multiplex PCR reactions. *Fresen J Anal Chem.* 369, 200–205. doi: 10.1007/s002160000641

Chambers, K. E., Reichard, U. H., and Moller, A. (2004). Cross-species amplification of human microsatellite markers using noninvasive samples from white-handed gibbons (*Hylobates lar*). *Am. J. Primatol.* 64, 19–27. doi: 10.1002/ajp.20058

David, H. R., and Richard, F. (2003). Correlation between fitness and genetic diversity. *Conserv. Biol.* 17:230e237. doi: 10.1046/j.1523-1739.2003.01236.x

Deng, H. Q., Zhang, M. X., and Zhou, J. (2015). Recovery of the critically endangered Hainan gibbon *Nomascus hainanus*. *Fau Flo In.* 51, 161–165. doi: 10.1017/S0030605315000678

Estrada, A., Garber, P. A., Rylands, A. B., Roos, C., Fernandez-Duque, E., Fiore, A., et al. (2017). Impending extinction crisis of the world's primates: why primates matter. *Sci Adv.* 3:e1600946. doi: 10.1126/sciadv.1600946

Fan, P. F., Fei, H. L., and Luo, A. D. (2013). Ecological extinction of the critically endangered northern white-checked gibbon *Nomascus* leucogenys in china. *Fau Flo In.* 48, 52–55. doi: 10.1017/S0030605312001305

Frankham, R. (1997). Do island populations have less genetic variation than mainland populations? *Heredity* 78, 311–327. doi: 10.1038/hdy.1997.46

Frankham, R. (2005). Genetics and extinction. *Biol. Conserv.* 126, 131–140.

Frankham, R., Ballou, J. D., and Briscoe, D. A. (2009). *An Introduction to Conservation Genetics*. Cambridge: Cambridge University Press.

Frankham, R., Bradshaw, C. J. A., and Brook, B. W. (2014). Genetics in conservation management: revised recommendations for the 50/500 rules. red list criteria and population viability analyses. *Biol. Conserv.* 170, 56–63. doi: 10.1016/j.biocon.2013.12.036

Goudet, J. (2001). *FSTAT, a program to estimate and test gene diversities and fixation indices (version 2.9.3)*. Available Online at: http://www.unil.ch/izea/softwares/fstat.html.

Groombridge, J. J., Dawson, D. A., Burke, T., Prys-Jones, R., Brooke, M., de, L., et al. (2009). Evaluating the demographic history of the Seychelles kestrel (Falco araea): genetic evidence for recovery from a population bottleneck following minimal conservation management. *Biol. Conserv.* 142, 2250–2257. doi: 10.1016/j.biocon.2009.04.026

Hartl, D. L., and Clark, A. G. (1997). *Principles of population genetics*, 3rd Edn. (Sutherland: Sinauer Associates).

Hedrick, P. W. (2000). *Genetics of populations*, 2nd Edn. (Sudbury: Jones and Bartlett).

Hemmings, N. L., Slate, J., and Birkhead, T. R. (2012). Inbreeding causes early death in apasserine bird. *Nat. Commun.* 3:863. doi: 10.1038/ncomms1870

Hoelzel, A. R. (1997). *Molecular ecology of pinnipeds. In: Molecular genetics of marine mammals. Special Publication, 3*. (Lawrence, USA: Society for Marine Mammalogy).

Hou, X., Xu, P. W., and Jackson, J. D. U. (2018). An integrated tool for microsatellite isolation and validation from the reference genome and their application in the study of breeding turover in an endangered avian population. *Integr. Zool.* 13, 553–568. doi: 10.1111/1749-4877.12305

Iucn (2004). *IUCN Red List Categories and Criteria: Version 3.1 Second edition*. (Gland, UK.: IUCN).

Iucn (2020). *The IUCN Red List of Threatened Species. Version 2020-2*. Available Online at: https://www.iucnredlist.org/

Jacob, C., Dunn, A. S. G., Jurgi, C. A., Liliana, C. O., Ernesto, R. L., and Leslie, A. K. (2014). Limited genetic diversity in the critically endangered mexican howler monkey (Alouatta palliata mexicana) in the selva zoque. *Mexico. Primates.* 55, 155–160. doi: 10.1007/s10329-013-0399-6

Jones, O. R., and Wang, J. L. (2010). COLONY: a program for parentage and sibship inference from multilocus genotype data. *Mol. Ecol. Resour.* 10, 551–555. doi: 10.1111/j.1755-0998.2009.02787.x

Li, B., Li, M., Li, J., Fan, P., Ni, Q., Lu, J., et al. (2018). The primate extinction crisis in china: immediate challenges and a way forward. *Biodivers. Conserv.* 27, 3301–3327. doi: 10.1007/s10531-018-1614-y

Li, Z. G., Wei, F. W., and Zhou, J. (2010). Sequence analysis of mitochondrial D-loop region of hainan gibbon and population rejuvenation. *Biodiversity* 18, 523–527. doi: 10.3724/SP.J.1003.2010.523

Lindsey, H. A., Gallie, J., Taylor, S., and Kerr, B. (2013). Evolutionary rescuefrom extinction is contingent on a lower rate of environmental change. *Nature* 494, 463–467. doi: 10.1038/nature11879

Liu, Z. H., Zhang, Y. Z., Jiang, H. S., and Southwick, C. H. (1989). Population structure of hylobates concolor in bawanglin nature reserve, hainan, china. *Am. J. Primatol.* 19, 247–254. doi: 10.1002/ajp.1350190406

Liu, Z. J., Liu, G. J., Roos, C., Wang, Z. M., Xiang, Z. F., Zhu, P. F., et al. (2015). Implications of genetics and current protected areas for conservation of 5 endangered primates in china. *Conserv. Biol.* 29, 1508–1517. doi: 10.1111/cobi.12581

Madsen, T., Shine, R., and Olsson, M. (1999). Conservation biology: restoration of an inbred adder population. *Nature.* 402, 34–35. doi: 10.1038/46941

Miquel, C., Bellemain, E., and Poillot, C. (2006). Quality indexes to assess the reliability of genotypes in studies using noninvasive sampling and multiple-tube approach. *Mol Ecol Notes.* 6, 985–988. doi: 10.1111/j.1471-8286.2006.01413.x

Oka, T., and Takenaka, O. (2001). Wild gibbons' parentage tested by non-invasive DNA sampling and PCR-amplified polymorphic microsatellites. *Primates* 42, 67–73. doi: 10.1007/BF02640690

Palle, V., and Tina, F. (2006). Fast and non-invasive PCR sexing of primates: apes, old world monkeys, new world monkeys and strepsirrhines. *BMC Ecol.* 6:8. doi: 10.1186/1472-6785-6-8

Park, S. J. (2001). *Microsatellite toolkit for Excel. Smurfit Institute of Genetics*. (Ireland: Trinity College. Universityof Dublin).

Siddle, H. V., Kreiss, A., Eldridge, M. D., Noonan, E., Clarke, C. J., Pyecroft, S., et al. (2007). Transmission of a fatal clonal tumor by biting occurs due to depleted MHC diversity in a threatened carnivorous marsupial. *PNAS* 104, 16221–16226. doi: 10.1073/pnas.0704580104

Storz, J. F., Bhat, H. R., and Kunz, T. H. (2001). Genetic consequences of polygyny and social structure in an indian fruit bat. cynopterus sphinx. i. inbreeding, outbreeding, and population subdivision. *Evolution* 55, 1215–1223. doi: 10.1111/j.0014-3820.2001.tb00641.x

Su, B., Monda, K., Wang, W., Jiang, X., Wang, Y., Woodruff, D. S., et al. (1995). "Molecular phylogeny of Chinese concolor gibbons (subgenus Nomascus) using noninvasive DNA genotyping," in *Primate Research and Conservation*, eds W. Xia and Y. Zhang (Beijing: China Forestry Publishing House).

Swinnerton, K. J., Groombridge, J. J., Jones, C. G., Burn, R. W., and Mungroo, Y. (2004). Inbreeding depression and founder diversity among captive and free-living populations of the endangered pink pigeon columba mayeri. *Anim. Conserv.* 7, 353–364. doi: 10.1017/S1367943004001556

Taberlet, P., and Luikart, G. (1999). Non-invasive genetic sampling and individual indentification. *Bio. J. Linn. Soci.* 68, 41–55. doi: 10.1111/j.1095-8312.1999.tb01157.x

Tajima, F. (1982). Evolutionary relationship of DNA sequences in finite populations. *Genetics* 105, 437–460.

Thinh, V. N., Mootnick, A. R., Geissmann, T., Li, M., Ziegler, T., Agil, M., et al. (2010a). Mitochondrial evidence for multiple radiations in the evolutionary history of small apes. *BMC Evol. Biol.* 10:74. doi: 10.1186/1471-2148-10-74

Thinh, V. N., Rawson, B., and Hallam, C. (2010b). Phylogeny and distribution of crested gibbons (genus *Nomascus*) based on mitochondrial cytochrome b gene sequence data. *Am. J. Primatol.* 72, 1047–1054. doi: 10.1002/ajp.20861

Thomas, O. (1892). XXIII.–Note on the gibbon of the island of hainan (*Hylobates hainanus* sp. n.). *J. Nat. Hist.* 9, 145–146. doi: 10.1080/00222939208677291

Valiere, N. (2002). GIMLET:a computer program for analysis genetic individual identification data. *Mol. Ecol. Notes* 2, 377–379. doi: 10.1046/j.1471-8286.2002.00228.x-i2

Waits, L. P., Luikart, G., and Taberlet, P. (2001). Estimating the probability of identity among genotypes in natural populations: cautions and guidelines. *Mol. Ecol.* 10, 249–256. doi: 10.1046/j.1365-294X.2001.01185.x

Wang, J., and Santure, A. W. (2009). Parentage and sibship inference from multilocus genotype data under polygamy. *Genetics* 181, 1579–1594. doi: 10.1534/genetics.108.100214

Wang, J. L. (2017). *User's guide for software COLONY Version 2.0.6.4*. (London: Zoological Society of London).

Wei, F. W., Hu, Y. B., Zhu, L., Bruford, M. W., Zhan, X., and Zhang, L. (2012). Black and white and read all over: the past, present and future of giant panda genetics. *Mol. Ecol.* 21, 5660–5674. doi: 10.1111/mec.12096

Wultsch, C., Waits, L. P., and Kelly, M. J. (2014). Noninvasive individual and species identification of jaguars (*Panthera onca*), pumas (*Puma concolor*) and ocelots (*Leopardus pardalis*) in Belize, Central America using cross-species microsatellites and faecal DNA. *Mol. Ecol. Res.* 14, 1171–1182. doi: 10.1111/1755-0998.12266

Yang, Y., Groves, C., Garber, P., Wang, X. W., Li, H., Long, Y. C., et al. (2019). First insights into the feeding habits of the Critically endangered black snub−nosed monkey, rhinopithecus strykeri (Colobinae, Primates). *Primates* 60, 143–153. doi: 10.1007/s10329-019-00717-0

Zhan, X. J., Zhang, Z. J., Wu, H., Goossens, B., Li, M., Jiang, S. W., et al. (2007). Molecualr analysis of dispersal in giant pandas. *Mol. Ecol.* 16, 3792–3800. doi: 10.1111/j.1365-294X.2007.03450.x

Zhang, Y. (1995). "A molecular phylogeny of gibbons based on DNA sequences," in *Primate Research and Conservation*, eds W. Xia and Y. Zhang (Beijing: China Forestry Publishing House), 50–54.

Zhou, J., Wei, F. W., and Li, M. (2005). Hainan black-crested gibbon is headed for extinction. *Am. J. Primatol.* 26, 453–465. doi: 10.1007/s10764-005-2933-x

Zhou, J., Wei, F. W., Li, M., Chan, B. P. L., and Wang, D. (2008). Reproductive characters and mating behaviour of wild *Nomascus hainanus*. *Am. J. Primatol.* 29, 1037–1046. doi: 10.1007/s10764-008-9272-7

Conflict of Interest: The authors declare that the research was conducted in the absence of any commercial or financial relationships that could be construed as a potential conflict of interest.

frontiers in Genetics

ORIGINAL RESEARCH
published: 15 December 2020
doi: 10.3389/fgene.2020.615926

Genetic Diversity, Inbreeding Level, and Genetic Load in Endangered Snub-Nosed Monkeys (*Rhinopithecus*)

*Weimin Kuang[1], Jingyang Hu[1], Hong Wu[1], Xiaotian Fen[2,3,4], Qingyan Dai[2,3,4], Qiaomei Fu[2,3,4], Wen Xiao[5], Laurent Frantz[6,7], Christian Roos[8], Tilo Nadler[9], David M. Irwin[10], Linchun Zhou[11], Xu Yang[12] and Li Yu[1]**

[1] State Key Laboratory for Conservation and Utilization of Bio-Resource in Yunnan, School of Life Sciences, Yunnan University, Kunming, China, [2] Key Laboratory of Vertebrate Evolution and Human Origins of Chinese Academy of Sciences, IVPP, CAS, Beijing, China, [3] Center for Excellence in Life and Paleoenvironment, Chinese Academy of Sciences, Beijing, China, [4] Beijing College of Life Science, University of Chinese Academy of Sciences, Beijing, China, [5] Institute of Eastern-Himalaya Biodiversity Research, Dali University, Dali, China, [6] School of Biological and Chemical Sciences, Queen Mary University of London, London, United Kingdom, [7] The Palaeogenomics and Bio-Archaeology Research Network, Department of Archaeology, University of Oxford, Oxford, United Kingdom, [8] Gene Bank of Primates and Primate Genetics Laboratory, German Primate Center, Leibniz Institute for Primate Research, Göttingen, Germany, [9] Wildlife Consultant, Ninh Binh, Vietnam, [10] Department of Laboratory Medicine and Pathobiology, University of Toronto, Toronto, ON, Canada, [11] Lushui Management and Conservation Branch of Gaoligong Mountain National Nature Reserve, Nujiang, China, [12] Lushui Forestry and Grassland Council, Nujiang, China

OPEN ACCESS

Edited by:
Deyan Ge,
Chinese Academy of Sciences (CAS), China

Reviewed by:
Xiao-Guang Qi,
Northwest University, China
Xuming Zhou,
Chinese Academy of Sciences (CAS), China

***Correspondence:**
Li Yu
yuli@ynu.edu.cn

Specialty section:
This article was submitted to Evolutionary and Population Genetics, a section of the journal Frontiers in Genetics

Received: 10 October 2020
Accepted: 17 November 2020
Published: 15 December 2020

Citation:
Kuang W, Hu J, Wu H, Fen X, Dai Q, Fu Q, Xiao W, Frantz L, Roos C, Nadler T, Irwin DM, Zhou L, Yang X and Yu L (2020) Genetic Diversity, Inbreeding Level, and Genetic Load in Endangered Snub-Nosed Monkeys (Rhinopithecus). Front. Genet. 11:615926. doi: 10.3389/fgene.2020.615926

The snub-nosed monkey genus (*Rhinopithecus*) comprises five closely related species (*R. avunculus*, *R. bieti*, *R. brelichi*, *R. roxellana*, and *R. strykeri*). All are among the world's rarest and most endangered primates. However, the genomic impact associated with their population decline remains unknown. We analyzed population genomic data of all five snub-nosed monkey species to assess their genetic diversity, inbreeding level, and genetic load. For *R. roxellana*, *R. bieti*, and *R. strykeri*, population size is positively correlated with genetic diversity and negatively correlated with levels of inbreeding. Other species, however, which possess small population sizes, such as *R. brelichi* and *R. avunculus*, show high levels of genetic diversity and low levels of genomic inbreeding. Similarly, in the three populations of *R. roxellana*, the Shennongjia population, which possesses the lowest population size, displays a higher level of genetic diversity and lower level of genomic inbreeding. These findings suggest that although *R. brelichi* and *R. avunculus* and the Shennongjia population might be at risk, it possess significant genetic diversity and could thus help strengthen their long-term survival potential. Intriguingly, *R. roxellana* with large population size possess high genetic diversity and low level of genetic load, but they show the highest recent inbreeding level compared with the other snub-nosed monkeys. This suggests that, despite its large population size, *R. roxellana* has likely been experiencing recent inbreeding, which has not yet affected its mutational load and fitness. Analyses of homozygous-derived deleterious mutations identified in all snub-nosed monkey species indicate that these mutations are affecting immune, especially in smaller population sizes, indicating that the long-term consequences of inbreeding may be resulting in an overall reduction of immune capability in the snub-nosed monkeys, which could provide a dramatic effect

on their long-term survival prospects. Altogether, our study provides valuable information concerning the genomic impact of population decline of the snub-nosed monkeys. We revealed multiple counterintuitive and unexpected patterns of genetic diversity in small and large population, which will be essential for conservation management of these endangered species.

Keywords: snub-nosed monkeys, population genomics, genetic diversity, inbreeding, genetic load, population decline

INTRODUCTION

The snub-nosed monkey genus (*Rhinopithecus*) comprises five closely related species. The golden snub-nosed monkey (*R. roxellana*), Yunnan snub-nosed monkey (*R. bieti*), and Guizhou snub-nosed monkey (*R. brelichi*) are endemic to China, while the Tonkin snub-nosed monkey (*R. avunculus*) is distributed in northern Vietnam, and the Myanmar/Nujiang snub-nosed monkey (*R. strykeri*) inhabits northern Myanmar and the Nujiang prefecture in China (Geissmann et al., 2011; Liedigk et al., 2012; Ma et al., 2014; Meyer et al., 2017) (**Figure 1**). Currently, all five species are classified as endangered or critically endangered on the International Union for Conservation of Nature (IUCN) Red List.

Fossil records indicate that the snub-nosed monkeys were widely distributed across East Asia during the Late Pleistocene and Early Holocene (Han, 1982; Jablonski and Pan, 1988; Jablonski, 1998). Environmental changes during the Holocene, however, led to habitat loss and fragmentation for all five species, and this process was likely accelerated by increasing human activities over the last 400 years (Li et al., 2002; Nuchel et al., 2018). In fact, recent field surveys indicated that the population sizes in these species were extremely low. For example, there are only 22,500 individuals of *R. roxellana*, the most numerous species, which are isolated in three fragmented populations in the Minshan and Qionglai mountains (SG; Sichuan/Gansu provinces), the Qinling mountain (QL; Shanxi province), and the Shennongjia National Nature Reserve (SNJ; Hubei province) (Quan and Xie, 2002; Liu et al., 2015; Li et al., 2018). Other species, such as *R. bieti* and *R. strykeri* are only ∼3,000 (Li et al., 2018; Zhao et al., 2019) and ∼950 individuals (Meyer et al., 2017; Ren et al., 2017; Yang et al., 2019), respectively, and there are fewer than 400 and 200 individuals of most endangered species *R. brelichi* (Guo et al., 2020) and *R. avunculus* (Nadler, 2018) left in the wild, respectively.

These dramatically low population sizes, if maintained long enough, may cause loss of genetic diversity, increase of inbreeding, and accumulation of deleterious mutations (genetic load), all of which can reduce adaptive potential and dramatically increase risk of extinction (Hansson and Westerberg, 2002; Frankham, 2005; Heller and Zavaleta, 2009; Jump et al., 2009). These issues, however, can be mitigated with appropriate conservation management that takes into account genetic diversity (Frankham, 2005). Yet, despite the fact that many studies have investigated the taxonomy, phylogeography, and deep evolutionary history of the snub-nosed monkeys based on mitochondrial DNA and microsatellites (Zhang and Ryder, 1997; Li et al., 2004, 2007; Liu et al., 2007, 2009, 2015; Chang et al., 2012; Liedigk et al., 2012; Yang et al., 2012; Kolleck et al., 2013; Hong et al., 2017), and more recently based on whole genome sequencing (Zhou et al., 2014, 2016; Yu et al., 2016; Kuang et al., 2019), little is known about the genetic diversity and levels of inbreeding in these populations.

To explore the genetic diversity, inbreeding level, and genetic load in these species, we analyzed 62 genome sequences representing individuals from all five snub-nosed monkeys. Our study provides valuable information concerning the genomic impact of population decline of the snub-nosed monkeys. In particular, we unravel unexpected patterns of genetic diversity in small and large population, which will be essential for conservation management of these endangered species.

MATERIALS AND METHODS

Data Collection and Genome Sequencing

Ninety-five published genomic data from all five snub-nosed monkeys, including 57 *R. roxellana*, 28 *R. bieti*, 1 *R. avunculus*, 5 *R. brelichi*, and 4 *R. strykeri* (Zhou et al., 2014, 2016; Yu et al., 2016; Kuang et al., 2019) were downloaded from the National Center for Biotechnology Information (NCBI). An additional, seven *R. bieti*, three *R. strykeri*, and one *R. avunculus* were sequenced in this study (**Supplementary Table 1**). A bone (R.strykeri-7) and two skin (R.strykeri-5 and R.strykeri-6) samples of *R. strykeri* individuals from the Gaoligong Mountain National Nature Reserve were provided by the Nujiang Forest Public Security Bureau and the Institute of Eastern-Himalaya Biodiversity Research, respectively. A skin (R.avunculus-2) sample of *R. avunculus* from the Ba Be National Park of northern Vietnam was provided by the Gene Bank of Primates at the German Primate Center. DNA samples of *R. bieti* from the Baima Mountain National Nature Reserve were provided by the Animal Branch of the Germplasm Bank of wild Species of Chinese Academy of Science. With the addition of these new samples, we obtained a total of 106 population genomes (average 12.02-fold coverage) representing all five snub-nosed monkeys. The genomic sequences from *Pygathrix nemaeus* (red shanked douc langur) and *Macaca mulatta* (rhesus macaque; SRS748669; Zhang et al., 2014) were used as outgroups. The DNA sample of *Pygathrix nemaeus* obtained from the Animal Branch of the Germplasm Bank of wild Species of Chinese Academy of Science was used to generate the genomic sequences (32.13-fold coverage).

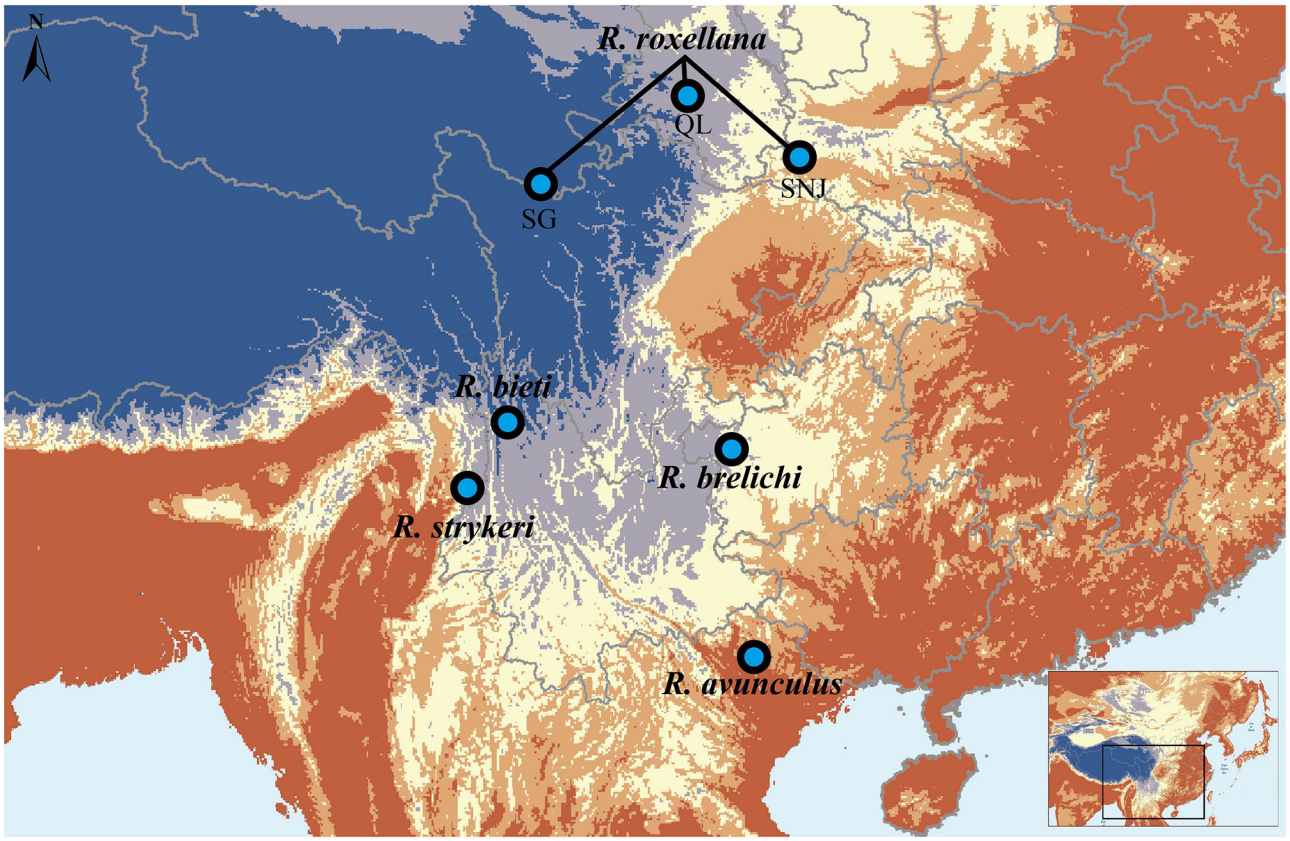

FIGURE 1 | Geographic distribution of the *Rhinopithecus* species. The map is drawn using ESRI ArcGIS 10.2.

Genomic DNAs from the skin and bone samples of *R. strykeri* and *R. avunculus* were extracted in the ancient DNA extraction facility of the Institute of Vertebrate Paleontology and Paleoanthropology (IVPP), Chinese Academy of Sciences, Beijing, China (for details, see **Supplementary Notes**). Sequencing libraries were produced using a double stranded library preparation protocol (Meyer and Kircher, 2010; Kircher et al., 2012) with uracil-DNA-glycosylase (UDG) and endonuclease (Endo VIII) treated (for details see **Supplementary Notes**). Sequencing libraries were sequenced using paired-end (PE) 150-bp reads on an Illumina HiSeq X-ten platform. Reads were demultiplexed by allowing one mismatch on each pair of reads. A modified version of SeqPrep (John, 2011) were used to collapse the PE reads (at least 11-bp overlap with one mismatch allowed), and base quality in the overlapping regions was set to the highest Phred score. Collapsed pairs were aligned using BWA samse v 0.6.1 (Li and Durbin, 2009) after stripping adapters. All duplicates were removed with bam-rmdup (https://github.com/mpieva/biohazard-tools) by keeping only the read for each set of duplicates with the highest quality bases.

Sequencing libraries based on high-quality genomic DNAs from *R. bieti* and *P. nemaeus* were constructed with an insert size of 350 bp and sequenced on an Illumina HiSeq 2500 platform using PE 100–150 bp reads. All newly sequenced genomic data generated for this study were deposited on the Short Read Archive (SRA) database under project number: PRJNA616055.

Reads Alignment, Genotype Calling, and Filtering

A high-quality reference genome is needed for population genomic studies. The published chromosome-level genome of the golden snub-nosed monkey (Wang et al., 2019a) was used as the reference genome here. Reads were aligned to the reference genome with BWA-MEM (Li and Durbin, 2009) and SAMtools v.1.3 to generate BAM files (Li et al., 2009). Aligned reads were realigned around inserts/deletions (INDELs) using GATK v3.8 indelRealigner (Mckenna et al., 2010) and duplicate reads were marked using Picard v2.10.3 (https://broadinstitute.github.io/picard).

We called single nucleotide polymorphism (SNPs) with GATK v3.8 HaplotypeCaller (Mckenna et al., 2010). Raw SNPs were then filtered for quality and depth using the following criteria: Variants failing the recommended GATK hard filters (QD $<$ 2.0 || FS $>$ 60.0 || MQ $<$ 40.0 || ReadPosRankSum $<$-8.0 || SB $>=$ $-$1.0 || DP $<$ 3), low Phred score (QUAL of $<$30), missingness above 20%, allele frequency $<$5% and sites identified within CpG islands using CpGIScan software (Jian et al., 2017) with default parameter values were excluded. Only biallelic autosomal SNPs

were analyzed in this study (i.e., triallelic SNPs and SNPs with mapping to the chromosomes X and Y were excluded).

Close Kinship Analyses

Given that the close relationship of samples has the potential to bias the heterozygosity, inbreeding, and genetic load results, so the kinship analyses among the collected genome sequences from the individuals for each species were performed with the Kinship-based Inference for Genome-wide association studies (KING) (Manichaikul et al., 2010) to remove the potential consanguineous individuals. Kinship coefficient was estimated with the "-kinship" command from KING v.2.2.5, which reflects the proportion of SNPs with identical state (IBS0, identity by state zero) between individuals. Negative coefficients indicate unrelated relationships, while positive coefficients indicate genealogy links between individuals. Nonconsanguineous individuals (kinship coefficients <0) were used in the subsequent analyses (**Supplementary Table 1**).

Whole Genome Heterozygosity and Nucleotide Mismatches Analyses

Whole genome heterozygosity (*He*) and pairwise nucleotide divergence were computed in 100-kb sliding-window size with no step using variant cell format (VCF) tools (Danecek et al., 2011) and in-house Perl scripts, respectively.

Runs of Homozygosity and Inbreeding Analyses

Run of homozygosity (ROHs) are contiguous homozygous segments of the genome where the two haplotypes inherited from the parents are identical (Gibson et al., 2006), which can be used to estimate inbreeding level (Keller et al., 2011). Since recombination events interrupt lengthy genome segment, thus long ROHs (long-ROHs) represent recent inbreeding events (Van Der Valk et al., 2019a). We used the physical length of ROHs as an approximation for genetic length and estimated that the long ROHs of 1-Mb trace back to <50 generations ago ($g = 100 / 2 * ROH_{Length}$, where g is the number of generations and ROH_{Length} is the ROHs length in centimorgans) (Thompson, 2013). ROHs were identified for each individual using the "run of homozygosity" function in the program PLINK v1.90 (Purcell et al., 2007). We ran sliding windows of 20 SNPs on the VCF files of all genomes, requiring at least one SNP per 10 kb. In each individual genome, we allowed for the maximum of one heterozygous and 50 missing calls per windows.

The proportion of the genome within ROHs, i.e., genomic inbreeding coefficient (F_{ROH}), was calculated as the total length of ROHs within an individual divided by the length of the genome (Mcquillan et al., 2008).

Genetic Load Analyses

Deleterious mutations (genetic load) are predicted to disrupt gene function, and therefore expected to substantially reduce the mean fitness of individuals in a species/population (Mattila et al., 2012). To estimate genetic load in the endangered snub-nosed monkeys, we used SnpEff v.4.3t (Cingolani et al., 2012) to annotate variant sites (in our multisample VCF) based on the mappings and genome annotation of the golden snub-nosed monkey (Wang et al., 2019a) and to identify loss-of-function (LOF), missense, and synonymous mutations. The major homozygous alleles (allele frequency above 0.5) in each species and also in at least one of the outgroup species were used to represent the ancestral state. As an indicator of mutational load, for each individual, we counted the number of genes containing one or more homozygous-derived LOF and the total number of homozygous-derived missense mutations divided by the number of synonymous mutations (Fay et al., 2001; Van Der Valk et al., 2020), respectively.

We identified candidate genes with deleterious mutations for each species/population as those satisfying the following criteria: (*i*) mutations classified as LOF and (*ii*) mutations being homozygous and derived alleles.

RESULTS AND DISCUSSION

Data, Sequencing, and SNP Calling

We analyzed a total of 106 individuals from all five snub-nosed monkey species and two outgroups, one *Pygathrix nemaeus* and one *Macaca mulatta* (**Supplementary Table 1**). Short reads from each individual were aligned to the high-quality chromosomal reference genome of the golden snub-nosed monkey (Wang et al., 2019a). An average mapping rate is 99.14% (78.73–100%), and average genomic depth is 12.02-fold coverage (5.04–35.25-fold coverage) (**Supplementary Table 1**). The high alignment rate and coverage ensures accurate identification of genetic variations. After stringent quality filtering, we identified a total of 108.28 million high-quality autosomal SNPs in the snub-nosed monkeys and the two outgroups.

Based on the kinship analyses, 44 potential consanguineous individuals (kinship coefficients > 0) were removed, resulting in a total of 62 individuals from all five snub-nosed monkeys used in the present analyses (kinship coefficients < 0). These included 40 individuals from *R. roxellana* (22 from SG, 13 from QL, and 5 from SNJ), 14 *R. bieti*, 4 *R. strykeri*, 2 *R. avunculus*, and 2 *R. brelichi* (**Supplementary Table 1**). After the removal of consanguineous individuals, we identified a total of 98.97 million high-quality autosomal SNPs in the 62 snub-nosed monkeys and the two outgroups.

Genetic Diversity Analyses

Whole genome heterozygosity (*He*) in snub-nosed monkeys ranged from 0.034 to 0.069% (**Figure 2A**). These estimates are similar to those obtained from other endangered and critically endangered primates, including aye-aye, Eastern lowland gorilla, mountain gorilla, Bornean orangutan, and pileated gibbon (0.051–0.073%) (Locke et al., 2011; Perry et al., 2012; Carbone et al., 2014; Xue et al., 2015), as well as estimated obtained from carnivores, including Bengal tiger, Amur tiger, white tiger, white lion, and African lion (0.040–0.073%) (Cho et al., 2013; Dobrynin et al., 2015). These estimates suggest that snub-nosed monkeys possess low genetic diversity, a pattern that may be

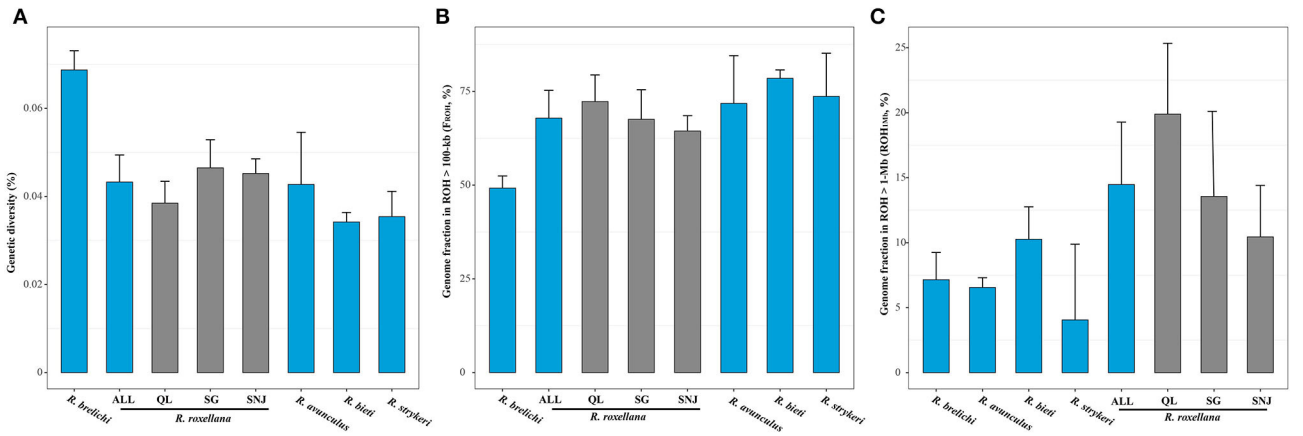

FIGURE 2 | Genetic diversity and inbreeding level in the snub-nosed monkeys. Error bars represent standard deviation (sd). **(A)** The whole genome heterozygosity (*He*) of *R. brelichi*, *R. roxellana*, *R. avunculus*, *R. bieti*, and *R. strykeri*. Within *R. roxellana*: ALL, three populations; QL, Qinling population; SG, Sichuan/Gansu population; SNJ, Shennongjia population. **(B)** Fraction of the genomes in all ROHs (>100 kb) representing the genomic inbreeding coefficient (F_{ROH}). **(C)** Fraction of genomes in long ROHs (>1 Mb; ROH_{1Mb}) representing the recent inbreeding levels of the snub-nosed monkeys.

related to recent environment change and human activities (Pan and Jablonski, 1987; Li et al., 2002; Zhou et al., 2016).

Contrary to the prevailing notion that smaller populations generally show lower levels of genetic diversity (Leffler et al., 2012; Cho et al., 2013; Prado Martinez et al., 2013; Díez-del-Molino et al., 2018), we found that *R. brelichi* possessed the highest genetic diversity ($He = 0.069\%$; $p < 0.05$, Wilcox test; **Figure 2A**), despite its population size being lower (<400 individuals) than most other species. The unexpectedly high genetic diversity found in *R. brelichi* may be caused by interspecific hybridization (Zhou et al., 2014) or only small population remained from a large population in the recent past (Kolleck et al., 2013). *R. roxellana* ($He = 0.043\%$) and *R. avunculus* ($He = 0.042\%$) showed the second highest levels of genetic diversity, both higher than *R. bieti* ($He = 0.034\%$) and *R. strykeri* ($He = 0.036\%$) ($p < 0.05$, Wilcox test). Lower genetic diversity estimates for *R. bieti* and *R. strykeri* are consistent with their small population sizes (∼3,000 individuals for *R. bieti* and 950 individuals for *R. strykeri*). The rather higher level of genetic diversity found in *R. roxellana* is consistent with their large population size (∼22,500 individuals). We found, however, that although its small population size (<200 individuals; the lowest of all five snub-nosed monkey species), *R. avunculus* possesses relatively high genetic diversity, possibly due to ancient introgression or only small population remained from a large population in the recent past, similarly to *R. brelichi*. Intriguingly, the average pairwise nucleotide mismatches in 100-kb windows across the genome was 0.154% within *R. avunculus*, which is larger than in other snub-nosed monkeys (0.052–0.093%), suggesting a substantial amount of genetic divergence within the *R. avunculus* population. The two individuals of *R. avunculus* were potentially originated from two substantially diverged populations. These findings are consistent with field surveys that found at least two noncontiguous subpopulations in northern Vietnam (Boonratana and Le, 1998; Zhang et al., 2016). Our results indicate that these populations are highly divergent in *R. avunculus*, suggesting that they should be managed independently.

As for *R. brelichi* and *R. avunculus*, we found that the smallest population of *R. roxellana*, i.e., SNJ population (∼1,200 individuals) also possessed relatively higher levels of genetic diversity ($He = 0.044\%$) compared with the QL population ($He = 0.038\%$, ∼5,500 individuals, $p = 0.0193$, Wilcox test) and even similarly do for the largest population of *R. roxellana*, i.e., SG population ($He = 0.046\%$, approximately 16,500 individuals, $p = 0.5695$, Wilcox test).

Genomic Inbreeding and Recent Inbreeding Analyses

We found that genomic inbreeding coefficient (F_{ROH}) of the snub-nosed monkeys to be between 49.37 and 78.86% (**Figure 2B**). Compared with other critically endangered or endangered species, the genomic inbreeding levels of the snub-nosed monkeys was higher than in the eastern gorillas ($F_{ROH} = 34–39\%$) (Xue et al., 2015; Van Der Valk et al., 2019a), vervets ($F_{ROH} = 6–12\%$) (Van Der Valk et al., 2019a), and pangolins ($F_{ROH} = 12–42\%$) (Hu et al., 2020). These high levels of inbreeding of the snub-nosed monkeys are consistent with recent dramatic population decline (Zhou et al., 2016).

We found that *R. brelichi* ($F_{ROH} = 49.37\%$) possessed the lowest level of genomic inbreeding and that *R. bieti* ($F_{ROH} = 78.86\%$) and *R. strykeri* ($F_{ROH} = 73.43\%$) have the highest level among the five snub-nosed monkey species ($F_{ROH} = 68.11–78.86\%$) ($p < 0.05$, Wilcox test). Those of *R. roxellana* ($F_{ROH} = 68.11\%$) and *R. avunculus* ($F_{ROH} = 68.17\%$) are in between. As for heterozygosity levels, we found that the SNJ population of *R. roxellana* also possessed the lowest level of genomic inbreeding ($F_{ROH} = 62.83\%$) compared with the SG ($F_{ROH} = 67.24\%$, $p = 0.2495$, Wilcox test) and QL populations ($F_{ROH} = 72.71\%$, $p = 0.00262$, Wilcox test). Analyses

of long-ROHs (>1 Mb; ROH_{1Mb}) indicated that although there are more individuals of *R. roxellana* than other snub-nosed monkey species, this species generally possessed more long-ROHs (ROH_{1Mb}, 14.78%) than other species (*R. brelichi*, 7.41%; *R. bieti*, 10.85%; *R. strykeri*, 3.92%; and *R. avunculus*, 7.18%) ($p < 0.05$, Wilcox test), which all have smaller population sizes. Within *R. roxellana*, the SNJ with the smallest population size possessed the lowest recent inbreeding level (ROH_{1Mb}, 10.19%) compared with the other two populations (SG, 13.01% and QL, 19.30%) ($p < 0.05$, Wilcox test) (**Figure 2C**).

It is generally thought that the smaller the population, the higher the inbreeding level (Keller and Waller, 2002). However, the results demonstrated that *R. brelichi*, *R. avunculus*, and the SNJ population of *R. roxellana*, which represented small populations, show high genetic diversity and low genomic and recent inbreeding. Thus, it seems that a potential mechanism could avoid inbreeding between close relatives, for example, the individual dispersal/transfer between social groups among these species/populations (Qi et al., 2009, 2014; Guo et al., 2010; Chang et al., 2014).

In comparison, *R. roxellana* has a large population size and demonstrates high genetic diversity and low genomic inbreeding, but high recent inbreeding. We speculate that the high recent inbreeding might result from the lower levels of population connectivity and habit utilization (∼0.528–0.587 km^2/individual) that was shaped by a recent increase in human activity for *R. roxellana* compared with the other snub-nosed monkeys (1–3.763 km^2/individual; **Supplementary Table 2**) (Liu et al., 2015; Meyer et al., 2017; Guo et al., 2020). Thus, *R. roxellana* populations have experienced dozens of recent generations of close inbreeding in spite of their largest population size in the wild compared with other snub-nosed monkeys (Zhou et al., 2016).

Genetic Load Analyses

High levels of inbreeding can lead to increased homozygosity of recessive deleterious mutations, especially for small and isolated species/populations (Charlesworth and Willis, 2009), which will disrupt gene function or reduce individual fitness. We found that among the snub-nosed monkeys, individuals of *R. roxellana* with the highest recent inbreeding level carried significantly fewer homozygous-derived LOF (homozygous LOF/synonymous, 0.36%) than the other snub-nosed monkey species (*R. brelichi*: homozygous LOF/synonymous, 0.45%; *R. strykeri*: homozygous LOF/synonymous, 0.49%; *R. avunculus*: homozygous LOF/synonymous, 0.49%; and *R. bieti*: homozygous LOF/synonymous, 0.55%) ($p < 0.001$, Wilcox test) (**Figure 3A**). A similar pattern was observed when analyzing homozygous-derived missense mutations (**Figure 3B**). This suggests that purging homozygous-derived deleterious mutations is more efficient in *R. roxellana* compared with the other snub-nosed monkeys with smaller population sizes.

Our finding that *R. roxellana* possess high levels of inbreeding and relatively lower levels of mutational load results suggest that inbreeding do not necessarily lead to higher level of mutational load as previously suggested (Reed and Frankham, 2003), which is corroborated by the evidence that there is very low overlapping of homozygous-derived deleterious mutation regions with the long-ROH regions (4.86 and 12.90% overlapping between the homozygous-derived LOF and missense mutations with the long-ROHs, respectively), but rather more overlap with the short-ROHs regions (47.18 and 54.99%, respectively) (**Figure 4**). The present observation in *R. roxellana* that recent inbreeding did not lead to an excessive accumulation of homozygous-derived deleterious mutations was also recently reported in the snow leopard, island fox, and cheetah (Van Der Valk et al., 2019b). Interestingly, although the three populations of *R. roxellana* possessed highly different ROHs and heterozygosity profiles, we found that their levels of mutational load were remarkably similar (SNJ: homozygous LOF/synonymous, 0.33%; SG: homozygous LOF/synonymous, 0.38%; QL: homozygous LOF/synonymous, 0.38%) ($p > 0.05$, Wilcox test). Altogether, these findings support the idea that mutational load may build up over much longer time frame than inbreeding (Van Der Valk et al., 2019b).

Our findings of a significantly fewer homozygous-derived deleterious mutations in *R. roxellana* than in the other snub-nosed monkey species contradict that of a previous study, which identified similar numbers of LOF and derived missense mutations in *R. roxellana*, *R. bieti*, and *R. brelichi* (Zhou et al., 2016). These differences are likely the results of difference in sample sizes (*R. roxellana*: 40 in the present study vs. 26 in Zhou et al., 2016; *R. bieti*: 14 in the present study vs. 8 in Zhou et al., 2016; *R. brelichi*: 2 in the present study vs. 3 in Zhou et al., 2016) and the use of a high-quality chromosome-level reference genome assembly in the present study.

Many of the genes containing homozygous LOF mutations in the snub-nosed monkey genomes were associated with functions related to immunity (three genes in *R. roxellana*, nine genes in *R. bieti*, eight genes in *R. strykeri*, nine genes in *R. brelichi*, and nine genes in *R. avunculus*, **Supplementary Table 3**). For example, we found LOF mutations at the coagulation factor II receptor-like 3 gene (*F2RL3*), which is involved in the recruitment and behavior of immune cells and blood coagulation (Vergnolle et al., 2002; Leger et al., 2006; Gomides et al., 2012; Hossain et al., 2015), segregating in all five species. In addition, more immune genes with LOF mutations were found in the snub-nosed monkey species with the smaller population sizes (i.e., *R. bieti*, *R. strykeri*, *R. brelichi*, and *R. avunculus*). These include genes such as calmodulin-like protein 6 (*CALML6*) and lymphocyte-specific protein tyrosine kinase genes (*LCK*), both of which play a key role in the activation of T/B lymphocytes and the maintenance of balance of the immune system (Tewari et al., 2006; Wang et al., 2019b; Sheng et al., 2020). Altogether, this suggests that inbreeding depression may manifest in the form of lowered immune capability in the snub-nosed monkeys.

CONCLUSION

Overall, this study provides new insights into the impact of population decline on genomic diversity in a set of highly endangered species, the snub-nosed monkeys

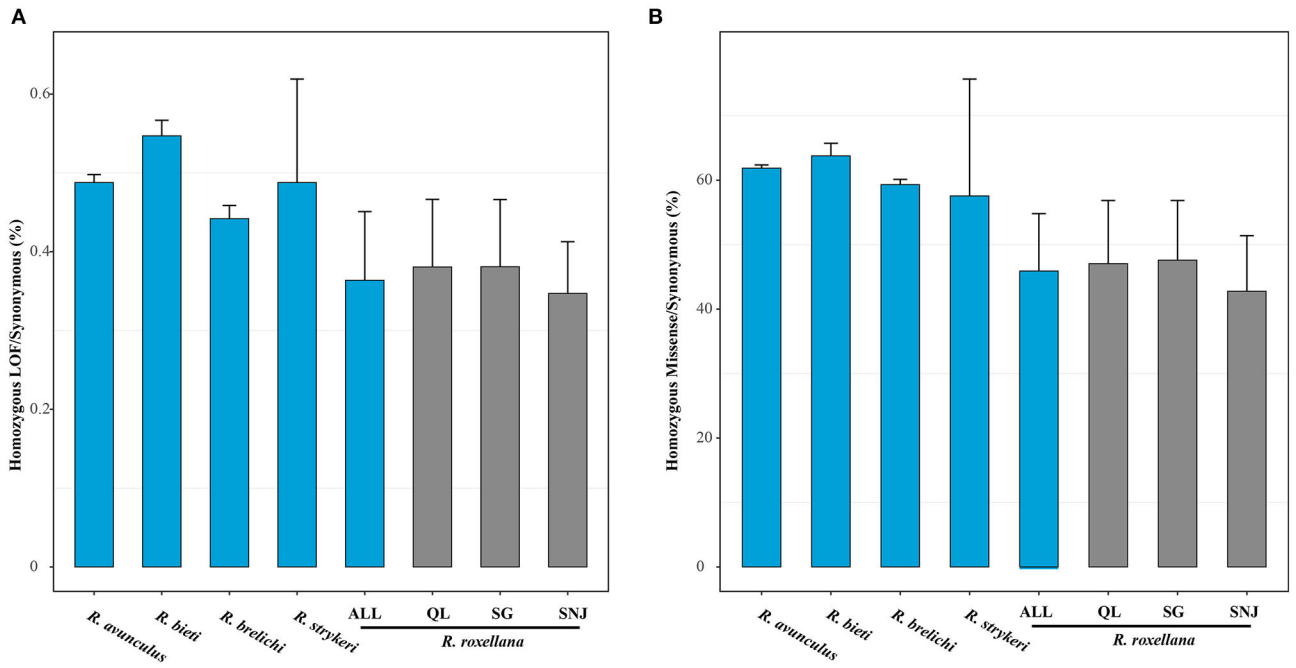

FIGURE 3 | Genetic load of the snub-nosed monkeys. Error bars represent standard deviation (sd). **(A)** The ratios of the total numbers of homozygous-derived loss of function (LOF) to synonymous mutations of the species/populations. **(B)** The ratios of the homozygous-derived missense to synonymous mutations.

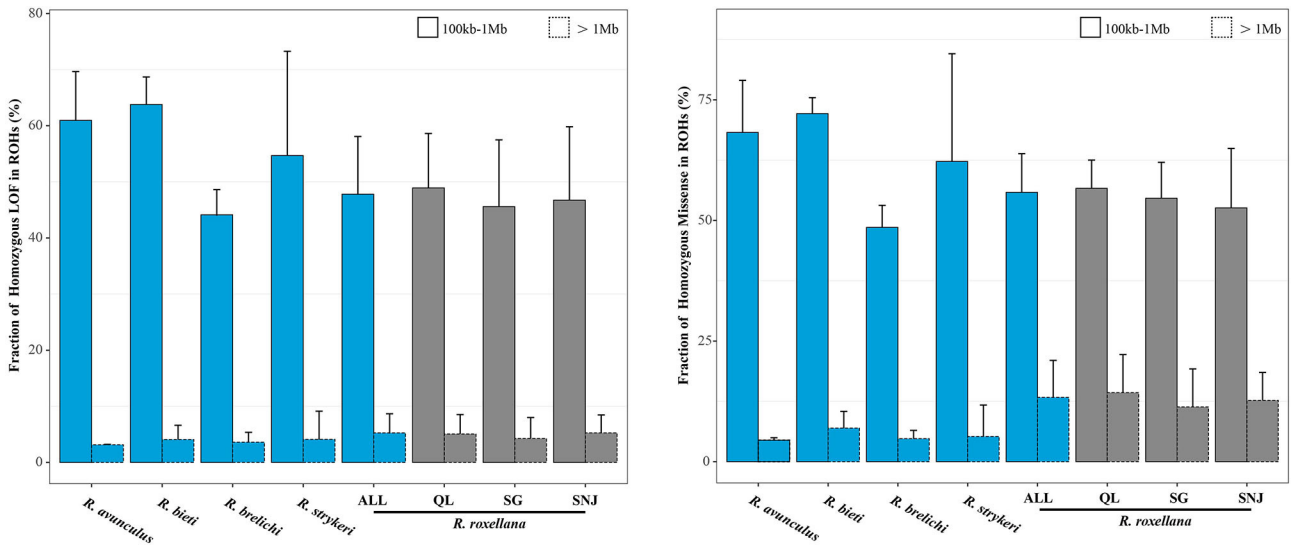

FIGURE 4 | Fractions of homozygous LOF and missense mutations in the ROHs. Error bars represent standard deviation (sd). Bars with solid lines represent short ROHs (100 kb−1 Mb), and bars with dashed lines represent long ROHs (>1 Mb).

(genus: *Rhinopithecus*). Our analyses demonstrated multiple counterintuitive patterns. For example, *R. brelichi*, *R. avunculus*, and SNJ population of *R. roxellana* with the small population size showed higher levels of genetic diversity, lower levels of genomic diversity, and recent inbreeding than other snub-nosed monkeys and other populations in *R. roxellana* with the larger population sizes. These findings suggest that, although their census population size is low, they have not yet lost much (if any) of their genetic variability over recent years. However, *R. roxellana* with the largest population size possesses high levels of recent breeding, despite low levels of genomic inbreeding and genetic load as well as high overall genetic diversity. This suggest that, despite its large population size, this species has likely been experiencing recent inbreeding, which has not yet affected its

overall mutational load, and perhaps has not yet affected its fitness. Analyses of homozygous-derived deleterious mutations identified in all snub-nosed monkeys, however, suggest that these types of mutations are affecting immune, especially in smaller population sizes. This suggests that the long-term consequences of inbreeding may be resulting in an overall reduction of immune capability in the snub-nosed monkeys, which could provide a dramatic effect on their long-term survival prospects.

DATA AVAILABILITY STATEMENT

The datasets presented in this study can be found in online repositories. The names of the repository/repositories and accession number(s) can be found below: https://www.ncbi.nlm.nih.gov/PRJNA616055.

ETHICS STATEMENT

The animal study was reviewed and approved by the Committee on Animal Research and Ethics of Yunnan University (No. yuncare20200370).

AUTHOR CONTRIBUTIONS

LY designed the study. WK performed the data analyses. WK, LY, and QF wrote the manuscript. XF and QD performed the genomic DNA extraction and preparation of sequencing libraries. WX, CR, TN, LZ, and XY provided the samples. JH, HW, LF, DI, CR, and TN reviewed and revised the manuscript. All authors read and approved the final manuscript.

FUNDING

This work was supported by a grant from the National Natural Science Foundation of China (No. 31925006), a grant from the Yunnan University's Research Innovation Fund for Graduate Students (2019z050) and the Academic Graduate Students Foundation of Yunnan Province.

SUPPLEMENTARY MATERIAL

The Supplementary Material for this article can be found online at: https://www.frontiersin.org/articles/10.3389/fgene.2020.615926/full#supplementary-material

REFERENCES

Boonratana, R., and Le, X. C. (1998). *Conservation of Tonkin Snub-Nosed Monkeys (Rhinopithecus avunculus) in Vietnam. The Natural History Of The Doucs And Snub-Nosed Monkeys*. Singapore: World Scientific.

Carbone, L., Harris, R. A., Gnerre, S., Veeramah, K. R., Lorente-Galdos, B., Huddleston, J., et al. (2014). Gibbon genome and the fast karyotype evolution of small apes. *Nature* 513, 195–201. doi: 10.1038/nature13679

Chang, Z. F., Luo, M. F., Liu, Z. J., Yang, J. Y., Xiang, Z. F., Li, M., et al. (2012). Human influence on the population decline and loss of genetic diversity in a small and isolated population of Sichuan snub-nosed monkeys (*Rhinopithecus roxellana*). *Genetica* 140, 105–114. doi: 10.1007/s10709-012-9662-9

Chang, Z. F., Yang, B. H., Vigilant, L., Liu, Z. J., Ren, B. P., Yang, J. Y., et al. (2014). Evidence of male-biased dispersal in the endangered Sichuan snub-nosed monkey (*Rhinopithexus roxellana*). *Am. J. Primatol.* 76, 72–83. doi: 10.1002/ajp.22198

Charlesworth, D., and Willis, J. H. (2009). The genetics of inbreeding depression. *Nat. Rev. Genet.* 10, 783–796. doi: 10.1038/nrg2664

Cho, Y. S., Hu, L., Hou, H., Lee, H., Xu, J., Kwon, S., et al. (2013). The tiger genome and comparative analysis with lion and snow leopard genomes. *Nat. Commun.* 4, 2433. doi: 10.1038/ncomms3433

Cingolani, P., Platts, A., Wang Le, L., Coon, M., Nguyen, T., Wang, L., et al. (2012). A program for annotating and predicting the effects of single nucleotide polymorphisms, SnpEff: SNPs in the genome of Drosophila melanogaster strain w1118; iso-2; iso-3. *Fly* 6, 80–92. doi: 10.4161/fly.19695

Danecek, P., Auton, A., Abecasis, G., Albers, C. A., Banks, E., Depristo, M. A., et al. (2011). The variant call format and VCFtools. *Bioinformatics* 27, 2156–2158. doi: 10.1093/bioinformatics/btr330

Díez-del-Molino, D., Sánchez-Barreiro, F., Barnes, I., Gilbert, M. T. P., and Dalén, L. (2018). Quantifying temporal genomic erosion in endangered species. *Trends Ecol. Evol.* 33, 176–185. doi: 10.1016/j.tree.2017.12.002

Dobrynin, P., Liu, S., Tamazian, G., Xiong, Z., Yurchenko, A. A., Krasheninnikova, K., et al. (2015). Genomic legacy of the African cheetah, Acinonyx jubatus. *Genome Biol.* 16:277. doi: 10.1186/s13059-015-0837-4

Fay, J. C., Wyckoff, G. J., and Wu, C. I. (2001). Positive and negative selection on the human genome. *Genetics* 158, 1227–1234. doi: 10.1002/gepi.1019

Frankham, R. (2005). Genetics and extinction. *Biol. Conserv.* 126, 0–140. doi: 10.1016/j.biocon.2005.05.002

Geissmann, T., Lwin, N., Aung, S. S., Aung, T. N., Aung, Z. M., Hla, T. H., et al. (2011). A new species of snub-nosed monkey, genus *Rhinopithecus* Milne-Edwards, 1872 (Primates, Colobinae), from northern Kachin state, northeastern Myanmar. *Am. J. Primatol.* 73, 96–107. doi: 10.1002/ajp.20894

Gibson, J., Morton, N. E., and Collins, A. (2006). Extended tracts of homozygosity in outbred human populations. *Hum. Mol. Genet.* 15, 789–795. doi: 10.1093/hmg/ddi493

Gomides, L. F., Duarte, I. D., Ferreira, R. G., Perez, A. C., Francischi, J. N., and Klein, A. (2012). Proteinase-activated receptor-4 plays a major role in the recruitment of neutrophils induced by trypsin or carrageenan during pleurisy in mice. *Pharmacology* 89, 275–282. doi: 10.1159/000337378

Guo, S. T., Ji, W. H., Li, M., Chang, H. L., and Li, B. G. (2010). The mating system of the Sichuan snub-nosed monkey (*Rhinopithecus roxellana*). *Am. J. Primatol.* 72, 25–32. doi: 10.1002/ajp.20747

Guo, Y., Ren, B., Dai, Q., Zhou, J., Paul, A. G., and Zhou, J. (2020). Habitat estimates reveal that there are fewer than 400 Guizhou snub-nosed monkeys, *Rhinopithecus brelichi*, remaining in the wild. *Glob. Ecol. Conserv.* 2020:e01181. doi: 10.1016/j.gecco.2020.e01181

Han, D. F. (1982). Mammalian fossils from Tashin country, Guangxi. *Vertebr. Palasiatica* 2, 58–63.

Hansson, B., and Westerberg, L. (2002). On the correlation between heterozygosity and fitness in natural populations. *Mol. Ecol.* 11, 2467–2474. doi: 10.1046/j.1365-294X.2002.01644.x

Heller, N. E., and Zavaleta, E. S. (2009). Biodiversity management in the face of climate change: a review of 22 years of recommendations. *Biol. Conserv.* 142, 14–32. doi: 10.1016/j.biocon.2008.10.006

Hong, Y., Duo, H., Hong, J., Yang, J., Liu, S., Yu, L., et al. (2017). Resequencing and comparison of whole mitochondrial genome to gain insight into the evolutionary status of the Shennongjia golden snub-nosed monkey (SNJ *R. roxellana). Ecol. Evol.* 7, 4456–4464. doi: 10.1002/ece3.3011

Hossain, M. B., Li, H. Q., Hedmer, M., Tinnerberg, H., and Broberg, K. (2015). Exposure to welding fumes is associated with hypomethylation of the F2RL3 gene: a cardiovascular disease marker. *Occup. Environ. Med.* 72, 845–851. doi: 10.1136/oemed-2015-102884

Hu, J. Y., Hao, Z. Q., Frantz, L., Wu, S. F., Chen, W., Jiang, Y. F., et al. (2020). Genomic consequences of population decline in critically endangered pangolins and their demographic histories. *Natl. Sci. Rev.* 7, 798–814. doi: 10.1093/nsr/nwaa031

Jablonski, N. G. (1998). The response of catarrhine primates to Pleistocene environmental fluctuations in East Asia. *Primates* 39, 29–37. doi: 10.1007/BF02557741

Jablonski, N. G., and Pan, Y. R. (1988). The evolution and palaeobiogeographic of monkeys in China. *Palaeoenviron. East Asia Midtert.* 2, 849–867.

Jian, Z., Du, L., Zhang, X., Yue, B., and Fan, Z. (2017). CpGIScan: an ultrafast tool for CpG islands identification from genome sequence. *Curr. Bioinform.* 12, 181–184. doi: 10.2174/1574893611666160907111325

John, J. S. (2011). Available online at: https://github.com/jstjohn/SeqPrep.

Jump, A. S., Marchant, R., and Penuelas, J. (2009). Environmental change and the option value of genetic diversity. *Trends Plant Sci.* 14, 51–58. doi: 10.1016/j.tplants.2008.10.002

Keller, L. F., and Waller, D. M. (2002). Inbreeding effects in wild populations. *Trends Ecol. Evol.* 17, 230–241. doi: 10.1016/S0169-5347(02)02489-8

Keller, M. C., Visscher, P. M., and Goddard, M. E. (2011). Quantification of inbreeding due to distant ancestors and its detection using dense single nucleotide polymorphism data. *Genetics* 189, 237–249. doi: 10.1534/genetics.111.130922

Kircher, M., Sawyer, S., and Meyer, M. (2012). Double indexing overcomes inaccuracies in multiplex sequencing on the Illumina platform. *Nucleic Acids Res.* 40:e3. doi: 10.1093/nar/gkr771

Kolleck, J., Yang, M., Zinner, D., and Roos, C. (2013). Genetic diversity in endangered Guizhou snub-nosed monkeys (*Rhinopithecus brelichi*): contrasting results from microsatellite and mitochondrial DNA data. *PLoS ONE* 8:e73647. doi: 10.1371/journal.pone.0073647

Kuang, W. M., Ming, C., Li, H. P., Wu, H., Frantz, L., Roos, C., et al. (2019). The origin and population history of the endangered golden snub-nosed monkey (*Rhinopithecus roxellana*). *Mol. Biol. Evol.* 36, 487–499. doi: 10.1093/molbev/msy220

Leffler, E. M., Bullaughey, K., Matute, D. R., Meyer, W. K., Segurel, L., Venkat, A., et al. (2012). Revisiting an old riddle: what determines genetic diversity levels within species? *PLoS Biol.* 10:e1001388. doi: 10.1371/journal.pbio.1001388

Leger, A. J., Covic, L., and Kuliopulos, A. (2006). Protease-activated receptors in cardiovascular diseases. *Circulation* 114, 1070–1077. doi: 10.1161/CIRCULATIONAHA.105.574830

Li, B., Li, M., Li, J., Fan, P., Ni, Q., Lu, J., et al. (2018). The primate extinction crisis in China: immediate challenges and a way forward. *Biodivers. Conserv.* 27, 3301–3327. doi: 10.1007/s10531-018-1614-y

Li, B., Pan, R., and Oxnard, C. E. (2002). Extinction of snub-nosed monkeys in China during the past 400 years. *Int. J. Primatol.* 23, 1227–1244. doi: 10.1023/A:1021122819845

Li, H., and Durbin, R. (2009). Fast and accurate short read alignment with Burrows-Wheeler transform. *Bioinformatics* 25, 1754–1760. doi: 10.1093/bioinformatics/btp324

Li, H., Handsaker, B., Wysoker, A., Fennell, T., Ruan, J., Homer, N., et al. (2009). The sequence alignment/map format and SAMtools. *Bioinformatics* 25, 2078–2079. doi: 10.1093/bioinformatics/btp352

Li, M., Liu, Z., Gou, J., Ren, B., Pan, R., Su, Y., et al. (2007). Phylogeography and population structure of the golden monkeys (*Rhinopithecus roxellana*): inferred from mitochondrial DNA sequences. *Am. J. Primatol.* 69, 1195–1209. doi: 10.1002/ajp.20425

Li, M., Wei, F., Huang, C., Pan, R., and Ruiter, J. D. (2004). Phylogeny of snub-nosed monkeys inferred from mitochondrial DNA, cytochrome B, and 12S rRNA sequences. *Int. J. Primatol.* 25, 861–873. doi: 10.1023/B:IJOP.0000029126.27618.88

Liedigk, R., Yang, M., Jablonski, N. G., Momberg, F., Geissmann, T., Lwin, N., et al. (2012). Evolutionary history of the odd-nosed monkeys and the phylogenetic position of the newly described Myanmar snub-nosed monkey *Rhinopithecus strykeri*. *PLoS ONE* 7:e37418. doi: 10.1371/journal.pone.0037418

Liu, Z., Liu, G., Roos, C., Wang, Z., Xiang, Z., Zhu, P., et al. (2015). Implications of genetics and current protected areas for conservation of 5 endangered primates in China. *Conserv. Biol.* 29, 1508–1517. doi: 10.1111/cobi.12581

Liu, Z., Ren, B., Wei, F., Long, Y., Hao, Y., and Li, M. (2007). Phylogeography and population structure of the Yunnan snub-nosed monkey (*Rhinopithecus bieti*) inferred from mitochondrial control region DNA sequence analysis. *Mol. Ecol.* 16, 3334–3349. doi: 10.1111/j.1365-294X.2007.03383.x

Liu, Z., Ren, B., Wu, R., Zhao, L., Hao, Y., Wang, B., et al. (2009). The effect of landscape features on population genetic structure in Yunnan snub-nosed monkeys (*Rhinopithecus bieti*) implies an anthropogenic genetic discontinuity. *Mol. Ecol.* 18, 3831–3846. doi: 10.1111/j.1365-294X.2009.04330.x

Locke, D. P., Hillier, L. W., Warren, W. C., Worley, K. C., Nazareth, L. V., Muzny, D. M., et al. (2011). Comparative and demographic analysis of orangutan genomes. *Nature* 469, 529–533. doi: 10.1038/nature09687

Ma, C., Huang, Z., Zhao, X., Zhang, L., Sun, W., Scott, M. B., et al. (2014). Distribution and conservation status of *Rhinopithecus strykeri* in China. *Primates* 55, 377–382. doi: 10.1007/s10329-014-0425-3

Manichaikul, A., Mychaleckyj, J. C., Rich, S. S., Daly, K., Sale, M., and Chen, W. M. (2010). Robust relationship inference in genome-wide association studies. *Bioinformatics* 26, 2867–2873. doi: 10.1093/bioinformatics/btq559

Mattila, A. L., Duplouy, A., Kirjokangas, M., Lehtonen, R., Rastas, P., and Hanski, I. (2012). High genetic load in an old isolated butterfly population. *Proc. Natl. Acad. Sci. U.S.A.* 109, E2496–2505. doi: 10.1073/pnas.1205789109

Mckenna, A., Hanna, M., Banks, E., Sivachenko, A., Cibulskis, K., Kernytsky, A., et al. (2010). The Genome Analysis Toolkit: a MapReduce framework for analyzing next-generation DNA sequencing data. *Genome Res.* 20, 1297–1303. doi: 10.1101/gr.107524.110

Mcquillan, R., Leutenegger, A. L., Abdel-Rahman, R., Franklin, C. S., Pericic, M., Barac-Lauc, L., et al. (2008). Runs of homozygosity in European populations. *Am. J. Hum. Genet.* 83, 359–372. doi: 10.1016/j.ajhg.2008.08.007

Meyer, D., Momberg, F., Matauschek, C., Oswald, P., Lwin, N., Aung, S., et al. (2017). *Conservation Status of the Myanmar or Black Snub-Nosed Monkey Rhinopithecus strykeri*. Yangon: Fauna & Flora International; Göttingen: Institute of Eastern-Himalaya Biodiversity Research, Dali, China; and German Primate Center.

Meyer, M., and Kircher, M. (2010). Illumina sequencing library preparation for highly multiplexed target capture and sequencing. *Cold Spring Harb. Protoc.* 2010:pdb.prot5448. doi: 10.1101/pdb.prot5448

Nadler, T. (2018). "Tonkin snub-nosed monkey" in Schwitzer, C., Mittermeier, R. A., Ryalnds, A. B., Chiozza, F., Williamson, E. A., Byler, D., Wich, S., Humle, T., Johnson, C., Mynott, H., and McCabe, G., eds. *IUCN SSC Primate Specialist Group*. International Primatological Society, Global Wildlife Conservation and Bristol Zoological Society. Manipal: Manipal Universal Press.

Nuchel, J., Bocher, P. K., Xiao, W., Zhu, A. X., and Svenning, J. C. (2018). Snub-nosed monkeys (*Rhinopithecus*): potential distribution and its implication for conservation. *Biodivers. Conserv.* 27, 1517–1538. doi: 10.1007/s10531-018-1507-0

Pan, Y. R., and Jablonski, N. G. (1987). The age and geographical distribution of fossil cercopithecids in China. *Hum. Evol.* 2, 59–69. doi: 10.1007/BF02436531

Perry, G. H., Reeves, D., Melsted, P., Ratan, A., Miller, W., Michelini, K., et al. (2012). A genome sequence resource for the aye-aye (*Daubentonia madagascariensis*), a nocturnal lemur from Madagascar. *Genome Biol. Evol.* 4, 126–135. doi: 10.1093/gbe/evr132

Prado Martinez, J., Sudmant, P. H., Kidd, J. M., Li, H., Kelley, J. L., Lorente Galdos, B., et al. (2013). Great ape genetic diversity and population history. *Nature* 499, 471–475. doi: 10.1038/nature12228

Purcell, S., Neale, B., Todd-Brown, K., Thomas, L., Ferreira, M. A., Bender, D., et al. (2007). PLINK: a tool set for whole-genome association and population-based linkage analyses. *Am. J. Hum. Genet.* 81, 559–575. doi: 10.1086/519795

Qi, X. G., Garber, P. A., Ji, W. H., Huang, Z. P., Huang, K., Zhang, P., et al. (2014). Satellite telemetry and social modeling offer new insights into the origin of primate multilevel societies. *Nat. Commun.* 5:5296. doi: 10.1038/ncomms6296

Qi, X. G., Li, B. G., Garber, P. A., Ji, W. H., and Watanabe, K. (2009). Social dynamics of the golden snub-nosed monkey (*Rhinopithecus roxellana*): female transfer and one-male unit succession. *Am. J. Primatol.* 71, 670–679. doi: 10.1002/ajp.20702

Quan, G., and Xie, J. (2002). *Research on the Golden Monkeys*. Beijing: Science and Education Publishing House, 79–92.

Reed, D. H., and Frankham, R. (2003). Correlation between fitness and genetic diversity. *Conserv. Biol.* 17, 230–237. doi: 10.1046/j.1523-1739.2003.01236.x

Ren, G. P., Yang, Y., He, X. D., Li, G. S., Gao, Y., Huang, Z. P., et al. (2017). Habitat evaluation and conservation framework of the newly discovered and critically endangered black snub-nosed monkey. *Biol. Conserv.* 209, 273–279. doi: 10.1016/j.biocon.2017.02.029

Sheng, C., Wang, Z., Yao, C., Chen, H. M., Kan, G., Wang, D., et al. (2020). CALML6 controls TAK1 ubiquitination and confers protection against acute inflammation. *J. Immunol.* 204, 3008–3018. doi: 10.4049/jimmunol.1901042

Tewari, K., Walent, J., Svaren, J., Zamoyska, R., and Suresh, M. (2006). Differential requirement for Lck during primary and memory CD8+ T cell responses. *Proc. Natl. Acad. Sci. U.S.A.* 103, 16388–16393. doi: 10.1073/pnas.0602565103

Thompson, E. A. (2013). Identity by descent: variation in Meiosis, across genomes, and in populations. *Genetics* 194, 301–326. doi: 10.1534/genetics.112.148825

Van Der Valk, T., Díez-del-Molino, D., Marques-Bonet, T., Guschanski, K., and Dalen, L. (2019a). Historical genomes reveal the genomic consequences of recent population decline in eastern gorillas. *Curr. Biol. 29*, 165-170 e166. doi: 10.1016/j.cub.2018.11.055

Van Der Valk, T., Gonda, C. M., Silegowa, H., Almanza, S., Sifuentes-Romero, I., Hart, T. B., et al. (2020). The genome of the endangered dryas monkey provides new insights into the evolutionary history of the vervets. *Mol. Biol. Evol.* 37, 183–194. doi: 10.1093/molbev/msz213

Van Der Valk, T., Manuel, M. D., Marques-Bonet, T., and Guschanski, K. (2019b). Estimates of genetic load in small populations suggest extensive purging of deleterious alleles. *bioRxiv [Preprint]*. doi: 10.1101/696831

Vergnolle, N., Derian, C. K., D'andrea, M. R., Steinhoff, M., and Andrade-Gordon, P. (2002). Characterization of thrombin-induced leukocyte rolling and adherence: a potential proinflammatory role for proteinase-activated receptor-4. *J. Immunol.* 169, 1467–1473. doi: 10.4049/jimmunol.169.3.1467

Wang, L., Wu, J., Liu, X., Di, D., Liang, Y., Feng, Y., et al. (2019a). A high-quality genome assembly for the endangered golden snub-nosed monkey (*Rhinopithecus roxellana*). *Gigascience* 8:98. doi: 10.1093/gigascience/giz098

Wang, Z., Sheng, C., Yao, C., Chen, H., Wang, D., and Chen, S. (2019b). The EF-Hand protein CALML6 suppresses antiviral innate immunity by impairing IRF3 dimerization. *Cell Rep.* 26, 1273-1285.e1275. doi: 10.1016/j.celrep.2019.01.030

Xue, Y., Prado-Martinez, J., Sudmant, P. H., Narasimhan, V., Ayub, Q., Szpak, M., et al. (2015). Mountain gorilla genomes reveal the impact of long-term population decline and inbreeding. *Science* 348, 242–245. doi: 10.1126/science.aaa3952

Yang, M., Yang, Y., Cui, D., Fickenscher, G., Zinner, D., Roos, C., et al. (2012). Population genetic structure of Guizhou snub-nosed monkeys (*Rhinopithecus brelichi*) as inferred from mitochondrial control region sequences, and comparison with *R. roxellana* and *R. bieti*. *Am. J. Phys. Anthropol.* 147, 1–10. doi: 10.1002/ajpa.21618

Yang, Y., Ren, G., Li, W., Huang, Z., Lin, A. K., Garber, P. A., et al. (2019). Identifying transboundary conservation priorities in a biodiversity hotspot of China and Myanmar: Implications for data poor mountainous regions. *Glob. Ecol. Conserv.* 20:e00732. doi: 10.1016/j.gecco.2019.e00732

Yu, L., Wang, G. D., Ruan, J., Chen, Y. B., Yang, C. P., Cao, X., et al. (2016). Genomic analysis of snub-nosed monkeys (*Rhinopithecus*) identifies genes and processes related to high-altitude adaptation. *Nat. Genet.* 48, 947–952. doi: 10.1038/ng.3615

Zhang, P., Hu, K., Yang, B., and Yang, D. (2016). Snub-nosed monkeys (*Rhinopithecus* spp.): conservation challenges in the face of environmental uncertainty. *Sci. Bull* 61, 345–348. doi: 10.1007/s11434-016-1008-z

Zhang, S. J., Liu, C. J., Yu, P., Zhong, X., Chen, J. Y., Yang, X., et al. (2014). Evolutionary interrogation of human biology in well-annotated genomic framework of rhesus macaque. *Mol. Biol. Evol.* 31, 1309–1324. doi: 10.1093/molbev/msu084

Zhang, Y., and Ryder, O. A. (1997). Mitochondrial DNA sequence evolution and conservation relevance of snub-nosed langurs. *Yi Chuan Xue Bao* 24, 116–121.

Zhao, X., Ren, B., Li, D., Xiang, Z., Garber, P. A., and Li, M. (2019). Effects of habitat fragmentation and human disturbance on the population dynamics of the Yunnan snub-nosed monkey from 1994 to 2016. *PeerJ.* 7:e6633. doi: 10.7717/peerj.6633

Zhou, X., Meng, X., Liu, Z., Chang, J., Wang, B., Li, M., et al. (2016). Population genomics reveals low genetic diversity and adaptation to hypoxia in snub-nosed monkeys. *Mol. Biol. Evol.* 33, 2670–2681. doi: 10.1093/molbev/msw150

Zhou, X., Wang, B., Pan, Q., Zhang, J., Kumar, S., Sun, X., et al. (2014). Whole-genome sequencing of the snub-nosed monkey provides insights into folivory and evolutionary history. *Nat. Genet.* 46, 1303–1310. doi: 10.1038/ng.3137

Conflict of Interest: The authors declare that the research was conducted in the absence of any commercial or financial relationships that could be construed as a potential conflict of interest.

frontiers in Genetics

ORIGINAL RESEARCH
published: 21 December 2020
doi: 10.3389/fgene.2020.609414

MHC-Based Mate Choice in Wild Golden Snub-Nosed Monkeys

Bing-yi Zhang[1], Han-yu Hu[1], Chun-mei Song[1], Kang Huang[1], Derek W. Dunn[1], Xi Yang[1], Xiao-wei Wang[2], Hai-tao Zhao[1,2], Cheng-liang Wang[1,2], Pei Zhang[1] and Bao-guo Li[1,3]**

[1] Shaanxi Key Laboratory for Animal Conservation, College of Life Sciences, Northwest University, Xi'an, China, [2] Shaanxi Institute of Zoology, Xi'an, China, [3] Xi'an Branch of Chinese Academy of Sciences, Xi'an, China

The genes of the major histocompatibility complex (MHC) are an important component of the vertebrate immune system and play a significant role in mate choice in many species. However, it remains unclear whether female mate choice in non-human primates is based on specific functional genes and/or genome-wide genes. The golden snub-nosed monkey (*Rhinopithecus roxellana*) lives in a multilevel society, which consists of several polygynous one-male-several-female units. Although adult females tend to mainly socialize with one adult male, females often initiate extra-pair copulations with other males resulting in a high proportion of offspring being fathered by extra-pair males. We investigated the effects of adaptive MHC genes and neutral microsatellites on female mate choice in a wild *R. roxellana* population. We sequenced 54 parent-offspring triads using two MHC class II loci (*Rhro-DQA1* and *Rhro-DQB1*) and 20 microsatellites from 3 years of data. We found that the paternities of offspring were non-randomly associated with male MHC compositions not microsatellite genotypes. Our study showed that the fathers of all infants had significantly less variance for several estimates of genetic similarity to the mothers compared with random males at both MHC loci. Additionally, the MHC diversity of these fathers was significantly higher than random males. We also found support for choice based on specific alleles; compared with random males, *Rhro-DQA1* 05* and *Rhro-DQB1* 08* were more common in both the OMU (one-male unit) males and the genetic fathers of offspring. This study provides new evidence for female mate choice for MHC-intermediate dissimilarity (rather than maximal MHC dissimilarity) and highlights the importance of incorporating multiple MHC loci and social structure into studies of MHC-based mate choice in non-human primates.

Keywords: mate choice, *Rhinopithecus roxellana*, major histocompatibility complex, extra-pair paternity, intermediate dissimilarity

OPEN ACCESS

Edited by:
Deyan Ge,
Institute of Zoology, Chinese Academy of Sciences (CAS), China

Reviewed by:
Sheng-Guo Fang,
Zhejiang University, China
Mathias Wegner,
Alfred Wegener Institute, Helmholtz Centre for Polar and Marine Research (AWI), Germany

***Correspondence:**
Pei Zhang
peizhang@nwu.edu.cn
Bao-guo Li
baoguoli@nwu.edu.cn

Specialty section:
This article was submitted to Evolutionary and Population Genetics, a section of the journal Frontiers in Genetics

Received: *23 September 2020*
Accepted: *23 November 2020*
Published: *21 December 2020*

Citation:
Zhang B-y, Hu H-y, Song C-m, Huang K, Dunn DW, Yang X, Wang X-w, Zhao H-t, Wang C-l, Zhang P and Li B-g (2020) MHC-Based Mate Choice in Wild Golden Snub-Nosed Monkeys. Front. Genet. 11:609414. doi: 10.3389/fgene.2020.609414

INTRODUCTION

Females usually invest more in each individual offspring than males and thus tend to be the choosier sex when determining mating partners (Searcy, 1982; Andersson, 1994; Kokko et al., 2003). Female mate choice can occur before, during and after mating. Females may choose males that offer them "direct" material benefits such as food, high-quality territories or paternal care that can translate into increased reproductive success. Alternatively, females may choose males that offer "indirect" genetic benefits such as "disassortative mating" and "good-genes-as-heterozygosity" (Trivers, 1972;

Andersson, 1994; Tregenza and Wedell, 2000; Moller and Jennions, 2001; Kokko et al., 2003; Neff and Pitcher, 2005; Kempenaers, 2007). "Disassortative mating" requires females to choose genetically dissimilar males by self-reference to their own genotypes in order to produce an excess of heterozygous offspring (Penn and Potts, 1999; Tregenza and Wedell, 2000; Mays and Hill, 2004). "Good-genes-as-heterozygosity" posits that females choose heterozygous males and can also result in the production of increased proportions of heterozygous offspring (Mays and Hill, 2004).

Several studies have examined specific functional loci effects and genome-wide effects of female mate choice. The genetic target(s) of female choice in most species thus generally remains unclear (Ferrandiz-Rovira et al., 2016). In most vertebrates, the highly polymorphic genes of the major histocompatibility complex (MHC) are key components of the immune system. These genes are involved in the recognition and presentation of intracellular (such as viruses) and extracellular (such as bacteria) antigens to T-cells, thereby contributing to a host immune response to pathogen attack (Doherty and Zinkernagel, 1975; Bernatchez and Landry, 2003). Several studies have shown that MHC genes are important for mate choice in several vertebrate species, with females not only benefiting directly by mating with "healthy" males (i.e., females may be less likely to be infected with pathogens from their mates) but also indirectly by producing offspring with enhanced capacity to fight pathogen infection (Landry et al., 2001; Richardson et al., 2005; Santos et al., 2017; Rekdal et al., 2019). MHC genes thus make an ideal study system to enable the identification of specific functional loci effects of female mate choice (Penn and Potts, 1999; Milinski, 2006; Schwensow et al., 2008a,b; Wedekind and Evanno, 2010).

A role for the MHC in mate choice has been found in a variety of vertebrate taxa (such as fish, reptiles, birds, rodents, and primates; Miller et al., 2009; Setchell et al., 2011; Evans et al., 2012; Paula Cutrera et al., 2012; Rekdal et al., 2019). There are three not necessarily mutually exclusive mechanisms by which MHC is relevant to mate choice. (1) Choice for dissimilarity by which one individual chooses a mating partner of a dissimilar MHC genotype. The benefits accrued are increased offspring heterozygosity with enhanced immunocompetence, and inbreeding avoidance (*Ailuropoda melanoleuca*, Zhu et al., 2019; *Microcebus murinus*, Huchard et al., 2013). Choice for intermediate dissimilarity is similar to choice for dissimilarity but is less pronounced. The chooser will benefit by producing offspring of intermediate rather than maximal MHC genetic diversity. This avoids any costs associated with excessive outbreeding depression, and/or locally adapted gene complexes affecting the immune systems of offspring being disrupted, and also avoids the consumption of mature T-cell repertoire in offspring with high MHC diversity (*Luscinia svecica*, Rekdal et al., 2019; *Mandrillus sphinx*, Setchell et al., 2016). (2) Choice for heterozygosity (diversity), in which heterozygous mating partners are preferred. Choosers benefit by associating with individuals with enhanced disease resistance and hence reduced infection, and by producing heterozygous offspring in variable environments (*Oceanodroma leucorhoa*, Hoover et al., 2018; *Microcebus murinus*, Schwensow et al., 2008a). (3) Choice for specific alleles in mating partners. Choosers can obtain benefits from associating with high-quality mates (such as reduced risk of contracting infection and higher intrasexual competitive ability) and produce more offspring with specific "good genes" (*Ctenomys talarum*, Paula Cutrera et al., 2012; *Cheirogaleus medius*, Schwensow et al., 2008b). Importantly, a lack of MHC-based mate choice in some species suggests that benefits associated with MHC-loci do not occur or may be context dependent (*Peromyscus californicus*, Melendez-Rosa et al., 2018; *Papio ursinus*, Huchard et al., 2010a).

The golden snub-nosed monkey (*Rhinopithecus roxellana*) is a good model system for investigating female mate choice, because this endangered primate species lives in a multi-level society (MLS). Each breeding band of up to 100 individuals is comprised of several one-male units (OMUs), each made up of a single adult male, and several adult females and their juvenile and infant offspring. The breeding band is followed by an all-male band (AMB), a group of former resident males, young males who have reached sexual maturity, and sub-adult males who have been ejected from the breeding band (Qi et al., 2014). These AMB males often challenge and attempt to usurp the OMU males and/or opportunistically engage in extra-pair copulations with adult females (Grueter et al., 2017; Qi et al., 2017). The *R. roxellana* social structure thus provides adult females with opportunities to exhibit mate choice between their own OMU male and the other adult males within the breeding band, and between their own OMU male and AMB males. In addition to the social status and competitiveness of adult males, female mate choice may play a major role in the usurpation of OMU males by AMB males (Qi et al., 2009; Fang et al., 2018). Moreover, previous field observations have found that females usually initiate extra-pair copulations when their OMU males are not present. Indeed, approximately 50% of offspring are fathered by a male other than the adult male of the same OMU as the mother (Guo et al., 2010; Qi et al., 2020). Female *R. roxellana* may also preferentially engage in extra-pair copulations with those males who have recently achieved OMU "leader" male status (Zhao et al., 2005; Qi et al., 2020).

Because female *R. roxellana* have ample opportunities to express their mating preferences in different ways, the high rates of extra-pair paternity in populations may not be the result of a single mechanism. We therefore tested alternative genetic mechanisms underlying female mate choice in *R. roxellana* using 3 years of social organization and genetic (20 microsatellites and two MHC loci: *DQA1* and *DQB1*) data. We made four *priori* predictions. (1) Females are likely to be members of OMUs headed by males based on the genetic traits of the OMU leader male, consistent with "choice for specific alleles" and "choice for heterozygosity." (2) Females use their own MHC genetic characteristics as a reference on which to choose the fathers of their offspring, and they will choose males who are most genetically different to themselves ("choice for dissimilarity"). (3) The MHC and/or microsatellite genetic diversity of males will affect the probability of a female producing offspring with her own OMU leader male or via extra-pair copulations. (4) MHC and/or microsatellite genetic diversity and compatibility will affect the likelihood of OMU males having infants present

within their OMU that they have not fathered [extra-pair offspring (EPO)].

MATERIALS AND METHODS

Study Site, Reproductive Data and Sample Collection

Field work was undertaken in the Zhouzhi National Nature Reserve (ZNNR), which is located on the northern edge of the Qinling Mountains (33°48′68″N, 108°16′18″E), Shaanxi Province, central China [see Li et al. (2000) and Li and Zhao (2007) for details]. Two *R. roxellana* troops are present in this area (East Ridge Troop: ERT and West Ridge Troop: WRT) (Li et al., 2000). We used the WRT for this study, which during the 3 years study period consisted of a breeding band of 10–13 one-male units (∼130–150 individuals) and one all-male band (∼ 40 individuals). These monkeys have been provisioned food every winter since October 2001 to enable close observation and recognition of individuals. Individual identification was made according to physical characteristics described previously (Qi et al., 2014).

Data were collected from September 2015 until May 2017. Data on the composition of the study troop OMUs were collected by focal animal sampling (Altmann, 1974) during the annual peak mating period (from September to December). The current fertility status of each female was determined from the subsequent breeding period (from March to May). Fecal and hair samples were collected non-invasively from 145 individuals. We sampled 80–90% of all individuals from the breeding band, samples that consisted of all adult OMU males (N = 16), all females that produced infants during the study period (N = 48), and all infants produced during the study period (N = 54). We also sampled approximately 70% of all AMB individuals, sampling that consisted of all adult (N = 21) and sub-adult males (N = 6). Juveniles were excluded because they cannot reproduce. In 2015, there were in total 20 mother-infant pairs. However, insufficient sampling for four infants prevented adequate PCR amplification for inclusion in the dataset. Therefore, only 16 mother-infant pairs were used for the subsequent data analysis. Samples from the infants, which were all born from 2015 to 2017, were collected by maternal-infant pairing (the mother-infant relationship is initially determined by the fact that infants are carried and fed by their mothers). All individuals were sampled repeatedly at least twice to ensure the accuracy of the genetic data.

DNA Extraction and Genotyping

DNA from hair follicles and fecal samples were extracted following methods described by Allen et al. (1998), and using QIAamp PowerFecal DNA Kits (QIAGEN, Germany), respectively.

We used 20 highly polymorphic microsatellite loci (D10s1432; D10s2483; D10s676; D12s375; D14s306; D18s1371; D19s1034; D19s582; D20s206; D21s2054; D3s1766; D6s1036; D6s501; D7s1804; D7s2204; D7s820; D8s1049; D9s252; D9s905; D6s49) to conduct paternity analysis for all 54 infants born from 2015 to 2017. The polymerase chain reaction (PCR) and the analysis of the microsatellite loci were conducted using an extended dataset, with the primers and conditions as described by Huang et al. (2016).

We genotyped 54 parent-offspring triads and adult and sub-adult males from the AMB (N = 27) at the highly polymorphic *Rhro-DQA1* and *Rhro-DQB1* exon 2 sequences. The primers, PCR amplifications, and genotyping were conducted using methods as previously described (Zhang et al., 2016).

Data Analysis

Parentage Analysis

For all infants, from whom information about their mothers and OMU males was available from field work, paternity analysis was performed using the software CERVUS 3.0.6 (Kalinowski et al., 2007), based on the 20 microsatellites. MHC genotype data concurred with the parentage results according to Mendelian inheritance.

Using parentage analysis, we categorized each adult male to one of the following two groups:

(i) OMU male: the resident male of the same OMU as the mother of each infant during the previous mating season.
(ii) Genetic father: the real father of each infant based on the result of parentage analysis. This could have been the resident OMU male of the same OMU as the mother, the resident male of a neighboring OMU to that of the mother, or an AMB male.

Using parentage analysis, we categorized each infant to one of the following two groups:

(i) Extra-pair offspring (EPO): an infant fathered by a male who was not the infant's OMU male.
(ii) Within-pair offspring (WPO): an infant fathered by its OMU male.

Test Parameters for Hypotheses

To test for mate choice based on MHC-dissimilarity, we estimated the following parameters: (1) the genetic similarity of MHC alleles between the individuals of adult male-female pairs (D_{FM}), calculated as $D_{FM} = 2N_{FM}/(N_F + N_M)$, where N_F and N_M are the number of MHC alleles in female and male, and N_{FM} is the number of these alleles shared by both individuals (Wetton et al., 1987); (2) the pairwise evolutionary amino acid distance (E_{aadis}), which was calculated as $E_{aadis} = E_{AB} + E_{Ab} + E_{aB} + E_{ab}$, where A, a, B, b represent the four alleles carried by the female and the male (Landry et al., 2001). The evolutionary distance between two alleles is calculated by MEGA 7.0 (Kumar et al., 2016); and (3) the pairwise functional amino acid distance (F_{aadis}). The physiochemical properties of each amino acid were represented by five z-descriptors: z1 (hydrophobicity), z2 (steric bulk), z3 (polarity), and z4 and z5 (electronic effects) (Sandberg et al., 1998). A matrix between alleles was constructed to enable the Euclidian distance of all amino acids to be calculated (Huchard et al., 2013). The formula used to calculate

F_{aadis} is similar to that used for E_{aadis}, as $F_{aadis} = F_{AB} + F_{Ab} + F_{aB} + F_{ab}$.

To test for mate choice based on MHC-heterozygosity, we calculated the MHC heterozygosity (H_{MHC}) of all adult OMU and AMB males (*DQA1* and *DQB1*). We used 0 to represent homozygotes and 1 to represent heterozygotes for each MHC locus. To test for mate choice based on MHC-diversity, two parameters were used: (1) the evolutionary amino acid distance (intra-E_{aadis}) and (2) the functional amino acid distance (intra-F_{aadis}) between two alleles within a locus for each adult OMU and AMB male.

To test for mate choice based on specific MHC genes, the MHC allele frequency (*AF*) of each locus in adult OMU and AMB males was used.

To test for mate choice based on overall heterozygosity, we calculated the microsatellite multi-locus heterozygosity in adult OMU and AMB males (*MLH*, the number of heterozygous microsatellite loci as a proportion of the total number of typed loci).

To test for inbreeding avoidance, we calculated Queller and Goodnight's (1989) relatedness *r* using the program SPAGeDi v1.5a (Hardy and Vekemans, 2002) to quantify the genetic relatedness of each actual mother of each infant to each OMU and AMB male combination (**Table 1**).

Randomization Tests

We conducted a randomization test based on Monte Carlo sampling to investigate three non-exclusive hypotheses on MHC-based mate choice. We simulated a random model of female choice by letting each female randomly select 10 000 times between all accessible adult males of the corresponding year. We then compared the observed mean value of OMU males or genetic fathers, to the simulated range of randomly "selected" males. We calculated *P*-values as the proportion of the total number of iterations greater or smaller than the observed mean. Observed values were significant if they fell outside of the 97.5–2.5% confidence interval (CI). If females prefer males with heterozygous or specific alleles as OMU males, we expected the mean of H_{MHC}, intra-E_{aadis}, intra-F_{aadis}, *MLH*, and *AF* for the OMU males would to be significantly higher than that of randomly assigned males. If females choose males based on their own MHC genotype as the genetic fathers of their offspring, A lower mean of D_{FM} and a higher mean of E_{aadis}, F_{aadis} for the genetic fathers to mothers than random suggests mate choice for maximum MHC-dissimilarity. However, the mean value for mate choice for intermediate MHC-dissimilarity cannot be distinguished from that for random mating. Therefore, in order to compare the variance of 54 observed mates with random mates, we produced 54 randomly selected "mates" and repeated the process 10,000 times to calculate the distribution of 10,000 variances. If the observed variance of pairwise MHC-dissimilarity is significantly lower than the random variance distribution, then this is consistent with mate choice for intermediate MHC-dissimilarity (Forsberg et al., 2007). If females are attempting to avoid the costs of inbreeding, we expected the mean of *r* for the genetic fathers and mothers to be significantly higher than that for random mating.

TABLE 1 | Summary table of the test parameters for alternative hypotheses.

Mate choice based on	Parameter	
MHC-dissimilarity	D_{FM}	the genetic similarity of MHC alleles between females and males
	E_{aadis}	the pairwise evolutionary amino acid distance between the MHC alleles of mates
	F_{aadis}	the pairwise functional amino acid distance between the MHC alleles of mates
MHC-heterozygosity (diversity)	H_{MHC}	MHC heterozygosity of individual male
	intra-E_{aadis}	the evolutionary amino acid distance between two alleles in males
	intra-F_{aadis}	the functional amino acid distance between two alleles in males
specific MHC genes	*AF*	the MHC allele frequency of each locus in males
overall heterozygosity	*MLH*	the microsatellite multi-locus heterozygosity in males
inbreeding avoidance	*r*	the genetic relatedness between females and males

Extra-Pair Copulation

To test if patterns of extra-pair copulation were consistent with female choice for MHC-based and/or genome-wide effects, we used a series of generalized linear mixed models (GLMM) to measure the probability of a male being an OMU male of an EPO or the genetic father of an EPO. Each model used a single explanatory measure. This was one of three female–male MHC-dissimilarity measures (D_{FM}, pairwise E_{aadis}, pairwise F_{aadis}), one of three MHC-heterozygosity (diversity) measures for males (H_{MHC}, intra-E_{aadis}, intra-F_{aadis}), the overall heterozygosity parameter of males (*MLH*), or the genetic relatedness between the female (mother) and either the OMU male of an EPO or the genetic father of an EPO (*r*). Each model used a binary response variable defined as 1 for an OMU male with an extra-pair offspring (EPO) or 0 for a genetic father of an EPO. To remove the effects of data pseudo-replication, female ID, male ID, and sampling year were all included as random factors.

We also used generalized linear mixed models (GLMM) to test for the effects of variation in genetic measurements (H_{MHC}, intra-E_{aadis}, intra-F_{aadis}, D_{FM}, pairwise E_{aadis}, pairwise F_{aadis}, *MLH*, and *r*) on the probability of individual offspring being the product of an extra-pair copulation. We used a binary response variable defined as 1 for an OMU male with an extra-pair offspring (EPO) or 0 for an OMU male with a within-pair offspring (WPO). To remove the effects of pseudo-replication, female ID, male ID, and sampling year were all included as random factors.

To account for any possible false discovery regarding multiple tests, we applied Bonferroni corrections (n = 8; p-threshold = 0.006). All GLMM analyses were conducted with R 3.6.1. (R-Core Team, 2019), either using the base package or with the additional package "lmerTest" (Kuznetsova et al., 2017).

RESULTS

Microsatellite Typing and Paternity Analysis

A total of 145 individuals were typed using 20 microsatellite loci and 54 parent-offspring triads were identified. For all infants, information about their mothers and OMU males was determined from behavioral observations. Thirty-three infants (61%) were fathered by their OMU male, the same male that headed their mother's OMU. The remaining 21 infants (39%) were the result of extra-pair copulations. Of these 21 infants, 14 (26% of all infants) were fathered by an OMU adult male from a different OMU to that of their mother, with 7 (13% of all infants) being fathered by an AMB male (**Supplementary Table 1**).

MHC Typing

The *DQA1* locus genotypes were determined for 144 individuals (16 OMU males, 27 AMB males, 48 adult females, and 53 infants) and the *DQB1* locus genotypes for 145 individuals (16 OMU males, 27 AMB males, 48 adult females, and 54 infants). For both *DQA1* and *DQB1* loci, we identified five previously reported alleles: *Rhro-DQA1*01*, *02*, *03*, *05*, and *08*, GenBank: JQ217107-JQ217115; *Rhro-DQB1*01*, *04*, *08*, *09*, and *17*, GenBank: JQ217116-JQ217131, KU184585 (Luo et al., 2012; Zhang et al., 2016).

There was no significant correlation between MHC heterozygosity and multi-locus heterozygosity. [H_{MHC}-*DQA1* vs. *MLH* ($N = 43$): Spearman's rho = −0.061, $p = 0.697$; H_{MHC}-*DQB1* vs. *MLH* ($N = 43$): Spearman's rho = −0.065, $p = 0.680$]. Our estimates of pairwise MHC genetic similarity did not correlate with relatedness as estimated from microsatellites [D_{FM}-*DQA1* vs. r ($N = 52$): Spearman's rho = −0.045, $p = 0.753$; D_{FM}-*DQB1* vs. r ($N = 52$): Spearman's rho = 0.017, $p = 0.906$].

Female Choice for OMU Males

No evidence of female choice for OMU males based on MHC dissimilarity, intermediate dissimilarity, heterozygosity, and diversity was detected at both loci (**Table 2**). However, the frequency of *Rhro-DQA1* 05* and *Rhro-DQB1* 08* for OMU

TABLE 2 | Results of randomization tests for differences in genetic parameters (MHC genes and microsatellites).

Hypotheses	Parameter	OMU males vs. randomly assigned males		Genetic fathers vs. randomly assigned males	
		DQA1	***DQB1***	***DQA1***	***DQB1***
MHC dissimilarity	D_{MF}	obs = 0.407	obs = 0.426	obs = 0.420	obs = 0.497
		sim = 0.478[0.395, 0.568]	sim = 0.463[0.370, 0.559]	sim = 0.478[0.395, 0.568]	sim = 0.463[0.370, 0.559]
	E_{aadis}	obs = 0.497	obs = 0.466	obs = 0.517	obs = 0.463
		sim = 0.506[0.463, 0.549]	sim = 0.491[0.447, 0.534]	sim = 0.506[0.463, 0.549]	sim = 0.491[0.447, 0.534]
	F_{aadis}	obs = 174.8	obs = 183.8	obs = 182.6	obs = 182.6
		sim = 180.0[164.2, 195.4]	sim = 193.7[176.4, 210.4]	sim = 180.0[164.2, 195.4]	sim = 193.7[176.4, 210.4]
MHC-heterozygosity	H_{MHC}	obs = 0.796	obs = 0.704	obs = 0.852	obs = 0.778
		sim = 0.833[0.741, 0.926]	sim = 0.741[0.630, 0.852]	sim = 0.833[0.741, 0.926]	sim = 0.741[0.630, 0.852]
(diversity)	intra-E_{aadis}	obs = 0.162	obs = 0.133	obs = 0.181	**obs = 0.155***
		sim = 0.155[0.127, 0.182]	sim = 0.129[0.102, 0.155]	sim = 0.155[0.127, 0.182]	**sim = 0.129[0.102, 0.155]**
	intra-E_{aadis}	obs = 57.45	obs = 52.32	obs = 64.56	**obs = 61.21***
		sim = 55.60[45.20, 65.34]	sim = 51.06[40.43, 61.17]	sim = 55.60[45.20, 65.34]	**sim = 51.06[40.43, 61.17]**
specific MHC genes	*AF*	*01*, obs = 0.315	*01*, obs = 0.102	*01*, obs = 0.426	*01*, obs = 0.102
		sim = 0.380[0.306, 0.463]	sim = 0.102[0.046, 0.167]	sim = 0.380[0.306, 0.463]	sim = 0.102[0.046, 0.167]
		02, obs = 0.278	***04*, obs = 0.315***	***02*, obs = 0.167****	*04*, obs = 0.435
		sim = 0.278[0.204, 0.361]	**sim = 0.407[0.324, 0.491]**	**sim = 0.278[0.204, 0.361]**	sim = 0.407[0.324, 0.491]
		03, obs = 0.083	***08*, obs = 0.231****	*03*, obs = 0.102	***08*, obs = 0.213***
		sim = 0.083[0.037, 0.130]	**sim = 0.139[0.074, 0.213]**	sim = 0.083[0.037, 0.130]	**sim = 0.139[0.074, 0.213]**
		05*, obs = 0.259*	*09*, obs = 0.093	***05*, obs = 0.241****	*09*, obs = 0.093
		sim = 0.139[0.074, 0.213]	sim = 0.139[0.074, 0.213]	**sim = 0.139[0.074, 0.213]**	sim = 0.139[0.074, 0.213]
		08*, obs = 0.065	*17*, obs = 0.259	***08*, obs = 0.065***	*17*, obs = 0.157
		sim = 0.111[0.065, 0.176]	sim = 0.204[0.139, 0.287]	**sim = 0.111[0.065, 0.176]**	sim = 0.204[0.139, 0.287]
		SSR			
overall heterozygosity	*MLH*	obs = 0.589		obs = 0.578	
		sim = 0.582[0.551, 0.612]		sim = 0.582[0.551, 0.612]	
inbreeding avoidance	*r*	obs = −0.000		obs = −0.010	
		sim = 0.002[−0.052, 0.059]		sim = 0.002[−0.052, 0.059]	

*Statistical significance is indicated in bold. obs, observed mean; sim, simulated mean [95% CI]. P ≤ 0.05 in the statistical tests is indicated with *; P ≤ 0.01 in the statistical tests is indicated with **.*

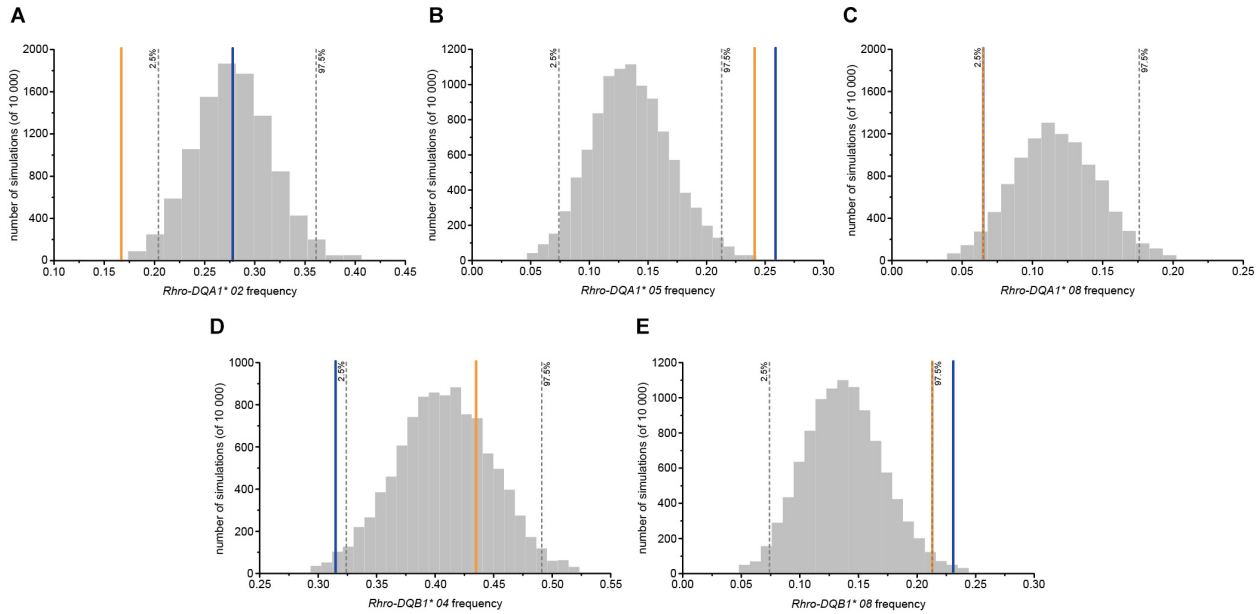

FIGURE 1 | Frequencies of MHC alleles for OMU males, genetic fathers, and randomly assigned males. Blue solid line: OMU males; orange solid line: genetic fathers; gray bars: frequency distributions of mean values generated from 10,000 simulations of random males. Two-tailed 95% confidence intervals are indicated by dashed lines which displayed cut-offs for significant departures from random mating. **(A)** *Rhro-DQA1* 02*, **(B)** *Rhro-DQA1* 05*, **(C)** *Rhro-DQA1* 08*, **(D)** *Rhro-DQB1* 04*, and **(E)** *Rhro-DQB1* 08*.

males was significantly higher than for randomly assigned males, and significantly lower frequencies of *Rhro-DQA1* 08* and *Rhro-DQB1* 04* (**Table 2** and **Figure 1**).

For female mate choice based on genome-wide effects, we found no difference between OMU males and randomly assigned males for microsatellite multi-locus heterozygosity (*MLH*), or relatedness (**Table 2**).

Female Choice for Genetic Fathers

The mean values of the genetic fathers-females did not significantly differ to the mean values for randomly assigned males-females in terms of D_{FM}, E_{aadis}, and F_{aadis} (**Table 2** and **Figure 2**). However, consistent with the intermediate dissimilarity hypothesis, variance for E_{aadis}, and F_{aadis} of the genetic fathers-females were significantly lower than the corresponding values for randomly selected mates at both loci (**Table 3**).

The genetic fathers had significantly higher value of evolutionary amino acid distances (intra-E_{aadis}) and functional amino acid distances (intra-F_{aadis}) than randomly assigned males at *DQB1* (**Table 2** and **Figure 3**).

The choice of specific MHC alleles for the genetic fathers was largely consistent with that for the OMU males. Both had significantly higher frequencies of *Rhro-DQA1* 05* and *Rhro-DQB1* 08* than randomly assigned males, but significantly lower frequencies of *Rhro-DQA1* 02* and *Rhro-DQA1* 08* (**Table 2** and **Figure 1**).

For choice based on genome-wide effects, we found no difference between genetic fathers and randomly assigned males for microsatellite multi-locus heterozygosities (*MLH*). The relatedness values for the genetic fathers and females did not differ to those of randomly assigned mates (**Table 2**).

Extra-Pair Paternity

We found no significant effect of each genetic variable on the probability of one male being an OMU male of an EPO or a genetic father of an EPO (GLMM; **Supplementary Tables 2–9**). Furthermore, we found no significant effect of each genetic variable on the probability of individual offspring being the product of an extra-pair copulation (GLMM; **Supplementary Tables 10–17**).

DISCUSSION

Although *R. roxellana* is generally regarded as being polygynous, its mating system is dynamic and is likely to change in response to various factors such as OMU take-overs and female transfers between different OMUs (Zhang et al., 2006; Qi et al., 2009). Moreover, our new parentage analysis showed a 39% rate of extra-pair paternity, which broadly concurs with the high rates in the same *R. roxellana* population in different years (57% in both 2005 and 2014–2015; Guo et al., 2010; Qi et al., 2020). Our results suggest that female *R. roxellana* choose the genetic fathers of their offspring non-randomly. Our data are consistent with female preference for mates of intermediate MHC dissimilarity and high MHC diversity, and showed evidence of choice for specific MHC genes. The measured values of MHC dissimilarity between females and the genetic fathers of their offspring was consistently close to the mean value of the random model, with a significantly

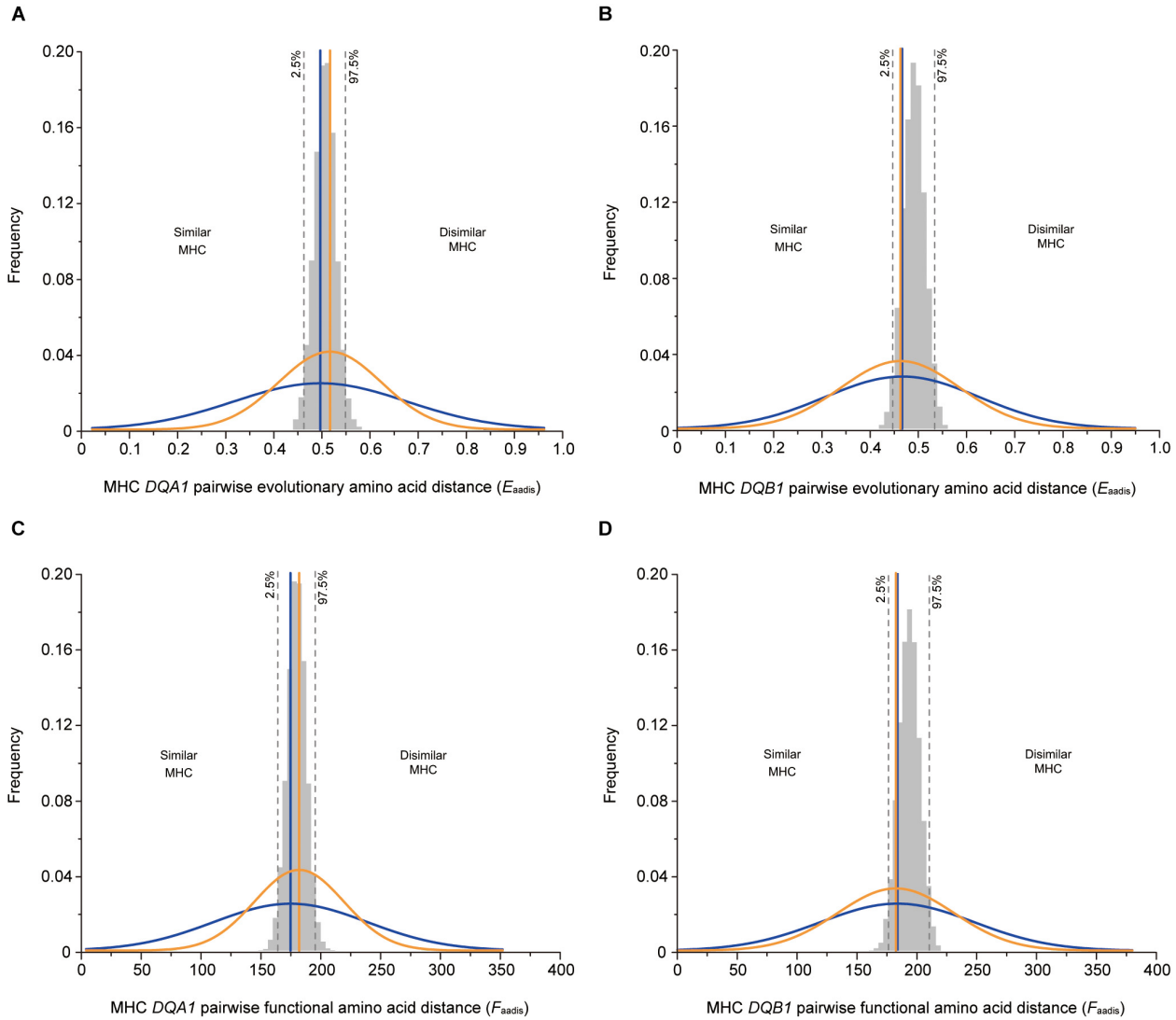

FIGURE 2 | MHC genetic similarity parameters between male and female for OMU males, genetic fathers and randomly assigned males. The observed values for the OMU males/genetic fathers and female are visualized as normalized curves in blue and orange. Blue solid line: mean of OMU males; orange solid line: mean of genetic fathers; gray bars: frequency distributions of mean values generated from 10,000 simulations of random mates. Two-tailed 95% confidence intervals are indicated by dashed lines which displayed cut-offs for significant departures from random mating. **(A,B)** pairwise evolutionary amino acid distance, **(C,D)** pairwise functional amino acid distance. **(A,C)** at *DQA1* locus, **(B,D)** at *DQB1* locus.

TABLE 3 | Results of randomization tests between OMU males/genetic fathers and randomly assigned males in measures of variance in MHC dissimilarity parameter.

Parameter	OMU males vs. randomly assigned males		Genetic fathers vs. randomly assigned males	
	DQA1	***DQB1***	***DQA1***	***DQB1***
variance in D_{MF}	obs = 0.095 sim = 0.111[0.073, 0.188]	obs = 0.095 sim = 0.132[0.081, 0.224]	obs = 0.087 sim = 0.111[0.073, 0.188]	obs = 0.128 sim = 0.132[0.081, 0.224]
variance in E_{aadis}	obs = 0.032 sim = 0.028[0.015, 0.043]	obs = 0.025 sim = 0.029[0.017, 0.042]	**obs = 0.011**** **sim = 0.028[0.015, 0.043]**	**obs = 0.015*** **sim = 0.029[0.017, 0.042]**
variance in F_{aadis}	obs = 4137.9 sim = 3626.2[1936.0, 5561.6]	obs = 4111.1 sim = 4421.0[2591.5, 6492.8]	**obs = 1394.9**** **sim = 3626.2[1936.0, 5561.6]**	**obs = 2345.8*** **sim = 4421.0[2591.5, 6492.8]**

*Statistical significance is indicated in bold. obs, observed mean; sim, simulated mean [95% CI]. $P \leq 0.05$ in the statistical tests is indicated with *; $P \leq 0.01$ in the statistical tests is indicated with **.*

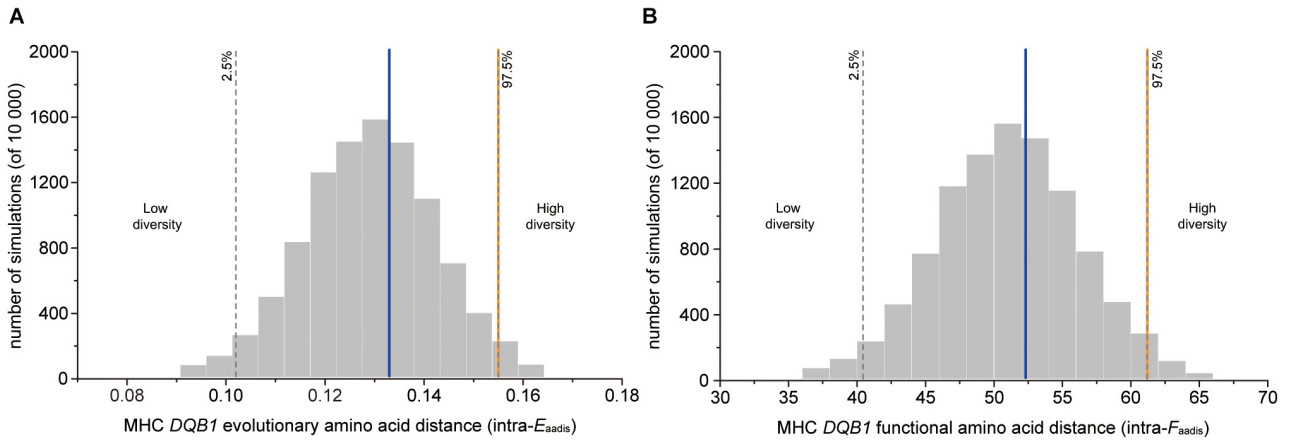

FIGURE 3 | MHC genetic diversity parameters for OMU males, genetic fathers and randomly assigned males. Blue solid line: OMU males; orange solid line: genetic fathers; gray bars: frequency distributions of mean values generated from 10,000 simulations of random males. Two-tailed 95% confidence intervals are indicated by dashed lines which displayed cut-offs for significant departures from random mating. **(A)** evolutionary amino acid distance of individual MHC alleles (intra-E_{aadis}), **(B)** functional amino acid distance of individual MHC alleles (intra-F_{aadis}).

reduced variance. The difference between individual MHC alleles of the genetic fathers of offspring was also significantly higher than for the randomly chosen males. In both the mothers' OMU males and the genetic fathers of offspring, the frequency of *Rhro-DQA1* 05* and *Rhro-DQB1* 08* was significantly higher than in randomly assigned males, and the frequency of *Rhro-DQB1* 08* was significantly lower than in randomly assigned males. Finally, our microsatellite data showed no evidence of choice for genome-wide heterozygosity advantage or inbreeding avoidance. Genes of the MHC or microsatellites convey different information, suggesting that the trends we observed regarding MHC class II genes were not due to genome-wide effects. The functional loci of the MHC are thus more likely to be the targets of female mate choice in *R. roxellana*.

Several studies have also reported evidence for intermediate dissimilarity choice at MHC loci (Bonneaud et al., 2006; Forsberg et al., 2007; Eizaguirre et al., 2009; Rekdal et al., 2019). This concurs with mate choice for MHC dissimilarity to produce offspring that can cope with a wide-range of pathogens. However, it is noteworthy that at some point the costs of choice for MHC genes will outweigh the benefits due to: (1) self-reactive autoimmune responses, (2) the cost of coadapted gene complex disruption, and (3) a consumption of mature T-cell repertoire in individual offspring with high MHC diversity (Nowak et al., 1992; Hendry et al., 2000; Woelfing et al., 2009). This concurs with the hypothesis that the optimal MHC diversity for offspring could be intermediate rather than maximal due to a trade-off between individual MHC alleles (Kalbe et al., 2009; Woelfing et al., 2009). Some experimental studies on infection by multiple parasites and pathogens have shown that high rates of MHC polymorphism may reduce the immune ability of individual hosts (Wegner et al., 2003; Ilmonen et al., 2007). Females may thus choose males with intermediate differences in genotypes as fathers of their offspring to avoid producing offspring with high MHC polymorphism. However, we found no evidence that any of the genetic variables in this study affected the probability of extra-pair copulation, and no evidence that any of the genetic variables affected the likelihood of OMU males fathering EPOs. This suggests that within the scope of our research, any benefits to females via extra-pair copulations may not be entirely genetic. In *R. roxellana*, extra-pair copulations are mostly initiated by females and are not confined to the mating season (Zhao et al., 2005). Extra-pair copulations may thus not always serve a direct reproductive function and may benefit females in other ways. For example, extra-pair copulations may help females establish a beneficial social relationship with a male (Lemasson et al., 2008). In *R. roxellana* multiple females from one OMU have been recorded engaging in extra-pair copulations with the same AMB male, which has successfully usurped the OMU male during the course of their pregnancies (Qi et al., 2020). Female *R. roxellana* may also produce extra-pair offspring as an infanticide avoidance strategy via paternity confusion (Qi et al., 2020). Female initiated extra-pair copulations are thus unlikely to be solely driven by genetic benefits to females.

Both human and non-human primate studies have shown evidence of mate choice for MHC-dissimilarity and diversity, with fewer reports of mate choice for intermediate MHC dissimilarity, optimal diversity, or specific MHC genes (Winternitz and Abbate, 2015). To date, there are relatively few reports of mate choice for specific MHC genes in non-human primates (Sauermann et al., 2001; Schwensow et al., 2008a,b; Setchell et al., 2009a, 2013, 2016; Huchard et al., 2010a, 2013; Yang et al., 2014; Sterck et al., 2017). In fat-tailed dwarf lemurs (*Cheirogaleus medius*), male and female formed life-long breeding pairs but with high rate of extra-pair paternity (44%), social males have higher frequency of *MHC-DRB* supertype S1 (20 MHC supertypes defined by hierarchical clustering based on amino acid sequence in the 50 different MHC-DRB alleles) than random males (Schwensow et al., 2008b). In mandrills (*Mandrillus sphinx*), a species that exhibits male mate-guarding

of females, males prefer to guard females who do not possess *MHC-DRB* supertype S1, an MHC supertype that is associated with decreased immune function in the study population (Setchell et al., 2016).

In another *R. roxellana* population, Yang et al. (2014) found no evidence for female mate choice based on MHC genotypes. Our study used similar statistical methods in order to quantify the effects of MHC variation on mate choice, as well as comparisons between real and random males. However, there are several differences between this present study and that of Yang et al. (2014). We found that both *DQA1* and *DQB1* loci of the MHC II gene significantly affected mate choice, whereas Yang et al. (2014) used the *DRB* locus of the MHC II gene and found no significant effects. Although any functional differences among the *DQA1*, *DQB1*, and *DRB* loci remain unknown for *R. roxellana*, there may be different mate choice selection pressures on different loci. For instance, in gray mouse lemurs (*Microcebus murinus*), disassortative mate choice was detected at *DRB* but not at *DQB* (Huchard et al., 2013).

An alternative explanation for the discrepancy between our new results and those of Yang et al. (2014) may be due to insufficient sample size, resulting in type II errors in the interpretation of highly polymorphic MHC genes (Hoover and Nevitt, 2016). The breeding band studied by Yang et al. (2014) was smaller than our study breeding band and contained only five adult males (four OMU leader males and a single AMU male) and 15 adult females. Moreover, Yang et al. (2014) also found extra-pair paternity, but only less than 10% of all infants were the result of an extra-pair copulation. Due to the larger number of adult males per female in the breeding band of our study, females thus had more opportunities to exhibit mate-choice and/or extra-pair copulation. In order to minimize conflict between adult males, interactions between the AMB and OMUs of the population studied by Yang et al. (2014) had been experimentally restricted so females would have had reduced opportunities for expressing their mate preferences (Qi et al., 2020). Studies of a wide variety of different taxa, including non-human primates, have shown that female mate choice is usually dependent on ecological conditions that alter the costs and benefits of being choosy (Andersson, 1994). For example, when dominant males are able to prevent other males from obtaining mating opportunities, such as in small groups, female mating preferences are constrained (Setchell and Huchard, 2010).

Major histocompatibility complex-based mate choice in *R. roxellana* posits the question: which phenotypic signals do females use to evaluate the genetic quality of potential mates? In some non-human primates, MHC profiles have been shown to correlate with variation in secondary sexual traits in both sexes. In Chacma baboons (*Papio ursinus*), the specific MHC supertype (S1) is associated with female physical condition and the size of sexual swellings, even there is no evidence of male mate choice for MHC dissimilarity, diversity or rare MHC genotypes (Huchard et al., 2010a,b). Female sexual swellings are a reliable indicator of female reproductive condition to males, and males preferring females with larger swellings (Huchard et al., 2009). In Mandrills (*Mandrillus sphinx*), male facial redness which were preferred by females, were positively correlated with MHC supertypes S4 and S11 (Setchell, 2005; Setchell et al., 2009b). *R. roxellana* exhibits several sexually dimorphic traits such as body size, facial color, and pelage color (Zhang et al., 2006). We speculate that females may assess male MHC quality using one or more of these traits. Additionally, olfactory cues to assess MHC dissimilarity may be involved, as have been found in diverse taxa such as sand lizards (*Lacerta agilis*), blue petrels (*Halobaena caerulea*), bank voles (*Myodes glareolus*), and humans (Jacob et al., 2002; Olsson et al., 2003; Thornhill et al., 2003; Radwan et al., 2008; Leclaire et al., 2017). In mandrills (*Mandrillus sphinx*), although male odors are not related to any specific MHC supertype, odor similarity is related to MHC similarity (Setchell et al., 2011).

Females may choose to mate with those extra-pair males that have a high likelihood of usurping an established OMU leader male, and may thus obtain future direct benefits from being a member of that male's OMU (Qi et al., 2020). Female mate choice may thus play an important role in the social organization of *R. roxellana*. The *R. roxellana* multilevel society provides opportunities for females to choose mates at different levels. The potential for female mate choice to contribute to the maintenance of this multilevel society may thus vary accordingly. The lack of cultural, socioeconomic, and technological factors, along with superficial similarities in social structure, makes the study of such non-human primates a more productive alternative to current human populations (Winternitz and Abbate, 2015).

CONCLUSION

To conclude, we investigated the effects of adaptive MHC genes and neutral microsatellites on female mate choice in *R. roxellana*. Our results are consistent with females basing their mate choice, at least in part, on benefits associated with intermediate MHC-dissimilarity, MHC-diversity, and specific MHC alleles but not on benefits associated with microsatellites. We emphasize that because we did not measure actual female mate choice in a behavioral context, our methods only enabled the evaluation of the effects of mate choice after choice had occurred (Andersson, 1994; Wagner, 1998; Qi et al., 2014). Finally, the differences in our results to those of another population of the same species emphasizes the importance of incorporating multiple MHC loci, large sample sizes, and variable social structures into studies of MHC-based mate choice in non-human primates.

DATA AVAILABILITY STATEMENT

The datasets presented in this study can be found in online repositories. The names of the repository/repositories and accession number(s) can be found below: https://www.ncbi.nlm.nih.gov/genbank/, JQ217107–JQ217115 and https://www.ncbi.nlm.nih.gov/genbank/, JQ217116–JQ217131.

ETHICS STATEMENT

The animal study was reviewed and approved by the Ethics Committee of the College of Life Sciences, Northwest University.

AUTHOR CONTRIBUTIONS

PZ and B-GL designed the study and helped to draft the manuscript. B-YZ, H-YH, and C-MS carried out the molecular genetic studies. B-YZ performed the statistical analysis and drafted the manuscript. KH and DWD edited the manuscript. XY provided data support in response to comments. X-WW, H-TZ, and C-LW participated in the sampling. All authors read and approved the final manuscript.

FUNDING

This study was funded by the Strategic Priority Research Program of the Chinese Academy of Sciences (XDB31000000), the National Natural Science Foundation of China (31730104, 31770425, 32071495, and 31770411), the National Key Program of Research and Development, Ministry of Science and Technology (2016YFC0503200), the Natural Science Basic Research Plan in Shaanxi Province of China (2019JM-258), and the "One Institute One Brand" Foundation of Shaanxi Academy of Sciences (2020k-01).

ACKNOWLEDGMENTS

We gratefully acknowledge Zhouzhi National Nature Reserve (ZNNR) for permission to carry out this research. We thank the staff of the Shaanxi Key Laboratory for Animal Conservation, College of Life Sciences, Northwest University. We also thank Northwest University students Yan-mei Duan and Hong-juan Sun for samples provision and laboratory work assistance.

SUPPLEMENTARY MATERIAL

The Supplementary Material for this article can be found online at: https://www.frontiersin.org/articles/10.3389/fgene.2020.609414/full#supplementary-material

REFERENCES

Allen, M., Engstrom, A. S., Meyers, S., Handt, O., Saldeen, T., von Haeseler, A., et al. (1998). Mitochondrial DNA sequencing of shed hairs and saliva on robbery caps: sensitivity and matching probabilities. *J. Forensic Sci.* 43, 453–464. doi: 10.1520/JFS16169J

Altmann, J. (1974). Observational study of behavior: sampling methods. *Behaviour* 49, 227–267.doi: 10.1163/156853974x00534

Andersson, M. (1994). *Sexual Selection*. Princeton, NJ: Princeton University Press.

Bernatchez, L., and Landry, C. (2003). MHC studies in nonmodel vertebrates: What have we learned about natural selection in 15 years? *J. Evol. Biol.* 16, 363–377.doi: 10.1046/j.1420-9101.2003.00531.x

Bonneaud, C., Chastel, O., Federici, P., Westerdahl, H., and Sorci, G. (2006). Complex Mhc-based mate choice in a wild passerine. *Proc. R. Soc. B Biol. Sci.* 273, 1111–1116. doi: 10.1098/rspb.2005.3325

Doherty, P. C., and Zinkernagel, R. M. (1975). Enhanced immunological surveillance in mice heterozygous at the H-2 gene complex. *Nature* 256, 50–52.doi: 10.1038/256050a0

Eizaguirre, C., Yeates, S. E., Lenz, T. L., Kalbe, M., and Milinski, M. (2009). MHC-based mate choice combines good genes and maintenance of MHC polymorphism. *Mol. Ecol.* 18, 3316–3329. doi: 10.1111/j.1365-294X.2009.04243.x

Evans, M. L., Dionne, M., Miller, K. M., and Bernatchez, L. (2012). Mate choice for major histocompatibility complex genetic divergence as a bet-hedging strategy in the Atlantic salmon (*Salmo salar*). *Proc. R. Soc. B Biol. Sci.* 279, 379–386.doi: 10.1098/rspb.2011.0909

Fang, G., Chen, J., Pan, R. L., Qi, X. G., and Li, B. G. (2018). Female choice impacts resident male takeover in golden snub-nosed monkeys (*Rhinopithecus roxellana*). *Zool. Res.* 39, 266–271. doi: 10.24272/j.issn.2095-8137.2018.035

Ferrandiz-Rovira, M., Allaine, D., Callait-Cardinal, M. P., and Cohas, A. (2016). Mate choice for neutral and MHC genetic characteristics in Alpine marmots: Different targets in different contexts? *Ecol. Evol.* 6, 4243–4257.doi: 10.1002/ece3.2189

Forsberg, L. A., Dannewitz, J., Petersson, E., and Grahn, M. (2007). Influence of genetic dissimilarity in the reproductive success and mate choice of brown trout - females fishing for optimal MHC dissimilarity. *J. Evol. Biol.* 20, 1859–1869.doi: 10.1111/j.1420-9101.2007.01380.x

Grueter, C. C., Qi, X. G., Li, B. G., and Li, M. (2017). Multilevel societies. *Curr. Biol.* 27, R984–R986. doi: 10.1016/j.cub.2017.06.063

Guo, S. T., Ji, W. H., Li, M., Chang, H. L., and Li, B. G. (2010). The mating system of the Sichuan snub-nosed monkey (*Rhinopithecus roxellana*). *Am. J. Primatol.* 72, 25–32.doi: 10.1002/ajp.20747

Hardy, O. J., and Vekemans, X. (2002). SPAGEDi: a versatile computer program to analyse spatial genetic structure at the individual or population levels. *Mol. Ecol. Notes* 2, 618–620.doi: 10.1046/j.1471-8286.2002.00305.x

Hendry, A. P., Wenburg, J. K., Bentzen, P., Volk, E. C., and Quinn, T. P. (2000). Rapid evolution of reproductive isolation in the wild: evidence from introduced salmon. *Science* 290, 516–518.doi: 10.1126/science.290.5491.516

Hoover, B., Alcaide, M., Jennings, S., Sin, S. Y. W., Edwards, S. V., and Nevitt, G. A. (2018). Ecology can inform genetics: disassortative mating contributes to MHC polymorphism in Leach's storm-petrels (*Oceanodroma leucorhoa*). *Mol. Ecol.* 27, 3371–3385.doi: 10.1111/mec.14801

Hoover, B., and Nevitt, G. (2016). Modeling the importance of sample size in relation to error in MHC-based Mate-choice studies on natural populations. *Integr. Comp. Biol.* 56, 925–933.doi: 10.1093/icb/icw105

Huang, K., Guo, S. T., Cushman, S. A., Dunn, D. W., Qi, X. G., Hou, R., et al. (2016). Population structure of the golden snub-nosed monkey *Rhinopithecus roxellana* in the Qinling Mountains, central China. *Integr. Zool.* 11, 350–360. doi: 10.1111/1749-4877.12202

Huchard, E., Baniel, A., Schliehe-Diecks, S., and Kappeler, P. M. (2013). MHC-disassortative mate choice and inbreeding avoidance in a solitary primate. *Mol. Ecol.* 22, 4071–4086.doi: 10.1111/mec.12349

Huchard, E., Benavides, J. A., Setchell, J. M., Charpentier, M. J. E., Alvergne, A., King, A. J., et al. (2009). Studying shape in sexual signals: the case of primate sexual swellings. *Behav. Ecol. Sociobiol.* 63, 1231–1242.doi: 10.1007/s00265-009-0748-z

Huchard, E., Knapp, L. A., Wang, J. L., Raymond, M., and Cowlishaw, G. (2010a). MHC, mate choice and heterozygote advantage in a wild social primate. *Mol. Ecol.* 19, 2545–2561. doi: 10.1111/j.1365-294X.2010.04644.x

Huchard, E., Raymond, M., Benavides, J., Marshall, H., Knapp, L. A., and Cowlishaw, G. (2010b). A female signal reflects MHC genotype in a social primate. *BMC Evol. Biol.* 10:96.doi: 10.1186/1471-2148-10-96

Ilmonen, P., Penn, D. J., Damjanovich, K., Morrison, L., Ghotbi, L., and Potts, W. K. (2007). Major histocompatibility complex heterozygosity reduces fitness in experimentally infected mice. *Genetics* 176, 2501–2508.doi: 10.1534/genetics.107.074815

Jacob, S., McClintock, M. K., Zelano, B., and Ober, C. (2002). Paternally inherited HLA alleles are associated with women's choice of male odor. *Nat. Genet.* 30, 175–179.doi: 10.1038/ng830

Kalbe, M., Eizaguirre, C., Dankert, I., Reusch, T. B. H., Sommerfeld, R. D., Wegner, K. M., et al. (2009). Lifetime reproductive success is maximized with optimal major histocompatibility complex diversity. *Proc. R. Soc. B Biol. Sci.* 276, 925–934.doi: 10.1098/rspb.2008.1466

Kalinowski, S. T., Taper, M. L., and Marshall, T. C. (2007). Revising how the computer program CERVUS accommodates genotyping error increases success in paternity assignment. *Mol. Ecol.* 16, 1099–1106.doi: 10.1111/j.1365-294X.2007.03089.x

Kempenaers, B. (2007). Mate choice and genetic quality: a review of the heterozygosity theory. *Adv. Study Behav.* 37, 189–278. doi: 10.1016/s0065-3454(07)37005-8

Kokko, H., Brooks, R., Jennions, M. D., and Morley, J. (2003). The evolution of mate choice and mating biases. *Proc. R. Soc. B Biol. Sci.* 270, 653–664. doi: 10.1098/rspb.2002.2235

Kumar, S., Stecher, G., and Tamura, K. (2016). MEGA7: molecular evolutionary genetics analysis Version 7.0 for bigger datasets. *Mol. Biol. Evol.* 33, 1870–1874.doi: 10.1093/molbev/msw054

Kuznetsova, A., Brockhoff, P. B., and Christensen, R. H. B. (2017). lmerTest Package: tests in linear mixed effects models. *J. Stat. Softw.* 82, 1–26. doi: 10.18637/jss.v082.i13

Landry, C., Garant, D., Duchesne, P., and Bernatchez, L. (2001). 'Good genes as heterozygosity': the major histocompatibility complex and mate choice in Atlantic salmon (*Salmo salar*). *Proc. R. Soc. B Biol. Sci.* 268, 1279–1285.doi: 10.1098/rspb.2001.1659

Leclaire, S., Strandh, M., Mardon, J., Westerdahl, H., and Bonadonna, F. (2017). Odour-based discrimination of similarity at the major histocompatibility complex in birds. *Proc. R. Soc. B Biol. Sci.* 284:20162466.doi: 10.1098/rspb.2016.2466

Lemasson, A., Palombit, R. A., and Jubin, R. (2008). Friendships between males and lactating females in a free-ranging group of olive baboons (*Papio hamadryas anubis*): evidence from playback experiments. *Behav. Ecol. Sociobiol.* 62, 1027–1035.doi: 10.1007/s00265-007-0530-z

Li, B., and Zhao, D. (2007). Copulation behavior within one-male groups of wild *Rhinopithecus roxellana* in the Qinling Mountains of China. *Primates* 48, 190–196.doi: 10.1007/s10329-006-0029-7

Li, B. G., Chen, C., Ji, W. H., and Ren, B. P. (2000). Seasonal home range changes of the StateSichuan snub-nosed monkey (*Rhinopithecus roxellana*) in the Qinling mountains of China. *Folia Primatol.* 71, 375–386. doi: 10.1159/000052734

Luo, M.-F., Pan, H.-J., Liu, Z.-J., and Li, M. (2012). Balancing selection and genetic drift at major histocompatibility complex class II genes in isolated populations of golden snub-nosed monkey (*Rhinopithecus roxellana*). *BMC Evol. Biol.* 12:207.doi: 10.1186/1471-2148-12-207

Mays, H. L., and Hill, G. E. (2004). Choosing mates: good genes versus genes that are a good fit. *Trends Ecol. Evol.* 19, 554–559.doi: 10.1016/j.tree.2004.07.018

Melendez-Rosa, J., Bi, K., and Lacey, E. A. (2018). Genomic analysis of MHC-based mate choice in the monogamous California mouse. *Behav. Ecol.* 29, 1167–1180.doi: 10.1093/beheco/ary096

Milinski, M. (2006). The major histocompatibility complex, sexual selection, and mate choice. *Annu. Rev. Ecol. Evol. Syst.* 37, 159–186.doi: 10.1146/annurev.ecolsys.37.091305.110242

Miller, H. C., Moore, J. A., Nelson, N. J., and Daugherty, C. H. (2009). Influence of major histocompatibility complex genotype on mating success in a free-ranging reptile population. *Proc. R. Soc. B Biol. Sci.* 276, 1695–1704.doi: 10.1098/rspb.2008.1840

Moller, A. P., and Jennions, M. D. (2001). How important are direct fitness benefits of sexual selection? *Naturwissenschaften* 88, 401–415.doi: 10.1007/s001140100255

Neff, B. D., and Pitcher, T. E. (2005). Genetic quality and sexual selection: an integrated framework for good genes and compatible genes. *Mol. Ecol.* 14, 19–38.doi: 10.1111/j.1365-294X.2004.02395.x

Nowak, M. A., Tarczy-Hornoch, K., and Austyn, J. M. (1992). The optimal number of major histocompatibility complex molecules in an individual. *Proc. Natl. Acad. Sci. U.S.A.* 89, 10896–10899. doi: 10.1073/pnas.89.22.10896

Olsson, M., Madsen, T., Nordby, J., Wapstra, E., Ujvari, B., and Wittsell, H. (2003). Major histocompatibility complex and mate choice in sand lizards. *Proc. R. Soc. B Biol. Sci.* 270, S254–S256. doi: 10.1098/rsbl.2003.0079

Paula Cutrera, A., Sol Fanjul, M., and Rita Zenuto, R. (2012). Females prefer good genes: MHC-associated mate choice in wild and captive tuco-tucos. *Anim. Behav.* 83, 847–856.doi: 10.1016/j.anbehav.2012.01.006

Penn, D. J., and Potts, W. K. (1999). The evolution of mating preferences and major histocompatibility complex genes. *Am. Nat.* 153, 145–164.doi: 10.1086/303166

Qi, X.-G., Garber, P. A., Ji, W., Huang, Z.-P., Huang, K., Zhang, P., et al. (2014). Satellite telemetry and social modeling offer new insights into the origin of primate multilevel societies. *Nat. Commun.* 5:5296. doi: 10.1038/ncomms6296

Qi, X.-G., Grueter, C. C., Fang, G., Huang, P.-Z., Zhang, J., Duan, Y.-M., et al. (2020). Multilevel societies facilitate infanticide avoidance through increased extrapair matings. *Anim. Behav.* 161, 127–137.doi: 10.1016/j.anbehav.2019.12.014

Qi, X.-G., Huang, K., Fang, G., Grueter, C. C., Dunn, D. W., Li, Y.-L., et al. (2017). Male cooperation for breeding opportunities contributes to the evolution of multilevel societies. *Proc. R. Soc. B Biol. Sci.* 284:20171480.doi: 10.1098/rspb.2017.1480

Qi, X.-G., Li, B.-G., Garber, P. A., Ji, W., and Watanabe, K. (2009). Social dynamics of the golden snub-nosed monkey (*Rhinopithecus roxellana*): female transfer and one-male unit succession. *Am. J. Primatol.* 71, 670–679.doi: 10.1002/ajp.20702

Queller, D. C., and Goodnight, K. F. (1989). Estimating relatedness using genetic markers. *Evolution* 43, 258–275.doi: 10.1111/j.1558-5646.1989.tb04226.x

Radwan, J., Tkacz, A., and Kloch, A. (2008). MHC and preferences for male odour in the bank vole. *Ethology* 114, 827–833.doi: 10.1111/j.1439-0310.2008.01528.x

R-Core Team (2019). *R: A Language and Environment for Statistical Computing*. Vienna: R Foundation for Statistical Computing.

Rekdal, S. L., Anmarkrud, J. A., Lifjeld, J. T., and Johnsen, A. (2019). Extra-pair mating in a passerine bird with highly duplicated major histocompatibility complex class II: preference for the golden mean. *Mol. Ecol.* 28, 5133–5144.doi: 10.1111/mec.15273

Richardson, D. S., Komdeur, J., Burke, T., and von Schantz, T. (2005). MHC-based patterns of social and extra-pair mate choice in the Seychelles warbler. *Proc. R. Soc. B Biol. Sci.* 272, 759–767.doi: 10.1098/rspb.2004.3028

Sandberg, M., Eriksson, L., Jonsson, J., Sjostrom, M., and Wold, S. (1998). New chemical descriptors relevant for the design of biologically active peptides. A multivariate characterization of 87 amino acids. *J. Med. Chem.* 41, 2481–2491.doi: 10.1021/jm9700575

Santos, P. S. C., Michler, F.-U., and Sommer, S. (2017). Can MHC-assortative partner choice promote offspring diversity? A new combination of MHC-dependent behaviours among sexes in a highly successful invasive mammal. *Mol. Ecol.* 26, 2392–2404.doi: 10.1111/mec.14035

Sauermann, U., Nurnberg, P., Bercovitch, F. B., Berard, J. D., Trefilov, A., Widdig, A., et al. (2001). Increased reproductive success of MHC class II heterozygous males among free-ranging rhesus macaques. *Hum. Genet.* 108, 249–254.doi: 10.1007/s004390100485

Schwensow, N., Eberle, M., and Sommer, S. (2008a). Compatibility counts: MHC-associated mate choice in a wild promiscuous primate. *Proc. R. Soc. B Biol. Sci.* 275, 555–564.doi: 10.1098/rspb.2007.1433

Schwensow, N., Fietz, J., Dausmann, K., and Sommer, S. (2008b). MHC-associated mating strategies and the importance of overall genetic diversity in an obligate pair-living primate. *Evol. Ecol.* 22, 617–636. doi: 10.1007/s10682-007-9186-4

Searcy, W. A. (1982). The evolutionary effects of mate selection. *Annu. Rev. Ecol. Syst.* 13, 57–85.doi: 10.1146/annurev.es.13.110182.000421

Setchell, J. M. (2005). Do female mandrills prefer brightly colored males? *Int. J. Primatol.* 26, 715–735. doi: 10.1007/s10764-005-5305-7

Setchell, J. M., Abbott, K. M., Gonzalez, J.-P., and Knapp, L. A. (2013). Testing for post-copulatory selection for major histocompatibility complex genotype in a semi-free-ranging primate population. *Am. J. Primatol.* 75, 1021–1031.doi: 10.1002/ajp.22166

Setchell, J. M., Charpentier, M. J. E., Abbott, K. M., Wickings, E. J., and Knapp, L. A. (2009a). Opposites attract: MHC-associated mate choice in a polygynous primate. *J. Evol. Biol.* 23, 136–148. doi: 10.1111/j.1420-9101.2009.01880.x

Setchell, J. M., Charpentier, M. J. E., Abbott, K. M., Wickings, E. J., and Knapp, L. A. (2009b). Is brightest best? Testing the Hamilton-Zuk hypothesis in mandrills. *Int. J. Primatol.* 30, 825–844. doi: 10.1007/s10764-009-9371-0

Setchell, J. M., and Huchard, E. (2010). The hidden benefits of sex: evidence for MHC-associated mate choice in primate societies. *Bioessays* 32, 940–948.doi: 10.1002/bies.201000066

Setchell, J. M., Richards, S. A., Abbott, K. M., and Knappe, L. A. (2016). Mate-guarding by male mandrills (*Mandrillus sphinx*) is associated with female MHC genotype. *Behav. Ecol.* 27, 1756–1766. doi: 10.1093/beheco/arw106

Setchell, J. M., Vaglio, S., Abbott, K. M., Moggi-Cecchi, J., Boscaro, F., Pieraccini, G., et al. (2011). Odour signals major histocompatibility complex genotype in an Old World monkey. *Proc. R. Soc. B Biol. Sci.* 278, 274–280.doi: 10.1098/rspb.2010.0571

Sterck, E. H. M., Bontrop, R. E., de Groot, N., de Vos-Rouweler, A. J. M., and Doxiadis, G. G. M. (2017). No postcopulatory selection against MHC-homozygous offspring: evidence from a pedigreed captive rhesus macaque colony. *Mol. Ecol.* 26, 3785–3793.doi: 10.1111/mec.14153

Thornhill, R., Gangestad, S. W., Miller, R., Scheyd, G., McCollough, J. K., and Franklin, M. (2003). Major histocompatibility complex genes, symmetry, and body scent attractiveness in men and women. *Behav. Ecol.* 14, 668–678.doi: 10.1093/beheco/arg043

Tregenza, T., and Wedell, N. (2000). Genetic compatibility, mate choice and patterns of parentage: invited review. *Mol. Ecol.* 9, 1013–1027.doi: 10.1046/j.1365-294x.2000.00964.x

Trivers, R. (1972). "Parental investment and sexual selection," in *Sexual Selection and the Descent of Man*, ed. B. Campbell (Chicago, StateIL: Aldine), 1378.

Wagner, W. E. (1998). Measuring female mating preferences. *Anim. Behav.* 55, 1029–1042.doi: 10.1006/anbe.1997.0635

Wedekind, C., and Evanno, G. (2010). "Mate choice, the major histocompatibility complex, and offspring viability," in *Human Evolutionary Biology*, ed. M. P. Muehlenbein (Cambridge: Cambridge University Press), 309–321. doi: 10.1017/cbo9780511781193.023

Wegner, K. M., Kalbe, M., Kurtz, J., Reusch, T. B. H., and Milinski, M. (2003). Parasite selection for immunogenetic optimality. *Science* 301, 1343–1343.doi: 10.1126/science.1088293

Wetton, J. H., Carter, R. E., Parkin, D. T., and Walters, D. (1987). Demographic study of a wild house sparrow population by DNA fingerprinting. *Nature* 327, 147–149.doi: 10.1038/327147a0

Winternitz, J. C., and Abbate, J. L. (2015). Examining the evidence for major histocompatibility complex-dependent mate selection in humans and nonhuman primates. *Res. Rep. Biol.* 6, 73–88.doi: 10.2147/rrb.S58514

Woelfing, B., Traulsen, A., Milinski, M., and Boehm, T. (2009). Does intra-individual major histocompatibility complex diversity keep a golden mean? *Philos. Trans. R. Soc. B Biol. Sci.* 364, 117–128. doi: 10.1098/rstb.2008.0174

Yang, B., Ren, B., Xiang, Z., Yang, J., Yao, H., Garber, P. A., et al. (2014). Major histocompatibility complex and mate choice in the polygynous primate: the Sichuan snub-nosed monkey (*Rhinopithecus roxellana*). *Integr. Zool.* 9, 598–612.doi: 10.1111/1749-4877.12084

Zhang, P., Song, X., Dunn, D. W., Huang, K., Pan, R., Chen, D., et al. (2016). Diversity at two genetic loci associated with the major histocompatibility complex in the golden snub-nosed monkey (*Rhinopithecus roxellana*). *Biochem. Syst. Ecol.* 68, 243–249. doi: 10.1016/j.bse.2016.07.014

Zhang, P., Watanabe, K., Li, B., and Tan, C. L. (2006). Social organization of StateSichuan snub-nosed monkeys (*Rhinopithecus roxellana*) in the Qinling Mountains, Central China. *Primates* 47, 374–382. doi: 10.1007/s10329-006-0178-8

Zhao, D. P., Li, B. G., Ja, Y. H., and Wada, K. (2005). Extra-unit sexual behaviour among wild StateSichuan snub-nosed monkeys (*Rhinopithecus roxellana*) in the Qinling Mountains of China. *Folia Primatol.* 76, 172–176.doi: 10.1159/000084379

Zhu, Y., Wan, Q.-H., Zhang, H.-M., and Fang, S.-G. (2019). Reproductive strategy inferred from major histocompatibility complex-based inter-individual, sperm-egg, and mother-fetus recognitions in giant pandas (*Ailuropoda melanoleuca*). *Cells* 8:257. doi: 10.3390/cells8030257

Conflict of Interest: The authors declare that the research was conducted in the absence of any commercial or financial relationships that could be construed as a potential conflict of interest.

frontiers in Ecology and Evolution

ORIGINAL RESEARCH
published: 23 December 2020
doi: 10.3389/fevo.2020.615862

Convergent Evolution of Locomotory Modes in Euarchontoglires

Wei-hang Geng[1,2,3†], Xiao-ping Wang[1†], Li-feng Che[4,5†], Xin Wang[1], Rui Liu[1], Tong Zhou[1], Christian Roos[6], David M. Irwin[7] and Li Yu[1]*

[1] State Key Laboratory for Conservation and Utilization of Bio-Resources in Yunnan, School of Life Sciences, Yunnan University, Kunming, China, [2] Kunming Institute of Zoology, Chinese Academy of Sciences, Kunming, China, [3] Kunming College of Life Science, University of Chinese Academy of Sciences, Kunming, China, [4] Shanxi Institute of Zoology, Xi'an, China, [5] Shanxi Key Laboratory for Animal Conservation, Xi'an, China, [6] Gene Bank of Primates and Primate Genetics Laboratory, German Primate Center, Leibniz Institute for Primate Research, Göttingen, Germany, [7] Department of Laboratory Medicine and Pathobiology, University of Toronto, Toronto, ON, Canada

OPEN ACCESS

Edited by:
Deyan Ge,
Chinese Academy of Sciences (CAS), China

Reviewed by:
Anderson Feijo,
Chinese Academy of Sciences (CAS), China
Yong-Gang Yao,
Kunming Institute of Zoology, China
Jia-Tang Li,
Chinese Academy of Sciences, China

***Correspondence:**
Li Yu
yuli@ynu.edu.cn

[†] These authors have contributed equally to this work

Specialty section:
This article was submitted to Behavioral and Evolutionary Ecology, a section of the journal Frontiers in Ecology and Evolution

Received: 10 October 2020
Accepted: 02 December 2020
Published: 23 December 2020

Citation:
Geng W-h, Wang X-p, Che L-f, Wang X, Liu R, Zhou T, Roos C, Irwin DM and Yu L (2020) Convergent Evolution of Locomotory Modes in Euarchontoglires. Front. Ecol. Evol. 8:615862. doi: 10.3389/fevo.2020.615862

The research of phenotypic convergence is of increasing importance in adaptive evolution. Locomotory modes play important roles in the adaptive evolution of species in the Euarchontoglires, however, the investigation of convergent evolution of the locomotory modes across diverse Euarchontoglire orders is incomplete. We collected measurements of three phalangeal indices of manual digit III, including metacarpal of digit III (MC3), manus proximal phalanx of digit III (MPP3), and manus intermediate phalanx of digit III (MIP3), from 203 individuals of 122 Euarchontoglires species representing arboreal (orders Scandentia, Rodentia, and Primates), terrestrial (orders Scandentia and Rodentia), and gliding (orders Dermoptera and Rodentia) locomotory modes. This data can be separated into seven groups defined by order and locomotory mode. Based on combination of the three phalangeal indices, the Principle component analyses (PCA), phylomorphospace plot, and C-metrics analyses clustered the arboreal species of Scandentia, Rodentia, and Primates together and the terrestrial species of Scandentia and Rodentia together, showing the convergent signal in evolution of the arboreal (C1 = 0.424, $P < 0.05$) and terrestrial (C1 = 0.560, $P < 0.05$) locomotory modes in Euarchontoglires. Although the gliding species from Dermoptera and Rodentia did not cluster together, they also showed the convergent signal (C1 = 0.563, $P < 0.05$). Our work provides insight into the convergent evolution of locomotory modes in Euarchontoglires, and reveals that these three indices contribute valuable information to identify convergent evolution in Euarchontoglires.

Keywords: convergent evolution, Euarchontoglires, metacarpal, manus proximal phalanx, manus intermediate phalanx, locomotory modes

INTRODUCTION

The relationship between morphology, locomotory modes and habitat has been receiving greater attention in evolutionary studies of phenotypic variation (Losos and Sinervo, 1989; Losos, 1990; Bonine and Garland, 1999; Vanhooydonck and Van Damme, 1999; Thorington and Santana, 2007; Goodman et al., 2008; Irschick et al., 2008; Pfaff et al., 2015; Kawashima et al., 2018). It has

been observed that differences in habitat trigger divergence in the evolution of the morphology of locomotory systems across many different taxonomic taxa (Losos, 1990; Runestad and Ruff, 1995; Irschick et al., 2005; Calsbeek and Irschick, 2007; Sargis et al., 2007; Samuels and Van Valkenburgh, 2008; Schmidt, 2008), and that convergent evolution of locomotory modes for the same habitat niche adaptation in phylogenetically unrelated taxa can lead to similar morphological traits (Lemelin and Grafton, 1998; Kingsolver and Huey, 2003; Samuels and Van Valkenburgh, 2008; Gleiss et al., 2011; Losos, 2011; Edwards et al., 2012; Chen and Wilson, 2015; Morris et al., 2018; Grossnickle et al., 2019, 2020). The morphological convergence provides clues to better understanding functional adaptation and how distantly related species evolved in a similar way.

The mammalian superorder Euarchontoglires is comprised of five orders and includes Lagomorpha (rabbit, pika, and hare), Rodentia (mouse, rat, squirrel, and beaver), Dermoptera (flying lemur), Scandentia (tree shrew), and Primates (human, monkey, and ape) (Murphy et al., 2001; Kriegs et al., 2006; Vander Linden et al., 2019). A great diversity in locomotory modes is observed among and within the Euarchontoglire orders, including fossorial, ricochetal, arboreal, terrestrial, and gliding (Macphee, 1993). Interestingly, the same locomotory modes are found in different orders of Euarchontoglire, including the arboreal mode in Scandentia, Rodentia, and Primates, the terrestrial mode in Scandentia and Rodentia, and the gliding mode in Dermoptera and Rodentia (Kirk et al., 2008; Meng et al., 2017; Vander Linden et al., 2019; Grossnickle et al., 2020; **Figure 1**). The sharing of locomotory modes among orders makes Euarchontoglires an intriguing group for the investigation of morphological convergence with locomotory modes. Previous studies with Euarchontoglires have focused on the convergence of forelimb evolution with several locomotory modes, but these studies only examined species within Rodentia (Samuels and Van Valkenburgh, 2008) or on skeletal convergence with the gliding mode in Dermoptera and Rodentia (Grossnickle et al., 2020). Therefore, knowledge on the convergent evolution of locomotory modes across Euarchontoglire orders is very limited and it remains unclear whether the underlying skeletal morphology of terrestrial and arboreal species from the different Euarchontoglire orders have converged.

In the present study, we collected three phalangeal indices of manual digit III from 203 individuals of 122 Euarchontoglires species that represent the arboreal (orders Scandentia, Rodentia, and Primates), terrestrial (orders Scandentia and Rodentia), and gliding (orders Dermoptera and Rodentia) locomotory modes to investigate the convergent evolution of locomotory modes across these Euarchontoglire orders. The three phalangeal indices include metacarpal of digit III (MC3), manus proximal phalanx of digit III (MPP3), and manus intermediate phalanx of digit III (MIP3), which represent the inherent properties of the manus (Corruccini, 1995; Hamrick, 2001; Bloch et al., 2007; Kirk et al., 2008) and have been used to illustrate the locomotory modes of mammals (Lemelin, 1999; Hamrick, 2001; Meng et al., 2006, 2017; Bloch et al., 2007; Kirk et al., 2008; Samuels and Van Valkenburgh, 2008; Venkataraman et al., 2013; Zheng et al., 2013; Chen and Wilson, 2015; Grossnickle et al., 2020; Young and Chadwell, 2020). Our morphometric analyses based on quantitative methods provide insights into the convergent evolution of locomotory modes in Euarchontoglires, and moreover, evaluate the potential of these indices for studies on the convergent evolution of locomotory modes in Euarchontoglires.

MATERIALS AND METHODS

Data Collection

Publicly available data for the three phalangeal indices of manual digit III, including MC3, MPP3, and MIP3, from a total of 152 individuals from 122 Euarchontoglire species belonging to the orders Scandentia, Rodentia, Dermoptera, and Primates were collected from published sources (Kirk et al., 2008; Samuels and Van Valkenburgh, 2008; Chen and Wilson, 2015; Meng et al., 2017). These species represent arboreal (99 individuals from 83 species of Scandentia, Rodentia, and Primates), terrestrial (33 individuals from 28 species of Scandentia and Rodentia), and gliding (20 individuals from 11 species of Dermoptera and Rodentia) locomotory modes. In addition, three phalangeal indices of manual digit III were measured from 51 individuals of the gliding complex-toothed flying squirrel (Rodentia, *Trogopterus xanthipes*) that were bred in the Runxing Planting and Breeding Cooperative, Liquan County, Xi'an, Shaanxi Province in the present study and were added to the relatively limited data available to represent the gliding locomotory mode. The three phalangeal indices measured using the electronic digital indicator for *Trogopterus xanthipes* were shown in **Supplementary Figure S1**. Chordal nodes for each bone element were measured from the nearest to the farthest end, and from the parallel to the midline of the axis on the sagittal plane based on the methods of Kirk et al. (2008). In total, three phalangeal indices from 203 individuals of 122 species were collected for the present study (**Supplementary Table S1**). Individuals were divided into seven groups for analyses according to their taxonomic order and their locomotory mode. The groups are: Rodentia Gliding (RG; 64 individuals of 9 species), Dermoptera Gliding (DG; 7 individuals of 2 species), Scandentia Terrestrial (ST; 8 individuals of 3 species), Rodentia Terrestrial (RT; 25 individuals of 25 species), Scandentia Arboreal (SA; 6 individuals of 4 species), Rodentia Arboreal (RA; 34 individuals of 27 species), and Primate Arboreal (PA; 59 individuals of 52 species). For the present analysis, the MC3, MPP3, and MIP3 indices used were the percentage of the length of each indices of the total combined length for these three elements, i.e., MC3(p), MPP3(p), and MIP3(p), as previously used (Corruccini, 1995; Elissamburu and Vizcaino, 2004). Statistical differences within the 3 indices among the different groups were detected using the Wilcoxon test.

Morphometric Analyses

To avoid the possible bias of morphological variations resulted from the unbalanced individual numbers for each species, we calculated the average values per species to perform the morphometric analyses based on species level.

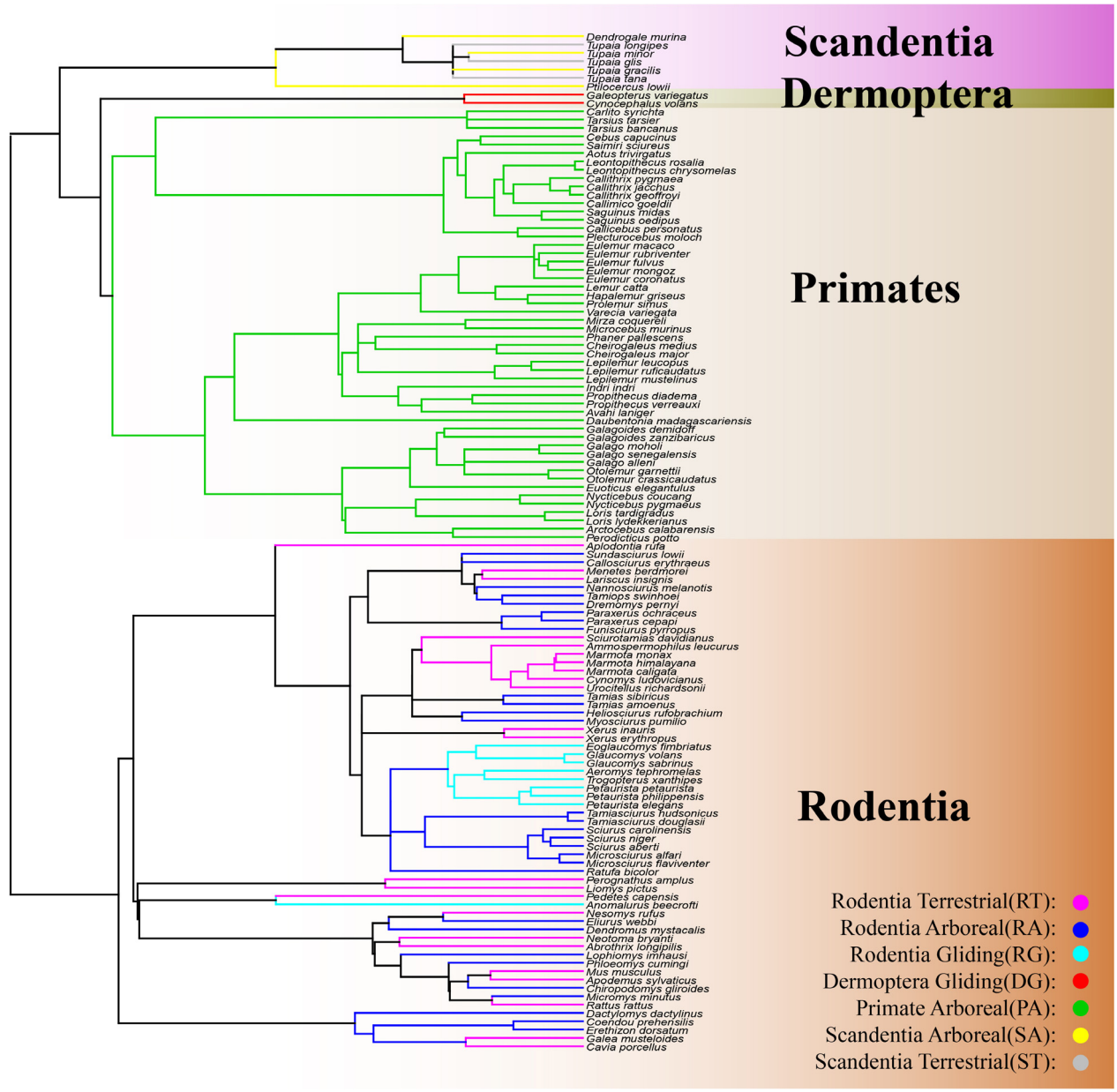

FIGURE 1 | Phylogeny of the 203 individuals from 122 Euarchontoglire species included in this study. Rectangle with a gradient of light brown color represents the order Rodentia; the rectangle with a gradient of green color represents the order Dermoptera; the rectangle with a gradient of light-yellow color represents the order Primate; the rectangle with a gradient of purple color represents the order Scandentia. The yellow lines represent the Scandentia Arboreal (SA) species; the gray lines represent the Scandentia Terrestrial (ST) species; the red lines represent the Dermoptera Gliding (DG) species; the green lines represent the Primate Arboreal (PA) species; the purple lines represent the Rodentia Terrestrial (RT) species; the blue lines represent the Rodentia Arboreal (RA) species; the indigo lines represent the Rodentia Gliding (RG) species.

First, a principle component analyses (PCA) was conducted using the *FactoMineR* and *factoextra* packages in R (Version 3.6.2) to visualize the overall distribution of the groups in the morphospace.

Then, taking into the phylogenetic effect, the principal components of the Procrustes coordinates were projected in the phylomorphospace plot by using the *phytools* package in R (Version 3.6.2). A well-accepted mammalian species tree of 122 species in our study from TimeTree database[1] was used as the input tree (**Figure 1**). This plot could detect the convergence based on the length and direction of branches in relation to their ancestral states (Feijó et al., 2020).

To statistically quantify the magnitude of convergence for the three locomotory modes from different orders, i.e., the gliding

[1]http://www.timetree.org/

(RG and DG), arboreal (RA, PA, and SA) and terrestrial (ST and RT) modes, the distance-based metric (C1–C4) were calculated (Stayton, 2015) by using the "convrat" function from *convevol* package in R (Version 3.6.2). C1 is the distance between the convergent tips of the taxa of interest (Dtip) divided by the maximum distance between any ancestral nodes (Dmax), which represents the proportion of the maximum distance between two lineages. This change of this value from 0 to 1 means the degree of convergence signal from non-convergence to convergence. C2 is obtained by Dtip minus Dmax and represent the magnitude of convergent change. C3 and C4 are the standardized value of C2 which were calculated by dividing C2 by the total morphological branch length of convergent taxa of interest (C3) and the total amount of branch length in the entire clade (C4) (Stayton, 2015), respectively. The significance of the metrics was assessed by the "convratsig" function of the same package with 1000 iterations.

RESULTS AND DISCUSSION

The three indices, i.e., MC3(p), MPP3(p), and MIP3(p), used for the seven groups, including Rodentia Gliding (RG), Dermoptera Gliding (DG), Scandentia Terrestrial (ST), Rodentia Terrestrial (RT), Scandentia Arboreal (SA), Rodentia Arboreal (RA), and Primate Arboreal (PA) are listed in **Supplementary Table S1**. Statistical tests for the three indices among the different groups revealed significant differences ($p < 0.05$) between most groups, with the exception of MIP3(p) for the same locomotory modes, including MIP3(p) between ST and RT ($p = 0.4774$), SA and RA ($p = 0.3449$), SA and PA ($p = 0.7868$), and RA and PA ($p = 0.089$), and MPP3(p) between RA and RG ($p = 0.5345$) (**Supplementary Table S2**).

A PCA of the three indices [MC3(p) + MPP3(p) + MIP3(p)] showed that PC1 explained 73.6% of variation and separated the terrestrial species of Scandentia and Rodentia (ST and RT groups) from the arboreal and gliding species (RA, PA, SA, RG, and DG groups) ($p < 0.05$). PC2 explained 26.4% of variation and separated the gliding species of Dermoptera (DG group) from the other species examined ($p < 0.05$) (**Figure 2**).

As seen from the phylomorphospace plot, the terrestrial species from Scandentia (ST group) and Rodentia (RT group) clustered together, suggesting that their similar phalangeal morphology may contribute to adapt to the same ground habitat. Likewise, the arboreal species from Scandentia (SA group), Rodentia (RA group), and Primate (PA group) clustered together, suggesting that their similar phalangeal morphology help them adapt to their grasping behavior. These results indicate the similarity of these morphological traits in the terrestrial and arboreal locomotory modes in Euarchontoglires. Interestingly, we found that the gliding species from Rodentia (RG group) were located between the arboreal species (RA, PA, and SA groups) and the gliding species from Dermoptera (DG group), consistent with the observation that the RG group species have evolved their morphological characteristics by not only adapting to tree-dwelling and branch-grasping life, but also to the gliding movement (Samuels and Van Valkenburgh, 2008; Grossnickle et al., 2020). The gliding species from Dermoptera are most distantly separated from the other species. Although the gliding species of Dermoptera (DG group) did not cluster with those from Rodentia (RG group) in the phylomorphospace plot (**Figure 2**), these two groups possess the same gliding locomotory mode and show a trend of closer proximity.

The C-metrics analyses of all three locomotory modes showed statistically significant convergence [gliding (DG and RG), C1 = 0.563, $P < 0.05$], arboreal (RA, PA, and SA), C1 = 0.424, $P < 0.05$) and terrestrial (ST and RT), C1 = 0.560, $P < 0.05$)], which indicate that evolution has reduced the distances in the gliding species and terrestrial species by showing more than 50% similarity than expected by chance, and in the arboreal species by more than 40% (**Table 1**). In addition, we also explore

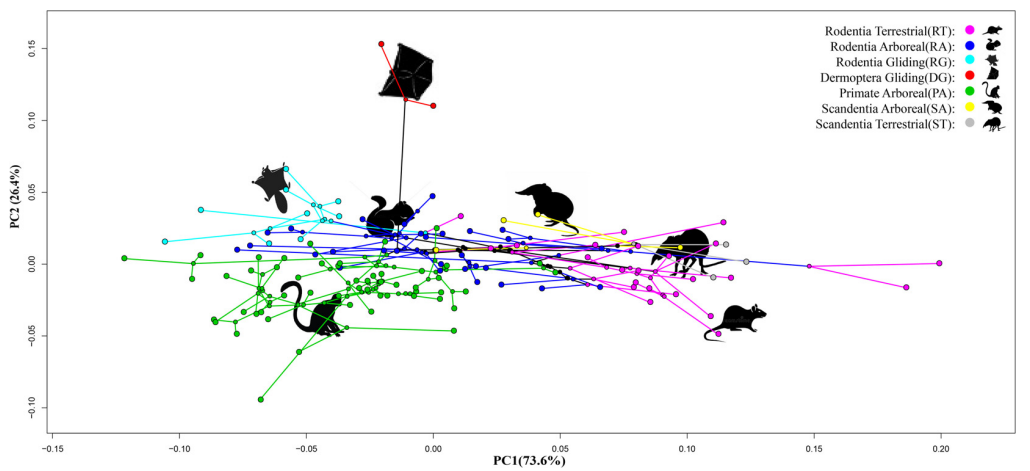

FIGURE 2 | Phylomorphospace plot of 122 Euarchontoglire species based on the scores of a principle component analysis (PCA) of three phalangeal indices of manual digit III. The yellow color represents the Scandentia Arboreal (SA) species; the gray color represents the Scandentia Terrestrial (ST) species; the red color represents the Dermoptera Gliding (DG) species; the green color represent the Primate Arboreal (PA) species; the purple color represents the Rodentia Arboreal (RT) species; the blue color represents the Rodentia Terrestrial (RT) species; the indigo color represents the Rodentia Gliding (RG) species.

TABLE 1 | The C-metrics analyses of three locomotory modes (C1–C4 metrics).

Locomotory modes	Groups	C1	C2	C3	C4
Gliding (11)	RG&DG	0.563*	0.082*	0.290*	0.008*
Terrestrial (28)	ST&RT	0.560*	0.083*	0.290*	0.009*
Arboreal (83)	SA&RA&PA	0.424*	0.054*	0.222*	0.006*

The numbers of species used in each locomotory modes were given in parentheses. The "" represents significant P-values among each locomotory modes with $P < 0.05$ generated from 1,000 simulations.*

the potential species that show more signals of convergence for the three locomotory modes, as used by the method of Stayton (2015). The phylomorphospace plot analyses and the C-metrics analyses identified and quantified at least 72 species in total showing more signals of convergence for the three locomotory modes, respectively (**Supplementary Table S3** and **Supplementary Figure S2**).

Therefore, our morphometric analyses based on quantitative methods provide insight into the convergent evolution of terrestrial, arboreal, and gliding locomotory modes in Euarchontoglires. In our analyses, the terrestrial species (ST and RT groups) demonstrate a relatively long metacarpal (MC3) and short phalange (MPP3 and MIP3) compared with the arboreal and gliding species ($P < 0.05$) (**Figure 3**), which would help increase their speed for hunting or feeding on the ground (Peng et al., 1991; Kirk et al., 2008; Samuels and Van Valkenburgh, 2008; Fuchs and Corbach-Söhle, 2010). In addition, previous studies have reported the possible genetic mechanisms at the gene level involving muscle contraction and skeletal morphogenesis for locomotory adaptation of terrestrial in Scandentia group (Fan et al., 2014). Our study not only confirmed the long metacarpal and short phalange in the terrestrial species of both Scandentia and Rodentia, but also demonstrated convergent evolution with the terrestrial locomotory mode in these two orders of Euarchontoglire.

In comparison, the arboreal species (RA, PA, and SA groups) show an elongated phalange MPP3 and MIP3 compared with terrestrial species ($P < 0.05$) (**Figure 3**), which would help them grasp branches while they are moving. This phenomenon has been demonstrated in arboreal Primates (Lemelin, 1999; Hamrick, 2001; Bloch et al., 2007; Kirk et al., 2008; Young and Chadwell, 2020) and Rodentia (Kirk et al., 2008; Samuels and Van Valkenburgh, 2008). Our study not only observed this in the arboreal species of Scandentia, Rodentia, and Primates, but also demonstrated convergent evolution with the arboreal locomotory mode in these three orders of Euarchontoglire.

The gliding species (DG and RG groups) demonstrated an elongation of the phalangeal MIP3 compared with arboreal and terrestrial species (**Figure 3**), which is likely associated with their unique attachment of the patagia to adapt the gliding locomotory habitat (Macphee, 1993) or to their roosting behavior (Grossnickle et al., 2020). Although they both possessed patagium, but they are different in that the former shows the patagium attachment by the styliform cartilages from the wrist or elbow while the latter's patagium are attached to the digits (Jackson, 2012). Further examination of the gliding species from these two orders showed that the gliding species from Rodentia have MPP3 lengths similar to those of arboreal species and have elongated MIP3, while the gliding species from Dermoptera have the shortest MPP3 and the most elongated MIP3 compared with species of the other two locomotory modes and the gliding species from Rodentia (**Supplementary Table S1**). According to these above observations, we speculate that the similarities and differences between these two orders make them both distant from the other locomotory modes, but prevent their clustering like that seen for the other two locomotory modes, although they do show a trend of having closer proximity in the phylomorphospace plot and do show the significant convergence signal in C-metrics analyses. Besides the phalangeal indices of manual digit III examined here, the gliding mammals also developed other morphological modifications for gliding adaptation, including the relatively elongated neck, longer forearms, lumbar, and shorter thoracic vertebrae, hands, feet bony as well as the more sensitivity of bony labyrinth morphometry in the inner ear (Thorington and Santana, 2007; Pfaff et al., 2015; Kawashima et al., 2018). So we hypothesized that additional morphological traits, in addition to the three indices used in the present study, are also necessary to address the convergence in the gliding locomotory mode. Indeed, a recent phylogenetic comparative analysis of 31 skeletal traits from

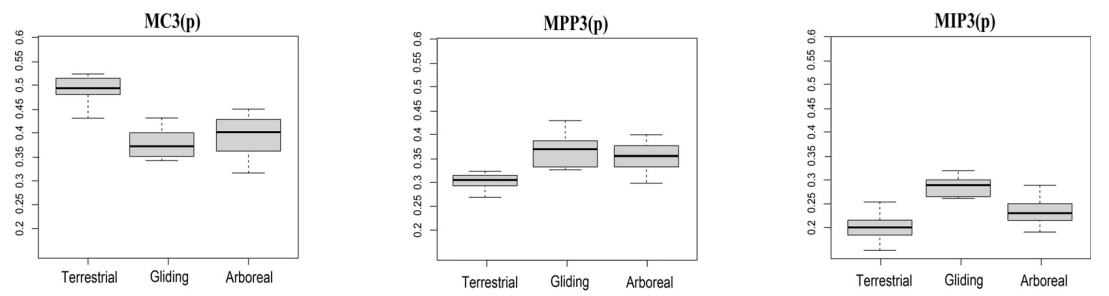

FIGURE 3 | The distribution of the three indices among each locomotory mode. The abscissa represents the locomotory modes and the ordinate represents the ratios of the indices. MC3(p): The proportion of MC3 in the total combined length of the three elements; MPP3(p): The proportion of MPP3 in the total combined length of the three elements; MIP3(p): The proportion of MIP3 in the total combined length of the three elements. Terrestrial mode includes ST and RT groups; Arboreal mode includes SA, RA, and PA groups; Gliding mode includes DG and RG groups. Wilcoxon tests of the three indices among each locomotry mode all show significant *P*-values ($P < 0.05$).

the gliding mammals has observed convergence, including the gliding Dermoptera and Rodentia (Grossnickle et al., 2020).

CONCLUSION

In the present study, we used morphometric analyses based on quantitative methods to explore the convergence of locomotory modes across diverse Euarchontoglires orders. Our results showed that the phalangeal morphology of species with terrestrial, arboreal, and gliding locomotory modes from multiple Euarchontoglire orders are convergent, supporting the convergent evolution of these three locomotory modes. This study adds evidence of phenotypic convergent evolution of the locomotory modes in Euarchontoglires by extending the investigation into the terrestrial, arboreal, and gliding locomotory modes across four Euarchontoglires orders, which had previously only been studied for the gliding mode of Euarchontoglires or for the other modes only within Primates and Rodentia. With these findings we provide a framework for future work on convergence in mammals, and the application of the phalangeal indices used here to allow the inference and interpretation of locomotory modes of unknown or fossil species.

DATA AVAILABILITY STATEMENT

The original contributions presented in the study are included in the article/**Supplementary Material**, further inquiries can be directed to the corresponding author/s.

ETHICS STATEMENT

The animal study was reviewed and approved by the Committee on Animal Research and Ethics of Yunnan University.

AUTHOR CONTRIBUTIONS

LY designed the study. W-HG, L-FC, TZ, XW, and RL measured and collected the data. X-PW and W-HG performed the data analyses. LY, X-PW, and W-HG wrote the manuscript. CR and DI revised the manuscript. All authors read and approved the final manuscript.

FUNDING

This work was supported by a grant from the National Natural Science Foundation of China (31760619) to XW, an Applied Basic Research General Project of Yunnan Science and Technology Department (202001BB050058) to XW and "One Institute One Product" Special Project of Shaanxi Academy of Sciences (2020K-02) to L-FC.

SUPPLEMENTARY MATERIAL

The Supplementary Material for this article can be found online at: https://www.frontiersin.org/articles/10.3389/fevo.2020.615862/full#supplementary-material

REFERENCES

Bloch, J. I., Silcox, M. T., Boyer, D. M., and Sargis, E. J. (2007). New Paleocene skeletons and the relationship of plesiadapiforms to crown-clade primates.*Proc. Natl. Acad. Sci. U.S.A.* 104, 1159–1164. doi: 10.1073/pnas.0610579104

Bonine, K. E., and Garland, T. (1999). Sprint performance of phrynosomatid lizards, measured on a high-speed treadmill, correlates with hindlimb length. *J. Zool.* 248, 255–265. doi: 10.1111/j.1469-7998.1999.tb01201.x

Calsbeek, R., and Irschick, D. J. (2007). The quick and the dead: correlational selection on morphology, performance, and habitat use in island lizards. *Evolution* 61, 2493–2503. doi: 10.1111/j.1558-5646.2007.00206.x

Chen, M., and Wilson, G. P. (2015). A multivariate approach to infer locomotor modes in Mesozoic mammals. *Paleobiology* 41, 280–312. doi: 10.1017/pab.2014.14

Corruccini, R. S. (1995). Of ratios and rationality. *Am. J. Phys. Anthropol.* 96, 189–191. doi: 10.1002/ajpa.1330960209

Edwards, S., Vanhooydonck, B., Herrel, A., Measey, G. J., and Tolley, K. A. (2012). Convergent evolution associated with habitat decouples phenotype from phylogeny in a clade of lizards. *PLoS One* 7:e51636. doi: 10.1371/journal.pone.0051636

Elissamburu, A., and Vizcaino, S. F. (2004). Limb proportions and adaptations in caviomorph rodents (Rodentia : Caviomorpha). *J. Zool.* 262, 145–159. doi: 10.1017/S0952836903004485

Fan, Y., Yu, D. D., and Yao, Y. G. (2014). Positively selected genes of the Chinese tree shrew (*Tupaia belangeri chinensis*) locomotion system. *Zool. Res.* 35, 240–248. doi: 10.11813/j.issn.0254-5853.2014.3.240

Feijó, A., Ge, D. Y., Wen, Z. X., Xia, L., and Yang, Q. S. (2020). Divergent adaptations in resource-use traits explain how *pikas* thrive on the roof of the world. *Funct. Ecol.* 34, 1826–1838. doi: 10.1111/1365-2435.13609

Fuchs, E., and Corbach-Söhle, S. (2010). "Tree shrews," in *The UFAW Handbook on the Care and Management of Laboratory and Other Research Animals*, eds R. Hubrecht and J. Kirkwood (Oxford: Wiley-Blackwell), 262–275. doi: 10.1002/9781444318777.ch20

Gleiss, A. C., Jorgensen, S. J., Liebsch, N., Sala, J. E., Norman, B., Hays, G. C., et al. (2011). Convergent evolution in locomotory patterns of flying and swimming animals. *Nat. Commun.* 2:352. doi: 10.1038/ncomms1350

Goodman, B. A., Miles, D. B., and Schwarzkopf, L. (2008). Life on the rocks: habitat use drives morphological and performance evolution in lizards. *Ecology* 89, 3462–3471. doi: 10.1890/07-2093.1

Grossnickle, D. M., Chen, M., Wauer, J. G. A., Pevsner, S. K., Weaver, L. N., Meng, Q. J., et al. (2020). Incomplete convergence of gliding-mammal skeletons. *Evolution* doi: 10.1111/evo.14094 [Online ahead of print].

Grossnickle, D. M., Smith, S. M., and Wilson, G. P. (2019). Untangling the multiple ecological radiations of early mammals. *Trends Ecol. Evol.* 34, 936–949. doi: 10.1016/j.tree.2019.05.008

Hamrick, M. W. (2001). Primate origins: evolutionary change in digital ray patterning and segmentation. *J. Hum. Evol.* 40, 339–351. doi: 10.1006/jhev.2001.0467

Irschick, D. J., Herrel, A. V., Vanhooydonck, B., Huyghe, K., and Van Damme, R. (2005). Locomotor compensation creates a mismatch between laboratory and field estimates of escape speed in lizards: a cautionary tale for performance-to-fitness studies. *Evolution* 59, 1579–1587. doi: 10.1111/j.0014-3820.2005.tb01807.x

Irschick, D. J., Meyers, J. J., Husak, J. F., and Le Galliard, J. F. (2008). How does selection operate on whole-organism functional performance capacities? A review and synthesis. *Evol. Ecol. Res.* 10, 177–196. doi: 10.1111/j.1558-5646.2007.00298.x

Jackson, S. M. (2012). *Gliding Mammals of the World*. Collingwood, VIC: Csiro Publishing.

Kawashima, T., Thorington, R. W. Jr., Bohaska, P. W., and Sato, F. (2018). Variability and constraint of vertebral formulae and proportions in colugos, tree shrews, and rodents, with special reference to vertebral modification by aerodynamic adaptation. *Folia Morphol.* 77, 44–56. doi: 10.5603/FM.a2017.0064

Kingsolver, J. G., and Huey, R. B. (2003). Introduction: the evolution of morphology, performance, and fitness. *Integr. Comp. Biol.* 43, 361–366. doi: 10.1093/icb/43.3.361

Kirk, E. C., Lemelin, P., Hamrick, M. W., Boyer, D. M., and Bloch, J. I. (2008). Intrinsic hand proportions of euarchontans and other mammals: implications for the locomotor behavior of plesiadapiforms. *J. Hum. Evol.* 55, 278–299. doi: 10.1016/j.jhevol.2008.02.008

Kriegs, J. O., Churakov, G., Kiefmann, M., Jordan, U., Brosius, J., and Schmitz, J. (2006). Retroposed elements as archives for the evolutionary history of placental mammals. *PloS. Biol.* 4:e91. doi: 10.1371/journal.pbio.0040091

Lemelin, P. (1999). Morphological correlates of substrate use in *Didelphid marsupials*: implications for primate origins. *J. Zool.* 247, 165–175. doi: 10.1017/S0952836999002046

Lemelin, P., and Grafton, B. W. (1998). "Grasping performance in *Saguinus midas* and the evolution of hand prehensility in primates," in *Primate Locomotion:Recent Advances*, eds E. Strasser, J. Fleagle, A. Rosenberger, and H. McHenry (New York, NY: Plenum Press), 131–144. doi: 10.1007/978-1-4899-0092-0_8

Losos, J. B. (1990). Concordant evolution of locomotor behavior, display rate and morphology in *Anolis* lizards. *Anim. Behav.* 39, 879–890. doi: 10.1016/S0003-3472(05)80952-2

Losos, J. B. (2011). Convergence, adaptation, and constraint. *Evolution* 65, 1827–1840. doi: 10.1111/j.1558-5646.2011.01289.x

Losos, J. B., and Sinervo, B. (1989). The effects of morphology and perch diameter on sprint performance of *Anolis* lizards. *J. Exp. Biol.* 145, 23–30.

Macphee, R. D. E. (1993). *Primates and Their Relatives in Phylogenetic Perspective*. New York, NY: Plenum Press, 63–90.

Meng, J., Hu, Y., Wang, Y., Wang, X., and Li, C. (2006). A Mesozoic gliding mammal from northeastern China. *Nature* 444, 889–893. doi: 10.1038/nature05234

Meng, Q. J., Grossnickle, D. M., Liu, D., Zhang, Y. G., Neander, A. I., Ji, Q., et al. (2017). New gliding mammaliaforms from the Jurassic. *Nature* 548, 291–296. doi: 10.1038/nature23476

Morris, P. J. R., Cobb, S. N. F., and Cox, P. G. (2018). Convergent evolution in the Euarchontoglires. *Biol. Lett.* 14:20180366. doi: 10.1098/rsbl.2018.0366

Murphy, W. J., Eizirik, E., O'brien, S. J., Madsen, O., Scally, M., Douady, C. J., et al. (2001). Resolution of the early placental mammal radiation using Bayesian phylogenetics. *Science* 294, 2348–2351. doi:10.1126/science.1067179

Peng, Y. Z., Ye, Z. Z., Zou, R. J., Wang, Y. X., Tian, B. P., Ma, Y. Y., et al. (1991). *Biology of Chinese Tree Shrews (Tupaia belangeri chinensis)*. Kunming: Yunnan Science and Technology Press.

Pfaff, C., Martin, T., and Ruf, I. (2015). Bony labyrinth morphometry indicates locomotor adaptations in the squirrel-related clade (Rodentia, Mammalia). *Proc. R. Soc. B Biol. Sci.* 282:20150744. doi:10.1098/rspb.2015.0744

Runestad, J. A., and Ruff, C. B. (1995). Structural adaptations for gliding in mammals with implications for locomotor behavior in Paromomyids. *Am. J. Phys. Anthropol.* 98, 101–119. doi: 10.1002/ajpa.1330980202

Samuels, J. X., and Van Valkenburgh, B. (2008). Skeletal indicators of locomotor adaptations in living and extinct rodents. *J. Morphol.* 269, 1387–1411. doi: 10.1002/jmor.10662

Sargis, E. J., Boyer, D. M., Bloch, J. I., and Silcox, M. T. (2007). Evolution of pedal grasping in Primates. *J. Hum. Evol.* 53, 103–107. doi: 10.1016/j.jhevol.2007.01.008

Schmidt, M. (2008). Forelimb proportions and kinematics: how are small primates different from other small mammals? *J. Exp. Biol.* 211, 3775–3789. doi: 10.1242/jeb.019802

Stayton, C. T. (2015). The definition, recognition, and interpretation of convergent evolution, and two new measures for quantifying and assessing the significance of convergence. *Evolution* 69, 2140–2153. doi: 10.1111/evo.12729

Thorington, R., and Santana, E. (2007). How to make a flying squirrel: *Glaucomys* anatomy in phylogenetic perspective. *J. Mammal.* 88, 882–896. doi: 10.1644/06-Mamm-S-325r2.1

Vander Linden, A., Hedrick, B. P., Kamilar, J. M., and Dumont, E. R. (2019). Atlas morphology, scaling and locomotor behaviour in primates, rodents and relatives (Mammalia: Euarchontoglires). *Zool. J. Linn. Soc.* 185, 283–299. doi: 10.1093/zoolinnean/zly042

Vanhooydonck, B., and Van Damme, R. (1999). Evolutionary relationships between body shape and habitat use in lacertid lizards. *Evol. Ecol. Res.* 1, 785–805.

Venkataraman, V. V., Rolian, C., Gordon, A. D., and Patel, B. A. (2013). A resampling approach and implications for estimating the phalangeal index from unassociated hand bones in fossil primates. *Am. J. Phys. Anthropol.* 151, 280–289. doi: 10.1002/ajpa.22278

Young, J. W., and Chadwell, B. A. (2020). Not all fine-branch locomotion is equal: grasping morphology determines locomotor performance on narrow supports. *J. Hum. Evol.* 142:102767. doi: 10.1016/j.jhevol.2020.102767

Zheng, X., Bi, S., Wang, X., and Meng, J. (2013). A new arboreal haramiyid shows the diversity of crown mammals in the Jurassic period. *Nature* 500, 199–202. doi: 10.1038/nature12353

Conflict of Interest: The authors declare that the research was conducted in the absence of any commercial or financial relationships that could be construed as a potential conflict of interest.

The reviewer, Y-GY, declared a shared affiliation with one of the authors, W-HG, to the handling editor at the time of review.

frontiers in Genetics

ORIGINAL RESEARCH
published: 20 January 2021
doi: 10.3389/fgene.2020.611914

Genetic Structure and Evolutionary History of *Rhinopithecus roxellana* in Qinling Mountains, Central China

Yuli Li[1†], *Kang Huang*[1†], *Shiyi Tang*[1], *Li Feng*[2], *Jia Yang*[3], *Zhonghu Li*[3] *and Baoguo Li*[1,4*]

[1] Shaanxi Key Laboratory for Animal Conservation, College of Life Sciences, Northwest University, Xi'an, China, [2] School of Pharmacy, Xi'an Jiaotong University, Xi'an, China, [3] Key Laboratory of Resource Biology and Biotechnology in Western China, Ministry of Education, College of Life Sciences, Northwest University, Xi'an, China, [4] Center for Excellence in Animal Evolution and Genetics, Chinese Academy of Sciences, Kunming, China

The Qinling mountainous region is one of the world's biodiversity hotspots and provides refuges for many endangered endemic animals. The golden snub-nosed monkeys (*Rhinopithecus roxellana*) are considered as a flagship species in this area. Here, we depicted the genetic structure and evolutionary history via microsatellite markers and combination with the ecological niche models (ENMs) to elucidate the intraspecific divergent and the impacts of the population demography on our focal species. Our results revealed three distinct subpopulations of *R. roxellana* and also uncovered asymmetric historical and symmetric contemporary gene flow that existed. Our evolutionary dynamics analyses based on diyabc suggested that the intraspecific divergence accompanied with effective population sizes changes. The ENM result implied that the distribution range of this species experienced expansion during the last glacial maximum (LGM). Our results highlighted that geological factors could contribute to the high genetic differentiation within the *R. roxellana* in the Qinling Mountains. We also provided a new insight into conservation management plans with endangered species in this region.

Keywords: ***Rhinopithecus roxellana*, population structure, gene flow, ecological niche models, evolutionary history**

OPEN ACCESS

Edited by:
Deyan Ge,
Chinese Academy of Sciences (CAS), China

Reviewed by:
Li Yu,
Yunnan University, China
Wei Wang,
Chinese Research Academy of Environmental Sciences, China

***Correspondence:**
Baoguo Li
baoguoli@nwu.edu.cn

[†]*These authors have contributed equally to this work*

Specialty section:
This article was submitted to Evolutionary and Population Genetics, a section of the journal Frontiers in Genetics

Received: *29 September 2020*
Accepted: *30 November 2020*
Published: *20 January 2021*

Citation:
Li Y, Huang K, Tang S, Feng L, Yang J, Li Z and Li B (2021) Genetic Structure and Evolutionary History of Rhinopithecus roxellana in Qinling Mountains, Central China. Front. Genet. 11:611914. doi: 10.3389/fgene.2020.611914

BACKGROUND

Historical processes such as geographic changes and human activities have greatly affected patterns of dispersal and genetic migration among populations; these processes could restrict gene flow and accelerate genetic differentiation through inbreeding and genetic drift (Waage and Greathead, 1988; Frankham, 2005) and consequently shape population structure and evolutionary history (Balkenhol et al., 2009). In many species, empirical studies have indicated that mountains (Lait and Burg, 2013), rivers (Chambers and Garant, 2010), and deserts (Astrid et al., 2012) could act as physical or ecological obstacles to prevent animal dispersal to mitigate gene flow. In addition, as humans continue to expand across the world, many once-continuous landscapes become divided into separate fragmented patches (Hanski, 1994; Newbold et al., 2015). Low genetic variations will decrease the adaptive abilities of species to circumstances, and then this species become more vulnerable when environmental conditions changes, which will finally lead to their extinction (Frankham, 2005; Willi et al., 2006; Burkey, 2010).

The golden snub-nosed monkey, *Rhinopithecus roxellana*, is an Asian colobine endemic to the temperate forests of the mountainous regions in central China (Li et al., 2002; Kirkpatrick and Grueter, 2010), which has a typical multi-level social structure discovered in primate (Kirkpatrick and Grueter, 2010). The society of this monkey consists of four levels: unit, band, herd, and troop

(Grueter et al., 2012). Furthermore, the bands can be classified into the breeding band (BB) and the all-male band (AMB) (Kirkpatrick and Grueter, 2010; Grueter et al., 2012). This primate once ranged widely across southern, southwestern, and central China (Li et al., 2003). However, due to the historical changes and continuous expansion of human populations and their corresponding activities, numbers and ranges of *R. roxellana* have been significantly reduced. In consequence, this primate today only distribute within the three isolated areas among four provinces (Shaanxi, Sichuan, Gansu, and Hubei), and its current estimated population size is no more than 20,000 individuals (Ren et al., 1998; Li et al., 2002, 2007).

In Shaanxi, *R. roxellana* occurs only in the Qinling Mountains (Li et al., 2000; Wang et al., 2014). This area is a major biodiversity hotspot of China with many unique and rare plant and/or animal species (Norton et al., 2011; Zhang et al., 2016). Within the mountains, 39 *R. roxellana* troops comprising a total of 4,000 individuals are distributed across the counties of Zhouzhi, Ningshan, Yangxian, Taibai, and Foping (**Figure 1**; Li et al., 2000). However, during the past few years, land reclamation, tree-felling, illegal hunting, and infrastructural development have all posed critical threats to the habitats of golden snub-nosed monkeys in these regions (Feng et al., 2009; Zhang et al., 2016). Previous research has shown that expanding human impact in nearby the Qinling Mountains has resulted in local extinction and population decline of *R. roxellana* (Li et al., 2002; Wang et al., 2014).

Based on the microsatellite data, Pan et al. (2005) showed the *R. roxellana* had relatively high intraspecific genetic diversity and formed different genetic structures at fine scale in China, e.g., the Minshan Mountains, the Shennongjia Mountains, and the Qinling Mountains. Also, Huang et al. (2016a) had detected that the genetic diversity and effective population size of *R. roxellana* in Qinling Mountains were not significantly decreased, which is in conflict with their expectations. In addition, a recent study has that, even under threat of habitat fragmentation, internal adjustment mechanisms in multilevel social systems can effectively avoid inbreeding due to the bridging role of certain social units (non-breeding groups: AMB) at a small scale within the Qinling Mountains (Li et al., 2020). However, the evolutionary history and demography of the *R. roxellana* inhabiting the Qinling Mountains remain poorly understood (Pan et al., 2005).

In this study, using microsatellite data, we evaluate the genetic diversity and gene flow within the Qinling populations and also investigated its complicated evolutionary history. We attempt to figure out the following: (i) whether the golden snub-nosed monkey was threatened by genetic homogeneity in fragmented habitat and, if so, (ii) whether the historical shifts facilitated the current genetic differentiation within *R. roxellana*, and (iii) whether and how the gene flow impacted its genetic structure.

METHODS

Genetic Sampling

We collected a total of 344 fecal and hair samples of five representative populations scattered among five counties (Zhouzhi, Foping, Taibai, Yangxian, and Ningshan), which spread over five National Nature Reserve [the Zhouzhi National Nature Reserve (ZNNR), the Foping National Nature Reserve (FNNR), the Taibaishan National Nature Reserve (TNNR), the Changqing Natioanl Nature Reserve (CNNR), and

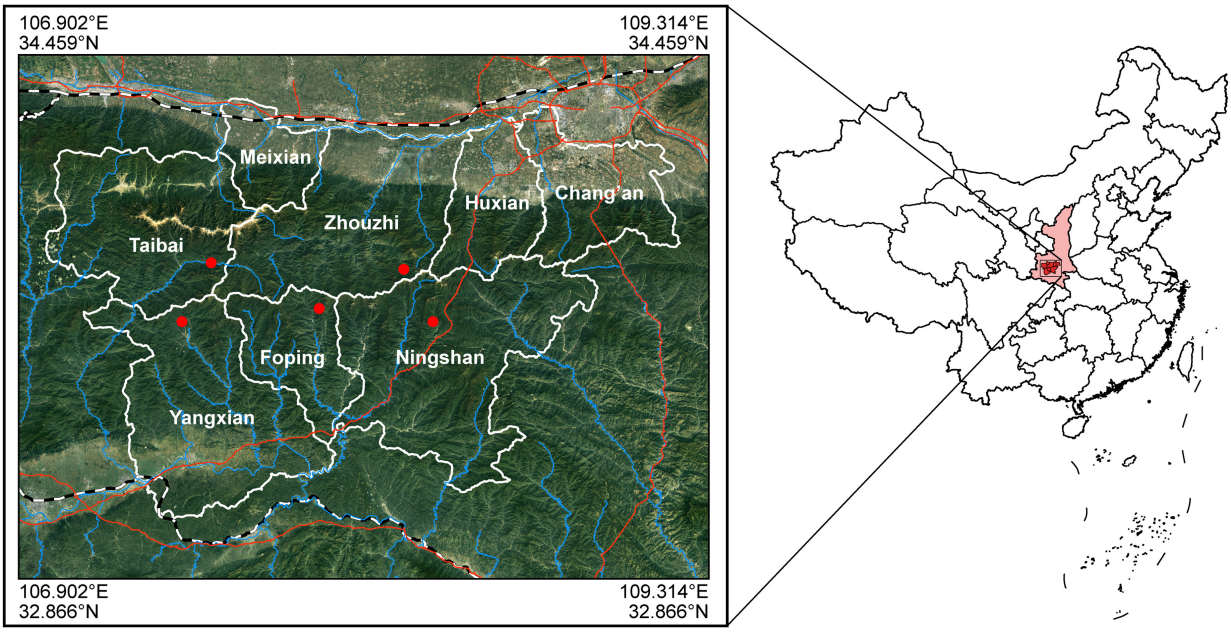

FIGURE 1 | Sampling sites: the range of coordinates were 107.52-108.38°E, 33.64-33.82°N.

TABLE 1 | Genetic diversities of five populations.

Band	Reserve	County	Longitude (°E)	Latitude (°N)	Population size	Sample size	F_{IS}	Genetic diversity				
								A_O	H_O	H_E	PIC	A_R
GNG	ZNNR	Zhouzhi	108.28	33.8	173	84	0.009	4.059	0.563	0.558	0.508	2.497
DPY	FNNR	Foping	107.99	33.68	133	71	0.081	5.353	0.566	0.629	0.473	2.342
SZZ	CNNR	Yangxian	107.52	33.64	142	67	0.065	5.765	0.607	0.650	0.538	2.642
HTP	TNNR	Tabai	107.62	33.82	118	62	0.095	5.176	0.614	0.672	0.527	2.539
CYG	NNR	Ningshan	108.38	33.64	72	33	0.031	4.882	0.624	0.605	0.510	2.532

F_{IS} denotes the Wright's inbreeding coefficient.
Six genetic diversity indices were presented, i.e., number of alleles (A_O), observed and expected heterozygosity (H_O and H_E, respectively), polymorphism information content (PIC)*, and allelic richness (A_R).*

Ningshan Nature Reserve (NNR); **Figure 1**: 107.52-108.38°E, 33.64-33.82°N]. These regions have semi-humid montane climate, and their elevations range from 1,100 to 2,930 m above sea level (Li et al., 2000, 2003). The average annual temperature of these areas is 8.59°C, with a minimum temperature in January (−17.7°C) and a maximum temperature in August (34.6°C). The average rainfall per annum is 577.64 mm. Details of the sample information are presented in **Table 1**; sampling locations are shown in **Figure 1**.

Because our focal species inhabit mountainous highlands and shy away from humans, it is quite hard to follow them across steep cliffs and precipitous valleys; it took us more than 1 year to collect the samples from March 2016 to April 2017. The percentage of fecal samples was 90 in our all samples, and they were stored in DETs [20% dimethyl sulfoxide (DMSO), 0.25 M of sodium-EDTA, 100 mM of Tris·HCl, pH 7.5, and NaCl to saturation] solution at −20°C (Allen et al., 1998). The hair samples, collected with a stick with adhesive tape by glue and fruit bait on an 80 × 6 cm wooden board, were mainly obtained from the Zhouzhi BB (because this band was half-habituated for 20 years on field observation) and then stored in silica gel for drying at room temperature.

Molecular Methods

Follicle DNA was extracted with proteinase *K* digestion in a PCR-compatible buffer, while fecal DNA was extracted using QIAamp DNA Stool Mini Kits (Qiagen, German). All samples were amplified based on the primers of 19 tetra-nucleotide microsatellite loci (see **Supplementary Table 1** for locus profile) in an ABI Veriti Thermal Cycler with the following protocol: 95°C for 5 min, followed by 30 cycles (94°C for 30 s, 55–60°C for 45 s, 72°C for 45 s), and 72°C for 10 min. PCR products were segregated with an ABI PRISM 3100 Genetic Analyser, and their sizes relative to the internal size standard (ROX-labeled HD400) were determined using GENEMAPPER V3.7 (Applied Biosystems). To prevent genotyping errors such as false allele and allelic dropout, homozygote genotypes were confirmed by five independent replicates, with all heterozygotes observed and confirmed by at least three separate reactions (Taberlet et al., 1996). Replicates were detected by POLYRELATEDNESS V1.6 (Huang et al., 2016b) and excluded from before subsequent analyses.

Genetic Diversity

We used MICROCHECKER v2.2.3 to test the presence of null alleles for all loci (van Oosterhout et al., 2010). For each population, we calculated the genetic diversity indices that included number of alleles (A_O), observed heterozygosity (H_O), expected heterozygosity (H_E), polymorphic information content (PIC), allelic richness (A_R), and Wright's inbreeding coefficient at each locus utilizing GENAIEX V6.5 (Peakall and Smouse, 2012). We performed a Hardy–Weinberg equilibrium (HWE) test for each band at each locus using Fisher's exact tests in GENEPOP V4.3 (Rousset, 2008). Significance thresholds were adjusted for multiple tests by the sequential Bonferroni procedure (Rice, 1989).

We employed two methods to test the presence of bottleneck effects within different populations. The first method was based on deviations of allele frequencies in calculations of heterozygosity, where we used the signed test and two-tailed Wilcoxon test in BOTTLENECK V1.2.02 (Piry et al., 1999). We considered two types of mutation models: (i) a two-phase model (*TPM*) with 95% stepwise mutations and a variance of 12 and (ii) a stepwise mutation model (*SMM*) with iteration number set to 1,000. The second method involved calculation of the *GW* coefficient in ARLEQUIN V3.6 (Excoffier and Lischer, 2010).

Population Differentiation and Structure

Genetic differentiation among populations was evaluated using θ (F_{ST}) across loci with the 100,000 permutations with ARLEQUIN V3.6 (Excoffier and Lischer, 2010). The number of steps in the Markov chain was set 100,000, and that of burn-in steps was 10,000. Moreover, we performed AMOVA analysis in ARLEQUIN V3.6 (Excoffier and Lischer, 2010) to estimate genetic variations among the populations. The significance of fixation indices was tested using 10,000 permutations.

Bayesian clustering was performed using STRUCTURE V2.3.4 (Pritchard et al., 2000) to examine the population genetic structure. We first assessed the occurrence of population subdivision under an admixture model and with allele frequencies correlated. The program was run for *K* from 1 to 10. For each run, we used 1,000,000 *MCMC* cycles following 500,000 burn-in cycles. Two alternative methods were utilized to estimate the most likely number (*K*) of genetic clusters with the program STRUCTURE HARVSTER (Earl and Vonholdt, 2012,

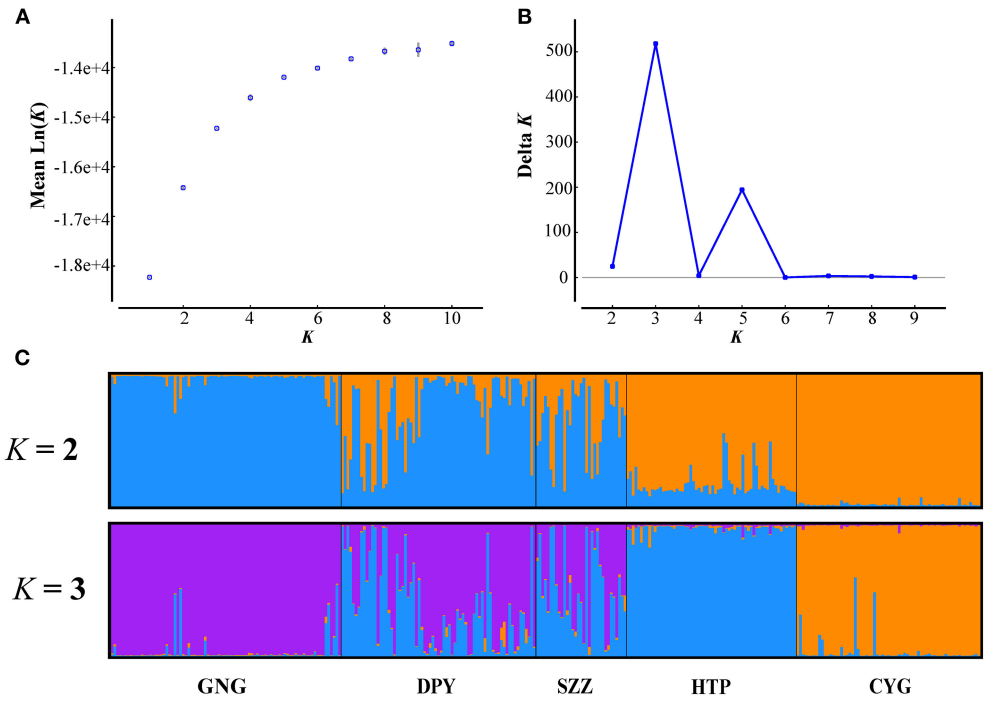

FIGURE 2 | Structure analyses using the LOCPRIOR model. **(A,B)** The mean estimated $L(K)$ and ΔK as a function of number of clusters (K). **(C)** The bar plots for $K = 2$ and 3.

i.e., by tracing the change in the average of log-likelihood $L(K)$ (Pritchard et al., 2000) and by calculating ΔK (Evanno et al., 2005).

Genetic Migration Analyses

To explore the historical genetic gene flow of *Rhinopithecus roxellana* in the Qinling Mountains, we used the program MIGRATE-N v3.6 (Beerli, 2006) to assess pairwise estimates of migration rates (Nm) among the five populations based on the microsatellite datasets. We performed maximum-likelihood analyses in MIGRATE-N v 3.6 using three long chains (100,000 runs) and 10 short chains (10,000 runs), and the burn-in was set as 10,000. We repeated this procedure five times to obtain the average maximum-likelihood estimates with 95% confidence intervals (CIs).

Moreover, in order to obtain the contemporary genetic migration among intraspecific lineages, we employed BAYESASS v3.0 (Wilson and Rannala, 2002) to calculate the intra-population migration rates. We conducted the analyses with burn-in of 1,000,000 iterations, setting 1,000 as the sampling frequency. Ten independent runs were executed to seek the model convergence.

Demographic History

In order to explore the plausible scenarios of divergence and population dynamics within *R. roxellana*, approximate Bayesian computation (ABC) was used in DIYABC v 2.04 (Cornuet et al., 2014). Based on the STRUCTURE results (**Figure 2**), 10 historical population divergence scenarios for these lineages were simulated by DIYABC analysis (**Supplementary Table 2**). We assumed uniform priors on all parameters, and then we used a goodness-of-fit test to check the priors of all parameters before implementing the simulations (**Figure 3A**). To estimate the divergence times among the lineages, the average generation time of *R. roxellana* was assumed to be 5 years, following Oleksyk et al. (2010).

Ecological Niche Modeling

Ecological niche modeling (ENM) analyses were performed with MAXENT v3.3.3k (Phillips et al., 2006) to assess the ecological niche of each lineage and to predict their potential range based on their georeferenced localities and environmental variables thereof. Only wild occurrences have been taken into account for the ENM analyses. The occurrence data of *R. roxellana* were obtained from our field observations, literature (Wen and Wen, 2006; Wen, 2009), and the records from two sources: the Global Biodiversity Information Facility (GBIF; https://www.gbif.org/) and the National Specimen Information Infrastructure (NSII; www.nsii.org.cn). In total, 131 georeferenced points were obtained.

We obtained 19 bioclimatic variables at 2.5 arc-minute resolutions from WorldClim (www.worldclim.org) (Hijmans et al., 2005) for four periods: the current, the Holocene (HOL; 12 ka–current), the last glacial maximum (LGM; 18–21 ka), and the last interglacial period (LIG; 120–140 ka). To avoid model over-fitting linked to correlated climatic parameters, only those seven variables that had low correlation coefficients with one another ($r < 0.8$) were retained for subsequent analyses (**Supplementary Table 3**).

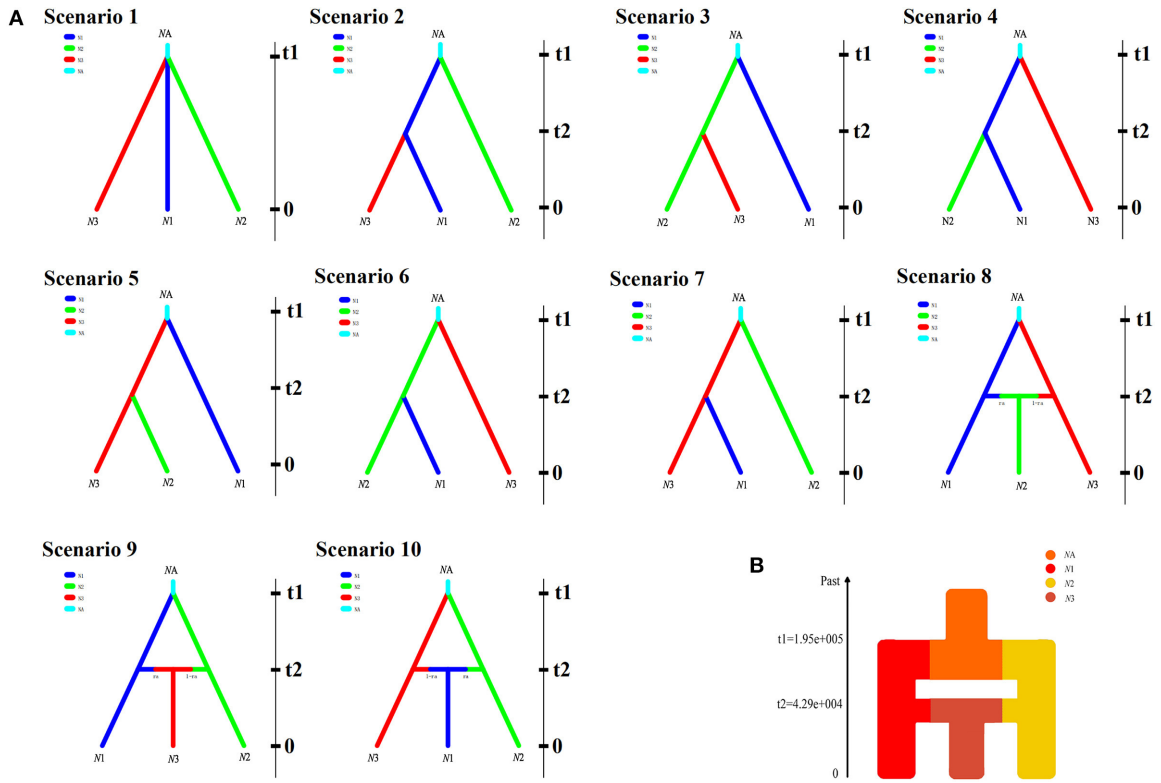

FIGURE 3 | (A) The 10 scenarios of population history of five populations in *Rhinopithecus roxellana* in Qinling Mountains with DIYABC V 2.04. *N*1, *N*2, and *N*3 denote the current population lineages, while *N*A represents the ancestral population lineage. t1 and t2 are divergence times for the depicted event. **(B)** Schematic representation of changes in population size tested within the three population lineages.

All ecological distribution models were visualized in ARCGIS 10.5.

RESULTS

Genetic Diversity

A total of 361 samples were collected. After exclusion of 44 repeated samples as determined by microsatellite profiles, we eventually established a dataset consisting 317 individuals. With the use of MICRO-CHECKER, the frequencies of null alleles at each of the 19 loci were found to be lower than the threshold frequency ($v = 0.15$) across the five populations. The location, population size, and sample size of each band are presented in **Table 1**.

The genetic diversity indices of each band are also presented in **Table 1**. On the whole, genetic variability was moderate at the population level. The number of alleles per locus ranged from 4 to 6, averaging 5.047; observed heterozygosity (H_O) ranged from 0.563 to 0.624, averaging 0.595; expected heterozygosity (H_E) was from 0.558 to 0.672, averaging 0.623; the polymorphism information content (PIC) was from 0.473 to 0.538, averaging 0.511; and allelic richness ranged from 2.342 to 2.642, averaging 2.511 for the populations. The values of Wright's inbreeding coefficient (F_{IS}) showed that the effect of inbreeding to five populations was weak.

No evidence of bottleneck effects has been found from the microsatellite data for each population. The results of bottleneck effects tests are shown in **Table 2**; none of the sign or Wilcoxon tests suggest heterozygosity excess or deficiency in either the SMM or TPM mutation models. The lowest *P*-value was 0.060 (Wilcoxon test under TPM model in DPY). The *GW* coefficients of all bands were above the empirical value 0.132 (Garza and Williamson, 2001), and the lowest *GW* coefficient was 0.846 ± 0.177 (CYG).

Population Differentiation and Structure

The results of F_{ST} and permutation test revealed a relatively low but significant genetic divergence among those five bands ($P < 0.05$, **Table 3**). The AMOVA analyses showed that genetic variation among and within five populations was 15.74 and 84.26%, respectively (**Table 4**). According to the STRUCTURE analysis of microsatellite data, the most likely number of genetic clusters was at 3, and the scenario of $K = 2$ was also given for comparison. The $L(K)$ (the probability of the data given K and the model) and ΔK (using the method of Evanno et al., 2005) as a function of selecting most likely *K*-value, and the bar plot of assignment matrix of LOCPRIOR analysis are shown in **Figure 2**.

TABLE 2 | Bottleneck effect tests of five populations.

Band	Sign text		Wilcoxon test		$M \pm SD$
	TPM	*SMM*	*TPM*	*SMM*	
GNG	0.528	0.076	0.865	0.325	0.880 ± 0.147
DPY	0.129	0.277	0.060	0.156	0.859 ± 0.164
SZZ	0.353	0.359	0.244	0.678	0.849 ± 0.197
HTP	0.430	0.428	0.329	0.644	0.858 ± 0.142
CYG	0.193	0.206	0.064	0.132	0.846 ± 0.177

No results were significant.
TPM denotes two-phase model, SMM denotes step-wise mutation model, and M is the Garza and Williamson (2001) coefficient.

TABLE 3 | Pairwise F_{ST} (lower triangular) and permutation test.

	GNG	DPY	SZZ	HTP
DPY	0.019*			
SZZ	0.030*	0.034*		
HTP	0.039*	0.037*	0.039*	
CYG	0.083*	0.066*	0.077*	0.051*

*$P < 0.05$.

TABLE 4 | Results of AMOVA.

Source of variation	*d. f.*	Sum of squares	Variance components	Variation %
Among populations	4	547.705	1.05401 *Va*	15.74
Within populations	629	3547.872	5.64050 *Vb*	84.26
Total	633	4095.577	6.69451	

Monkeys from three populations (e.g., GNG, DPY, and SZZ) were collectively classified into a single cluster, while the remaining two monkey populations, HTP and CYG, were each assigned to a separate cluster.

Gene Flow

Our study revealed asymmetrical historical gene flow among the five populations by MIGRATE, with the greatest gene migration between CYG and DPY (54.1218; **Table 5**) and the lowest between GNG and CYG (6.8760; **Table 5**). Moreover, BAYESASS analysis revealed contemporary genetic migration was symmetrical among the 10 related pairs. Estimated population sizes according to Bayesian modes, with 95% CI, were 0.3074 (95% CI: 0.2936–0.3661) for GNG, 0.4262 (95% CI: 0.4038–0.4502) for DPY, 0.2567 (95% CI: 0.2427–0.2719) for SZZ, 0.6696 (95% CI: 0.6341–0.7078) for HTP, and 1.4484 (95% CI: 1.3051–1.5423) for CYG.

Evolutionary Dynamics History

In the DIYABC analysis, the posterior probability for scenario 8 (with 95% CI) was 0.914 (95% CI: 0.906–0.942), much higher than that of the other nine scenarios (**Supplementary Figure 1**). Our ABC demographic analysis detected that the first divergence in our focal species formed *N*1 and *N*3 lineages and the second divergence formed *N*2, which originated from the second contact of the *N*1 and *N*3 lineages (**Figure 3B**). The median values of the effective population sizes of *N*1, *N*2, and *N*3 were 2.18×10^5, 1.69×10^5, and 1.44×10^5, respectively, whereas *N*A was 1.85×10^6 (**Table 6**). In addition, the mean values of effective populations of *N*1, *N*2, and *N*3 were 2.61×10^5, 2.07×10^5, and 1.75×10^5, respectively, whereas *N*A was 1.96×10^6 (**Table 6**). The estimated median time of divergence between *N*1 (GNG, DPY, and SZZ populations) and *N*3 (CYG populations) (t1) from the common ancestor was 1.95×10^5 generations ago, *N*2 (HTP populations) diverged from the *N*1, and *N*3 (t2) was 4.51×10^4 generations ago (**Table 6**).

Ecological Niche Modeling

We obtained four distributions tendencies of the *Rhinopithecus roxellana*, including the LIG, LGM, HOL, and current models by MAXENT (**Figure 4**). All models had high predictive ability [area under the receiver operating characteristic curve (AUC) > 0.9]. The predicted model for the present potential range of *R. roxellana* was fairly congruent with the current distribution of the species. The ENMs suggested that the *R. roxellana* had population expansion during the LIG to LGM. Compared with the HOL and the current distributions, the current pattern had little diminished.

DISCUSSION

The present distributions of animal populations depend upon the historical processes and human activities. The habitat range of *Rhinopithecus roxellana* is a consequence of variation in ecological factors such as climatic change and intensity of human disturbance. In this study, we firstly used the interdisciplinary approaches to address the evolutionary dynamics of *R. roxellana* in Qinling Mountains. We examined genetic diversity, gene flow, genetic structures, and evolutionary history combination with the ENMs to elucidate ecological factors on the population demography.

Genetic Diversity and Genetic Differentiation

We used microsatellite data to analyze the genetic diversity and population structure of *R. roxellana*. A relatively high level of genetic diversity had been found. Compared with previous studies based on the microsatellite profiles, the expected heterozygosity in all populations from our investigation (0.628) was close to that of the other studies of this species (0.559 in Li et al., 2020; 0.625 in Huang et al., 2016a; 0.591 in Chang et al., 2013; and 0.631 in Pan et al., 2005). In addition, there was no evidence of any past genetic bottlenecks in any of the sampled monkey bands (**Table 2**), revealing that these populations have not suffered significant population size reduction. This result was consistent with that of Li et al. (2020) and Huang et al. (2016a), which also focused on the monkeys in the Qinling Mountains. The F_{ST} and permutation test results revealed a genetic differentiation among different populations ($P < 0.05$)

TABLE 5 | Rates of contemporary and historical gene flows among five populations using microsatellite data with the programs bayesass, migrate, and bidirectional gene flow (*N*m = immigrants per generation).

	GNG	DPY	SZZ	HTP	CYG
Bayesass					
GNG	–	0.0045 (0.0013–0.0094)	0.0038 (0–0.0078)	0.0038 (0.0017–0.0077)	0.0041 (0.0023–0.0060)
DPY	0.0097 (0.0054–0.0176)	–	0.0056 (0.0021–0.0084)	0.0044 (0–0.0143)	0.0053 (0.0027–0.0092)
SZZ	0.0051 (0.0022–0.0105)	0.0055 (0.0009–0.0094)	–	0.0050 (0–0.0117)	0.0072 (0.0014–0.0128)
HTP	0.0046 (0–0.0096)	0.0046 (0.0023–0.0075)	0.0046 (0–0.0089)	–	0.0047 (0.0018–0.0077)
CYG	0.0093 (0–0.0197)	0.0091 (0.0030–0.0176)	0.0023 (0–0.0067)	0.0056 (0–0.0083)	–
Migrate					
GNG	–	17.2104 (15.6694–18.8496)	26.1928 (24.2800–28.2037)	24.6458 (22.7858–26.6049)	12.963 (11.6314–14.3922)
DPY	20.1345 (18.6601–21.6870)	–	26.7072 (25.0050–28.4849)	17.1630 (15.8051–18.5953)	54.1218 (51.6823–26.6378)
SZZ	18.7277 (17.1183–20.4326)	38.0089 (21.4185–25.1390)	–	23.2310 (21.4185–25.1390)	26.3535 (24.4257–28.3757)
HTP	13.7162 (12.6706–14.8180)	16.3020 (15.1622–17.4970)	13.9972 (12.9361–15.1145)	–	9.8459 (8.9673–10.7804)
CYG	6.8760 (6.2652–7.5248)	26.0904 (24.8841–27.3354)	9.8011 (9.0647–10.5769)	8.6441 (7.9570–9.3706)	–
***N*m**					
GNG	–	10.5810 (8.3546–12.6872)	16.1033 (14.8424–18.437)	15.1522 (13.6046–17.7099)	7.9697 (5.4052–9.8011)
DPY	17.1626 (15.0317–19.2484)	–	22.7652 (20.4299–24.5679)	14.6297 (12.6118–16.1843)	16.1334 (14.1217–18.3535)
SZZ	19.6148 (17.3025–21.5698)	19.5138 (17.2316–21.9637)	–	11.9268 (9.2373–13.9993)	13.5299 (11.3314–15.3275)
HTP	18.3687 (16.0359–20.6790)	21.8316 (19.117–23. 4606)	18.7451 (16. 998–20.5518)	–	13.1856 (11. 221–15.4657)
CYG	19.4866 (17.3668–21.6047)	13.9402 (11.2919–15.3879)	17.7763 (15.0038–19.0291)	14.4974 (12.4778–17.1034)	–

95% confidence intervals are presented in parentheses.

TABLE 6 | Demographic approximate Bayesian computation (ABC) models for *Rhinopithecus roxellana* in Qinling Mountains.

Parameters	*N*1	*N*2	*N*3	*N*A	t1 (generations)	t2 (generations)	μ	*P*
Median	2.18E+005	1.69E+005	1.44E+005	1.85E+006	1.34E+005	4.51E+004	1.92E−006	0.5
Mean	2.61E+005	2.07E+005	1.75E+005	1.96E+006	1.95E+005	4.29E+004	2.22E−006	0.5
Lower bound	7.04E+004	5.09E+004	5.24E+004	4.21E+005	6.67E+004	2.82E+004	1.13E−006	0.254
Upper bound	6.07E+005	5.12E+005	3.94E+005	3.94E+006	5.71E+005	4.96E+004	4.36E−006	0.685

N1, effective population size of GNG, DPY, and SZZ; N2, effective population size of HTP; N3, effective population size of SZZ; NA, effective population size of ancestral population; t1, divergence time of N1 and N2 from ancestral population; t2, divergence time of N3 from N1 and N2; μ, mutation rate (per generation per locus).

associated with topographical barriers such as mountain ridges, which might lead to the reduced gene flow between populations (Chang et al., 2013).

Genetic Admixture and Gene Flow

The Bayesian clustering revealed three major subpopulations that strongly coincide with the major topographical ridge features in the study area. Our results indicated that the contemporary gene flow among the five populations was symmetric and low, whereas the historical gene flow for all pairs seemed asymmetric (**Table 5**). The possible explanations for the low contemporary gene flow were the more and more frequent human activities in this area. Human-constructed barriers such as rivers, villages, logging roads, and farmlands have limited the ability of BBs to freely

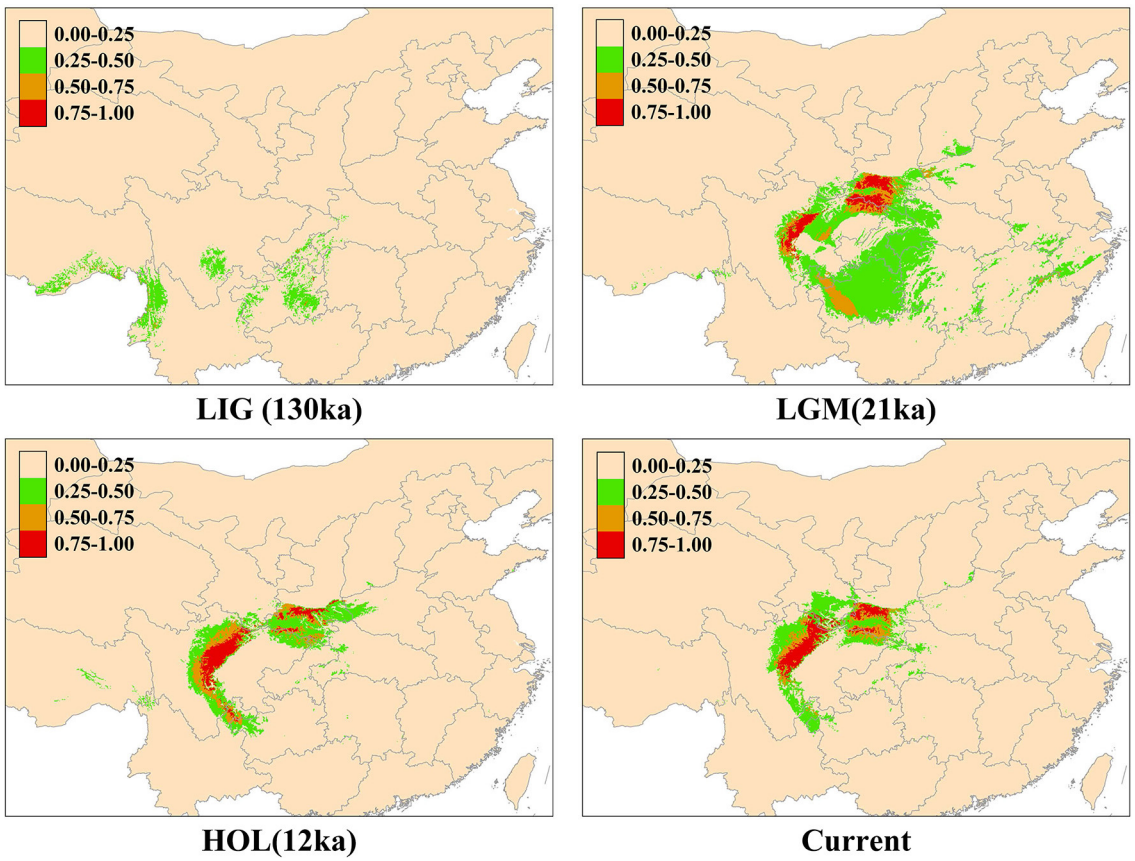

FIGURE 4 | Predicted past and current distributions of *Rhinopithecus roxellana* based on ecological niche modeling using MAXENT: the current, the Holocene (HOL; 12 ka–current), the last glacial maximum (LGM; 18–21 ka), and the last interglacial period (LIG; 120–140 ka).

move across these fragment landscapes for decades (Li et al., 2002; Wang et al., 2014). Moreover, the topography of the Qinling Mountains, which is dominated by high altitude temperate forest habitats, and open areas of fragmented and cleared forests containing villages and agricultural fields, may greatly increase the genetic differentiation of *R. roxellana* and restrict gene flow by decreasing the opportunities for successful dispersal (Wang et al., 2014). Nevertheless, satellite telemetry data indicated that some neighbor populations had small overlaps of their home ranges with occasional group fission–fusions (Qi et al., 2017). Meanwhile, the AMBs of *R. roxellana* played critical roles, which connected, gathered, and allocated gene flow among nearby populations (Li et al., 2020). But these only happened at a fine scale, which may explain the genetic migration of the bands between GNG, DPY, and SZZ (**Figure 2C**).

In general, gene flow is critical for mitigating the impacts of local adaptation by homogenizing populations from differing conditions or by spreading deleterious alleles across populations, and it also could spread favorable alleles to populations and increase genetic diversity (Welt et al., 2015; Epps and Keyghobadi, 2016). Previous research had reported that historical and contemporary gene migration was low among populations that often existed in highly fragmented habitats (Chiucchi and Gibbs, 2010), but if genetic structure was admixture, it might cause intense historical gene flow (Epps et al., 2013). However, whether the genetic structure of the Qinling Mountains was due to historical gene flow rather than contemporary ones needs further investigation.

Demographic History

Our ABC demographic analysis detected three lineages (*N*1, *N*2, and *N*3) existing within the monkeys of the Qinling Mountains (*N*1: GNG, DPY, and SZZ; *N*2: CYG; and *N*3: HTP). The first divergence in our focal species that formed *N*1 and *N*3 lineages from ancestral linage was at 0.975 Ma [95% highest posterior density (HPD): 0.33–2.86 Ma]. Based on the genetic analysis and fossil data from existing populations, snub-nosed monkeys are distributed across eastern, central, southern, and southwestern China in the past 2 million years (Liedigk et al., 2003). In addition, our initial divergence time in the Qinling Mountains might occur at the Late Pleistocene. Due to climate change and orogenic movement, lots of numbers of animals have declined population sizes and even became extinct during this period (Buuveibaatar et al., 2016; Olsoy et al., 2016). Some species have been forced to shift their range to resist environmental changes

and/or habit conversion (Ceballos, 2002; Cleland et al., 2012). The first divergence time estimation coincided with this historical period.

Moreover, the second divergence was at 0.23 Ma (95% HPD: 0.14–0.25 Ma), and formed *N*2, which originated from the second contact of the *N*1 and *N*3 lineages. Since the habitat fragmentation and ecological barriers could lead to restrict gene migration, some species would resist the threat of genetic homogeneity (Lenormand, 2002). It had been reported the monkeys would disperse long distance and build their families in another population (Huang et al., 2017). But so far, since our understanding of the mechanism against genetic homogeneity is still limited, further research would be needed. In addition, according to previous studies (Yu et al., 2016; Zhou et al., 2016; Kuang et al., 2019), one lineage of the Sichuan (SG) population was closely clustered with the Qinling (QL) population. This result indicated that the SG population may have contributed to the genetic structure of the QL population; for our subsequent research, this part would also be taken into account.

The ENM analyses also suggested that the golden snub-nosed monkeys had expanded their ranges during the LIG (0.14–0.12 Ma) to LGM. At the end of the largest glaciation (ca. 1.2–0.6 Ma), the temperature increased, and also, the relatively cold climate may have continued until the late Ionian stage (0.3–0.126 Ma) (Goldewijk et al., 2001). Thus, because the golden snub-nosed monkey could adapt to cold habitats (Yu et al., 2016), it is feasible that they expanded their ranges and increased their population sizes during this period.

It is necessary for us to raise the issues on a conservation strategy for the *R. roxellana*, in addition to carrying out further survey and studies on its ecology, behavior, and dietary selection. At the moment, what we know about the most possible threats could include road accidents (traffic is heavy in the areas), habitat loss, human's intentional killing due to economic reasons from the local culture, and natural disasters (Li et al., 2002; Wang et al., 2014). Although a series of natural reserve have been established in the Mt. Qinling, rapid tourism development would inevitably lead to the expanding of roads and other artificial constructions, while increasing human disturbance in this area. A monitoring system on their dynamic population profiles should be established, so that emergency strategies for their conservation could be applied if a significant population decline was detected. On the other hand, more technical programs for captive breeding are also required.

The Qinling Mountains are famous for their global biodiversity hotspot and refugia for many endangered mammals and birds, particularly during the last glaciation (Wang et al., 2014). The Chinese Government has invested a great deal of manpower to the conservation of "four precious species in the Mts. Qinling" (the giant panda, *Ailuropoda melanoleuca*; the golden snub-nosed monkey, *Rhinopithecus roxellana*; the crested ibis, *Nipponia nippon*; and the takin, *Budorcas taxicolor*). Our new results of the evolutionary history with the *R. roxellana* could also shed light on species with the same geographical distribution, as well as other threatened or endangered amphibians and reptiles in this area.

DATA AVAILABILITY STATEMENT

The datasets presented in this study can be found in online repositories. The names of the repository/repositories and accession number(s) can be found in the article/**Supplementary Material**.

ETHICS STATEMENT

The animal study was reviewed and approved by Wildlife Protection Society of China.

AUTHOR CONTRIBUTIONS

BL and YL conceived the study. YL and KH performed the experiments. YL, LF, JY, and ZL contributed materials and analysis tools. BL, YL, and ST wrote the manuscript. LF and JY revised the manuscript. All authors approved the final version of the manuscript.

FUNDING

This work was funded by the Strategic Priority Research Program of the Chinese Academy of Sciences (XDB31020302), the National Natural Science Foundation of China (31730104, 31572278, and 31770411), the National Key Program of Research and Development, the Ministry of Science and Technology of China (2016YFC0503200), the Young Elite Scientists Sponsorship Program by CAST (2017QNRC001), and the Natural Science Foundation of Shaanxi Province (2018JM3024).

ACKNOWLEDGMENTS

We thanked four National Nature Reserves of the Qinling Mountains for the permission of this study.

SUPPLEMENTARY MATERIAL

The Supplementary Material for this article can be found online at: https://www.frontiersin.org/articles/10.3389/fgene.2020.611914/full#supplementary-material

Supplementary File 1 | Genepop genotype file.

Supplementary Figure 1 | The posterior probabilities of the 10 scenarios.

Supplementary Table 1 | Microsatellite marker information.

Supplementary Table 2 | Prior distributions for model parameters used in divergence model comparisons (**Figure 3A**).

Supplementary Table 3 | The seven bioclimatic variables that were used in ecological niche modeling.

REFERENCES

Allen, M., Engström, A. S., Meyers, S., Handt, O., and Gyllensten, U. (1998). Mitochondrial DNA sequencing of shed hairs and saliva on robbery caps: sensitivity and matching probabilities. *J. Forensic Sci.* 43, 453–464. doi: 10.1520/JFS16169J

Astrid, V. S., Nathan, H. S., Graham, J. F., Paul, C. P., and Ryan, K. B. (2012). Landscape resistance to dispersal: simulating long-term effects of human disturbance on a small and isolated wolf population in southwestern Manitoba, Canada. *Environ. Monit. Assess.* 184, 6923–6934. doi: 10.1007/s10661-011-2469-9

Balkenhol, N., Gugerli, F., Cushman, S. A., Waits, L. P., Coulon, A., Arntzen, J. W., et al. Participants of the landscape genetics research agenda workshop 2007 (2009). Identifying future research needs in landscape genetics: where to from here? *Landsc. Ecol.* 24, 455–463. doi: 10.1007/s10980-009-9334-z

Beerli, P. (2006). Comparison of Bayesian and maximum-likelihood inference of population genetic parameters. *Bioinformatics* 22, 341–345. doi: 10.1093/bioinformatics/bti803

Burkey, T. V. (2010). Extinction rates in archipelagoes: implications for populations in fragmented habitats. *Conserv. Biol.* 9, 527–541. doi: 10.1046/j.1523-1739.1995.09030527.x

Buuveibaatar, B., Mueller, T., Strindberg, S., Leimgruber, P., Kaczensky, P., and Fuller, T. K. (2016). Human activities negatively impact distribution of ungulates in the Mongolian Gobi. *Biol. Conserv.* 203, 168–175. doi: 10.1016/j.biocon.2016.09.013

Ceballos, G. (2002). Mammal population losses and the extinction crisis. *Science* 296, 904–907. doi: 10.1126/science.1069349

Chambers, J. L., and Garant, D. (2010). Determinants of population genetic structure in eastern Chipmunks (*Tamias striatus*): the role of landscape barriers and sex-biased dispersal. *J. Hered.* 101, 413–422. doi: 10.1093/jhered/esq029

Chang, Z. F., Yang, B. H., Vigilant, L., Liu, Z. J., and Li, M. (2013). Evidence of male-biased dispersal in the endangered Sichuan snub-nosed monkey (*Rhinopithexus roxellana*). *Am. J. Primatol.* 76, 72–83. doi: 10.1002/ajp.22198

Chiucchi, J. E., and Gibbs, H. L. (2010). Similarity of contemporary and historical gene flow among highly fragmented populations of an endangered rattlesnake. *Mol. Ecol.* 19, 5345–5358. doi: 10.1111/j.1365-294X.2010.04860.x

Cleland, E. E., Allen, J. M., Crimmins, T. M., Dunne, J. A., Pau, S., Travers, S. E., et al. (2012). Phenological tracking enables positive species responses to climate change. *Ecology* 93, 1765–1771. doi: 10.1890/11-1912.1

Cornuet, J. M., Pudlo, P., Veyssier, J., Dehne-Garcia, A., Gautier, M., Leblois, R., et al. (2014). DIYABC v2.0: a software to make approximate Bayesian computation inferences about population history using single nucleotide polymorphism, DNA sequence and microsatellite data. *Bioinformatics* 30, 1187–1189. doi: 10.1093/bioinformatics/btt763

Earl, D. A., and Vonholdt, B. M. (2012). Structure Harvest: a website and program for visualizing structure output and implementing the Evanno method. *Conserv. Genet. Resour.* 4, 359–361. doi: 10.1007/s12686-011-9548-7

Epps, C. W., Castillo, J. A., Anne, S. K., Pierre, D. P., Greg, S. H., Mark, J., et al. (2013). Contrasting historical and recent gene flow among African buffalo herds in the Caprivi Strip of Namibia. *J. Hered.* 104, 172–181. doi: 10.1093/jhered/ess142

Epps, C. W., and Keyghobadi, N. (2016). Landscape genetics in a changing world: disentangling historical and contemporary influences and inferring change. *Mol. Ecol.* 24, 6021–6040. doi: 10.1111/mec.13454

Evanno, G. S., Regnaut, S. J., and Goudet, J. (2005). Detecting the number of clusters of individuals using the software STRUCTURE: a simulation study. *Mol. Ecol.* 14, 2611–2620. doi: 10.1111/j.1365-294X.2005.02553.x

Excoffier, L., and Lischer, H. E. (2010). Arlequin suite ver 3.5: a new series of programs to perform population genetics analyses under Linux and Windows. *Mol. Ecol. Resour.* 10, 564–567. doi: 10.1111/j.1755-0998.2010.02847.x

Feng, T. T., Manen, F. T., Zhao, N. X., and Wei, L. F. (2009). Habitat assessment for giant pandas in the qinling mountain region of China. *J. Wildl. Manage.* 73, 852–858. doi: 10.2193/2008-186

Frankham, R. (2005). Genetics and extinction. *Biol. Conserv.* 126, 131–140. doi: 10.1016/j.biocon.2005.05.002

Garza, J. C., and Williamson, E. G. (2001). Detection of reduction in population size using data from microsatellite loci. *Mol. Ecol.* 10, 305–318. doi: 10.1046/j.1365-294x.2001.01190.x

Goldewijk, K. K., Beusen, A., van Drecht, G., and de Vos, M. (2001). The HYDE 3.1 spatially explicit database of human-induced global land-use change over the past 12,000 years. *Glob. Ecol. Biogeogr.* 20, 73–86. doi: 10.1111/j.1466-8238.2010.00587.x

Grueter, C. C., Chapais, B., and Zinner, D. (2012). Evolution of multilevel social systems in nonhuman primates and humans. *Int. J. Primatol.* 33, 1002–1037. doi: 10.1007/s10764-012-9618-z

Hanski, I. (1994). Patch-occupancy dynamics in fragmented landscapes. *Trends Ecol. Evol.* 9, 131–135. doi: 10.1016/0169-5347(94)90177-5

Hijmans, R. J., Cameron, S. E., Parra, J. L., Jones, P. G., and Andy, J. (2005). Very high resolution interpolated climate surfaces for global land areas. *Int. J. Biometeorol.* 25, 1965–1978. doi: 10.1002/joc.1276

Huang, K., Guo, S. T., Cushman, S. A., Dunn, D. W., Qi, X. G., Hou, R., et al. (2016a). Population structure of the golden snub-nosed monkey *Rhinopithecus roxellana* in the Qinling Mountains, central China. *Integr. Zool.* 11, 350–360. doi: 10.1111/1749-4877.12202

Huang, K., Ritland, K., Dunn, D. W., Qi, X. G., Guo, S. T., and Li, B. G. (2016b). Estimating relatedness in the presence of null alleles. *Genetics* 201, 247–260. doi: 10.1534/genetics.114.163956

Huang, Z. P., Bian, K., Liu, Y., Pan, R. L., Qi, X. G., and Li, B. G. (2017). Male dispersal pattern in golden snub-nosed monkey (*Rhinopithecus roxellana*) in qinling mountains and its conservation implication. *Sci. Rep.* 7:46217. doi: 10.1038/srep46217

Kirkpatrick, R. C., and Grueter, C. C. (2010). Snub-nosed monkeys: multilevel societies across varied environments. *Evol. Anthropol. Issues News Rev.* 19, 98–113. doi: 10.1002/evan.20259

Kuang, W. M., Ming, C., Li, H. P., Wu, H., Frantz, L., Roos, C., et al. (2019). The origin and population history of the endangered golden snub-nosed monkey (*Rhinopithecus roxellana*). *Mol. Biol. Evol.* 36, 487–499. doi: 10.1093/molbev/msy220

Lait, L. A., and Burg, T. M. (2013). When east meets west: population structure of a high-latitude resident species, the boreal chickadee (*Poecile hudsonicus*). *Heredity* 1, 321–329. doi: 10.1038/hdy.2013.54

Lenormand, T. (2002). Gene flow and the limits to natural selection. *Trends Ecol. Evol.* 17, 183–189. doi: 10.1016/S0169-5347(02)02497-7

Li, B. G., Chen, C., Ji, W. H., and Ren, B. P. (2000). Seasonal home range changes of the Sichuan snub-nosed monkey (*Rhinopithecus roxellana*) in the Qinling mountains of China. *Folia Primatol.* 71, 375–386. doi: 10.1159/000052734

Li, B. G., Jia, Z. Y., Pan, R. L., and Ren, B. P. (2003). "Changes in distribution of the snub-nosed monkey in China," in *Primates in Fragments: Ecology and Conservation*. ed L. K. Marsh (New York, NY: Kluwer Academic/Plenum Press), 29–51. doi: 10.1007/978-1-4757-3770-7_4

Li, B. G., Pan, R. L., and Oxnard, C. E. (2002). Extinction of snub-nosed monkeys in China during the Past 400 Years. *Int. J. Primatol.* 23, 1227–1244. doi: 10.1023/A:1021122819845

Li, M., Liu, Z. J., Gou, J. X., Ren, B. P., Pan, R. L., Su, Y. J., et al. (2007). Phylogeography and population structure of the golden monkeys (*Rhinopithecus roxellana*): inferred from mitochondrial DNA sequences. *Am. J. Primatol.* 69, 1195–1209. doi: 10.1002/ajp.20425

Li, Y. L., Wang, L., Wu, J. W., Ye, X. P., Garber, G. A., Yan, Y., et al. (2020). Bachelor groups in primate multilevel society facilitate gene flow across fragmented habitats. *Curr. Zool.* 66, 113–122. doi: 10.1093/cz/zoaa006

Liedigk, R., Yang, M. Y., Jablonski, N. G., Momberg, F., Geissmann, T., Lwin, N., et al. (2003). Evolutionary history of the odd-nosed monkeys and the phylogenetic position of the newly described Myanmar snub-nosed monkey *Rhinopithecus strykeri*. *PLoS ONE* 7:e37418. doi: 10.1371/journal.pone.0037418

Newbold, T., Hudson, L. N., Hill, S. L., Contu, S., Lysenko, I., Senior, R. A., et al. (2015). Global effects of land use on local terrestrial biodiversity. *Nature* 520, 45–50. doi: 10.1038/nature14324

Norton, C. J., Jin, C. Z., Wang, Y., and Zhang, Y. Q. (2011). "Rethinking the palearctic-oriental biogeographic boundary in Quaternary China," in *Asian Paleoanthropology: From Africa to China and Beyond*, eds C. J. Norton, and D. R. Braun (Dordrecht: Springer Press), 81–100. doi: 10.1007/978-90-481-9094-2_7

Oleksyk, T. K., Smith, M. W., and O'Brien, S. J. (2010). Genome-wide scans for footprints of natural selection. *Philos. Trans. R. Soc. Lond. Ser. B.* 365, 185–205. doi: 10.1098/rstb.2009.0219

Olsoy, P. J., Zeller, K. A., Hicke, J. A., Quigley, H. B., Rabinowitz, A. R., and Thornton, D. H. (2016). Quantifying the effects of deforestation and fragmentation on a range-wide conservation plan for jaguars. *Biol. Conserv.* 203, 8–16. doi: 10.1016/j.biocon.2016.08.037

Pan, D., Li, Y., Hu, H. X., Meng, S. J., Men, Z. M., Fu, Y. X., et al. (2005). Microsatellite polymorphisms of Sichuan golden monkeys. *Chin. Sci. Bull.* 50, 2850–2855. doi: 10.1007/BF02899655

Peakall, R., and Smouse, P. E. (2012). GenAlEx 6.5: genetic analysis in Excel. Population genetic software for teaching and research-an update. *Bioinformatics* 28, 2537–2539. doi: 10.1093/bioinformatics/bts460

Phillips, S. J., Anderson, R. P., and Schapire, R. E. (2006). Maximum entropy modeling of species geographic distributions. *Ecol. Modell.* 190, 231–259. doi: 10.1016/j.ecolmodel.2005.03.026

Piry, S., Luikart, G., and Cornuet, J. M. (1999). Bottleneck: a computer program for detecting recent reductions in the effective size using allele frequency data. *J. Hered.* 90, 502–503. doi: 10.1093/jhered/90.4.502

Pritchard, J. K., Stephens, M., and Donnelly, P. (2000). Inference of population structure using multilocus genotype data. *Genetics* 155, 945–959. Available online at: https://www.genetics.org/content/155/2/945

Qi, X. G., Huang, K., Fang, G., Grueter, C. C., Dunn, D. W., Li, Y. L., et al. (2017). Male cooperation for breeding opportunities contributes to the evolution of multilevel societies. *Proc. R. Soc. B* 284:20171480. doi: 10.1098/rspb.2017.1480

Ren, R. M., Su, Y. J., Yan, K. H., Li, J. J., and Hu, Y. F. (1998). *Preliminary Survey of the Social Organization of Rhinopithecus Roxellana in Shennongjia National Natural Reserve*. Hubei: World Scientific Press. doi: 10.1142/9789812817020_0014

Rice, W. R. (1989). Analyzing tables of statistical tests. *Evolution* 43, 223–225. doi: 10.1111/j.1558-5646.1989.tb04220.x

Rousset, F. (2008). Genepop'007: a complete re-implementation of the genepop software for Windows and Linux. *Mol. Ecol. Resour.* 8, 103–106. doi: 10.1111/j.1471-8286.2007.01931.x

Taberlet, P., Griffin, S., Goossens, B., Questiau, S., Manceau, V., Escaravage, N., et al. (1996). Reliable genotyping of samples with very low DNA quantities using PCR. *Nucleic Acids Res.* 24, 3189–3194. doi: 10.1093/nar/24.16.3189

van Oosterhout, C., Hutchinson, W. F., Wills, D. P., and Shipley, P. (2010). Micro-checker: software for identifying and correcting genotyping errors in microsatellite data. *Mol. Ecol. Resour.* 4, 535–538. doi: 10.1111/j.1471-8286.2004.00684.x

Waage, J. K., and Greathead, D. J. (1988). Biological control: challenges and opportunities. *Philos. Trans. R. Soc. Lond. B. Biol. Sci.* 318, 111–128. doi: 10.1098/rstb.1988.0001

Wang, C. L., Wang, X. W., Qi, X. G., Guo, S. T., zhao, H. T., Wei, W., et al. (2014). Influence of human activities on the historical and current distribution of Sichuan snub-nosed monkeys in the Qinling Mountains, China. *Folia Primatol.* 85, 343–357. doi: 10.1159/000368398

Welt, R. S., Amy, L., and Franks, S. J. (2015). Analysis of population genetic structure and gene flow in an annual plant before and after a rapid evolutionary response to drought. *AoB Plants* 7, 632–641. doi: 10.1093/aobpla/plv026

Wen, H., and Wen, R. (2006). *The Change of the Plant and Animal in China During Different Historical Period*. Chongqing: Chongqing Press.

Wen, R. (2009). *The Distributions and Changes of Rare Wild Animals in China*. Jinan: Shandong Science and Technology Press.

Willi, Y., Van Buskirk, J., and Hoffmann, A. A. (2006). Limits to the adaptive potential of small populations. *Annu. Rev. Ecol. Evol. Syst.* 37, 433–458. doi: 10.1146/annurev.ecolsys.37.091305.110145

Wilson, G., and Rannala, B. (2002). Bayesian inference of recent migra-tion rates using multilocus genotypes. *Genetics* 163, 1177–1191. Available online at: https://www.genetics.org/content/163/3/1177

Yu, L., Wang, G. D., Ruan, J., Chen, Y. B., Yang, C. P., Cao, X., et al. (2016). Genomic analysis of snub-nosed monkeys (*Rhinopithecus*) identifies genes and processes related to high-altitude adaptation. *Nat. Genet.* 48, 947–952. doi: 10.1038/ng.3615

Zhang, Y. B., Wang, Y. Z., Phillips, N., Ma, K. P., Li, J. S., and Wang, W. (2016). Integrated maps of biodiversity in the Qinling Mountains of China for expanding protected areas. *Biol. Conserv.* 210, 64–71. doi: 10.1016/j.biocon.2016.04.022

Zhou, X. M., Meng, X. H., Liu, Z. J., Chang, J., Wang, B. S., Li, M. Z., et al. (2016). Population genomics reveals low genetic diversity and adaptation to hypoxia in snub-nosed monkeys. *Mol. Biol. Evol.* 33, 2670–2681. doi: 10.1093/molbev/msw150

Conflict of Interest: The authors declare that the research was conducted in the absence of any commercial or financial relationships that could be construed as a potential conflict of interest.

frontiers in Ecology and Evolution

ORIGINAL RESEARCH
published: 17 February 2021
doi: 10.3389/fevo.2021.634757

CT-Informed Skull Osteology of *Palaeolagus haydeni* (Mammalia: Lagomorpha) and Its Bearing on the Reconstruction of the Early Lagomorph Body Plan

Andrzej S. Wolniewicz[1†] *and Łucja Fostowicz-Frelik*[1,2,3*†]

[1] *Department of Evolutionary Paleobiology, Institute of Paleobiology, Polish Academy of Sciences, Warsaw, Poland,* [2] *Key Laboratory of Vertebrate Evolution and Human Origins, Institute of Vertebrate Paleontology and Paleoanthropology, Chinese Academy of Sciences, Beijing, China,* [3] *Center for Excellence in Life and Paleoenvironment, Chinese Academy of Sciences, Beijing, China*

OPEN ACCESS

Edited by:
K. Christopher Beard, University of Kansas, United States

Reviewed by:
John Wible, Carnegie Museum of Natural History, United States
Ornella C. Bertrand, University of Edinburgh, United Kingdom

***Correspondence:**
Łucja Fostowicz-Frelik
lfost@twarda.pan.pl

†ORCID:
Andrzej S. Wolniewicz
orcid.org/0000-0002-6336-8916
Łucja Fostowicz-Frelik
orcid.org/0000-0002-1266-1178

Specialty section:
This article was submitted to Paleontology, a section of the journal Frontiers in Ecology and Evolution

Received: *03 December 2020*
Accepted: *25 January 2021*
Published: *17 February 2021*

Citation:
Wolniewicz AS and Fostowicz-Frelik Ł (2021) CT-Informed Skull Osteology of Palaeolagus haydeni (Mammalia: Lagomorpha) and Its Bearing on the Reconstruction of the Early Lagomorph Body Plan. Front. Ecol. Evol. 9:634757. doi: 10.3389/fevo.2021.634757

Lagomorpha is a clade of herbivorous mammals nested within Euarchontoglires, one of the major placental groups represented today. It comprises two extant families with markedly different body plans: the long-eared and long-limbed Leporidae (hares and rabbits) and the short-eared and short-limbed Ochotonidae (pikas). These two lagomorph lineages diverged probably during the latest Eocene/early Oligocene, but it is unclear whether the last common ancestor of crown lagomorphs was more leporid- or more ochotonid-like in morphology. *Palaeolagus*, an early lagomorph dominant in western North America from the late Eocene to Oligocene is of particular importance for addressing this controversy. Here, we present new and comprehensive data on the cranial anatomy of *Palaeolagus haydeni*, the type species for the genus, based on micro-computed tomography (μCT). Our μCT data allow us to confirm, revise and score for the very first time the states of several leporid-like and ochotonid-like characters in the skull of *Palaeolagus*. This mixed cranial architecture differentiates *Palaeolagus* from the crown groups of Lagomorpha and supports its phylogenetic status as a stem taxon.

Keywords: skull, Lagomorpha, Leporidae, Ochotonidae, *Palaeolagus*, cranial base, micro-computed tomography

INTRODUCTION

Lagomorpha is a highly conservative clade of Glires, known in the fossil record since the early Eocene (Li et al., 2007; Fostowicz-Frelik et al., 2015; Lopatin and Averianov, 2020). Nowadays, Lagomorpha comprise leporids (hares and rabbits) and ochotonids (pikas); both families differ considerably in their external morphology, especially in the limb length and proportions, and the

Abbreviations: AMNH, American Museum of Natural History, New York, NY, United States; FMNH, Field Museum of Natural History, Chicago, IL, United States; IBS (formerly ZBS), Institute of Mammal Research, Polish Academy of Sciences, Białowieża, Poland; ISEZ, Institute of Systematics and Evolution of Animals, Polish Academy of Sciences, Cracow, Poland; MCZ, Museum of Comparative Zoology, Harvard University, Cambridge, MA, United States; USNM, National Museum of Natural History, Smithsonian Institution, Washington D.C., United States; ZPAL, Institute of Paleobiology, Polish Academy of Sciences, Warsaw, Poland.

size and shape of the pinnae. These two families also show marked differences in the skull structure and dentition (e.g., Wible, 2007; Dawson, 2008; Fostowicz-Frelik and Meng, 2013; Wilson et al., 2016), some of them due to parallel evolution and frequent homoplasy (Fostowicz-Frelik and Meng, 2013; Fostowicz-Frelik, 2017).

Most of the Paleogene fossil record of Lagomorpha is represented by stem taxa (e.g., Fostowicz-Frelik, 2013; Fostowicz-Frelik and Meng, 2013; Fostowicz-Frelik et al., 2015), and the precise ancestry and the time of origination of the crown lagomorph lineages remains uncertain. *Palaeolagus*, a speciose genus of the Paleogene North American lagomorph seems to be of particular importance for addressing this conundrum. Although *Palaeolagus* was historically regarded as an early leporid (mostly based on its dental morphology), the most recent phylogenetic analyses have recovered it as a stem lagomorph, even if close to the crown taxa (e.g., Wible, 2007; Fostowicz-Frelik and Meng, 2013; Lopatin and Averianov, 2020; but see Asher et al., 2019).

Currently, *Palaeolagus* includes nine species and spans from the late Eocene through the earliest Miocene interval (Dawson, 1958, 2008). This work concerns the type species *Palaeolagus haydeni*, known from the Oligocene of the Great Plains (e.g., Wood, 1940; Dawson, 1958, 2008). *P. haydeni* was a ubiquitous and abundant species of the genus and is represented by numerous remains, including well-preserved skulls (**Figures 1**, **2**) and postcranial skeletons from the fossiliferous sediments of the White River Formation (see Wood, 1940; Dawson, 1958). Its abundance in the fossil record may be compared to the broad prevalence of extant *Oryctolagus cuniculus*, which, however, is related to *Palaeolagus* only distantly. These features position *Palaeolagus* as one of the most important taxa for understanding early lagomorph morphology and evolution. Despite the availability of material, very few contributions deal with the cranial anatomy of *Palaeolagus* (see Troxell, 1921; Dice, 1933; Wood, 1940; Dawson, 1958). Moreover, these studies leave out the details of the base of the skull and the braincase, due to past technical limitations of studying the fossil material. Some detailed aspects of the cranial anatomy of *Palaeolagus* were provided by Wible (2007), but his observations were not supported with relevant drawings or photographs.

Here, we present new data on the cranial anatomy of *P. haydeni*, based on micro-computed tomography (μCT). Our anatomical observations provide information important for inferring the character states present in the probable last common ancestor of ochotonids and leporids. They will also be of great importance in phylogenetic studies focusing on resolving the relationships at the base of Lagomorpha in particular, and Glires in general.

MATERIALS AND METHODS

This study is based on CT-scan data from an almost complete cranium with mandible in occlusion of *Palaeolagus haydeni* (FMNH PM9476) from the early Oligocene of the Brule Formation, Nebraska (**Figures 1**, **3**). The skull roof is partially missing in this specimen (posterior frontals and parietals were lost during sedimentation), the anterior nasals and the left zygomatic arch are also largely damaged. To complement the study of the external cranial morphology, several partial skulls of *P. haydeni* were examined as comparative material: AMNH FM106111, a cranium with a slightly distorted muzzle and missing nasals; AMNH FM143956, an almost complete cranium with missing zygomatic arches (**Figure 2**); FMNH PM43030, an anterior part of a skull with a complete muzzle and orbit, associated with both anterior mandible bodies; MCZ 3373, a complete skull with both parts of the mandible *in situ* and partly missing parietals; USNM PAL 243590 and USNM 2530-49, both complete crania without mandibles, partly embedded in matrix. Additionally, we consulted the morphology of several extant lagomorphs (see Supplementary Material).

FMNH PM9476 was CT-scanned in a high-resolution Phoenix v| tome| x L 240 scanner (GE Measurement & Control Solutions) at the AMNH. The specimen was scanned in a single scan with the following parameters: voltage 170 kV, current 170 μA and a 0.1 mm Cu filter to minimize beam hardening. The CT-data were reconstructed with Phoenix datos| x 2.0 software obtaining a total of 1401 images at a resolution of 0.0365 mm (isometric voxels). The reconstruction of the raw data generated a 16-bit TIFF image stack comprising 980 slices (570 × 515 pixels). The original image stack was first uploaded into ImageJ 1.52a (Schneider et al., 2012) to remove beam hardening artifacts and increase the contrast between fossilized bone and rock matrix using the Brightness and Contrast tool (Image → Adjust → Brightness/Contrast). The adjusted images were then saved as an 8-bit TIFF image stack and uploaded into AvizoLite 2019.4 (Thermo Fischer Scientific 1995–2019) installed on a FUJITSU Celsius M740 workstation (processor: Intel Xeon CPU E5-2620 v4 2.10 GHz, RAM: 128 GB, graphics card: GeForce GTX 1050 Ti, hard drive: Samsung SSD 860 EVO 500 GB) operating on Windows 10 Pro (Microsoft 2019). Manual segmentation involved using the Lasso and Magic Wand tools. Because of extensive bone fusion, it was not possible to determine the position of sutures between: (1) the maxillae and the zygomatic bones; (2) the orbital portions of the frontals, the presphenoid, the orbitosphenoids, the alisphenoids, the pterygoids and the basisphenoid; and (3) the interparietal and supraoccipital. As a result, these bones were segmented not as individual elements, but as bone complexes, and the external sutures between them were inferred from observations of the external and internal surfaces of the 3D models, as well as from comparisons with additional specimens of *Palaeolagus* and extant lagomorphs. 3D models of individual bones and bone complexes were generated using the Unconstrained Smoothing option (smoothing extent = 2.5). Images of the 3D models were created using the Snapshot tool and compiled into figures using Adobe Photoshop Elements (Adobe 2020). The 3D models of FMNH PM9476 and digitally separated bones are available from the Dryad Digital Repository[1] (Fostowicz-Frelik and Wolniewicz, 2021).

[1]https://doi.org/10.5061/dryad.crjdfn338

FIGURE 1 | Skull of *Palaeolagus haydeni* (FMNH PM9476) from the early Oligocene of Nebraska in **(A)** anterior, **(B)** posterior, **(C)** dorsal, **(D)** ventral, and **(E)** right lateral views. Life reconstruction **(F)** of the head of *Palaeolagus* drawn by A. Kapuścińska. Scale bar = 10 mm.

Anatomical Terminology

The cranial anatomy of *P. haydeni* was described with reference to three previously published, comprehensive and well-illustrated accounts of extant lagomorph cranial anatomy: two historical descriptions of *Oryctolagus cuniculus* by Krause (1884) and Craigie (1948), and a more recent, comparative description of *Ochotona princeps* and *Romerolagus diazi* (Wible, 2007). The description of the cranial anatomy of the dog by Evans and de Lahunta (2013), a widely cited source for mammal anatomical nomenclature, was used as an additional reference. Because some of the anatomical structures were given markedly different names in all four studies (see **Supplementary Table 1**), for our description we decided to use the anatomical terms that were: (1) derived from English, rather than Latin [e.g., 'nasoturbinate crest' (Evans and de Lahunta, 2013) rather than 'crista nasalis' (Krause, 1884)]; (2) the least descriptive [e.g., ethmoidal fossa (Evans and de Lahunta, 2013) rather than 'small pocket open posteriorly' (Wible, 2007)]; and (3) anatomically most accurate [e.g., 'apex of premaxillary process of nasal' (this work) rather than 'triangular process of nasal' (Wible, 2007)]. We also avoided phrases taken from common language [e.g., 'nasoturbinate crest' rather than 'nasoturbinal scroll' (Craigie, 1948)]. In addition, Wible and Shelley (2020) were consulted for nomenclature on the anatomy of the petrosal.

OSTEOLOGICAL DESCRIPTION

Nasal

The paired nasals form the dorsal surface of the rostrum and the roof of the nasal cavity. Their anterior margins also contribute to the dorsal margin of the external nasal aperture. In most specimens, including FMNH PM9476, only the posterior parts of the nasals are preserved, whereas their anterior portions are abraded due to their overall fragility (**Figures 3A–C,E**, **4A–E**). However, the complete nasals can be observed in AMNH FM143956 (**Figures 2A–C**). Their general morphology does not depart from the description of Wood (1940, p. 279). Also, the anterior tips of the bones, not connected to the premaxillae, slightly narrow mediolaterally and protrude anterior to the incisors, overhanging the external nasal aperture.

The nasal is a dorsoventrally flattened bone that is much longer anteroposteriorly than it is wide mediolaterally. It forms a premaxillary process, laterally, and a frontal process, posteriorly.

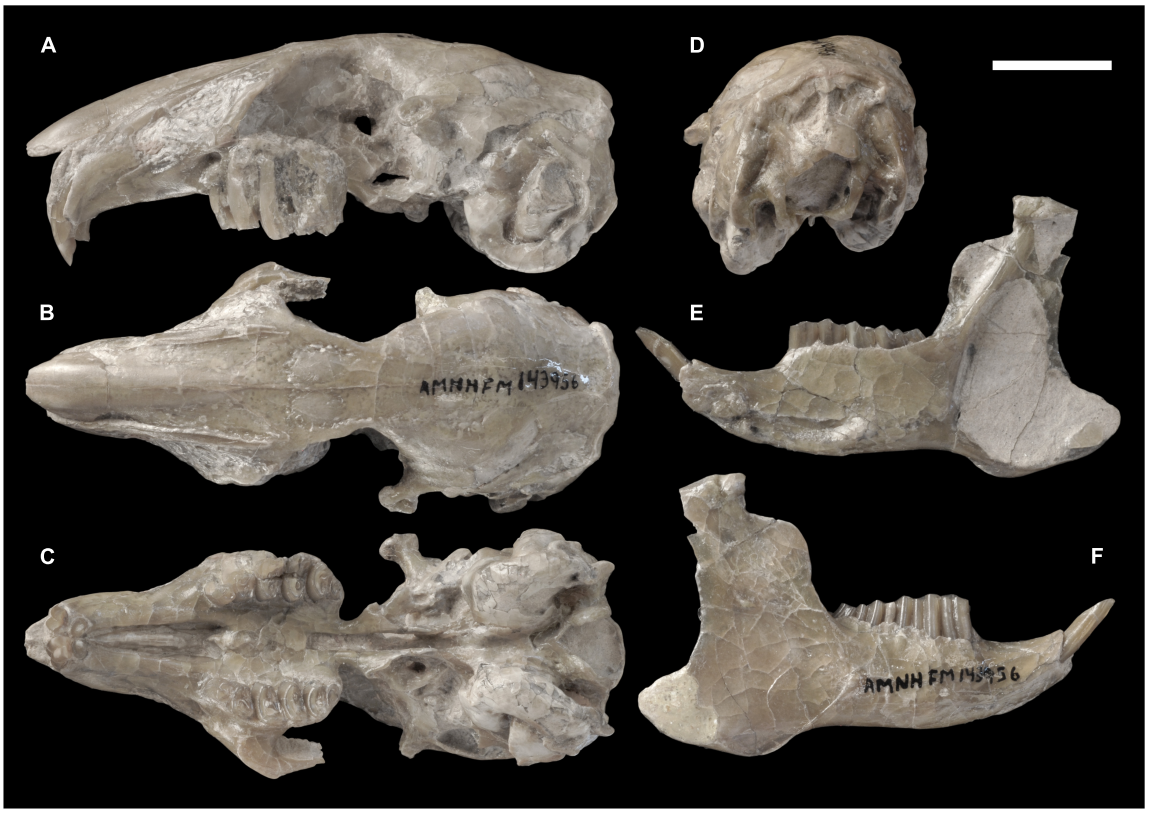

FIGURE 2 | Skull of *Palaeolagus haydeni* (AMNH FM143956) from the early Oligocene of Wyoming in **(A)** left lateral, **(B)** dorsal, **(C)** ventral, and **(D)** posterior views. Mandible of the same specimen in **(E)** medial and **(F)** lateral views. Note the well-preserved nasal region and the completely preserved mandible. Scale bar = 10 mm.

The mediolateral width of the nasal increases posteriorly along its anteroposterior length, until the nasal attains its greatest mediolateral width at the base of the frontal process. This is similar to the condition present in extant leporids, but differs from *Ochotona*, in which the mediolateral width of the nasal decreases posteriorly or remains approximately constant throughout its entire anteroposterior length (Wible, 2007, char. 1; Fostowicz-Frelik et al., 2010). The dorsal surfaces of the preserved portions of the nasals in FMNH PM9476 are slightly concave throughout most of their anteroposterior length, but their orientation becomes sub-horizontal at the base of the frontal process. At the lateral border of the dorsal surface of each nasal a field of neurovascular foramina is present, arranged along the nasal process of the premaxilla (AMNH FM143956; **Figure 2A**). Our observations stand in opposition to those of Wood (1940, p. 279), who stated that *Palaeolagus* does not have any nutritive foramina located on the nasals, which are usually observed in extant leporids. Furthermore, Wood (1940, p. 279) considered it a primitive feature, similar to the state observed in *Ochotona*. According to our observations, the vascularization of the nasals was present in all studied *Palaeolagus* specimens that preserve the anterior nasals, although its extent was variable. It was similarly expressed in all skulls of *Lepus europaeus* consulted by us, as well as in the skulls of *Oryctolagus cuniculus*, *Sylvilagus aquaticus*, and *S. floridanus*, but absent in all studied specimens of *Ochotona* (see **Supplementary Material**). Thus, this character in *Palaeolagus* shows similarity to leporids (not ochotonids), and the variability in the extent of this character in *P. haydeni* is comparable to the intraspecific variability in *L. europaeus* or *O. cuniculus*.

The ventral surface of the nasal bears a longitudinal nasoturbinate (ethmoidal) crest, which contacts the nasoturbinate and extends posteriorly just anterior to the base of the frontal process. The nasoturbinate crest separates the posterior portion of the ventral surface of the nasal into two concave areas: the medially located dorsal nasal meatus and the laterally located roof of the ethmoidal fossa. The ethmoidal fossa spans above the dorsal surface of the lateral part of the ethmoid labyrinth and is also bordered anteriorly by an anteriorly convex transverse septum, and laterally by the premaxillary process of the nasal. The ethmoidal fossa in *P. haydeni* is relatively shallow dorsoventrally, a condition similar to that in *Ochotona* (*O. dauurica*; ISEZ M/1674/60), but in marked contrast to *Oryctolagus cuniculus*, in which the ethmoidal fossa is greatly expanded dorsoventrally and mediolaterally and forms the 'marsupium nasale' (Krause, 1884).

The premaxillary process of the nasal is a vertically oriented, mediolaterally flattened and slightly laterally convex sheet of bone. Its dorsoventral height is greatest at approximately its anteroposterior mid-length, where the premaxillary process contacts the anterior wall of the ethmoidal fossa and forms

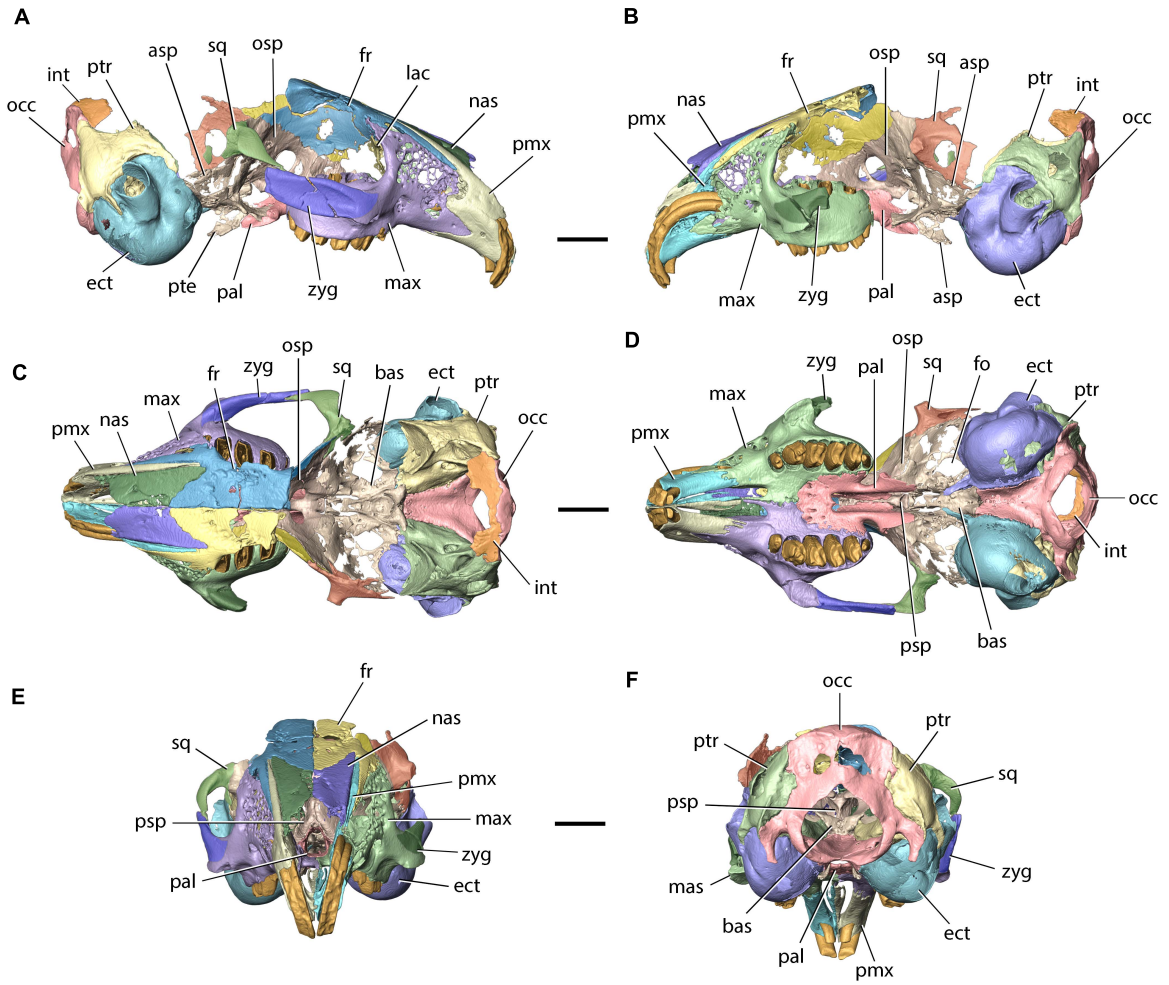

FIGURE 3 | Model of the cranium of *Palaeolagus haydeni* (FMNH PM9476) in **(A)** left lateral, **(B)** right lateral, **(C)** dorsal, **(D)** ventral, **(E)** anterior, and **(F)** posterior views. asp, alisphenoid; bas, basisphenoid; ect, ectotympanic; fo, foramen ovale; fr, frontal; int, interparietal; lac, lacrimal; mas, masseteric spine; max, maxilla; nas, nasal; occ, occipital; osp, orbitosphenoid; pal, palatine; pmx, premaxilla; psp, presphenoid; pte, pterygoid; ptr, petrosal; sq, squamosal; zyg, zygomatic. Scale bars = 10 mm.

a sharp apex in lateral view. A similar, sharp apex of the premaxillary process is also present in *Ochotona* (*O. dauurica*; ISEZ M/1674/60). Wible (2007, p. 216) also recognized the presence of a sharp apex formed by the nasal in *Ochotona*, but mistook it as part of the nasoturbinate crest. The dorsoventral height of the premaxillary process decreases both anteriorly and posteriorly. The lateral surface of the premaxillary process contacts the medial surface of the nasal process of the premaxilla throughout its entire anteroposterior length.

Posteriorly, the nasal produces a frontal process, which tapers into a sharp apex, posterolaterally, and overlaps a dedicated facet on the anterior portion of the frontal. The posteromedial margins of the frontal processes form a V-shaped suture with the anterolateral margins of the nasal processes of the frontals, a condition similar to that present in leporids, but different from *Ochotona*, in which the frontal processes are rounded posteriorly (Wood, 1940; Wible, 2007, char. 1; Fostowicz-Frelik et al., 2010). The medial margins of both nasals form a straight internasal suture extending along the dorsal midline of the skull, and a nasoethmoidal suture with the dorsal margin of the nasal septum, ventrally.

Premaxilla

The paired premaxillae form the anterolateral portions of the rostrum, contribute to the anterior part of the palate and carry both pairs of upper incisors (**Figures 3**, **4F–J**). In FMNH PM9476, the right premaxilla is well preserved, with the exception of its anterior surface, which is slightly abraded, whereas the right premaxilla is extensively damaged, anteriorly. The premaxilla can be divided into a corpus (body) and three processes: a nasal process, a palatine process, and a maxillary process.

The premaxillary corpus bears the alveoli for both pairs of upper incisors. The anterior openings of both alveoli are located anteroventrally. The alveolus for the anterior upper incisor (nominally dI2) is proportionally larger and located more anteriorly and dorsally relative to the alveolus for the

posterior upper incisor (I3). Both alveoli are dorsally curved and extend posteriorly along the entire anteroposterior length of the premaxillary corpus; the dI2 alveolus forms a posterior opening and continues inside the corpus of the maxilla, whereas the I3 alveolus is contained entirely within the body of the premaxilla and extends posteriorly to the base of the maxillary process. The position of both incisors on the lateral surface of the corpus is indicated by the presence of distinct alveolar juga, with the jugum for dI2 being much more prominent. The lateral surface of the premaxillary corpus bears several minuscule neurovascular foramina, dorsally. In some specimens (e.g., USNM PAL 243590 or 2530-49) the dorsal foramina may be extended to a form of substantial fenestration, whereas foramina occurring more ventrally may become more frequent but maintain their minuscule size. The anterodorsal margin of the corpus of the premaxilla, above the incisor alveoli, forms a thin erect lamella confluent with the base of the nasal process. It arises toward the nasals, participating in the formation of the lateral wall of the nasal cavity. Anteriorly, the margin of the lamella is slightly indented (concave) but this 'concavity' does not extend posteriorly beyond the external exposure of dI2. Wood (1940, p. 282) referred to the structure described here as a 'notch' between the nasals and the premaxilla. He also noted that the extent of this concavity and the height of the vertical lamella differentiated *P. haydeni* from extant leporids, which he considered to possess a much more extensive concavity, extending further posteriorly. Furthermore, Wood (1940) stated that this lack of a well-developed 'notch' in *Palaeolagus* resembles the condition found in ochotonids (namely, extant *Ochotona*), and perceived it as a primitive feature. The observations made by Wood (1940) generally hold true; all specimens of *Palaeolagus* studied by us have indeed a very poorly developed 'notch' in which they are similar to *Ochotona* and *Prolagus* (Dawson, 1969). On the other hand, comparisons with a broad sample of extant lagomorphs indicate that this character is much more variable within Leporidae. Most genera have higher and well-developed vertical laminae and the anterior concavity (see Ge et al., 2015), which makes the external nasal aperture higher and the anterior part of the nasal cavity potentially more spacious. The exception is *Romerolagus diazi*, which has the 'notch' very poorly expressed (Wible, 2007) and is similar in this respect to *Ochotona* (Fostowicz-Frelik et al., 2010).

Posterolaterally, the premaxillary corpus forms a triangularly incised suture with the anterior prongs formed by the corpus of the maxilla, with the facet for the dorsal prong exhibiting a small degree of fenestration. The medial surface of the premaxillary corpus contacts the maxilloturbinal, posteriorly, and bears a deep, dorsally curved fossa, which separates the upper incisors and forms the premaxillary portion of the nasolacrimal canal (see **Figure 5E**; Frahnert, 1999; Wible, 2007, char. 11). Anteromedially, the body of the premaxilla forms a mediolaterally compressed vertical plate, which bears a series of anteroposteriorly elongate ridges and troughs. These interlock tightly with ridges and troughs located on the contralateral premaxilla and form the anterior portion of the interpremaxillary suture. As a result, the interpremaxillary suture forms shallow interdigitations in anterior view (**Figure 3E**), whereas it is straight in palatal view (**Figure 3D**). The anterior margins of the premaxillary corpora form the ventral margin of the external nasal aperture. Their ventromedial margins form the anterolateral margins of the incisive foramina and their posteroventral surfaces contribute to the anterior portions of the diastemata.

The nasal process of the premaxilla [=frontal process of Krause (1884) and Craigie (1948); =posterodorsal process of Wible (2007)] extends posterodorsally from the corpus. It is anteroposteriorly elongate, dorsally curved and sub-triangular in cross-section, forming a sharp, ventral margin. In *P. haydeni*, the nasal process of the premaxilla terminates just anterior to the apex of the frontal process of the nasal, resembling the condition in leporids, but differs from ochotonids, in which the nasal process terminates well anterior to the posterior margin of the nasal (Wood, 1940; Wible, 2007). The medial surface of the nasal process contacts the lateral surface of the premaxillary process of the nasal along its entire anteroposterior length. The ventrolateral surface of the nasal process contacts the maxillary process of the frontal, which separates the premaxilla from the maxilla in dorsal view.

The palatine process of the premaxilla extends posteriorly from the anteromedial surface of the premaxillary corpus. It is anteroposteriorly elongate, mediolaterally narrow and terminates in a blunt apex, posteriorly. It attains its greatest mediolateral width at approximately the anterior three-fourths of its anteroposterior length. In *P. haydeni*, the base of the palatine process of the premaxilla is located at the level of dI2, which differs markedly from the condition in extant leporids and ochotonids, in which the base of the palatine process is located well posterior to I3 (Troxell, 1921; Wood, 1940; Wible, 2007). The palatine process produces a dorsoventrally short, horizontal medial wall and a proportionally taller, laterally convex lateral wall. The dorsal surface of the palatine process is concave and forms a dorsal sulcus [=palatine semisulcus of Krause (1884); =palatine groove of Craigie (1948)], which receives the ventral portion of the cartilaginous internasal septum. Posterolaterally, the palatine process is perforated by an anteroposteriorly elongate foramen, which in extant leporids is filled with a thin layer of connective tissue and does likely not transmit any nerves or vessels (*O. cuniculus*, ZPAL comparative collection). The medial surfaces of both contralateral palatine processes contact each other and form a straight posterior portion of the interpremaxillary suture. The palatine processes separate the anterior portions of both incisive foramina along the ventral cranial midline. The incisive foramen is anteroposteriorly elongate and mediolaterally narrow, anteriorly, but becomes mediolaterally broad posterior to the premaxillary–maxillary suture. It is similar in outline to the incisive foramen in extant leporids, but differs markedly from the bipartite incisive foramen of extant ochotonids (Wible, 2007, char. 32). The incisive foramen is bordered by the premaxilla, anteromedially (palatine process) and anterolaterally (corpus), and by the maxilla (palatine process), posteriorly.

The maxillary process of the premaxilla originates from the posteroventral portion of the premaxillary corpus. It is anteroposteriorly much shorter than the nasal process,

dorsoventrally compressed, and tapers posteriorly into a broad apex. The maxillary process bears several longitudinal ridges, separated by troughs, both dorsally and ventrally. The posterior portion of the maxillary process is entirely encompassed by the anteroventral portion of the maxillary corpus, with the two bones forming an interdigitating premaxillary-maxillary suture in ventral view. The maxillary process of the premaxilla differentiates *P. haydeni* from extant leporids and ochotonids, in which the premaxilla does not form a distinct maxillary process (Wood, 1940; Wible, 2007).

Frontal

The paired frontals occupy the anterior part of the skull roof and form the posterior roof of the nasal cavity. They also form the dorsal portions of the orbital walls. In FMNH PM9476, both frontals are well preserved anteriorly, but the supraorbital processes, as well as the posterior parts of the frontal squamae, are missing (**Figures 3A–C**, **4K–L**) [compare with Wood, 1940, pl. XXXIV, Figures 2–2a].

The frontal can be divided into a frontal squama and an orbital portion, which are separated from each other by the supraorbital rim (infraorbital margin). The frontal squama forms the anterior part of the skull roof and the posterior portion of the dorsal wall of the nasal cavity. It is dorsoventrally compressed and has an approximately flat dorsal surface, resembling in this respect the frontal of extant ochotonids, but it differs from leporids, in which the part posterior to the supraorbital processes is markedly convex (Wood, 1940; Wible, 2007). This feature is immediately related to the degree of the skull arching, which is much stronger in leporids (Wible, 2007; Fostowicz-Frelik et al., 2010; Fostowicz-Frelik and Meng, 2013) and results in the rounded roof of the braincase in this group. Anteromedially, the frontal squama in *Palaeolagus* forms a nasal process, which is approximately triangular in outline and tapers anteriorly into a broad apex. This differs from the condition present in most leporids, in which the nasal process terminates with a pointed nasal spine (Krause, 1884; Wood, 1940; Craigie, 1948; Wible, 2007), although in some speciose genera (e.g., *Lepus*) the exact morphology of the nasal spine of the frontal may vary from more to less pointed (Koby, 1959). Anterolaterally, the frontal squama forms an anteroposteriorly elongate and laterally curved maxillary process, which is approximately triangular in cross-section and tapers anteriorly into a sharp apex. The maxillary process contacts the nasal process of the premaxilla, medially, and the dorsal margin of the maxillary corpus, ventrolaterally, separating both bones from each other in dorsal view. Posterolaterally, the maxillary process produces an anterolateral prong, which has a rugose posterolateral surface and contacts the dorsomedial surface of the frontal process of the maxilla. The frontal squama also forms a dorsoventrally thin facet for the reception of the frontal process of the nasal, which is much thinner than the remainder of the bone and spans between the lateral margin of the nasal process and the medial margin of the maxillary process. The dorsal surface of the frontal squama is pitted, although not as extensively as in *Romerolagus* or *Sylvilagus* (Wood, 1940; Wible, 2007), and differentiates *Palaeolagus* from extant ochotonids, in which the dorsal surface of the frontal is smooth (Wible, 2007, char. 6). The pitting of the frontals in *Palaeolagus* clearly delineates the position of the olfactory bulbs (see **Figures 4K–L**).

In ventral view, the anterior part of the frontal squama forms two concave surfaces (**Figure 4L**). The medial surface forms the posterior extension of the dorsal nasal meatus, whereas the lateral surface forms an articular surface for the ethmoid. Posteriorly, the ventral surface of the frontal squama forms well-developed fossae for the olfactory bulbs, anteriorly, and the anterior portion of the cerebral fossa, posteriorly (compare with López-Torres et al., 2020). Both fossae are separated from each other by a well-developed transverse ridge, which extends onto the medial wall of the orbital portion of the frontal. The frontal squamae form an approximately straight suture along the dorsal cranial midline.

The orbital portion of the frontal is a medially concave, mediolaterally compressed sheet of bone which forms the dorsal part of the orbital wall. The lateral surface of the orbital portion bears a single ethmoidal foramen, which extends into an ethmoidal sulcus, posteroventrally. Anteriorly, the orbital portion of the frontal abuts against the posterior surface of the frontal process of the maxilla. The orbital portion of the frontal also contacts (from anterior to posterior): the lacrimal, the orbitosphenoid, the squamosal, and the parietal.

Maxilla

The paired maxillae form the posterolateral portions of the rostrum and the central portion of the palate. They also bear all the cheek teeth, contribute to the anterior orbital margin and comprise the ventral and ventromedial portions of the orbital walls (**Figures 3A–E**, **5**). In FMNH PM9476, both maxillae are well preserved, except for the anterior portion of the left maxillary corpus, which is extensively damaged.

The maxilla can be divided into a corpus (body) and four processes: a frontal process, an alveolar process, a palatine process, and a zygomatic process. The corpus of the maxilla is approximately trihedral in shape and produces two prongs, anteriorly, which insert into dedicated facets on the posterolateral surface of the corpus of the premaxilla. The dorsal prong has a rounded anterior margin (contra Wood, 1940, pl. XXXIV, Figure 2), whereas the ventral prong is anteroposteriorly longer than the dorsal one and tapers anteriorly into a pointed apex. The presence of two anterior maxillary prongs was said to differentiate *P. haydeni* from extant leporids and ochotonids (Wood, 1940), but whereas the maxilla does not bifurcate anteriorly in leporids, it does produce two prongs in some ochotonids, although the ventral prong is not as well developed as in *P. haydeni* (Wible, 2007; Fostowicz-Frelik et al., 2010). The anteroventral portion of the maxillary corpus also bears a dorsoventrally narrow fissure, bordered by a series of anteroposteriorly elongate ridges and troughs, which interlock tightly with a series of corresponding structures located on the dorsal and ventral surfaces of the maxillary process of the premaxilla and produce an interdigitating premaxillary-maxillary suture in ventral view. The posterior portion of the maxillary corpus [=orbital process of maxilla of Craigie (1948)], is thickened and concave, and forms the anterior orbital margin. In addition, it forms the lateral border of the 'pars orbitalis' of the maxillary fenestra (Wible, 2007, char. 9).

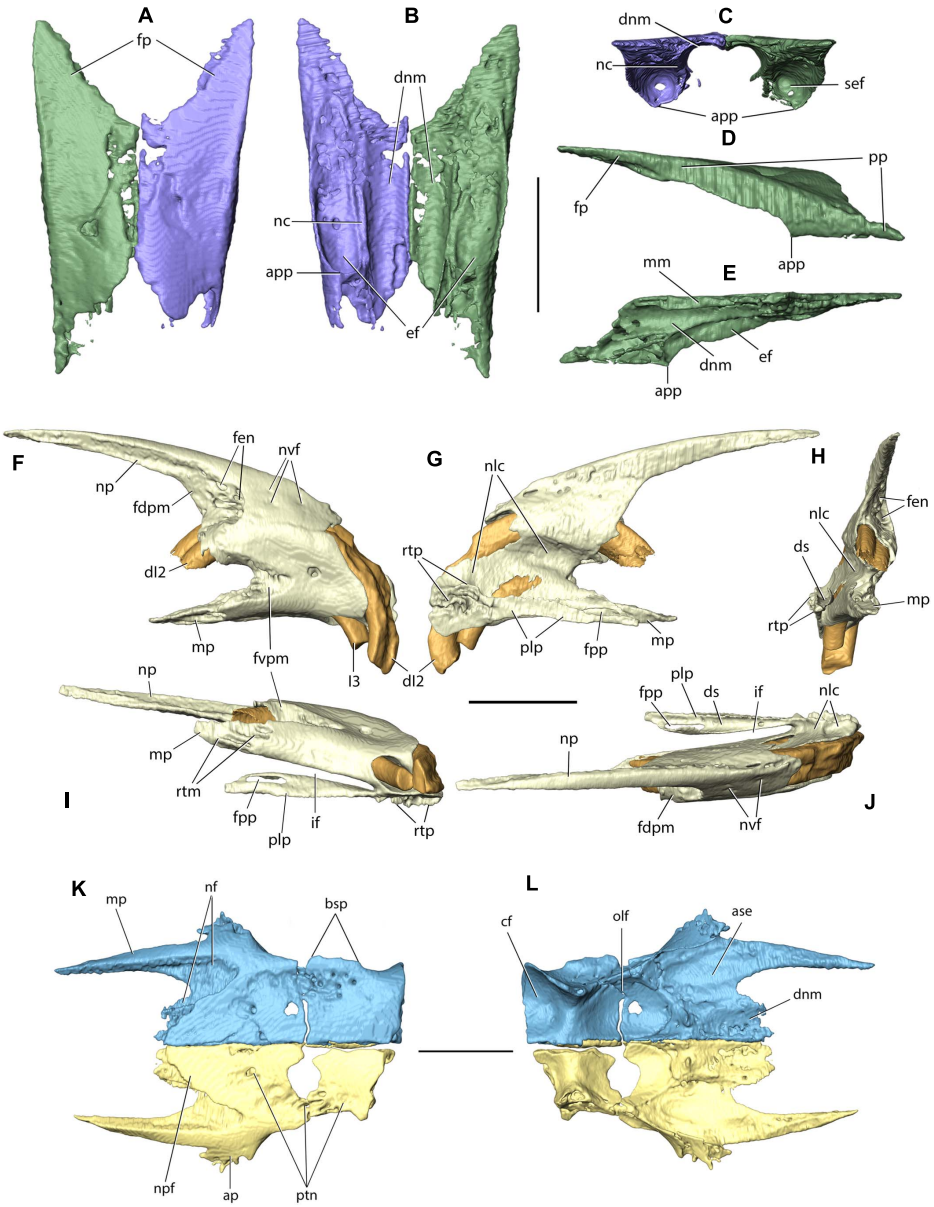

FIGURE 4 | Nasal, premaxilla (incisive), and frontal of *Palaeolagus haydeni* (FMNH PM9476). Posterior portions of the left (purple) and right (green) nasals in **(A)** dorsal, **(B)** ventral, and **(C)** posterior views. Right nasal in **(D)** lateral and **(E)** medial views. Right premaxilla in **(F)** lateral, **(G)** medial, **(H)** posterior, **(I)** ventral, and **(J)** dorsal views. Left (yellow) and right (blue) frontals in **(K)** dorsal and **(L)** ventral views (orbital portions removed). ap, anterior prong; app, apex of premaxillary process; ase, articular surface for ethmoid; bsp, base of supraorbital process (broken); cf, cerebral fossa; dnm, dorsal nasal meatus; ds, dorsal sulcus; ef, ethmoidal fossa; fdpm, facet for dorsal prong of maxilla; fen, fenestration; fp, frontal process; fpp, foramen in palatine process; fvpm, facet for ventral prong of maxilla; dl2, anterior upper incisor; l3, posterior upper incisor; if, incisive foramen; mm, medial margin; mp, maxillary process; nc, nasoturbinate (ethmoidal) crest; nf, nasal facet; nlc, nasolacrimal canal; np, nasal process of premaxilla; npf, nasal process of frontal; nvf, neurovascular foramen; olf, olfactory bulb fossa; plp, palatine process; pp, premaxillary process; ptn, pitting; rtm, ridges and troughs for maxilla; rtp, ridges and throughs for contralateral premaxilla; sef, anterior septum of ethmoidal fossa. Scale bars = 5 mm.

The lateral wall of the maxillary corpus is perforated by a lacework of small openings, similar to that present in extant leporids, but different from ochotonids, in which the lateral wall of the maxillary corpus produces a large, single opening ('pars facialis' of the maxillary fenestra; Wible, 2007, char. 8). Posteroventrally, the lateral surface of the maxillary corpus bears a large, sub-circular infraorbital foramen for the passage of the infraorbital nerve (branch of the maxillary nerve [CN V_2]) and associated blood vessels. Anteriorly, the infraorbital foramen opens into the maxillary fossa located on the external surface of the bone, whereas posterodorsally it extends into the infraorbital canal located on the medial surface of the lateral wall

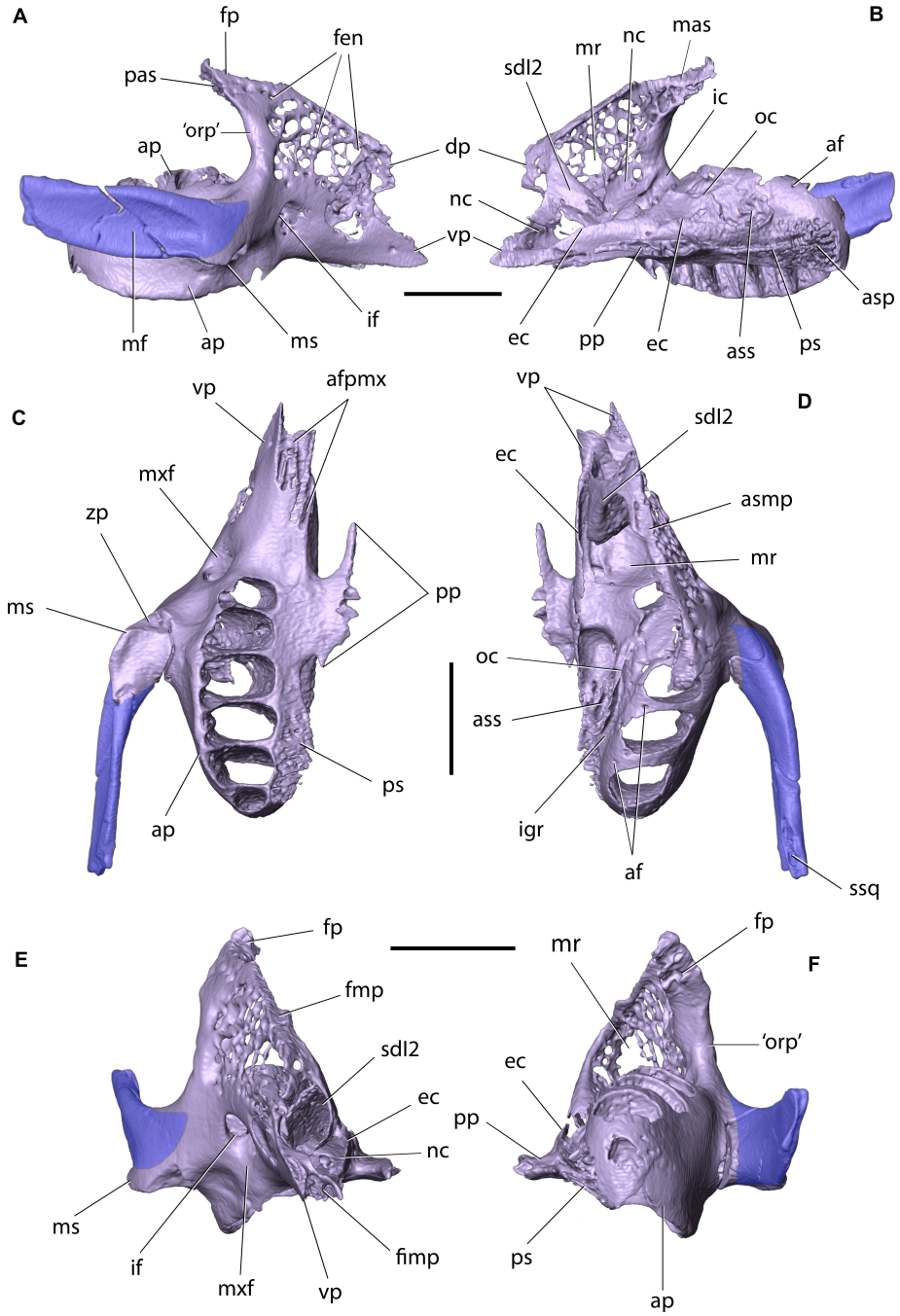

FIGURE 5 | Right maxilla and zygomatic of *Palaeolagus haydeni* (FMNH PM9476) in: **(A)** lateral, **(B)** medial, **(C)** ventral, **(D)** dorsal, **(E)** anterior, and **(F)** posterior views. Dentition removed for clarity. af, alveolar foramen; afpmx, articular facet for maxillary process of premaxilla; ap, alveolar process; asp, articular surface for horizontal lamina of palatine; ass, articular surface for ethmoidal process of presphenoid; dp, dorsal prong; ec, ethmoidal crest; fen, fenestrations; fimp, fissure for maxillary process of premaxilla; fmp, facet for maxillary process of frontal; fp, frontal process; ic, infraorbital canal; if, infraorbital foramen; igr, infraorbital groove; mas, dorsomedial articular surface of frontal process; mf, masseteric fossa; mr, maxillary recess (sinus); ms, masseteric spine; mxf, maxillary fossa; nc, nasolacrimal canal; oc, orbital crest; 'orp', 'orbital process' (posterior part of the corpus); pas, posterior articular surface of frontal process; pp, palatine process; ps, palatine shelf; sdl2, sheath for dl2; ssq, sulcus for zygomatic process of squamosal; vp, ventral prong; zp, zygomatic process. Scale bars = 5 mm.

of the premaxillary corpus. Anterodorsal to the infraorbital canal, the medial surface of the lateral wall of the maxillary corpus forms the maxillary portion of the nasolacrimal canal, which extends anteroventrally from the level of the 'pars orbitalis' of the maxillary fenestra, and attains a sub-sagittal orientation at the level of the posterior end of dI2, as in extant leporids (**Figure 6E**;

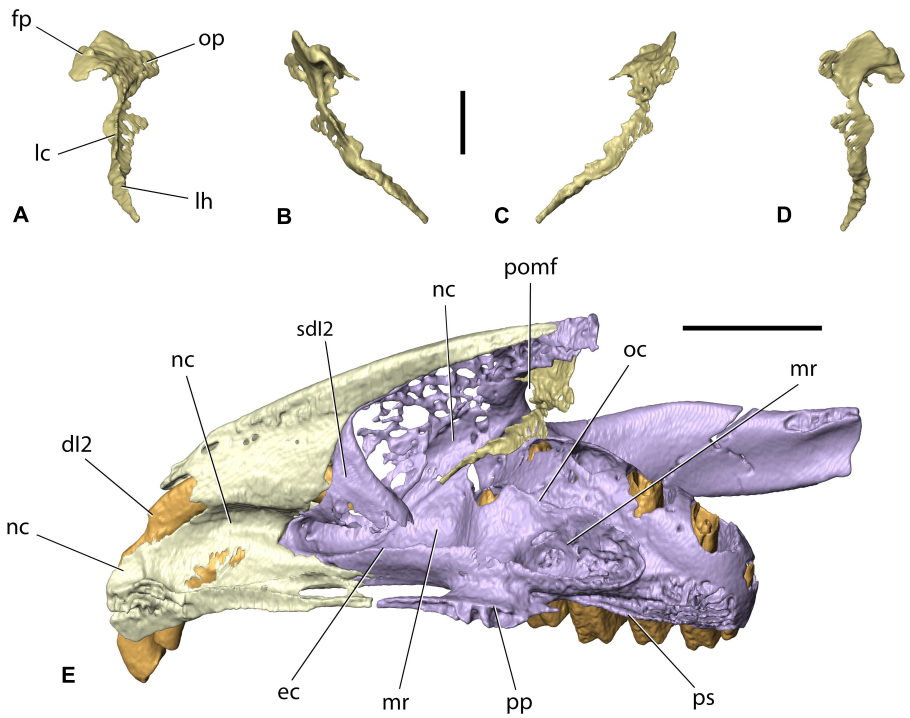

FIGURE 6 | Right lacrimal of *Palaeolagus haydeni* (FMNH PM9476) in **(A)** anterior, **(B)** lateral, **(C)** medial, and **(D)** posterior views. Note the incompleteness of the facial process and orbital plate. **(E)** Right premaxilla (light yellow), lacrimal (gold) and maxilla-zygomatic complex (light purple) in dorsomedial view, highlighting the position of the nasolacrimal canal. Teeth marked with orange. fp, facial process; dI2, anterior upper incisor; lc, lacrimal crest; lh, lacrimal hamulus; mr, maxillary recess (sinus); nc, nasolacrimal canal; oc, orbital crest; op, orbital plate; pomf, 'pars orbitalis' of maxillary fenestra; pp, palatine process; ps, palatine shelf; sdI2, sheath for dI2. Scale bar in **(A–D)** = 2 mm; scale bar in **(E)** = 5 mm.

Frahnert, 1999; Wible, 2007, char. 11). Dorsally, the maxillary corpus bears a longitudinal facet for the reception of the maxillary process of the frontal. The posterior surface of the maxillary corpus abuts against the facial process of the lacrimal, dorsally. The ventral surface of the maxillary corpus forms the posterior portion of the diastema, and its ventromedial margin forms the posterolateral margin of the incisive foramen.

Anteromedially, the maxillary corpus forms a sheath for the posterior portion of dI2. Ventromedially, it bears a longitudinal, dorsoventrally low ethmoidal crest, which contacts the ethmoid, anterolaterally and dorsally, and the palatine, posteromedially. Adjacent to the alveolar process, the body of the maxilla forms an orbital crest, which contacts the orbitosphenoid, medially. The external exposure of the crest is anteroposteriorly much more elongate than that visible in lagomorphs and ochotonids (Wible, 2007, char. 14), but is similar to the anteroposteriorly elongate orbital crest (=process) visible in the medial orbital wall in *Rhombomylus turpanensis* (Meng et al., 2003, Figure 31). Several recesses are present within the maxillary corpus, which collectively form the maxillary recess (sinus). Posterodorsally, the maxillary corpus produces a frontal process (=sphenoorbital process of Craigie, 1948). The dorsomedial and posterior surfaces of the frontal process are rugose and abut against corresponding surfaces on the anterior prong of the maxillary process of the frontal, and the orbital portion of the frontal, respectively. The lateral wall of the frontal process is fenestrated and perforated by several small foramina.

The alveolar process carries the cheek teeth and is located posterolateral to the maxillary corpus. The alveolar process in *P. haydeni* represents a morphology somewhat intermediate between that in extant leporids and ochotonids, in that it is not as mediolaterally broad as in ochotonids, in which the process forms the ventral portion of the orbital wall, but it is also not as medially shifted as in leporids. The alveolar process is also relatively lower than in extant leporids, which is related to proportionally lower tooth crowns in *Palaeolagus*.

Posteriorly, the alveolar process in *P. haydeni* remains relatively broad mediolaterally and possesses a convex, posterior surface, resembling the alveolar process of *Ochotona*. In contrast, in extant leporids the mediolateral width of the alveolar process decreases posteriorly (Wood, 1940; Wible, 2007; Fostowicz-Frelik and Meng, 2013). The alveolar process bears six alveoli (P2–4 and M1–3). The alveolus for M1 is the largest and the size of the remaining alveoli decreases both anteriorly and posteriorly, with the M3 alveolus being the smallest. Several small alveolar foramina are present on the dorsal surface of the alveolar process. Medially, the alveolar process is separated from the orbital crest by a deep, oblique infraorbital groove for the infraorbital nerve and vessels (Fostowicz-Frelik and Meng, 2013). The infraorbital groove in *P. haydeni* resembles the deep groove present in leporids but differs markedly from the shallow groove present in

ochotonids (Fostowicz-Frelik and Meng, 2013). This character is related to the degree of mediolateral displacement of the alveolar process (see above). The infraorbital groove ends anteriorly at the infraorbital foramen, through which the infraorbital nerve and vessels pass onto the external surface of the maxilla (Fostowicz-Frelik and Meng, 2013). The pulp cavities of the cheek teeth are exposed on the dorsal surface of the alveolar process in FMNH PM9476, a feature which has been demonstrated to vary within *P. haydeni* (Wood, 1940) and is also present in most leporids, but has not been observed in ochotonids (Wible, 2007, char. 16). Posteroventromedially, the alveolar process forms a complex palatomaxillary suture with the perpendicular portion of the palatine, comprising of: (1) an anteroposteriorly elongate, slightly medially inclined palatine shelf, which inserts into a deep groove located in the lateral surface of the palatine, and (2) a series of anteroposteriorly elongate projections, which interlock tightly with corresponding projections located on the lateral surface of the perpendicular portion of the palatine.

The palatine process extends laterally from the ventral portion of the maxillary corpus and forms the anterior portion of the hard palate (palatine bridge). The palatine process is dorsoventrally flattened and produces a mediolaterally narrow spine, anteromedially, which ends with a blunt apex that almost contacts the apex of the palatine process of the premaxilla. As a result, the left and right incisive foramina are almost completely separated from each other along the ventral midline of the skull in *P. haydeni*, a condition similar to that present in leporids, but markedly different from the condition present in ochotonids, in which the palatine processes of the premaxilla and maxilla are well separated from each other (Wible, 2007, char. 32; Ge et al., 2015). Posterodorsally, the palatine process is overlapped by the horizontal portion of the palatine. Medially, each palatine process produces a series of prominent prongs which interlock tightly with the prongs present on the contralateral palatine process and form the intermaxillary suture. The lateral and posterior margins of the palatine process form the medial and posterior margins of the incisive foramen, respectively.

The zygomatic process of the maxilla extends laterally from the maxillary body, at the level of P2–P3. Anteroventrolaterally, it forms a well-developed masseteric spine, which served as the attachment for the ligament of the masseteric muscle, as in *O. cuniculus* (Craigie, 1948). Like in osteologically mature specimens of extant lagomorphs, the zygomatic process of *P. haydeni* is tightly co-ossified with the anterior portion of the zygomatic, so that the suture between both elements is usually not discernible (Craigie, 1948; Wible, 2007).

Lacrimal

The lacrimal lies apressed against the anterior wall of the orbit. It comprises an anteroposteriorly compressed orbital plate, a facial (lateral) process, and the lacrimal hamulus. In FMNH PM9476, only the right lacrimal is partially preserved (**Figures 3B**, **6A–D**). Its orbital plate and facial process are abraded to a large extent, whereas the lacrimal hamulus is well preserved. Wood (1940, p. 281) noted that the orbital plate of the lacrimal in *P. haydeni* was extensive, like in extant lagomorphs, and occupied much of the anteromedial orbital wall. However, the lacrimal in *P. haydeni* was not figured either by him or by earlier authors (see Troxell, 1921; Dice, 1933). Even though the orbital plate is not preserved in the right lacrimal in FMNH PM9476, its presence can be inferred from the presence of large openings in the anteromedial walls of both orbits, which resemble the openings visible in extant leporid specimens with disarticulated lacrimals (Wood, 1940; Wible, 2007). The lacrimal hamulus extends anteroventrally from the orbital plate and tapers into a pointed apex. Laterally, the hamulus forms the medial wall of the posterior portion of the nasolacrimal canal (**Figure 6E**). Dorsally, the hamulus produces a lacrimal crest, which extends along its entire anteroposterior length. The concave, lateral margin of the lacrimal forms the medial margin of the orbital portion ('pars orbitalis') of the maxillary fenestra (Wible, 2007). The orbital portion of the maxillary fenestra is a dorsoventrally tall and mediolaterally narrow opening, which is bordered medially by the posterior part of the maxillary corpus forming the anterior orbital rim. Ventrally, the orbital portion of the maxillary fenestra becomes confluent with the infraorbital and nasolacrimal canals.

Zygomatic (=Jugal)

The zygomatic comprises the anterior portion of the zygomatic arch and forms approximately the anterior two-thirds of the ventral margin of the orbit (**Figures 3A–D**, **5**). In FMNH PM9476, only a small portion of the left zygomatic, adjacent to the zygomatic process of the maxilla, is preserved. In contrast, the right zygomatic is almost completely preserved, with the exception of its posterior portion.

Anteriorly, the zygomatic is extensively fused with the zygomatic process of the maxilla, like in osteologically mature specimens of extant lagomorphs (Craigie, 1948; Wible, 2007). The zygomatic is mediolaterally and dorsoventrally broadest anteriorly. Its dorsoventral height gradually decreases posteriorly, whereas its mediolateral width decreases abruptly posterior to its anterior end and remains constant throughout the remainder of its anteroposterior length. Its dorsal margin is slightly thicker mediolaterally than its ventral margin, which forms a sharp crest. Both the lateral and medial surfaces of the zygomatic are concave, with the concavity on the lateral surface forming a prominent zygomatic fossa, which acted as an attachment site for the lateral masseter muscle. In contrast to extant leporids and ochotonids, the lateral surface of the zygomatic does not bear any neurovascular foramina (Krause, 1884; Wible, 2007, char. 20). The posterodorsal margin of the zygomatic bears a sulcus for the reception of the zygomatic process of the squamosal. The posterior portions of the zygomatic bones are not preserved in FMNH PM9476, but in more complete specimens of *P. haydeni* (Dice, 1933; Wood, 1940), the zygomatic forms a short, posterior process, similar to that present in the majority of extant leporids, but unlike the elongate posterior process in *R. diazi* and ochotonids (Wible, 2007, char. 21).

Palatine

The palatine comprises a single, unpaired element, located posterior to the maxillae along the ventral cranial midline (**Figures 3D**, **7**). The unpaired palatine arises as a result of the anterior fusion of paired, embryonic ossifications

(Insom et al., 1990). It forms the posterior portion of the hard palate (palatal bridge), the anteromedial walls of the pterygopalatine fossae and the lateral walls of the nasopharyngeal duct. In FMNH PM9476, the palatine is completely preserved, enabling a detailed description of its anatomy. Each hemipalatine is divided into a medial horizontal lamina (portion) and a lateral perpendicular lamina. The horizontal lamina forms approximately the posterior two-thirds of each half of the hard palate. It has a palatine (ventral) surface, a nasal (dorsal) surface, a convex anterior margin, and a concave posterior margin. The anterior margin, located at the level of the interalveolar septum separating P3 and P4, bears a groove that receives the posterior margin of the palatine process of the maxilla. The posterior margin bears a prominent nasal spine, medially. Anterolaterally, the palatine surface bears a large, sub-circular major palatine foramen. Posteromedially and posteriorly to the major palatine foramen, the palatine surface has two (right) and three (left) additional foramina – the accessory palatine foramina. The posteromedial accessory palatine foramina are small and are preceded anteriorly by anteroposteriorly elongated grooves, whereas the posterior accessory palatine foramina are larger and sub-circular in outline. The presence of a single major palatine foramen, enclosed entirely within the palatine in *P. haydeni*, resembles the condition present in numerous extant leporids, with the exception of *Pronolagus* and *Lepus*, in which the major palatine foramen is bordered anteriorly by the maxilla. In ochotonids, a single major palatine foramen cannot be recognized, but multiple small foramina occupy the anterolateral palatine surface, instead (Wible, 2007, char. 33). All palatine foramina form the ventral openings of palatine canals which perforate the horizontal lamina and open into the sphenopalatine canal.

The perpendicular lamina of the palatine extends dorsally from the lateral border of the horizontal lamina at an approximately right angle. The dorsal margins of both perpendicular laminae converge posteromedially, so that each perpendicular lamina forms a slightly concave lateral wall of the nasopharyngeal canal, medially, and an oblique wall of the pterygopalatine fossa, laterally. The dorsal margin of each perpendicular lamina bifurcates into a medial and lateral crest, which border a deep groove for the reception of the ethmoidal process of the presphenoid, anteriorly, and the presphenoid corpus, posteriorly. The posterodorsal margin of the perpendicular plate is concave and forms the anteromedial boundary of the superior orbital fissure. Anterolaterally, the perpendicular lamina forms an oblique crest, which abuts against the medial wall of the ethmoidal crest of the maxilla, laterally. Ventrolaterally, the perpendicular lamina forms a series of medially projecting shelves, grooves and protrusions, which tightly interlock with corresponding structures present on the medial surface of the alveolar process of the maxilla to form the palatomaxillary suture. Dorsolaterally, the perpendicular plate bears an oblique sphenopalatine canal, which connects the pterygopalatine fossa with the nasal cavity. The canal is bordered by the perpendicular lamina of the palatine, ventrally and medially, by the alveolar process of the maxilla, laterally, and by the ethmoidal process of the presphenoid, dorsally. Anteriorly, the sphenopalatine canal opens with the sphenopalatine foramen, which is bordered by the alveolar process of the maxilla, laterally, and the horizontal lamina of the palatine, medially, like in extant lagomorphs (Wible, 2007, char. 13; contra Asher et al., 2005, char. 133). Ventrally, the sphenopalatine canal is perforated by minute openings of palatine canals, which lead to the nasal surface of the horizontal lamina and open externally as accessory palatine foramina. Anteriorly, the sphenopalatine canal bifurcates into a large, anteroventral canal, which opens externally as the major palatine foramen, and an anteromedial groove, which leads into the dorsal opening of a canal which opens ventrally as one of the accessory palatine foramina. Posteroventrally, the perpendicular lamina produces a pyramidal (sphenoidal) process, which is separated from the main portion of the lamina by a concave surface. In dorsal or ventral view, this surface forms the palatine notch (incisure) (=posterior maxillary notch of Wahlert, 1974) that transmits the minor palatine nerve and associated vessels. The deep, concave palatine notch in *P. haydeni* resembles the condition present in extant ochotonids, but differs markedly from extant leoprids, in which the palatine notch forms a pointed apex (Wible, 2007). The posterior margin of the pyramidal process contacts the medial lamina of the pterygoid and forms the anterior portion of the entopterygoid crest. Posterolaterally, the pyramidal process bears a deep fissure, which receives the anterior portion of the lateral lamina of the pterygoid. The posterior part of the dorsolateral surface of the pyramidal process contributes to the anteromedial wall of the pterygoid fossa.

Presphenoid

The presphenoid is an unpaired element, which occupies the anterior portion of the cranial floor and contributes to the ventral portions of the orbital walls (**Figures 3A,B**, **8**). In FMNH PM9476, the presphenoid is almost complete, except for the dorsal portion of the right ethmoidal process, which is not preserved. The presphenoid comprises a median corpus (body) and paired ethmoidal processes. The corpus of the presphenoid, which has the form of an anteroposteriorly elongate cylinder, is located along the ventral midline of the skull, anterior to the basisphenoid and posterior to the ethmoid. Posteroventrally, the presphenoid corpus forms a concave facet, which is approximately hexagonal in outline, and forms the anterior boundary of the intersphenoidal synchondrosis. Ventrally, the presphenoid corpus bears a median ridge, bordered laterally by articular surfaces for the perpendicular portions of the palatine. Anterolaterally, the presphenoid forms paired ethmoidal processes. Each ethmoidal process comprises a dorsoventrally tall lateral wall and a concave ventral wall. The lateral wall abuts against the orbital crest of the maxilla, anterolaterally. The ventral wall forms a sharp, ventral crest, which inserts into an anteroposteriorly elongate groove located on the perpendicular lamina of the palatine. The anteroventral corner of the ethmoidal process is encompassed by the maxillary corpus. The anteriorly open space bordered laterally and ventrally by both ethmoidal processes comprises the sphenoidal fossa (sinus). Posterior to the ethmoidal processes, the presphenoid forms the sphenoidal yoke (jugum sphenoidale), which forms the ventral surface of the anterior cranial fossa. Posteroventral to

the optic canal, the presphenoid forms the sulcus chiasmatis for the optic chiasma.

Orbitosphenoid

The orbitosphenoids (lesser wings) extend posterodorsally from the presphenoid corpus. Posterior to the sphenoidal yoke, the medial margins of the orbitosphenoids bear notches which form the lateral margins of a single optic canal. Posteroventrally to the optic canal, the internal (medial) surfaces of the orbitosphenoids form the sulcus chiasmatis for the optic chiasma. The external (lateral) surfaces of the orbitosphenoids contribute to the posterior portions of the orbital walls, whereas their internal (medial) surfaces form a considerable portion of the anterolateral surface of the middle cranial fossa (**Figures 3A,B**, **8**). The orbitosphenoid also forms the posteromedial boundary of the superior orbital fissure. The orbitosphenoid contacts the orbital portions of the frontal, anterodorsally, the alisphenoid, posteriorly, and fuses with the squamosal, posterolaterally.

Basisphenoid

The basisphenoid, the alisphenoids and the pterygoids are well preserved in FMNH PM9476, because of limited preparation performed on the external surfaces of the basis cranii (**Figure 1D**). This is in stark contrast to most other cranial specimens of *P. haydeni*, in which the basisphenoid, alisphenoids and pterygoids are damaged or not preserved (Wood, 1940, p. 285).

The basisphenoid occupies the base of the middle cranial fossa and is located anterior to the basioccipital and posterior to the presphenoid. Its dorsal surface forms a central hypophyseal fossa, bordered posteriorly by the dorsum sellae, which is elevated considerably beyond the dorsal surface of the middle cranial fossa. Anterolaterally, the dorsum sellae produces a pair of prominent posterior clinoid processes, which, together with the hypophyseal fossa and the dorsum sellae, comprise the sella turcica. Lateral to the hypophyseal fossa, the basisphenoid bears a pair of carotid sulci, which mark the passage of the internal carotid arteries, entering the middle cranial fossa though the carotid canal enclosed between the petrosal and ectotympanic bones. The anterior portion of the basisphenoid is mediolaterally narrow and anteroposteriorly elongate and is bordered laterally by sphenopalatine vacuities, which become confluent with the superior orbital fissures, anteriorly. The sphenopalatine vacuity transmits the nerve of the pterygoid canal, which occupies a weakly demarcated groove located posterior to the sphenopalatine vacuity on the ventral surface of the basisphenoid (visible on the left side of FMNH PM9476). *P. haydeni* shares the presence of anteroposteriorly elongate, medially positioned sphenopalatine vacuities with ochotonids and the leporid *Pronolagus*, but differs in this respect from the majority of leporids, in which the sphenopalatine vacuity is smaller and more laterally positioned or is entirely absent (Wible, 2007, char. 36). The ventral surface of the basisphenoid bears a small midline foramen (=foramen cavernosum of Krause, 1884) for the craniopharyngeal canal, which is also present in extant leporids, but absent in ochotonids and *Rhombomylus turpanensis* (Wible, 2007, char. 43). The foramen cavernosum opens internally into the extensive sphenoidal sinus, clearly visible in FMNH PM9476 because of extensive damage to the anterodorsal surfaces of the basisphenoid. Posterolateral to the posterior margin of the medial lamina of the pterygoid, the basisphenoid is perforated by two (right side) and one (left side) transverse canal foramina, which are also present in both leporids and ochotonids (Wible, 2007, char. 42). Anteriorly, the basisphenoid forms a sub-oval, concave surface, which forms the posterior limit of the intersphenoidal synchondrosis. Posteriorly, it forms a pair of ventrally projecting tuberosities, the posterior surfaces of which abut against the anterior surface of the basioccipital. Posterolaterally, the basisphenoid is underlapped by the styliform processes of the ectotympanic bones.

Alisphenoid

The alisphenoids (greater wings) extend laterally from the basisphenoid and form the ventrolateral walls of the middle cranial fossa and continue anterodorsally to form the posterior wall of the orbit (**Figures 3A,B**, **8**, **9**). Ventromedially to the base of the zygomatic process of the squamosal, the alisphenoid produces a low, sub-transverse ridge, which forms the alisphenoid crest [=crista alae magnae of Craigie (1948)]. In extant lagomorphs, the alisphenoid surface located immediately medial and ventral to the crest is formed by very thin, semi-transparent sheets of connective tissue (*O. cuniculus*, ZPAL comparative collection). Therefore, the large, irregular openings located ventromedially and posterolaterally to the alisphenoid crest in FMNH PM9476 are interpreted as similar areas covered in life by thin connective tissue rather than as any neurovascular openings (**Figures 8**, **9**).

The alisphenoid is perforated by several foramina that connect the middle cranial fossa with the external surface of the cranium and serve as the passageways of important nerves and vessels. The largest opening, located immediately lateral to the basisphenoid, is the sub-oval foramen ovale, which serves as the passageway for the mandibular nerve (CN V_3). Posterior to the foramen ovale, the dorsal surface of the alisphenoid bears a mediolaterally broad and anteroposteriorly short groove, which indicates the position of the root of the mandibular nerve and the associated semilunar ganglion (Craigie, 1948). The foramen ovale in *P. haydeni* is located entirely within the alisphenoid, whereas in leporids it is bordered posteriorly by the petrosal, as a result of the foramen ovale being confluent with the piriform fenestra; the condition in ochotonids is variable (Wible, 2007, char. 40). FMNH PM9476 does not possess a piriform fenestra posterior to the foramen ovale, but it is possible that some of the spaces preserved lateral to the foramen ovale represent fenestrations homologous to the piriform fenestra present in some lagomorphs (e.g., *Lepus*, ZPAL comparative collection).

The anteromedial margin of the alisphenoid is concave and forms the lateral margin of the superior orbital fissure, which represents both the superior orbital fissure and foramen rotundum present in other mammals and serves as the passage way for CN III, IV, V_1, V_2 and VI (Craigie, 1948) (**Figures 8**, **9**). The superior orbital fissure does not possess a dedicated medial wall and is bordered medially by the basisphenoid and anteriorly by the posterior margin of the perpendicular lamina

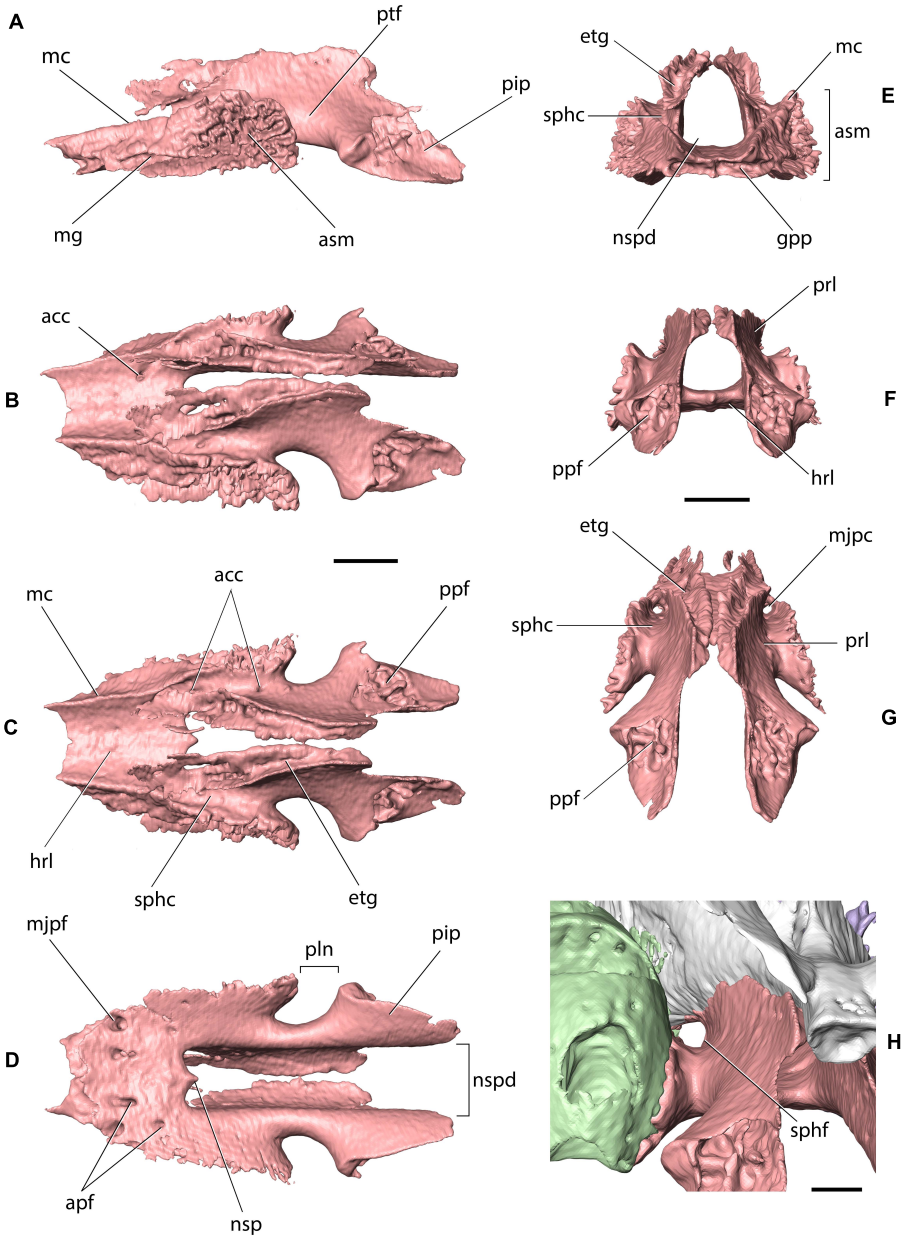

FIGURE 7 | Palatine of *Palaeolagus haydeni* (FMNH PM9476) in **(A)** left lateral, **(B)** left dorsolateral, **(C)** dorsal, **(D)** ventral, **(E)** anterior, **(F)** posterior, **(G)** posterodorsal, and **(H)** left posterolateral views. Left maxilla shown in light green, presphenoid shown in white. acc, dorsal opening of accessory palatine canal; apf, accessory palatine foramen; asm, articular surface for alveolar process of maxilla; etg, ethmoidal groove; gpp, groove for palatine process of maxilla; hrl, horizontal lamina; mc, maxillary crest; mg, maxillary groove; mjpc, major palatine canal; mjpf, major palatine foramen; nsp, nasal spine; nspd, nasopharyngeal duct; pip, pyramidal process; pln, palatine notch; ppf, fissure for pterygoid process of basisphenoid; prl, perpendicular lamina; ptf, pterygopalatine fossa; sphc, sphenopalatine canal; sphf, sphenopalatine foramen. Scale bars for **(A–G)** = 2 mm, scale bar for **(E)** = 1 mm.

of the palatine. Posterolateral to the superior orbital fissure, the base of the lateral lamina of the pterygoid is perforated by the alisphenoid canal, which forms the passage for the maxillary artery and vein (Wible, 2007, char. 38). Lateral to the alisphenoid canal, the base of the lateral lamina of the pterygoid bears a subcircular foramen, which likely represents the masseteric foramen for the masseterico-temporal ramus of the mandibular nerve, also present in extant lagomorphs (Wible, 2007, char. 39). The presence of the buccinator foramen cannot be confirmed in FMNH PM9476, due to the incompletely preserved surface of the alisphenoid in the adjacent region.

Pterygoid

The paired pterygoids, which comprise medial and lateral laminae, extend anterolaterally to the basisphenoid. The medial lamina [=entopterygoid crest of Wible (2007)] is vertical

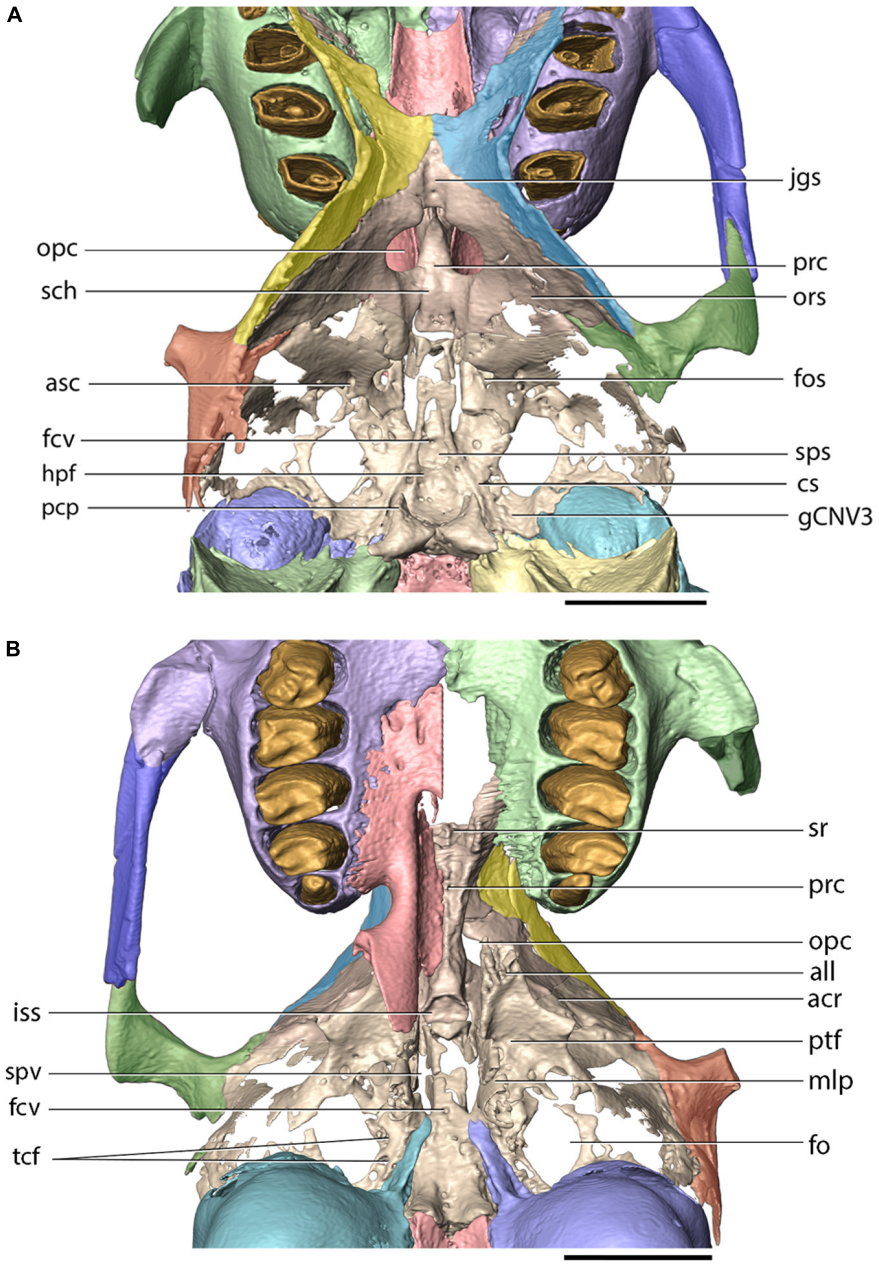

FIGURE 8 | Cranial base of *Palaeolagus haydeni* (FMNH PM9476) in **(A)** dorsal and **(B)** ventral views. Frontal (orbital portion)-presphenoid-basisphenoid-squamosal figured as complex (internal sutures not visible in CT data). acr, alisphenoid crest; all, apex of lateral lamina of pterygoid process; asc, alisphenoid canal; cs, carotid sulcus; fcv, foramen cavernosum; fo, foramen ovale; fos, superior orbital fissure; gCNV3, groove for root of CN V3 and semilunar ganglion; hpf, hypophyseal fossa; iss, presphenoid surface of intersphenoidal synchondrosis; jgs, jugum sphenoidale; mlp, medial lamina of pterygoid process of palatine; opc, optic canal; ors, orbitosphenoid; pcp, posterior clinoid process; prc, presphenoid corpus; ptf, pterygoid fossa; sch, sulcus chiasmatis; sps, sphenoidal sinus; spv, sphenopalatine vacuity; sr, sphenoidal recess; tcf, transverse canal foramina. Scale bar = 5 mm.

and forms the posterior extension of the medial margin of the pyramidal process of the palatine. Its medial surface forms the posterolateral surface of the nasopharyngeal duct. Posteroventrally, the medial lamina terminates with a pointed hamular process. The lateral lamina [=ectopterygoid crest of Wible (2007)] extends anteroventrally from the lateral part of the basisphenoid and tapers anteriorly into a rugose apex, which inserts into a fissure in the pyramidal process of the palatine. The lateral lamina of the pterygoid does not extend as far posteriorly as the medial lamina, which is similar to the condition present in ochotonids and leporids (contra Dice, 1933; Wible, 2007, char. 37). The medial and lateral laminae of the pterygoids form the posteromedial and anterolateral boundaries of the pterygoid fossa, respectively.

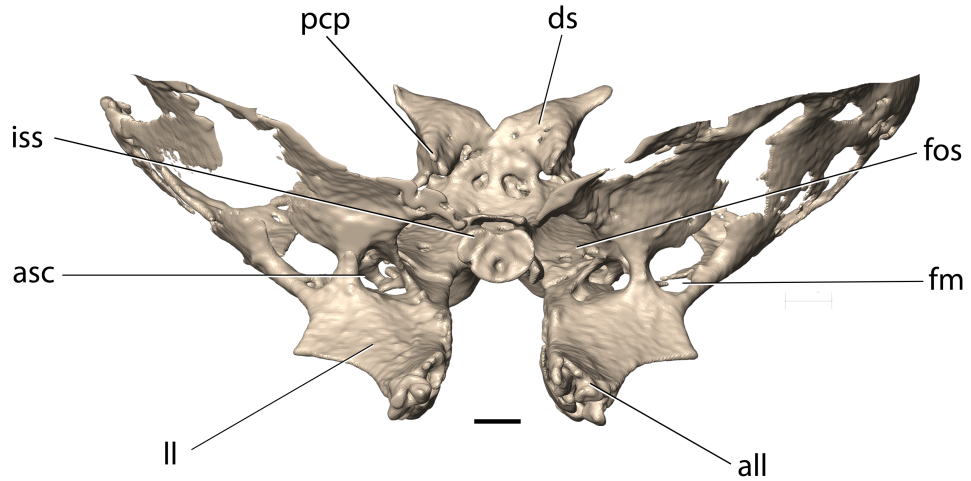

FIGURE 9 | Basisphenoid of *Palaeolagus haydeni* (FMNH PM9476) in anterior view (portions adjacent to alisphenoid crests removed). asc, alisphenoid canal; all, apex of lateral lamina of pterygoid; ds, dorsum sellae; fm, masseteric foramen; fos, superior orbital fissure; iss, presphenoid surface of intersphenoidal synchondrosis; ll, lateral lamina of pterygoid; pcp, posterior clinoid process. Scale bar = 1 mm.

Squamosal

The squamosal occupies the lateral part of the braincase and forms the lateral surface of the middle cranial fossa, internally. It comprises the squama of the squamosal and an anterolaterally projecting zygomatic process. The posterior portion of the zygomatic process contributes to the cranial part of the craniomandibular joint. In FMNH PM9476, the squamosals are incompletely preserved; the left squamosal is preserved partially, with the anterior portion of the zygomatic process broken, whereas the right squamosal is represented only by its zygomatic process (**Figures 3A,B**, **8**). The morphology of the squamosal in *P. haydeni* is somewhat intermediate between the squamosal of leporids, which is approximately quadrangular in outline in lateral view, and the dorsoventrally narrow squamosal present in ochotonids (Krause, 1884; Craigie, 1948; Wible, 2007). Anteriorly, the squama of the squamosal projects medially onto the orbital wall, where it contacts the frontal, dorsally, and the orbitosphenoid, ventrally. Dorsally, the main portion of the squamosal forms a weakly interdigitating suture with the parietal, whereas ventrally it contacts the alisphenoid. In FMNH PM9476, the squama of the squamosal is perforated by a large, oval opening, but it is difficult to determine whether this opening is entirely artifical, or it represents indeed the postglenoid foramen enlarged as a result of damage.

The zygomatic process forms a root which extends anteroventrolaterally, and an anterior portion which extends anteroventromedially. The root bears a prominent transverse ridge, anteroventrally, which separates the anteromedial surface of the squamosal from the concave glenoid cavity (mandibular fossa). The posterior surface of the root of the zygomatic process, together with part of the ventrolateral surface of the squama, form the temporal fossa, which is demarcated dorsally by a prominent, sub-longitudinal ridge, located dorsally to the mentioned large opening (postglenoid foramen). The anteroventral portion of the zygomatic process is triangular in outline in lateral view, mediolaterally flattened and laterally concave. Ventrally, it forms a sharp crest, which inserts into a groove located on the posterodorsal margin of the zygomatic and the two bones form a straight, sub-longitudinal suture. The posterior portion of the squamosal is incompletely preserved in FMNH PM9476, but the mastoid portions of the petrosals of the specimen bear prominent facets for the posteroventral process of the squamosal, located anterodorsally to the dorsal margin of the external acoustic meatus (**Figure 10B**).

Petrosal

The petrosal occupies the posterodorsolateral portion of the cranium and is approximately pyramidal in shape, with an anteromedially directed apex (**Figure 10**). On the dorsal surface, a prominent petrosal crest (=crista petrosa) extends from the apex, posterolaterally, and separates the cerebral and cerebellar surface of the petrosal into anterior and medial portions; it also separates the medial and posterior cranial fossae. The medial surface possesses a large, sub-oval opening of the subarcuate fossa, which houses the petrosal lobule of the cerebellum. Ventral to the subarcuate fossa, the medial surface bears the internal acoustic meatus, which is divided by the transverse crest into the anterodorsal opening of the facial canal and the posteroventral area occupied predominantly by the cochlear nerve. Anteroventral to the internal acoustic meatus, the petrosal bears an anteroposteriorly short and mediolaterally broad groove for the passage of the trigeminal nerve (CN V), which continues onto the dorsal surface of the basisphenoid. Ventromedially, the medial surface possesses a prominent petrobasilar sulcus for the ventral (inferior) petrosal sinus. Ventral to the petrobasilar sulcus, the petrosal is overlapped by the basilar portion of the occipital.

The posteromedial surface of the petrosal bears an approximately triangular articular surface for the occipital bone, demarcated anteromedially and posterodorsally by low

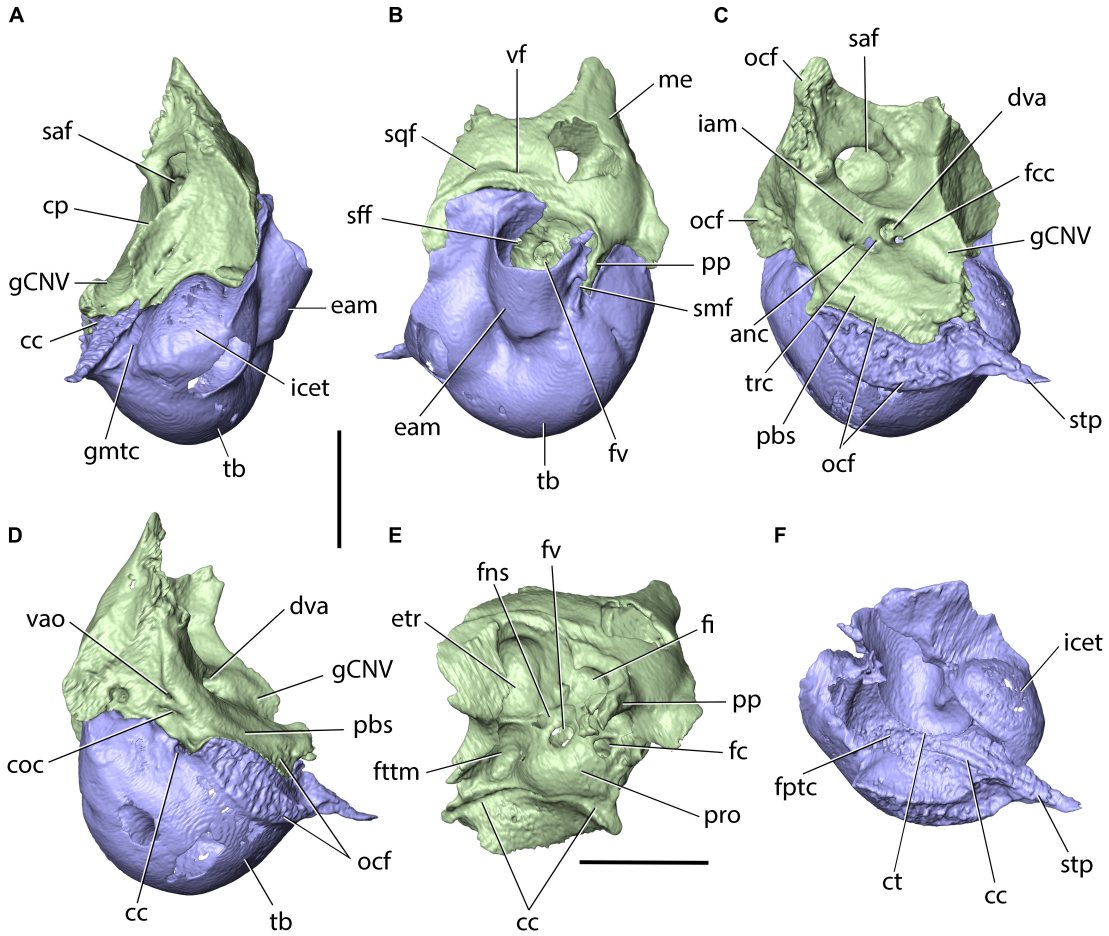

FIGURE 10 | Petrosal (light green) and ectotympanic (dark blue) of *Palaeolagus haydeni* (FMNH PM9476) in **(A)** anterior, **(B)** lateral, **(C)** medial, **(D)** posteromedial, **(E)** ventral and **(F)** dorsal views. anc, canal for acoustic nerve; cc, carotid canal; coc, external opening of the cochlear aqueduct; cp, crista petrosa; ct, crista tympanica; dva, dorsal vestibular area; eam, external acoustic meatus; etr, epitympanic recess; fc, fenestra cochleae; fi, fossa incudis; fns, facial nerve (CN VII) sulcus; fptc, fundic part of tympanic cavity; fttm, fossa for tensor tympani muscle; fv, fenestra vestibuli; gCNV, groove for trigeminal nerve (CN V); gmtc, groove leading into musculotubal canal; iam, internal acoustic meatus; icet, intracranial exposure of ectotympanic; me, mastoid exposure; ocf, occipital facet; pbs, petrobasilar groove; pp, paroccipital process; pro, promontory; saf, subarcuate fossa; sff, secondary facial foramen; sqf, squamosal facet; smf, stylomastoid foramen; stp, styliform process; tb, tympanic bulla; trc, transverse crest; vao, external opening of the vestibular aqueduct; vf, venous foramen. Scale bars = 5 mm.

ridges. Immediately ventral to the anteromedial ridge, the petrosal bears the external opening for the vestibular aqueduct. Ventral to this opening, the petrosal produces a small, but deep cleft, containing the external opening of the cochlear aqueduct. The ventral portion of the posteromedial surface of the petrosal forms the anterolateral border of the jugular foramen.

The tympanic (ventral) surface of the petrosal forms the dorsal roof of the tympanic cavity. In its central portion, the tympanic surface bears an eminence, the promontory (=promontorium), which indicates the position of the basal turn of the cochlea situated immediately dorsally. Lateral to the promontory, the petrosal is perforated by the fenestra vestibuli (=vestibular [oval] window), which is closed by the footplate of the stapes in life. Posteromedial to the fenestra vestibuli, the petrosal bears the fenestra cochleae (=cochlear [round] window), which is closed by the secondary tympanic membrane in life. The tympanic surface also bears three distinct fossae: the fossa for the tensor tympani muscle, located anteromedial to the fenestra vestibuli; the epitympanic recess, which lies dorsolaterally to the tensor tympani fossa and is occupied by the incus and the head of the malleus in life; and a fossa lying posteromedially to the fenestra cochleae, which represents the fossa incudis for the short process (=crus breve) of the incus. A sulcus representing the dorsal portion of the carotid canal is also present in the tympanic surface. The sulcus extends anterolaterally from a notch representing the dorsal portion of the posterior carotid foramen. On the lateral surface of the promontory, the sulcus changes its orientation to anteroventral and extends toward the carotid groove on the dorsal surface of the basisphenoid.

The lateral surface of the petrosal was partly overlapped by the thin, posteroventral process of the squamosal, as indicated by the presence of a dedicated, squamosal facet, and the extent of the squamosal in more complete skulls (**Figure 2**; see also Wood, 1940, pl. XXXIV, Figure 2). This condition

resembles Leporidae (Wible, 2007), although the posteroventral process of the squamosal is shorter in *Palaeolagus* than in extant leporids. The lateral exposure of the mastoid portion in *P. haydeni* is more extensive than in leporids, but most probably the posteroventral process of the squamosal separated the dorsal side of the tympanic bulla and the mastoid, as in Leporidae. The surface of the mastoid exposure is smooth, a feature *P. haydeni* shares with ochotonids, whereas in leporids the mastoid exposure is extensively pitted (Wible, 2007). The mastoid exposure forms a prominent mastoid (paroccipital) process, which inserts into a fissure located in the dorsal surface of the ectotympanic and forms the posterior boundary of the stylomastoid foramen, through which the facial nerve (CN VII) leaves the petrosal. The mastoid process is shorter in *Palaeolagus* than in leporids, displaying a somewhat intermediate morphology between ochotonids and leporids.

Ectotympanic

The ectotympanic is located in the posteroventrolateral portion of the cranium and forms the greatly expanded tympanic bulla (**Figures 3A,B,D–F**, **10A–D,F**). Laterally, the ectotympanic bears the osseous external acoustic meatus, which has the form of a posterolaterally directed canal leading from the external ear to the tympanic membrane, and resembles the external acoustic meatus of leporids, but differs markedly from the short, laterally directed meatus in ochotonids (Wible, 2007, char. 26). Posterior to the external acoustic meatus, the dorsal surface of the ectotympanic forms a fissure for the mastoid process. Ventromedially, the external acoustic meatus terminates with the crista tympani, which in life forms the base of the tympanic membrane.

Anteromedially, the ectotympanic forms an oblique styliform process which underlaps the basisphenoid. Immediately lateral to the styliform process, the tympanic forms the musculotubal canal, which is occupied by the eustachian tube in life and forms a connection between the middle ear and the nasopharynx. Following Evans and de Lahunta (2013), the tympanic cavity can be divided into three parts: the fundic part, which is the largest and most ventrally positioned; the proper tympanic cavity, located opposite the tympanic membrane; and a dorsal part for the incus, part of the stapes and head of the malleus, formed by the epitympanic recess. The carotid canal for the internal carotid artery (ICA) is located entirely between the petrosal and tympanic, which form their dorsal and ventral portions, respectively. The carotid canal opens posteriorly with the posterior carotid foramen located anteroventrolaterally to the jugular foramen in the petrobasilar fissure. It then extends anterolaterally toward the medial surface of the promontory, where the orientation of the canal changes to anteromedial. The carotid canal opens toward the middle cranial fossa via the internal carotid foramen, located medial to the styliform process. The ICA position in *P. haydeni* differs from that in extant lagomorphs. In ochotonids, the ICA is more medial and it enters the middle cranial fossa via a carotid notch. In leporids, on the other hand, the carotid canal is present, but is located within the wall of the ectotympanic, posteriorly, and is bordered by the petrosal and ectotympanic only anteriorly (Meng, 1991; Wible, 2007, char. 44). An anterodorsal portion of the wall of the tympanic bulla is exposed in the middle cranial fossa in *P. haydeni*, in contrast to extant lagomorphs (Meng, 1991).

Occipital

The occipital occupies the posterior portion of the cranium and forms a bony ring around the foramen magnum (**Figure 11**). The occipital comprises four portions: the ventral, unpaired basilar portion (basioccipital), the paired lateral portions (exoccipitals) and the unpaired, dorsal squamous portion (supraoccipital). All four portions develop as separate ossifications and fuse into a single occipital bone during ontogeny (Craigie, 1948).

The basilar portion (basioccipital) occupies the posterior portion of the cranial base. It is mediolaterally narrowest anteriorly, and its mediolateral width increases posteriorly toward the foramen magnum. In this respect, the basioccipital of *P. haydeni* resembles that in *Rhombomylus*, *Gomphos*, *Prolagus*, and *Ochotona*, but differs from the basioccipital in leporids, which is mediolaterally broadest anteriorly (Wible, 2007, char. 45). The dorsal surface of the basioccipital is exposed in the ventral part of the posterior cranial fossa and bears an anteroposteriorly elongate pontine impression. Posteroventrally, the basioccipital bears a subtle, median ridge (compare with Dice, 1933, Figure 2). A similar median ridge is also present in *Rhombomylus* (Meng et al., 2003, Figure 33), *Gomphos* (Asher et al., 2005, Figure 2), leporids and *Ochotona* (Wible, 2007, Figure 4), but whereas it is also weakly developed in leporids, *Rhombomylus*, and *Gomphos*, it is much more prominent in *Ochotona* and extends further anteriorly. In addition, lateral to the median ridge, the ventral surface of the basioccipital forms prominent grooves for the rectus capitis anterior in leporids and *Ochotona* (Wible, 2007), which are only weakly developed in *P. haydeni*. Anteriorly, the basioccipital bears a transverse, rugose articular surface, which is apressed against a similar surface located on the basisphenoid corpus, with both surfaces comprising the sphenooccipital synchondrosis. The lateral surface of the basioccipital gives rise to two pairs of crests: a dorsolateral pair and a ventrolateral pair (=tympanic processes of Wible, 2007). The oblique lateral surfaces of these crests are rugose and whereas the anterolateral crests overlap the medial surfaces of the petrosals, immediately ventral to the petrobasilar groove, the ventrolateral crests overlap the tympanic bones, medially, and contribute to the medial walls of the tympanic bullae. In leporids, the tympanic crests are oriented dorsally and laterally, instead of dorsolaterally and ventrolaterally. Furthermore, the dorsal crest does not overlap the medial surface of the petrosal, but abuts against its medial margin, and the ventrolateral crest does not overlap the tympanic bulla, but contacts an articular surface that is separated from the bulla by a deep groove (*O. cuniculus*, ZPAL comparative collection). In *Ochotona*, the ventromedial crests overlap the medial walls of the tympanic bullae as in *P. haydeni*, but the exact morphology of the dorsal or dorsolateral crests is unknown (Wible, 2007, char. 46). Posterolaterally, the basioccipital forms the ventral portions of the occipital condyles, whereas posteriorly it bears a sharp, concave posterior margin, which forms the intercondylar notch and the ventral margin of the foramen magnum. Immediately anterior to the intercondylar notch, the ventral surface of the

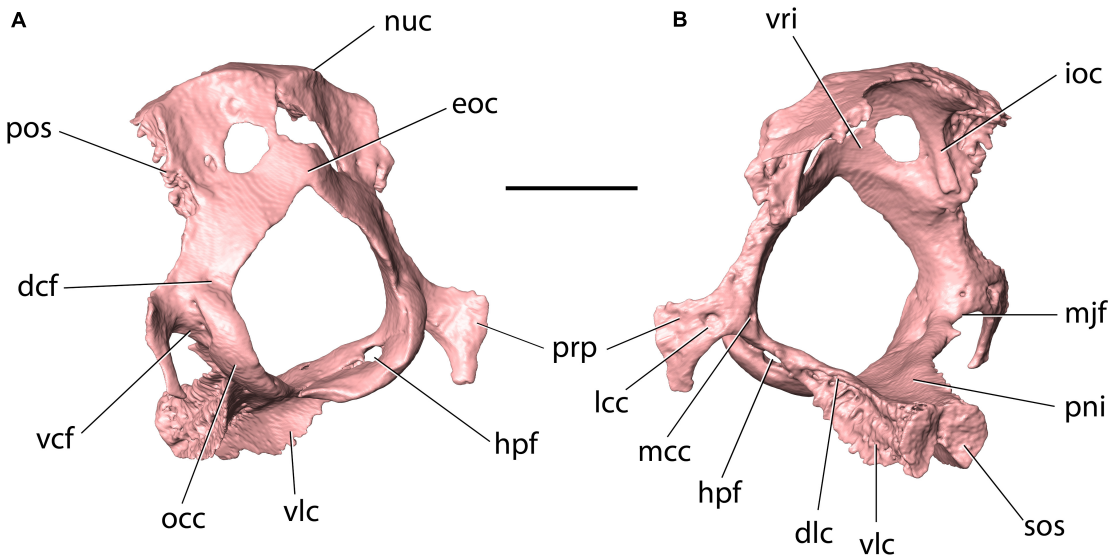

FIGURE 11 | Occipital of *Palaeolagus haydeni* (FMNH PM9476) in **(A)** posteroventrolateral and **(B)** anterodorsolateral views. Note the ventral condyloid fossa perforated by two foramina. dcf, dorsal condyloid fossa; dlc, dorsolateral crest; eoc, external occipital crest; hpf, hypoglossal foramen; ioc, intraoccipital crest; lcc, lateral opening of condyloid canal; mcc, medial opening of condyloid canal; mjf, posteromedial margin of jugular foramen; nuc, nuchal crest; occ, occipital condyle; pni, pontine impression; pos, petrosooccipital suture; prp, paracondylar process; sos, sphenooccipital synchondrosis; vcf, ventral condyloid fossa; vlc, ventrolateral crest; vri, vermiform impression. Scale bar = 5 mm.

basioccipital bears a small pharyngeal tubercle in *O. cuniculus* (ZPAL, comparative collection), which is absent in *P. haydeni* and *Ochotona*.

The paired lateral portions (exoccipitals) form the lateral margins of the foramen magnum and bear the main parts of the occipital condyles. Lateral to the dorsal portion of the occipital condyle, the exoccipital forms a slender paracondylar (=jugular, =paramastoid) process, which extends ventrolaterally, and then ventromedially. This resembles the condition in leporids, but differs from *Ochotona*, in which the paracondylar process extends ventrolaterally and is much broader (Wible, 2007, Figure 4). The paracondylar process in *P. haydeni* is anteroposteriorly compressed, has a convex anterior surface and a concave posterior surface and extends about halfway down the tympanic bulla, like in *Ochotona*, but unlike leporids, in which the paracondylar process extends almost along the entire dorsoventral height of the bulla (Wible, 2007, char. 29). The paracondylar process in *P. haydeni* is widely separated from the paroccipital process of the mastoid by the posterior surface of the tympanic (contra Wible, 2007, char. 30). A similar condition is present in *Ochotona*, but differs from the condition in leporids, in which both processes almost abut against each other, ventrally (Wible, 2007, char. 30). The anterior surface of the paracondylar process bears two foramina, possibly representing the external openings of the condyloid canal – a larger, lateral foramen and a smaller, medial foramen (compare with Evans and de Lahunta, 2013, p. 89). The anterior surface of the paracondylar process is pressed against the posteromedial surface of the petrosal and the posterodorsal surface of the tympanic bulla. A small, pointed process extends anterolaterally from the base of the paracondylar process, so that the concave margin of the exoccipital between them forms the posteromedial margin of the jugular foramen, bound anterolaterally by the petrosal. Between the dorsal portion of the occipital condyle and the paracondylar process, the exoccipital forms a ventral condyloid fossa, perforated by a pair of ventral condyloid foramina on each side. The presence of ventral condyloid foramina is variable in *Ochotona* and within Leporidae (Wible, 2007, char. 48). The exoccipital also bears a dorsal condyloid fossa, which does not bear any foramina. This resembles the condition in *Ochotona* and some leporids, but differs from *Lepus* and *Oryctolagus*, in which the dorsal condyloid fossa bears numerous small foramina (Wible, 2007, char. 49). Posteromedial to the jugular foramen, the exoccipital is perforated by a single hypoglossal foramen, like in *Ochotona*, *Gomphos,* and *Rhombomylus*. This is in contrast to the condition in leporids, in which the exoccipital bears two hypoglossal foramina (Wible, 2007, char. 47).

The squamous part (supraoccipital) forms the dorsolateral borders of the foramen magnum. It comprises a posteriorly convex, anteroventrally flattened sheet of bone, which bifurcates ventrally to fuse with the dorsal part of each exoccipital. Laterally, the supraoccipital forms an interdigitating suture with the posteromedial surface of the petrosal. At the intersection of the skull roof and the posterior cranial wall, the supraoccipital produces a prominent nuchal crest. Anterior to the nuchal crest, it forms an anteroposteriorly narrow dorsal exposure. Between the nuchal crest and the dorsal apex of the foramen magnum, a weakly developed external occipital crest is present. In all these respects, the supraoccipital of *P. haydeni* is remarkably similar to that in *Ochotona*. However, it differs markedly from the supraoccipital in leporids, in which it forms: (1) a nuchal crest well anterior to the intersection of the skull roof and posterior

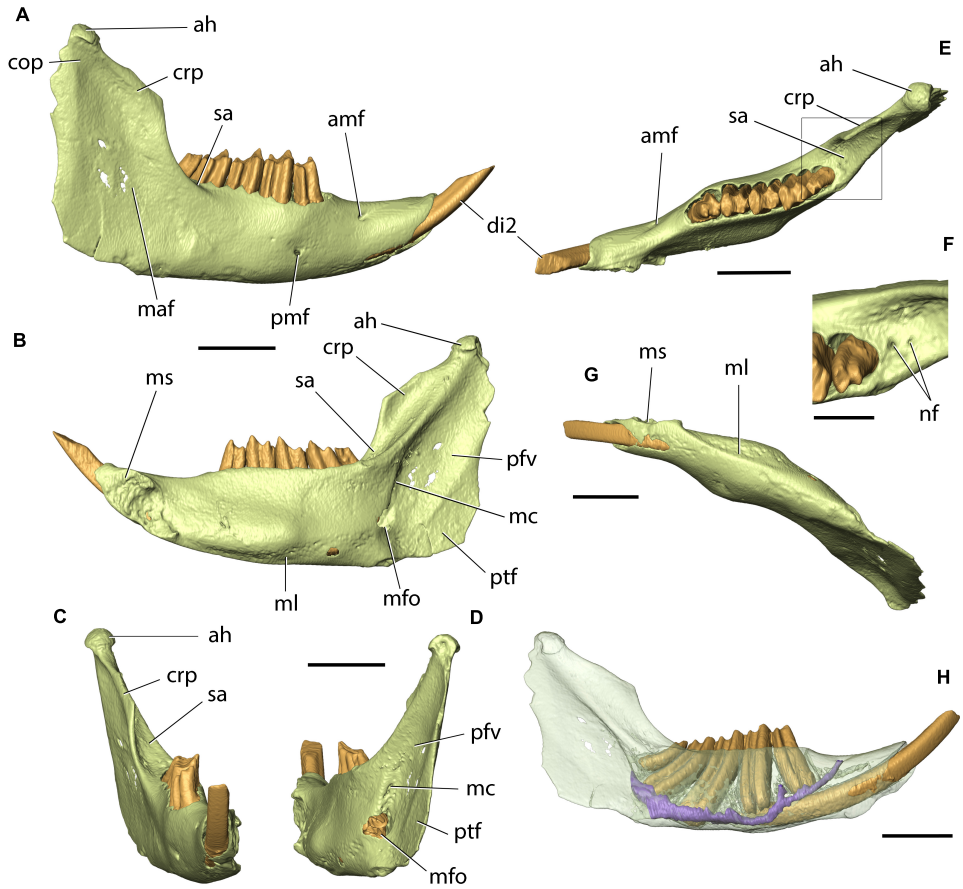

FIGURE 12 | Right mandible of *Palaeolagus haydeni* (FMNH PM9476) in **(A)** lateral, **(B)** medial, **(C)** anterior, **(D)** posterior, **(E)** dorsal, and **(G)** ventral views. Inset in **(F)** shows detail of area posterior to m3 outlined in **(E)**. **(H)** Shows the position of teeth and mandibular canal (purple) within the bone. ah, articular head; cop, condyloid process (broken); crp, coronoid process (broken); di2, lower incisor; maf, masseteric fossa; mc, external foramina of maxillary canal; amf, anterior mental foramen; ml, mylohyoid line; mfo, mandibular foramen; ms, mandibular symphysis; nf, neurovascular foramina; pfv, pterygoid fovea; pmf, posterior mental foramen; ptf, pterygoid fossa; sa, ascending sulcus. Scale bars for **(A–E,G)** = 5 mm, **(F)** = 2 mm.

cranial wall; (2) an extensive exposure on the dorsal surface of the skull; and (3) a prominent external occipital protuberance extending posteriorly to the nuchal crest (Wible, 2007, char. 7). The external surface of the supraoccipital is smooth in *P. haydeni*, and differs from both ochotonids, in which the external surface of the supraoccipital bears only a minute, single neurovascular foramen, dorsally, and from leporids, in which the surface is extensively pitted (Wible, 2007). The internal surface of the supraoccipital forms a concave vermiform impression, bounded laterally by prominent, internal occipital crests.

The foramen magnum, located within the occipital, comprises the passageway through which the medulla oblongata leaves the cranial fossa to form the spinal cord. The foramen magnum in *P. haydeni* differs from that in other lagomorphs in that it is approximately sub-circular in outline, and produces a pointed, dorsal apex. In contrast, in ochotonids and leporids, the foramen magnum forms a round, dorsal apex, and the supraoccipital also bears a pair of prominent nuchal tubercles, ventromedially, which give the foramen magnum a pentagonal outline (Wible, 2007, Figure 4).

Mandible

The mandible is well-preserved in FMNH PM9476, except for the posterior portions of both mandibular rami and the right coronoid process, which are broken (**Figure 12**; compare with **Figures 2E,F**).

The mandible is formed by two hemimandibles joined anteriorly at the mandibular symphysis. Each hemimandible comprises a horizontal portion and an approximately perpendicular mandibular ramus. The horizontal portions of both contralateral hemimandibles form the body (corpus) of the mandible. Anteriorly, the body of the mandible lies in a sagittal plane, and becomes obliquely oriented posterior to the mandibular symphysis, so that both contralateral mandibular bodies form an angle of approximately 40°. Anteriorly, the mandibular body bears the alveolus for di2. Posteriorly, the dorsal surface of the mandibular body bears alveoli for p3–p4 and m1–m3, which are approximately equal in size, except for the alveolus for m3, which is markedly smaller. Posterior to the di2 alveolus, and anterior to the p3 alveolus, the dorsal surface of the mandibular body is concave and

contributes to the ventral part of the diastema. There are two mental foramina in each mandibular body: an anterior mental foramen, located approximately at the posterior one-third of the anteroposterior length of the diastema, which is likely homologous with the mental foramen in leporids located in a similar position, and a posterior mental foramen, placed below the posterior part of p3, likely homologous with the more posteriorly placed (m3 level) mental foramen present in ochotonids (Wible, 2007). Ventrally, the mandibular body bears a prominent mylohyoid line for the insertion of the mylohyoid muscle.

The lateral surface of the mandibular ramus is concave and forms an extensive masseteric fossa. Anteroventrally to the masseteric fossa, the mandibular ramus bears a tuberosity, which is only slightly demarcated in FMNH PM9476, but is much more prominent in other specimens of *P. haydeni* (**Figure 2F**; see also Troxell, 1921; Wood, 1940). The medial surface of the mandibular ramus bears two depressions: an anterodorsal pterygoid fovea, which marks the attachment site for the lateral pterygoid muscle, and a posteroventral pterygoid fossa, for the insertion of the medial pterygoid muscle. Both depressions are separated from each other by a weakly demarcated, oblique ridge, which is also present in extant leporids, but is absent in ochotonids (Wible, 2007, char. 57). Anteromedially, a prominent, oblique ridge separates the pterygoid fovea from the anteromedial surface of the mandibular ramus [=sulcus ascendens of Krause (1884)]. Posterior to m3, the anteromedial surface of the mandibular ramus is perforated by a single (left side) or two (right side) minute foramina. Posterodorsally to the mylohyoid line, the mandibular ramus bears a mandibular foramen, which is located at a level below the mandibular tooth row (contra Asher et al., 2005, char. 48). Dorsal to the mandibular foramen, the medial surface of the mandibular ramus is perforated by a minute foramen, possibly representing the posterior opening of the maxillary canal. Anterodorsally, the mandibular ramus bears a prominent, dorsomedially directed coronoid process, which is much more prominent than the coronoid process present in extant lagomorphs (**Figures 2E,F**). The condylar processes in FMNH PM9476 are broken posteriorly, but preserve the prominent articular heads, which extend posteriorly into a mediolaterally narrow crest in more complete specimens (**Figures 2E,F**). Posteroventrally, the mandibular ramus produces an anteroposteriorly elongate angular process, which has a convex ventral margin, a concave dorsal margin and tapers to a point, posteriorly. A prominent masseteric line extends from the ventrolateral surface of the angular process onto the lateral surface of the angular process, resembling the prominent massteric line in leporids, but differing markedly from the masseteric line in ochotonids, which is restricted to the ventrolateral surface of the angular process (Wible, 2007). The extent of the pterygoid shelf on the medial surface of the angular process is difficult to determine in the specimens of *P. haydeni* examined in this study because of incomplete preservation, but seems to be restricted to the posteroventral portion of the mandible, as in ochotonids, unlike the anteroposteriorly elongate pterygoid shelf present in extant leporids (Wible, 2007, char. 59).

The mandibular canal opens posteriorly at the mandibular foramen and extends anteriorly below the roots of m1–m3. It then extends ventromedially to the root of p4, and continues anterodorsally, lying ventral to the root of p3. The mandibular canal opens anteriorly at the anterior mental foramen. The mandibular canal also forms a mediolaterally short, lateral branch located between the p3 and p4 alveoli, which opens laterally at the posterior mental foramen.

DISCUSSION

There are only few contributions that treated the cranial morphology of fossil lagomorphs in some detail. Among them, Wood (1940), Dawson (1958), and Fostowicz-Frelik (2013) concern North American Paleogene lagomorphs, in particular *Palaeolagus* (Wood, 1940; Dawson, 1958) or closely related genera (Fostowicz-Frelik, 2013). Other works covered mostly Neogene fossil ochotonids: *Alloptox* (Wu, 2003), *Austrolagomys* (=*Kenyalagomys* in MacInnes, 1953), and *Prolagus* (Dawson, 1969).

Ever since Dice (1929), *Palaeolagus* was recognized as belonging to Leporidae on the basis of the dentition, mandible, and muzzle morphology, the parts most frequently preserved in the fossil record (Dice, 1933; Wood, 1940; Dawson, 1958). However, recent phylogenetic studies of lagomorphs and Glires have, in general, supported the position of *Palaeolagus* as a stem lagomorph (Asher et al., 2005; Wible, 2007; Fostowicz-Frelik and Meng, 2013; Lopatin and Averianov, 2020).

Thus, the current study aimed at the reappraisal of the cranial morphology of *P. haydeni* in order to provide new morphological data as a base for deciding between the two phylogenetic hypotheses. Micro-CT scanning allowed us to study the internal cranial structures and scrutinize the whole skull, bone by bone, comparing it with the crown taxa in detail, using Wible's (2007) character matrix as the basis for our comparisons. Our study of *Palaeolagus* revealed that its cranial morphology shares characters not only with extant leporids but also with *Ochotona* (**Table 1**). Out of 46 characters analyzed by us, in 21 *Palaeolagus* showed features characteristic of extant Leporidae, in 13 the features characteristic of Ochotonidae (represented by *Ochotona* and *Prolagus*) and in seven, shared with both clades. However, in five characters *Palaeolagus* displayed morphology unlike any of the crown groups of Lagomorpha. These were: the morphology of the orbital process of maxilla, which is elongated in *Palaeolagus*, the absence of the zygomatico-orbital canal, a broader posterior squamosal, the absence of piriform fenestra, and the presence of two mental foramina (**Table 1**). This last combination of features can be viewed as plesiomorphic for all Glires, because *Palaeolagus* shares them with *Rhombomylus* (see Meng et al., 2003; Wible, 2007), a basal gliroid mammal which is neither a lagomorph nor a rodent (Asher et al., 2005).

The skull of *P. haydeni* shows a leporid-like structure of the muzzle, including the nasals, premaxilla–maxilla articulation, frontals with nascent postorbital processes, as well as the most part of the maxilla, showing extended lateral fenestration and leporid-like arrangement of the alveolar processes. Furthermore,

TABLE 1 | Comparison of cranial character states based mostly on the character-taxon matrix of Wible (2007), between Ochotonidae (represented by *Ochotona* and *Prolagus*), Leporidae [represented by sample studied by Wible (2007) and the comparative material for the present study], and *Palaeolagus haydeni*.

No.	Character	Ochotonidae	Leporidae	*Palaeolagus haydeni*
1	Shape of the nasals	*Narrow posteriorly and expanded anteriorly or narrow with sides parallel	Broad posteriorly, with V-shaped frontal articulation	Broad posteriorly, with V-shaped frontal articulation
2	Dorsal margin of the premaxilla	Smooth, convex	Dorsal extension well developed	Dorsal extension weak
3	Premaxilla/maxilla suture	Premaxilla wedges into maxilla	Maxilla wedges into premaxilla	Maxilla wedges into premaxilla
4	Postorbital process	Absent	Present	Present
5	Supraorbital notch	Absent	Present	Absent
6	Braincase pitting	Absent	Present	Absent
7	External occipital protuberance and nuchal crest	Does not dominate dorsal occiput; nuchal crest absent	Dominates dorsal occiput; nuchal crest present	Does not dominate dorsal occiput; nuchal crest absent
8	Maxillary fenestra, pars facialis	Single, large opening	Numerous, small openings	Numerous, small openings
9	Maxillary fenestra, pars orbitalis	Present	Absent	Present
10	Lacrimal facial process	Reduced	Reduced, but with pointed lacrimal tubercle	Reduced, but with pointed lacrimal tubercle
11	Position of nasolacrimal canal	Lateral to incisor	Position not related to incisor	*Position not related to incisor
12	Anteroventral orbital rim	Round	Square	Square
13	Sphenopalatine foramen	Between the palatine and maxilla	Within the palatine	*Between the palatine and maxilla
14	'Orbital process' of maxilla	Narrow	Narrow	*Elongated anteroposteriorly
15	Alveolar process of maxilla	Close to the lateral wall of the orbit	Close to the medial wall of the orbit	Close to the medial wall of the orbit
16	Root exposure in orbit wall	Absent	Present	Weakly present
17	Zygomatico-orbital canal	Present	Present	Absent
18	Masseteric crest	Short, formed as a pronounced tubercle	Long, extended along the ventrolateral margin of the anterior zygomatic root	Long, extended along the ventrolateral margin of the anterior zygomatic root
19	Posterior process of zygomatic	Substantially elongated	Present, but not very long (with rounded tip)	Present, but not very long (with rounded tip)
20	Posterior squamosal	Long and narrow	Narrow with processes quamosum	Broader but with posterior process external to the acoustic meatus
21	Exernal acoustic meatus	Tube very short and laterally directed	Tube elongate and posterolaterally directed	Tube elongate and posterolaterally directed
22	Lateral exposure of mastoid	Present, immediately dorsal to external acoustic meatus	Present, immediately dorsal to external acoustic meatus	*Present, dorsal to the acoustic meatus
23	Paracondylar process	Short, extends not longer than a halfway down posterior bullar wall	Long, extends halfway or completely down posterior bullar wall	*Intermediate, extends halfway down posterior bullar wall
24	Paroccipital and paracondylar process relationship	Distant	Close, (approximating)	*Distant
25	Incisive foramen	Elongated and partitioned into two openings; posteriorly at the level of P4	Elongated, single; posteriorly reaching P2	Elongated, single, reaching P2 or P2/P3 alveolar septum
26	Major palatine foramen	Multiple openings in palatine	Single opening within palatine or between palatine and maxilla	Single opening within palatine
27	Premolar foramen	Present	Absent (generally)	Absent
28	Posterior palate	Level with M1	Level with M1	Level with M1/M2
29	Sphenopalatine vacuity	Present, near midline	Absent or present, near midline, or present, laterally positioned	*Present, near midline
30	Ento- and ectopterygoid crests	Ectopterygoid crest of variable length in relation to the entopterygoid crest; shorter (*Ochotona*) or longer (*Prolagus*); ends anterior or posterior to the entopterygoid crest, respectively	Ectopterygoid crest shorter, ends anterior to the entopterygoid crest	*Ectopterygoid crest short, ends anterior to the entopterygoid crest
31	Foramen ovale	Placed within alisphenoid or between alisphenoid and petrosal	Placed between alisphenoid and petrosal	Placed within alisphenoid
32	Piriform fenestra anterior to auditory bulla	Present	Present	Absent

(Continued)

TABLE 1 | Continued

No.	Character	Ochotonidae	Leporidae	*Palaeolagus haydeni*
33	Craniopharyngeal canal	Absent	Present	Present
34	Carotid canal	Absent	Present	Present
35	Basioccipital	Long, broadens posteriorly	Short, broadest anteriorly	Long, broadens posteriorly
36	Lateral margin of the basioccipital	Bearing prominent tympanic process overlapping medial wall of auditory bulla	With thick, flattened prominence meeting the downturned lip from the auditory bulla	Baring prominent tympanic process overlapping medial wall of auditory bulla
37	Hypoglossal foramen	One	Two or more	One
38	Ventral condyloid foramen	Present or absent	Present or absent	Present
39	Dorsal condyloid foramen	Absent	Present or absent	Absent
40	Number of mental foramina	One	One	*Two
41	Anterior most position of mental foramen	At the level of ultimate molar	At the back of diastema	The anterior one at the back of diastema
42	Masseteric line	Restricted posteriorly on ramus	Along ventral margin of the mandibular ramus	Along ventral margin of mandibular ramus
43	Maxillary canal	Present	Present	*Probably present
44	Mandibular foramen	Inferior to occlusal surface of tooth row	Inferior to occlusal surface of tooth row	*Inferior to occlusal surface of tooth row
45	Pterygoid fovea	Not delineated	Prominently delineated	*Prominently delineated
46	Pterygoid shelf	Restricted posteriorly on ramus	Along ventral margin of mandibular ramus	*Restricted posteriorly on the ramus

Asterisk denotes modified character state change from that in Wible (2007).

the structure of the zygomatic root of the maxilla and the zygomatic are typical of leporids. The ochotonid features can be found in the basicranium and, generally, in the posterior part of the skull (**Table 1**). The basioccipital is ochotonid-like in having the tympanic processes encroaching the wall of the auditory bullae; furthermore, the structure of the petrosal mastoid exposure is more ochotonid-like than leporid-like, although its condition is overall intermediate. The posterior part of the skull with the relatively level parietals and lack of the nuchal crest at the occipital also resembles more that of *Ochotona* than of any modern leporid.

The described cranial characters of *Palaeolagus* are not characteristic of only one of the crown clades; thus, this lagomorph is better considered as a stem lagomorph. Its apparent mosaic morphology has at least two important implications. First, the fact that the early lagomorph *Palaeolagus*, which does not have an immediate relationship to either of the crown clades, exhibits a mixture of morphological characters typically associated either with ochotonids or leporids, indicates its independent position, already suggested by Fostowicz-Frelik and Meng (2013). Second, it allows us to assume that some of the cranial characters observed in extant taxa and regarded thus far as synapomorphies for the recent clades are most likely plesiomorphic.

The *Palaeolagus* lineage most probably originated in the late middle Eocene (see Fostowicz-Frelik and Tabrum, 2009), and it was already well represented in the early late Eocene (Dawson, 2008). Therefore, the skull of *Palaeolagus haydeni* is a very good reference point for advanced stem lagomorphs, which most probably gave rise to Leporidae in North America (see Fostowicz-Frelik, 2013). However, to reconstruct the ancestral cranial morphotype of Ochotonidae more data is needed from the Eocene Asian taxa, of which our knowledge is at present very fragmentary.

DATA AVAILABILITY STATEMENT

The original contributions presented in the study are included in the article/**Supplementary Material**, further inquiries can be directed to the corresponding author/s.

AUTHOR CONTRIBUTIONS

ŁF-F designed the study. AW processed and visualized the CT-data. Both authors analyzed the data, wrote the manuscript, and approved the final version.

FUNDING

This research was funded by National Science Centre (Cracow, Poland) grant number 2015/18/E/NZ8/00637, a visiting scholarship from FMNH, and an AMNH Roosevelt Research Fellowship to ŁF-F.

ACKNOWLEDGMENTS

We are grateful to W. Simpson (FMNH) and R. J. Emry (USNM) for access to the *Palaeolagus* specimens and to M. Hill (AMNH) for CT-scanning the FMNH PM9476 skull. The senior author is especially indebted to J. Meng (AMNH) for valuable discussions, support for this study, and access

to the AMNH *Palaeolagus* material. We thank F. Ippolito (previously AMNH) for the photos of the skulls used in **Figures 1**, **2**. A. Kapuścińska (ZPAL) kindly created a visualization of the head of *Palaeolagus*, and A. Hołda-Michalska (ZPAL) helped us edit **Figures 1**, **2**.

SUPPLEMENTARY MATERIAL

The Supplementary Material for this article can be found online at: https://www.frontiersin.org/articles/10.3389/fevo.2021.634757/full#supplementary-material

REFERENCES

Asher, R. J., Meng, J., Wible, J. R., McKenna, M. C., Rougier, G. W., Dashzeveg, D., et al. (2005). Stem Lagomorpha and the antiquity of Glires. *Science* 307, 1091–1094. doi: 10.1126/science.1107808

Asher, R. J., Smith, M. R., Rankin, A., and Emry, R. J. (2019). Congruence, fossils and the evolutionary tree of rodents and lagomorphs. *R. Soc. Open Sci.* 6:190387. doi: 10.1098/rsos.190387

Craigie, E. H. (1948). *Bensley's Practical Anatomy of the Rabbit: An Elementary Laboratory Text-Book in Mammalian Anatomy*, 8th Edn. Toronto, ONT: University of Toronto Press.

Dawson, M. R. (1958). Later Tertiary Leporidae of North America. *Univ. Kansas Paleontol. Contrib. Vertebrata* 6, 1–75.

Dawson, M. R. (1969). Osteology of *Prolagus sardus*, a Quaternary ochotonid (Mammalia. Lagomorpha). *Palaeovertebrata* 2, 157–190. doi: 10.18563/pv.2.4.157-190

Dawson, M. R. (2008). "Lagomorpha," in *Evolution of Tertiary Mammals of North America*, Vol. 2, eds C. M. Janis, G. F. Gunnell, and M. D. Uhen, (Cambridge: Cambridge University Press), 293–310.

Dice, L. R. (1929). The phylogeny of the Leporidae, with description of a new genus. *J. Mammal.* 10, 340–344. doi: 10.2307/1374124

Dice, L. R. (1933). Some characters of the skull and skeleton of the fossil hare, *Palaeolagus haydeni*. *Papers Mich. Acad. Sci. Art. Lett.* 18, 301–306.

Evans, H. E., and de Lahunta, A. (2013). *Miller's Anatomy of the Dog*. St. Louis, MO: Elsevier-Saunders.

Fostowicz-Frelik, Ł. (2013). Reassessment of *Chadrolagus* and *Litolagus* (Mammalia: Lagomorpha) and a new genus of North American Eocene lagomorph from Wyoming. *Am. Mus. Novit.* 3773, 1–76. doi: 10.1206/3773.2

Fostowicz-Frelik, Ł. (2017). "Convergent and parallel evolution in early Glires (Mammalia)," in *Evolutionary Biology: Self/Nonself Evolution, Species and Complex Traits Evolution, Methods and Concepts*, ed. P. Pontarotti, (Cham: Springer), 199–216. doi: 10.1007/978-3-319-61569-1_11

Fostowicz-Frelik, Ł., Frelik, G. J., and Gasparik, M. (2010). Morphological phylogeny of pikas (Lagomorpha: *Ochotona*), with a description of a new species from the Pliocene/Pleistocene transition of Hungary. *Proc. Acad. Nat. Sci. Phila.* 159, 97–118. doi: 10.1635/053.159.0107

Fostowicz-Frelik, Ł., Li, C.-K., Li, Q., Meng, J., and Wang, Y.-Q. (2015). *Strenulagus* (Mammalia: Lagomorpha) from the middle Eocene Irdin Manha Formation of the Erlian Basin, Nei Mongol, China. *Acta Geol. Sin. (Eng. Ed.)* 89, 12–26. doi: 10.1111/1755-6724.12391

Fostowicz-Frelik, Ł., and Meng, J. (2013). Comparative morphology of premolar foramen in lagomorphs (Mammalia: Glires) and its functional and phylogenetic implications. *PLoS One* 8:e79794. doi: 10.1371/journal.pone.0079794

Fostowicz-Frelik, Ł., and Tabrum, A. R. (2009). Leporids (Mammalia, Lagomorpha) from the Diamond O Ranch local fauna, latest middle Eocene of southwestern Montana. *Ann. Carnegie Mus.* 78, 253–271. doi: 10.2992/007.078.0303

Fostowicz-Frelik, Ł., and Wolniewicz, A. S. (2021). CT-informed skull osteology of *Palaeolagus haydeni* (Mammalia: Lagomorpha). *Dryad Dataset*. doi: 10.5061/dryad.crjdfn338

Frahnert, S. (1999). Morphology and evolution of the Glires rostral cranium. *Mitt. Mus. Nat. Berlin* 75, 229–246. doi: 10.1002/mmnz.19990750205

Ge, D., Yao, L., Xia, L., Zhang, Z., and Yang, Q. (2015). Geometric morphometric analysis of skull morphology reveals loss of phylogenetic signal at the generic level in extant lagomorphs (Mammalia: Lagomorpha). *Contrib. Zool.* 84, 267–284. doi: 10.1163/18759866-08404001

Insom, E., Magnoni, M. L., and Simonetta, A. M. (1990). Etudes sur la morphologie évolutive des Ochotonidés (Mammalia, Lagomorpha). 1. La morphologie crânienne d'*Ochotona rufescens* et d'*Ochotona roylei*. *Mammalia* 54, 633–651.

Koby, F. E. (1959). Contribution au diagnostic ostéologique différentiel de *Lepus timidus* Linné et *L. europaeus* Pallas. *Ver. Nat. Gesell. Basel* 70, 1–44.

Krause, W. (1884). *Die Anatomie des Kaninchens in Topographischer und Operativer Rücksicht*. Leipzig: Wilhelm Engelmann.

Li, C.-K., Meng, J., and Wang, Y.-Q. (2007). *Dawsonolagus antiquus*, a primitive lagomorph from the Eocene Arshanto Formation. Nei Mongol, China. *Bull. Carnegie Mus. Nat. Hist.* 39, 97–110. doi: 10.2992/0145-9058(2007)39[97:daaplf]2.0.co;2

Lopatin, A., and Averianov, A. (2020). *Arnebolagus*, the oldest eulagomorph, and phylogenetic relationships within the Eocene Eulagomorpha new clade (Mammalia, Duplicidentata). *J. Paleontol.* 1–12. doi: 10.1017/jpa.2020.94

López-Torres, S., Bertrand, O. C., Lang, M. M., Silcox, M. T., and Fostowicz-Frelik, Ł (2020). Cranial endocast of the stem lagomorph *Megalagus* and brain structure of basal Euarchontoglires. *Proc. R. Soc. B Biol. Sci.* 287:20200665. doi: 10.1098/rspb.2020.0665

MacInnes, D. G. (1953). The Miocene and Pleistocene Lagomorpha of East Africa. *Foss. Mamm. Afr.* 6, 1–30.

Meng, J. (1991). Ear features of *Palaeolagus* (Mammalia, Lagomorpha) and some character polarities. *J. Vertebr. Paleontol.* 11(Suppl. 3):47A.

Meng, J., Hu, Y., and Li, C.-K. (2003). The osteology of *Rhombomylus* (Mammalia, Glires): implications for phylogeny and evolution of Glires. *Bull. Am. Mus. Nat. Hist.* 275, 1–247. doi: 10.1206/0003-0090(2003)275<0001:toormg>2.0.co;2

Schneider, C. A., Rasband, W. S., and Eliceiri, K. W. (2012). NIH image to ImageJ: 25 years of image analysis. *Nat. Methods* 9, 671–675. doi: 10.1038/nmeth.2089

Troxell, E. L. (1921). *Palaeolagus*, an extinct hare. *Am. J. Sci.* 1, 340–348. doi: 10.2475/ajs.s5-1.4.340

Wahlert, J. H. (1974). The cranial foramina of protrogomorphous rodents, an anatomical and phylogenetic study. *Bull. Mus. Comp. Zool.* 146, 363–410.

Wible, J. R. (2007). On the cranial osteology of the Lagomorpha. *Bull. Carnegie Mus. Nat. Hist.* 39, 213–234. doi: 10.2992/0145-9058(2007)39[213:otcoot]2.0.co;2

Wible, J. R., and Shelley, S. L. (2020). Anatomy of petrosal and middle ear of the brown rat, *Rattus norvegicus* (Berkenhout, 1769) (Rodentia, Muridae). *Ann. Carnegie Mus.* 86, 1–35. doi: 10.2992/007.086.0101

Wilson, D. E., Lacher, T. E., and Mittermeier, R. A. (eds) (2016). *Handbook of the Mammals of the World: Lagomorphs and Rodents I*. Barcelona: Lynx Edicions.

Wood, A. E. (1940). The mammalian fauna of the White River Oligocene. Part III. Lagomorpha. *Trans. Am. Philos. Soc.* 28, 271–362. doi: 10.2307/1005524

Wu, S.-Y. (2003). The cranial morphology and phylogenetic relationship of *Alloptox gobiensis* (Lagomorpha, Ochotonidae). *Vert. PalAsiat.* 41, 115–130.

Conflict of Interest: The authors declare that the research was conducted in the absence of any commercial or financial relationships that could be construed as a potential conflict of interest.

The reviewer, OB, declared a past co-authorship with one of the authors, ŁF-F, to the handling editor.

frontiers in Genetics

ORIGINAL RESEARCH
published: 26 February 2021
doi: 10.3389/fgene.2021.622724

Comparison of the Microsatellite Distribution Patterns in the Genomes of Euarchontoglires at the Taxonomic Level

Xuhao Song[1,2†], Tingbang Yang[1,2†], Xinyi Zhang[1], Ying Yuan[1], Xianghui Yan[1], Yi Wei[1,2], Jun Zhang[1,2] and Caiquan Zhou[1,2]*

[1] Key Laboratory of Southwest China Wildlife Resources Conservation (Ministry of Education), China West Normal University, Nanchong, China, [2] Institute of Ecology, China West Normal University, Nanchong, China

Microsatellite or simple sequence repeat (SSR) instability within genes can induce genetic variation. The SSR signatures remain largely unknown in different clades within Euarchontoglires, one of the most successful mammalian radiations. Here, we conducted a genome-wide characterization of microsatellite distribution patterns at different taxonomic levels in 153 Euarchontoglires genomes. Our results showed that the abundance and density of the SSRs were significantly positively correlated with primate genome size, but no significant relationship with the genome size of rodents was found. Furthermore, a higher level of complexity for perfect SSR (P-SSR) attributes was observed in rodents than in primates. The most frequent type of P-SSR was the mononucleotide P-SSR in the genomes of primates, tree shrews, and colugos, while mononucleotide or dinucleotide motif types were dominant in the genomes of rodents and lagomorphs. Furthermore, (A)n was the most abundant motif in primate genomes, but (A)n, (AC)n, or (AG)n was the most abundant motif in rodent genomes which even varied within the same genus. The GC content and the repeat copy numbers of P-SSRs varied in different species when compared at different taxonomic levels, reflecting underlying differences in SSR mutation processes. Notably, the CDSs containing P-SSRs were categorized by functions and pathways using Gene Ontology and Kyoto Encyclopedia of Genes and Genomes annotations, highlighting their roles in transcription regulation. Generally, this work will aid future studies of the functional roles of the taxonomic features of microsatellites during the evolution of mammals in Euarchontoglires.

Keywords: Euarchontoglires, genome, microsatellite distribution pattern, taxonomic features, functional annotation

OPEN ACCESS

Edited by:
Irina Ruf,
Senckenberg Research Institute and Natural History Museum Frankfurt, Germany

Reviewed by:
Jie Qiu,
Shanghai Normal University, China
Xiuyue Zhang,
Sichuan University, China

***Correspondence:**
Caiquan Zhou
drcqzhou1@163.com

† These authors have contributed equally to this work

Specialty section:
This article was submitted to Evolutionary and Population Genetics, a section of the journal Frontiers in Genetics

Received: *29 October 2020*
Accepted: *05 February 2021*
Published: *26 February 2021*

Citation:
Song X, Yang T, Zhang X, Yuan Y, Yan X, Wei Y, Zhang J and Zhou C (2021) Comparison of the Microsatellite Distribution Patterns in the Genomes of Euarchontoglires at the Taxonomic Level. Front. Genet. 12:622724. doi: 10.3389/fgene.2021.622724

INTRODUCTION

Microsatellites, or simple sequence repeats (SSRs) are tandem repetitions of relatively short DNA motifs present in perfect (P-SSR), compound (C-SSR), and imperfect (I-SSR) forms in nearly all known genomes (Du et al., 2018; Du et al., 2020). Polymorphic microsatellites have been widely utilized as popular molecular markers for studying neutral genetic variation in diverse fields,

including individual identification (Huang et al., 2015), population genetics (Zepeda et al., 2019), and other genetic studies (Highnam et al., 2012; Aristizábal et al., 2018). Recently, SSR instability in functional genes has been shown to be associated with many human diseases, such as neurological disorders (Rohilla and Gagnon, 2017) and colorectal cancers (Yamamoto and Imai, 2019). In particular, SSRs could also play an important role in generating the genetic variation underlying the adaptive evolution of organisms. There are substantial data indicating that SSR mutability can affect gene regulation as well as transcription and protein function, which ultimately confer phenotypic flexibility/plasticity (Holder et al., 2015; Bagshaw et al., 2017; Press et al., 2018).

Aside from the ubiquity and functional significance of SSRs, tremendous progress has been made in characterizing the distribution patterns of SSRs in diverse eukaryotic genomes (Qin et al., 2015; Ding et al., 2017; Srivastava et al., 2019). Indeed, comparative genomics approaches have aided the exploration of microsatellite conservation footprints in eukaryotic species evolution. More specifically, previous analyses of SSRs within 136 insect genomes revealed that common genomic features of SSRs were detectable at the family level (Ding et al., 2017). Furthermore, an investigation of P-SSRs in 719 eukaryotic species revealed several taxon-specific P-SSR characteristics as well as some evolutionary differences in the context of length and GC content of these P-SSRs (Srivastava et al., 2019). Meanwhile, profound interspecific variability in SSR distribution patterns in genomes has also been reported in insects, which suggests that variation might play an important role in the adaptation and evolution of insects (Behura and Severson, 2012; Song et al., 2020). Microsatellites present various degrees of taxon-specific enrichment in different lineages; thus, comparative analyses of SSRs at different taxonomic levels could therefore provide insight into the significance of evolutionarily relevant SSRs.

Euarchontoglires is a superclade of placental mammals that includes primates, rodents, lagomorphs, tree shrews, and colugos. Dynamic evolutionary signatures of microsatellites in Euarchontoglires genomes may be present because many species in this group are characterized by their successful adaptive radiation to various ecological niches. Although over 150 Euarchontoglires genomes are now available in the GenBank database, the SSR distribution patterns have only been studied in a handful of species in this clade (Liu et al., 2017; Xu et al., 2018; Srivastava et al., 2019). Thus, a genome-wide characterization of the microsatellite distribution patterns in Euarchontoglires genomes remains to be completed. Here, we investigated the distribution patterns of SSRs in 153 species, representing five taxonomic orders of Euarchontoglires (Rodentia, Lagomorpha, Primates, Scandentia, and Dermoptera). Comparisons of the distribution patterns of SSRs among different taxonomic levels were made to characterize taxonomic patterns of the microsatellite distributions in Euarchontoglires. Furthermore, the potential functions of microsatellite-containing CDSs were further surveyed using Gene Ontology (GO) enrichment analysis and Kyoto Encyclopedia of Genes and Genomes (KEGG) pathway analysis. We present a detailed characterization of the taxon-specific distribution pattern of SSRs among 153 species and provides insight into the biological significance of SSRs in this clade.

MATERIALS AND METHODS

Genome Dataset

Currently, the genomes of 153 species (57 primates, 88 rodents, four lagomorphs, three tree shrews, and one colugo) within Euarchontoglires are publicly available (**Supplementary Table 1**). All currently available Euarchontoglires genomes were downloaded from GenBank[1] for microsatellite identification and analysis. Ambiguous nucleotides were removed from the genomes prior to analysis. Detailed taxonomic information of these organisms was gathered from the National Center of Biotechnology Information (NCBI) database. The features of these genomes are presented in **Supplementary Table 1**. Among the 153 genomes, 57 genomes (26 primates, 27 rodents, two lagomorphs, one tree shrew, and one colugo) were annotated with protein-coding genes accompanied by gff3 annotation files containing positional information for exons and introns (**Supplementary Table 1**). The hierarchical classification provided by TimeTree (Kumar et al., 2017) was downloaded as a Newick file and was used for visualization through the iTOL (interactive Tree of Life) web server (Letunic and Bork, 2016).

Microsatellite Identification

According to the methods described previously (Qi et al., 2020), SSRs (i.e., P-SSRs, C-SSRs, and I-SSRs) were screened and localized using Krait v1.0.3 software (Du et al., 2018). Furthermore, the P-SSRs located within intergenic regions were further identified by a Python script according to the annotation file. Repeats with unit patterns of circular permutations and/or reverse complementation to each other were grouped together as a single type for statistical analysis as described previously (Xu et al., 2016). Overall, 5356 possible permutations of SSR motifs 1–6 bp in length were divided into 501 stand motif types as described by Srivastava et al. (2019). In addition, the relative positions of exons, introns, and CDSs were extracted from the annotation files for genomic annotation of P-SSRs, C-SSRs, and I-SSRs by Krait v1.0.3.

Microsatellite Attribute Investigation

In this study, the prevalence of SSRs in the genome was assessed by SSR abundance (loci/Mb) and SSR density (bp/Mb) as described by Qi et al. (2016). The abundance of the 501 stand repeat motif types in each genome was calculated by a custom Python script. A heatmap was generated based on the density of all SSR motif classes in each organism as described by Srivastava et al. (2019) with slight modifications, which could reveal repeat class-specific enrichment trends among different taxon groups. First, we ranked all of the repeat motif classes based on their density in each species. Furthermore, we first gave -2 to those repeats that had a frequency of < 10 in a given organism, to reduce sampling bias. Next, we assigned scores of

[1] http://www.ncbi.nlm.nih.gov/

3, 2, and 1 to repeats with the top 5, 20, and 35 ranks in the genome, respectively. Repeats in the bottom 20 ranks and with a frequency of at least 10 were given a score of −1. All other repeats were assigned a score of 0. A matrix was built using the score information, where each row represents an organism and the columns represent the repeated classes. The clustered matrix was visualized using TBtools (Chen et al., 2020). The color scale on the heatmap ranged from a maximum score of 3 (red) to a minimum score of −2 (blue).

The GC content of mono- to hexanucleotide P-SSRs was also calculated for the GC composition analysis in each organism using in-house Python scripts. Meanwhile, the preference analysis of the repeat copy numbers (RCNs) and analysis of the coefficient of variability (CV) of the P-SSRs were analyzed according to the methods described by Qi et al. (2020), which was able to reveal the degree of variation in the RCNs of different SSRs.

Functional Annotation of the P-SSRs

To characterize the functional roles of the CDSs containing P-SSRs, these sequences were aligned with the NCBI non-redundant database and the SWISS-PROT database using Diamond (Buchfink et al., 2015) with a cutoff E-value of 1E-5. Gene Ontology (GO) term mapping was conducted by TBtools. The mapping results were submitted to WEGO (Ye et al., 2018) for GO classification, and TBtools was further used to perform GO enrichment analysis. Kyoto Encyclopedia of Genes and Genomes (KEGG) pathway analysis was carried out by a KEGG automatic annotation server called KAAS (KEGG Automatic Annotation Server[2]; Moriya et al., 2007). The output contains KO (KEGG Orthology) assignments that were used for KEGG enrichment analysis by TBtools.

Statistical Analysis

SPSS (Statistical Product and Service Solutions, version 17.0) was used for the calculation of the Pearson correlation coefficient and the significance test. Figures were produced using Microsoft Office Excel 2013, ImageGP[3], and R (version 3.5.1) with the "ggplot2" package.

RESULTS

Occurrence of SSRs in Euarchontoglires Genomes

The basic attributes of different SSR categories derived from our analysis along with the taxonomic classification of each organism are presented in **Supplementary Table 2**. A total of 702,828,080 SSR loci (P-SSRs, C-SSRs, and I-SSRs) were identified from the genome data of 153 species. The length proportions of the SSRs covered from 3.19% (*Daubentonia madagascariensis*) to 9.87% (*Myocastor coypus*) of the Euarchontoglires genomes. Of these, I-SSRs were the dominant SSR category (62.05–82.58%) of the SSRs recovered, followed by P-SSRs (16.77–34.64%), and C-SSRs (0.60–4.17%). **Supplementary Table 3** shows that both the total number and length of SSRs (including P-SSRs, C-SSRs, and I-SSRs) were positively correlated with genome size (SSR numbers: Pearson, $r = 0.619$, $p < 0.01$; SSR length: Pearson, $r = 0.495$, $p < 0.01$). Moreover, the total number and total length of the SSRs in rodents, primates, lagomorphs, and tree shrews were positively correlated with genome size (**Supplementary Table 3**). However, the abundance and density of SSRs were not significantly correlated with the genome size of Euarchontoglires (SSR abundance: Pearson, $r = 0.092$, $p = 0.534$; SSR density: Pearson, $r = 0.028$, $p = 0.73$). Although the abundance and density of SSRs in rodent genomes were not significantly correlated with genome size (SSR abundance: Pearson, $r = 0.082$, $p = 0.449$; SSR density: Pearson, $r = 0.068$, $p = 0.53$), the abundance and density of SSRs in primate genomes were significantly positively correlated with genome size (SSR abundance: Pearson, $r = 0.534$, $p < 0.001$; SSR density: Pearson, $r = 0.528$, $p < 0.001$). Furthermore, no significant relationship between genome size and SSR abundance or SSR density was found in lagomorphs and tree shrews. In the genic regions, the abundance of SSRs also followed the pattern I-SSRs > P-SSRs > C-SSRs (**Supplementary Table 4**). Moreover, the abundance of SSRs in different genic regions followed the pattern intron > exon > CDS.

Variation Characteristics of P-SSRs Across the Evolutionary Landscape

As presented in **Figure 1**, the most frequent categories of P-SSRs in primates, tree shrews, and colugo were identical (i.e., mononucleotide P-SSRs), while mono- or dinucleotide motif types were the most abundant P-SSRs in both rodents and lagomorphs. In rodents, SSR abundance varied among the studied genomes. For example, the dominant P-SSR category tends to be conserved within most genera, such as *Peromyscus*, *Mus, Rattus*, or *Cavia* (**Figure 1**). In the *Microtus* genus (4 species), however, dinucleotide P-SSRs dominated in *Microtus agrestis*, *Microtus ochrogaster*, and *Microtus oeconomus* but not in *Microtus arvalis*, in which the proportion of mononucleotide P-SSRs (36.74%) was slightly higher than that of dinucleotide P-SSRs (35.69%). Next, the numbers of P-SSRs in the CDS, exon, and intron regions of the Euarchontoglires genomes were further analyzed (**Table 1**). As expected, trinucleotide P-SSRs dominated in the CDS regions of all species analyzed in this study. Similarly, the most prevalent P-SSR categories in the exon and intron regions of primates, tree shrews, and colugos were mononucleotide P-SSRs, while the most common P-SSR types in rodents and lagomorphs were mono- or dinucleotide P-SSRs. The predominant P-SSR type in most rodents within the same genus was conserved in the exon and intron regions, but the dominant P-SSR type in the exon regions varied among species within *Mus* (**Table 1**).

The top five most abundant repeat motifs and the most dominant repeat motifs with different lengths are shown in **Supplementary Table 5**. Our results demonstrated that the most predominant P-SSR motifs showed some taxon-specific features. (A)n was the most recurrent motif in primates, lagomorphs, tree shrews, and colugo, while (A)n, (AC)n, or (AG)n was the

[2]http://www.genome.jp/kegg/kaas/

[3]http://www.ehbio.com/Cloud_Platform/front/#/

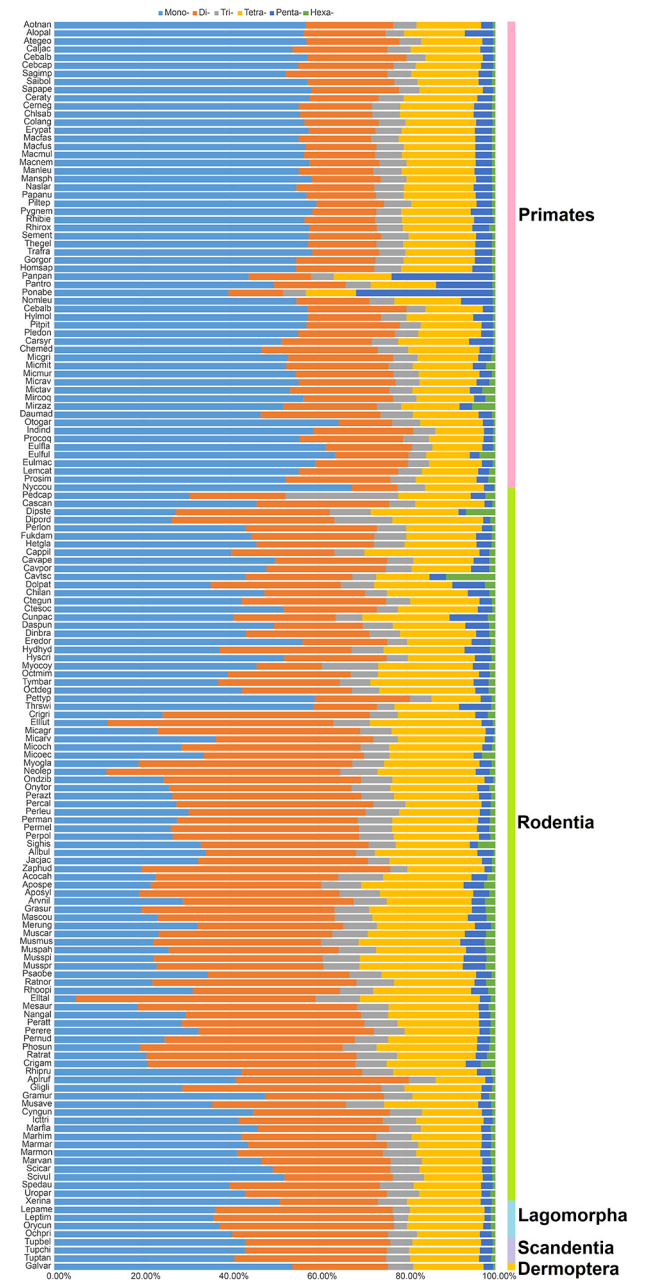

FIGURE 1 | Percentage of six categories of P-SSRs in the 153 Euarchontoglires genomes. Percentages were calculated according to the total number of each P-SSR type divided by the total number of P-SSRs in that species.

most abundant motif in rodent genomes. Furthermore, the most dominant SSR motifs within some genera in Rodentia varied (e.g., *Peromyscus*). On the other hand, the results showed that the most frequent repeated motif in each P-SSR category (mono- to hexanucleotide P-SSRs) exhibited different levels of variation among the mammals studied. Moreover, such variation was greater in rodents than in primates (**Supplementary Table 5**). For the most frequent repeat motifs of mononucleotide P-SSRs, (A)n dominated in all Euarchontoglires genomes. The dominant dinucleotide repeat motif was (AC)n in primates and colugos. The most frequent dinucleotide motif in rodent and lagomorph genomes was (AC)n and (AG)n, whereas (AG)n repeats rarely occurred. The most frequent dinucleotide motif in tree shrews was (AG)n. Additionally, (AAT)n and (AAC)n dominated in primate and lagomorph genomes; (AAT)n, (AAC)n, and (AGG)n were the most common trinucleotide repeat motifs; and (AAT)n was the most dominant motif in tree shrews and colugos. For tetranucleotide P-SSRs, the predominant motif in the genomes of primates, lagomorphs, tree shrews, and colugo was (AAAT)n, while the predominant motifs of tetranucleotides in rodents were (AAAG)n, (AAAT)n, and (AAAC)n. However, the predominant motifs of penta- or hexanucleotide P-SSRs differed considerably among these Euarchontoglires genomes. It is noteworthy that the dominant repeat motif might differ among species belonging to the same genus in different clades, for instance, the dominant hexanucleotide P-SSR motifs in *Peromyscus* (**Supplementary Table 5**). However, the similarity of the dominant motif among species in the same genus did not coincide with the topological structure of the tree (**Figure 2**).

Although the dominant P-SSR repeat motif in genic regions (especially in CDS regions) varied within Euarchontoglires, a few taxon-specific features were observed (**Supplementary Table 5**). For example, (C)n was the most frequent mononucleotide P-SSR motif in genic regions (CDS, exon, and intron regions) of all Euarchontoglires genomes (**Supplementary Table 5**). Furthermore, (AC)n was the most abundant dinucleotide P-SSR motif in intron regions of primates and colugo; (AC)n or (AG)n was the most frequent motifs in rodents and lagomorphs; and (AG)n was dominant in tree shrews. Notably, the dominant triplet P-SSR motif types in the CDS regions showed more diversity than those in the exon and intron regions. For example, (AAAAAC)n was dominant in intron regions of most primates, while striking variability of the dominant hexanucleotide repeat motif was observed in the CDS regions of rodent genomes. Nevertheless, the most dominant trinucleotide repeat motifs in the CDS regions of all genomes were (ACG)n, (AGG)n, (CCG)n, and (AGG)n.

As described by Srivastava et al. (2019), a ranked P-SSR density heat map was plotted to illustrate the density-based abundance trends of the 501 SSRs (columns) across all 153 genomes (rows) in our study (**Figure 3** and **Supplementary Table 6**). Our results demonstrated that some clear patterns of abundance that were distinct for different subgroups of Euarchontoglires could be detected in the heat map. As seen along the left-most columns of the **Figure 3**, a few P-SSR motifs are highly abundant across most organisms, such as A, AC, AG, AAAT, AAAG, and other polyA repeat classes. Moreover, the density of some motif types was relatively higher in specific groups, but relatively rare in other groups. For example, the density of (AAGAGG)n was relatively higher in rodents than that in other clades, as indicated by arrow in **Figure 3**. Furthermore, comparison of microsatellite motifs demonstrated that clade-specific motifs were only found in rodents: (AAGCGT)n, (ATCGCG)n, (AACGGT)n, (AACGTC)n, (AACGAT)n, (ATGCTC)n, (AGCTCG)n, and (AAACGT)n. However, such motifs were only shared by several

TABLE 1 | The proportion of mono- to hexanucleotide P-SSRs in genic regions.

Order	Suborder	Family	Species	CDS						Exon						Intron					
				Mono-	Di-	Tri-	Tetra-	Penta-	Hexa-	Mono-	Di-	Tri-	Tetra-	Penta-	Hexa-	Mono-	Di-	Tri-	Tetra-	Penta-	Hexa-
Primates	Haplorrhini	Aotidae	*Aotus nancymaae*	2.51%	2.17%	88.69%*	1.66%	0.57%	4.40%	55.23%*	19.90%	13.74%	8.33%	2.09%	0.715%	60.88%*	18.01%	4.78%	13.28%	2.50%	0.55%
	Haplorrhini	Cebidae	*Saimiri boliviensis*	4.94%	3.05%	84.01%*	1.89%	0.51%	5.60%	62.65%*	17.56%	10.20%	6.28%	2.41%	0.91%	61.61%*	17.36%	4.75%	12.69%	2.86%	0.72%
	Haplorrhini	Cebidae	*Sapajus apella*	3.21%	2.07%	88.60%*	1.43%	0.30%	4.39%	58.88%*	18.47%	12.50%	7.49%	1.99%	0.69%	62.52%*	17.95%	4.13%	12.71%	2.27%	0.42%
	Haplorrhini	Cercopithecidae	*Cercocebus atys*	22.90%	5.14%	63.97%*	4.47%	0.58%	2.94%	56.01%*	18.46%	12.59%	9.30%	2.89%	0.75%	61.52%*	14.27%	5.60%	14.69%	3.31%	0.61%
	Haplorrhini	Cercopithecidae	*Chlorocebus sabaeus*	4.38%	4.97%	83.40%*	2.44%	1.22%	3.58%	55.58%*	19.59%	11.13%	9.68%	3.20%	0.82%	59.81%*	14.81%	5.67%	15.02%	3.98%	0.71%
	Haplorrhini	Cercopithecidae	*Colobus angolensis*	2.81%	2.04%	88.95%*	1.90%	0.35%	3.94%	61.00%*	17.71%	10.63%	7.37%	2.60%	0.69%	61.11%*	14.90%	5.56%	14.41%	3.48%	0.53%
	Haplorrhini	Cercopithecidae	*Macaca mulatta*	1.50%	1.86%	90.27%*	1.99%	0.58%	3.81%	55.72%*	17.88%	13.56%	9.06%	2.98%	0.80%	60.86%*	14.55%	5.51%	14.85%	3.62%	0.62%
	Haplorrhini	Cercopithecidae	*Macaca nemestrina*	2.48%	3.05%	87.97%*	2.29%	0.53%	3.68%	54.93%*	18.81%	12.82%	9.52%	3.04%	0.88%	60.87%*	14.91%	5.55%	14.45%	3.56%	0.66%
	Haplorrhini	Cercopithecidae	*Mandrillus leucophaeus*	2.84%	3.19%	87.79%*	1.66%	0.49%	4.02%	62.24%*	16.27%	10.33%	7.49%	2.78%	0.88%	60.15%*	14.96%	5.67%	14.76%	3.78%	0.68%
	Haplorrhini	Cercopithecidae	*Papio anubis*	3.11%	3.02%	87.88%*	1.74%	0.46%	3.80%	54.53%*	20.34%	11.32%	10.09%	2.97%	0.76%	61.27%*	14.33%	5.56%	14.56%	3.67%	0.62%
	Haplorrhini	Cercopithecidae	*Piliocolobus tephrosceles*	22.11%	1.61%	71.44%*	0.81%	0.20%	3.83%	61.92%*	16.18%	11.73%	7.25%	2.08%	0.84%	63.03%*	13.82%	5.29%	13.88%	3.42%	0.56%
	Haplorrhini	Cercopithecidae	*Rhinopithecus bieti*	3.07%	2.49%	88.61%*	1.68%	0.58%	3.59%	54.22%*	18.58%	13.78%	8.81%	3.98%	0.63%	61.86%*	13.90%	5.45%	14.35%	4.18%	0.26%
	Haplorrhini	Cercopithecidae	*Rhinopithecus roxellana*	1.95%	1.57%	90.56%*	1.76%	0.33%	3.81%	57.67%*	15.47%	15.38%	7.64%	2.86%	0.97%	62.89%*	13.45%	5.27%	14.22%	3.54%	0.63%
	Haplorrhini	Cercopithecidae	*Theropithecus gelada*	2.27%	1.93%	90.16%*	1.40%	0.24%	4.00%	58.71%*	14.88%	15.53%	7.59%	2.47%	0.82%	62.34%*	13.72%	5.34%	14.28%	3.66%	0.65%
	Haplorrhini	Cercopithecidae	*Trachypithecus francoisi*	2.31%	2.26%	89.50%*	1.46%	0.66%	3.81%	56.70%*	16.52%	14.95%	8.35%	2.70%	0.79%	63.17%*	13.42%	5.34%	14.12%	3.35%	0.61%
	Haplorrhini	Hominidae	*Gorilla gorilla*	1.29%	1.93%	90.85%*	1.48%	0.49%	3.96%	53.81%*	17.32%	15.86%	9.06%	2.97%	0.98%	59.76%*	15.85%	5.65%	14.59%	3.46%	0.70%
	Haplorrhini	Hominidae	*Homo sapiens*	1.74%	1.69%	90.25%*	2.60%	0.45%	3.26%	54.54%*	18.65%	11.44%	11.21%	3.18%	0.97%	58.40%*	16.74%	5.61%	15.02%	3.52%	0.71%
	Haplorrhini	Hominidae	*Pan paniscus*	4.33%	1.93%	86.46%*	3.11%	0.88%	3.28%	59.31%*	15.15%	11.32%	10.13%	3.28%	0.82%	58.56%*	16.25%	5.77%	14.99%	3.80%	0.63%
	Haplorrhini	Hominidae	*Pan troglodytes*	2.87%	3.18%	87.16%*	2.03%	1.10%	3.66%	52.61%*	19.73%	13.33%	10.45%	3.10%	0.78%	59.01%*	16.03%	5.74%	15.01%	3.59%	0.61%
	Haplorrhini	Hominidae	*Pongo abelii*	1.46%	1.99%	90.00%*	1.55%	0.58%	4.42%	55.03%*	16.04%	16.95%	8.48%	2.66%	0.84%	60.07%*	15.45%	6.22%	14.37%	3.24%	0.64%
	Haplorrhini	Hylobatidae	*Nomascus leucogenys*	2.15%	1.77%	90.11%*	1.68%	0.47%	3.82%	55.37%*	16.93%	16.14%	7.87%	2.92%	0.78%	61.90%*	15.12%	5.34%	13.93%	3.20%	0.50%
	Haplorrhini	Hylobatidae	*Hylobates moloch*	3.00%	2.47%	88.34%*	1.76%	0.57%	3.85%	56.44%*	17.27%	14.88%	7.88%	2.81%	0.72%	62.73%*	14.74%	5.23%	13.61%	3.18%	0.51%
	Haplorrhini	Tarsiidae	*CarlitoCarlit syrichta*	3.47%	2.45%	85.70%*	1.78%	0.68%	5.92%	55.28%*	20.19%	14.58%	6.64%	2.27%	1.03%	60.08%*	17.74%	5.01%	13.76%	3.00%	0.40%
	Strepsirrhini	Cheirogaleidae	*Microcebus murinus*	2.34%	1.69%	89.56%	1.92%	0.27%	4.21%	50.85%*	21.17%	15.27%	10.00%	2.23%	0.47%	58.89%*	20.09%	4.89%	12.89%	2.80%	0.44%
	Strepsirrhini	Galagidae	*Otolemur garnettii*	2.39%	1.55%	89.18%*	2.60%	0.35%	3.94%	57.55%*	14.42%	17.19%	8.01%	2.14%	0.69%	69.01%*	10.20%	5.70%	12.56%	2.24%	0.30%
	Strepsirrhini	Indriidae	*Propithecus coquereli*	1.55%	1.44%	91.58%*	1.39%	0.16%	3.89%	50.41%*	15.17%	24.39%	7.77%	1.69%	0.56%	61.38%*	20.04%	4.88%	11.35%	1.97%	0.38%
Rodentia	Castorimorpha	Castoridae	*Castor canadensis*	1.62%	1.91%	88.41%*	2.49%	0.81%	4.75%	53.05%*	25.01%	5.62%	14.06%	1.88%	0.40%	53.53%*	25.26%	4.75%	14.24%	1.87%	0.36%
	Castorimorpha	Heteromyidae	*Dipodomys ordii*	1.77%	1.82%	90.69%*	1.93%	0.48%	3.32%	34.77%	36.04%*8*	8.54%	18.60%	1.65%	0.40%	34.85%	36.27%*	8.08%	18.77%	1.65%	0.38%
	Hystricomorpha	Bathyergidae	*Fukomys damarensis*	2.26%	3.63%	84.84%*	2.66%	0.48%	6.13%	44.77%*	26.83%	12.81%	11.33%	3.41%	0.84%	48.97%*	24.79%	6.43%	15.43%	3.61%	0.76%
	Hystricomorpha	Bathyergidae	*Heterocephalus glaber*	3.01%	2.34%	85.79%*	1.78%	1.06%	6.02%	49.24%*	21.19%	12.79%	12.09%	3.59%	1.09%	51.16%*	23.20%	6.00%	15.43%	3.49%	0.72%
	Hystricomorpha	Caviidae	*Cavia porcellus*	2.32%	1.84%	84.59%*	2.11%	1.09%	8.04%	50.34%*	21.86%	13.30%	9.19%	3.67%	1.63%	54.37%*	22.68%	5.00%	13.24%	3.70%	1.01%
	Hystricomorpha	Chinchillidae	*Chinchilla lanigera*	1.92%	1.47%	85.60%*	2.50%	0.64%	7.87%	52.06%*	21.75%	11.00%	10.11%	3.91%	1.18%	51.43%*	20.70%	4.46%	17.52%	4.72%	1.17%
	Hystricomorpha	Octodontidae	*Octodon degus*	1.29%	1.60%	87.29%*	1.96%	0.31%	7.55%	51.17%*	17.37%	18.61%	8.78%	2.63%	1.43%	48.43%*	22.70%	5.19%	19.61%	2.84%	1.22%
	Myomorpha	Cricetidae	*Cricetulus griseus*	4.49%	3.18%	82.12%*	2.78%	0.90%	6.53%	44.36%*	30.07%	8.13%	13.17%	3.17%	1.11%	28.77%	42.90%*	5.99%	17.93%	2.94%	1.47%
	Myomorpha	Cricetidae	*Microtus ochrogaster*	1.29%	1.53%	92.51%*	1.13%	0.16%	3.38%	47.09%*	25.41%	12.05%	12.40%	2.55%	0.50%	31.43%	38.39%*	6.00%	21.25%	2.26%	0.67%
	Myomorpha	Cricetidae	*Neotoma lepida*	1.09%	2.69%	89.44%*	2.69%	0.95%	3.13%	15.53%	48.36%*	8.87%	22.65%	3.45%	1.14%	15.53%	48.36%*	8.87%	22.65%	3.45%	1.14%
	Myomorpha	Cricetidae	*Peromyscus leucopus*	1.60%	0.95%	92.59%*	1.60%	0.39%	2.86%	42.46%*	24.22%	18.38%	11.77%	2.49%	0.68%	32.48%	38.69%*	7.14%	18.39%	2.39%	0.91%
	Myomorpha	Cricetidae	*Peromyscus maniculatus*	2.08%	1.44%	91.14%*	1.34%	0.54%	3.47%	43.98%*	24.26%	15.72%	12.34%	2.89%	0.81%	26.61%	46.91%*	6.45%	16.78%	2.26%	0.98%
	Myomorpha	Dipodidae	*Jaculus jaculus*	2.39%	1.53%	89.73%*	2.08%	0.86%	3.41%	46.91%*	12.93%	27.11%	8.87%	2.56%	1.62%	34.63%	36.29%*	4.40%	21.61%	2.40%	0.66%
	Myomorpha	Muridae	*Arvicanthis niloticus*	4.42%	1.62%	85.66%*	1.35%	0.11%	6.85%	49.78%*	21.45%	12.74%	11.85%	3.07%	1.12%	31.23%	37.43%*	6.59%	19.88%	3.04%	1.83%
	Myomorpha	Muridae	*Grammomys surdaster*	1.79%	1.46%	90.45%*	1.92%	0.33%	4.05%	42.77%*	26.38%	14.61%	12.45%	2.76%	1.03%	23.38%	41.10%*	6.94%	23.64%	3.14%	1.80%
	Myomorpha	Muridae	*Mastomys coucha*	0.82%	1.87%	89.72%*	2.42%	0.38%	4.78%	36.01%*	28.80%	15.23%	14.35%	4.42%	1.20%	25.80%	38.75%*	7.75%	21.76%	4.19%	1.75%
	Myomorpha	Muridae	*Meriones unguiculatus*	1.68%	1.22%	92.16%*	1.31%	0.32%	3.31%	49.83%*	19.31%	16.24%	10.99%	3.18%	0.46%	35.16%*	31.91%	6.54%	21.91%	3.69%	0.78%
	Myomorpha	Muridae	*Mus caroli*	1.90%	2.38%	90.07%*	1.49%	0.36%	3.80%	39.48%*	25.73%	15.12%	14.21%	4.41%	1.05%	26.23%	38.16%*	7.73%	21.48%	4.64%	1.75%
	Myomorpha	Muridae	*Mus musculus*	2.24%	4.02%	83.54%*	3.37%	0.75%	6.08%	31.61%	33.03%*	10.49%	18.49%	4.84%	1.54%	23.52%	38.42%*	7.84%	22.78%	5.22%	2.23%
	Myomorpha	Muridae	*Mus pahari*	1.77%	1.50%	90.08%*	1.44%	0.17%	5.04%	44.15%*	23.22%	15.19%	11.98%	4.27%	1.19%	28.45%	37.23%*	7.77%	20.21%	4.38%	1.96%
	Myomorpha	Muridae	*Rattus norvegicus*	3.01%	3.12%	84.99%*	2.41%	0.60%	5.86%	39.31%*	30.84%	10.12%	14.70%	3.73%	1.31%	24.82%	44.49%*	7.57%	18.59%	2.68%	1.86%
	Myomorpha	Muroidea	*Mesocricetus auratus*	1.13%	1.45%	91.81%*	1.51%	0.31%	3.78%	29.57%	35.81%*	15.12%	15.54%	3.12%	0.85%	22.29%	46.89%*	6.53%	20.76%	2.26%	1.26%
	Myomorpha	Muroidea	*Nannospalax galili*	2.31%	1.75%	88.93%*	2.69%	0.25%	4.07%	47.86%*	25.15%	13.87%	9.68%	2.67%	0.76%	35.24%	36.55%*	5.59%	19.19%	2.59%	0.83%
	Myomorpha	Muroidea	*Rattus rattus*	2.24%	1.59%	90.14%*	1.42%	0.18%	4.43%	43.46%*	23.78%	15.68%	12.14%	3.81%	1.14%	23.32%	46.22%*	8.12%	18.15%	2.52%	1.67%
	Sciuromorpha	Sciuridae	*Ictidomys tridecemlineatus*	2.06%	1.56%	90.22%*	1.35%	0.14%	4.68%	58.38%*	19.03%	11.24%	8.02%	2.89%	0.43%	46.72%*	29.34%	6.64%	14.89%	2.00%	0.42%

(Continued)

TABLE 1 | Continued

Order	Suborder	Family	Species	CDS						Exon						Intron					
				Mono-	Di-	Tri-	Tetra-	Penta-	Hexa-	Mono-	Di-	Tri-	Tetra-	Penta-	Hexa-	Mono-	Di-	Tri-	Tetra-	Penta-	Hexa-
	Sciuromorpha	Sciuridae	*Marmota flaviventris*	2.02%	1.36%	91.12%*	0.98%	0.27%	4.25%	59.10%*	16.13%	15.47%	6.80%	1.98%	0.51%	51.66%*	26.50%	6.17%	13.43%	1.86%	0.38%
	Sciuromorpha	Sciuridae	*Urocitellus parryii*	1.53%	0.60%	90.84%*	0.98%	0.49%	5.56%	48.28%*	28.66%	6.77%	13.90%	1.91%	0.48%	48.42%*	28.95%	6.23%	14.05%	1.90%	0.45%
Lagomorpha		Leporidae	*Oryctolagus cuniculus*	2.78%	2.04%	88.03%*	1.30%	0.46%	5.38%	2.69%	45.12%*	28.23%	16.14%	4.87%	2.95%	40.70%*	36.27%	2.67%	17.60%	1.74%	1.02%
		Ochotonidae	*Ochotona princeps*	1.38%	1.44%	93.46%*	0.96%	0.36%	2.40%	57.15%*	15.63%	17.24%	7.32%	2.49%	0.17%	44.43%*	32.69%	6.60%	13.27%	2.56%	0.45%
Dermoptera		Cynocephalidae	*Galeopterus variegatus*	2.75%	2.12%	89.90%*	1.91%	0.49%	2.82%	60.22%*	17.34%	12.19%	7.69%	2.04%	0.52%	62.30%*	17.77%	4.58%	13.01%	1.98%	0.36%
Scandentia		Tupaiidae	*Tupaia chinensis*	6.55%	2.55%	82.55%*	1.36%	1.02%	5.96%	55.44%*	21.75%	9.59%	8.91%	3.26%	1.05%	45.50%*	30.97%	4.66%	15.63%	2.70%	0.54%

**the dominant P-SSR type.*

rodent species. For example, (AACGTC)n was shared by four rodent species, while (AAGCGT)n was only found in *Peromyscus maniculatus*. The specific repeat motifs in genic and intergenic regions of different clades were further analyzed (not shown), which revealed that the number of the specific repeat motif categories in rodents was higher than that in other clades of Euarchontoglires.

Analysis of the Coefficient of Variability of the P-SSRs

The variation characteristics of RCNs of different SSR types in Euarchontoglires genomes are shown in **Supplementary Table 7**. The CV of the RCN of P-SSRs with the same motif length (e.g., mononucleotide P-SSRs) varied differentially among the species in Euarchontoglires. In *Peromyscus* genus, for example, the CV of the RCN of the hexanucleotide P-SSR in genomes varied from 30.39% (*Peromyscus nudipes*) to 343.14% (*Peromyscus eremicus*). Furthermore, the trend line for the CV of the mono- to hexanucleotide P-SSRs among different species also differed considerably (**Supplementary Table 8**). Nonetheless, a few common characteristics of the CV of the RCN of P-SSRs were detected in the CDS and exon regions. For example, the CVs of tetra- and pentanucleotide P-SSRs were relatively lower compared with those of trinucleotide P-SSRs in most species. Moreover, the mean CV of the mono- to hexanucleotide P-SSR among the five subclades of Euarchontoglires exhibited comparable trends (**Figure 4**). From di- to hexanucleotide P-SSRs in exon regions, for example, the CV decreased as the P-SSR motif length increased. Furthermore, the patterns of CV of P-SSRs in genomes showed similar pattern to that in intergenic regions, while the CV of P-SSRs in CDS and exon regions showed similar pattern.

GC Content of P-SSRs in Euarchontoglires Genomes

Assessment of the GC content variation of P-SSRs in different subgroups of Euarchontoglires was also performed in this study (**Figure 5** and **Supplementary Table 9**), which demonstrated that the P-SSR categories containing the highest or the lowest GC were relatively conserved. As shown in **Figure 5** and **Supplementary Table 9**, mononucleotide P-SSRs had the lowest GC content in all genomes studied, while dinucleotide or hexanucleotide P-SSRs had the highest GC content across most genomes. However, different levels of GC content variation could be observed in different clades when compared at different taxonomic levels. The P-SSR category that had the highest GC content varied within some genera; for example, mononucleotide P-SSRs in *Eulemur flavifrons* and *Eulemur macaco* had the highest GC content, whereas hexanucleotide P-SSRs had the highest GC content in *Eulemur fulvus*. This pattern in GC content was not consistent with the topological structure of the evolutionary relationships within *Eulemur*. In genic regions, the P-SSR category containing the highest GC content in the exon and intron regions was relatively conserved in primates compared with rodents (**Supplementary Table 9**). For example, trinucleotide P-SSRs had the highest GC content in exon regions

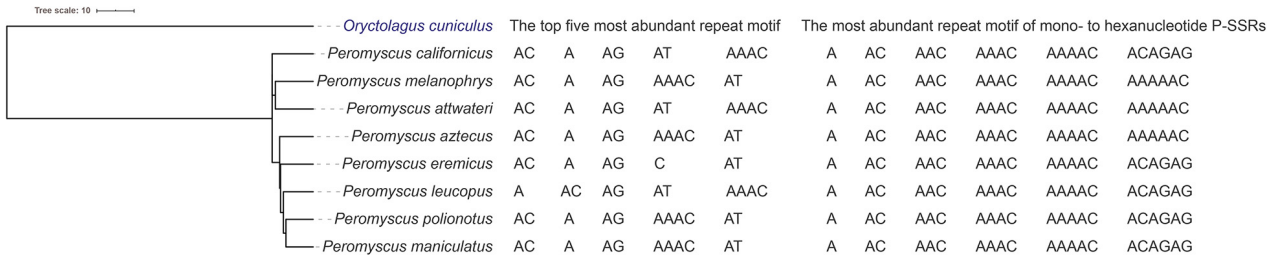

FIGURE 2 | The top five most abundant repeat motifs and the most common repeat motif in each P-SSR category in the *Peromyscus* genus. The phylogenetic tree was derived from TimeTree (http://www.timetree.org/), and *Oryctolagus cuniculus* was used as the outgroup. *Peromyscus nudipes* could not be found in Timetree and therefore is not shown in this tree.

FIGURE 3 | The enrichment trend of the 501 P-SSRs across 153 genomes. The P-SSR density-based ranking is used to generate a heat map per the color scale indicated. The 501 P-SSR motifs are arranged in columns, and the 153 organisms are arranged in rows. Arrows mark the positions for uniquely abundant (enriched) SSR signatures described in the text.

of most primates (except for *Rhinopithecus bieti*), while di- (12 species) or hexanucleotide P-SSRs (15 species) had the highest GC content in rodents (**Supplementary Table 9**). In addition, the GC content was higher for tetra-, penta-, or hexanucleotide P-SSRs than for other P-SSR categories, which was caused by the small amount of tetra- to hexanucleotide P-SSRs in the CDS regions. In intergenic regions, the P-SSR category with the lowest GC content was mononucleotide P-SSRs in most Euarchontoglires species. Furthermore, the GC content of mono- to hexanucleotide P-SSRs in most rodents was higher than that in primates.

Functional Analysis of CDSs With P-SSRs in the Genomes of Euarchontoglires

To characterize the functional roles of the CDSs possessing P-SSRs, we performed GO and KEGG pathway enrichment analyses. Surprisingly, GO and KEGG pathway enrichment analyses for the CDS containing P-SSRs in different clades of Euarchontoglires obtained similar results (**Supplementary Table 10**, **Supplementary Table 11**). As shown in **Supplementary Table 10**, the molecular function (MF) category of the GO analysis showed that the CDSs containing P-SSRs in all genomes were significantly enriched in "binding" and "transcription regulator activity." For the biological process (BP) category of the GO analysis, these CDSs were mainly associated with developmental process, immune system process, and metabolic process. Furthermore, these sequences were involved with "cell," "intracellular," or "protein-containing complex" in the cellular component (CC) categories. **Supplementary Table 11** shows the results of the KEGG analysis, and **Figure 6** shows the KEGG analysis results of *Homo sapiens*, *Mus musculus*, *Oryctolagus cuniculus*, *Tupaia chinensis*, and *Galeopterus variegatus*. The CDSs containing P-SSRs in the genomes of *Homo sapiens*, *Mus musculus*, *Oryctolagus cuniculus*, *Tupaia chinensis*, and *Galeopterus variegatus* were mainly enriched in transcription factors (**Figure 6B**).

Transcription factors, which bind preferentially to certain DNA sequences, play the central role of transcriptional regulation

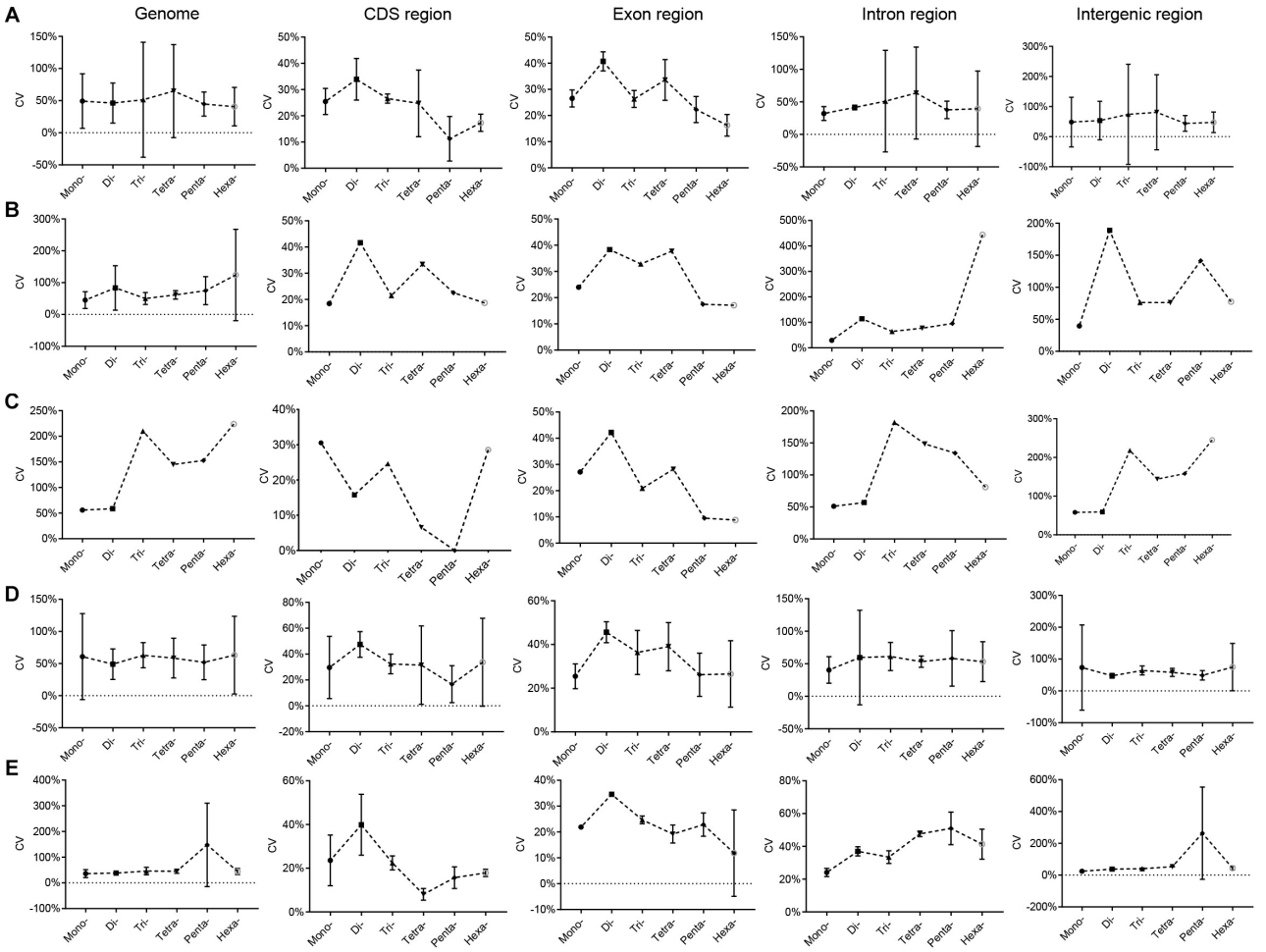

FIGURE 4 | CV analysis of the RCNs of P-SSRs in Euarchontoglires genomes. **(A)**, Primates; **(B)**, Scandentia; **(C)**, Dermoptera; **(D)**, Rodentia; **(E)**, Lagomorpha.

in all organisms (Imlay, 2015; Symonenko et al., 2018; Mejhert et al., 2020). In this study, the transcription factors containing SSRs were further identified from the annotation files and the results in **Supplementary Table 11** by a Python script. Our results revealed that the most abundant transcription factors containing P-SSRs in different clades of Euarchontoglires were zinc finger protein and forkhead-box protein (**Supplementary Table 12**).

DISCUSSION

The Distribution Patterns of SSRs in Euarchontoglires Genomes

Although the contributions of SSRs to variation in genome size remain unclear, the genome size variation among eukaryotic species is more closely correlated with the amount of repetitive DNA rather than the number of coding genes (Bennetzen et al., 2005; Blommaert et al., 2019). Our results showed that the number and length of SSRs were positively correlated with genome size, which is consistent with previous studies (Zhao et al., 2012; Qi et al., 2016; Ding et al., 2017). However, differences in the relationships between genome size and SSR abundance or SSR density were observed for primates and rodents. Our findings revealed a significant positive relationship between genome size and SSR abundance or density in primates, but no significant relationship was observed for rodents (**Supplementary Table 3**). Likewise, variable results have been derived from different taxon groups. For example, a negative relationship between genome size and SSR abundance has been observed in insects (Ding et al., 2017), but no correlation or no significant relationship has been observed in fungi (Wang et al., 2014), birds (Huang et al., 2016), or primates (Xu et al., 2018). In addition to the SSR detection criteria and sampling size, we suggested that the relationship between genome size and SSR density (or SSR abundance) might differ in different clades. Indeed, our results supported this hypothesis. Moreover, a significant positive relationship between SSR abundance (or density) and the genome size of species in Euarchontoglires was observed. Consequently, such a relationship (e.g., the relationship between SSR abundance and genome size) derived from a higher taxonomic level might not hold within its subgroups.

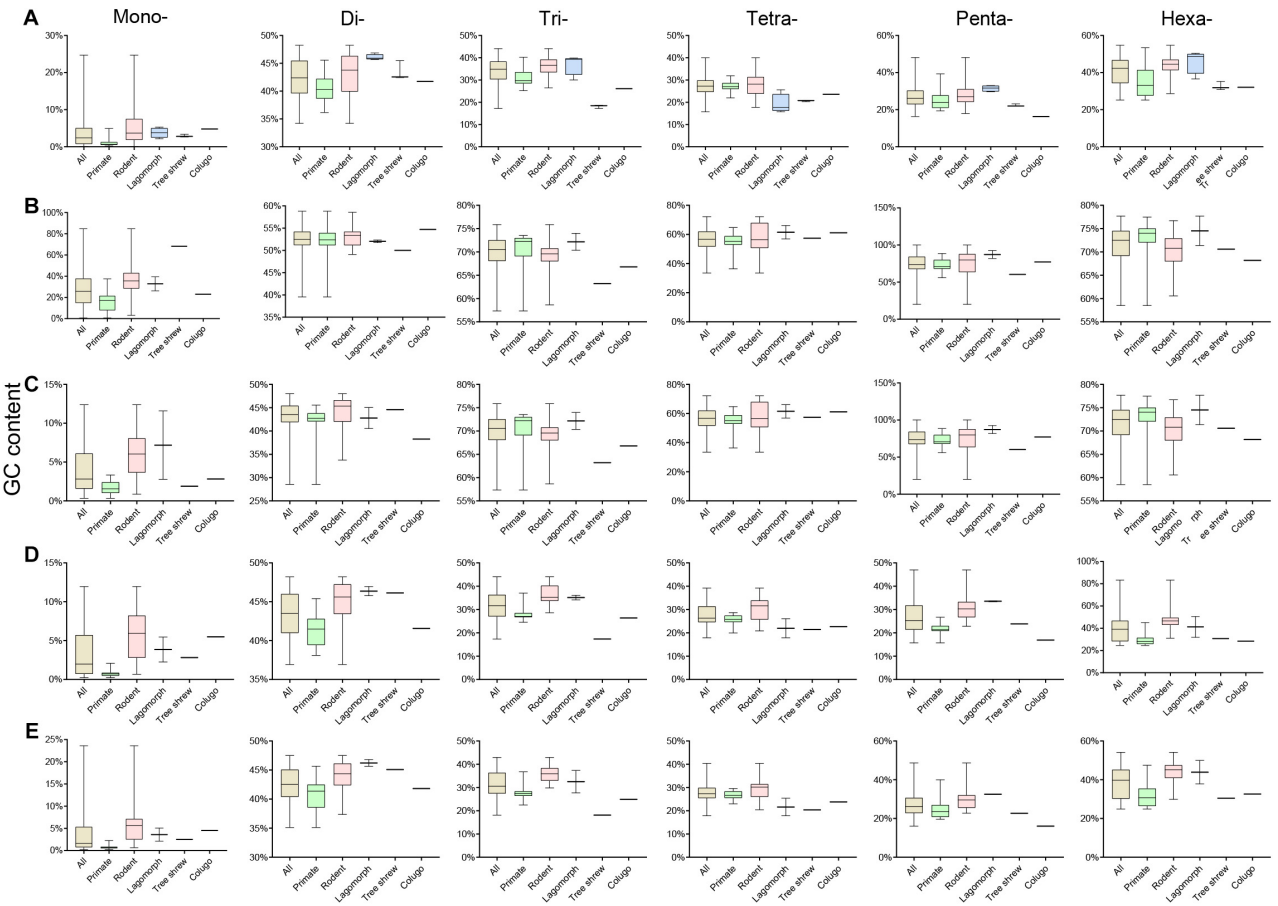

FIGURE 5 | The GC contents of P-SSRs in genomes and in genomic regions of different taxon clades within Euarchontoglires. **(A)**, genomes; **(B)**, CDSs; **(C)**, exons; **(D)**, introns; **(E)**, intergenic regions.

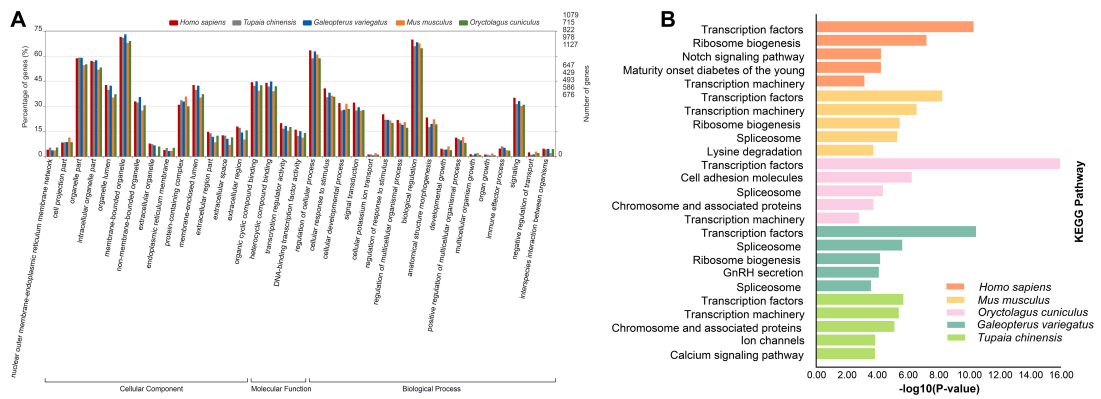

FIGURE 6 | The results of GO **(A)** and KEGG **(B)** analysis for the CDSs containing SSRs in genomes of five representatives within Euarchontoglires (*Homo sapiens*, *Tupaia chinensis*, *Galeopterus variegatus*, *Mus musculus*, and *Oryctolagus cuniculus*).

The proportion of different SSR categories was highly conserved in genomes or in genic regions across species in Euarchontoglires and showed the pattern I-SSRs > P-SSRs > C-SSRs (**Supplementary Tables 2**, **4**), which is consistent with patterns observed in beetles that used the same SSR detection criteria (Song et al., 2020). Better insight into the occurrence of SSRs in a range of taxa under an evolutionary scenario is important for understanding the differential abundance of SSRs. It remains to be seen whether the prevalence of I-SSR is common in other lineages with the same SSR detection

criteria. Changes in motif units by insertions, substitutions, and deletions of nucleotides produce I-SSRs and C-SSRs, which show decreased mutation rates compared with P-SSRs (Sainudiin et al., 2004). The dominance of I-SSRs in CDS regions has been suggested to play an important role in preventing coding-region frameshifts induced by microsatellite instability (Song et al., 2016). Therefore, the prevalence of I-SSRs in the genome might reflect the important role that the DNA repair system plays in the regulation of microsatellite instability. Moreover, the I-SSRs concentrated at certain locus in potyvirus genomes (e.g., HC-Pro helper component proteinase and coat protein) could be involved in recombination, producing genetic variation that drives host adaptation (Alam et al., 2013). Additional study of the dominance of I-SSRs in genomes may be useful for better understanding of genetic variation in Euarchontoglires species.

Taxon-Specific Features of P-SSRs in Euarchontoglires Genomes

Taxon-specific P-SSR distribution patterns have been detected in some lineages of organisms (Qin et al., 2015; Ding et al., 2017; Srivastava et al., 2019). However, few studies have examined variation in the distribution of microsatellites in Euarchontoglires at different taxonomic levels. Despite the controversial placement of Scandentia (Kumar et al., 2013), the most abundant P-SSR category in the genomes of the primate, tree shrew, and colugo clade (mononucleotide P-SSR) was different from that in the clade including rodents and lagomorphs (mono- or dinucleotide P-SSR dominated; **Figure 1**). A similar observation was made based on a comparison of the dominant P-SSR category in intron and exon regions (**Table 1**). It is possible that the dominant category of P-SSRs in genomes or in the intron and exon regions of different clades has the potential to be used as markers for phylogenetic analysis at the order level in Euarchontoglires. However, the dominant P-SSR category should be used with caution for phylogenetic analysis given that most genomes of Scandentia species remain unavailable. As expected, trinucleotide motif repeats prevailed in CDS regions. Microsatellites are thought to be under selection in genomes, which is reflected in their distribution and abundance, both of which are much higher than expected by chance or random accumulation (Ellegren, 2004). Our results showed that (ACG)n, (CCG)n, and (AGG)n were the dominant trinucleotide repeat motifs across all Euarchontoglires genomes (**Supplementary Table 5**), which indicated that these preferred motifs might be transcribed repeatedly in the same amino acids and further affect the physical and chemical properties of the proteins (as reviewed by Saeed et al., 2016). Moreover, the prevalence of some specific repeat motifs in genomes has been shown to have specific effects on genome function (Deback et al., 2009; Behura and Severson, 2012; Bagshaw, 2017). Comparative analysis demonstrated that rodent genomes had more specific repeat motif categories in genic and intergenic regions than that of other clades. Therefore, one intriguing question that needs to be resolved in the further is the function of the high frequencies of these amino acids in specific species or clades of Euarchontoglires.

A previous comprehensive analysis constructed phylogenetic trees using SSR frequency and revealed that the distribution patterns of SSRs were evolutionarily conserved at the family level in insects (Ding et al., 2017). In this study, we are wondering whether the dominant repeat motif is also correlated with the phylogenetic relationships within Euarchontoglires. Surprisingly, we found that the dominant repeat motif type of P-SSR (mono- to hexanucleotide P-SSR) was highly conserved at all taxonomic levels in primates, but was more variable in rodents (**Supplementary Table 5**). However, the similarity in the dominant P-SSR motif types (e.g., hexanucleotide P-SSRs) among rodent species precludes their use as a molecular marker for phylogenetic studies within the genus in Rodentia (**Figure 2**). A possible mechanistic explanation for these taxon-specific signatures in primates and rodents is that SSRs could evolve differently among different lineages. There is a general consensus that the presence of SSRs in the genomes of organisms is biased toward certain specific repeat motifs in different clades (Alam et al., 2019; Manee et al., 2020; Qi et al., 2020). In this study, an enrichment trend of P-SSR density for certain motif types was observed among the five taxonomic orders (**Figure 3**), which was similar to the findings of a previous study (Srivastava et al., 2019). Primates are rich in (AT)n repeats, whereas in rodents, (A)n, (AC)n, or (AG)n repeats are the most common (**Supplementary Table 5**). It is noteworthy that the dominant motif types could be different within the same genus in rodents (e.g., *Microtus*). This is likely explained by the fact that genome nucleotide composition could shape the prevalence of certain repeat units (Tian et al., 2010). Furthermore, the variation in prevalent taxon-specific repeat units might exhibit different biological functions in different taxon clades. In human genomes, for example, dinucleotide microsatellites with repeat units consisting of 50% A or T show higher recombination rates than other types of dinucleotide microsatellites (Guo et al., 2009).

The GC content of mononucleotide P-SSRs was the lowest across all Euarchontoglires genomes studied in the present investigation, which was consistent with previous studies of bovids (Qi et al., 2018), beetles (Song et al., 2020), and forest musk deer (Qi et al., 2020), suggesting that similar selective constraints might operate upon the GC content of mononucleotides in different clades. However, the P-SSR category containing the highest GC content displayed no taxon-specific features in Euarchontoglires (**Supplementary Table 10**). Indeed, P-SSR categories containing the highest GC contents may even vary in phylogenetically related species, such as *Eulemur macaco* and *Eulemur fulvus*. Various relationships have been observed between the polymorphism levels of P-SSRs and its GC content in different species (Kelkar et al., 2008; Brandström and Ellegren, 2008; Payseur et al., 2011). For example, relationships between GC content and SSR polymorphism levels for di- and tetranucleotides are opposite in chickens (Brandström and Ellegren, 2008). Although the relationship between GC content and SSR polymorphism level in different taxonomic groups requires further investigation, the observed GC content variation suggests that the polymorphism of P-SSR varies widely and gives an indication of the genetic variation among Euarchontoglires species. Moreover, the average GC content of trinucleotide

P-SSRs in genomes was 34.34%, while that in the CDS regions was 69.84% (**Supplementary Table 9**). Numerous studies have shown that the GC content of the DNA sequence is functionally important (Guo et al., 2009; Bhati et al., 2015; Kenigsberg et al., 2016); for example, some GC-rich SSRs may affect influence replication *via* their effects on DNA secondary structure (Nakagama et al., 2006; Bhati et al., 2015). Considering that trinucleotide P-SSRs are dominant in CDS regions, the GC content might be negatively associated with SSR variability to limit repeat number variation. The biological significance of the GC-rich bias of trinucleotides in CDS regions of Euarchontoglires requires further study.

SSRs with variable-length repeating motifs cause many human diseases (Yim et al., 2006; Wilkins et al., 2009; Sznajder et al., 2018). As expected, our scatter plot analyses revealed that the abundance of P-SSRs in different genomic regions decreased as the RCNs increased, and the RCNs of the microsatellites of corresponding motif lengths in the coding regions were lower than those in introns or in the whole genome (**Supplementary Table 7**). These results are consistent with the notion that the growth of long microsatellites is constrained by an upper length boundary that, when reached, sometimes results in large deletions (Vowles and Amos, 2006). The CV analysis of the RCN of P-SSRs demonstrated that patterns varied among different clade organisms. For example, a similar pattern was observed in bovids (Qi et al., 2018), but large variation was observed in beetles (Song et al., 2020). A possible explanation for this could be that the CVs of the RCNs of P-SSRs in species could be taxon-specific (Song et al., 2020), but the sample size could also considerably affect the results. Indeed, if all CV results derived from the 153 species are shown in one figure, no clear pattern of the CV could be observed (**Supplementary Table 8**). Moreover, a different pattern of CVs of P-SSRs was detected at every taxonomic level in Euarchontoglires (e.g., in *Eulemur* and *Microcebus*). Nonetheless, comparable results in genomes or in genomic regions of the five clades in this study could be observed when we plotted our results by using the average value of CV, e.g., the CVs of the RCNs of P-SSRs in CDS regions (**Figure 4**). Microsatellites are one of the most important sources of genetic variation, and the polymorphism levels are highly correlated with the repeat copy numbers of motif (Bagshaw, 2017). Therefore, interspecific differences in the CVs of P-SSRs can generate functional variability, and the variation in the CVs of RCNs could reflect fundamental differences among different organisms. Replication slippage (Saeed et al., 2016), heterozygosity (Amos, 2016) and varied environmental selection pressure are possible forces that could drive variation in CV trends among different species (**Figure 4** and **Supplementary Table 8**).

Functional Analysis of CDSs Harboring P-SSRs in Euarchontoglires Genomes

Recent studies have shown that the functional significance of SSRs in the modulation of gene expression and genome organization implies their functional conservation across species. An increasing number of SSRs have been developed from the transcriptomes of many organisms because of their importance as a source of functional markers (Park et al., 2019; Souza et al., 2020). However, the expression patterns of genes affected by many factors; thus, the SSRs derived from the transcriptome might be incomplete. In this study, we investigated the potential functions of CDSs containing P-SSRs in genomes of Euarchontoglires species by conducting GO and KEGG pathway enrichment analysis. It was intriguing that all the CDSs in different species containing P-SSRs were enriched in binding (GO:0005488) and transcription regulator activity function (GO:0140110), which is similar to the potential functions of the CDSs containing P-SSRs in beetles (Song et al., 2020). Moreover, KEGG enrichment analysis of genes containing SSRs indicated that transcription factors were the most well-represented pathways among Euarchontoglires species (**Figure 6** and **Supplementary Table 11**). Transcription factors are key regulatory elements that affect gene expression which coordinate a lot of biological processes, such as development (Yan et al., 2018) and metabolism (Chisato et al., 2018). Therefore, it is reasonable to speculate that the genes containing P-SSRs might regulate the selective synthesis of certain proteins. In this study, our results demonstrated that the two most abundant transcription factor categories that containing P-SSRs in different clades of Euarchontoglires were identical (i.e., zinc finger protein and forkhead-box protein; **Supplementary Table 12**). Previous studies revealed that zinc finger transcription factors and forkhead-box transcription factors have key roles in various aspects of immune regulation (Coffer and Burgering, 2004; Sakaguchi et al., 2010; Zhang et al., 2019). Although some SSRs in genes could facilitate the binding of transcription factors (reviewed by Bagshaw, 2017), the potential roles of SSRs in transcription factors in Euarchontoglires species remain to be further explored. Moreover, SSRs can be regarded as mutational hot spots in genome sequences, and the resulting genetic variation has been reported to play a positive role in adaptive evolution (Kashi and King, 2006; Li et al., 2008; Gemayel et al., 2010). A similar analysis performed in the giant panda revealed that the genes possessing polymorphic coding SSRs were involved in digestion and metabolism, which may contribute to its special adaptive evolution to its specialized diet of bamboo (Cheng et al., 2019). Taken together, our work paves the way for further understanding and validating the function roles of the genes containing P-SSRs. Additional large-scale comparative functional analyses of CDSs containing P-SSRs in different organisms should be performed to assess the generality of the results documented in our study.

CONCLUSION

Taxon-specific microsatellite distribution patterns were observed among different clades within Euarchontoglires. The dominant P-SSR categories in primates, tree shrews, and colugos were identical, but varied in rodents and lagomorphs. The enrichment of the most prevalent repeat motifs in specific clades was detected at the order level. However, the GC content and CV of P-SSRs varied greatly among different species at all taxonomic levels, suggesting that SSR variation might contribute to genetic

variation among these mammals. We showed that the CDSs containing P-SSRs across all Euarchontoglires genomes were enriched for functions related to transcription. However, more work is needed to clarify the precise evolution and functional roles of taxon-specific P-SSRs in Euarchontoglires.

DATA AVAILABILITY STATEMENT

The original contributions presented in the study are included in the article/**Supplementary Material**, further inquiries can be directed to the corresponding author/s.

AUTHOR CONTRIBUTIONS

XS, CZ, and YW: conceptualization. XS and TY: writing-original draft. XS, TY, XZ, and YY: data curation. TY, XY, and JZ: formal analysis. All authors contributed to the article and approved the submitted version.

FUNDING

This work was supported by the Department of Science and Technology of Sichuan Province (grant number 2020YFS0322) and the Doctoral Scientific Research Funds of China West Normal University (grant number 18Q055).

SUPPLEMENTARY MATERIAL

The Supplementary Material for this article can be found online at: https://www.frontiersin.org/articles/10.3389/fgene.2021.622724/full#supplementary-material

REFERENCES

Alam, C. M., George, B., Sharfuddin, C., Jain, S. K., and Chakraborty, S. (2013). Occurrence and analysis of imperfect microsatellites in diverse potyvirus genomes. *Gene* 521, 238–244. doi: 10.1016/j.gene.2013.02.045

Alam, C. M., Iqbal, A., Sharma, A., Schulman, A. H., and Ali, S. (2019). Microsatellite diversity, complexity, and host range of mycobacteriophage genomes of the Siphoviridae family. *Front. Genet*. 10:207. doi: 10.3389/fgene.2019.00207

Amos, W. (2016). Heterozygosity increases microsatellite mutation rate. *Biol. Lett*. 12:20150929. doi: 10.1098/rsbl.2015.0929

Aristizábal, A., Tuberquia, D. J., and Sanín, M. J. (2018). Conservation genetics of two highly endangered and poorly known species of *Zamia* (Zamiaceae: Cycadales) in Colombia. *J. Hered*. 109, 438–445.

Bagshaw, A. T. (2017). Functional mechanisms of microsatellite DNA in eukaryotic genomes. *Genome Biol. Evol*. 9, 2428–2443. doi: 10.1093/gbe/evx164

Bagshaw, A. T. M., Horwood, L. J., Fergusson, D. M., Gemmell, N. J., and Kennedy, M. A. (2017). Microsatellite polymorphisms associated with human behavioural and psychological phenotypes including a gene-environment interaction. *BMC Med. Genet*. 18:12. doi: 10.1186/s12881-017-0374-y

Behura, S. K., and Severson, D. W. (2012). Genome-wide comparative analysis of simple sequence coding repeats among 25 insect species. *Gene* 504, 226–232. doi: 10.1016/j.gene.2012.05.020

Bennetzen, J. L., Ma, J., and Devos, K. M. (2005). Mechanisms of recent genome size variation in flowering plants. *Ann. Bot*. 95, 127–132. doi: 10.1093/aob/mci008

Bhati, J., Sonah, H., Jhang, T., Singh, N. K., and Sharma, T. R. (2015). Comparative analysis and EST mining reveals high degree of conservation among five Brassicaceae species. *Comp. Funct. Genomics*. 2010:520238 doi: 10.1155/2010/520238

Blommaert, J., Riss, S., Hecox-Lea, B., Mark Welch, D. B., and Stelzer, C. P. (2019). Small, but surprisingly repetitive genomes: transposon expansion and not polyploidy has driven a doubling in genome size in a metazoan species complex. *BMC Genomics* 20:466. doi: 10.1186/s12864-019-5859-y

Brandström, M., and Ellegren, H. (2008). Genome-wide analysis of microsatellite polymorphism in chicken circumventing the ascertainment bias. *Genome Res*. 18, 881–887. doi: 10.1101/gr.075242.107

Buchfink, B., Xie, C., and Huson, D. H. (2015). Fast and sensitive protein alignment using diamond. *Nat. Methods* 12, 59–60. doi: 10.1038/nmeth.3176

Chen, C. J., Chen, H., Zhang, Y., Thomas, H. R., Frank, M. H., He, Y. H., et al. (2020). Tbtools - an integrative toolkit developed for interactive analyses of big biological data. *Mol. Plant* 13, 1194–1202. doi: 10.1016/j.molp.2020.06.009

Cheng, M. L., Ren, J. Y., Shen, F. J., Huang, Y., Fan, Z. X., Price, M., et al. (2019). Genome-wide investigation of microsatellite polymorphism in coding region of the giant panda (*Ailuropoda melanoleuca*) genome: a resource for study of phenotype diversity and abnormal traits. *Mamm. Res*. 64, 353–363. doi: 10.1007/s13364-019-00418-5

Chisato, S., Akihisa, O., Hiromasa, T., Munenori, K., Tomohiro, S., Takeo, U., et al. (2018). Suppression of mitochondrial oxygen metabolism mediated by the transcription factor HIF-1 alleviates propofol-induced cell toxicity. *Sci. Rep*. 8:8987. doi: 10.1038/s41598-018-27220-8

Coffer, P. J., and Burgering, B. M. T. (2004). Forkhead-box transcription factors and their role in the immune system. *Nat. Rev. Immunol*. 4, 889–899. doi: 10.1038/nri1488

Deback, C., Boutolleau, D., Depienne, C., Luyt, C. E., Bonnafous, P., Gautheret-Dejean, A., et al. (2009). Utilization of microsatellite polymorphism for differentiating herpes simplex virus type 1 strains. *J. Clin. Microbiol*. 47, 533–540. doi: 10.1128/JCM.01565-08

Ding, S., Wang, S. P., He, K., Jiang, M. X., and Li, F. (2017). Large-scale analysis reveals that the genome features of simple sequence repeats are generally conserved at the family level in insects. *BMC Genomics* 18:848. doi: 10.1186/s12864-017-4234-0

Du, L. M., Liu, Q., Zhao, K. L., Tang, J., Zhang, X. Y., Yue, B. S., et al. (2020). PSMD: an extensive database for pan-species microsatellite investigation and marker development. *Mol. Ecol. Resour*. 20, 283–291. doi: 10.1111/1755-0998.13098

Du, L. M., Zhang, C., Liu, Q., Zhang, X. Y., and Yue, B. S. (2018). Krait: an ultrafast tool for genome-wide survey of microsatellites and primer design. *Bioinformatics* 34, 681–683. doi: 10.1093/bioinformatics/btx665

Ellegren, H. (2004). Microsatellites: simple sequences with complex evolution. *Nat. Rev. Genet*. 5, 435–445. doi: 10.1038/nrg1348

Gemayel, R., Vinces, M. D., Legendre, M., and Verstrepen, K. J. (2010). Variable tandem repeats accelerate evolution of coding and regulatory sequences. *Annu. Rev. Genet*. 44, 445–477. doi: 10.1146/annurev-genet-072610-155046

Guo, W. J., Ling, J., and Li, P. (2009). Consensus features of microsatellite distribution: microsatellite contents are universally correlated with recombination rates and are preferentially depressed by centromeres in multicellular eukaryotic genomes. *Genomics* 93, 323–331. doi: 10.1016/j.ygeno.2008.12.009

Highnam, G., Franck, C. T., Martin, A., Stephens, C., Puthige, A., and Mittelman, D. (2012). Accurate human microsatellite genotypes from high-throughput resequencing data using informed error profiles. *Nucleic Acids Res*. 41:e32. doi: 10.1093/NAR/GKS981

Holder, I. T., Wagner, S., Xiong, P., Sinn, M., Frickey, T., Meyer, A., et al. (2015). Intrastrand triplex DNA repeats in bacteria: a source of genomic instability. *Nucleic Acids Res*. 43, 10126–10142. doi: 10.1093/nar/gkv1017

Huang, J., Li, W. J., Jian, Z. Y., Yue, B. S., and Yan, Y. F. (2016). Genome-wide distribution and organization of microsatellites in six species of birds. *Biochem. Syst. Ecol*. 67, 95–102. doi: 10.1016/j.bse.2016.05.023

Huang, J., Li, Y. Z., Du, L. M., Yang, B., Shen, F. J., Zhang, H. M., et al. (2015). Genome-wide survey and analysis of microsatellites in giant panda (*Ailuropoda*

melanoleuca), with a focus on the applications of a novel microsatellite marker system. *BMC Genomics* 16:61. doi: 10.1186/s12864-015-1268-z

Imlay, J. A. (2015). Transcription factors that defend bacteria against reactive oxygen species. *Annu. Rev. Microbiol*. 69, 93–108. doi: 10.1146/annurev-micro-091014-104322

Kashi, Y., and King, D. G. (2006). Simple sequence repeats as advantageous mutator in evolution. *Trends Genet*. 22, 253–259. doi: 10.1016/j.tig.2006.03.005

Kelkar, Y. D., Tyekucheva, S., Chiaromonte, F., and Makova, K. D. (2008). The genome-wide determinants of human and chimpanzee microsatellite evolution. *Genome Res*. 18, 30–38. doi: 10.1101/gr.7113408

Kenigsberg, E., Yehuda, Y., Marjavaara, L., Keszthelyi, A., Chabes, A., Tanay, A., et al. (2016). The mutation spectrum in genomic late replication domains shapes mammalian GC content. *Nucleic Acids Res*. 44, 4222–4232. doi: 10.1093/nar/gkw268

Kumar, S., Stecher, G., Suleski, M., and Hedges, S. B. (2017). TimeTree: a resource for timelines, timetrees, and divergence times. *Mol. Biol. Evol*. 34, 1812–1819. doi: 10.1093/molbev/msx116

Kumar, V., Hallström, B. V., and Janke, A. (2013). Coalescent-based genome analyses resolve the early branches of the Euarchontoglires. *PLoS One* 8:e60019. doi: 10.1371/journal.pone.0060019

Letunic, I., and Bork, P. (2016). Interactive tree of life (iTOL) v3: an online tool for the display and annotation of phylogenetic and other trees. *Nucleic Acids Res*. 44, W242–W245. doi: 10.1093/nar/gkw290

Li, Y. C., Korol, A. B., Fahima, T., Beiles, A., and Nevo, E. (2008). Microsatellites, genomic distribution, putative functions and mutational mechanisms, a review. *Mol. Ecol*. 11, 2453–2465. doi: 10.1046/j.1365-294X.2002.01643.x

Liu, S. X., Hou, W., Sun, T. L., Xu, Y. T., Li, P., Yue, B. S., et al. (2017). Genome-wide mining and comparative analysis of microsatellites in three macaque species. *Mol. Genet. Genomics* 292, 537–550. doi: 10.1007/s00438-017-1289-1

Manee, M. M., Algarni, A. T., Alharbi, S. N., Al-Shomrani, B. M., Ibrahim, M. A., Binghadir, S. A., et al. (2020). Genome-wide characterization and analysis of microsatellite sequences in camelid species. *Mamm. Res*. 65, 359–373. doi: 10.1007/s13364-019-00458-x

Mejhert, N., Kuruvilla, L., Gabriel, K. R., Elliott, S. D., Guie, M., Wang, H., et al. (2020). Partitioning of MLX-family transcription factors to lipid droplets regulates metabolic gene expression. *Mol. Cell* 77, 1251–1264. doi: 10.1016/j.molcel.2020.01.014

Moriya, Y., Itoh, M., Okuda, S., Yoshizawa, A., and Kanehisa, M. (2007). KAAS: an automatic genome annotation and pathway reconstruction server. *Nucleic Acids Res*. 35, W182–W185. doi: 10.1093/nar/gkm321

Nakagama, H., Higuchi, K., Tanaka, E., Tsuchiya, N., Nakashima, K., Katahira, M., et al. (2006). Molecular mechanisms for maintenance of G-rich short tandem repeats capable of adopting G4 DNA structures. *Mutat. Res. Fundam. Mol. Mech. Mutagen*. 598, 120–131. doi: 10.1016/j.mrfmmm.2006.01.014

Park, S., Son, S., Shin, M., Fujii, N., Hoshino, T., and Park, S. J. (2019). Transcriptome-wide mining, characterization, and development of microsatellite markers in *Lychnis kiusiana* (Caryophyllaceae). *BMC Plant Biol*. 19:14. doi: 10.1186/s12870-018-1621-x

Payseur, B. A., Peicheng, J., and Haasl, R. J. (2011). A genomic portrait of human microsatellite variation. *Mol. Biol. Evol*. 28, 301–312. doi: 10.1093/molbev/msq198

Press, M. O., McCoy, R. C., Hall, A. N., Akey, J. M., and Queitsch, C. (2018). Massive variation of short tandem repeats with functional consequences across strains of *Arabidopsis thaliana*. *Genome Res*. 28, 1169–1178. doi: 10.1101/GR.231753.117

Qi, W. H., Jiang, X. M., Yan, C. C., Zhang, W. Q., Xiao, G. S., Yue, B. S., et al. (2018). Distribution patterns and variation analysis of simple sequence repeats in different genomic regions of bovid genomes. *Br. Antarct. Surv. Sci. Rep*. 8, 1–13. doi: 10.1038/s41598-018-32286-5

Qi, W. H., Lu, T., Zheng, C. L., Jiang, X. M., Jie, H., Zhang, X. Y., et al. (2020). Distribution patterns of microsatellites and development of its marker in different genomic regions of forest musk deer genome based on high throughput sequencing. *Aging* 12:4445. doi: 10.18632/AGING.102895

Qi, W. H., Yue, B. S., Li, J., Hu, T. Z., Zhang, X. Y., Li, G. Z., et al. (2016). Distinct patterns of simple sequence repeats and GC distribution in intragenic and intergenic regions of primate genomes. *Aging* 8, 2635–2650. doi: 10.18632/aging.101025

Qin, Z., Wang, Y. P., Wang, Q. M., Li, A. X., Hou, F. Y., and Zhang, L. M. (2015). Evolution analysis of simple sequence repeats in plant genome. *PLoS One* 10:e0144108. doi: 10.1371/journal.pone.0144108

Rohilla, K. J., and Gagnon, K. T. (2017). RNA biology of disease-associated microsatellite repeat expansions. *Acta Neuropathol. Commun*. 5:63. doi: 10.1186/s40478-017-0468-y

Saeed, A. F., Wang, R. Z., and Wang, S. H. (2016). Microsatellites in pursuit of microbial genome evolution. *Front. Microbiol*. 6:1462. doi: 10.3389/fmicb.2015.01462

Sainudiin, R., Durrett, R. T., Aquadro, C. F., and Nielsen, R. (2004). Microsatellite mutation models: insights from a comparison of humans and chimpanzees. *Genetics* 168, 383–395. doi: 10.1534/genetics.103.022665

Sakaguchi, S., Hombauer, M., Bilic, I., Naoe, Y., Schebesta, A., and Taniuchi, I. (2010). The zinc finger protein MAZR is part of the transcription factor network controlling CD4/CD8 cell fate decision of DP thymocytes. *Nat. Immunol*. 11, 442–448. doi: 10.1038/ni.1860

Song, X. H., Shen, F. J., Huang, J., Huang, Y., Du, L. M., Wang, C., et al. (2016). Transcriptome-derived tetranucleotide microsatellites and their associated genes from the giant panda (*Ailuropoda melanoleuca*). *J. Hered*. 107, 423–430. doi: 10.1093/jhered/esw024

Song, X. H., Yang, T. B., Yan, X. H., Zheng, F. K., Xu, X. Q., and Zhou, C. Q. (2020). Comparison of microsatellite distribution patterns in twenty-nine beetle genomes. *Gene* 757:144919. doi: 10.1016/j.gene.2020.144919

Souza, M. C. P. D., Silva, M. D. D., Binneck, E., Cabral, G. A. D. L., Iseppon, A. M. B., Pompelli, M. F., et al. (2020). RNA-seq transcriptome analysis of *Jatropha curcas* L. accessions after salt stimulus and unigene-derived microsatellite mining. *Ind. Crops Prod*. 147:112168. doi: 10.1016/j.indcrop.2020.112168

Srivastava, S., Avvaru, A. K., Sowpati, D. T., and Mishra, R. K. (2019). Patterns of microsatellite distribution across eukaryotic genomes. *BMC Genomics* 20:153. doi: 10.1186/s12864-019-5516-5

Symonenko, A. V., Roshina, N. V., Krementsova, A. V., and Pasyukova, E. G. (2018). Reduced neuronal transcription of *Escargot*, the *Drosophila* gene encoding a snail-type transcription factor, promotes longevity. *Front. Genet*. 9:151. doi: 10.3389/fgene.2018.00151

Sznajder, ŁJ., Thomas, J. D., Carrell, E. M., Reid, T., McFarland, K. N., Cleary, J. D., et al. (2018). Intron retention induced by microsatellite expansions as a disease biomarker. *Proc. Natl. Acad. Sci. U.S.A*. 115, 4234–4239. doi: 10.1073/pnas.1716617115

Tian, X., Strassmann, J. E., and Queller, D. C. (2010). Genome nucleotide composition shapes variation in simple sequence repeats. *Mol. Biol. Evol*. 28, 899–909. doi: 10.1093/molbev/msq266

Vowles, E. J., and Amos, W. (2006). Quantifying ascertainment bias and species-specific length differences in human and chimpanzee microsatellites using genome sequences. *Mol. Biol. Evol*. 23, 598–607. doi: 10.1093/molbev/msj065

Wang, Y., Chen, M. J., Wang, H., Wang, J. F., and Bao, D. P. (2014). Microsatellites in the genome of the edible mushroom, *Volvariella volvacea*. *BioMed. Res. Int*. 2014:281912. doi: 10.1155/2014/281912

Wilkins, J. M., Southam, L., Mustafa, Z., Chapman, K., and Loughlin, J. (2009). Association of a functional microsatellite within intron 1 of the *BMP5* gene with susceptibility to osteoarthritis. *BMC Med. Genet*. 10:141. doi: 10.1186/1471-2350-10-141

Xu, Y. T., Hu, Z. X., Wang, C., Zhang, X. Y., Li, J., and Yue, B. S. (2016). Characterization of perfect microsatellite based on genome-wide and chromosome level in rhesus monkey (*Macaca mulatta*). *Gene* 592, 269–275. doi: 10.1016/j.gene.2016.07.016

Xu, Y. T., Li, W. J., Hu, Z. X., Zeng, T., Shen, Y. M., Liu, S. X., et al. (2018). Genome-wide mining of perfect microsatellites and tetranucleotide orthologous microsatellites estimates in six primate species. *Gene* 643, 124–132. doi: 10.1016/j.gene.2017.12.008

Yamamoto, H., and Imai, K. (2019). An updated review of microsatellite instability in the era of next-generation sequencing and precision medicine. *Semin. Oncol*. 46, 261–270. doi: 10.1053/j.seminoncol.2019.08.003

Yan, J. Y., Li, J., Hu, J., Zhang, L., Wei, C. G., Sultana, N., et al. (2018). Smad4 deficiency impairs chondrocyte hypertrophy via the Runx2 transcription factor in mouse skeletal development. *J. Biol. Chem*. 293, 9162–9175. doi: 10.1074/jbc.RA118.001825

Ye, J., Zhang, Y., Cui, H. H., Liu, J. W., Wu, Y. Q., Cheng, Y., et al. (2018). Wego 2.0: a web tool for analyzing and plotting GO annotations, 2018 update. *Nucleic Acids Res*. 46, W71–W75. doi: 10.1093/nar/gky400

Yim, J. J., Lee, H. W., Lee, H. S., Kim, Y. W., Han, S. K., Shim, Y. S., et al. (2006). The association between microsatellite polymorphisms in intron II of the human Toll-like receptor 2 gene and tuberculosis among Koreans. *Genes Immun*. 7, 150–155. doi: 10.1038/sj.gene.6364274

Zepeda, P. S., Rodríguez-Serrano, E., Torres-Pérez, F., Celis-Diez, J. L., and Palma, R. E. (2019). Genetic variability and structure of the Olive Field Mouse: a sigmodontine rodent in a biodiversity hotspot of southern Chile. *PeerJ* 7:e6955. doi: 10.7717/peerj.6955

Zhang, J., Luo, J. L., Jiang, H. L., Xie, T., Zheng, J. L., and Tian, Y. H. (2019). The tumor suppressor role of zinc finger protein 671 (*znf671*) in multiple tumors based on cancer single-cell sequencing. *Front. Oncol*. 9:1214. doi: 10.3389/fonc.2019.01214

Zhao, X. Y., Tian, Y. L., Yang, R. H., Feng, H. P., Ouyang, Q. J., Tian, Y., et al. (2012). Coevolution between simple sequence repeats (SSRs) and virus genome size. *BMC Genomics* 13:435. doi: 10.1186/1471-2164-13-435

Conflict of Interest: The authors declare that the research was conducted in the absence of any commercial or financial relationships that could be construed as a potential conflict of interest.

The reviewer XZ declared a past co-authorship with one of the authors XS to the handling editor.

frontiers in Ecology and Evolution

ORIGINAL RESEARCH
published: 04 March 2021
doi: 10.3389/fevo.2021.631417

Effects of Hierarchical Steepness on Grooming Patterns in Female Tibetan Macaques (*Macaca thibetana*)

Dong-Po Xia[1,2†], Xi Wang[2,3†], Paul A. Garber[4,5], Bing-Hua Sun[2,3], Lori K. Sheeran[6], Lixing Sun[7] and Jin-Hua Li[2,3*]*

[1] School of Life Sciences, Anhui University, Hefei, China, [2] International Collaborative Research Center for Huangshan Biodiversity and Tibetan Macaque Behavioral Ecology, Hefei, China, [3] School of Resources and Environmental Engineering, Anhui University, Hefei, China, [4] Department of Anthropology and Program in Ecology, Evolution, and Conservation Biology, University of Illinois at Urbana–Champaign, Urbana, IL, United States, [5] International Centre of Biodiversity and Primate Conservation, Dali University, Dali, China, [6] Department of Anthropology and Museum Studies, Central Washington University, Ellensburg, WA, United States, [7] Department of Biological Sciences, Central Washington University, Ellensburg, WA, United States

OPEN ACCESS

Edited by:
Lucja A. Fostowicz-Frelik, Institute of Paleobiology (PAN), Poland

Reviewed by:
Małgorzata Arlet, Adam Mickiewicz University, Poland
Jundong Tian, Zhengzhou University, China

***Correspondence:**
Dong-Po Xia
dpxia@ahu.edu.cn
Jin-Hua Li
jhli@ahu.edu.cn

† These authors have contributed equally to this work

Specialty section:
This article was submitted to Behavioral and Evolutionary Ecology, a section of the journal Frontiers in Ecology and Evolution

Received: *20 November 2020*
Accepted: *16 February 2021*
Published: *04 March 2021*

Citation:
Xia DP, Wang X, Garber PA, Sun BH, Sheeran LK, Sun L and Li JH (2021) Effects of Hierarchical Steepness on Grooming Patterns in Female Tibetan Macaques (Macaca thibetana). Front. Ecol. Evol. 9:631417. doi: 10.3389/fevo.2021.631417

Hierarchical steepness, defined as status asymmetries among conspecifics living in the same group, is not only used as a main characteristic of animal social relationships, but also represents the degree of discrepancy between supply and demand within the framework of biological market theory. During September and December 2011, we studied hierarchical steepness by comparing variation in grooming patterns in two groups of Tibetan macaques (*Macaca thibetana*), a primate species characterized by a linear dominance hierarchy. Using a focal sampling method, we collected behavioral data from two provisioned, free-ranging groups (YA1 and YA2) at Mt. Huangshan, China. We found that female dominance hierarchies were steeper in the YA1 group (0.81 based on the proportion of wins-losses and 0.66 based on dyadic dominance indices) than among members of the YA2 group (0.76 based on the proportion of wins-losses and 0.56 based on dyadic dominance indices). Females in the YA1 group groomed more frequently and for longer duration than females in YA2. Further analysis showed that grooming patterns of high- and low-ranking females did not differ between the two groups. However, middle-ranking females in YA1 groomed conspecifics more frequently and for longer duration than middle-ranking females in YA2. Our results suggest that the steepness of a dominance hierarchy plays an important role in the set of social strategies used by middle-ranking females to avoid a reduction in rank, as well as to increase their rank (the dilemma of middle class hypothesis). We suggest that future studies focus on individuals of middle-rank in order to better understand how the dynamics of rank stability and rank changes influence social relationships, and affiliative and competitive interactions in non-human primates.

Keywords: hierarchical steepness, grooming, biological market, dilemma of the middle class, primates

INTRODUCTION

In many species of gregarious animals, individuals form strong social bonds and alliances based on a dynamic set of reciprocal and mutualistic interactions with conspecifics as well competitive interactions associated with access to limited resources (van Schaik, 1989; Aureli et al., 2002; Silk, 2007). These affiliative relationships can enhance the collective benefits of social group living to individuals and their offspring (Sussman and Garber, 2011), (e.g., baboon, *Papio cynocephalus*, Silk et al., 2003, 2009, 2010).

Social grooming (hereafter grooming), defined as an individual cleaning another individual's fur with hand or mouth, has been considered a fundamental component of primate social interactions (see Sussman and Garber, 2011). Given that grooming is a common and widespread affiliative behavior present in all primate species and relatively easy to observe and measure, grooming relationships have traditionally been used as an index of social and sexual bonds among members of the same social group (Henzi and Barrett, 1999). In non-human primates, grooming accounts for 10–20% of an individual's daily activity budget and is the most extensively studied affiliative behavior (Dunbar, 2010; Schino and Aureli, 2010; Sussman and Garber, 2011). In addition to a hygienic function (Zamma, 2002), grooming plays important role in establishing and maintaining social bonds and promoting social cohesion among partners (Lehmann et al., 2007; Schino and Aureli, 2008).

Reciprocity and biological market theory provide alternative explanation for primate grooming patterns (Trivers, 1971; Noë and Hammerstein, 1994, 1995). Several studies have shown that grooming, especially among kin and individuals of similar social rank, is reciprocal, both across individual grooming bouts and over time (Schino and Aureli, 2008). In other studies, grooming was found to be interchanged for rank-related benefits (tolerance at feeding sites: Gumert and Ho, 2008; Carne et al., 2011; Tiddi et al., 2011; Kurihara, 2016; access to infants in response to aunting behavior: Henzi and Barrett, 2002; Tiddi et al., 2010; Fruteau et al., 2011; agonistic support: Hemelrijk and Ek, 1991; Carne et al., 2011; or increased mating opportunities: Gumert, 2007; Sonnweber et al., 2015).

Over the past two decades, several primate researchers has focused on the mutual benefits gained from exchange/interchange with group mates (Noë, 2001, 2016). Given that across many primate species individuals reside in the same social group for months, years, and decades, individuals are expected to alter their social interactions with individual group members based on changes in age, group size and composition, reproductive condition, resource availability, and social rank (Noë and Hammerstein, 1995; de Waal, 2000). In this regard, the degree to which a species is characterized by a rigid or relaxed dominance hierarchy is considered an important factor in balancing the frequency and context of cooperative interactions and competitive interactions among group members. For example, in species characterized by a strict or linear hierarchy, individuals may target grooming partners of similar social rank or attempt to groom up the hierarchy in an attempt to form alliances that enhance their social rank within the group (Xia et al., 2013; Kurihara, 2016). Within such a system, higher-ranking individuals typically receive more grooming than they give (e.g., mandrills, *Mandrillus sphinx,* Schino and Pellegrini, 2011; Tibetan macaques, *M. thibetana*, Xia et al., 2012, 2013). Individuals of higher-rank also may direct grooming down the hierarchy (captive *Cebus apella*; Parr et al., 1997). However, low-ranking individuals may have little opportunity to groom the group's highest-ranked individuals because of competition for access to these preferred grooming partners (Seyfarth, 1977).

Biological market principles offer a productive framework for proposing and testing hypotheses to explain variation in grooming interactions in non-human primates. In primate societies characterized by high levels of within-group contest competition and linear or steep dominance hierarchies, higher-ranking individuals are expected to maintain access to monopolizable commodities. Social strategies used by lower-ranking individuals are expected to include the interchange of different services. For example, lower-ranking individuals might groom higher-ranking individuals in exchange for agonistic support at feeding sites. In contrast, when within-group competition is low and rank gradients shallow, grooming relationships are expected to be more time-matched and reciprocal.

It has been proposed, that as the steepness of a hierarchy increases, investment patterns change so that the interchange of grooming for agonistic support increases (Balasubramaniam et al., 2012). This added benefit (increased grooming frequency and/or increased duration of grooming bouts) for the individuals being groomed, in response to higher demand, should provide an incentive for *all* market participants to increase their supply of grooming. Such behavioral sensitivity to social circumstance in macaques can be viewed as an adaptive reaction to different market conditions in the trading of social grooming (Dunbar, 2010). Because an increment in the steepness of a hierarchy drives up the levels of both top-down (from higher-ranking individuals to lower-ranking individuals) and bottom-up (from lower-ranking individuals to higher-ranking individuals), the demand for grooming as a social tool is expected to increase as well. Accordingly, biological market theory integrates competitive regimes, dominance gradients, and grooming relationships (Barrett et al., 1999). Here we examine the predictive strength of biological market theory by comparing individual social strategies in two groups of Tibetan macaques (*Macaca thibetana*) that differ in hierarchical steepness.

Tibetan macaques offer an instructive model for investigating the relationships between biological markets, hierarchical steepness, and grooming relationships. Tibetan macaques are endemic to China and live in multi-male and multi-female social groups [number of adult males: 8.52 ± 0.67, number of adult females: 9.35 ± 0.51 (data from 1987 to 2017) (Li et al., 2020)]. They are characterized by male dispersal and female philopatry (Li et al., 2020). Males typically disperse from their natal group after reaching puberty (about 6–7 years of age), whereas females remain in their natal groups (Li et al., 2020). Although initial studies proposed that they showed a tolerant

or relaxed dominance style based on the presence of ritualized greetings (Ogawa, 1995), more recent studies provide strong evidence that Tibetan macaque groups maintain a more despotic dominance style, a strict linear dominance hierarchy, with low levels of reconciliation and counter-aggression (Berman et al., 2004, 2006; Zhu et al., 2013; Li et al., 2020). Berman et al. (2006) report that among female-female dyads there was no evidence that tolerant interaction was disrupted after conflicts suggesting that dominance hierarchies may be relatively stable or that after disputes females are able to re-establish social relationships without the need for reconciliatory behavior. Moreover, females prefer to groom members of their matriline (Berman et al., 2008), and grooming up the hierarchy serves to reduce aggression from higher-ranking females (Xia et al., 2012).

The aim of this study is to examine the effects of hierarchical steepness on grooming interactions in two groups of free-ranging Tibetan macaques. We expect that with increased hierarchical steepness, females would groom more frequently or for longer duration. Moreover, we also expected that low-ranking individuals use grooming (for high- and middle-rankings) to promote upward social mobility, whereas high-ranking individuals use grooming to consolidate their current social relationships with middle- and low-rankings. In contrast, mid-ranking individuals are expected to use a broader range of social grooming tactics, use the biological market condition to gain favor with individuals above them in the hierarchy (high-rankings) and to maintain relationships with individuals below them in the hierarchy (low-rankings). Consequently, middle-ranking females might invest more grooming than both high- and low-ranking females within group. In addition, the steeper the social hierarchy, the more grooming the mid-ranking individuals would invest.

MATERIALS AND METHODS

Ethical Note

Our study took place in the Huangshan Scenic District, Anhui Province, China. Our data were collected using non-invasive, observational methods, so no review by an Institutional Animal Care and Use Committee was required according to the Chinese wildlife law. Our methods of data collection complied with the Wildlife Protection Law of the People's Republic of China and the regulatory requirements of Huangshan Garden Forest Bureau.

Study Site

This study was conducted at Mt. Huangshan National Reserve located in Anhui Province, China. Mt. Huangshan (118.3 E, 30.2 N, elevation 1841 m) is a scenic area and tourist destination in east-central China. It consists of steep, sparsely treed peaks at high elevations and mixed deciduous and evergreen forests in middle and lower elevations. The study site is adjacent to Mt. Huangshan. Additional details of our study site can be found in Li et al. (2020). Several groups of Tibetan macaques are found throughout the reserve (Berman and Li, 2002). Groups appear to have non-overlapping home ranges (Wada et al., 1987).

Study Groups

Our two study groups are the Yulinkeng A1 group (YA1) and the Yulinkeng A2 group (YA2). Researchers began monitoring and studying YA1 in 1986. The local government provisioned YA1 at the beginning of our study in order to open the reserve to ecotourism (Li et al., 1996; Berman and Li, 2002). YA2 naturally fissioned from YA1 in 1996 (Li et al., 1996). In October 2010, YA2 experienced a second natural fissioning event and group size decreased from 74 to 41. Each group is provisioned in virtually the same manner; with a total of *ca.* 6 kg of dried corn per day at feeding sites set up by the reserve. The monkeys are provisioned four times per day, and feeding duration usually lasted approximately 30 min per provisioning event. After feeding, the monkeys leave the provisioned area and continue their natural and undisturbed activities in the forest.

All individuals of the two subject groups were individually recognizable based on distinct physical features such as facial or body characteristics (Li, 1999; Li et al., 2020). The compositions of two subject social groups can be found in **Table 1**. Matrilineal kin relationships are known for all female members of both the YA1 and YA2 groups as demographic data have been collected on a daily basis since 1986 (for YA1) and 2004 (for YA2) (Li, 1999; Li et al., 2020).

Data Collection

We collected behavioral data from all adult females in each group (≥5 years old; N = 8 in YA1; N = 11 in YA2). To avoid the possibility of rank changes during our study, we collected data over a limited period (108 days from September to December 2011) during which the social hierarchy remained stable. We alternated and followed the two groups from dawn to dusk. We began observations at approximately 0700–0800 and ended at 1700–1800 each day (depending on the season of year). We used focal animal sampling (with 20 min for each sample duration) and continuous recording (with a digital voice recorder, model Newsmy RV50) to collect the following behavioral data (Altmann, 1974; Xia et al., 2012): the identities of individuals in a grooming dyad, and the frequency and duration of grooming given and grooming received by identity.

Prior to daily recording, we randomly selected an ordered list of focal females for observation (Xia et al., 2012). If a preselected focal female was lost from view during the sampling interval, we observed the next female from the randomized list (Shutt et al., 2007; Xia et al., 2012). To minimize the potential influence of tourists on macaque behavior, we collected all focal animal data in the forest, where tourists were absent. In total, we recorded 133.7 h of data from group YA1 and 184 h from YA2 with

TABLE 1 | Composition of YA1 and YA2 groups during the study period.

Group	Group size	Adult males[a]	Adult females[b]
YA1	27	4	8
YA2	43	9	11

[a]Adult males (≥7 years old) and [b]adult females (≥5 years old) based on Li (1999).

approximately equal distribution of time among all adult females (16.7 ± 0.12, Mean ± SE hours per female, n = 19 females).

We defined to grooming as any act in which a macaque (groomer) uses its hand or mouth to touch, clean, or manipulate the fur of another individual (groomee) for a continuous period lasting at least 5 s (Berman et al., 2008; Xia et al., 2012, 2013). We recorded a grooming bout when an individual initiated grooming a conspecific. When the groomer and the groomee separated or if no grooming was exchanged for more than 30 s, and then grooming resumed, this was scored as a new grooming bout. Within a grooming bout, when the groomer and groomee reversed their roles, we scored this as new grooming bout (Wei et al., 2012). If individual A groomed individual B and then B groomed A grooming bout, we considered this to be two bouts (Chancellor and Isbell, 2009). For each grooming bout, we recorded the identities of the participants and the time spent grooming and being groomed.

We also recorded aggressive and submissive interactions *ad libitum* and used the frequency and direction of these among identified female dyads to determine dominance relationships. Aggressive behavior was defined as one individual threatening, chasing, slapping, grabbing, or biting another individual (Berman et al., 2007). Submissive behavior was defined as an individual showing fearful behaviors, such as a fear grin, cower, mock leave, avoid, flee, or scream as defined in Berman et al. (2004).

Dominance Hierarchy

We calculated hierarchical steepness in each group. This was accomplished by building an aggressive/submission matrix according to the direction of agonistic interactions given and received. Each aggression matrix generated a matrix of Dyadic Dominance Index (DDI) values corrected for chance (D_{ij} scores) (de Vries et al., 2006). From these scores, we generated a David's Score for each individual as a measure of relative aggressive success. We defined hierarchical steepness as the absolute slopes of plots of NDS (Normalized David's Score) and the rank of each resident female (Gammell et al., 2003; de Vries et al., 2006). The greater the NDS, the higher the individual's social rank. We also calculated hierarchical steepness values from wins-losses matrices containing the dyadic proportion of wins (P_{ij}) (scores can be found in **Supplementary Table S1**) (see de Vries et al., 2006). We used both Dij- and Pij-based scores to quantify and compare the steepness of the dominance hierarchy for both YA1 and YA2 social groups, according to Balasubramaniam et al. (2012). Based on Pij and Dij of the YA1 and YA2, we calculated a best-fit equation line for each. Following Barrett et al. (2002), the greater the absolute slope, the higher degree of steepness in the dominance hierarchy.

In order to analyze the effects of social rank on grooming, we assigned all adult female subjects to high-ranking, middle-ranking, and low-ranking categories. According to Zhang et al. (2010) and Xia et al. (2012), we used hierarchical cluster analysis to assign these categorize. Each females was assigned to one of the following rank classes: high-ranking (TR, YZ in YA1; HON, HM, HT in YA2), middle-ranking (TT, HHU, YH, YM in YA1; HPG, BLN, HHA, GZ, HMG in YA2), and low-ranking (TH, HH in YA1; HZ, HY, LAN in YA2) (see **Table 2**).

TABLE 2 | Female social ranks in group YA1/YA2 during the study period.

Group	Female/ID	Age[a]	Parity[b]	Rank[c]
YA1	TR	Young	Middle fecundity	High
YA1	YZ	Old	High fecundity	High
YA1	TT	Old	High fecundity	Middle
YA1	HHU	Young	Middle fecundity	Middle
YA1	YH	Young	Middle fecundity	Middle
YA1	YM	Old	High fecundity	Middle
YA1	TH	Young	Middle fecundity	Low
YA1	HH	Young	Middle fecundity	Low
YA2	HON	Old	High fecundity	High
YA2	HM	Young	Middle fecundity	High
YA2	HT	Young	Middle fecundity	High
YA2	HPG	Middle	Middle fecundity	Middle
YA2	BLN	Young	High fecundity	Middle
YA2	HHA	Young	Nulliparous	Middle
YA2	GZ	Young	Middle fecundity	Middle
YA2	HMG	Young	Middle fecundity	Middle
YA2	HZ	Young	Nulliparous	Low
YA2	HY	Young	Middle fecundity	Low
YA2	LAN	Old	High fecundity	Low

[a]*Young (>5 years old and ≤10 years old); Middle (>10 years old and ≤20 years old); Old (>20 years old).* [b]*Nulliparous: no infant; Middle fecundity: less than or equal to 3 infants; High fecundity: more than 3 infants.* [c]*Rank was determined by David's score.*

Data Analysis

We reported data as mean (±SE) grooming frequency (episodes/h within bouts) and grooming duration (min/h). We used Wilcoxon ranked test to analyze the difference between groups, among ranks within groups, and the variation of the same rank-classes between groups. All analyses, unless otherwise specified, were two-tailed with alpha set at 0.05 *a priori*. We used SPSS 13.0 software (SPSS Inc., Chicago, IL, United States; see Norusis, 2005) to perform all tests. Finally, to prevent false positive results due to multiple pairwise comparisons, we calculated adjusted P-values (q-values) based on the "Graphically Sharpened" false discovery rate method (FDR-adjust) in R (version 3.2.4 for windows; TUNA Team, 2016). The use of q-values was to avoid biases using the Bonferroni correction, which tends to be too conservative (Pike, 2011).

RESULTS

Hierarchical Steepness

The equations for hierarchical steepness in group YA1 were $Y = -0.81X + 7.16$ (based on P_{ij}) and $Y = -0.66X + 6.45$ (based on D_{ij}). For females in the YA2 group, the equations were $Y = -0.76X + 9.56$ (based on P_{ij}) and $Y = -0.56X + 8.37$ (based on D_{ij}) (see **Figure 1**). Because the slope for YA1 (0.66) was higher than that for YA2 (0.56), the female dominance hierarchy in YA1 was judged to be steeper than in YA2.

Social Grooming

At the group level, adult females in YA1 groomed at a rate of 0.30 ± 0.09 bouts/h and 0.96 ± 0.15 min/h in duration. For

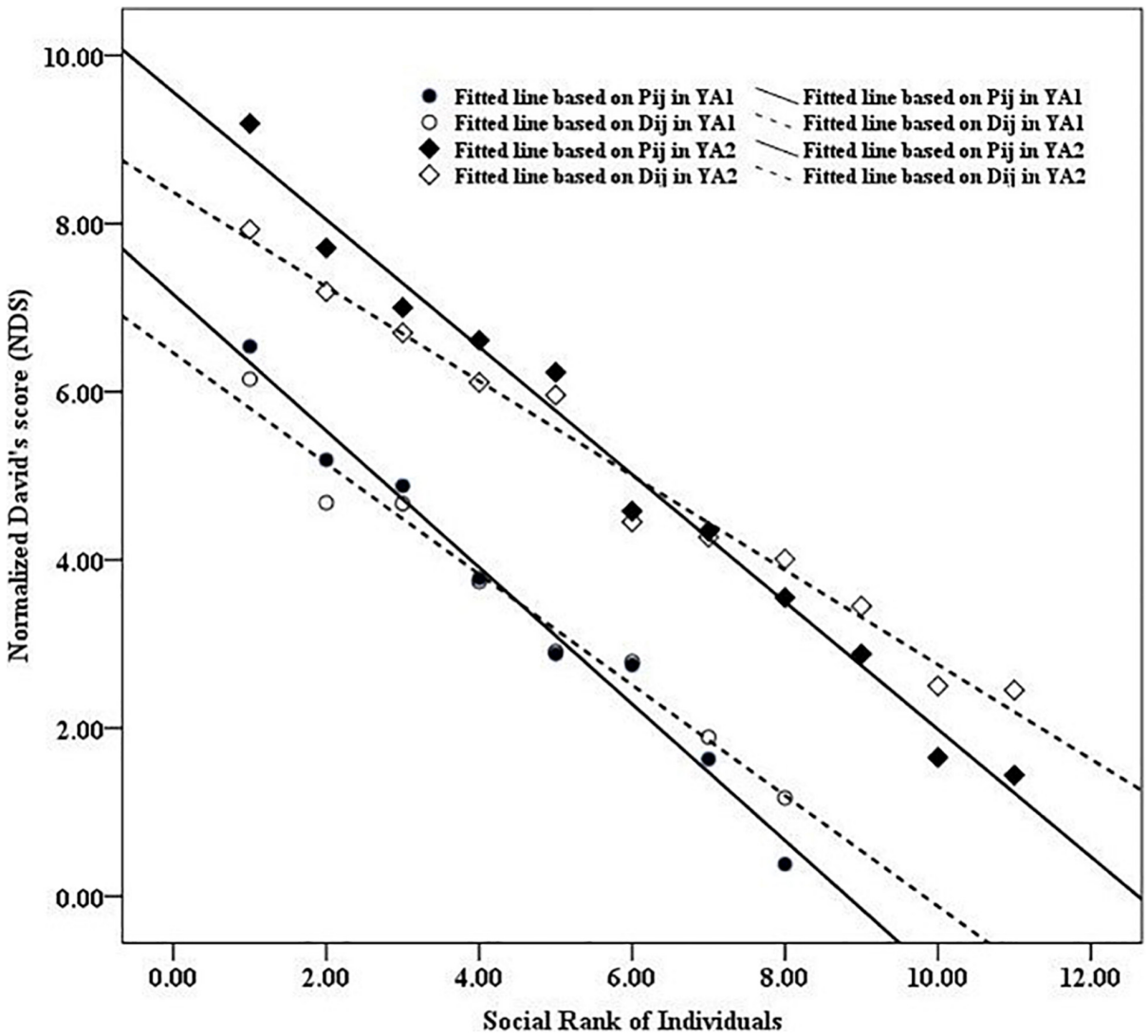

FIGURE 1 | Plots between NDS and ranks of members for YA1 and YA2 of hierarchical stability based on Dij and Pij values, respectively. Steepness for each group was measured as the absolute slopes of these regression lines.

females in YA2, these values were 0.12 ± 0.06 bouts/h and 0.48 ± 0.09 min/h. Overall, females in YA1 invested more effort in grooming than did females in YA2 (frequency: $Z = 7.684$, $N_1 = 8$, $N_2 = 12$, $P < 0.01$; duration: $Z = 6.459$, $N_1 = 8$, $N_2 = 12$, $P < 0.01$; see **Figure 2**).

Within-Group Grooming Patterns

In YA1, middle-ranking females groomed more frequently (0.38 ± 0.09 bouts/h) and for a longer duration (1.30 ± 0.09 min/h) than both high-ranking (frequency: 0.30 ± 0.07 bouts/h, $Z = -5.332$, adjusted P-values: $q < 0.05$; duration: 0.78 ± 0.12 min/h, $Z = -8.301$, adjusted P-values: $q < 0.01$) and low-ranking females (frequency: 0.13 ± 0.07 bouts/h, $Z = -6.445$, adjusted P-values: $q < 0.05$; duration: 0.46 ± 0.08 min/h, $Z = -7.101$, adjusted P-values: $q < 0.05$). In YA2, middle-ranking females groomed less frequently and for a shorter duration (frequency: 0.12 ± 0.09 bouts/h; duration: 0.55 ± 0.08 min/h) than high-ranking females (frequency: 0.17 ± 0.08 bouts/h, $Z = 3.442$, adjusted P-values: $q < 0.05$; duration: 0.60 ± 0.08 min/h, $Z = 4.011$, adjusted P-values: $q < 0.05$). However, in the group, mid-ranking females groomed others more frequently and for longer duration than did low-ranking females (frequency: 0.07 ± 0.02 bouts/h, $Z = 6.703$, adjusted P-values: $q < 0.05$; 0.30 ± 0.06 min/h, $Z = 6.559$, adjusted P-values: $q < 0.05$).

Between-Group Grooming Patterns

A comparison between groups indicates no statistical difference in either the frequency or duration of grooming bouts among high-ranking females (frequency: $Z = 1.103$, adjusted P-values: $q > 0.05$; duration: $Z = 0.981$, adjusted P-values: $q > 0.05$) or among low-ranking females (frequency: $Z = 1.005$, adjusted

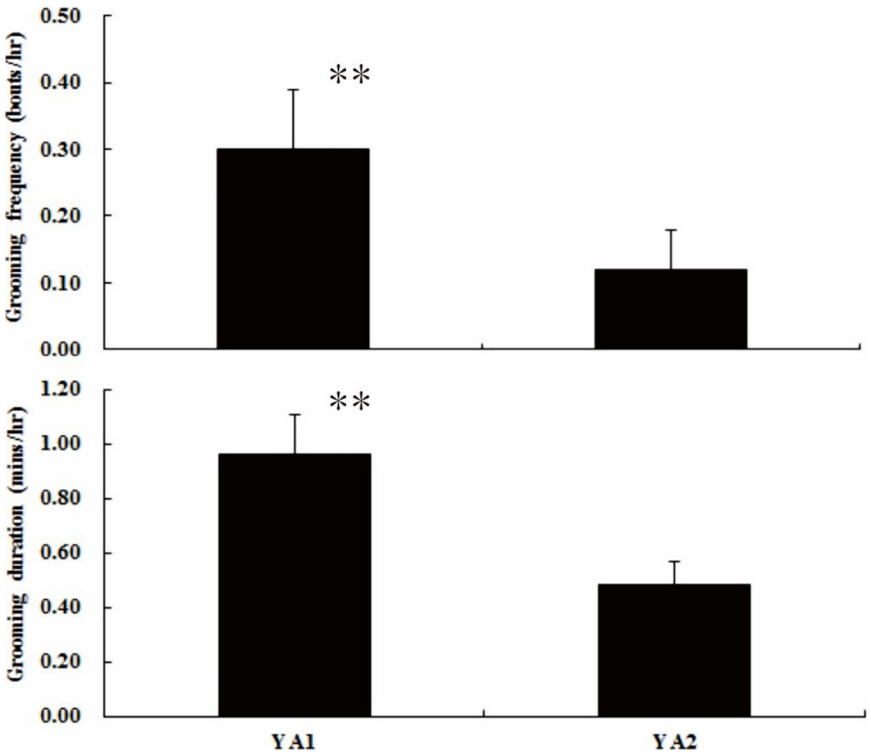

FIGURE 2 | Difference in grooming investment between the YA1 and YA2 groups. $^{**}P < 0.01$.

P-values: $q > 0.05$; duration: $Z = 1.014$, adjusted *P*-values: $q > 0.05$). However, middle-ranking females in YA1 groomed other females more frequently ($Z = 8.216$, adjusted *P*-values: $q < 0.01$, see **Figure 3A**) and for a greater duration ($Z = 8.409$, adjusted *P*-values: $q < 0.05$; see **Figure 3B**) compared to middle-ranking females in YA2.

DISCUSSION

To our knowledge, this is the first study to investigate variation in female grooming patterns in the context of hierarchical steepness in Tibetan macaques. Our results provide evidence that Tibetan macaque females residing in social groups characterized by increased hierarchical steepness groomed others more frequently and for longer duration than females residing in a neighboring group characterized by a shallower hierarchy. Moreover, middle-ranking individuals invested more time in grooming than both high- and low-ranking individuals, and the steeper the group's social hierarchy, the more grooming the middle-ranking females invested. This study offers new insights into the set of social strategies used by Tibetan macaques to form social bonds and social alliances within the context of a linear dominance hierarchy.

Among female primates living in matrilineal groups, social grooming has been used extensively to enhance and maintain social relationships (Dunbar, 2010). Previous studies have shown that factors such as group size and kinship influence grooming relationships (Chapais, 2006; Lehmann et al., 2007). In this regard, Dunbar (1991) who tested the group cohesion hypothesis and Lehmann et al. (2007) using a meta-analysis found that grooming tends to increase with group size across primate species. However, in this study, we found that females in smaller social group (YA1: 27 individuals) groomed more frequently and for longer duration than females in larger social group (YA2: 43 individuals). It indicated that effect of group size might be offset by the steepness of dominance hierarchy, which is one of the main variables we examined in this study. Moreover, although kinship was considered as an important factor to influence grooming patterns, reciprocity and interchange for other behavioral services (such as increasing tolerance from higher rankings) appeared to play a more critical role than kinship in explaining social grooming relationships in primates with linear dominance hierarchy (Schino and Aureli, 2010; Xia et al., 2012). Thus, multiple lines of evidence indicate that primates use social grooming as an effective tool to form, maintain, and alter social relationships. The results of our study add to our understanding of primate sociality and by providing evidence that female Tibetan macaques alter their grooming behavior based on the hierarchical steepness of their group in an attempt to improve their social rank.

In Tibetan macaques, grooming is a valuable behavioral service used for strengthening bonds among adult females (Xia et al., 2012). Assuming hierarchical steepness is a response to increased females competition for access to limited food

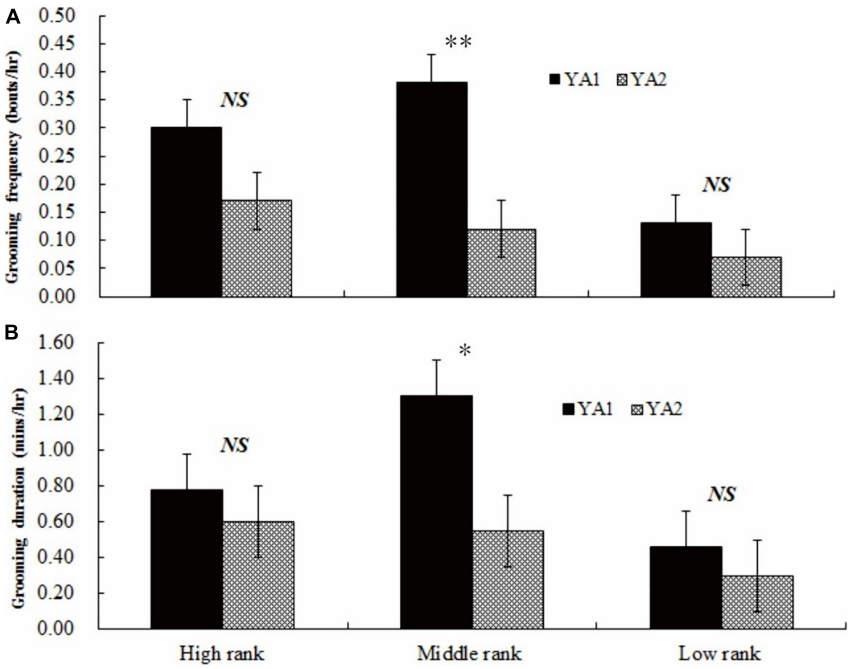

FIGURE 3 | Grooming frequency **(A)** and duration **(B)** of individuals of similar ranks between the two groups. High rank, middle rank, and low rank represents high-ranking, middle-ranking, and low-ranking females. NS, no significant difference; $^{*}P < 0.05$; $^{**}P < 0.01$.

resources, resident females are expected to select high-ranking grooming partners who will provide coalitionary support or be more socially tolerant at feeding sites (van Schaik, 1989; Sterck et al., 1997). Although two study groups are provisioned and therefore food could not be important limited factor, we found that females in YA1 (with steeper linear dominance hierarchy) groomed more frequently and for longer duration than females in YA2 (with shallower linear dominance hierarchy). A similar relationship between dominance style and grooming patterns have been reported in lion-tailed macaques (*Macaca silenus*) (Singh et al., 2006) and bonobos (*Pan paniscus*) (Stevens et al., 2005). Singh et al. (2006) found that female lion-tailed macaques residing in a group characterized by a despotic social hierarchy groomed each other more than female lion-tailed macaques living in an egalitarian group. Stevens et al. (2005) showed that grooming among female bonobos was more reciprocal in groups characterized by a shallow dominance hierarchy, compared to groups exhibiting a more steep dominance hierarchy. As such, hierarchical steepness could be considered as one of the alternative indicators to explain social grooming and social relationships between groups.

Importantly, we found that in Tibetan macaques, middle-ranking females invested more in grooming than both higher- and lower-ranking females. The steeper the group's social hierarchy, the more frequent and the longer middle-ranking females invested in grooming. As suggested by Parr et al.(1997:336) for captive brown capuchins, middle-ranking females ". . .play the pivotal role by grooming both up and down the hierarchy, and may provide an affiliative link between the top and bottom divisions of the female hierarchy." In the case of wild chacma baboons (*Papio hamadryas*), middle-ranking female have been observed to trade increased minutes of grooming with both high- and low-ranking group members (Henzi et al., 2003). Thus, middle-ranking females may increase their effort and groom their preferred partners to maintain affiliative bonds with both high- and low-ranking females. These females may groom low ranking females as a strategy to maintain their current social rank *or* groom higher ranking females in an attempt to improve their position in the hierarchy (Sun, 2013).

Furthermore, Tibetan macaques is described as a seasonal breeder, with the mating season lasting from July to January (see Li et al., 2020). Our study period was a peak of the mating season, both males and females competed for mating partners during this period from September to December. Female intrasexual competitions for access to adult males was higher, especially for high- and middle-rankings with high or middle fecundity with the effects of male mate choice (Zhang et al., 2010). Previous study has demonstrated that, to reduce aggression from higher-ranking females, lower-ranking females groomed more frequently and for longer duration to high-rankings than vice versa (Seyfarth, 1977). Empirical study showed that these patterns occurred between high- and middle-ranking, and middle- and low-ranking dyads (Xia et al., 2012). The grooming interactions of middle-ranking females lies in contrast to both high- and low-ranking females, who are found to direct grooming at either low- or high-ranking females, but not both. Berghaenel et al. (2010) noted a higher level of grooming in middle-rankings in *Macaca sylvanus*. Our study provides evidence that grooming frequency and duration of middle-ranking female Tibetan macaques increases with hierarchical steepness of the group,

and that these females might strategically adjust their supply of grooming services to the demands of their group's biological market. That is, if a steeper hierarchy increases the demand for grooming as a tool to reduce social anxiety, increase tolerance from high-rankings, or re-establish social bonds, middle-ranking females who most readily adjusted their behavior. In groups characterized by a shallower hierarchy, and presumed lower for grooming as a social tool, middle-ranking females supplied less grooming. Recent study at the same study site showed that middle-rankings displayed higher cortisol levels than both high- and low-ranking individuals (Wu et al., unpublished data). It provided supportive evidence that middle-rankings might devote more grooming to reduce social anxiety.

Social grooming is not only the indicator to represent dyadic social relationships, but also a process to establish and maintain dyadic social relationships. Complex factors might be involved, and thus there is no simple model to describe. Based on our results, although sample size limited, we provided an alternative explanation for grooming patterns between social groups within the framework of hierarchical steepness. We also hypothesize that middle-ranking females across a number of primate species, and possibly in other social mammals, alter their grooming behavior in response to the steepness of a social hierarchy. We suggest that in response to the dilemma faced by the middle class, these females adjust their grooming behavior in order to form and maintain social bonds with particular conspecifics. Future studies, with a larger number of sample size and a longer study period, will need pay more attention to conspecifics occupying middle social rank among more primate species in order to better understand the joint effects of rank, dominance style, social affiliation, grooming relationships and fitness in non-human primates.

DATA AVAILABILITY STATEMENT

The raw data supporting the conclusions of this article will be made available by the authors, without undue reservation. Further inquiries can be directed to the corresponding author/s.

ETHICS STATEMENT

Ethical review and approval was not required for the animal study because our data were collected using non-invasive, observational methods, so no review by an Institutional Animal Care and Use Committee was required according to the Chinese wildlife law. In our data collection we complied with the Wildlife Protection Law of the People's Republic of China and the regulatory requirements of Huangshan Garden Forest Bureau.

AUTHOR CONTRIBUTIONS

DPX and JHL designed the study. DPX and XW performed the experiments. DPX, XW, BHS, and LKS contributed to analysis. DPX, XW, PG, LS, and JHL contributed to writing and editing the manuscript. All authors contributed to the article and approved the submitted version.

FUNDING

DPX acknowledges support from the National Natural Science Foundation of China (Nos. 32070455 and 31772475). JHL acknowledges support from the National Natural Science Foundation of China (No. 31672307). XW acknowledges support from the National Natural Science Foundation of China (No. 31801983). LKS acknowledges support from National Science Foundation-IRES (#1065589).

ACKNOWLEDGMENTS

We are grateful to the Huangshan Garden Forest Bureau for their permission to and support our research. We acknowledge Mr. H. B. Cheng's family for logistic support. PG wishes to thank Chrissie, Sara, Jenni, and Dax for their love and support.

SUPPLEMENTARY MATERIAL

The Supplementary Material for this article can be found online at: https://www.frontiersin.org/articles/10.3389/fevo.2021.631417/full#supplementary-material

REFERENCES

Altmann, J. (1974). Observational study of behavior: sampling methods. *Behaviour* 49, 227–267. doi: 10.1163/156853974x00534

Aureli, F., Cords, M., and van Schaik, C. P. (2002). Conflict resolution following aggression in gregarious animals: a predictive framework. *Anim. Behav.* 64, 325–343. doi: 10.1006/anbe.2002.3071

Balasubramaniam, K. N., Berman, C. M., Ogawa, H., and Li, J. H. (2012). Using biological markets principles to examine patterns of grooming exchange in *Macaca thibetana*. *Am. J. Primatol.* 73, 1269–1279. doi: 10.1002/ajp.20999

Barrett, L., Gaynor, D., and Henzi, S. P. (2002). A dynamic interaction between aggression and grooming reciprocity among female chacma baboons. *Animal Behaviour* 63, 1047–1053. doi: 10.1006/anbe.2002.3008

Barrett, L., Henzi, S. P., Weingrill, T., Lycett, J. E., and Hill, R. A. (1999). Market forces predict grooming reciprocity in female baboons. *Proc. R. B. Biol. Sci.* 266, 665–670. doi: 10.1098/rspb.1999.0687

Berghaenel, A., Schülke, O., and Ostner, J. (2010). Coalition formation among Barbary macaque males: the influence of scramble competition. *Anim. Behav.* 80, 675–682. doi: 10.1016/j.anbehav.2010.07.002

Berman, C. M., Ionica, C., and Li, J. H. (2004). Dominance style among *Macaca thibetana* on Mt. Huangshan, China. *Int. J. Primatol.* 25, 1283–1312. doi: 10.1023/b:ijop.0000043963.77801.c3

Berman, C. M., Ionica, C., and Li, J. H. (2007). Supportive and tolerant relationships among male Tibetan macaques at Huangshan. *China. Behav.* 144, 631–661. doi: 10.1163/156853907781347790

Berman, C. M., Ionica, C. S., Dorner, M., and Li, J. H. (2006). Postconflict affiliation between former opponents in *Macaca thibetana* on Mt. Huangshan, China. *Int. J. Primatol.* 27, 827–854. doi: 10.1007/s10764-006-9039-y

Berman, C. M., and Li, J. H. (2002). Impact of translocation, provisioning and range restriction on a group of *Macaca thibetana*. *Int. J. Primatol.* 23, 283–297.

Berman, C. M., Ogawa, H., Ionica, C., Yin, H., and Li, J. H. (2008). Variation in kin bias over time in a group of Tibetan macaques at Huangshan. China: contest competition, time constraints or risk reponse? *Behaviour* 145, 863–896. doi: 10.1163/156853908784089252

Carne, C., Wiper, S., and Semple, S. (2011). Reciprocation and interchange of grooming, agonistic support, feeding tolerance, and aggression in semi-free-ranging barbary macaques. *Am. J. Primatol.* 73, 1127–1133. doi: 10.1002/ajp.20979

Chancellor, R. L., and Isbell, L. A. (2009). Female grooming markets in a polulation of gray-cheeked mangabeys (*Lophocebus albigena*). *Behav. Ecol.* 20, 79–86. doi: 10.1093/beheco/arn117

Chapais, B. (2006). "Kinship, competence and cooperation in primates," in *Cooperation in primates and humans: Mechanisms and evolutions*, eds P. M. Kappeler and C. P. van Schaik (New York: Springer), 47–64. doi: 10.1007/3-540-28277-7_3

de Vries, H., Stevens, J. G., and Vervaecke, H. (2006). Measuring and testing the steepness of domiance hierarchies. *Anim. Behav.* 71, 585–592. doi: 10.1016/j.anbehav.2005.05.015

de Waal, F. B. M. (2000). Primates: a natural heritage of conflict resolution. *Science* 289, 586–590. doi: 10.1126/science.289.5479.586

Dunbar, R. I. M. (1991). Functional significance of social grooming in primates. *Folia Primatologica* 57, 121–131. doi: 10.1159/000156574

Dunbar, R. I. M. (2010). The social role of touch in humans and primates: Behavioural function and neurobiological mechanisms. *Neurosci. Biobehav. Rev.* 34, 260–268. doi: 10.1016/j.neubiorev.2008.07.001

Fruteau, C., van de Waal, E., van Damme, E., and Noë, R. (2011). Infant access and handling in sooty mangabeys and vervet monkeys. *Anim. Behav.* 81, 153–161. doi: 10.1016/j.anbehav.2010.09.028

Gammell, M. P., De Vries, H., Jennings, D. J., Carlin, C. M., and Hayden, T. J. (2003). David's score: a more appropriate dominance ranking method than Clutton-Brock et al.'s index. *Anim. Behav.* 66, 601–605. doi: 10.1006/anbe.2003.2226

Gumert, M. D. (2007). Payment for sex in a macaque mating market. *Anim. Behav.* 74, 1655–1667. doi: 10.1016/j.anbehav.2007.03.009

Gumert, M. D., and Ho, M. R. (2008). The trade balance of grooming and its coordination of reciprocation and tolerance in Indonesian long-tailed macaques (*Macaca fascicularis*). *Primates* 49, 176–185. doi: 10.1007/s10329-008-0089-y

Hemelrijk, C. K., and Ek, A. (1991). Reciprocity and interchange of grooming and 'support' in captive chimpanzees. *Anim. Behav.* 41, 923–935. doi: 10.1016/s0003-3472(05)80630-x

Henzi, S. P., and Barrett, L. (1999). The value of grooming to female primates. *Primates* 40, 47–59. doi: 10.1007/bf02557701

Henzi, S. P., and Barrett, L. (2002). Infants as a commodity in a baboon market. *Anim. Behav.* 63, 915–921. doi: 10.1006/anbe.2001.1986

Henzi, S. P., Barrett, L., Gaynor, D., Greeff, J., Weingrill, T., et al. (2003). Effect of resource competition on the long-term allocation of grooming by female baboons: evaluating Seyfarth's model. *Anim. Behav.* 66, 931–938. doi: 10.1006/anbe.2003.2244

Kurihara, Y. (2016). Low-ranking female Japanese macaques make efforts for social grooming. *Curr. Zool.* 62, 99–108. doi: 10.1093/cz/zow006

Lehmann, J., Korstjens, A. H., and Dunbar, R. I. M. (2007). Group size, grooming and social cohesion in primates. *Anim. Behav.* 74, 1617–1629. doi: 10.1016/j.anbehav.2006.10.025

Li, J. H. (1999). *The Tibetan Macaque Society: A Field Study*. Hefei: Anhui University Press.

Li, J. H., Sun, L., and Kappeler, P. M. (2020). *The behavioral ecology of the Tibetan macaque*. Berlin: Springer.

Li, J. H., Wang, Q. S., and Li, M. (1996). Migration of male Tibetan macaques (*Macaca thibetana*) at Mt. Huangshan, Anhui province, China. *Acta Theriolog. Sinca* 16, 1–6. doi: 10.1007/s10329-011-0276-0

Norusis, M. (2005). *SPSS 13.0 Advanced Statistical Procedures Companion*. Upper Saddle River, NJ: Prentice Hall.

Noë, R. (2001). "Biological markets: partner choice as the driving force behind the evolution of mutualisms," in *Nature: Social Dilemmas, Mate Choice and Biological Markets*, eds R. Noë, J. van Hooff, P. Hammerstein, and Economics (Cambridge: Cambridge University Press).

Noë, R. (2016). *How do biological markets compare to the markets of economics? Mpra Paper*. France: Université de Strasbourg. 72509.

Noë, R., and Hammerstein, P. (1994). Biological market: supply and demand determine the effect of partner choice in cooperation, mutualism and mating. *Behav. Ecol. Sociobiol.* 35, 1–11. doi: 10.1007/s002650050063

Noë, R., and Hammerstein, P. (1995). Biological markets. *Trends Ecol. Evol.* 10, 336–339.

Ogawa, H. (1995). Recognition of social relationships in bridging behavior among Tibetan macaques (*Macaca thibetana*). *Am. J. Primatol.* 35, 305–310. doi: 10.1002/ajp.1350350406

Parr, L. A., Matheson, M. D., Bernstein, I. S., and de Waal, F. B. M. (1997). Grooming down the hierarchy: Allogrooming in captive brown capuchin monkeys. Cebus paella. Anim. Behav. 54, 361–367. doi: 10.1006/anbe.1996.0419

Pike, N. (2011). Using false discovery rates for multiple comparisons in ecology and evolution. *Methods Ecol. Evol.* 2, 278–282. doi: 10.1111/j.2041-210x.2010.00061.x

Schino, G., and Aureli, F. (2008). Tradeoffs in primate grooming reciprocity: testing behavioral flexibility and correlated evolution. *Biol. J. Linnean Soc.* 95, 439–446. doi: 10.1111/j.1095-8312.2008.01067.x

Schino, G., and Aureli, F. (2010). The relative roles of kinship and reciprocity in explaining primate altruism. *Ecol. Lett.* 13, 45–50. doi: 10.1111/j.1461-0248.2009.01396.x

Schino, G., and Pellegrini, B. (2011). Grooming and the expectation of reciprocation in mandrills (*Mandrillus sphinx*). *Int. J. Primatol.* 32, 406–414. doi: 10.1007/s10764-010-9477-4

Seyfarth, R. M. (1977). A model of social grooming among adult female monkeys. *J. Theor. Biol.* 65, 671–698. doi: 10.1016/0022-5193(77)90015-7

Shutt, K., MacLarnon, A., Heistermann, M., and Semple, S. (2007). Grooming in Barbary macaques: better to give than to receive? *Biol. Lett.* 3, 231–233. doi: 10.1098/rsbl.2007.0052

Silk, J. B. (2007). The adaptive value of sociality in mammalian groups. *Philosop. Transac. R Soc. London B* 362, 539–559. doi: 10.1098/rstb.2006.1994

Silk, J. B., Alberts, S. C., and Altmann, J. (2003). Social bonds of female baboons enhance infant survival. *Science* 302, 1231–1234. doi: 10.1126/science.1088580

Silk, J. B., Beehner, J. C., Bergman, T. J., Crockford, C., Engh, A. L., Moscovice, L. R., et al. (2009). The benefits of social captital: Close social bonds among female baboons enhance offspring survival. *Proc. R Soc. B* 276, 3099–3104. doi: 10.1098/rspb.2009.0681

Silk, J. B., Beehner, J. C., Bergman, T. J., Crockford, C., Engh, A. L., Moscovice, L. R., et al. (2010). Female chacma baboons form strong, equitable, and enduring social bonds. *Behav. Ecol. Sociobiol.* 64, 1733–1747. doi: 10.1007/s00265-010-0986-0

Singh, M., Krishna, B. A., and Singh, M. (2006). Dominance hierarchy and social grooming in female lion-tailed macaques (*Macaca silenus*) in the Western Ghats, India. *J. Biosci.* 31, 369–377. doi: 10.1007/bf02704110

Sonnweber, R. S., Massen, J. J. M., and Fitch, W. T. (2015). Post-copulatory grooming: a conditional mating strategy? *Behav. Ecol. Sociobiol.* 69, 1749–1759. doi: 10.1007/s00265-015-1987-9

Sterck, E. H. M., Watts, D. P., and van Schaik, C. P. (1997). The evolution of female social relationships in nonhuman primates. *Behav. Ecol. Sociobiol.* 41, 291–309.

Stevens, J. M. G., Vervaeche, H., de Vries, H., and Van Elsacher, L. (2005). The influence of the steepness of dominance hierarchies on reciprocity and interchange in captive groups of bonobos (*Pan paniscus*). *Behaviour* 142, 941–960. doi: 10.1163/1568539055010075

Sun, L. (2013). *The fairness instinct: the robin hood mentality and our biological nature. New York*. Amherst: Prometheus Books.

Sussman, R. W., and Garber, P. A. (2011). "Cooperation, collective action, and competition in primate social interactions," in *Primates in Perspective*, Vol. 2, eds C. J. Campbell, A. Fuentes, K. C. MacKinno, S. Bearder, and R. Stumpf (New York: Oxford University Press), 587–599.

Tiddi, B., Aureli, F., di Sorrentino, E. P., Janson, C. H., and Schino, G. (2011). Grooming for tolerance? Two mechanisms of exchange in wild tufted capuchin monkeys. *Behav. Ecol.* 22, 663–669. doi: 10.1093/beheco/arr028

Tiddi, B., Aureli, F., and Schino, G. (2010). Grooming for infant handling in tufted capuchin monkeys: a reappraisal of the primate infant market. *Anim. Behav.* 79, 1115–1123. doi: 10.1016/j.anbehav.2010.02.008

Trivers, R. L. (1971). The evolution of reciprocal altruism. *Q. Rev. Biol.* 46, 35–57. doi: 10.1086/406755

van Schaik, C. P. (1989). "The ecology of social relationships amongst female primates," in *Comparative socioecology: the behavioural ecology of humans and other animals*, eds V. Standen and R. A. Foley (Oxford: Blackwell Scientific), 195–218.

Wada, K., Xiong, C. P., and Wang, Q. S. (1987). On the distribution of Tibetan and rhesus monkeys in Southern Anhui province. China. *Acta Theriolog. Sinica* 7, 148–176.

Wei, W., Qi, X. G., Guo, S. T., Zhao, D. P., Zhang, P., et al. (2012). Market powers predict reciprocal grooming in Golden Snub-nosed monkeys (*Rhinopithecus roxellana*). *PLoS One* 7:e36802. doi: 10.1371/journal.pone.0036802

Xia, D. P., Li, J. H., Garber, P. A., Matheson, M. D., Sun, B. H., et al. (2013). Grooming reciprocity in male Tibetan macaques. *Am. J. Primatol.* 75, 1009–1020. doi: 10.1002/ajp.22165

Xia, D. P., Li, J. H., Garber, P. A., Sun, L., Zhu, Y., et al. (2012). Grooming reciprocity in female Tibetan macaques *Macaca thibetana*. *Am. J. Primatol.* 74, 569–579. doi: 10.1002/ajp.21985

Zamma, K. (2002). Grooming site preferences determined by lice infection among Japanese macaques in Arashiyama. *Primates* 43, 41–49. doi: 10.1007/bf02629575

Zhang, M., Li, J. H., Zhu, Y., Wang, X., and Wang, S. (2010). Male mate choice in Tibetan macaques *Macaca thibetana* at Mt. Huangshan, China. *Curr. Zool.* 56, 213–221.

Zhu, L., Li, J. H., Xia, D. P., Zhu, Y., Wang, X., et al. (2013). Stability of the female dominance hierarchy in free-ranging, provisioned adult Tibetan macaques (*Macaca thibetana*) at Mt. Huangshan, China. *Acta Theriolog. Sinica* 33, 238–245.

Conflict of Interest: The authors declare that the research was conducted in the absence of any commercial or financial relationships that could be construed as a potential conflict of interest.

frontiers in Ecology and Evolution

ORIGINAL RESEARCH
published: 15 March 2021
doi: 10.3389/fevo.2021.642814

Tempo and Mode: Evidence on a Protracted Split From a Dense Fossil Record

Yuri Kimura[1,2,3†], Lawrence J. Flynn[4†] and Louis L. Jacobs[5†]*

[1] National Museum of Nature and Science, Tsukuba, Japan, [2] Department of Geology and Paleontology, National Museum of Nature and Science, Tsukuba, Japan, [3] Institut Català de Paleontologia Miquel Crusafont, ICTA-ICP, Edifici Z. Carrer de les Columnes, s/n., Campus de la Universitat Autònoma de Barcelona, Barcelona, Spain, [4] Department of Human Evolutionary Biology, Harvard University, Cambridge, MA, United States, [5] Roy M. Huffington Department of Earth Sciences, Southern Methodist University, Dallas, TX, United States

Fossil records generally inform paleobiologists about extinct taxa and rates of evolution measured at the scale of millions of years. Good records that are densely sampled through time can reveal species level details such as longevity in local sections. Yet fossil data normally do not address details of lineage microevolution because the density through time of lineage sampling is insufficient to perceive patterns at a precision finer than 10^6 years in most cases. This study concerns details of a splitting event in the evolution of murine rodents, an event for which multiple fossil samples dated to a precision of 10^5 years fortuitously document the tempo and mode of origin of sister species, the stems of two extant tribes of mice. Evolution of early Murinae in the northern part of the biogeographically restricted Indian subcontinent between 11.6 and 10.5 Ma involved cladogenesis of two crown taxa, the extant tribes Murini and Arvicanthini. Large samples of fossil rodent teeth document their divergence from a common morphological pool. Definitive basal Murini and Arvicanthini at 10.5 Ma are similar in size and differ by subtle features of the dentition. Those features occur sporadically in the common pool of older fossil teeth at 11.2, 11.4, and 11.6 Ma as inconsistent polymorphisms. Interpreted as a single lineage in the 11.6–11.2 Ma interval, variability of this abundant murine incorporated the roots of the two crown tribes. The pattern through time suggests morphological stasis for several hundred thousand years prior to splitting. This special case informs us on one example of evolution and shows that the tempo of splitting evolution in some cases may be measured in hundreds of thousands of years, followed by stasis once daughter species have differentiated morphologically.

Keywords: speciation, evolution, Murinae, Miocene, Siwaliks, morphology

Edited by:
Irina Ruf,
Senckenberg Research Institute and Natural History Museum Frankfurt, Germany

Reviewed by:
Paloma López-Guerrero, Universidad Complutense de Madrid, Spain
Wilma Wessels, Utrecht University, Netherlands

****Correspondence:***
Lawrence J. Flynn
ljflynn@fas.harvard.edu

† These authors have contributed equally to this work and share first authorship

Specialty section:
This article was submitted to Paleontology, a section of the journal Frontiers in Ecology and Evolution

Received: *16 December 2020*
Accepted: *19 February 2021*
Published: *15 March 2021*

Citation:
Kimura Y, Flynn LJ and Jacobs LL (2021) Tempo and Mode: Evidence on a Protracted Split From a Dense Fossil Record. Front. Ecol. Evol. 9:642814. doi: 10.3389/fevo.2021.642814

INTRODUCTION

Gould (1985) and Reznick and Ricklefs (2009) discussed the importance of the fossil record for evolutionary biology in unveiling major events, especially those under the category of macroevolution. Generally, paleontology does not address details on how evolution proceeds at the population level because relevant data are not sampled densely enough in space and time. In special circumstances, however, the fossil record may be detailed enough to address aspects of evolution

that lie between macro- and microevolution, such as species longevity, changes in abundance, and rates of morphological change. The potential for approaching microevolutionary patterns through the fossil record is great for muroid rodents in cases where stratigraphy and dating are well resolved, and multiple large samples of individuals are available.

Resolution of muroid rodent phylogenetics has had a quantum advance with the application of mitochondrial and nuclear genetic analyses. Steppan and Schenk (2017) resolved a massive amount of data to develop a well-supported hypothesis on relationships of over 900 species. This and previous works (e.g., Lecompte et al., 2008) distinguished major clades of muroids at the family, subfamily, and tribe levels, including tribes Arvicanthini and Murini, both of which have fossil members in South Asia.

Here we set out to interpret a unique fossil record for its relevance to a splitting event that marked the origin of the extant murine rodent tribes Arvicanthini and Murini. Sediments from the Siwalik Group of Pakistan yield a well dated and resolved series of fossil mouse assemblages. We have developed the alpha taxonomy of these species in a series of papers (Jacobs, 1977, 1978; Cheema et al., 2000; Kimura et al., 2015, 2017) and specified the timing of morphological divergence and the emergence of features involved in that divergence (Kimura et al., 2013a,b; Flynn et al., 2020). Early late Miocene Siwalik species assigned to the stem genera *Karnimata* and *Progonomys*, respectively, fortuitously capture the rise of distinctive morphological features that by 10.5–10 million years ago (Ma) characterize dentitions of members of the tribes Arvicanthini and Murini. These features occur in fossil samples from the same geographic area before 11 Ma (Flynn et al., 2020), but inconsistently so that species level taxonomy at that age is problematic.

We contend that the common origin of the Arvicanthini and Murini was recorded in South Asia in Siwalik fossil samples between 12 and 11 Ma. The distinct morphologies of the tribes expressed clearly in fossil species of *Karnimata* and *Progonomys* dating to 10.5 Ma and younger occur across a mix of individuals in the 11.6–11.2 Ma interval that are otherwise inseparable. These appear to be polymorphisms that were stable for hundreds of thousands of years and later characterized the extant tribes.

Our purpose is to document the simultaneous existence of arvicanthin and murinin morphologies in a series of samples from single localities of early late Miocene age, discuss the relevance of their splitting origin within a refined chronology of mouse evolution, and thereby address the tempo and mode of this special event recorded in the fossil record. We interpret these fossils to represent the common ancestral lineage for the two living mouse tribes. Possibly, they represent individuals of closely related cryptic species that did not differ in any other features preserved in the fossils. In either case the time frame for morphological separation of the two tribes is measured in hundreds of thousands of years.

The significance of understanding the tempo and mode of the specific cladogenic event we are studying is that it provides a more confident and precise date for an evolutionary divergence that is relevant for calibrating the molecular phylogeny of essentially every living species of one of the most diverse and speciose groups of mammals in existence, the true mice or Murinae. This group is native to the Old World, including Africa, Australia, and Pacific islands, and global as commensals. It contains the laboratory mouse (*Mus*) and laboratory rat (*Rattus*), long the subject of innumerable studies (da Costa et al., 2019), the former with more than forty living wild species (Suzuki, 2020) and the latter with a confusingly large number of cryptic species (Pages et al., 2010; Rowe et al., 2011). Because fossil murines are known mainly from isolated teeth, the spectrum of morphological characters is limited, which restricts the application of standard morphology-based cladistic analysis. However, the backbone provided by molecular phylogenies of the vast number of living species allows fossil mice to be related confidently.

The fossil mice from Pakistan have long been recognized as relevant to calibrating molecular evolutionary hypotheses (Jacobs and Pilbeam, 1980; Jacobs and Flynn, 2005), but earlier studies have been much improved upon by more comprehensive work (e.g., Kimura et al., 2015; Aghová et al., 2018) and the addition of newly studied fossil samples (e.g., Kimura et al., 2017). Divergence dates from Pakistan have been useful in molecular sequence studies applied to biogeography, ecology, and evolutionary patterns (e.g., Rowe et al., 2016, 2019; Bryja et al., 2017), as well as studies of pathogens and genetic mechanisms (e.g., Casola, 2018; Ma et al., 2018), and many other topics. This study contributes by providing a more explicit description of a fossil-based cladogenic event in a precise chronological framework.

MATERIALS AND METHODS

The source of the fossil data is a biostratigraphy of successive rodent sites from the Miocene formations of the Siwalik Group of South Asia. Here we focus on Miocene age sites that are dated 12.5–10 Ma. Each site produces a sample of isolated rodent teeth concentrated most likely by avian predators of the time. Sites contain remains of individuals that died (and are time-averaged) over a decadal to centennial scale. The fossil rodent fauna is represented by squirrels, primitive burrowing rats, hamsters, gerbils, gundis, dormice, and dominant true mice. The series of sites that captures the cladogenic event spans at least 400,000 years from 11.6 to 11.2 Ma. Fossil sites are concentrated in a relatively small area of 200 km^2 near Chinji and Nagri villages on the Potwar Plateau of northern Pakistan (area B in Barry et al., 2002: their Figure 1).

Geology

The Potwar Plateau in northern Pakistan presents an extraordinarily continuous record of Siwalik sediments shed from deformed highlands to the north, the present day mountain ranges bordering the Tibetan Plateau. Drainages carrying detritus southward continue to the present day as components of the mighty Indus River system. The highlands, principally related to the Himalayan and Hindu Kush mountain ranges, have been uplifted continuously throughout the Cenozoic Era by the tectonic forces that thrust the Indian Plate northward under the southern margin of Asia. Currently at 33° North

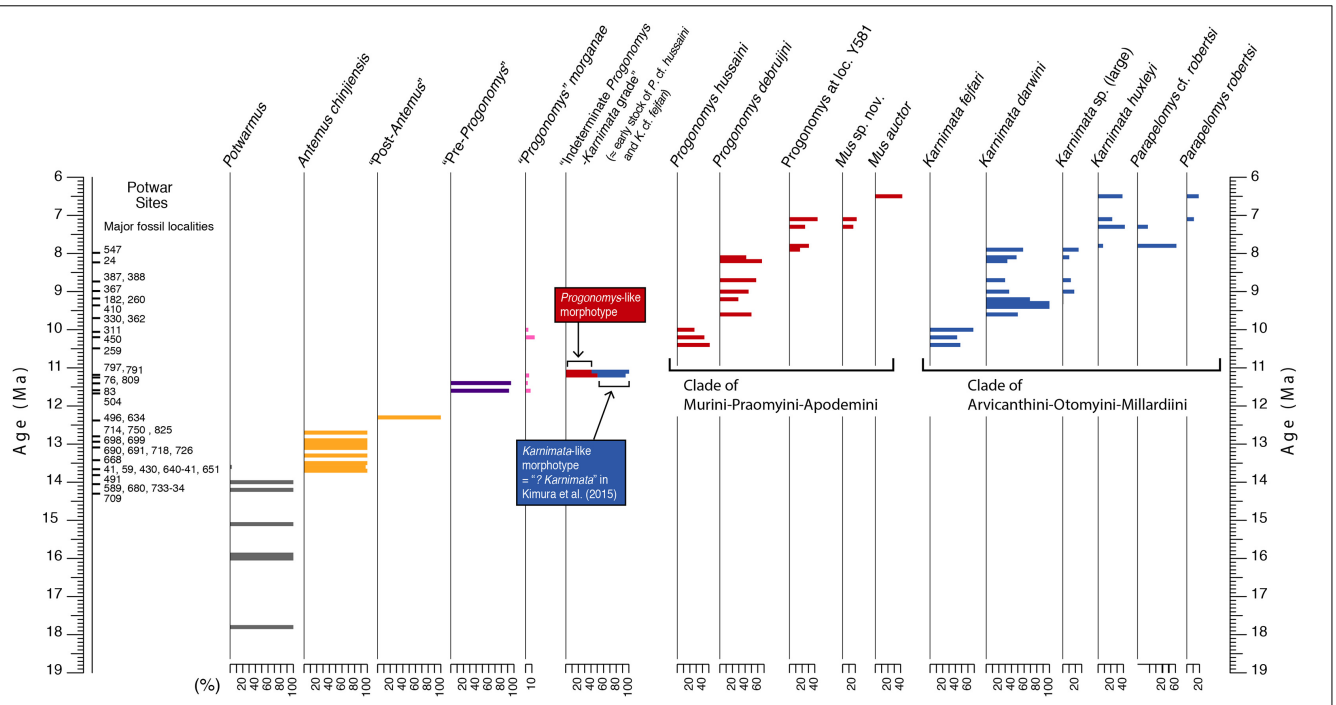

FIGURE 1 | Age and stratigraphic sequence of Potwar Plateau rodent localities of the middle and late Miocene with a time scale in millions of years (Ma); key localities plotted on left. Relative abundances of each taxon and morphotype shown for each stratigraphic level. Pattern reflects evolutionary divergence and diversification of Siwalik Murinae based on species distributions through time. Stem Murinae are succeeded after 11 Ma by crown Murini represented on the one hand by *Progonomys* and its more derived sister clades (Aghová et al., 2018) and on the other hand by crown Arvicanthini represented by *Karnimata* and its more derived sister clades. Columns indicate relative abundances among all contemporary murines. The color scheme is maintained in later figures.

latitude, the area has moved northward with the Indian plate by about 4° since 11 Ma (Tauxe and Opdyke, 1982). Erosional detritus carried southward and accumulating on pre-Indus floodplains (over 3000 m thick on the Potwar Plateau; Tauxe and Opdyke, 1982) comprise layers of rock of varied lithology, formations of the Siwalik Group. The layers of rock of most interest here, mainly Miocene in age, occur in a broad belt across Indo-Pakistan and as exposed on the Potwar Plateau are ∼18–6 million years old (18–6 Ma). The Siwaliks are important for evolutionary biology because the sediments entomb rich samples of the vertebrate biota that populated the region through the Miocene. Fossil bones and teeth are preserved at many levels in the sequence, with the potential that remains of populations in single lineages can be sequentially sampled through time.

The dating of terrestrial fossils through magnetic polarity stratigraphy began in the early 1970's. At that time a consortium of universities began paleontological, stratigraphic, and paleomagnetic studies on the Potwar Plateau because of its fossil abundance known since the 19th Century, its very long fossiliferous stratigraphic section related to the uplift of the Himalaya, and as a focus to develop and validate magnetic polarity stratigraphy in developing a global polarity timescale. From those beginnings, the tradition of precise dating applied to terrestrial paleontology, evolution, and paleoecological studies in the Siwaliks has continued (Keller et al., 1977; Tauxe and Opdyke, 1982; Johnson et al., 1985).

This analysis crucially depends on dated fossil sites with resolution up to 100,000 year precision (see Barry et al., 2002). The dating method involves careful stratigraphic correlation of fossil sites to a master stratigraphic section, in which the paleomagnetic properties of successive samples of rock throughout the stratigraphic sequence build a composite magnetostratigraphy for the Siwaliks. Due to the completeness of the Potwar record, the magnetostratigraphy can be matched to the dated global geomagnetic polarity time scale, yielding age estimates for the rocks (Barry et al., 2013). Estimates are not direct dates, but the dates are relative to one another and distinguishable at a scale of 10^5 years. Because Siwalik strata are generally well exposed, individual fossil localities can be dated in this fashion. This method is widely applied globally (e.g., Garcés et al., 2003; Tedford et al., 2013; Van Dam et al., 2014; García-Paredes et al., 2016).

Siwalik Rodent Fossils

Small mammal fossils accumulated under special conditions at a number of Potwar localities. They are dominantly dental remains presumably accumulated by raptors (mostly owls) in riparian settings. Such conditions did not occur everywhere, so fossil sites are not uniformly distributed through the composite geological section (**Figure 1**)–but they occur densely enough in time to sample details of lineage evolution. Fossils were recovered by wet screening large quantities of fossiliferous sediment from promising localities that usually showed small bone fragments

TABLE 1 | Potwar Plateau rodent localities utilized in this study, their ages, and fossil sample sizes.

Age (Ma)	Locality Number	Total Rodent Fossils	Murine Fossils
10.1	Y311	283	205
10.2	Y450	91	41
10.5	Y259	607	395
11.2	Y797	321	108
11.2	Y791	67	48
11.4	Y076	377	142
11.4	Y809	127	67
11.6	Y083	51	17
11.6	Y504	146	52
12.3	Y634	85	32
12.4	Y496	218	88

on the ground surface. After sieving, the concentrate was sorted under magnification and isolated teeth were retrieved. Samples of individual species range from a few to several tens of teeth per site. For the stratigraphic interval capturing the time of divergence of major murine groups, **Table 1** shows the ages of localities, the number of rodent fossils recovered from each, and the number of those rodents that are murines. With fossils, more complete is always better than less complete, but our use of isolated teeth was necessitated because that is the nature of the samples and is mitigated by the observation that living murine rodent taxa are commonly characterized by molars (e.g., Misonne, 1969).

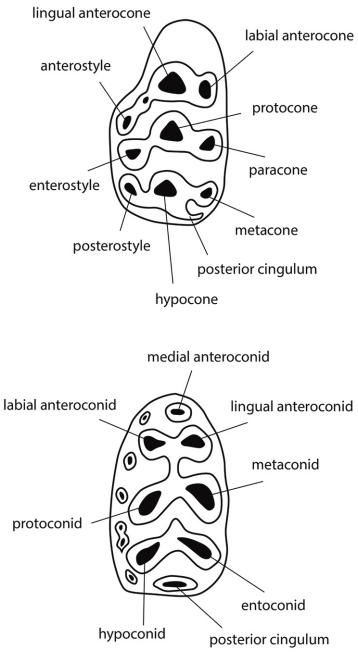

FIGURE 2 | Diagrams of typical murine first molars, upper (above, M1) and lower (below, m1), with cusp nomenclature. Major cusps are labeled, anterior is to the left. Upper molar shows cusps arranged in transverse chevrons; lower molar shows six major cusps in opposed pairs. The axis of the upper molar metacone-hypocone complex is termed a "metaloph."

Morphology

Siwalik fossil teeth recovered by screening represent mostly rodents, but include hedgehogs, shrews, bats, and a few other mammals. The most abundant rodents retrieved are murine mice, and these, like all crown muroids, have only molars in each quadrant behind the enlarged procumbent incisor. The largest and best represented of the molars is the first upper molar (M1). Because it is large (by mouse standards) and relatively complex, this tooth locus presents diagnostic characters and is the most informative of the molars for systematic study. In some cases, the first lower molar (m1) is also useful.

Middle Miocene fossils represent stem murines, but exhibit the apomorphic characteristics of the subfamily, namely extra cusps in M1 and a twinned anteroconid plus labial cingulum in m1 (**Figure 2**). These features are derived, absent in muroid outgroups. The extra cusps in M1 (anterostyle and enterostyle behind it) are lingual in position and constitute, with neighboring cusps, transverse sectorial chevrons. In middle Miocene taxa, the chevrons are poorly developed: most *Potwarmus* (bottom of **Figure 1**) lack the anterostyle, and in *Antemus* the enterostyle is unconnected with its chevron. Jacobs et al. (1989) described the considerable morphological variation in *Antemus* M1 for a large sample from locality Y491 (13.8 Ma). Toward the end of the middle Miocene (12.3 Ma) the early murine lineage, by then advanced over *Antemus*, exhibited full chevrons on M1, but with low ridges weakly connecting neighboring cusps. In none of these samples do we observe definitive features of crown murine tribes.

Beginning with samples at 11.6 Ma, the debut of the late Miocene, we observe sporadic occurrence of advanced M1 features (as below) that characterize crown mouse tribes. Yet these traits occur in samples of teeth that are otherwise homogeneous. Characteristic features of Murini and Arvicanthini appear to be randomly distributed among the specimens. These mouse teeth represent either a single lineage with considerable variation, or two lineages that are cryptic as far as fossil teeth are concerned.

Murini

The key feature of the M1 that characterizes the Murini concerns the anterostyle (Jacobs, 1978). This lingual cusp is associated with the first chevron. In Murini the cusp is shifted posteriorly, its crest running anterolabially to the double anterocone. The anterior part of the M1 is therefore transversely narrow. In addition to its posterior position, the anterostyle is not a circular cusp, but relatively laterally compressed. Molar cusps are distinctly inclined posteriorly.

This combination of features appears in some teeth as a variation in fossil samples of 11.6–11.2 Ma. By 10.5–10.1 Ma, it is stable. Samples of that age and younger are readily assigned to the genus *Progonomys*. By the end of the Miocene, the derivative living genus *Mus* shows a strongly shifted anterostyle, a narrow anterior shelf surmounted by the double anterocone, and a reduced posterior cingulum (Jacobs, 1978).

Arvicanthini

This group conserved the primitive anterostyle position, not strongly repositioned posterolingual to the double anterocone. However, arvicanthins developed progressively a separately derived feature; this concerns the metacone cusp (Kimura et al., 2015). A large metacone that is posteriorly inclined, similar to the paracone, is a primitive condition for mice. The posterior inclination is most obvious in lateral view. Arvicanthins progressively fix a derived condition of the metacone, which is vertical and diminished in size. Most specimens older than 11 Ma show the primitive metacone condition, but some have a modified metacone, smaller than the paracone. By 9.2 Ma, approximately 25% of *Karnimata darwini* show the fully transformed metacone. Progressive development of the derived metacone in the *Karnimata* lineage without similar change in the posterostyle, led Kimura et al. (2015) to recognize that the genus represents a stem in the Arvicanthini-Otomyini-Millardiini clade.

Relative Abundances of Siwalik Murines

Temporal change in the relative abundances of the major components of the Siwalik murine rodents in **Figure 1** is based on the Harvard University-Geological Survey of Pakistan database (e.g., Barry et al., 2013), which is continuously updated. Although the master database includes fossils representing all tooth positions, we analyzed a subset (extracted December, 2020) of only upper first molars (M1) for those taxa with total number of specimens of ten or more. Complexity of M1 maximizes precision of taxonomic assignment for that tooth. The relative abundance of M1 was calculated as the number of fossils in a species (taxonomic unit) relative to the total number of murine fossils. The stratigraphic diagrams were generated with 0.1 m.y. (10^5 year) time bins by the *strat.plot* function in the package *rioja* (Juggins, 2020) implemented in R (R Core Team, 2020).

Crown Morphology in Transition

To visualize change through time of dental characters as they were fixed in the *Mus-Arvicanthis* divergence (**Figure 3** and **Tables 2–5**), we obtained the measurements of four morphometric traits of M1 from time-ordered and sequential samples: the ratio of the major and minor axes of the anterostyle; the acute angle of the anterostyle relative to the longitudinal tooth axis; the acute angle between a line connecting the protocone-enterocone and the longitudinal tooth axis; and the acute angle of the metaloph (line through the major axis of the metacone) relative to the longitudinal tooth axis. The datasets of Kimura et al. (2013b) are combined with the latter feature, which is newly obtained for this study. Taxonomic assignments of Kimura et al. (2013b) are updated following Kimura et al. (2015, 2016, 2017) and Flynn et al. (2020). Previously, in Kimura et al. (2013b), we calculated the 95% bias-corrected and accelerated bootstrap (BCa) confidence intervals for groups with more than three entries (i.e., taxa in different time slices are treated as separate groups), and only these data are plotted in Figure 9 of Kimura et al. (2013b). In this study, we calculated both 95% bootstrap confidence intervals for groups with more than two entries. The choice of the bootstrap method did not affect our conclusions. In the bootstrap permutation, 9999 replicates were resampled. The bootstrap confidence intervals were calculated in the R package *boot* (Canty and Ripley, 2020) using the *boot.ci* function. All data are plotted in **Figure 3**. Due to updates in taxonomic assignments, the different bootstrap calculation method, and the selection of groups plotted in **Figure 3**, some details differ slightly from that of Kimura et al. (2013b, Figure 9).

Stratigraphic Age and the Molecular Clock

A time-calibrated tree (discussed below) was generated using "Stratigraphic Tree Analysis for Paleontology" (strap) in R package for proposed relationships of Siwalik murines. We constructed a tree file (.tre) with a single tree as our hypothesis by manually editing tree shape in Mesquite version 3.04 (Maddison and Maddison, 2017) based against an updated review of ranges of Siwalik fossils. For time calibration, first and last appearances were compiled as the lowermost and uppermost stratigraphic occurrences of the taxa. In the R package "strap," the equal scaling method was used in the *DatePhylo* function with a root length (i.e., length of the base of the tree) of 1 million. Although the time-scaling algorithm of the "equal" method is tuned to avoid zero-length branches instead of generating best estimates of divergence times, the model ages of the fossil calibration points are consistent with our previous proposals and molecular estimates (Lecompte et al., 2008; Aghová et al., 2018), and support the proposition that the density of sampled Siwalik fossils may be sufficient to capture transitional morphological changes near divergences.

RESULTS

Previously, we (Flynn et al., 2020) found a good match between the stratigraphic record of clade appearances and the node age estimates from the molecular time tree of Lecompte et al. (2008). Nevertheless, the Siwalik murine record has obtained more detail in recent years from review and analysis of carefully controlled data for over 3600 specimens and therefore the evolution of murines can be traced in more detail. In samples of 9.2 Ma (locality Y182), Jacobs (1978) recognized two clearly separate species, *Progonomys debruijni* and *K. darwini*, now recognized to represent Murini in the former case and Arvicanthini in the latter (**Figure 4**). *P. debruijni* had the murine anterostyle shifted and laterally compressed. All cusps showed posterior inclination and *P. debruijni* was the smaller of the two. The other mouse *K. darwini* was clearly larger with a plesiomorphic anterostyle. Kimura et al. (2013b, 2015) recognized the significance of the morphological distinctions between *Progonomys* and *Karnimata* and distinguished a number of other dental features, including isotopic differences (Kimura et al., 2013a), that set the lineages apart especially after 9 Ma.

In older samples dating to 10.5–10.1 Ma (localities Y259, 450, 311), the murines resembled the 9.2 Ma samples, but represented more primitive species, which Kimura et al. (2017) recognized as *Progonomys hussaini* and *Karnimata fejfari* (**Figure 5**). These earlier representatives of the *Progonomys* and *Karnimata*

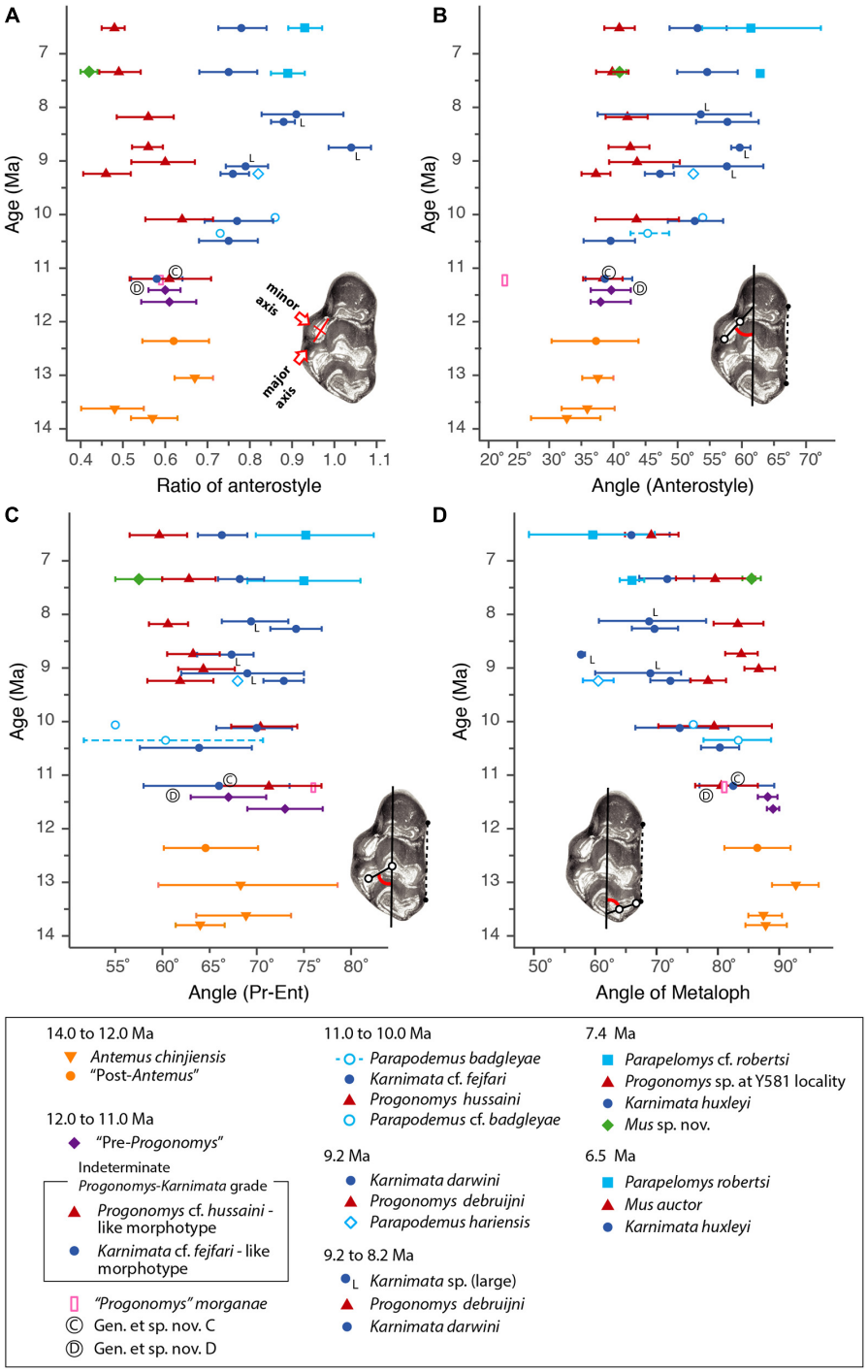

FIGURE 3 | Temporal change and variation in four morphometric characters in Siwalik murines. **(A)** Axis ratio of anterostyle shape (length of the minor axis relative to that of the major axis). **(B)** Acute angle between the anterostyle and the longitudinal axis of the tooth. **(C)** Acute angle formed by a line connecting the centers of protocone and enterostyle with the longitudinal axis of the tooth. **(D)** Acute angle between the major axis of the metacone (forms a metaloph with the hypocone) and the longitudinal axis of the tooth. Error bars indicate 95% bootstrap confidence intervals. The specimen illustrated is *Progonomys debruijni* (YGSP 7740) in early wear. Versions of panels **(A–C)** initially in Kimura et al. (2013b), updated here with revised taxonomy; panel **(D)** is new. Error bars represent 95% confidence intervals.

lineages, the stems of Murini and Arvicanthini, were less distinct, showed lower frequency of derived character states, and were much closer in size.

If the older *P. hussaini* and *K. fejfari* were more similar to each other than younger members of these genera (at least in features that could be perceived in the dentition), would

TABLE 2 | Summary statistics for anterostyle ratio in Siwalik murine rodents, corresponding to **Figure 3A**.

Taxonomic Unit	*N*	Average Age (Ma) GTS2012	Mean	Min	Max	SD	Lower CI basic	Upper CI basic	Lower CI BCa	Upper CI BCa
Karnimata huxleyi	10	6.52	0.78	0.60	0.90	0.09	0.73	0.84	0.72	0.83
Mus auctor	12	6.52	0.48	0.40	0.58	0.05	0.45	0.50	0.45	0.51
Parapelomys robertsi	5	6.52	0.93	0.87	0.98	0.04	0.89	0.97	0.89	0.96
Mus sp. nov.	2	7.34	0.42	0.40	0.44	0.03	0.40	0.44	0.40	0.44
Karnimata huxleyi	20	7.34	0.75	0.45	0.94	0.15	0.68	0.82	0.67	0.81
Progonomys sp. at Y581 locality	11	7.34	0.49	0.37	0.58	0.08	0.44	0.54	0.44	0.53
Parapelomys cf. *robertsi*	2	7.37	0.89	0.85	0.93	0.06	0.85	0.93	0.85	0.93
Karnimata sp. (large)	5	8.13	0.91	0.80	1.02	0.10	0.83	1.02	0.81	1.00
Progonomys debruijni	12	8.18	0.56	0.41	0.87	0.12	0.49	0.62	0.51	0.66
Karnimata darwini	12	8.27	0.88	0.81	0.97	0.05	0.85	0.91	0.85	0.91
Progonomys debruijni	16	8.74	0.56	0.45	0.68	0.07	0.52	0.59	0.52	0.60
Karnimata sp. (large)	3	8.75	1.04	1.00	1.10	0.05	0.99	1.09	1.00	1.10
Progonomys debruijni	3	9.02	0.60	0.53	0.68	0.08	0.52	0.67	0.53	0.68
Karnimata sp. (large)	3	9.10	0.79	0.73	0.83	0.05	0.74	0.84	0.73	0.83
Karnimata darwini	31	9.24	0.76	0.56	0.95	0.10	0.73	0.80	0.73	0.80
Parapodemus hariensis	2	9.24	0.82	0.69	0.95	0.18	0.69	0.95	0.69	0.95
Progonomys debruijni	15	9.24	0.46	0.26	0.61	0.11	0.41	0.52	0.40	0.52
Parapodemys cf. *badgleyae*	1	10.06	0.86	0.86	0.86	NA	NA	NA	NA	NA
Progonomys hussaini	5	10.09	0.64	0.57	0.76	0.09	0.55	0.71	0.58	0.74
Karnimata fejfari	9	10.12	0.77	0.58	0.97	0.12	0.69	0.86	0.69	0.85
Parapodemus badgleyae	3	10.35	0.73	0.73	0.74	0.01	0.73	0.74	0.73	0.74
Karnimata fejfari	9	10.49	0.75	0.62	0.91	0.10	0.68	0.82	0.68	0.82
Gen. et sp. nov. C	1	11.18	0.62	0.62	0.62	NA	NA	NA	NA	NA
"Indeterminate *Progonomys-Karnimata* grade" (*Progonomys*-like morphotype)	7	11.20	0.61	0.46	0.81	0.13	0.52	0.71	0.52	0.72
"Indeterminate *Progonomys-Karnimata* grade" (*Karnimata*-like morphotype)	6	11.20	0.58	0.50	0.68	0.07	0.52	0.64	0.52	0.64
"*Progonomys*" *morganae*	1	11.23	0.59	0.59	0.59	NA	NA	NA	NA	NA
"Pre-*Progonomys*"	21	11.41	0.60	0.49	0.83	0.09	0.56	0.64	0.57	0.65
Gen. et sp. nov. D	1	11.41	0.53	0.53	0.53	NA	NA	NA	NA	NA
"Pre-*Progonomys*"	3	11.63	0.61	0.54	0.67	0.07	0.54	0.67	0.54	0.67
"Post-*Antemus*"	7	12.36	0.62	0.46	0.79	0.11	0.55	0.70	0.55	0.71
Antemus chinjiensis	7	13.05	0.67	0.60	0.75	0.06	0.62	0.71	0.63	0.72
Antemus chinjiensis	14	13.62	0.48	0.31	0.74	0.14	0.40	0.55	0.41	0.56
Antemus chinjiensis	12	13.80	0.57	0.40	0.69	0.10	0.52	0.63	0.51	0.63

CI: 95% confidence interval. BCa: bias-corrected and accelerated bootstrap.
SD: standard deviation.

still older samples (those available to us being 11.6–11.2 Ma) show more subtle differences, or appear to merge? Localities Y797 and Y791, dating to 11.2 Ma, have abundant murines, all about the same size and resembling *Progonomys* and *Karnimata* (plus a few teeth representing small "*Progonomys*" *morganae* and two unnamed mice; Flynn et al., 2020). Most individual specimens appear comparable to *P. hussaini* and *K. fejfari*, but the collections, taken as biological samples, do not sort readily into more than one species. These fossils were considered a single population also in model-based Bayesian cluster analysis

TABLE 3 | Summary statistics for anterostyle angle in Siwalik murine rodents, corresponding to **Figure 3B**.

Taxonomic Unit	*N*	Average Age (Ma) GTS2012	Mean	Min	Max	SD	Lower CI basic	Upper CI basic	Lower CI BCa	Upper CI BCa
Karnimata huxleyi	10	6.52	53	43	62	7.0	48.7	57.6	48.4	57.3
Mus auctor	12	6.52	41	34	49	4.1	38.6	43.3	38.5	43.2
Parapelomys robertsi	5	6.52	61	50	70	10.0	53.8	72.3	50.3	69.0
Mus sp. nov.	2	7.34	41	40	42	1.4	40.0	42.0	40.0	42.0
Karnimata huxleyi	20	7.34	55	37	72	10.6	49.9	59.4	50.0	59.4
Progonomys sp. at Y581 locality	11	7.34	40	34	45	4.3	37.3	42.3	37.3	42.3
Parapelomys cf. *robertsi*	2	7.37	63	54	72	12.7	69.0	81.0	69.0	81.0
Karnimata sp. (large)	5	8.13	54	45	81	15.4	37.5	61.4	46.3	81.0
Progonomys debruijni	12	8.18	42	34	53	5.7	38.8	45.3	39.2	45.8
Karnimata darwini	12	8.27	58	40	73	8.5	52.9	62.6	52.7	62.4
Progonomys debruijni	16	8.74	43	32	57	6.5	39.3	45.6	39.8	46.2
Karnimata sp. (large)	3	8.75	60	58	61	1.5	58.3	61.3	58.0	61.0
Progonomys debruijni	3	9.02	44	37	48	5.9	39.3	50.3	37.0	48.0
Karnimata sp. (large)	3	9.10	58	52	66	7.4	49.3	63.3	52.0	66.0
Karnimata darwini	31	9.24	47	40	64	6.4	44.9	49.4	45.2	49.8
Parapodemus hariensis	2	9.24	53	45	60	10.6	45.0	60.0	45.0	60.0
Progonomys debruijni	15	9.24	37	31	45	4.5	35.0	39.5	35.1	39.6
Parapodemys cf. *badgleyae*	1	10.06	54	54	54	NA	NA	NA	NA	NA
Progonomys hussaini	5	10.09	44	36	53	6.9	37.2	50.2	37.0	50.0
Karnimata fejfari	9	10.12	53	40	62	6.6	48.5	57.1	47.6	56.5
Parapodemus badgleyae	3	10.35	45	42	48	3.1	42.7	48.7	42.0	48.0
Karnimata fejfari	9	10.49	40	31	51	6.0	35.4	43.4	36.1	44.4
Gen. et sp. nov. C	1	11.18	39	39	39	NA	NA	NA	NA	NA
"Indeterminate *Progonomys-Karnimata* grade" (*Progonomys*-like morphotype)	7	11.20	38	31	43	4.1	35.3	41.4	34.2	40.8
"Indeterminate *Progonomys-Karnimata* grade" (*Karnimata*-like morphotype)	6	11.20	39	30	43	4.6	35.7	42.9	31.8	41.0
"Progonomys" morganae	1	11.23	23	23	23	NA	NA	NA	NA	NA
"Pre-*Progonomys*"	21	11.41	40	28	54	7.3	36.5	42.7	36.7	43.0
Gen. et sp. nov. D	1	11.41	44	44	44	NA	NA	NA	NA	NA
"Pre-*Progonomys*"	3	11.63	38	38	38	0.0	36.5	42.7	36.7	43.0
"Post-*Antemus*"	7	12.36	37	26	51	8.9	30.4	43.9	31.0	44.6
Antemus chinjiensis	7	13.05	38	33	43	3.3	35.1	40.0	35.2	40.2
Antemus chinjiensis	14	13.62	36	22	50	7.9	31.9	40.2	31.4	39.7
Antemus chinjiensis	12	13.80	33	21	50	9.5	27.2	38.0	27.7	38.6

CI: 95% confidence interval. BCa: bias-corrected and accelerated bootstrap.
SD: standard deviation.

(Kimura et al., 2016). Some M1's have the murinin (*Progonomys*-like) morphology and some present the arvicanthin morphology (**Figures 1**, **3**, **6**). The array of morphologies observed among the M1 is not bimodal–there are intermediates. Further, other molars in the dentition (m1, second and third molars) comprise samples that show no consistent differentiation and no pattern for taxonomic association with M1. For the 11.2 Ma samples Flynn et al. (2020) could not defend two species and opted for an informal designation of "indeterminate *Progonomys–Karnimata* grade." There is no record of *P. hussaini* and *K. fejfari* on

TABLE 4 | Summary statistics for angle formed by the protocone and enterostyle in Siwalik murine rodents, corresponding to **Figure 3C**.

Taxonomic Unit	*N*	Average Age (Ma) GTS2012	Mean	Min	Max	SD	Lower CI basic	Upper CI basic	Lower CI BCa	Upper CI BCa
Karnimata huxleyi	10	6.52	66	60	72	4.2	63.8	69.0	63.5	68.7
Mus auctor	12	6.52	60	52	69	5.3	56.5	62.6	56.8	63.0
Parapelomys robertsi	5	6.52	75	63	81	7.5	69.9	82.4	63.0	80.0
Mus sp. nov.	2	7.34	58	55	60	3.5	55.0	60.0	55.0	60.0
Karnimata huxleyi	20	7.34	68	53	77	5.6	65.9	70.8	65.3	70.2
Progonomys sp. at Y581 locality	11	7.34	63	55	70	4.8	60.0	65.6	60.0	65.8
Parapelomys cf. *robertsi*	2	7.37	75	69	81	8.5	69.0	81.0	69.0	81.0
Karnimata sp. (large)	5	8.13	69	63	73	4.0	66.3	73.3	63.0	72.0
Progonomys debruijni	12	8.18	61	55	66	3.7	58.6	62.7	58.3	62.5
Karnimata darwini	12	8.27	74	67	81	4.8	71.4	76.9	71.4	76.8
Progonomys debruijni	16	8.74	63	55	75	5.7	60.5	66.1	60.4	66.1
Karnimata sp. (large)	3	8.75	67	65	71	3.2	63.7	69.7	65.0	71.0
Progonomys debruijni	3	9.02	64	61	67	3.1	61.7	67.7	61.0	67.0
Karnimata sp. (large)	3	9.10	69	63	76	6.6	62.0	75.0	63.0	76.0
Karnimata darwini	31	9.24	73	59	87	6.0	70.7	75.0	70.8	75.1
Parapodemus hariensis	2	9.24	68	66	70	2.8	66.0	70.0	66.0	70.0
Progonomys debruijni	15	9.24	62	51	75	6.8	58.4	65.4	58.4	65.4
Parapodemys cf. *badgleyae*	1	10.06	55	55	55	NA	NA	NA	NA	NA
Progonomys hussaini	5	10.09	70	64	74	4.0	67.3	74.3	64.0	73.0
Karnimata fejfari	9	10.12	70	61	83	6.2	65.7	73.8	66.6	74.9
Parapodemus badgleyae	3	10.35	60	50	69	9.6	51.7	70.7	50.0	69.0
Karnimata fejfari	9	10.49	64	50	82	8.9	57.6	69.5	58.8	70.8
Gen. et sp. nov. C	1	11.18	67	67	67	NA	NA	NA	NA	NA
"Indeterminate *Progonomys-Karnimata* grade" (*Progonomys*-like morphotype)	7	11.20	71	59	82	7.1	65.9	76.9	65.3	76.3
"Indeterminate *Progonomys-Karnimata* grade" (*Karnimata*-like morphotype)	6	11.20	66	56	80	9.3	58.0	73.5	58.7	74.2
"Progonomys" morganae	1	11.23	76	76	76	NA	NA	NA	NA	NA
"Pre-*Progonomys*"	21	11.41	67	51	83	9.3	63.0	71.0	62.9	70.9
Gen. et sp. nov. D	1	11.41	61	61	61	NA	NA	NA	NA	NA
"Pre-*Progonomys*"	3	11.63	73	69	77	4.0	69.0	77.0	69.0	75.7
"Post-*Antemus*"	7	12.36	65	53	70	6.6	60.1	70.1	57.4	68.5
Antemus chinjiensis	7	13.05	68	48	84	12.4	59.6	78.6	57.6	76.6
Antemus chinjiensis	14	13.62	69	54	93	9.8	63.6	73.6	64.5	74.7
Antemus chinjiensis	12	13.80	64	57	71	4.5	61.4	66.6	61.3	66.5

CI: 95% confidence interval. BCa: bias-corrected and accelerated bootstrap.
SD: standard deviation.

the Potwar Plateau prior to 10.5 Ma. The roots of distinct *Progonomys* and of *Karnimata* lineages appear to lie in samples captured at 11.2 Ma.

The mice from Y791 and Y797, 11.2 Ma, were very close to the crown murine genera *Progonomys* and *Karnimata* but did not show one or the other derived morphologies consistently. Morphologies observed from somewhat older localities were yet more variable, but with inconsistently derived morphologies (**Figure 7**). Our field surveys in subjacent strata located fossil localities Y76 and Y809 at 11.4 Ma, and below these (therefore

TABLE 5 | Summary statistics for axis angle through metacone in Siwalik murine rodents, corresponding to **Figure 3D**.

Taxonomic Unit	*N*	Average Age (Ma) GTS2012	Mean	Min	Max	SD	Lower CI basic	Upper CI basic	Lower CI BCa	Upper CI BCa
Karnimata huxleyi	10	6.52	66	47	81	9.5	60.2	72.1	59.0	71.3
Mus auctor	12	6.52	69	56	80	7.6	64.9	73.6	64.3	73.0
Parapelomys robertsi	5	6.52	60	41	73	12.1	49.2	69.7	46.3	68.1
Mus sp. nov.	2	7.34	86	84	87	2.1	84.0	87.0	84.0	87.0
Karnimata huxleyi	20	7.34	72	59	97	10.4	67.2	76.1	67.8	76.8
Progonomys sp. at Y581 locality	11	7.34	80	64	91	10.8	73.2	86.1	72.9	85.8
Parapelomys cf. *robertsi*	2	7.37	66	64	68	2.8	64.0	68.0	64.0	68.0
Karnimata sp. (large)	5	8.13	69	56	79	9.3	60.6	78.1	58.3	76.3
Progonomys debruijni	12	8.18	83	71	91	7.3	79.3	87.4	78.6	86.9
Karnimata darwini	12	8.27	70	55	80	6.7	66.0	73.5	65.4	73.1
Progonomys debruijni	16	8.74	84	75	91	5.4	81.2	86.5	81.0	86.3
Karnimata sp. (large)	3	8.75	58	57	58	0.6	57.3	58.3	57.0	58.0
Progonomys debruijni	3	9.02	87	84	89	2.5	84.3	89.3	84.0	89.0
Karnimata sp. (large)	3	9.10	69	64	78	7.8	60.0	74.0	64.0	78.0
Karnimata darwini	31	9.24	72	55	89	9.2	69.0	75.4	69.2	75.7
Parapodemus hariensis	2	9.24	61	58	63	3.5	58.0	63.0	58.0	63.0
Progonomys debruijni	15	9.24	78	67	87	5.6	75.6	81.3	75.4	81.2
Parapodemys cf. *badgleyae*	1	10.06	76	76	76	NA	NA	NA	NA	NA
Progonomys hussaini	5	10.09	79	70	90	9.3	70.3	88.8	70.0	88.0
Karnimata fejfari	9	10.12	74	53	91	11.4	66.6	81.7	65.4	80.8
Parapodemus badgleyae	3	10.35	83	78	89	5.5	77.7	88.7	78.0	89.0
Karnimata fejfari	9	10.49	80	74	86	4.7	77.3	83.5	77.0	83.2
Gen. et sp. nov. C	1	11.18	83	83	83	NA	NA	NA	NA	NA
"Indeterminate *Progonomys-Karnimata* grade" (*Progonomys*-like morphotype)	7	11.20	81	66	87	7.0	76.3	86.5	71.3	84.0
"Indeterminate *Progonomys-Karnimata* grade" (*Karnimata*-like morphotype)	6	11.20	83	72	90	7.6	77.0	89.2	74.0	87.7
"Progonomys" morganae	1	11.23	81	81	81	NA	NA	NA	NA	NA
"Pre-*Progonomys*"	21	11.41	88	81	96	3.7	86.5	89.7	86.6	89.8
Gen. et sp. nov. D	1	11.41	78	78	78	NA	NA	NA	NA	NA
"Pre-*Progonomys*"	3	11.63	89	88	90	1.0	88.0	90.0	88.0	89.7
"Post-*Antemus*"	7	12.36	86	78	97	7.0	81.1	91.9	81.0	91.8
Antemus chinjiensis	7	13.05	93	86	100	5.0	88.8	96.4	89.2	96.8
Antemus chinjiensis	14	13.62	87	74	92	5.3	85.0	90.5	83.2	89.5
Antemus chinjiensis	12	13.80	88	76	98	5.9	84.5	91.3	84.0	90.8

CI: 95% confidence interval. BCa: bias-corrected and accelerated bootstrap.
SD: standard deviation.

older) sites Y83 and Y504 at 11.6 Ma. The collections presented a medley of features, some specimens showing a displaced, pinched anterocone, others showing variably inclined cusps. Individual M1 were occasionally reminiscent of *Progonomys* in having the anterostyle displaced backward (**Figure 7C**), but most molars lacked derived conditions of extant mouse tribes. The M1 resembled their "post-*Antemus*" predecessors of 12.3 Ma, many with anterocones not elongated antero-posteriorly, and connections between adjacent cusps generally undeveloped. These "pre-*Progonomys*" mice were basal crown murines (stem species) containing the roots of later tribe-level radiations, but themselves undifferentiated along modern lines.

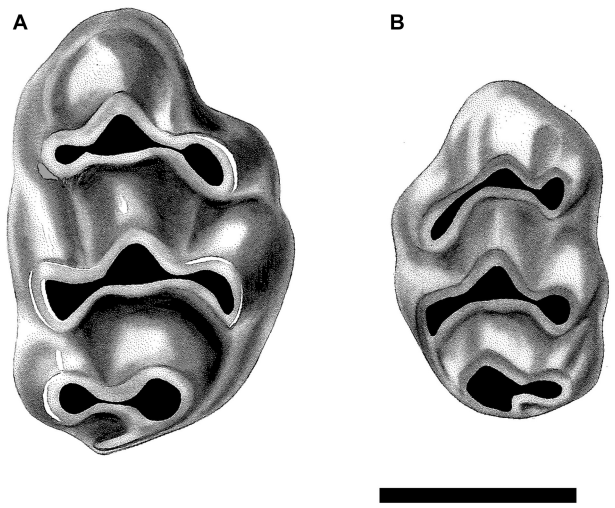

FIGURE 4 | Upper first molars of the dominant murines present at locality Y182, 9.2 Ma. **(A)** Right M1 of *Karnimata darwini*, specimen YGSP 7720, and **(B)** smaller left M1 of *Progonomys debruijni*, YGSP 7736. Both at same 1 mm scale, anterior is upward.

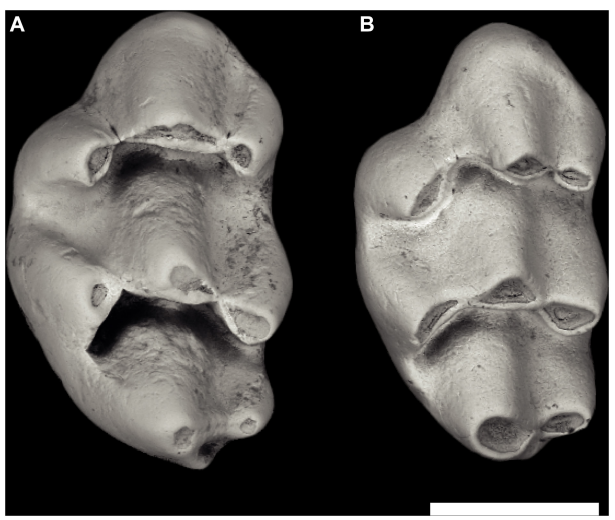

FIGURE 5 | Early *Karnimata* and *Progonomys* from locality Y311, 10.1 Ma. **(A)** *Karnimata fejfari* left M1 YGSP 54147 and **(B)** *Progonomys hussaini* left M1 YGSP 541443. *Progonomys* is slender with more inclined cusps but is near the size of *Karnimata*. Both at same 1 mm scale, anterior is upward.

The documentation of multiple, sequentially progressive transitional samples, whether of mixed cryptic species or of consecutive individually variable species, provides a timescale for this cladistic event and a view of its mode. In either case, the 11 Ma divergence provided by "*strap*"-based stratigraphic age estimation (**Figure 8**) is congruent with the most recent molecular estimates of the Murini-Arvicanthini split provided by Aghová et al. (2018).

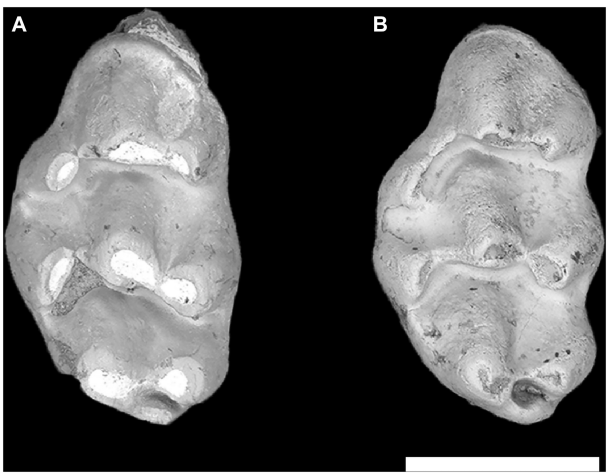

FIGURE 6 | Indeterminate *Karnimata–Progonomys* grade molars from locality Y797, 11.2 Ma. **(A)** *Karnimata*-like left M1 YGSP 36826 and **(B)** *Progonomys*-like left M1 YGSP 33878. Both at same 1 mm scale, anterior is upward.

DISCUSSION

It is well worth emphasizing the unique set of conditions that allowed this evaluation of tempo and mode in evolution using the fossil record. Siwalik Group rocks or their equivalents span a vast area along the Himalaya front from Pakistan to Myanmar. Correlative fossils from India largely complement and corroborate the Siwalik murine record in Pakistan (Patnaik, 2014, 2020). Older fossils are not relevant to this study because they are phylogenetically distant from the problem; younger fossil taxa are more derived members of Murini and Arvicanthini (e.g., Jacobs, 1978; Musser, 1987; Patnaik et al., 1993, 2018; Kotlia, 2008; Patnaik, 2020). Although fossil murines and other fossil rodents have been known in Europe (Schaub, 1938; Michaux, 1971) and globally for many years, no murine fossil known is older than the oldest murines of Pakistan. Flynn et al. (2020) have discussed this restricted biogeographic setting of the Siwaliks as the "murine cradle."

Moreover, Siwalik murines and other small mammals were linked with the remainder of the fauna as part of a large, evolving ecosystem that responded to global conditions (Barry et al., 1985; Blois and Hadley, 2009; Figueirido et al., 2012) and to more regional abiotic and climatic changes (Flynn and Jacobs, 1982; Badgley et al., 2008; López-Antoñanzas et al., 2015). Stable isotopes have been used to track changes in Siwalik murine diets and tooth morphology has been correlated with dietary changes (Kimura et al., 2013a,b, 2016). These aspects of paleobiology, all of which have a temporal component, reiterate the importance of high-quality geologic dating and dense sampling of fossils in the Siwaliks. Finally, the group of animals being studied, with an enormous modern diversity and broad geographic range, renders the study of their deep roots both multidisciplinary and highly significant.

FIGURE 7 | Four left M1 from locality Y76, 11.4 Ma, showing stem murinin-arvicanthin morphology. **(A)** YGSP 33586, **(B)** 33571, **(C)** 33591, and **(D)** 33572. Of these four, panel **(C)** is *Progonomys*-like; the others resemble *Karnimata*. Same 1 mm scale, anterior upward.

The middle and late Miocene age murine fossil record is rich throughout the Old World, but the oldest fossils of the subfamily are from the early Miocene of South Asia (Flynn et al., 2020). Significant events in early murine evolution appear to be centered in southern Asia, and the best fossil record that captures part of that radiation is being developed in the Siwaliks of the Indian Subcontinent (Jacobs and Downs, 1994; Jacobs and Flynn, 2005; Patnaik, 2014). This exceptional fossil record bears on the origin of two extant tribes, Murini and Arvicanthini. We contend that while the fossil record does not address population microevolution, it is relevant to fine scale evolutionary phenomena between the microevolutionary and macroevolutionary levels.

The Siwalik deposits of the Potwar Plateau contain a record of superposed fossil samples that is continuous and well dated on the scale of 100,000 years especially for the time span discussed here, 14–8 Ma. We have applied this precise biostratigraphy to a special episode in murine evolution. The relative ages of fossils are consistent with the pattern of evolution of crown clades (Lecompte et al., 2008; Aghová et al., 2018; Flynn et al., 2020).

Major morphological features are in this case an insufficient basis for tracing microevolution so we dissected molar crown morphology into distinct, definable traits and traced change through time (**Figure 3**). We selected four features (see section "Materials and Methods") and quantified change from 14 to 6 Ma. These features show considerable variation until about 11 Ma, when they diverge, slowly at first, as Murini and Arvicanthini (and other minor lineages). We contend that this faithfully reflects growing divergence in morphology consistent with the scenario of a split of the two lineages from a common ancestor, with clear separation by 10.5 Ma.

Fossil samples at 9.2 Ma and younger securely represent early Murini and Arvicanthini in morphological features and dietary preferences (Kimura et al., 2015, 2016). Key species at that age are the distinct *P. debruijni* and *K. darwini*. Predecessor species, *P. hussaini* and *K. fejfari*, occur in rocks one million years older. These species were morphologically closer to each other than their successors were to their contemporaries, but still distinct, and are closer in time to the origins of the tribes. The oldest records of *P. hussaini* and *K. fejfari* are from locality Y259 at 10.5 Ma; they may well have been distinct before that. However, at 11.2 Ma we find that while the species were not yet present, samples are consistent with the hypothetical origin of Murini and Arvicanthini. Fossil samples at 11.2 Ma comprise morphological variants that resemble *Progonomys* and *Karnimata* but appear to represent a single lineage of rodents. The samples do not present a bimodal distribution of shape or size. Hypothetical cryptic species may be a possibility but cannot be distinguished morphologically.

These data speak to the *mode* of evolution in these murines. The split of the modern tribes was incremental. It began in a common pool of morphological variants. Extremes in variation, e.g., the murinin anterostyle, became hallmarks of mice exploiting one part of the range of variation, in contrast to the arvicanthin strategy of retained vertical cusps and broadened molars. Absolute change in M1 morphology is greater in arvicanthins, which later exploited preferentially a C4 diet. Our data suggest such a scenario but are not sufficient to claim that the tribes originated at 11.2 Ma exactly. Indeed, the lineages may have been close, but not yet morphologically distinct at that age in the features we can perceive. The fossils at 11.2 Ma may sample two cryptic species, *Progonomys* and *Karnimata* ancestors.

The Siwalik fossil record also addresses the *tempo* of the origin of Murini and Arvicanthini. Prior to 11.2 Ma, fossil samples show similar variation embracing early murinin and arvicanthin morphology. This suggests a very long interval of time during which basal crown murines experimented with diversification as Murini and Arvicanthini. Hundreds of thousands of years passed before the definitive tribe-equivalent morphologies emerged. Even if *Progonomys* and *Karnimata* had diverged by 11.2 Ma, the completion of their splitting process was protracted over a very long time, at least 400,000 years during this interval.

What may have gone on during these 100,000 years? While the clear separation of crown tribes may be arbitrary within tight limits, it is quite feasible that gene flow, even if limited, continued between their earliest species members for some time after their genetic divergence. The phenomenon of genetic

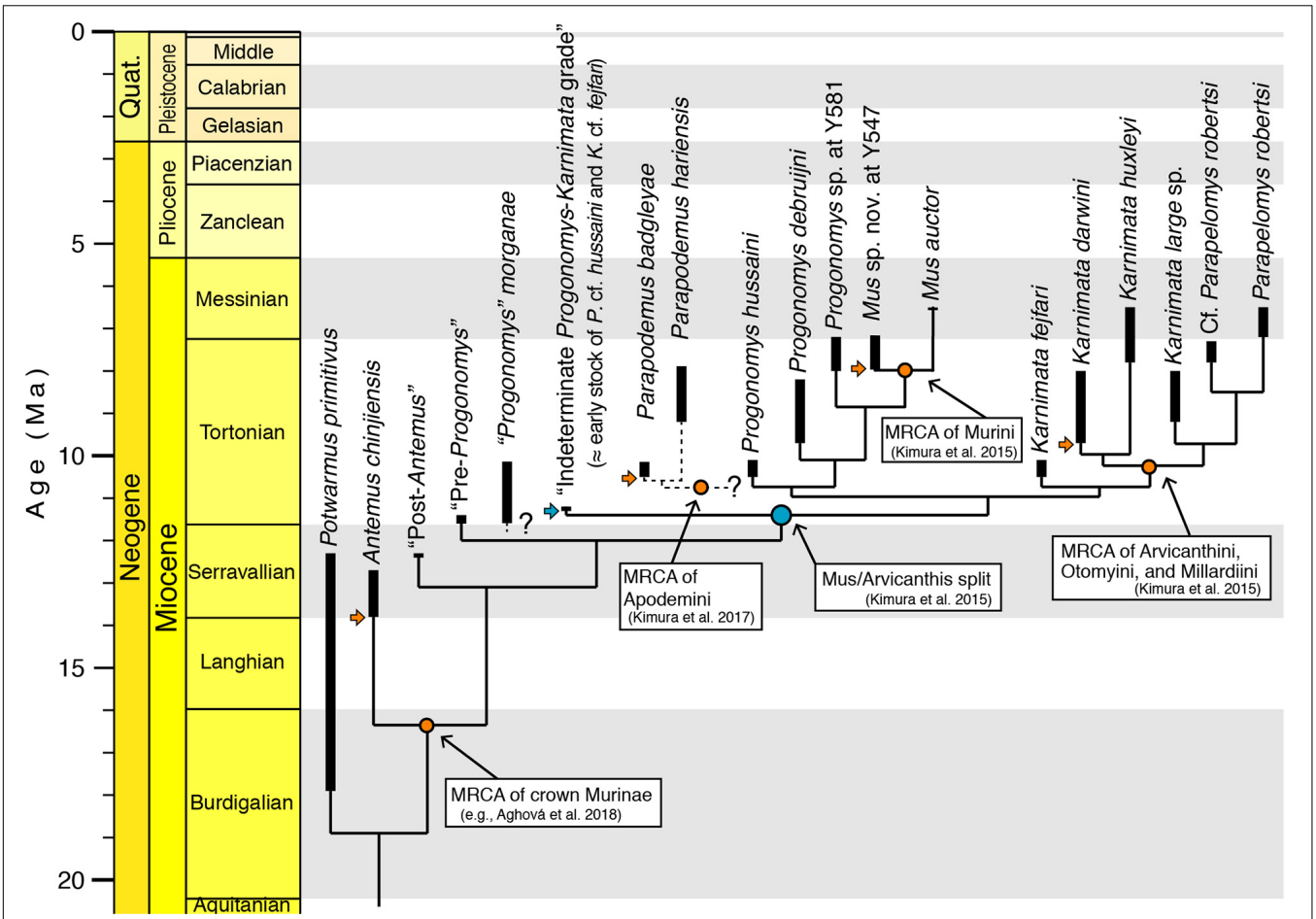

FIGURE 8 | Time-tree for proposed phylogenetic relationships of major Siwalik murine rodents with well-defined time calibration points on the standard time scale, modeled with the "*strap*" package in R (Bell and Lloyd, 2015). Stem murines *Potwarmus primitivus* and *Antemus chinjiensis* are succeeded on the tree by basal crown murines, followed by a grade labeled "indeterminate *Progonomys–Karnimata*" (the cf. *Progonomys hussaini* and cf. *Karnimata fejfari* of Flynn et al., 2020). These are succeeded by the *Progonomys* and *Karnimata* clades, which are basal to subclades Murini-Praomyini-Apodemini and Arvicanthini-Otomyini-Millardiini, respectively. The bold lines connect range-through occurrences of the taxa in the Potwar record. The light blue node indicates a fossil calibration point evidenced by an initial split into two clades. The orange nodes indicate calibration points defined by the earliest occurrence of stem species of the clade. Horizontal arrows show the earliest occurrences of stem fossils. "*Strap*"-based ages of fossil calibration points are consistent with those previously proposed by Bayesian-based molecular divergence estimates in Aghová et al. (2018). Considering that the "equal" time-scaling algorithm in "*strap*" is tuned to avoid zero-length branches and that the molecular phylogeny is based on a framework of Bayesian statistics, the consistent age estimates between the two approaches indicate that Siwalik fossil sampling is dense enough to capture transitional morphological changes. Best practices for the use of fossils in molecular phylogenetics proposed by Parham et al. (2012) and followed by Aghová et al. (2018) yield credible divergence estimates for the Murinae tree. MRCA: most recent common ancestor.

introgression within a temporal murine metacommunity over a long interval before complete isolation of daughter species (Presgraves and Yi, 2009) has important implications for interpreting age of lineage splitting and therefore the molecular clock. The timing of cladogenesis as perceived by paleontologists from preserved morphology may post-date significantly a protracted interval of gene exchange at the base of the split. We have been fortunate to be able to view the results of one cladogenic event in detail, the split of Tribes Murini and Arvicanthini. That process may unfold quickly or take hundreds of thousands of years for significant morphological change to accumulate. Judging from our case, morphological change following sporadic genetic divergence may be a significantly protracted process.

DATA AVAILABILITY STATEMENT

The original contributions presented in the study are included in the article/supplementary material, further inquiries can be directed to the corresponding author/s.

AUTHOR CONTRIBUTIONS

All authors contributed equally to this work and each agrees to be accountable for the content of the work. YK developed much of the original comparative data and developed the temporo-stratigraphic analyses. LJ integrated the morphological

and molecular patterns into a coherent whole, and organized specimen imaging. LF applied this special case for the fossil record to current molecular records and revised specimen identifications and locality dating.

FUNDING

JSPS KAKENHI Grant Number JP15H06884 (Grant-in-Aid for Young Scientists Start-up), JSPS KAKENHI Grant Number 18K13650, ISEM at SMU, and the American School of Prehistoric Research.

ACKNOWLEDGMENTS

Many collaborators in the field worked to build the fossil collections on which his study is based. Scientists from the Geological Survey of Pakistan and the Pakistan Museum of Natural History, and from various institutions in the United States, especially our small mammal colleague, Will Downs, made this study possible. Roy Beavers of Southern Methodist University skillfully produced SEM images. David Pilbeam, John Barry, and Michèle Morgan supplied both feedback and data, reviewers stimulated improvements, and we thank the editors and the series editors for their patience and encouragement.

REFERENCES

Aghová, T., Kimura, Y., Bryja, J., Dobigny, G., Granjon, L., and Kergoat, G. J. (2018). Fossils know it best: using a new set of fossil calibrations to improve the temporal phylogenetic framework of murid rodents (Rodentia: muridae). *Mol. Phylogenet. Evol.* 128, 98–111. doi: 10.1016/j.ympev.2018.07.017

Badgley, C., Barry, J. C., Morgan, M. E., Nelson, S. V., Behrensmeyer, A. K., Cerling, T. E., et al. (2008). Ecological changes in Miocene mammalian record show impact of prolonged climatic forcing. *Proc. Natl. Acad. Sci. U.S.A.* 105, 12145–12149. doi: 10.1073/pnas.0805592105

Barry, J. C., Behrensmeyer, A. K., Badgley, C. E., Flynn, L. J., Peltonen, H., Cheema, I. U., et al. (2013). "The neogene siwaliks of the potwar plateau, Pakistan," in *Fossil Mammals of Asia: Neogene Biostratigraphy and Chronology*, eds X. Wang, L. J. Flynn, and M. Fortelius (New York, NY: Columbia University Press), 373–398. doi: 10.7312/columbia/9780231150125.003.0015

Barry, J. C., Johnson, N. M., Raza, S. M., and Jacobs, L. L. (1985). Neogene mammalian faunal change in Southern Asia: correlations with climatic, tectonic, and eustatic events. *Geology* 13, 637–640. doi: 10.1130/0091-7613(1985)13<637:nmfcis>2.0.co;2

Barry, J. C., Morgan, M. E., Flynn, L. J., Pilbeam, D., Behrensmeyer, A. K., Raza, S. M., et al. (2002). Faunal and environmental change in the late Miocene Siwaliks of northern Pakistan. *Paleobiol. Memoir.* 28, 1-71.

Bell, M. A., and Lloyd, G. T. (2015). STRAP: an R package for plotting phylogenies against stratigraphy and assessing their stratigraphic congruence. *Palaeontology* 58, 379–389. doi: 10.1111/pala.12142

Blois, J. L., and Hadley, E. A. (2009). Mammalian response to Cenozoic climatic change. *Annu. Rev. Earth Planet. Sci.* 37, 181–208. doi: 10.1146/annurev.earth.031208.100055

Bryja, J., Sumbera, R., Peterhans, J. C. K., Aghová, T., Bryjova, A., Mikula, O., et al. (2017). Evolutionary history of the, thicket rats (genus *Grammomys*) mirrors the evolution of African forests since late Miocene. *J. Biogeogr.* 44, 182–194. doi: 10.1111/jbi.12890

Canty, A., and Ripley, B. D. (2020). *Boot: Bootstrap R (S-Plus) Functions. R Package Version 1.3-25*.

Casola, C. (2018). From de novo to "de Nono": the majority of novel protein coding genes identified with phylostratigraphy are old genes or recent duplicates. *Genome Biol. Evol.* 10, 2906–2918. doi: 10.1093/gbe/evy231

Cheema, I. U., Raza, S. M., Flynn, L. J., Rajpar, A. R., and Tomida, Y. (2000). Miocene small mammals from Jalalpur (District Jhelum) and their biochronologic implications. *Natl. Sci. Mus. Bull.* 26, 57–77. Tokyo,

da Costa, S. M., Rossi, M. I. D., Evangelista, A. A., and Oliveira, G. M. (2019). Origin, phylogeny and natural behavior of mice: what is their influence on welfare during their maintenance in the house facilities? *Amer. J. Biomed. Sci.* 5:AJBSR.MS.ID.000946. doi: 10.34297/AJBSR.2019.05.000946

Figueirido, B., Janis, C. M., Pérez-Claros, J. A., De Renzi, M., and Palmqvist, P. (2012). Cenozoic climate change influences mammalian evolutionary dynamics. *Proc. Natl. Acad. Sci. U.S.A.* 109, 722–727. doi: 10.1073/pnas.1110246108

Flynn, L. J., and Jacobs, L. L. (1982). Effects of changing environments on Siwalik rodent faunas of northern Pakistan. *Palaeogeogr. Palaeoclimatol. Palaeoecol.* 38, 129–139. doi: 10.1016/0031-0182(82)90067-0

Flynn, L. J., Kimura, Y., and Jacobs, L. L. (2020). "The murine cradle," in *Biological Consequences of Plate Tectonics: New Perspectives on Post-Gondwanaland Break-Up*, eds G. V. R. Prasad, and R. Patnaik (Cham: Springer), 347–362.

Garcés, M., Krijgsmann, W., Paláez-Campomanes, P., Álvarez-Sierra, M. A., and Daams, R. (2003). *Hipparion* dispersal in Europe: magnetostratigraphic constraints from the Daroca area (Spain). *Coloq. Paleontol.* 1, 171–178.

García-Paredes, I., Álvarez-Sierra, M. A., van den Hoek Ostende, L. W., Hernández-Ballarin, V., Hordijk, K., López-Guerro, P., et al. (2016). The Aragonian and Vallesian high-resolution micromammal succession from the Calatayud-Montalbán Basin (Aragón, Spain). *C. R. Palevol* 15, 781–789. doi: 10.1016/j.crpv.2015.09.014

Gould, S. J. (1985). The paradox of the first tier: an agenda for paleobiology. *Paleoiology* 11, 2–12. doi: 10.1017/s0094837300011350

Jacobs, L. L. (1977). A new genus of murid rodent from the Miocene of Pakistan and comments on the origin of the Muridae. *Paleobios* 25, 1–11.

Jacobs, L. L. (1978). Fossil rodents (Rhizomyidae and Muridae) from Neogene Siwalik deposits, Pakistan. *Mus. North. Arizona Press Bull.* 52, 1–103.

Jacobs, L. L., and Downs, W. R. (1994). "The evolution of murine rodents in Asia," in *Rodent and Lagomorph Families of Asian Origins and Diversification*, Vol. 8, eds Y. Tomida, C.-k. Li, and T. Setoguchi (Tokyo: National Science Museum Monograph), 149–156.

Jacobs, L. L., and Flynn, L. J. (2005). "Of mice again: the Siwalik rodent record, murine distribution, and molecular clocks," in *Interpreting the Past: Essays on Human, Primate, and Mammal Evolution in Honor of David Pilbeam*: American School of Prehistoric Research Monograph Series 5, eds D. E. Lieberman, R. J. Smith, and J. Kelley (Boston, MA: Brill Academic Publishers, Inc.), 63–80.

Jacobs, L. L., Flynn, L. J., and Downs, W. R. (1989). "Neogene rodents of southern Asia," in *Papers on Fossil Rodents in Honor of Albert Elmer Wood*, Vol. 33, eds C. C. Black, and M. R. Dawson (Los Angeles, CA: Natural History Museum of Los Angeles County), 157–177.

Jacobs, L. L., and Pilbeam, D. (1980). Of mice and men: fossil-based divergence dates and molecular "clocks". *J. Hum. Evol.* 9, 551–555. doi: 10.1016/0047-2484(80)90062-7

Johnson, N. M., Stix, J., Tauxe, L., Cerveney, P. F., and Tahirkheli, R. A. K. (1985). Paleomagnetic chronology, fluvial processes, and tectonic implications of the Siwalik deposits near Chinji Village, Pakistan. *J. Geol.* 93, 27–40. doi: 10.1086/628917

Juggins, S. (2020). *rioja: Analysis of Quaternary Science Data. R Package Version 0.9-26*. Available online at: https://cran.r-project.org/package=rioja (accessed December 15, 2020).

Keller, H. M., Tahirkheli, R. A. K., Mirza, M. A., Johnson, G. D., Johnson, N. M., and Opdyke, N. D. (1977). Magnetic polarity stratigraphy of the Upper Siwalik Deposits, Pabbi Hills, Pakistan. *Earth Planet. Sci. Lett.* 36, 187–201. doi: 10.1016/0012-821x(77)90198-4

Kimura, Y., Flynn, L. J., and Jacobs, L. L. (2016). A palaeontological case study for species delimitation in diverging fossil lineages. *Hist. Biol.* 28, 189–198. doi: 10.1080/08912963.2015.1022175

Kimura, Y., Flynn, L. J., and Jacobs, L. L. (2017). Early late Miocene murine rodents from the upper part of the Nagri Formation, Siwalik Group, Pakistan, with a new fossil calibration point for the Tribe Apodemurini (*Apodemus*/*Tokudaia*). *Fossil Imprint* 73, 197–212. doi: 10.2478/if-2017-0011

Kimura, Y., Hawkins, M. T. R., McDonough, M. M., Jacobs, L. L., and Flynn, L. J. (2015). Corrected placement of *Mus-Rattus* fossil calibration forces precision in the molecular tree of rodents. *Sci. Rep.* 5:14444. doi: 10.1038/srep14444

Kimura, Y., Jacobs, L. L., Cerling, T. E., Uno, K. T., Ferguson, K. M., Flynn, L. J., et al. (2013a). Fossil mice and rats show isotopic evidence of niche partitioning and change in dental ecomorphology related to dietary shift in late Miocene of Pakistan. *PLoS One* 8:e69308. doi: 10.1371/journal.pone.0069308

Kimura, Y., Jacobs, L. L., and Flynn, L. J. (2013b). Lineage-specific responses of tooth shape in murine rodents (Murinae, Rodentia) to late Miocene dietary change in the Siwaliks of Pakistan. *PLoS One* 8:e76070. doi: 10.1371/journal.pone.0076070

Kotlia, B. S. (2008). A new species of fossil *Mus* (Rodentia, Muridae) from the Indian Himalaya: evolutionary and phylogenetic implications. *Palaeoworld* 17, 47–56. doi: 10.1016/j.palwor.2007.08.004

Lecompte, E., Aplin, K., Denys, C., Catzeflis, F., Chades, M., and Chevret, P. (2008). Phylogeny and biogeography of African Muridae based on mitochondrial and nuclear gene sequences, with a new tribal classification of the subfamily. *BMC Evol. Biol.* 8:199. doi: 10.1186/1471-2148-8-199

López-Antoñanzas, R., Knoll, F., Wan, S., and Flynn, L. J. (2015). Causal evidence between monsoon and evolution of rhizomyine rodents. *Sci. Rep.* 5:9008. doi: 10.1038/srep09008

Ma, L., Cisse, O. H., and Kovacs, J. A. (2018). A molecular window into the biology and epidemiology of *Pneumocystis* spp. *Clin. Microbiol. Rev.* 31:e00009-18. doi: 10.1128/CMR.00009-18

Maddison, W. P., and Maddison, D. R. (2017). *Mesquite: A Modular System for Evolutionary Analysis. Version 3.04*. Available online at: http://mesquiteproject.org (accessed December 12, 2020).

Michaux, J. (1971). Muridae (Rodentia) neogenes d'Europe Sud-Occidentale: evolution et rapports avec les formes actuelles. *Paleobiol. Continentale* 2, 1–67.

Misonne, X. (1969). *African and Indo-Australian Muridae Evolutionary Trends*: Annales. Sciences Zoologique 8. Tervuren: Musée Royal de l'Afrique Centrale, 1–219.

Musser, G. G. (1987). The occurrence of *Hadromys* (Rodentia: muridae) in early Pleistocene Siwalik strata in northern Pakistan and its bearing on biogeographic affinities between Indian and northeastern African murine faunas. *Am. Mus. Novitates* 2883, 1–36.

Pages, M., Chaval, Y., Herbreteau, V., Waengsothorn, S., Cosson, J.-F., Hugot, J.-P., et al. (2010). Revisiting the taxonomy of the Rattini tribe: a phylogeny-based delimitation of species boundaries. *BMC Evol. Biol.* 10:184. doi: 10.1186/1471-2148-10-184

Parham, J. F., Donoghue, P. C., Bell, C. J., Calway, T. D., Head, J. J., Holroyd, P. A., et al. (2012). Best practices for justifying fossil calibrations. *Syst. Biol.* 61, 346–359.

Patnaik, R. (2014). Phylogeny of Siwalik murine rodents: implications for *Mus-Rattus* divergence time. *J. Palaeontol. Soc. India* 59, 15–28.

Patnaik, R. (2020). "New data on the Siwalik murines, rhizomyines and ctenodactylines (Rodentia) from the Indian subcontinent," in *Biological Consequences of Plate Tectonics: New Perspectives on Post-Gondwanaland Break-Up*, eds G. V. R. Prasad, and R. Patnaik (Cham: Springer), 363–391. doi: 10.1007/978-3-030-49753-8_16

Patnaik, R., Bahadur, M., Sharma, T., and Sahni, A. (1993). A comparative analysis of the molars of *Mus booduga*, *Mus dunni* and fossil *Mus* of the Indian subcontinent: phylogenetic and palaeobiogeographic implications. *Curr. Sci.* 65, 782–786.

Patnaik, R., Kotla, S. S., Singh, N. P., Singla, A., and Kaur, J. (2018). A new murid rodent assemblage from the Upper Siwaliks, Himachal Pradesh, India: biostratigraphic, phylogenetic and paleobiogeographic implications. *J. Asian Earth Sci.* 162, 93–106. doi: 10.1016/j.jseaes.2017.05.030

Presgraves, D. C., and Yi, S. V. (2009). Doubts about complex speciation between humans and chimpanzees. *Trends Ecol. Evol.* 24, 533–540. doi: 10.1016/j.tree.2009.04.007

R Core Team (2020). *R: A Language and Environment for Statistical Computing*. Vienna: R. Foundation for Statistical Computing.

Reznick, D. N., and Ricklefs, R. E. (2009). Darwin's bridge between microevolution and macroevolution. *Nature* 457, 837–842. doi: 10.1038/nature07894

Rowe, K. C., Achmadi, A. S., and Esselstyn, J. A. (2016). Repeated evolution of carnivory among Indo-Australian rodents. *Evolution* 70, 653–665. doi: 10.1111/evo.12871

Rowe, K. C., Achmadi, A. S., Fabre, P.-H., Schenk, J. J., Steppen, S. J., and Esselstyn, J. A. (2019). Oceanic islands of Wallacea as a source for dispersal and diversification of murine rodents. *J. Biogeogr.* 46, 2752–2768. doi: 10.1111/jbi.13720

Rowe, K. C., Aplin, K. P., Baverstock, P. R., and Moritz, C. (2011). Recent and rapid speciation with limited morphological disparity in the genus Rattus. *Syst. Biol.* 60, 188–203. doi: 10.1093/sysbio/syq092

Schaub, S. (1938). Tertiäre und quartäre Murinae. *Abh. Schweiz. Palaeontologischen Ges.* 61, 1–37.

Steppan, S. J., and Schenk, J. J. (2017). Muroid rodent phylogenetics: 900-species tree reveals increasing diversification rates. *PLoS One* 12:e0183070. doi: 10.1371/journal.pone.0183070

Suzuki, H. (2020). "Evolutionary history of the subgenus *Mus* in Eurasia with special emphasis on the house mouse *Mus musculus*," in *Papers in Honour of Ken Aplin. Records Australian Mus*, Vol. 72, eds J. Louys, S. O'Connor, and K. M. Helgen (Darlinghurst NSW: Australian Museum) 317–323. doi: 10.3853/j.2201-4349.72.2020.1727.

Tauxe, L., and Opdyke, N. D. (1982). A time framework based on magnetostratigraphy for the Siwalik sediments of the Khaur area, northern Pakistan. *Palaeogeogr. Palaeoclimatol. Palaeoecol.* 37, 43–61. doi: 10.1016/0031-0182(82)90057-8

Tedford, R. H., Qiu, Z.-x, and Flynn, L. J. (2013). "Late Cenozoic Yushe Basin, Shanxi Province, China: geology and fossil mammals," in *History, Geology, and Magnetostratigraphy*, Vol. I (Dordrecht: Springer).

Van Dam, J. A., Krijgsmann, W., Abels, H., Álvarez-Sierra, M. A., García-Paredes, I., López-Guerro, P., et al. (2014). Updated chronology for the middle to late Miocene mammal sites of the Daroca area (Calatayud-Mont Albán Basin, Spain). *Géobios* 47, 325–334. doi: 10.1016/j.geobios.2014.07.002

Conflict of Interest: The authors declare that the research was conducted in the absence of any commercial or financial relationships that could be construed as a potential conflict of interest.

frontiers in Ecology and Evolution

ORIGINAL RESEARCH
published: 06 April 2021
doi: 10.3389/fevo.2021.636039

Mechanics of Arboreal Locomotion in Swinhoe's Striped Squirrels: A Potential Model for Early Euarchontoglires

*Jan Wölfer[1], Tina Aschenbach[1], Jenny Michel[1,2] and John A. Nyakatura[1]**

[1] AG Vergleichende Zoologie, Institut für Biologie, Humboldt-Universität zu Berlin, Berlin, Germany, [2] Abteilung Zoologie, Staatliches Museum für Naturkunde Stuttgart, Stuttgart, Germany

Differences between arboreal and terrestrial supports likely pose less contrasting functional demands on the locomotor system at a small body size. For arboreal mammals of small body size, asymmetrical gaits have been demonstrated to be advantageous to increase dynamic stability. Many of the extant arboreal squirrel-related rodents display a small body size, claws on all digits, and limited prehensility, a combination that was proposed to have characterized the earliest Euarchontoglires. Thus, motion analysis of such a modern analog could shed light onto the early locomotor evolution of eurarchontoglirans. In this study, we investigated how Swinhoe's striped squirrels (*Tamiops swinhoei*; Scuiromorpha) adjust their locomotion when faced with different orientations on broad supports and simulated small branches. We simultaneously recorded high-Hz videos (501 trials) and support reaction forces (451 trials) of squirrels running on two types of instrumented trackways installed at either a 45° incline (we recorded locomotion on inclines and declines) or with a horizontal orientation. The striped squirrels almost exclusively used asymmetrical gaits with a preference for full bounds. Locomotion on simulated branches did not differ substantially from locomotion on the flat trackway. We interpreted several of the quantified adjustments on declines and inclines (in comparison to horizontal supports) as mechanisms to increase stability (e.g., by minimizing toppling moments) and as adjustments to the differential loading of fore- and hind limbs on inclined supports. Our data, in addition to published comparative data and similarities to the locomotion of other small arboreal rodents, tree shrews, and primates as well as a likely small body size at the crown-group node of Euarchontoglires, render a preference for asymmetrical gaits in early members of the clade plausible. This contributes to our understanding of the ancestral lifestyle of this mammalian 'superclade'.

Keywords: *Tamiops*, locomotion, support reaction forces, gait, asymmetrical locomotion

OPEN ACCESS

Edited by:
Irina Ruf,
Senckenberg Research Institute and Natural History Museum Frankfurt, Germany

Reviewed by:
Michael Granatosky,
New York Institute of Technology, United States
Andrew R. Lammers,
Cleveland State University, United States

****Correspondence:***
John A. Nyakatura
john.nyakatura@hu-berlin.de

Specialty section:
This article was submitted to Behavioral and Evolutionary Ecology, a section of the journal Frontiers in Ecology and Evolution

Received: *30 November 2020*
Accepted: *25 February 2021*
Published: *06 April 2021*

Citation:
Wölfer J, Aschenbach T, Michel J and Nyakatura JA (2021) Mechanics of Arboreal Locomotion in Swinhoe's Striped Squirrels: A Potential Model for Early Euarchontoglires. Front. Ecol. Evol. 9:636039. doi: 10.3389/fevo.2021.636039

INTRODUCTION

Evidence from the fossil record suggests stem placentals (i.e., eutherian mammals) to have been small scansorial animals. For example, *Juramaia sinensis* from the Jurassic of China (ca. 160 million years ago, mya) was a small, approx. mouse-sized animal which featured wrist bones that are similar to those of modern arboreal mammals (Luo et al., 2011). *Eomaia scansoria* (ca. 125 mya)

from China was characterized by very similar body proportions and overall small size (Ji et al., 2002). Within placentals, the 'superclades' or 'grandorders' Laurasiatheria and Euarchontoglires form well-accepted monophyletic sister taxa (Murphy et al., 2001; Asher et al., 2009; Zhou et al., 2015). Euarchontoglires include the Lagomorpha (rabbits and pikas) and Rodentia (rodents), which together constitute the Glires (Simpson, 1945; Novacek, 1992; Murphy et al., 2001; Meredith et al., 2011). Also part of the Euarchontoglires are the taxa that together form the Euarchonta (Adkins and Honeycutt, 1991; Springer et al., 2004; Bininda-Emonds et al., 2007). The Euarchonta include the Dermoptera (colugos), the Scandentia (treeshrews), and the Primates (monkeys, apes and humans). Similarly to stem placentals, body size of early euarchontans (e.g., plesiadapiforms) was likely small, too (Silcox and López-Torres, 2017). A consensus regarding the phylogenetic affinities of the taxa forming the Euarchontoglires has not been reached despite considerable effort over recent years (reviewed in Nyakatura, 2019).

To help conceptualize the evolution of the Euarchontoglires (and specifically early primates), Sargis et al. (2007) proposed a small, clawed, and non-grasping mammal to represent the Euarchontoglires node. For the Euarchonta node, a clawed arboreal mammal with pedal grasping was suggested (Sargis et al., 2007). It can thus be expected that these small scansorial animals were not dissimilar to even earlier stem eutherians such as *J. sinensis* or *E. scansoria*. Since functional demands acting on the locomotor-system of small scansorial mammals and small arboreal mammals have been proposed to be highly similar (Jenkins, 1974), we here hypothesize that a small (∼100 g), clawed, scansorial or arboreal mammal could be regarded as a modern analog to early Euarchontoglires (or even stem placentals). Motion analysis to assess kinematic and dynamic adjustments could help to gain an improved understanding of the functional demands acting on the locomotor system of such an animal when confronted with simulated arboreal supports.

Small representatives of the squirrel-related clade (Sciuromorpha) combine many of the characteristics that Sargis et al. (2007) proposed for the Euarchontoglires and Euarchonta nodes. Sciuromorpha is the sister clade to all other rodents (Fabre et al., 2012) and it is likely that its most recent common ancestor was characterized by an arboreal lifestyle (Wölfer et al., 2019). Swinhoe's striped squirrels (*Tamiops swinhoei*) live in forests consisting of evergreen broadleaf trees or conifers that spread from central China to northern Vietnam/Laos (Smith and Xie, 2013). They are characterized by an arboreal lifestyle including feeding on young shoots, fruits, and insects, and long jumps between trees, but are also found on the ground (Smith and Xie, 2013). Swinhoe's striped squirrels are of relatively small size, with non-grasping (i.e., non-divergent) hallux and pollex, and with a crown-rump length of ca. 10 cm and a total mass of approx. 100 g. *T. swinhoei* also has claws on all digits. Moreover, striped squirrels almost entirely employ asymmetrical gaits, i.e., the species relies on full bounds, half-bounds, and gallops (Mielke et al., 2018).

Chadwell and Young (2015) proposed the existence of an evolutionary trade-off between the benefits and drawbacks of asymmetrical gaits which is related to body mass and support diameter. Asymmetrical gaits offer the advantages of generally higher locomotor speeds, the possibility to bridge gaps in the discontinuous arboreal habitat during the aerial phases of leaps, and the possibility to 'grasp' a thin support (e.g., a terminal branch) between the left and right appendage of each girdle without the necessity of grasping autopodia with opposable fingers or toes (cf. Lammers and Zurcher, 2011). However, high speeds and substantial aerial phases will incur large support reaction forces and could result in breaking thin arboreal supports (terminal branches) or in oscillations that complicate locomotor control. Thus, the authors proposed that arboreal species using asymmetrical locomotion in the terminal branch habitat should be restricted to small body size (Chadwell and Young, 2015).

We here employ motion analysis (kinematics and dynamics) on simulated arboreal supports of Swinhoe's striped squirrels (*Tamiops swinhoei*, Sciuromorpha, Rodentia), a viable modern analog for the Euarchonta and Euarchontoglires nodes, to inform the reconstruction of functional demands that might have acted on early representatives of this mammalian 'superclade'. Specifically, we tested whether the following expectations regarding the adjustments of spatio-temporal and dynamic parameters of locomotion, when confronted with simulated arboreal supports (narrow and/or inclined) were met (**Table 1**).

1. When comparing locomotion on thin simulated branches with locomotion on flat supports, we expected running speed, jumping distance, jumping height (normal to the support), and peak support reaction force (SRF) in the normal and fore-aft direction to be reduced and duty factor (DF) to be increased for both, fore- and hind limbs. This would facilitate better control over the oscillations of the center of mass as previously proposed based on analyses of larger arboreal species (different primates and Eastern gray squirrels Schmitt, 1999; Dunham et al., 2019). These previously observed adjustments are usually interpreted to increase aspects of static stability. Since it has been pointed out that the difference between terrestrial and arboreal supports is less consequential for smaller animals (Jenkins, 1974), we expected to find less emphasized differences between the flat trackway and the simulated branch in the small species we analyzed.
2. When comparing downhill and uphill to horizontal locomotion on both, simulated branches and flat trackways, we expected the avoidance of whole-body suspensions, increases in limb contact duration, and increases in the time interval between the landing of trailing and leading limbs as observed for the asymmetrical locomotion of mouse lemurs on similarly challenging supports (Shapiro et al., 2016). Again, similar trends have also been documented in the spatio-temporal parameters of Eastern gray squirrels and were proposed to promote stability (Dunham et al., 2019).
3. We further expected that the striped squirrels of our study would grasp further around the simulated branch with their feet than with their hands when running

TABLE 1 | Investigated variables and associated expectations.

Variables	Expectation when comparing		
	Pole to trackway	Decline to horizontal	Incline to horizontal
Used as a dependent variable in a regression model			
Speed [ms^{-1}]	–	–	–
Mean duty factor of the forelimbs [%]	+	+	+
Mean duty factor of the hind limbs [%]	+	+	+
Mean duty factor ratio (forelimbs/hind limbs)		+	–
Jumping distance [cm]	–	–	–
Jumping height [cm]	–	–	–
Distance between hands [mm]			+
Distance between feet [mm]		+	
Distance ratio (hands/feet)		+	–
Position of MCPJ III [%]			–
Position of MTPJ III [%]		–	
Position ratio (MCPJ III/MTPJ III)		+	–
Used for qualitative analysis			
Peak normal support reaction force [BW units]	–	Forelimbs + Hind limbs –	Forelimbs – Hind limbs +
Peak fore-aft support reaction force [BW units]	–	Forelimbs + Hind limbs –	Forelimbs – Hind limbs +

MCPJ: Metacarpophalangeal joint.
MTPJ: Metatarsophalangeal joint.
+: increase.
–: decrease.

down a decline to allow a secure grip of the support between both feet and to avoid toppling forwards. We expected the opposite kinematic adjustment during incline locomotion to avoid toppling backwards as shown for considerably larger European red squirrels by Schmidt and Fischer (2011). These expectations are based on Siberian chipmunks (*Tamias sibiricus*) on a horizontal pole, which used the autopodia of both limbs of a girdle to grasp a simulated branch on opposite sides (Lammers and Zurcher, 2011). By this, the subjects controlled rolling torques of the body's center of mass (CoM) to stay within a range even though net-rolling torque was usually non-zero over just one stride (Lammers and Zurcher, 2011). Grasping further around the pole can thus be expected to emphasize this control strategy on more demanding supports. On a declined flat trackway, we expected the squirrels to abduct their hind limbs more than their forelimbs based on a similar consideration. This 'leaning backward' adjustment would shift the center of mass posteriorly and toward the support, and would reduce the chance of toppling over forwards. Accordingly, we expected the squirrels to abduct their forelimbs more than their hindlimbs during inclined locomotion on the flat trackway. This 'leaning forward' adjustment would shift the CoM forwards and closer to the support, and would reduce the chance of toppling over backwards.

4. Regarding SRFs, we expected that the peak normal components of the SRF are slightly larger in the forelimbs than in the hind limbs during steady speed on a horizontal support as is usual in non-primate quadrupedal mammals, in contrast to the opposite pattern regularly observed in primates (cf. Schmidt, 2005; Lammers and Gauntner, 2008; Hesse et al., 2015). Further, we expected generally smaller peak normal and fore-aft SRF components to occur on the narrow, simulated branch when compared to the flat trackway to minimize dangerous impacts on potentially flexible and easily breaking narrow terminal branches (Schmitt, 1999). When confronted with declines, we expected to observe a shift toward larger peak normal SRFs and a larger peak braking force during forelimb support to facilitate deceleration as has been observed in symmetrical gaits of tamarins on declined simulated branches (Hesse et al., 2015) and in asymmetrical gaits of short-tailed opossums on a declined flat trackway (Lammers et al., 2006). We expected larger peak normal SRFs and a larger peak accelerating force during hind limb support when running up an incline to facilitate acceleration against gravity.

MATERIALS AND METHODS

Animals

Four adult male individuals of *Tamiops swinhoei*, aged between 2 and 4 years, were filmed. They were born in captivity and kept in a cage (300 cm × 200 cm × 120 cm) with numerous hiding places and branches imitating an arboreal habitat. The animals were provided with food and water *ad libitum*. It was ensured that each animal was well rested before each recording session. Recording occurred 3 days a week at maximum with at least 1 day of rest in between from November 2017 until March 2018. The weights of the animals were documented before each session. The four individuals with the IDs a1-a4 had an average body mass ± standard deviation of 98.6 ± 2.4 g, 107 ± 4 g, 101 ± 4.7 g, and 106 ± 2.5 g, respectively. Two hours of filming in the morning were followed by 2 h in the afternoon after at least a 1-h break, in which the animals were kept in their transport cages. All procedures involving live animals were approved by the Humboldt-Universität zu Berlin and in correspondence with the regulations of animal welfare in Berlin, Germany, and approved by the relevant authority (LAGeSo reg. no.: 0098/16).

Experimental Setup

We recorded the locomotion on two different setups, which were additionally installed at different slopes (**Figure 1**). The first support was a trackway of approximately 2 m which was covered with a thin layer of cork to facilitate enough friction during fast locomotion. We assumed the cork to be thin enough to not dampen the impact during the support phase. A force plate was implemented into the center of the trackway with a small gap around it in order to minimize the transfer of oscillations. The

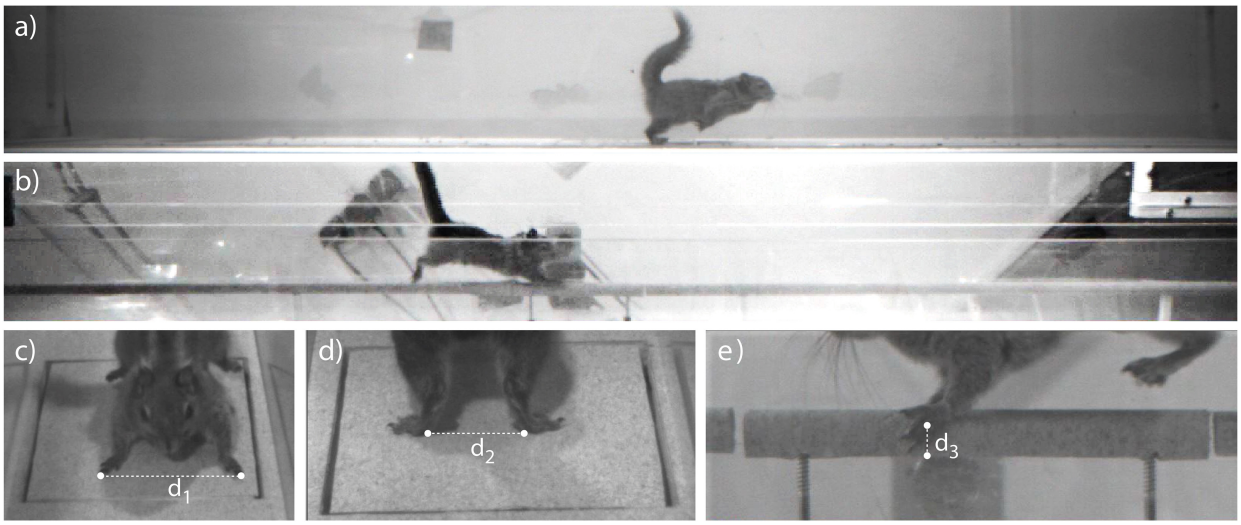

FIGURE 1 | Camera views used for kinematic analysis of the experimental setups. Overview on **(A)** the flat trackway (here oriented horizontally) and **(B)** on the branch-like pole (here inclined by 45°, the squirrel is heading downwards). **(C,D)** Close-up views on the trackway to measure the distance (d1) between the claws of the phalanges III of the hands and the distance (d2) between the metatarsophalangeal joints III, respectively. **(E)** Close-up view on the pole to measure the distance (d3) between the metacarpo- and metatarsophalangeal joint III, respectively, and the lower margin of the pole.

second support covered with the same type of cork was a raised dowel to simulate a branch (diameter = 13.3 mm). It had a similar length of approximately 2 m and was mounted on the trackway. The central part of this pole with a length of 14.6 cm was mounted separately on the force plate underneath leaving a small gap to the adjoining dowels, thus also minimizing the transfer of oscillations. The trackway was covered by an acrylic glass enclosure high enough to not restrain the maximum jumping height of the animals [we previously studied the influence of the enclosure size on locomotor parameters (Mielke et al., 2018)].

Both supports were then either fixed on a table or inclined to form a slope of 45°. The subjects were filmed using three high speed CamPhF 2000 cameras (Photonfocus AG, Lachen, Switzerland). Recording was accomplished using the software Contemplas Templo (Contemplas GmbH, Kempten, Germany). One camera was positioned at the side of the setup in a right angle for an overview of the entire trackway. It recorded with a framerate of initially 200 and later 300 frames per second (fps), which was finally increased to 350 fps (used for the vast majority of the trials). This camera was used to analyze running speed, jumping distance, jumping height, and DF.

For the flat trackway set up, the other two cameras were positioned to facilitate a close-up view on the force plate. They were used to measure limb abduction (**Figure 1**). Regarding the pole setup, the other two cameras were placed closer on both sides of the central pole to measure the positioning of the hand and feet during touchdown. These two cameras always recorded with a framerate of 600 fps. They were additionally used to determine if the animals put all four limbs 'cleanly' on the force plate (or the pole mounted on top of it) or if they stepped over a margin, resulting in incomplete force measurements. This facilitated a selection of appropriate trials for the analysis of SRFs. For the experiments, two individuals were placed inside the setup at a time as we noticed that subjects were more motivated to move around when not alone, resulting in more recorded trials. However, only trials were used during which a single individual was contacting the force plate. Normal, fore-aft, and mediolateral (not used in this study) SRFs were recorded for all limbs combined using a single AMTI HE6X6-1 force plate (Advanced Mechanical Technology, Inc., Watertown, MA, United States) at a rate of 1800 Hz (**Figure 1**). A completely separate recording of single limb forces was not possible as ipsilateral fore- and hind limbs overlapped in their stem phases and were additionally placed closely adjacent to each other. Camera- and force plate recordings allowed for a visual matching of touchdown/lift-off events and SRF changes since both devices were not perfectly synchronized electronically.

Data Preparation

We aimed at only including trials approximating a steady running speed. Swinhoe's striped squirrels are non-cursorial animals characterized by fast acceleration and deceleration within a few stride cycles (Mielke et al., 2018). We only analyzed the two cycles ending and beginning with contacting the force plate, respectively. A stride cycle was defined as starting with a touchdown of the first forelimb and ending with the last frame before the subsequent touchdown of the first forelimb. The videos from the overview camera were imported, calibrated, and the kinematics were analyzed in Vicon Motus 3D (Contemplas GmbH, Kempten, Germany). The tip of the nose of the respective subject was digitized with a landmark in each frame of interest. To obtain a measure of running speed, the x-coordinate of each landmark was subtracted from the x-coordinate of the landmark of the previous frame and then multiplied by the frame rate to obtain the speed (the

x-axis was defined as being parallel to the support). The speed values of a stride cycle were then averaged, labeled just speed in the following. According to our criterion, all trials with a speed difference of more than 25% between the two analyzed stride cycles were discarded, with 501 trials remaining for analysis (**Supplementary Table 1**). In case a sequence adhered to our steady speed criterion, the landmarks of the second cycle (starting with the first forelimb touchdown on the force plate) were used for analysis. The absolute difference between the x-coordinates of the last and first landmarks placed during the second stride cycle was used as the jumping distance. Jumping height was obtained by selecting the landmark with the largest y-coordinate value. Note that in the inclined setup, the camera was also tilted by 45° to the side. Thus, this variable refers to the maximum distance of the tip of the animal's nose from the support and not to the height in line with gravitational acceleration.

Frames associated with the touchdowns (including the ones of the consecutive cycle) and lift-offs of all limbs were recorded for the computation of DFs and lead duration. The DFs of the limbs of a girdle were averaged to obtain the mean DFs of the fore- and hind limbs (DF-FL and DF-HL, respectively). The ratio between DF-FL and DF-HL was also computed (DF-R). The leads of the fore- and hind limbs were computed to evaluate the gait type.

The close-up camera videos were imported to ImageJ2 (Rueden et al., 2017). Regarding the trackway, the force plate's width was used for calibration to measure limb abduction. Forelimb abduction was quantified by measuring the distance between the claws of left and right phalanx III and hind limb abduction was measured as the distance between the centers of the metatarsophalangeal joints (as the phalanges were not visible; **Figure 1**). The ratio between the former and the latter was computed, but the raw measures were also analyzed to determine the contribution of forelimb and hind limb adjustments to changes in the ratio. On the pole, the distance between the metacarpophalangeal or metatarsophalangeal joints III (MCPJ III or MTPJ III) and the lower margin of the pole was measured to quantify hand and foot positioning, respectively (**Figure 1**). Only the camera on one side was used to obtain these data. The distance was normalized by the diameter of the pole. Values above 100% were possible when the hand/foot was placed close to the top or on top of the pole. A ratio between MCPJ III and MTPJ III positioning was computed. Hence, we also analyzed the ratio as well as the two distances themselves.

The SRF data were directly exported from Templo. The normal force (normal to the support), as well as accelerating and decelerating forces (fore-aft forces, in line with the running direction) were analyzed, as well as their relative timings within the duration from the first forelimb touchdown to the last hind limb lift-off. 451 of 501 trials contained appropriate force data, which were trimmed to match this duration. Forces were then smoothed using a simple moving average filter including three consecutive time points and standardized by the body weight of the animal. The support phase duration (from forelimb touchdown to hind limb lift-off) was standardized to 100%. SRFs of all limbs combined were evaluated just graphically in terms of their trajectory. We did not calculate peak forces or impulses and thus, we did not include inferential statistics, as fore- and hind limbs generally overlapped in their contacts with the force plate (see above).

Statistical Analysis

All statistical analyses were conducted with the software R (R Core Team, 2020). The following additional packages were used for data preparation, visualization, and analysis: readxl (Wickham and Bryan, 2019), tidyverse (Wickham et al., 2019), psych (Lenth, 2020), nlme (Pinheiro et al., 2020), and emmeans (Lenth, 2020).

The gaits were classified using forelimb and hind limb lead duration, respectively, in percent of the stride cycle duration of the left hindlimb. Cut-off lead percentages were defined according to Hildebrand (1977). Linear regression modeling was used to investigate the influence of support orientation, support type, and speed on the respective parameters. We followed the guidelines provided by Zuur et al. (2009) to obtain regression models with significant explanatory variables that also sufficiently fulfill the necessary modeling assumptions. The following procedure was applied to each dependent variable (**Table 1**).

Firstly, a simple linear regression including all fixed effects and possible interaction effects among them was conducted. Residual outliers were assessed via boxplots and removed if considered too extreme, i.e., they were distinctly separated from all other data points in the residual distribution.

Secondly, the animal ID was included as a random effect using the lme function. To avoid overfitting, differences among animals regarding the effects of support type, support orientation, and speed on the dependent variable were assessed graphically while disregarding interactions. The most complex combination of random effects that seemed meaningful was included. The random term was then simplified via backwards elimination, using likelihood ratio tests to compare the more complex model to the simpler model at each step. If the p-value was above 0.05, the simpler model was selected; otherwise the complex model was retained. If two different simpler models were both considered more appropriate than the more complex parent model, they were compared using the Akaike information criterion (AIC; Burnham and Anderson, 2002) and the model with the lower value was retained. In case the random effect did not significantly contribute to model likelihood, it was removed completely.

Thirdly, the homoscedasticity of the residuals was assessed graphically. Again, the most complex model adjustments that appeared to be necessary were included using the weights argument in the lme function (or the gls function in case a random effect was not retained). The model was simplified using backwards elimination as outlined above until the most parsimonious adjustment for heteroscedasticity was achieved.

Finally, the fixed effects and their interaction were removed via backwards elimination as outlined above, always removing interaction effects before the associated main effects. The final model was checked in regard of normality and homoscedasticity of within-subject residuals. If extreme outliers were present again, they were removed. All in all, outliers were removed for three dependent variables, with five outliers being the maximum.

Estimated marginal means of support orientations and support types were compared *post hoc* using the contrast function of the emmeans package and the Tukey method for adjusting p-values. In case interactions with speed were significant, *post hoc* tests for support type and support orientation were conducted at three speed values (low, moderate, and high, see Results). A significance level of 0.05 was chosen for all analyses. See **Supplementary Data Sheets 1, 2** for the R script and data, respectively, to reproduce all regression results.

Regression results are presented in the following way: (1) descriptive statistics of the dependent variables (see also **Supplementary Table 2**), (2) specifications of the final regression models (see also **Supplementary Table 3**), (3) comparisons between pole and trackway for all support orientations, (4) comparisons between downhill and horizontal locomotion on both support types, and (5) comparisons between uphill and horizontal locomotion on both support types. An overview of the regression results including the coefficient table, the variance function estimates, the estimated marginal means, and all pairwise *post hoc* comparisons is provided in **Supplementary Tables 4–15**.

RESULTS

Gait and Speed of Locomotion on Different Setups

Out of 501 stride cycles used for kinematic analysis, 500 showed asymmetrical gaits; One stride cycle was characterized by an asymmetrical forelimb pattern and a symmetrical hind limb pattern (hind limb lead > 40%; **Figure 2**). The asymmetrical gaits could be distinguished into full bound (456 times, common for all setups), half bound (31 times, observed during downhill locomotion irrespective of the support type), crutch walk (6 times) and gallop (7 times), both modes mostly being used during declined locomotion on the trackway.

The average speed across all observations was 1.7 ± 0.4 ms^{-1}. The minimum speed was 0.8 ms^{-1} and the maximum speed was 3.4 ms^{-1}. However, the latter value was an extreme value and speeds above 2.5 ms^{-1} were generally rare (**Figure 2**). The following three values were chosen for all other locomotion parameters (i.e., the dependent variables except for speed) to compare support types and support orientation levels *post hoc* in case of significant interactions with speed: 1.2 m/s – low, 1.8 m/s – medium, 2.4 m/s – high. This was considered a meaningful range with a doubling in speed from smallest to largest value. Furthermore, all three speed values lay within the range of four of the six combinations of support types and support orientations. A speed of 2.4 ms^{-1} was not observed during downhill locomotion on the trackway and the pole (**Figure 2**). Hence, comparisons involving downhill locomotion at this speed were not interpreted.

The final regression model included support type and support orientation and their interaction as fixed effects and animal specific effects of support orientation as a random effect. The variance function accounted for heterogeneity by including different variances for all combinations of support orientation and support type.

The speed was significantly lower on average on the pole compared to the trackway when running horizontally ($p < 0.001$; **Figure 2** and **Table 2**). Running down the decline, the opposite case was observed with a significantly higher speed being observed on the pole ($p < 0.001$). There was no significant difference between the two support types during uphill locomotion ($p = 0.783$). The speed was significantly lower on average on the trackway when the squirrels ran downhill compared to horizontally ($p < 0.001$), but this was not the case on the pole ($p = 0.138$). Comparing uphill to horizontal locomotion, the speed was significantly lower during uphill locomotion on both support types ($p \leq 0.002$).

Duty Factor on Different Setups

The DF-FL was 41.8 ± 10.5% on average, with a minimum of 18.8% and a maximum of 71.2%. The DF-HL was 42 ± 9.9% on average, with a minimum of 19.4% and a maximum of 70.2%. The DF-R was 1 ± 0.2 on average, with a minimum of 0.5 and a maximum of 1.9.

All three final models included support type and support orientation as fixed effects and speed as a covariate. The regression models with DF-FL and DF-HL as a dependent variable, respectively, included all possible interactions and different effects of speed and support orientation on the DF per animal as a random effect. The variance function for the model with DF-HL accounted for heterogeneity by including a dependence of the variance of the DF-HL on speed that differed between all combinations of support orientations and support types. The regression model with DF-R as a dependent variable included two two-way-interactions (support type x speed and support orientation x speed) and different effects of support orientation on the DF-R per animal as a random effect. The variance function accounted for heterogeneity by including a different variance of the DF-R for each support orientation.

The DF-FL as well as the DF-HL were significantly larger on the pole compared to the trackway at all three speeds when the squirrels ran horizontally (p-always < 0.001; **Figure 3** and **Table 3**). During downhill locomotion, the DF-FL was only significantly larger on the pole at a low speed ($p < 0.001$), but not at a medium speed ($p = 0.114$), whereas the DF-HL was never significantly different ($p \geq 0.290$). Regarding uphill locomotion, the DF-FL was significantly larger on the pole at medium and high speeds (p-always < 0.001), but not at a low speed ($p = 0.615$).

On the trackway, the DF-FL and the DF-HL were significantly increased during downhill compared to horizontal locomotion at both, low and medium speeds (p-always < 0.001). On the pole, no significant differences were observed for both between declined and horizontal locomotion at these speeds ($p \geq 0.527$). The DF-R was only significantly larger during downhill compared to horizontal locomotion at a low speed irrespective of support type ($p < 0.001$), but not at a medium speed ($p = 0.257$).

Comparing uphill to horizontal locomotion on the trackway, the DF-FL was significantly larger at a low speed ($p = 0.007$) but not at medium and high speeds ($p \geq 0.431$), whereas the

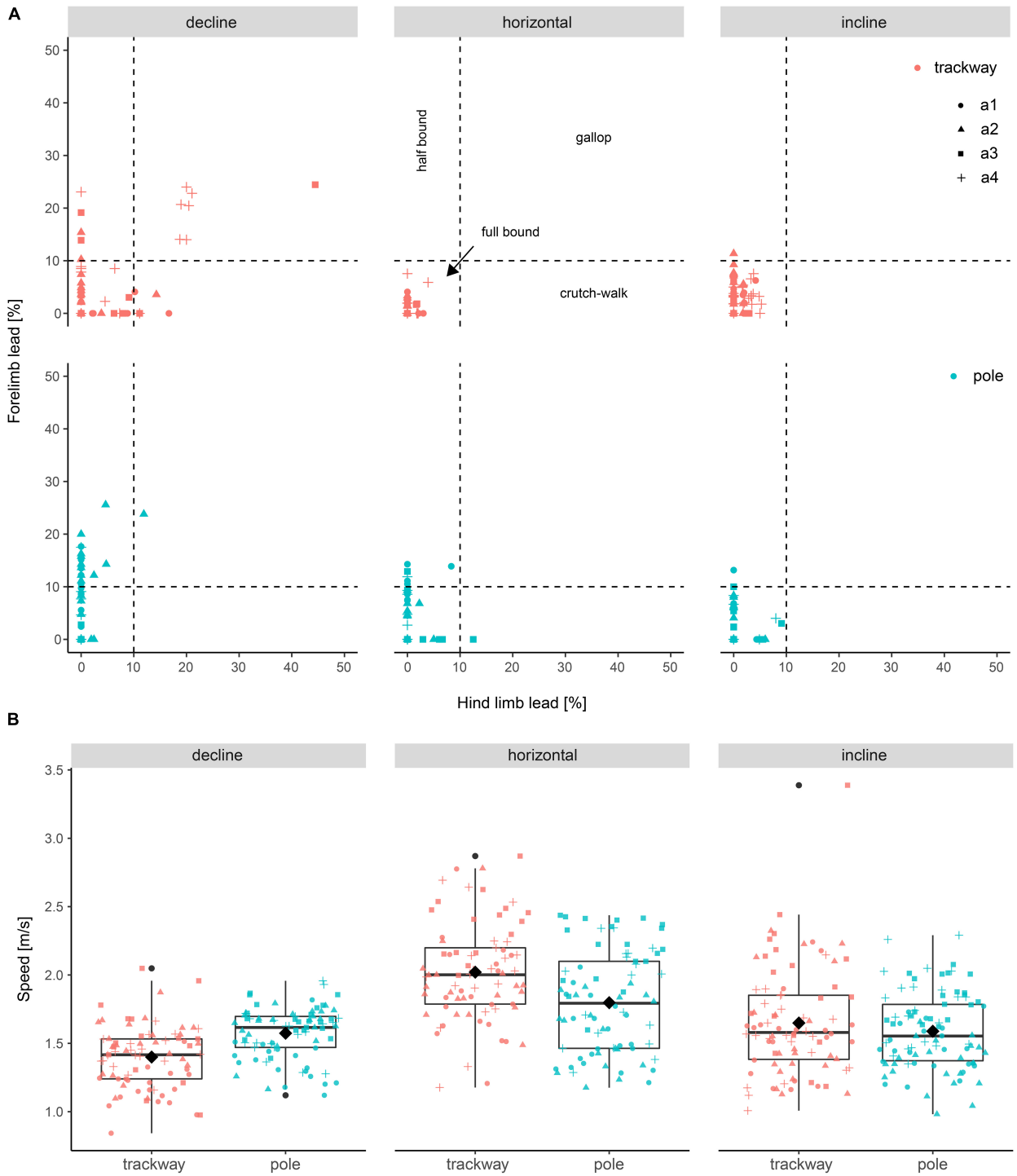

FIGURE 2 | Forelimb lead versus hind limb lead and speed differences among setups. **(A)** Lead used to quantify asymmetrical gaits. Cut-off values according to Hildebrandt (1977). Trials with a forelimb and hind limb lead < 10% are categorized as full bounds, trials with forelimb lead > 10% and hind limb lead < 10% are categorized as half bounds, trials with forelimb lead < 10% and hind limb lead > 10% are categorized as crutch walks, and trials with forelimb and hind limb lead > 10% are categorized as gallops. **(B)** Speed distributions shown as boxplots. a1–a4 refer to the studied individuals.

DF-HL was significantly larger at low and medium speeds (p-always < 0.001) but not at a high speed ($p = 0.731$). On the pole, the animals displayed a similar DF-FL pattern, with it being significantly larger at a low speed ($p = 0.034$) but not at medium and high speeds ($p \geq 0.122$). However, the DF-HL did not differ significantly between uphill and horizontal locomotion

TABLE 2 | *Post hoc* contrasts for the regression of speed.

Contrast	Support type	Support orientation	Estimate	SE	d.f.	Lower 95% CL	Upper 95% CL	*t*	*p*
Pole – trackway		Decline	0.17	0.03	491	0.09	0.24	6.29	**<0.001**
		Horizontal	−0.24	0.05	491	−0.37	−0.12	−5.19	**<0.001**
		Incline	−0.05	0.04	491	−0.16	0.07	−1.1	0.783
Horizontal – decline	Trackway		0.64	0.1	491	0.36	0.92	6.19	**<0.001**
	Pole		0.23	0.1	491	−0.04	0.5	2.29	0.138
Incline – horizontal	Trackway		−0.4	0.07	491	−0.58	−0.22	−6.11	**<0.001**
	Pole		−0.2	0.06	491	−0.35	−0.05	−3.69	**0.002**

SE: standard error.
d.f.: degrees of freedom.
CL: confidence limit.
t: t-value.
p: p-value (significant p-values in bold).

at all three speeds ($p \geq 0.994$). The DF-R was significantly smaller during uphill locomotion irrespective of the support type (p-always < 0.001).

Aerial Phases (Jumping) on Different Setups

The average jumping distance was 20.8 ± 7 cm, with a minimum of 10.8 cm and a maximum of 51.3 cm. The final model included support type, support orientation, speed and all possible interactions as fixed effects/covariate and different effects of support orientation and speed on jumping distance per animal as a random effect. The variance function accounted for heterogeneity by including a dependence of variance in jumping distance on speed that differed between support types.

The jumping distance was always significantly lower on average on the pole compared to the trackway ($p \leq 0.001$; **Figure 4** and **Table 4**). Comparing downhill to horizontal locomotion, the squirrels jumped a significantly shorter distance on average on the trackway ($p \leq 0.001$), but not on the pole ($p \geq 0.988$). When comparing uphill to horizontal locomotion at all three speeds, the squirrels jumped a significantly shorter distance on average only at a medium running speed while on the trackway ($p = 0.001$, else $p \geq 0.140$), whereas jumping distance was significantly shorter for both, low and medium speeds on the pole ($p \geq 0.002$, else 0.309).

The jumping height was 4.1 ± 1.1 cm on average, with a minimum of 2.3 cm and a maximum of 8.2 cm. The final model included support type and support orientation as well as their interaction as fixed effects and different effects of support orientation and speed on jumping height per animal as a random effect. The variance function accounted for heterogeneity by including a dependence of the variance of jumping height on speed that differed between all combinations of support orientations and support types.

The jumping height was significantly lower on average on the pole compared to the trackway for all three support orientations (p-always < 0.001). It was also significantly lower when comparing downhill to horizontal locomotion on both support types (p-always < 0.001). When running uphill, jumping height was significantly lower compared to the horizontal support orientation on the trackway ($p < 0.001$), but not on the pole ($p > 0.999$).

Autopodial Positioning on Different Setups

The distance between the hands was 44.4 ± 11.3 mm on average, with a minimum of 23.2 mm and a maximum of 75 mm. The distance between the feet was 49.2 ± 7.3 mm on average, with a minimum of 33.9 mm and a maximum of 70 mm. The ratio of hand to foot distance was 0.9 ± 0.3 on average, with a minimum of 0.4 and a maximum of 1.9.

All three final models included support orientation as a fixed effect. The models with forelimb distance and the ratio of forelimb to hind limb distance, respectively, additionally included speed as a covariate and its interaction with support orientation as a fixed effect. All three models accounted for different effects of support orientation on forelimb distance per animal as a random effect and included a variance function accounting for heterogeneity by including different variances for all support orientations.

There was no significant difference in the average distance between hands ($p \geq 0.567$ at low and medium speeds) or between feet ($p = 0.082$) when comparing declined to horizontal trackway, although the distance between feet appeared to be larger when running downhill (**Supplementary Image 1** and **Supplementary Tables 10, 11**). Contrary to our expectation, the ratio was not significantly smaller when comparing locomotion on the declined trackway to that on the horizontal trackway at low and medium speeds ($p \geq 0.053$), although a trend in this direction was observable at a low speed (**Figure 5** and **Table 5**). There was a significant difference in the average distance between hands (p-always < 0.001, larger distance on the incline) as well as between feet ($p < 0.001$, smaller distance on the incline) when comparing uphill to horizontal locomotion. As expected, the ratio was significantly larger on the incline at all three speeds (p-always < 0.001).

The relative position of the MCPJ III from the lower margin of the pole was 99.7 ± 19.2% on average, with a minimum of 32.7% and a maximum of 131.3%. The relative position of the MTPJ III on the pole was 95.3 ± 21.9% on average, with a minimum of 33.9% and a maximum of 138.3%. The ratio between hand and

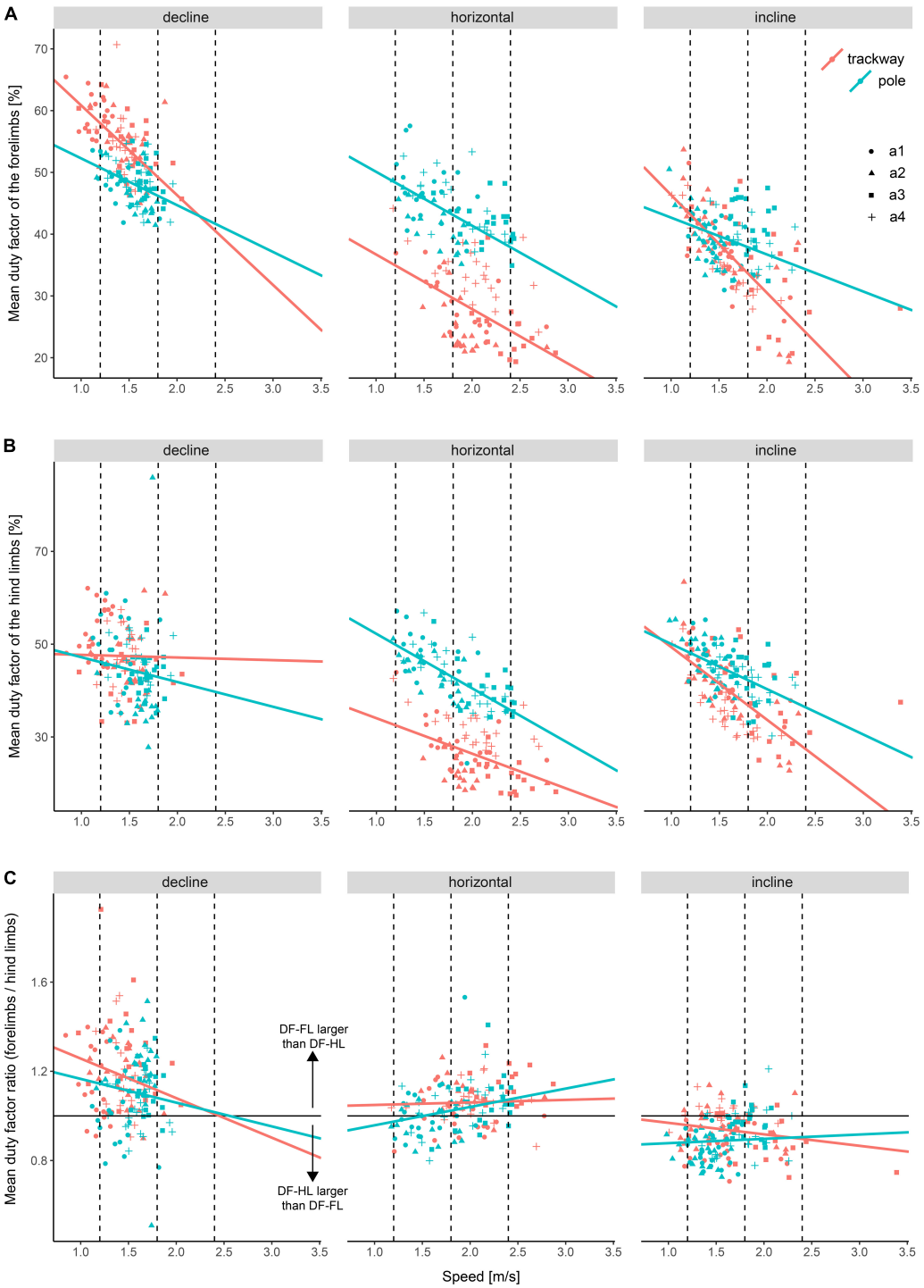

FIGURE 3 | Duty factor differences among experimental setups. **(A)** Mean duty factor of the forelimbs (DF-FL), **(B)** mean duty factor of the hind limbs (DF-HL), and **(C)** Ratio between the two mean duty factors. Dashed lines indicate the speed values at which setups were compared statistically *post hoc*. a1–a4 refer to the studied individuals.

foot positioning was 1.1 ± 0.4 on average, with a minimum of 0.3 and a maximum of 2.9.

The three final models included support orientation as a fixed effect. Except for the ratio regression model, speed was considered a significant covariate. The regression model for MCPJ III included different intercepts per animal as a random effect, whereas the other two regression models included a variance formula that accounted for

TABLE 3 | *Post hoc* contrasts for the regressions of duty factors and their ratio.

Contrast	Support type	Support orientation	Speed [ms^{-1}]	Estimate	SE	d.f.	Lower 95% CL	Upper 95% CL	*t*	*p*
Mean duty factor of the forelimbs [%]										
Pole - trackway		Decline	1.2	−7.19	1.09	482	−10.51	−3.88	−6.59	**<0.001**
			1.8	−3.02	1.11	482	−6.37	0.34	−2.73	0.114
			2.4	1.16	2.75	482	−7.17	9.5	0.42	> 0.999*
		Horizontal	1.2	13.41	1.37	482	9.25	17.56	9.79	**<0.001**
			1.8	13.48	0.68	482	11.4	15.55	19.72	**<0.001**
			2.4	13.55	1.07	482	10.3	16.8	12.64	**<0.001**
		Incline	1.2	−1.7	0.95	482	−4.57	1.17	−1.79	0.615
			1.8	4.24	0.69	482	2.15	6.34	6.14	**<0.001**
			2.4	10.18	1.62	482	5.28	15.08	6.3	**<0.001**
Horizontal - decline	Trackway		1.2	−23	1.99	482	−29.04	−16.97	−11.57	**<0.001**
			1.8	−19.58	1.82	482	−25.09	−14.07	−10.78	**<0.001**
			2.4	−16.16	2.58	482	−24	−8.32	−6.26	**<0.001***
	Pole		1.2	−2.4	1.99	482	−8.43	3.62	−1.21	0.925
			1.8	−3.09	1.68	482	−8.2	2.02	−1.83	0.588
			2.4	−3.77	2.60	482	−11.65	4.1	−1.45	0.824*
Incline - horizontal	Trackway		1.2	8.23	2.26	482	1.37	15.1	3.64	**0.007**
			1.8	4.01	1.94	482	−1.88	9.91	2.07	0.431
			2.4	−0.21	2.15	482	−6.74	6.31	−0.1	> 0.999
	Pole		1.2	−6.87	2.17	482	−13.47	−0.28	−3.16	**0.034**
			1.8	−5.22	1.94	482	−11.1	0.65	−2.7	0.122
			2.4	−3.58	2.47	482	−11.06	3.9	−1.45	0.826
Mean duty factor of the hind limbs [%]										
Pole - trackway		Decline	1.2	−1.47	1.45	485	−5.87	2.94	−1.01	0.971
			1.8	−4.33	1.88	485	−10.05	1.39	−2.3	0.290
			2.4	−7.2	4.28	485	−20.18	5.79	−1.68	0.691*
		Horizontal	1.2	17.36	1.50	485	12.82	21.9	11.6	**<0.001**
			1.8	14.89	0.77	485	12.56	17.23	19.35	**<0.001**
			2.4	12.43	1.27	485	8.57	16.28	9.78	**<0.001**
		Incline	1.2	1.88	1.21	485	−1.8	5.56	1.55	0.773
			1.8	5.44	0.96	485	2.53	8.35	5.68	**<0.001**
			2.4	9	2.23	485	2.23	15.77	4.03	**0.002**
Horizontal - decline	Trackway		1.2	−15.07	1.74	485	−20.35	−9.8	−8.66	**<0.001**
			1.8	−19.33	2.05	485	−25.54	−13.11	−9.43	**<0.001**
			2.4	−23.58	3.73	485	−34.9	−12.25	−6.32	**<0.001***
	Pole		1.2	3.76	1.95	485	−2.17	9.68	1.92	0.527
			1.8	−0.1	1.54	485	−4.77	4.57	−0.07	> 0.999
			2.4	−3.96	3.20	485	−13.65	5.74	−1.24	0.915*
Incline - horizontal	Trackway		1.2	13.69	2.36	485	6.52	20.86	5.8	**<0.001**
			1.8	8.87	2.05	485	2.65	15.1	4.33	**<0.001**
			2.4	4.06	2.51	485	−3.55	11.67	1.62	0.731
	Pole		1.2	−1.79	2.34	485	−8.89	5.31	−0.77	0.994
			1.8	−0.58	2.02	485	−6.71	5.55	−0.29	> 0.999
			2.4	0.63	2.76	485	−7.75	9.01	0.23	> 0.999
Mean duty factor ratio (forelimbs/hind limbs)										
Horizontal - decline			1.2	−0.17	0.04	485	−0.26	−0.08	−4.45	**<0.001**
			1.8	−0.06	0.04	485	−0.14	0.03	−1.58	0.257
			2.4	0.06	0.06	485	−0.09	0.21	0.88	0.653*
Incline - horizontal			1.2	−0.09	0.02	485	−0.14	−0.04	−4.45	**<0.001**
			1.8	−0.13	0.01	485	−0.16	−0.1	−8.92	**<0.001**
			2.4	−0.17	0.02	485	−0.22	−0.12	−7.46	**<0.001**

SE: standard error.
d.f.: degrees of freedom.
CL: confidence limit.
t: t-value.
p: p-value (significant p-values in bold).
**: comparison falls outside of data range.*

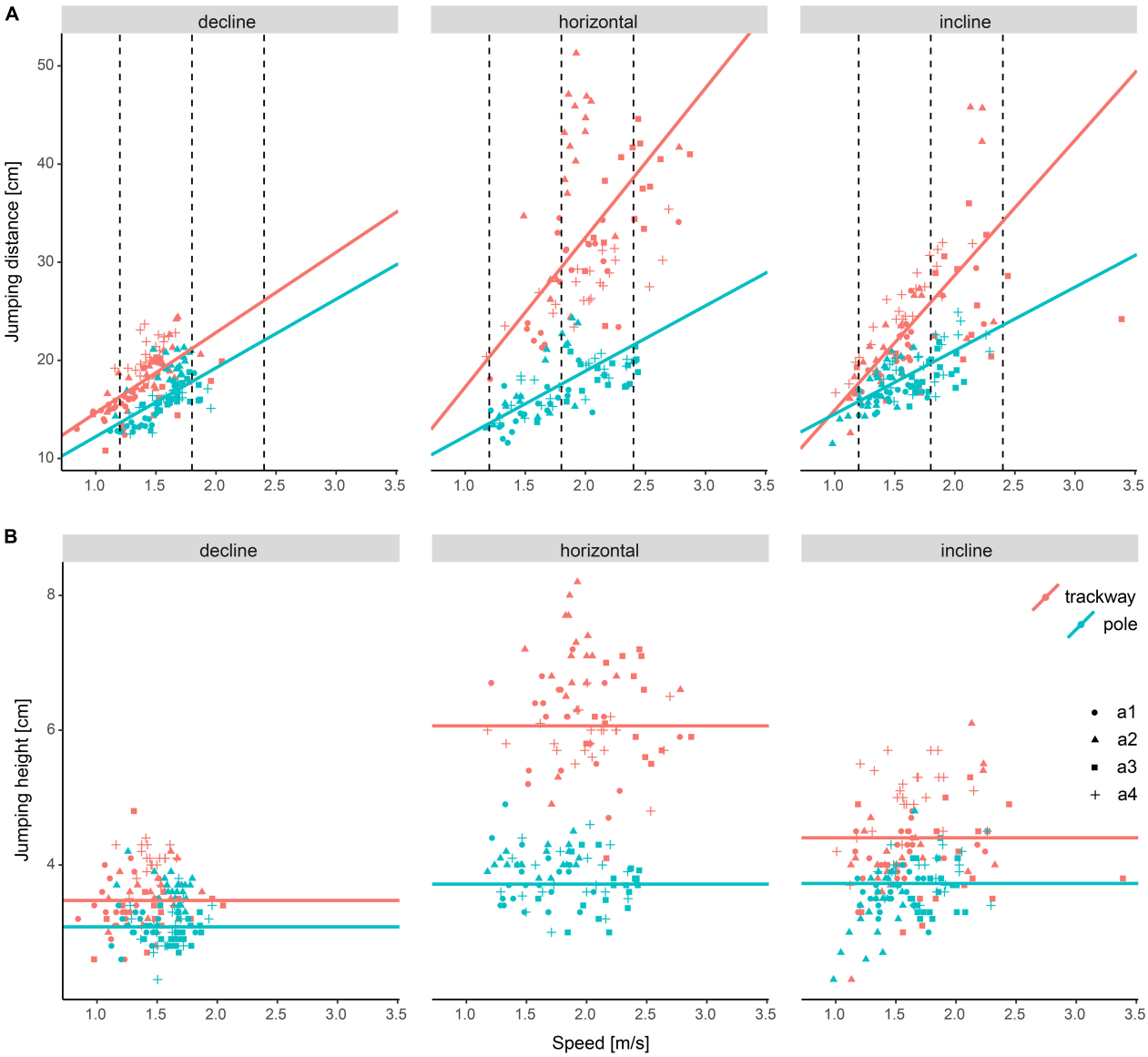

FIGURE 4 | Differences in jumping distance and jumping height among experimental setups. **(A)** Jumping distance and **(B)** Jumping height. Dashed lines indicate the speed values at which setups were compared statistically *post hoc* (not relevant for jumping height as speed had no significant effect and hence was removed from the final regression model). a1–a4 refer to the studied individuals.

heterogeneity by including a different variance for each support orientation.

There was no significant difference in the average hand positioning on the pole between running down a decline and horizontal locomotion ($p = 0.993$), but the foot was positioned significantly closer to the lower margin of the pole when running on a decline compared to horizontal locomotion ($p < 0.001$; **Supplementary Image 2** and **Supplementary Tables 13, 14**). The ratio was significantly larger when comparing downhill to horizontal locomotion ($p < 0.001$; **Figure 5** and **Table 5**), supporting the previous finding. Running on an incline, the hand was positioned significantly lower on average compared to horizontal locomotion ($p < 0.001$), whereas the foot was positioned significantly higher on average ($p = 0.02$), although the estimated difference was a lot smaller for the latter (∼6% compared to ∼18%). Using the ratio to compare foot to hand placement, the ratio was significantly smaller when comparing inclined to horizontal locomotion ($p < 0.001$), supporting these findings.

Support Reaction Forces on Different Setups

Overall, the average SRF patterns were very similar between pole and trackway. On both supports, the normal force on a horizontal support is characterized on average by two large peaks (**Figure 6**). Each is representing the support phase of a limb girdle of which the forelimbs exert a higher maximum force on average. When

TABLE 4 | *Post hoc* contrasts for the regressions of jumping distance/jumping height.

Contrast	Support type	Support orientation	Speed [ms^{-1}]	Estimate	SE	d.f.	Lower 95% CL	Upper 95% CL	*t*	*p*
Jumping distance [cm]										
Pole - trackway		Decline	1.2	−2.66	0.36	486	−3.76	−1.56	−7.35	**<0.001**
			1.8	−3.37	0.58	486	−5.12	−1.61	−5.82	**<0.001**
			2.4	−4.07	1.23	486	−7.81	−0.33	−3.30	**0.022***
		Horizontal	1.2	−6.75	0.98	486	−9.72	−3.78	−6.90	**<0.001**
			1.8	−11.90	0.61	486	−13.74	−10.06	−19.59	**<0.001**
			2.4	−17.04	1.30	486	−21.00	−13.09	−13.07	**<0.001**
		Incline	1.2	−1.84	0.43	486	−3.16	−0.52	−4.24	**0.001**
			1.8	−6.22	0.57	486	−7.94	−4.50	−10.97	**<0.001**
			2.4	−10.60	1.25	486	−14.38	−6.82	−8.51	**<0.001**
Horizontal - decline	Trackway		1.2	4.04	0.95	486	1.16	6.92	4.25	**0.001**
			1.8	8.27	0.78	486	5.89	10.65	10.54	**<0.001**
			2.4	12.51	1.63	486	7.57	17.45	7.68	**<0.001***
	Pole		1.2	−0.05	0.44	486	−1.39	1.28	−0.12	> 0.999
			1.8	−0.26	0.30	486	−1.17	0.65	−0.87	0.988
			2.4	−0.46	0.76	486	−2.77	1.84	−0.61	0.999*
Incline - horizontal	Trackway		1.2	−2.67	1.06	486	−5.89	0.55	−2.51	0.188
			1.8	−3.55	0.87	486	−6.19	−0.91	−4.08	**0.001**
			2.4	−4.44	1.68	486	−9.53	0.66	−2.64	0.140
	Pole		1.2	2.24	0.61	486	0.38	4.10	3.66	**0.007**
			1.8	2.13	0.53	486	0.53	3.72	4.04	**0.002**
			2.4	2.01	0.89	486	−0.68	4.70	2.26	0.309
Jumping height [cm]										
Pole - trackway		Decline		−0.39	0.06	492	−0.55	−0.23	−6.64	**<0.001**
		Horizontal		−2.35	0.09	492	−2.59	−2.1	−25.98	**<0.001**
		Incline		−0.68	0.07	492	−0.87	−0.48	−9.37	**<0.001**
Horizontal - decline	Trackway			2.59	0.11	492	2.29	2.89	23.11	**<0.001**
	Pole			0.63	0.07	492	0.44	0.82	9.01	**<0.001**
Incline - horizontal	Trackway			−1.66	0.15	492	−2.07	−1.25	−10.99	**<0.001**
	Pole			0.01	0.12	492	−0.32	0.34	0.08	> 0.999

SE: standard error.
d.f.: degrees of freedom.
CL: confidence limit.
t: t-value.
p: p-value (significant p-values in bold).
**: comparison falls outside of data range.*

running down a decline, the peak of the forelimbs is larger compared to that of hind limbs, whereas the opposite is the case for running up an incline. On a horizontal support, fore-aft forces of each girdle are characterized by an initial deceleration which is later followed by an acceleration. It appears from **Figure 6** that the forelimbs are net decelerating and the hind limbs are net accelerating.

When comparing the average SRFs among setups, it is important to take into account the average running speeds. The average peak normal and fore-aft forces during locomotion on a decline appear to be similar between trackway and pole according to **Figure 6**. As the speed was significantly higher on average on the pole (see **Table 2**), this suggests that peak normal forces tended to be decreased on the pole. A similar reasoning can be applied to the inclined locomotion. The average peak normal and fore-aft forces during inclined locomotion tended to be higher on the trackway than on the pole according to **Figure 6**, but the speed did not differ significantly between support types (see **Table 2**), indicating that this difference is not an effect of speed.

When running down the decline, the animals instantly exerted a braking force at touchdown, followed by a short and, on average, much smaller acceleration phase by the forelimbs (**Figure 6**). The hind limbs also exerted a braking force, followed by a weak acceleration phase. In contrast, when running up the incline, the animals on average immediately exerted an accelerating force with the forelimbs after touchdown, sometimes followed by a relatively short and small deceleration phase. This was followed by an emphasized acceleration phase by the hind limbs.

DISCUSSION

In order to gain insight into the locomotion of the ancestor of Euarchontoglires, one strategy is to analyze the locomotion of

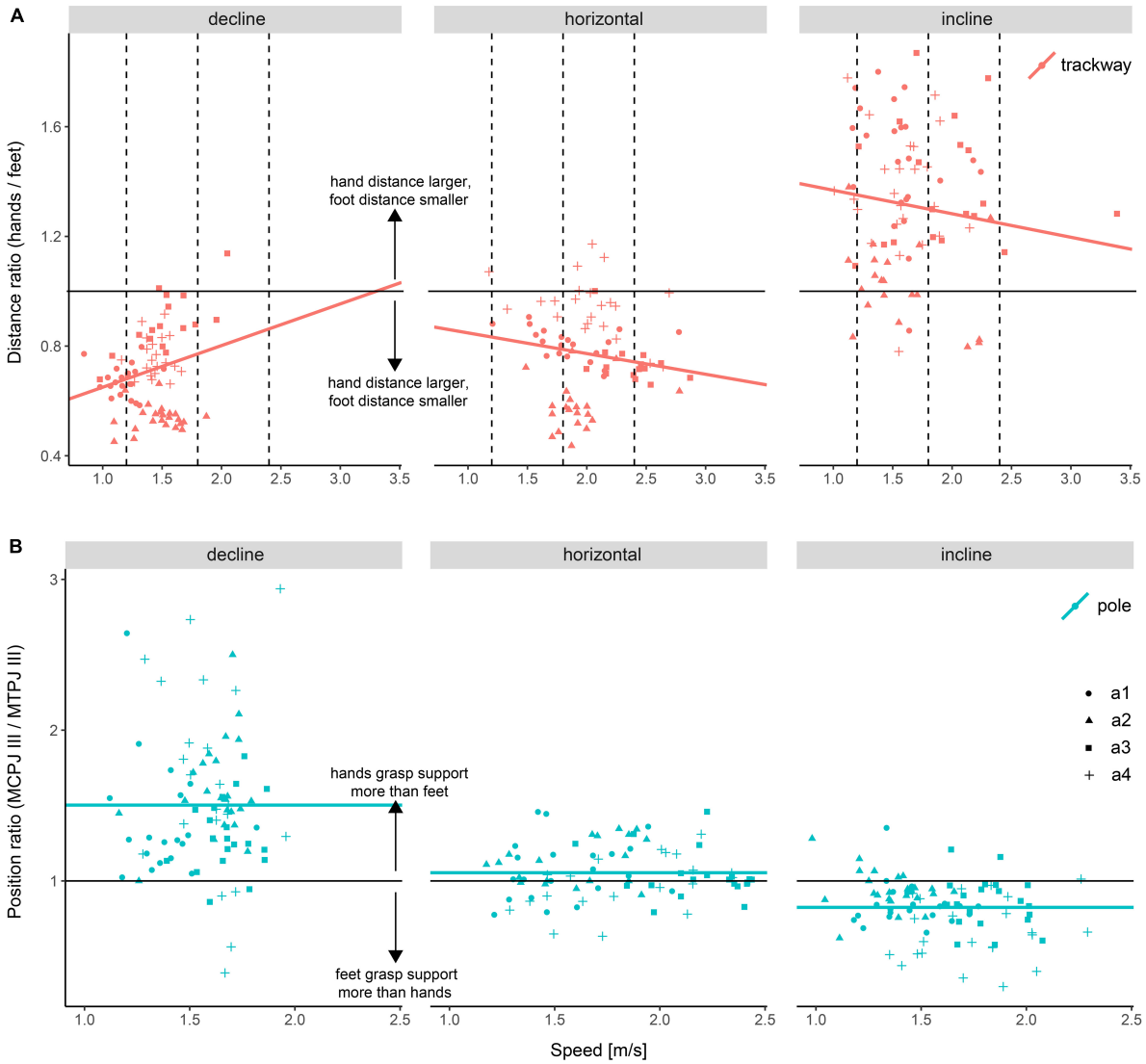

FIGURE 5 | Differences in autopodial placement depending on support orientation. **(A)** Ratio of the distance between hands to the distance between feet on the flat trackway. **(B)** Ratio between the position of the metacarpophalangeal joint III (MCPJ III) and metatarsophalangeal joint III (MTPJ III) on the pole. Position was measured as the distance from the lower margin of the pole. Dashed lines indicate the speed values at which setups were compared statistically *post hoc* (not relevant for **(B)** as speed had no significant effect and hence was removed from the final regression model). a1–a4 refer to the studied individuals.

extant species that share the morphological features assumed to have been characteristic of the crown-group node, i.e., conducting an analysis of identified modern analogs. Here, we analyzed the locomotion of *Tamiops swinhoei*, a small arboreal squirrel species displaying many of the postcranial features proposed for the last common ancestor of Euarchontoglires (Sargis et al., 2007). We studied how the squirrels adjust their locomotion when faced with a flat trackway and a narrow branch-like support and when confronted with different orientations.

We found our expectations to be supported by the data in most of the cases. However, when our hypotheses were not supported, it was due to a more complex relationship between the independent and dependent variables, including interaction effects among support type, support orientation, and running speed. Our findings for a relatively small squirrel species sometimes contrast and thus expand on the findings of Schmidt and Fischer (2011) and Dunham et al. (2019), who studied adjustments of the locomotor kinematics in the larger squirrel species *Sciurus vulgaris* (∼350 g) and *Sciurus carolinensis* (∼500 g), respectively, on poles of varying support orientations and diameters.

Locomotor Adjustments of Striped Squirrels to Diverse Supports

We found that *Tamiops swinhoei* more often increases leads (except when running on the declined support), and reduces speed, jumping distance and jumping height as well as peak

TABLE 5 | *Post hoc* contrasts for the regressions of the ratio of hand/foot distance on the trackway and the ratio of the positions of the MCPJ III and MTPJ III on the pole.

Contrast	Speed [ms^{-1}]	Estimate	SE	d.f.	Lower 95% CL	Upper 95% CL	*t*	*p*
Distance ratio (hand/feet)								
Horizontal - decline	1.2	0.15	0.07	235	0	0.31	2.33	0.053
	1.8	0.02	0.06	235	−0.13	0.16	0.26	0.963
	2.4	−0.12	0.07	235	−0.29	0.05	−1.64	0.233*
Incline - horizontal	1.2	0.52	0.08	235	0.34	0.7	6.72	**<0.001**
	1.8	0.51	0.07	235	0.35	0.67	7.55	**<0.001**
	2.4	0.51	0.08	235	0.31	0.7	6.19	**<0.001**
Position ratio (MCPJ III/MTPJ III)								
Horizontal - decline		−0.45	0.05	110.94	−0.57	−0.32	−8.45	**<0.001**
Incline - horizontal		−0.23	0.03	167.44	−0.3	−0.16	−8.07	**<0.001**

SE: standard error.
d.f.: degrees of freedom.
CL: confidence limit.
t: t-value.
p: p-value.
**: comparison falls outside of data range.*
MCPJ: Metacarpophalangeal joint.
MTPJ: Metatarsophalangeal joint.

SRFs when running along a pole compared to the trackway. Moreover, the squirrels increase DF on the branch-like support. This indicates the need for more grounded gaits that reduce the oscillations of the CoM (Schmitt et al., 2006; Young, 2009). Many of these kinematic and dynamic adjustments, however, were relatively subtle on inclines and declines and generally locomotion did not differ dramatically between the flat trackway and the simulated branch. This corroborates the notion of Jenkins (1974) that functional demands posed on the locomotor system by these support types become more similar with decreasing body size. However, on the horizontal support, mechanical adjustments were comparably more pronounced (**Figures 2–4**, **6**), though *T. swinhoei* still rarely departed from using full bounds on this support orientation, too (**Figure 1**).

The retention of asymmetrical gaits on the pole is also likely to be determined by the relation between body size and substrate size as found in other rodents (e.g., Karantanis et al., 2017a,b). A narrower pole diameter somewhere below 13 mm might have forced the squirrels in our study to switch to symmetrical gaits as observed for species used in these two studies by Karantanis et al. (2017c). Nevertheless, narrower substrates come with increased compliance, a confounding factor when comparing pole to trackway that was not of interest in this study. The relevance of substrate compliance for *T. swinhoei* during foraging in the fine-branch niche and when jumping between trees is not known by now. Dedicated behavioral and performance studies could give insight into how this non-grasping species adapts its biomechanics to such conditions.

Many of the final regression models included animal ID as a random effect, suggesting that the extent of biomechanical adjustments to speed, support type, and support orientation can differ among individuals. This becomes also evident from the more or less separated point clouds of the individuals in **Figures 2–5**. Larger interindividual differences appear to occur during locomotion on the trackway, indicating that a flat surface poses less constraints on the biomechanics compared to the branch-like substrate.

A comparison of locomotion on inclines and declines with horizontal locomotion revealed more pronounced gait differences, too, suggesting the need for more complex adjustments. During locomotion on declines, it appeared that on the pole, the lead of both girdles was less variable. The squirrel might have been more comfortable controlling the descent by the means of establishing a firm grip via grasping the branch-like support between the autopodia of a girdle than using their pronated autopodia to brake on a flat support. When running up an inclined support, leads and average speed were fairly similar on the pole and on the trackway. Similar adjustments were also observed in mouse lemurs and gray squirrels when confronted with different inclines and declines (Shapiro et al., 2016; Dunham et al., 2019).

More specifically, when faced with a decline, the squirrels' gaits exhibited a suite of 'security promoting' adjustments in overall slower trials with reduced jumping height (trackway and pole) and distance (trackway only), and larger DFs with an emphasis of the forelimbs (reflected in the DF-R). By and large, similar combinations of kinematic adjustments to declines have been documented for several small euarchontogliran species including primates (Hesse et al., 2015; Shapiro et al., 2016) and rodents (Karantanis et al., 2017a,c, 2018). Moreover, similar adjustments have been observed in small arboreal marsupials (Shapiro et al., 2014). SRFs reflect the increased net-braking role of the forelimbs and the decreased net-propulsive role of the forelimbs which has similarly been observed in opossums (Lammers et al., 2006) and cotton-top tamarins (Hesse et al., 2015). In accordance with our expectation, also the posture was adjusted to mitigate large forward toppling moments. For example, hindlimb abduction tended to be increased on the declined trackway, bringing the posterior body closer to the support, most likely to avoid toppling over forwards. Similarly, the feet played a larger role in grasping further around the pole on the decline. Generally, hand and foot

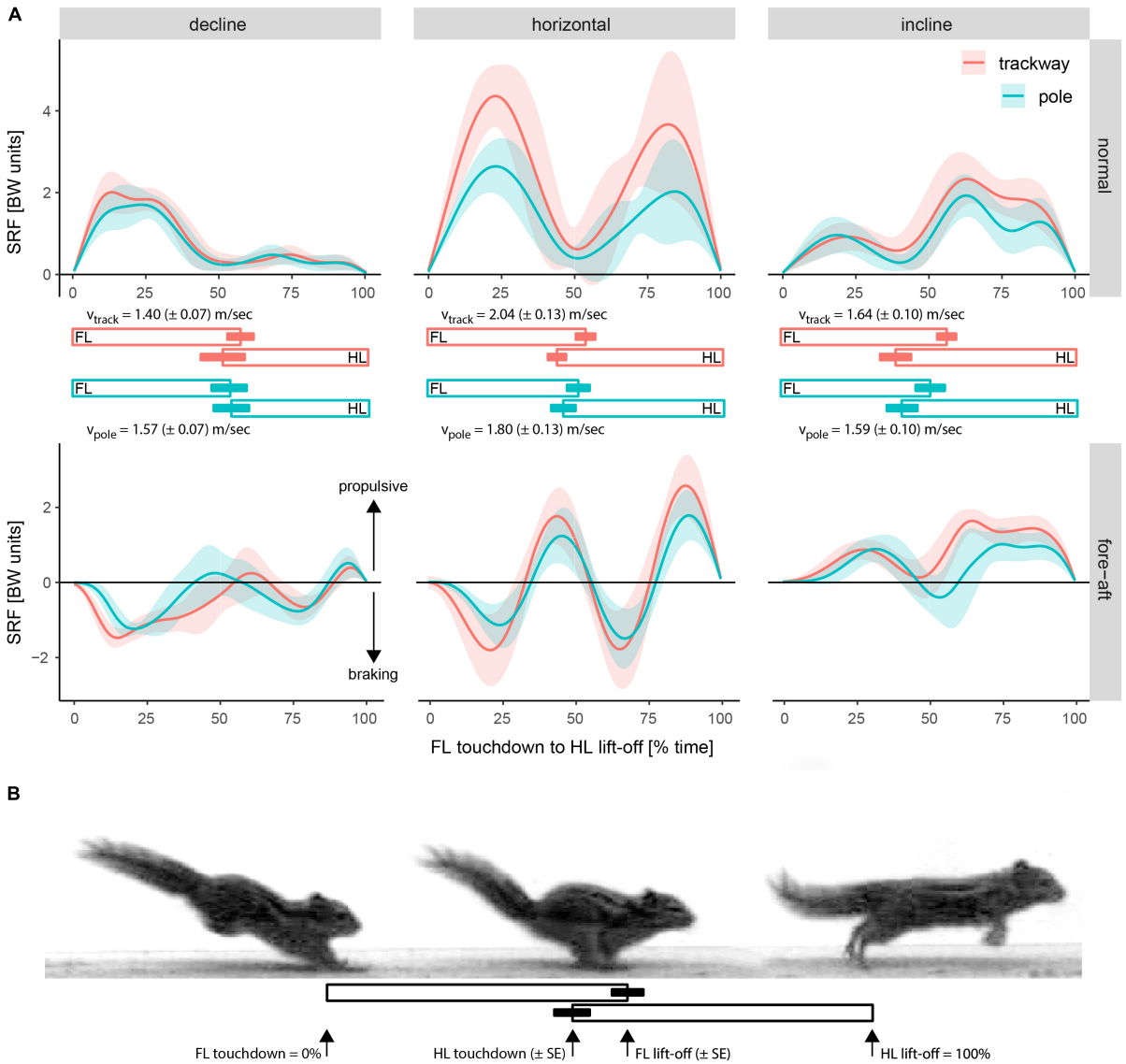

FIGURE 6 | Differences in the average support reaction force trajectories over time among setups. **(A)** Support reaction force (SRF) of all limbs combined in percentage of body weight (BW units) depending on time from forelimb (FL) touchdown to hind limb (HL) lift-off [%]. Shaded areas represent values within a range of ± one standard deviation from the mean SRF. Bars indicate the average support duration [%] ± one standard deviation from the mean for the forelimbs and hind limbs on each setup. The average running speed (v) ± one standard error is reported for each setup to facilitate the comparison of SRFs (see Results). **(B)** Illustration of typical touchdown and lift-off events.

postures are adjusted to accommodate differences of supports in all arboreal species analyzed in detail so far (e.g., Toussaint et al., 2020), but the specific functional significance of these often-overlooked kinematic adjustments requires more dedicated research, for example with use of new spatially-resolved force sensors (Llamosi and Toussaint, 2019).

When confronted with inclines, the striped squirrels displayed a few similar adjustments, but also a few notable kinematic and dynamic differences. Comparable to declines, the subjects reduced their jumping distance (trackway and pole) and height (only on trackway) when comparing similar speeds. These adjustments, in combination with an overall decrease of speed and peak SRFs, suggest a reduction of whole-body suspensions and a stronger emphasis on locomotor control. Also, as in the opossum (Lammers et al., 2006), the forelimb DF of striped squirrels was larger, similar to the adjustment to the decline. Nevertheless, the DF-R on inclines reflects the more pronounced hind limb contact phase as has been observed in several species previously (Vilensky et al., 1994; Nyakatura et al., 2008; Shapiro et al., 2016). This pronounced contact relates to the increased need for acceleration to overcome the additional gravitational pull on a decline (Preuschoft, 2002; Birn-Jeffery and Higham, 2014) and was also observed in opossums (Lammers et al., 2006) and cotton-top tamarins (Hesse et al., 2015). Autopodial

positioning displayed a contrary pattern compared to the adjustments to the declined support. For example, increased forelimb abduction and decreased hind limb abduction were observed on the inclined trackway, both contributing to shifting the CoM to the forelimbs, perhaps reducing the chance of toppling over backwards. On the pole, the hands grasped further around the pole while the feet were placed more on top of it. Thus, despite its general significance, it appears that autopodial repositioning plays a more extensive role for *T. swinhoei* when shifting from a horizontal to an inclined support than from a horizontal to a declined support.

Implications for the Reconstruction of the Locomotion of the Euarchontogliran Ancestor

According to Jenkins (1974) and due to their small body size, ancestral mammals were likely well-suited to exploit both, terrestrial and arboreal supports. For small, non-cursorial, and relatively generalized mammals in a forest habitat, the distinction between arboreal and terrestrial locomotion is rather artificial, because the uneven and disordered supports for locomotion (relative to the size of the animals) require an identical locomotor repertoire (Jenkins, 1974; reviewed in Nyakatura, 2019). Thus, the small early Euarchontoglires likely were not yet specialized climbers and probably lacked salient morphological adaptations to arboreal locomotion. In accordance with this view, Sargis et al. (2007) proposed a non-grasping mode of arboreal locomotion to be representative for the ancestor of Euarchontoglires. Hence, small, arboreal squirrels appear to be a well-suited model system for the understanding of the locomotor mechanics of the earliest Euarchontoglires and perhaps even stem placentals, as they are found in the fine branch niche (Orkin and Pontzer, 2011; Youlatos and Samaras, 2011; Dunham et al., 2019), but also display different degrees of terrestriality when it comes, for example, to foraging (Thorington et al., 2012). This might have constrained them to relatively minor modifications compared to, e.g., primates (Orkin and Pontzer, 2011; Dunham et al., 2019).

Studies of locomotor kinetics and kinematics in arboreal squirrels are relatively rare (e.g., Orkin and Pontzer, 2011; Schmidt, 2011; Schmidt and Fischer, 2011; Lammers and Sufka, 2013; Dunham et al., 2019), but these studies, albeit analyzing larger species than the small *Tamiops swinhoei* studied here, together with our results suggest that these clawed animals without grasping abilities are able to adjust biomechanically to the challenges of different support types and orientations while maintaining fast asymmetrical gaits. In accordance with Jenkins' considerations, *Tamiops swinhoei* showed rare deviations from a full bound, displayed similar speeds on the flat trackway and the branch-like support during inclined locomotion and even higher speeds on the latter when running on declines. This supports the idea that squirrels, similar to relatively small clawed callitrichids and even smaller mouse lemurs, exploit dynamic stability during asymmetrical gaits (Young, 2009; Schmidt and Fischer, 2011; Chadwell and Young, 2015; Shapiro et al., 2016). For example, synchronous use of both limbs of a girdle during asymmetrical gaits allows them to pinch the branch simultaneously between left and right autopodia, which has been proposed to mitigate large roll torques around the CoM, with small disturbances canceled out over several rapid subsequent stride cycles (Lammers and Zurcher, 2011; Schmidt and Biknevicius, 2014).

Considering the likely small body size as suggested by stem placental fossils (Ji et al., 2002; Luo et al., 2011; Youlatos et al., 2015) and early members of the Euarchontoglires (e.g., plesiadapiforms, Silcox and López-Torres, 2017), small body size should be one of the main considerations when identifying potential modern analogs for early primates and further early Euarchontoglires (Nyakatura, 2019). This is especially important considering the size threshold for effective asymmetrical locomotion proposed by Chadwell and Young (2015). The authors described an evolutionary trade-off between the benefits and drawbacks of asymmetrical locomotion which is related to both body mass and support diameter (Chadwell and Young, 2015). While asymmetrical gaits offer benefits such as locomotion with relatively high speeds combined with aerial phases that can be used to bridge gaps between supports in a discontinuous habitat, this locomotor type also involves relatively high forces that are exerted onto the supports (peak forces of several times the body mass documented in our study). Asymmetrical gaits are therefore either limited to larger, more robust branches, or the animals must be lightweight to be able to use asymmetrical gaits on fine branches.

Still, little comparative kinematic and dynamic data for small (below ∼100 g), arboreal members of the Euarchontoglires on simulated arboreal supports are available. But strikingly, all available data for such potential modern analogs documents ubiquitous occurrence of asymmetrical gaits. This includes the small scandentian *Dendrogale murina* (Youlatos et al., 2017), the small primate *Microcebus murinus* (Shapiro et al., 2016; Herbin et al., 2018), and small arboreal rodents such as *Apodemus flavicollis* (Karantanis et al., 2017c) and *Tamiops swinhoei* (our study). The lagomorphs are usually larger and only non-arboreal pikas can be smaller than 100 g. Similarly, members of the Dermoptera are larger. While more comparative data is necessary to consolidate the database for the development of evolutionary scenarios, this points to asymmetrical gaits being present at the origin of Euarchontoglires. Further, our results on a viable modern analog suggests that small-bodied, early crown group members of the Euarchontoglires have already been capable of exploiting the arboreal habitats including the fine, terminal branches and other challenging supports using asymmetrical gaits.

CONCLUSION

Fossil evidence points to a small body size in stem placentals and early Euarchontoglires. Small, arboreal squirrels arguably represent viable modern analogs for early Euarchontoglires and help to conceptualize the locomotor characteristics at the crown-group node. When confronted with narrow, branch-like supports, striped squirrels studied here do not dramatically alter their kinematics and especially dynamics when compared to a flat trackway, albeit some minor adjustments of spatio-temporal parameters in accordance to other published accounts of small arboreal mammal locomotion. This underscores the notion

of Jenkins (1974) that the difference between terrestrial and arboreal supports is largely inconsequential for small mammals. Adjustments to different orientations involved kinematic changes that increased security, while changes in the dynamic data reflected an emphasis on hind limb acceleration on inclines and forelimb braking on declines. In line with a proposed size-related threshold up to which the benefits of asymmetrical locomotion outweigh the drawbacks of it (Chadwell and Young, 2015), limited available comparative kinematic and dynamic data for locomotion on simulated arboreal supports suggests a strong preference of asymmetrical locomotion in small (less than 100 g), arboreal Euarchontoglires. This apparent preference of asymmetrical gaits in small arboreal and scansorial eurarchontoglirans lets us assume that asymmetrical locomotion has been an important part of the locomotor repertoire of the animals at the crown-group node of this mammalian 'superclade'.

DATA AVAILABILITY STATEMENT

The original contributions presented in the study are included in the article/**Supplementary Material**, further inquiries can be directed to the corresponding author/s.

ETHICS STATEMENT

The animal study was reviewed and approved by Landesamt für Gesundheit und Soziales, Berlin.

AUTHOR CONTRIBUTIONS

JW and JN conceived of the study. TA, JM, and JW conducted the experiments and acquired and analyzed the data. JW conducted the statistical analysis. JW and JN drafted the manuscript and all authors contributed to the final version of the manuscript.

FUNDING

We are grateful for funding by the German Research Council (DFG EXC 1027 to JW and JN and DFG NY 63/2-1 to JN).

ACKNOWLEDGMENTS

We thank N. Erickson, S. Thiel and S. Grübel for their help with keeping the animals at the animal facility of the Humboldt University. Finally, we thank all members of the Comparative Zoology lab at HU for critical comments and inspiring discussions.

SUPPLEMENTARY MATERIAL

The Supplementary Material for this article can be found online at: https://www.frontiersin.org/articles/10.3389/fevo.2021.636039/full#supplementary-material

REFERENCES

Adkins, R. M., and Honeycutt, R. L. (1991). Molecular phylogeny of the superorder archonta. *Proc. Natl. Acad. Sci.* 88, 10317–10321. doi: 10.1073/pnas.88.22.10317

Asher, R. J., Bennett, N., and Lehmann, T. (2009). The new framework for understanding placental mammal evolution. *Bioessays* 31, 853–864. doi: 10.1002/bies.200900053

Bininda-Emonds, O. R., Cardillo, M., Jones, K. E., MacPhee, R. D., Beck, R. M., Grenyer, R., et al. (2007). The delayed rise of present-day mammals. *Nature* 446, 507–512. doi: 10.1038/nature05634

Birn-Jeffery, A. V., and Higham, T. E. (2014). The scaling of uphill and downhill locomotion in legged animals. *Integ. Comp. Biol.* 54, 1159–1172. doi: 10.1093/icb/icu015

Burnham, K. P., and Anderson, D. R. (2002). *Model selection and multimodel inference: a practical information-theoretic approach*, 2 Edn. New York, NY: Springer Science & Business Media.

Chadwell, B. A., and Young, J. W. (2015). Angular momentum and arboreal stability in common marmosets (Callithrix jacchus). *Am. J. Phys. Anthropol.* 156, 565–576. doi: 10.1002/ajpa.22683

Dunham, N. T., McNamara, A., Shapiro, L., Phelps, T., Wolfe, A. N., and Young, J. W. (2019). Locomotor kinematics of tree squirrels (*Sciurus carolinensis*) in free-ranging and laboratory environments: Implications for primate locomotion and evolution. *J. Exp. Zool. Part A Ecol.Integ. Physiol.* 331, 103–119. doi: 10.1002/jez.2242

Fabre, P. H., Hautier, L., Dimitrov, D., and Douzery, E. J. (2012). A glimpse on the pattern of rodent diversification: a phylogenetic approach. *BMC Evol. Biol.* 12:88. doi: 10.1186/1471-2148-12-88

Herbin, M., Hommet, E., Hanotin-Dossot, V., Perret, M., and Hackert, R. (2018). Treadmill locomotion of the mouse lemur (*Microcebus murinus*); kinematic parameters during symmetrical and asymmetrical gaits. *J. Comp. Physiol. A* 204, 537–547. doi: 10.1007/s00359-018-1256-2

Hesse, B., Nyakatura, J. A., Fischer, M. S., and Schmidt, M. (2015). Adjustments of limb mechanics in cotton-top tamarins to moderate and steep support orientations: significance for the understanding of early primate evolution. *J. Mammal. Evol.* 22, 435–450. doi: 10.1007/s10914-014-9283-4

Hildebrand, M. (1977). Analysis of asymmetrical gaits. *J. Mammal.* 58, 131–156. doi: 10.2307/1379571

Jenkins, F. A. (1974). "Tree shrew locomotion and the origins of primate arborealism," in *Primate locomotion*, ed. F. A. Jenkins (New York: Academic Press), 85–115. doi: 10.1016/B978-0-12-384050-9.50008-8

Ji, Q., Luo, Z. X., Yuan, C. X., Wible, J. R., Zhang, J. P., and Georgi, J. A. (2002). The earliest known eutherian mammal. *Nature* 416, 816–822. doi: 10.1038/416816a

Karantanis, N.-E., Rychlik, L., Herrel, A., and Youlatos, D. (2017a). Arboreality in acacia rats (*Thallomys paedulcus*; Rodentia, Muridae): gaits and gait metrics. *J. Zool.* 303, 107–119. doi: 10.1111/jzo.12473

Karantanis, N.-E., Rychlik, L., Herrel, A., and Youlatos, D. (2017b). Comparing the arboreal gaits of *Muscardinus avellanarius* and *Glis glis* (gliridae, rodentia): a first quantitative analysis. *Mammal Study* 42, 161–172. doi: 10.3106/041.042.0306

Karantanis, N. E., Rychlik, L., Herrel, A., and Youlatos, D. (2017c). Arboreal gaits in three sympatric rodents *Apodemus agrarius*, *Apodemus flavicollis* (rodentia, muridae) and *Myodes glareolus* (rodentia, cricetidae). *Mammalian Biol.* 83, 51–63. doi: 10.1016/j.mambio.2016.12.004

Karantanis, N. E., Rychlik, L., Herrel, A., and Youlatos, D. (2018). Vertical locomotion *in Micromys minutus* (Rodentia: Muridae): insights into the evolution of eutherian climbing. *J. Mammalian Evol.* 25, 277–289. doi: 10.1007/s10914-016-9374-5

Lammers, A. R., Earls, K. D., and Biknevicius, A. R. (2006). Locomotor kinetics and kinematics on inclines and declines in the gray short-tailed opossum *Monodelphis domestica*. *J. Exp. Biol.* 209, 4154–4166. doi: 10.1242/jeb.02493

Lammers, A. R., and Gauntner, T. (2008). Mechanics of torque generation during quadrupedal arboreal locomotion. *J. Biomech.* 41, 2388–2395. doi: 10.1016/j.jbiomech.2008.05.038

Lammers, A. R., and Sufka, K. M. (2013). Turning the corner in quadrupedal arboreal locomotion: kinetics of changing direction while running in the siberian chipmunk (*Tamias sibiricus*). *J. Exp. Zool. Part A Ecol. Genet. Physiol.* 319, 99–112. doi: 10.1002/jez.1775

Lammers, A. R., and Zurcher, U. (2011). Torque around the center of mass: dynamic stability during quadrupedal arboreal locomotion in the siberian chipmunk (*Tamias sibiricus*). *Zoology* 114, 95–103. doi: 10.1016/j.zool.2010.11.004

Lenth, R. (2020). *emmeans: Estimated Marginal Means, aka Least-Squares Means. Version*.

Llamosi, A., and Toussaint, S. (2019). Measuring force intensity and direction with a spatially resolved soft sensor for biomechanics and robotic haptic capability. *Soft Robotics* 6, 346–355. doi: 10.1089/soro.2018.0044

Luo, Z. X., Yuan, C. X., Meng, Q. J., and Ji, Q. (2011). A Jurassic eutherian mammal and divergence of marsupials and placentals. *Nature* 476, 442–445. doi: 10.1038/nature10291

Meredith, R. W., Janečka, J. E., Gatesy, J., Ryder, O. A., Fisher, C. A., Teeling, E. C., et al. (2011). Impacts of the cretaceous terrestrial revolution and KPg extinction on mammal diversification. *Science* 334, 521–524. doi: 10.1126/science.1211028

Mielke, F., Schunke, V., Wölfer, J., and Nyakatura, J. A. (2018). Motion analysis of non-model organisms using a hierarchical model: influence of setup enclosure dimensions on gait parameters of Swinhoe's striped squirrels as a test case. *Zoology* 129, 35–44. doi: 10.1016/j.zool.2018.05.009

Murphy, W. J., Eizirik, E., Johnson, W. E., Zhang, Y. P., Ryder, O. A., and O'Brien, S. J. (2001). Molecular phylogenetics and the origins of placental mammals. *Nature* 409, 614–618. doi: 10.1038/35054550

Novacek, M. J. (1992). Mammalian phylogeny: shaking the tree. *Nature* 356, 121–125. doi: 10.1038/356121a0

Nyakatura, J. A. (2019). Early primate evolution: insights into the functional significance of grasping from motion analyses of extant mammals. *Biol. J. Linnean Soc.* 127, 611–631. doi: 10.1093/biolinnean/blz057

Nyakatura, J. A., Fischer, M. S., and Schmidt, M. (2008). Gait parameter adjustments of cotton-top tamarins (*Saguinus oedipus*, callitrichidae) to locomotion on inclined arboreal substrates. *Am. J. Phys. Anthropol.* 135, 13–26. doi: 10.1002/ajpa.20699

Orkin, J. D., and Pontzer, H. (2011). The narrow niche hypothesis: gray squirrels shed new light on primate origins. *Am. J. Phys. Anthropol.* 144, 617–624. doi: 10.1002/ajpa.21450

Pinheiro, J., Bates, D., DebRoy, S., Sarkar, D., and R Core Team. (2020). *nlme: Linear and Nonlinear Mixed Effects Models_. R package version 3.1-149*.

Preuschoft, H. (2002). What does "arboreal locomotion" mean exactly and what are the relationships between "climbing", environment and morphology? *Zeitschrift für Morphologie und Anthropologie* 83, 171–188.

R Core Team. (2020). *R: A language and environment for statistical computing. R Foundation for Statistical Computing, Vienna, Austria. Revelle, W. (2020) psych: Procedures for Personality and Psychological Research*. Illinois, USA: Northwestern University, Evanston.

Rueden, C. T., Schindelin, J., Hiner, M. C., DeZonia, B. E., Walter, A. E., Arena, E. T., et al. (2017). ImageJ2: imagej for the next generation of scientific image data. *BMC Bioinform.* 18:529. doi: 10.1186/s12859-017-1934-z

Sargis, E. J., Boyer, D. M., Bloch, J. I., and Silcox, M. T. (2007). Evolution of pedal grasping in Primates. *J. Hum. Evol.* 53, 103–107. doi: 10.1016/j.jhevol.2007.01.008

Schmidt, A. (2011). Functional differentiation of trailing and leading forelimbs during locomotion on the ground and on a horizontal branch in the european red squirrel (*Sciurus vulgaris*, rodentia). *Zoology* 114, 155–164. doi: 10.1016/j.zool.2011.01.001

Schmidt, A., and Biknevicius, A. R. (2014). Structured variability of steady-speed locomotion in rats. *J. Exp. Biol.* 217, 1402–1406. doi: 10.1242/jeb.092668

Schmidt, A., and Fischer, M. S. (2011). The kinematic consequences of locomotion on sloped arboreal substrates in a generalized (*Rattus norvegicus*) and a specialized (*Sciurus vulgaris*) rodent. *J. Exp. Biol.* 214, 2544–2559. doi: 10.1242/jeb.051086

Schmidt, M. (2005). Quadrupedal locomotion in squirrel monkeys (Cebidae *Saimiri sciureus*): a cineradiographic study of limb kinematics and related substrate reaction forces. *Am. J. Phys. Anthropol.* 128, 359–370. doi: 10.1002/ajpa.20089

Schmitt, D. (1999). Compliant walking in primates. *J. Zool.* 248, 149–160. doi: 10.1111/j.1469-7998.1999.tb01191.x

Schmitt, D., Cartmill, M., Griffin, T. M., Hanna, J. B., and Lemelin, P. (2006). Adaptive value of ambling gaits in primates and other mammals. *J. Exp. Biol.* 209, 2042–2049. doi: 10.1242/jeb.02235

Shapiro, L. J., Kemp, A. D., and Young, J. W. (2016). Effects of substrate size and orientation on quadrupedal gait kinematics in mouse lemurs (*Microcebus murinus*). *J. Exp. Zool.* 325, 329–343. doi: 10.1002/jez.2020

Shapiro, L. J., Young, J. W., and VandeBerg, J. L. (2014). Body size and the small branch niche: using marsupial ontogeny to model primate locomotor evolution. *J. Hum. Evol.* 68, 14–31. doi: 10.1016/j.jhevol.2013.12.006

Silcox, M. T., and López-Torres, S. (2017). Major questions in the study of primate origins. *Ann. Rev. Earth Planetary Sci.* 45, 113–137. doi: 10.1146/annurev-earth-063016-015637

Simpson, G. G. (1945). The principles of classification and a classification of mammals. *Bull. Amer. Mus. Nat. Hist.* 85:350.

Smith, A. T., and Xie, Y. (2013). *Mammals of China*. Princeton, NJ: Princeton University Press.

Springer, M. S., Stanhope, M. J., Madsen, O., and de Jong, W. W. (2004). Molecules consolidate the placental mammal tree. *Trends Ecol. Evol.* 19, 430–438. doi: 10.1016/j.tree.2004.05.006

Thorington, R. W. Jr., Koprowski, J. L., Steele, M. A., and Whatton, J. F. (2012). *Squirrels of the world*. Baltimore, MD: John Hopkins University Press.

Toussaint, S., Llamosi, A., Morino, L., and Youlatos, D. (2020). The central role of small vertical substrates for the origin of grasping in early primates. *Curr. Biol.* 30, 1600–1613. doi: 10.1016/j.cub.2020.02.012

Vilensky, J. A., Moore, A. M., and Libii, J. N. (1994). Squirrel monkey locomotion on an inclined treadmill: implications for the evolution of gaits. *J. Hum. Evol.* 26, 375–386. doi: 10.1006/jhev.1994.1024

Wickham, H., Averick, M., Bryan, J., Chang, W., McGowan, L., François, R., et al. (2019). Welcome to the tidyverse. *J. Open Source Software* 4:1686. doi: 10.21105/joss.01686

Wickham, H., and Bryan, J. (2019). *readxl: Read Excel Files. R package version 1.3.1*.

Wölfer, J., Amson, E., Arnold, P., Botton-Divet, L., Fabre, A. C., van Heteren, A. H., et al. (2019). Femoral morphology of sciuromorph rodents in light of scaling and locomotor ecology. *J. Anat.* 234, 731–747. doi: 10.1111/joa.12980

Youlatos, D., Karantanis, N. E., Byron, C. D., and Panyutina, A. (2015). Pedal grasping in an arboreal rodent relates to above-branch behavior on slender substrates. *J. Zool.* 296, 239–248. doi: 10.1111/jzo.12237

Youlatos, D., Karantanis, N. E., and Panyutina, A. (2017). Pedal grasping in the northern smooth-tailed treeshrew *Dendrogale murina* (tupaiidae, scandentia): insights for euarchontan pedal evolution. *Mammalia* 81, 61–70. doi: 10.1515/mammalia-2015-0113

Youlatos, D., and Samaras, A. (2011). Arboreal locomotor and postural behaviour of European red squirrels (*Sciurus vulgaris* L.) in northern Greece. *J. Ethol.* 29, 235–242. doi: 10.1007/s10164-010-0248-7

Young, J. W. (2009). Substrate determines asymmetrical gait dynamics in marmosets (*Callithrix jacchus*) and squirrel monkeys (*Saimiri boliviensis*). *Am. J. Phys. Anthropol.* 138, 403–420. doi: 10.1002/ajpa.20953

Zhou, X., Sun, F., Xu, S., Yang, G., and Li, M. (2015). The position of tree shrews in the mammalian tree: comparing multi-gene analyses with phylogenomic results leaves monophyly of Euarchonta doubtful. *Integrative Zool.* 10, 186–198. doi: 10.1111/1749-4877.12116

Zuur, A. F., Ieno, E. N., Walker, N., Saveliev, A. A., and Smith, G. M. (2009). *Mixed effects models and extensions in ecology with R*. New York, NY: Springer Science & Business Media. doi: 10.1007/978-0-387-87458-6

Conflict of Interest: The authors declare that the research was conducted in the absence of any commercial or financial relationships that could be construed as a potential conflict of interest.

frontiers in Ecology and Evolution

ORIGINAL RESEARCH
published: 10 June 2021
doi: 10.3389/fevo.2021.636110

Anatomy of the Nasal and Auditory Regions of the Fossil Lagomorph *Palaeolagus haydeni*: Systematic and Evolutionary Implications

Irina Ruf[1†], *Jin Meng*[2†] *and Łucja Fostowicz-Frelik*[3,4,5*†]

[1] Abteilung Messelforschung und Mammalogie, Senckenberg Forschungsinstitut und Naturmuseum Frankfurt, Frankfurt, Germany, [2] Division of Paleontology, American Museum of Natural History, New York, NY, United States, [3] Key Laboratory of Vertebrate Evolution and Human Origins, Institute of Vertebrate Paleontology and Paleoanthropology, Chinese Academy of Sciences, Beijing, China, [4] Chinese Academy of Sciences, Center for Excellence in Life and Paleoenvironment, Beijing, China, [5] Department of Evolutionary Paleobiology, Institute of Paleobiology, Polish Academy of Sciences, Warsaw, Poland

OPEN ACCESS

Edited by:
Nathalie Bardet,
UMR 7207 Centre de Recherche sur la Paléobiodiversité et les Paléoenvironnements (CR2P), France

Reviewed by:
Timothy B. Rowe,
University of Texas at Austin, United States
Ingrid Lundeen,
University of Texas at Austin, United States

***Correspondence:**
Łucja Fostowicz-Frelik
lfost@twarda.pan.pl

†ORCID:
Irina Ruf
orcid.org/0000-0002-9728-1210
Jin Meng
orcid.org/0000-0002-3385-8383
Łucja Fostowicz-Frelik
orcid.org/0000-0002-1266-1178

Specialty section:
This article was submitted to Paleontology, a section of the journal Frontiers in Ecology and Evolution

Received: 09 December 2020
Accepted: 11 May 2021
Published: 10 June 2021

Citation:
Ruf I, Meng J and Fostowicz-Frelik Ł (2021) Anatomy of the Nasal and Auditory Regions of the Fossil Lagomorph Palaeolagus haydeni: Systematic and Evolutionary Implications. Front. Ecol. Evol. 9:636110. doi: 10.3389/fevo.2021.636110

Palaeolagus, a late Eocene to early Miocene North American lagomorph genus, represented by numerous and well-preserved specimens, has been long considered a basal leporid, although it is currently understood as a stem lagomorph. Based on micro-computed tomography (μCT) data and 3D reconstructions, here we present the first description of intracranial structures of the nasal and auditory regions of a complete skull of *Palaeolagus haydeni* from the early Oligocene of Nebraska. Although *Palaeolagus haydeni* shows a puzzling mixture of extant leporid and ochotonid characters, it helps to polarize and re-evaluate already known lagomorph intracranial characters based on outgroup comparison with Rodentia and Scandentia. Common derived features of *Palaeolagus haydeni* and extant Lagomorpha are the dendritic maxilloturbinal and the excavated nasoturbinal that contacts the lamina semicircularis. Generally, *Palaeolagus haydeni* and Leporidae have several characters in common, some of which are certainly plesiomorphic (e.g., thin wall of bulla tympani and flat conic cochlea). *Palaeolagus haydeni* resembles Leporidae in having an interturbinal between the two frontoturbinals, and three ethmoturbinals plus one interturbinal between ethmoturbinal I and II. Now, this should also be regarded as a plesiomorphic grundplan pattern for Leporidae whereas ochotonids are derived from the lagomorph grundplan as concerns the number of frontoturbinals. Concerning the middle ear, *Palaeolagus haydeni* significantly contributes to the polarization of the anterior anchoring of the malleus in extant lagomorphs. *Palaeolagus haydeni* resembles the pattern observed in early ontogenetic stages of Ochotonidae, i.e., the attachment of the malleus to the ectotympanic via a short processus anterior. The patterns in adult ochotonids and leporids now can be regarded as two different and apomorphic character states. Autapomorphic characters of *Palaeolagus haydeni* are the reduced frontoturbinal 2 and the additional anterolaterally oriented process of the lamina semicircularis. Interestingly, among the investigated intracranial structures the loss of the secondary crus commune is the only apomorphic grundplan character of crown Lagomorpha.

Keywords: computed tomography, lagomorph skull, auditory ossicles, bony labyrinth, bulla tympani, malleus, petrosal, turbinals

INTRODUCTION

Intracranial bony structures of the mammalian nasal and auditory regions provide proxies for sense organs of smell (the olfactory turbinals), balance (vestibular part of the inner ear bony labyrinth) and hearing (the auditory ossicles and cochlear part of the inner ear bony labyrinth) as well as for thermoregulation (the respiratory turbinals). Thus, they can significantly contribute to a deeper understanding of morphofunctional and ecological adaptations as demonstrated in extant and fossil mammal species (e.g., Spoor et al., 2007; Pfaff et al., 2017; Martinez et al., 2018, 2020; Wagner and Ruf, 2019). Furthermore, characters, especially those related to the auditory region, are frequently used in mammalian phylogeny to reconstruct relationships among major clades (Meng et al., 2003; Wible et al., 2009; Mennecart et al., 2016).

Lagomorpha have been rarely subject to detailed studies of these structures and the existing contributions concern almost exclusively extant taxa, particularly the domesticated form of *Oryctolagus cuniculus* (Voit, 1909; Frick and Heckmann, 1955; Hoyte, 1961; King et al., 2007). However, recent studies on extant Lagomorpha revealed phylogenetically relevant characters of the nasal and ear regions. Ochotonidae and Leporidae can clearly be distinguished by specific characters of the turbinal skeleton and of the middle ear such as the pattern of the processus anterior and the processus praearticularis internus of the malleus (Ruf, 2014; Maier et al., 2018).

When fossils are considered, the synapomorphy schemes for lagomorphs and their related groups (Duplicidentata as a whole) may be contradicted; a derived feature shared by living taxa may turn out to be secondary or convergent if fossil relatives do not possess that feature. Since Lagomorpha has been generally considered as a monophyletic (e.g., Asher et al., 2005; Fostowicz-Frelik and Meng, 2013) and morphologically conservative group (Fostowicz-Frelik, 2017; López-Torres et al., 2020), characters that we collect from fossil lagomorphs may help us to evaluate characters and their polarity obtained from the living lagomorph relatives.

The subject of this study is *Palaeolagus haydeni*, the most common and widespread fossil lagomorph of North America (Dawson, 1958, 2008) and arguably the best known fossil lagomorph to date. For decades, the phylogenetic position of *Palaeolagus* has remained somewhat disputed. Traditionally it has been considered a basal leporid (Dawson, 2008). In contrast, recent phylogenetic analyses consequently place this genus outside of the crown Lagomorpha (Asher et al., 2005; Wible, 2007; Fostowicz-Frelik, 2013; Fostowicz-Frelik and Meng, 2013; but see Asher et al., 2019). Nevertheless, *Palaeolagus* with its eight species, spanning from the late Eocene to the early Miocene is a key genus for a deeper understanding of lagomorph evolution. *Palaeolagus haydeni*, the type species of *Palaeolagus,* is represented by a large number of well-preserved specimens available for us to study, as compared to other fossil taxa. Recently, a detailed study of the skull anatomy of *Palaeolagus haydeni* supported a basal position based on a mixed pattern of ochotonid and leporid characters (Wolniewicz and Fostowicz-Frelik, 2021).

Here we present the first description of intracranial structures of the nasal and auditory regions of *Palaeolagus haydeni* and compare our observations to the pattern in extant Lagomorpha. We also discuss some character transformations based on new evidence, and consider the plausible ancestral character set for extant Lagomorpha. Our study complements the work by Wolniewicz and Fostowicz-Frelik (2021) that is based on the same specimen.

MATERIALS AND METHODS

The study is based on μCT data obtained from the skull of an adult *Palaeolagus haydeni* (FMNH PM9476) housed in the Field Museum of Natural History (FMNH, Chicago, IL, United States). The skull was μCT scanned using a high-resolution GE phoenix| x-ray v|tome|x L 240 scanner (GE Measurement & Control Solutions) at the American Museum of Natural History (AMNH, New York, NY, United States). The parameters of the scan of the entire skull were as follows: voltage 170 kV, current 170 mA, and 0.1 mm Cu filter. The total of 1401 images were acquired at a resolution of 50.69 μm (isotropic voxels). A second scan of the posterior part of the skull (orbitotemporal and otical regions) has the following scan parameters: voltage 170 kV, current 170 mA, and 0.1 mm Cu filter, resolution 36.49 μm. Raw data were further reconstructed with GE phoenix| x-ray datos| x 2.0 software resulting in 16-bit TIFFs (1900 × 1000 pixel in size). Based on the μCT data virtual 3D reconstructions were performed with Avizo 9.0.1 (Thermo Fisher Scientific). Turbinals were segmented with the manual segmentation tool; hereby the entire turbinal structure up to the contact with the lateral wall of the nasal cavity, the lamina horizontalis and the lamina cribrosa was considered. The bony labyrinth and the auditory ossicles were segmented with the manual and automatic (magic wand) segmentation tools. The first scan was used for reconstruction of the selected structures (in **Figures 1–3**). The μCT image in **Figure 4** as well as the auditory ossicles in **Figure 5** are based on the second scan. The μCT data (image stacks) and the 3D models are deposited in the Dryad Digital Repository (Fostowicz-Frelik et al., 2021).

Terminology of the described structures follows Ekdale (2013, 2016), Ruf (2014), Maier and Ruf (2014), and Maier et al. (2018). The results concerning *Palaeolagus haydeni* are discussed in comparison to extant Lagomorpha based on data from literature (e.g., Ruf, 2014; Maier et al., 2018) and against the background of combined phylogeny from Matthee et al. (2004), and Fostowicz-Frelik and Meng (2013). For grundplan reconstruction that allows defining all characters (apomorphic and plesiomorphic) of the last common ancestor of a respective taxon we follow the definition by Hennig (1984). The same scans of adult extant Lagomorpha included in the study on the auditory ossicles in Maier et al. (2018) are used to discuss characters of the middle ear and the bony labyrinth.

For outgroup comparison recent studies on the nasal region of further members of Euarchontoglires are considered: Rodentia (Ruf, 2014, 2020; Martinez et al., 2018), Scandentia (Ruf et al., 2015; Lundeen and Kirk, 2019),

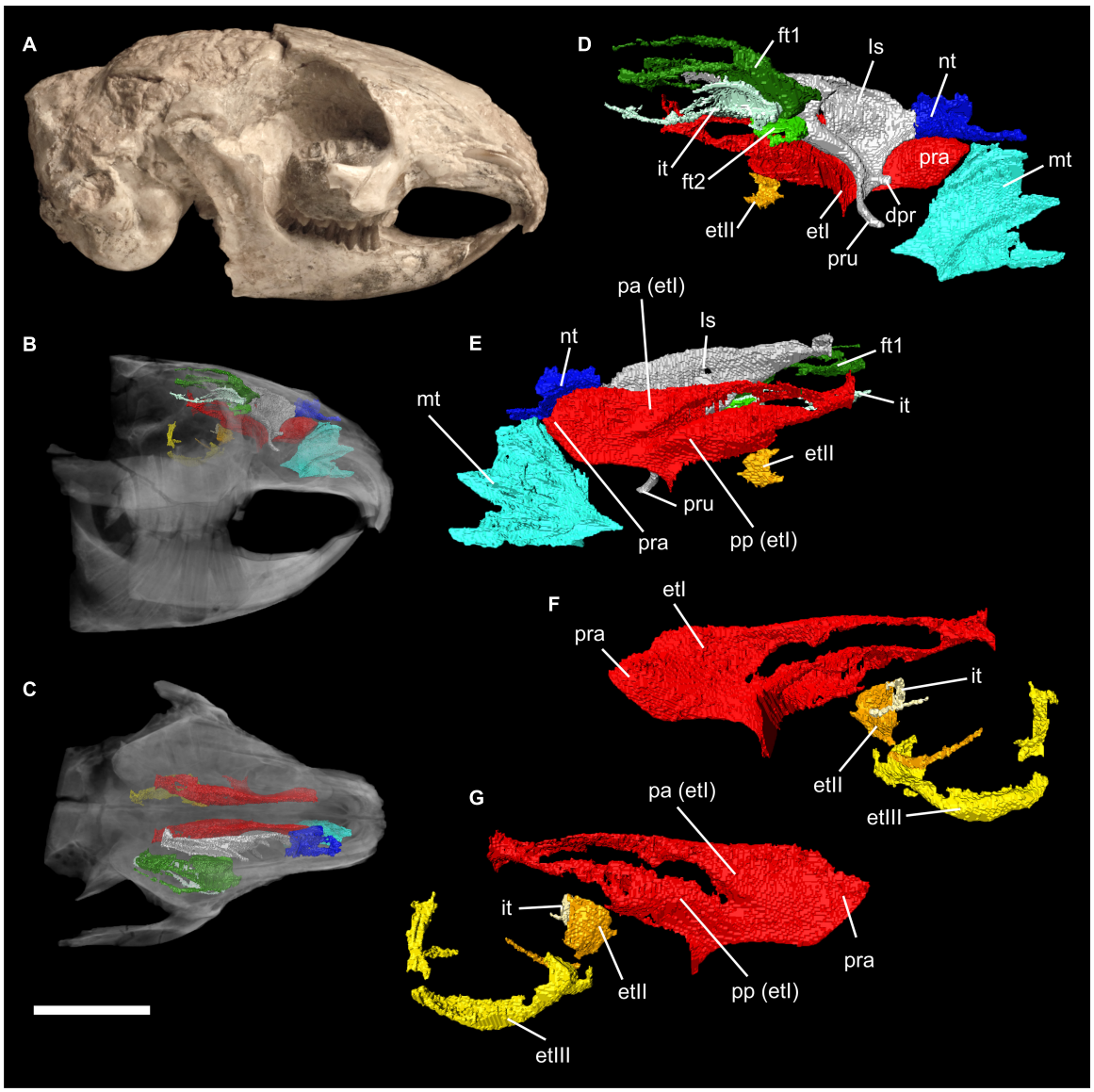

FIGURE 1 | Virtual 3D reconstructions of the turbinal skeleton of *Palaeolagus haydeni* (FMNH PM9476). Actual skull in mirrored lateral view **(A)**. Rostrum with highlighted turbinal skeleton in lateral **(B)** and dorsal **(C)** views. The skull bones are transparent. Right turbinal skeleton in lateral **(D)** and medial **(E)** views. The ethmoturbinals are incomplete. Left turbinal skeleton in lateral **(F)** and medial **(G)** views. Only the fronto- ethmo-, and interturbinals are reconstructed. Abbreviations: et I-III, ethmoturbinal I-III; dpr, dorsal process; ft 1-2, frontoturbinal 1-2; it, interturbinal; ls, lamina semicircularis; mt, maxilloturbinal; nt, nasoturbinal; pa, pars anterior; pp, pars posterior; pra, processus anterior; pru, processus uncinatus. Scale bar = 10 mm refers to **(A–C)**; **(D–G)** not to scale.

Dermoptera (Maier and Ruf, 2014; Lundeen and Kirk, 2019), and Primates (Maier and Ruf, 2014; Smith et al., 2016; Lundeen and Kirk, 2019).

RESULTS

Palaeolagus haydeni FMHN PM9476 comprises a complete skull including the articulated mandible. The cavities inside the skull are completely filled by sediment. The specimen is mostly intact, although some parts are missing or have been damaged. These are the anterior nasal roof, the left zygomatic arch, the orbital wall of the nasal cavity, and the roof of the braincase (**Figure 1A**; see also Wolniewicz and Fostowicz-Frelik, 2021). In addition, the auditory bullae show some defects, resulting in their fenestration. Thus, the following anatomical description refers to the better preserved side, left or right depending on the completeness of the respective structure.

Nasal Region

The turbinal skeleton of FMHN PM9476 is incomplete because all turbinals show defects or are broken. This affects especially the structures located in the most anterior and posterior parts of

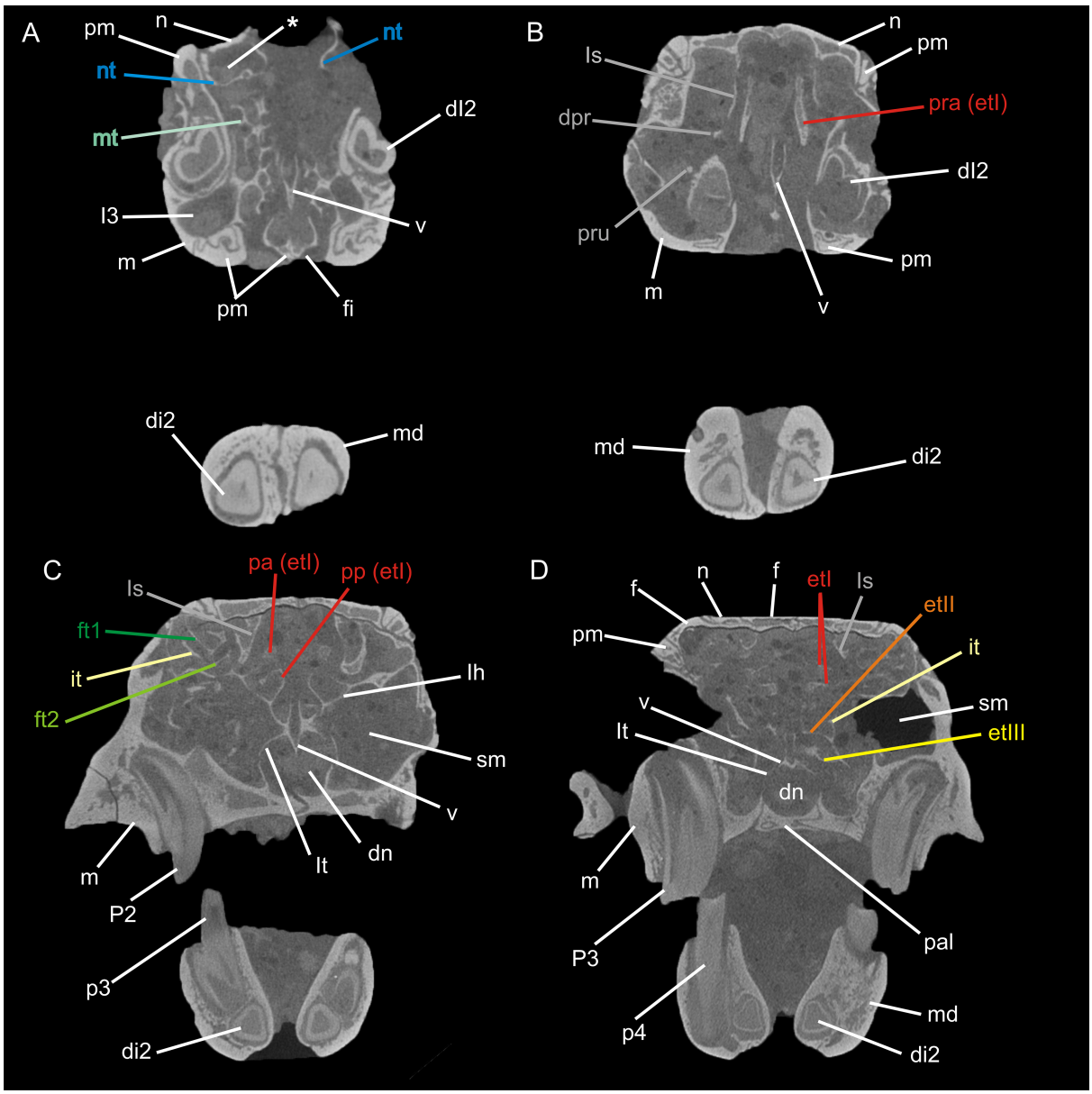

FIGURE 2 | Transversal μCT images through the nasal cavity of *Palaeolagus haydeni* (FMNH PM9476) from anterior **(A)** to posterior **(D)**. The asterisk (*) indicates the cavity formed by the nasoturbinal and the nasal. Abbreviations: dl2, deciduous upper incisor 2; di2, deciduous lower incisor 2; dn, ductus nasopharyngeus; dpr, dorsal process; et I-III, ethmoturbinal I–III; ft1-2, frontoturbinal 1–2; f, frontal; fi, foramen incisivum; l3, upper incisor 3; it, interturbinal; lh, lamina horizontalis; ls, lamina semicircularis; lt, lamina terminalis; m, maxilla; md mandible; mt, maxilloturbinal; n, nasal; nt, nasoturbinal; p3–4, lower premolars 3 and 4; P2–3, upper premolars 2 and 3; pa, pars anterior; pal, palatine; pm, premaxilla; pp, pars posterior; pra, processus anterior; pru, processus uncinatus; sm, sinus maxillaris; v, vomer. Not to scale.

the nasal cavity. However, the number of turbinals can be clearly deduced from both sides of the nasal cavity, although the detailed anatomy remains uncertain in some parts. Ethmoturbinals II and III as well as the interturbinal of the pars posterior are much better preserved on the left side (**Figures 1B–G**).

The pars anterior of the nasal cavity houses a large and dendritic maxilloturbinal whose anterior portion is not preserved (**Figures 1B–E**, **2A**). It covers the canalis nasolacrimalis that houses the ductus nasolacrimalis medially and ends ventral to the processus anterior of ethmoturbinal I. The anterior part of the nasoturbinal is also not preserved. The remnant of the nasoturbinal is a short straight lamella. Posteriorly, the nasoturbinal forms the floor of a deep cavity whose roof is the nasal bone (**Figures 1B–E**, **2A**). The lamina semicircularis separates the pars posterior of the nasal cavity from the pars lateralis. It is a long lamella projecting from the nasal roof that ends at the anterior rim of the lamina cribrosa. This lamella corresponds to the dorsal lamella or flank of

a typical sickle-shaped lamina semicircularis. Ventrally, the lamina semicircularis projects into the sinus maxillaris via the hiatus semilunaris. This ventral projection that might comprise a vestigial ventral lamina, shows two anterolaterally oriented processus. The dorsal process is short. The ventral one is more prominent and interpreted as the processus uncinatus (**Figures 1D,E**, **2B**). The posterior margin of the lamina semicircularis is rolled-up laterally. The lamina semicircularis and the nasoturbinal are not fused but together form a continuous lamella and therefore, a functional unit attached to the nasal roof.

The recessus frontoturbinalis of the pars lateralis houses three turbinals, which are not completely preserved (**Figures 1B–D**, **2C**). Of the three turbinals, the dorsal one can be identified as frontoturbinal 1. It is attached to the nasal roof (mostly the frontal bone) and merges posteriorly into the lamina cribrosa. The shape can be reconstructed as a double-scroll. The second turbinal is almost as long as frontoturbinal 1 and is similar in shape. It starts at the lateral rim of the lamina horizontalis and attaches to the lateral wall of the nasal cavity in its further course; the posterior end merges into the lamina cribrosa. We interpret this turbinal as the interturbinal. The third turbinal, most likely frontoturbinal 2, is very short and small. It is attached to the lamina horizontalis and its posterior end is in contact with the root of ethmoturbinal I. Frontoturbinal 2 probably shows only a lateral scroll but the exact shape is not preserved. The homology of the interturbinal and frontoturbinal is discussed below.

The pars posterior of the nasal cavity houses four turbinals that are only partly preserved except for ethmoturbinal I (**Figures 1B–G**, **2B–D**). Ethmoturbinal I is attached to the lamina horizontalis and has a broad massive processus anterior that projects far into the pars anterior of the nasal cavity (**Figures 1C–G**, **2B**). The two major lamellae of ethmoturbinal I, pars anterior and pars posterior, can be clearly separated. While the pars anterior is a straight lamella, the pars posterior is rolled-up laterally (**Figures 1E,G**, **2C**). Posteriorly, both parts fuse to form a funnel-shaped recess that is attached to the lamina cribrosa. The following turbinals all arise from the lamina horizontalis and more posterior from the lateral sidewall of the nasal cavity. Ethmoturbinal II and the interturbinal between the former and ethmoturbinal I are represented only by their anteriormost part (**Figures 1B,D–G**, **2D**). Their length and morphology cannot be determined from these remnants. However, it is visible that the interturbinal forms at least partly a double-scroll. Ethmoturbinal III extends far into the posterior nasal cavity and forms a prominent ventrally convex lamella. However, only the distal part of ethmoturbinal III is preserved and thus its detailed shape and number of lamellae remain unclear (**Figures 1B,F,G**, **2D**).

The nasal septum is only partly preserved with its dorsoposterior part being attached to the lamina cribrosa as well as the very most end inside the cupula nasi posterior.

Middle Ear

Palaeolagus haydeni shows a well-developed bulla tympani that completely encloses the tympanic cavity (**Figure 3**). In ventral view, the bulla is oval, with its long axis oriented anteromedially.

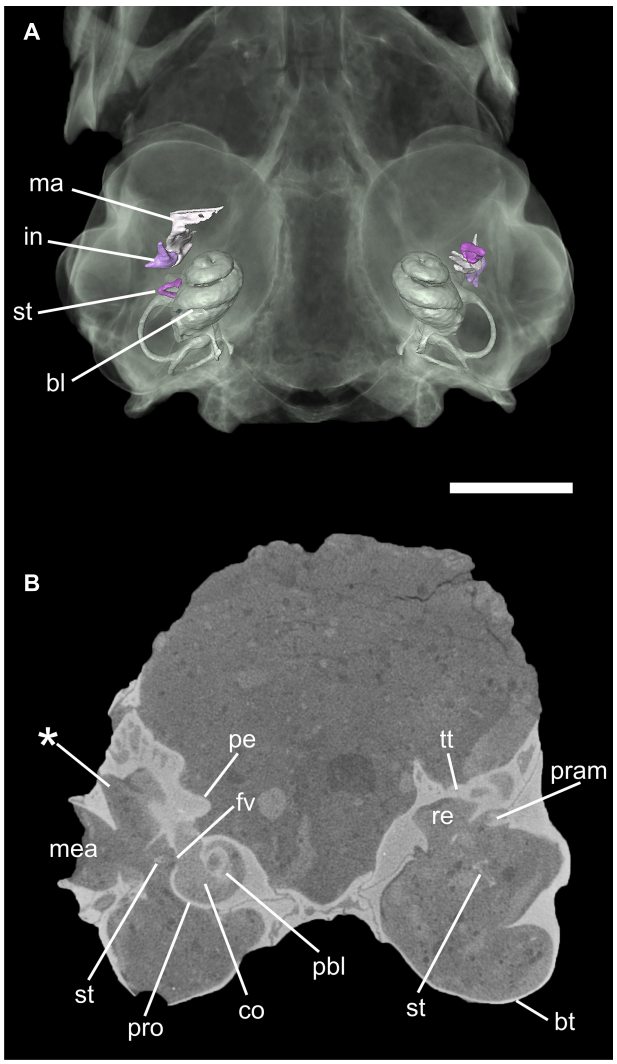

FIGURE 3 | Virtual 3D reconstruction of the auditory region of *Palaeolagus haydeni* (FMNH PM9476) in ventral views **(A)**. The skull bones are transparent in order to show the auditory ossicles and bony labyrinth. **(B)** transversal μCT image through the auditory region. Note the small processus anterior (pram) of the malleus below the tegmen tympani in the left ear. The asterisk (*) indicates the lateral expansion of the epitympanic recess. Abbreviations: bl, bony labyrinth; bt, bulla tympani; co, cochlea; re, epitympanic recess; fv, fenestra vestibuli; in, incus; ma, malleus; mea; meatus acusticus externus; pbl, primary bony lamina; pe, petrosal; pram, processus anterior of malleus; pro, promontorium; st, stapes; tt, tegmen tympani. Scale bar = 5 mm.

The bulla is built exclusively by the ectotympanic, which laterally forms a short external auditory canal (meatus acusticus externus), projecting and opening dorsolaterally (**Figure 3B**). Anteriorly, a horizontal septum divides the cavum tympani into a dorsal and a ventral chamber. This septum continues into the bony ring that supports the tympanic membrane and forms the entrance of the meatus acusticus externus. There is no additional septum inside the bulla. On the dorsal side of the tympanic cavity, the epitympanic recess is situated posterolateral to the fenestra cochleae. The medial part of the epitympanic recess is a small,

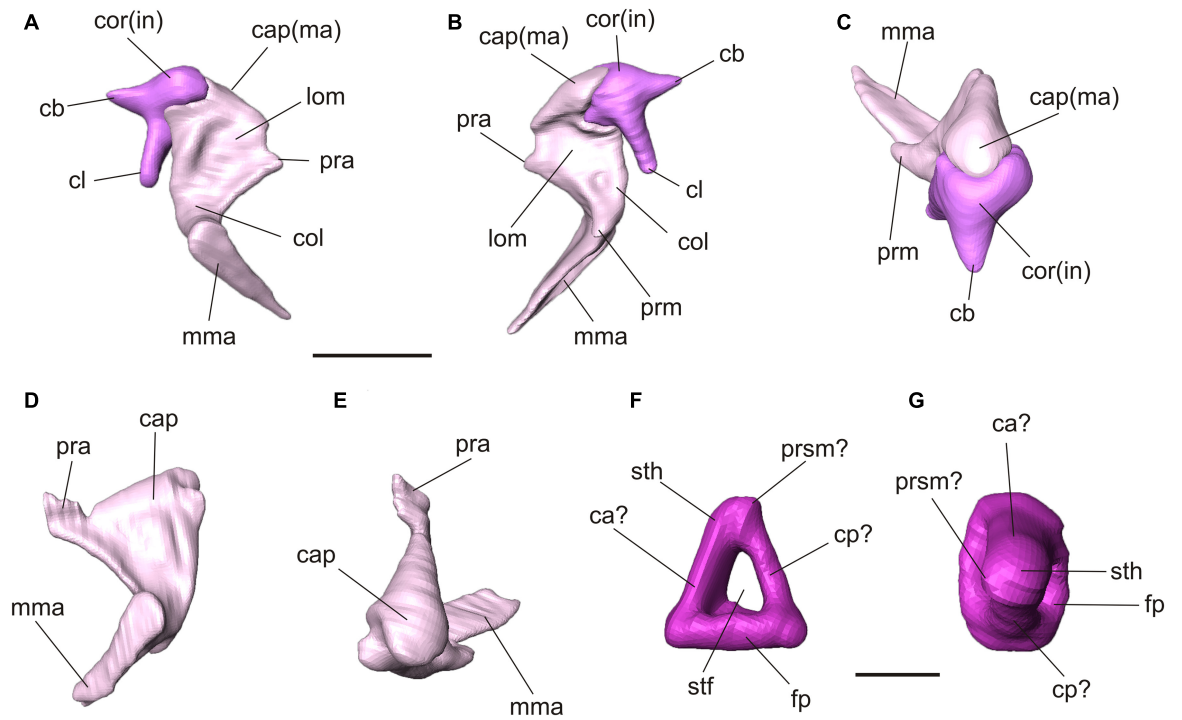

FIGURE 4 | Virtual 3D reconstructions of the auditory ossicles of *Palaeolagus haydeni* (FMNH PM9476). Color code refers to **Figure 3**. Articulated right malleus and incus in lateral **(A)**, medial **(B)** and dorsal **(C)** views. Note the incomplete processus anterior of the malleus. Left malleus in lateral **(D)** and dorsal **(E)** views. Ventral **(F)** and medial **(G)** views of the left stapes. Interpretation of orientation is tentative due to displacement and weaker preservation of the right stapes. Abbreviations: ca, crus anterior; cap, caput; cb, crus breve; cl, crus longum; cp, crus posterior; col, collum; cor, corpus; fp, footplate; in, incus; lom, lamina ossea mallei; ma, malleus; mma, manubrium mallei; pra, processus anterior; prm, processus muscularis; prsm, process for stapedial muscle; stf, stapedial foramen; sth, stapedial head. Scale bar for **(A–E)** = 2 mm, **(F–G)** = 1mm.

shallow fossa in the petrosal whereas, in contrast, its lateral part is expanded into a large chamber, extending anteriorly, laterally and dorsally (**Figure 3B**). This chamber is laterally bounded by the ectotympanic so that the squamosal is entirely excluded from the tympanic cavity. In ventral view, most of the lateral tympanic recess is covered by a bony lamina of the ectotympanic, which forms the dorsal wall of the external auditory canal and continuous anteriorly into the lamina anterior (**Figure 3B**). Anterolateral to the fossa for the tensor tympani muscle and anterior to the expanded epitympanic recess there is a large spherical chamber that develops entirely within the ectotympanic. This chamber is identified as the epitympanic sinus. On the intracranial side of the skull, the dorsal wall of the epitympanic sinus is exposed as an oval, convex patch between the petrosal and alisphenoid; thus, the ectotympanic contributes to the floor of the braincase.

The three auditory ossicles are preserved on both sides, mostly intact but displaced (**Figures 3**, **4**). The malleus and incus are still in articulation on both sides. They are embracing each other with their criss-cross articulation facets (**Figures 4A–C**). The malleus has a distinct caput that shows a smooth convex dorsal surface. Anteroventrally, it continues into a broad lamina ossea mallei. The collum and manubrium mallei form an angle about 90°; the manubrium is bent anteromedially and its lateral surface, which was attached to the tympanic membrane, is broadened. On the medial side, a prominent processus muscularis for attachment of the musculus tensor tympani is present (**Figures 4A–C**). Dorsal to this process the neck bears a distinct fossa (**Figure 4B**). The manubrium mallei of the left malleus is incomplete distally. The processus anterior is incomplete in the right malleus but intact in the left one (**Figures 4A–E**). In the higher resolution μCT scan, the attachment of the processus anterior to the roof of the middle ear cavity can be traced. The processus anterior is short but bends dorsolaterally and ends as a free rod in a small cavity between the tegmen tympani and ectotympanic (**Figures 3B**, **4D,E**). This cavity opens medially. A processus internus praearticularis is lacking. The incus shows a distinct crus breve and a significantly longer crus longum. A processus lenticularis is not visible because it may be broken (**Figures 4A–C**).

The right stapes is *in situ* but not well preserved and slightly projecting through the foramen vestibuli (**Figure 3**). Its footplate is incomplete. The left stapes is complete but displaced. The stapedial footplate is oval and flat. Both crura are prominent, positioned quite symmetrically at the rim of the footplate and embracing a distinct stapedial foramen. We tentatively interpret a small process next to the head of the left stapes as the process for the stapedial muscle. In the left stapes one crus is stronger and forms a half tube (**Figures 4F,G**). Although the right stapes is *in situ*, it can hardly be used for orientation as both crura show the same thickness and no stapedial muscle process is visible.

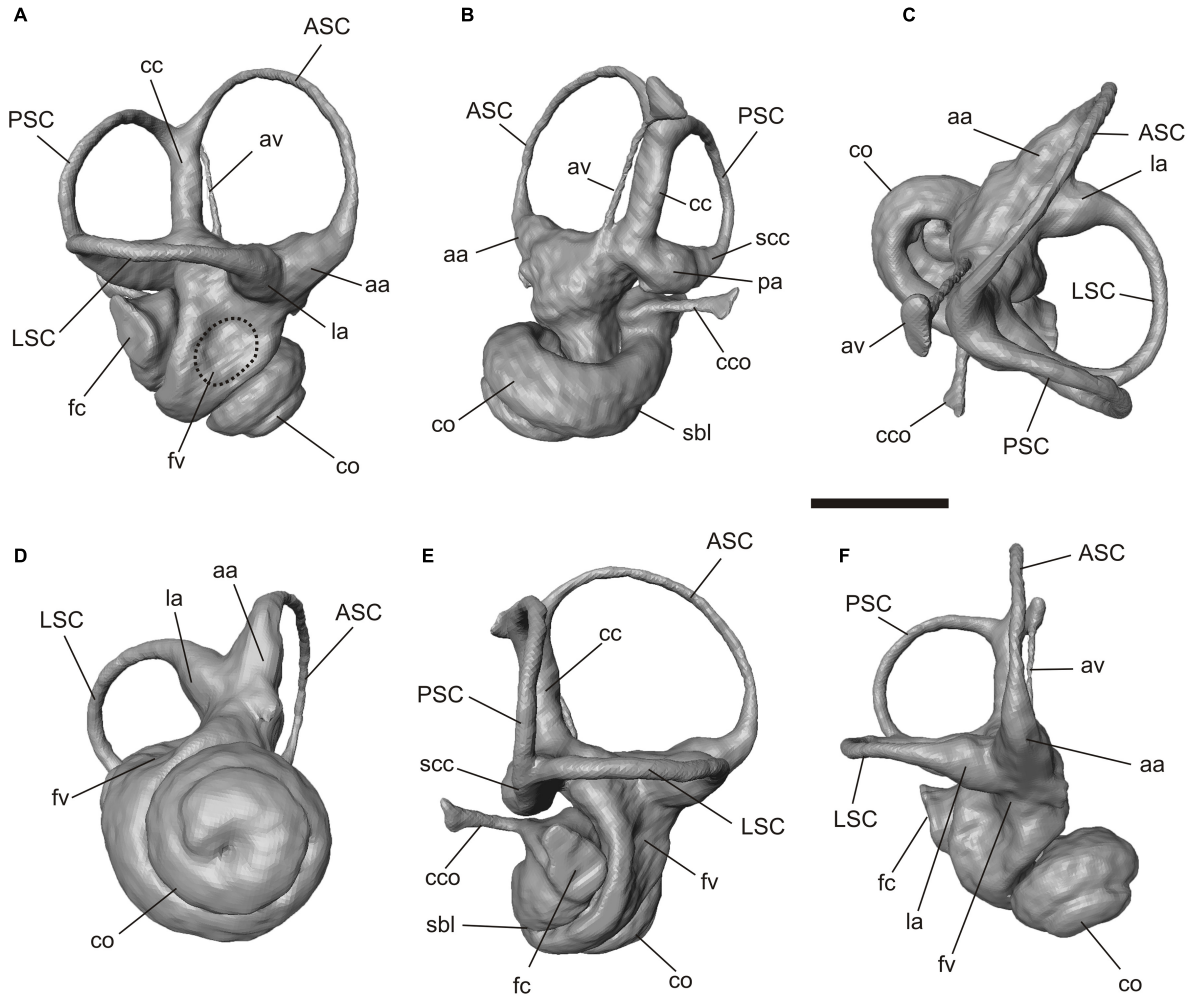

FIGURE 5 | Virtual 3D reconstruction of the right bony labyrinth of *Palaeolagus haydeni* (FMNH PM9476). **(A)** lateral, **(B)** medial, **(C)** dorsal, **(D)** ventral, **(E)** posterolateral and **(F)** anterolateral views. Abbreviations: aa, anterior ampulla; ASC, anterior semicircular canal; av, aquaeductus vestibuli; cc, crus commune; cco, canaliculus cochleae; co, cochlea; la, lateral ampulla; fc, fenestra cochleae; fv, fenestra vestibuli; LSC, lateral semicircular canal; pa, posterior ampulla; PSC, posterior semicircular canal; sbl, secondary bony lamina; scc, secondary crus commune. Scale bar = 2 mm.

Inner Ear

The ventral surface of the promontorium is gently rounded (**Figure 3B**). At its posterior end a nearly circular fenestra cochleae (*sive* rotunda) is present, not concealed by any bony outgrowth of the petrosal. On the lateral side of the promontorium there is a small, oval fenestra vestibuli (*sive* ovalis), facing lateroventrally (**Figure 3B**). The petrosal houses the bony labyrinth, a hollow space that is filled with the soft tissue structures and perilymphatics and endolymphatic fluids of the inner ear in the living animal.

The bony labyrinth is complete on both sides. The cochlea is tightly coiled, conic but relatively flat; it has 2.25 turns (**Figures 3A**, **5**). The secondary bony lamina that supports the basilar membrane together with the primary bony lamina extends up to a quarter of the basal turn (**Figures 5B,E**). The canaliculus cochleae is thin and relatively short. The pathways of the cochlear nerves that enter the internal auditory meatus and spread through the primary lamina can be traced. The three semicircular canals are thin but show a well pronounced curvature. In perpendicular view to their planes the anterior and lateral semicircular canals show an oval shape whereas the posterior semicircular canal is almost circular (**Figure 5**). The anterior semicircular canal is by far the largest in diameter (curvature) and its dorsalmost point is significantly higher than the crus commune, the joint section of the anterior and posterior semicircular canal (**Figures 5A,E**). This canal borders the entrance into a large and deeply excavated fossa subarcuata. The lateral semicircular canal forms a secondary crus commune together with the posterior semicircular canal (**Figures 5B,D**). This joint canal does only comprise the bony structures, but not the soft tissue ducts. While the anterior and lateral semicircular canal show almost no planar deviation the posterior semicircular canal is slightly undulating (**Figures 5C,E**). The ampullae of the canals are distinct but not significantly inflated. The aquaeductus

vestibuli leaves the vestibulum anterior to the crus commune and runs as a thin canal in a gentle curve next to the latter (**Figure 5B**).

DISCUSSION

Nasal Region

The turbinal pattern of *Palaeolagus haydeni* generally resembles that of extant Lagomorpha. Key characters of Lagomorpha, as revealed by extant species, are a dendritic maxilloturbinal, an excavated nasoturbinal that is continuous with the lamina semicircularis, two frontoturbinals, three ethmoturbinals and one interturbinal between ethmoturbinal I and II (see Ruf, 2014). All these characters are also present in *Palaeolagus haydeni*.

The highly dendritic maxilloturbinal observed in *Palaeolagus haydeni* and extant lagomorphs can be tentatively regarded as an apomorphic character. Some rodents (e.g., *Sciurus vulgaris*, *Castor canadensis*, *Cricetus cricetus*, and *Myocastor coypus*) also show a complex and up to highly dendritic maxilloturbinal that is constrained by functional adaptations at least in semiaquatic species (Ruf, 2014, 2020; Martinez et al., 2020). However, the grundplan pattern in Rodentia remains ambiguous. In Scandentia, Primates and Dermoptera the maxilloturbinal is a straight, scrolled or double-scrolled structure that can show further epiturbinals (additional lamellae) in the former (Maier and Ruf, 2014; Ruf, 2014; Ruf et al., 2015; Lundeen and Kirk, 2019) although such morphological complexity as in *Palaeolagus haydeni* and extant Lagomorpha is not achieved.

The lamina semicircularis of *Palaeolagus haydeni* shows a puzzling pattern. Similar to all extant Leporidae, the posterior margin of the lamina semicircularis is scrolled. Based on the present phylogeny, the straight lamina semicircularis of Ochotonidae has to be regarded a derived feature (**Figure 6**). However, a distinct ventral lamella is lacking in *Palaeolagus haydeni*, a trait shared with Ochotonidae. Because this pattern is also present in *Sciurus vulgaris* and muroid rodents, it can be regarded as a plesiomorphic feature for extant Lagomorpha as well as *Palaeolagus haydeni* (Ruf, 2014, 2020). In Scandentia, the lamina semicircularis has a distinct ventral lamella and a pronounced processus uncinatus (Ruf, 2014, 2020; Ruf et al., 2015; Lundeen and Kirk, 2019: lamina semicircularis labeled as nasoturbinal). A ventral lamina as well as processus uncinatus are also present at least in some primates (Maier, 1993; Maier and Ruf, 2014; Lundeen and Kirk, 2019: lamina semicircularis labeled

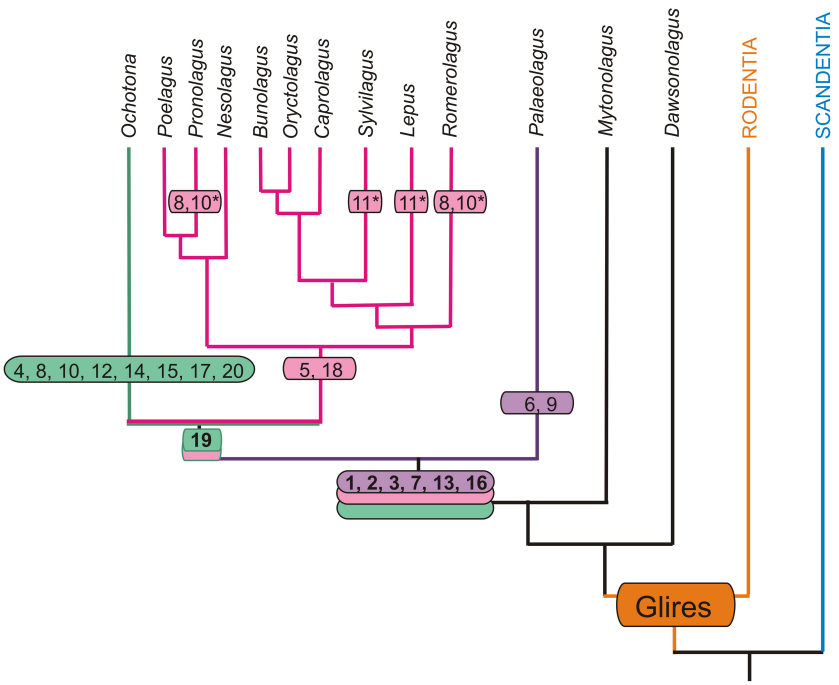

FIGURE 6 | Autapomorphic characters of the nasal and auditory regions in *Palaeolagus haydeni* and extant Lagomorpha mapped onto phylogeny of Matthee et al. (2004) and Fostowicz-Frelik and Meng (2013). Only those extant genera that have been previously investigated are considered (Ruf, 2014; Maier et al., 2018). Note that for *Nesolagus* data on the turbinal skeleton are not available. Apomorphic characters based on outgroup comparison (Rodentia + Scandentia): 1, dendritic maxilloturbinal; 2, excavated nasoturbinal contacts lamina semicircularis; 3, scrolled posterior margin of lamina semicircularis; 4, straight posterior margin of lamina semicircularis; 5, lamina semicircularis has a ventral lamina; 6, lamina semicircularis with anterolaterally projecting additional process; 7, interturbinal between frontoturbinal 1 and 2; 8, loss of interturbinal between frontoturbinal 1 and 2; 9, reduced frontoturbinal 2; 10, loss of ethmoturbinal III; 11, additional interturbinals; 12, bulla tympani strongly pneumatized; 13, contribution of ectotympanic to cranial floor (unclear in Ochotonidae); 14, caput mallei with distinct cristae; 15, loss of musculus tensor tympani; 16, anchoring of malleus via short processus anterior that ends in cavity formed by the ectotympanic and tegmen tympani; 17, anchoring of malleus via short processus anterior fused to bony trabeculae of pneumatized tegmen tympani (adult stages); 18, anchoring of malleus via extensive processus internus praearticularis fused to ectotympanic; 19, loss of secondary crus commune; 20, high cylindric cochlea; asterisk (*) denotes characters restricted to certain species.

as nasoturbinal). Unfortunately, detailed descriptions of the lamina semicircularis in adult stages are generally scarce and thus, information needs to be mostly drawn from the published figures. The processus uncinatus is proportionally longer in *Palaeolagus haydeni* than in Ochotonidae. The second processus of the lamina semicircularis as well as the anteroventrally orientation can be regarded as an apomorphic feature of *Palaeolagus haydeni*, as they are not known in any extant lagomorph species or outgroup member investigated so far (Maier and Ruf, 2014; Ruf, 2014, 2020; Ruf et al., 2015).

Similar to all extant species of Leporidae (except for *Pronolagus* spp. and *Romerolagus diazi*) *Palaeolagus haydeni* has three turbinals inside the frontoturbinal recess (two frontoturbinals and one large interturbinal in between), which is regarded as an apomorphic feature of this family. Ochotonids resemble the lagomorph grundplan in having only two frontoturbinals and lacking an interturbinal (Ruf, 2014).

Observations on prenatal stages of *Oryctolagus cuniculus* clearly show that after the development of the two frontoturbinals an additional turbinal, the interturbinal, occurs in-between in later fetal stages (Voit, 1909; Frick and Heckmann, 1955). In leporids both frontoturbinals are quite similar in size and the interturbinal is shorter than frontoturbinal 2 (Ruf, 2014). *Palaeolagus haydeni* shows a different pattern in that frontoturbinal 2 is very small. However, based on the comparison of the attachment and location of the three turbinals we conclude that *Palaeolagus haydeni* shows the leporid pattern with a highly reduced frontoturbinal 2 as an apomorphic character. Furthermore, given the likely systematic position of *Palaeolagus* outside crown Lagomorpha, three turbinals in the frontoturbinal recess could resemble the plesiomorphic grundplan pattern for Leporidae and instead the ochotonid pattern needs to be regarded apomorphic (**Figure 6**), although convergent evolution of the interturbinal in *Palaeolagus* and Leporidae would be equally parsimonious. Among Rodentia, Scandentia and Dermoptera two frontoturbinals are a common feature (Maier and Ruf, 2014; Ruf et al., 2015; Martinez et al., 2018; Lundeen and Kirk, 2019; Ruf, 2020) and likely represent the grundplan pattern of Euarchontoglires. In some species the recessus frontoturbinalis houses additional small interturbinals that tend to be variable (e.g., Maier and Ruf, 2014; Ruf, 2014). In primates the recessus frontoturbinalis becomes reduced in concert with the reduction and loss of the frontoturbinals; some strepsirrhines still show two or more frontoturbinals (Maier, 1993; Maier and Ruf, 2014; Smith et al., 2016; Lundeen and Kirk, 2019). Further investigation of stem lagomorphs would help elucidate the polarization of this character.

At first glance, it is tempting to interpret the small frontoturbinal 2 of *Palaeolagus haydeni* as an evolving third turbinal within the recessus frontoturbinalis. Regardless of whether this structure is interpreted as the frontoturbinal or interturbinal, this hypothesis would have considerable consequences for the homology of the respective turbinals. Interturbinals develop later in ontogeny and are hidden by the fronto- and ethmoturbinals in medial view; in many mammals they are smaller than the adjacent turbinals (Paulli, 1900; Reinbach, 1952a,b; Ruf, 2020). This pattern is supported by the prenatal ontogeny of *Oryctolagus cuniculus* as described above. Furthermore, in Ochotonidae both frontoturbinals are also of the same size (Ruf, 2014). Thus, evolutionary reduction of frontoturbinal 2 in *Palaeolagus haydeni* would be the most parsimonious hypothesis.

Although the turbinals of the ethmoturbinal recess are not fully preserved in *Palaeolagus haydeni*, their number (three ethmoturbinals and one interturbinal between ethmoturbinals I and II) resembles a common pattern observed in many Lagomorpha and Rodentia, all Scandentia, and some strepsirrhine primates, e.g., *Eulemur collaris* and *Galago senegalensis* (Ruf, 2014, 2020; Martinez et al., 2018; Lundeen and Kirk, 2019). At least for Glires this pattern might represent the grundplan character state. Four ethmoturbinals are present in Dermoptera and some Strepsirrhini, e.g., *Daubentonia madagascariensis* and *Indri indri* (Maier and Ruf, 2014; Lundeen and Kirk, 2019), and may reflect a basal pattern for Euarchontoglires. Haplorhini show a reduced number of ethmo- and interturbinals (Maier, 1993; Maier and Ruf, 2014; Lundeen and Kirk, 2019).

Auditory Region

The bulla tympani of *Palaeolagus haydeni* has a thin wall, similar to that generally present in extant Leporidae, but differs from the heavily pneumatized bulla in extant Ochotonidae (Cockerell et al., 1914; Maier et al., 2018). *Oryctolagus cuniculus* has also a thin wall of the bulla tympani but the lateral part is only slightly pneumatized (this study). The pattern observed in *Palaeolagus haydeni* and Leporidae can be regarded as plesiomorphic for Lagomorpha because it is a common pattern in mammals and also present in sciuromorph rodents and scandentians (Wible, 2009; Pfaff et al., 2015b). However, the sciuromorph rodents show a specific pattern of septa not comparable to that of the lagomorphs under study. The anterodorsal exposure of the ectotympanic at the floor of the braincase is also present in *Romerolagus diazi* and *Oryctolagus cuniculus* (this study). As this pattern is uncommon in mammals, it might be regarded as an apomorphic feature of *Palaeolagus haydeni* and Leporidae (Novacek, 1977). However, the contribution of the ectotympanic to the cranial floor has also been observed in *Desmodillus auricularis*, a small desert murid with heavily expanded auditory bullae (Mason, 2016: fig. 3B). In Ochotonidae, the dorsal extension of the ectotympanic cannot be discerned as the petrosal bone is also mostly pneumatized and no sutures can be traced (see figures in Maier et al., 2018). Investigation of perinatal stages could help to elucidate the origin of the roof of the cavum tympani. However, for the given phylogeny we tentatively regard this character as apomorphic for the clade comprising *Palaeolagus* and crown Lagomorpha (**Figure 6**).

In general, the auditory ossicles of *Paleolagus haydeni* resemble those of extant Lagomorpha, especially Leporidae (Doran, 1878; Cockerell et al., 1914; Fleischer, 1973; Maier et al., 2018). Similar to leporids, the stapes shows a flat footplate and no stapedial muscle process and the dorsal surface of the mallear head is smooth. The musculus tensor tympani was certainly also present in *Palaeolagus haydeni* as this species shows a prominent processus muscularis. The auditory ossicles of Ochotonidae differ in several respects: the stapes has a convex footplate and a small process for the stapedial muscle, a processus muscularis of the

malleus is missing due to the lack of the musculus tensor tympani, and the mallear head shows distinct cristae (Cockerell et al., 1914; Ruf et al., 2009; Maier et al., 2018). The cristae are most probably a derived character of the family. In this respect, *Palaeolagus haydeni* shows the plesiomorphic lagomorph pattern.

The most striking feature of the lagomorph auditory ossicles in terms of phylogenetic and morphofunctional implications is the processus anterior of the malleus, especially the processus internus praearticularis of Leporidae (Maier et al., 2018). According to Fleischer (1978), the auditory ossicles of Lagomorpha resemble the "freely mobile type" that is common in terrestrial mammals with medium-sized to large tympanic membrane. Here, the anterior process of the malleus is short and loosely attached to the roof of the tympanic cavity via the anterior ligament; the incus is also attached to the roof of the fossa incudis with a short ligament. Maier et al. (2018) clearly demonstrated that Lagomorpha show a much more complicated anatomy of the processus anterior of the malleus. In both living families a specific independently evolved pattern has been described. In Leporidae the thin processus internus praearticularis of the processus anterior is distally inflated (already in prenatal stages) and fused to the ectotympanic inside a bony cavity of the tympanic roof. In contrast, the processus internus praearticularis of Ochotonidae is very small and only present in prenatal stages; in adults the processus anterior is fused to bony trabeculae of the tegmen tympani (Maier et al., 2018). Until now, the two patterns in Lagomorpha could not have been polarized. *Palaeolagus haydeni* resembles the pattern in adult Ochotonidae in having a short processus anterior and no processus internus praearticularis and that of prenatal stages in having a laterally oriented tip of the processus anterior approaching the ectotympanic (see Maier et al., 2018: fig. 7i). The anterior attachment of the malleus in *Palaeolagus haydeni* resembles the pattern in Leporidae in certain aspects, although achieved with different parts of the malleus: a processus projecting into a small cavity formed by the ectotympanic bone. Furthermore, the processus anterior of *Palaeolagus haydeni* shows a different orientation than in extant Lagomorpha. It is clearly attached more laterally to the tympanic roof; a distortion of the delicate process during decomposition of the body cannot be excluded as this connection is very flexible (Mason, 2016; Maier et al., 2018). In certain rodents, the processus anterior is also a short tapering lamella attached to the roof of the tympanic cavity but no details on the attachment site are given (Mason, 2016). Thus, *Palaeolagus haydeni* resembles the plesiomorphic lagomorph pattern still present in early ontogenetic stages of Ochotonidae. In adult pikas the attachment would be adapted to the derived pattern of the highly pneumatized ectotympanic and petrosal. The extensive processus internus praearticularis of Leporidae is obviously derived from the lagomorph grundplan (see **Figure 6**). As proposed by Maier et al. (2018) for the auditory ossicles of Lagomorpha, *Palaeolagus haydeni* also resembles the "bone elasticity type."

The bony labyrinth of *Palaeolagus haydeni* shows some plesiomorphic features compared to the extant lagomorph species. It still has a secondary crus commune, a character absent in extant Lagomorpha and regarded to be plesiomorphic for Theria (Ekdale, 2013, 2016; Ruf et al., 2016). In *Romerolagus diazi*, *Oryctolagus cuniculus*, *Lepus californicus*, *Sylvilagus floridanus* and *Ochotona alpina*, the lateral semicircular canal has a separate entrance into the vestibule resulting in a plane of the canal dorsal to the ampulla of the posterior semicircular canal (Ekdale, 2013; this study). Among the investigated structures of the present study this is the only apomorphy of crown Lagomorpha (**Figure 6**).

Furthermore, the extant leporids have relatively thin semicircular canals with great curvatures, as observed in *Palaeolagus haydeni*, whereas the pikas show more eliptical semicircular canals (Ekdale, 2013; this study). Shape and size of the semicircular canals are constrained by the type of locomotion and agility of the respective species (e.g., Spoor et al., 2007; Billet et al., 2012; Malinzak et al., 2012; Berlin et al., 2013; Pfaff et al., 2015a, 2017). Thus, the thin and prominently arcuated semicircular canals of *Palaeolagus haydeni* indicate a more agile locomotion compared to leporids but different from ochotonids. In that regard, a detailed morphometric study of the semicircular canals of living and fossil Lagomorpha is needed to elucidate their locomotory adaptations and allow reconstructions of the behavior for fossil species. The flat and conic cochlea of *Palaeolagus haydeni* resembles the flat and conic shape observed in living Leporidae but differs from the high and cylindric cochlea in Ochotonidae (Ekdale, 2013; this study).

SUMMARY

In conclusion, the intracranial structures of the nasal and auditory regions of *Palaeolagus haydeni* contribute to our understanding of early lagomorph evolution and reveal a closer affinity to Leporidae than to Ochotonidae or members of the outgroup. In several characters, some of which are certainly plesiomorphic in lagomorphs, this fossil species resembles modern Leporidae. Common characters are the number of olfactory turbinals, the general morphology of the bulla tympani, shape and proportions of the semicircular canals and cochlea. However, *Palaeolagus haydeni* differs from modern Leporidae by plesiomorphic characters (e.g., the attachment of the malleus via its processus anterior, secondary crus commune) that still could justify a basal position within the lagomorph clade as proposed by Wolniewicz and Fostowicz-Frelik (2021). Apomorphic features of *Palaeolagus haydeni* are the reduced frontoturbinal 2 and the dorsal process at the lamina semicircularis. Future phylogenetic analyses including the presented herein characters of the nasal and auditory regions as well as data from further well-preserved fossil Lagomorpha could finally decide the phylogenetic position of *Palaeolagus haydeni* and its relatives.

DATA AVAILABILITY STATEMENT

The original contributions presented in the study are included in the article and the Dryad Digital Repository (https://doi.org/10.5061/dryad.kh189325r), further inquiries can be directed to the corresponding author/s.

AUTHOR CONTRIBUTIONS

ŁF-F and JM made the μCT scans. IR made the virtual 3D reconstructions. IR and ŁF-F wrote the manuscript and prepared the figures. All authors designed the project, analyzed data, discussed the results, and read and approved the final version.

FUNDING

This research was funded by National Science Centre (Cracow, Poland), Grant No. 2015/18/E/NZ8/00637 and an AMNH Roosevelt Research Fellowship to ŁF-F, and Deutsche Forschungsgemeinschaft DFG (German Research Foundation) Grant No. DFG RU 1496/4-1 to IR.

ACKNOWLEDGMENTS

We thank W. Simpson (FMNH) for access to the *Palaeolagus* FMNH PM9476 specimen and M. Hill (AMNH) for μCT-scanning of the skull, and the following colleagues for access to extant lagomorph specimens: R. Hutterer (Zoologisches Forschungsmuseum Alexander Koenig, Bonn, Germany), D. Möricke (Staatliches Museum für Naturkunde Stuttgart, Germany), F. Mayer (Museum für Naturkunde Berlin), A.A. Cohen (NCB Naturalis, Leiden, Netherlands), L. Costeur (Naturhistorisches Museum Basel, Switzerland), and D. Kalthoff and U. Johansson (Naturhistoriska riksmuseet, Stockholm, Sweden). We are grateful to J. Eberhardt (Senckenberg Forschungsinstitut und Naturmuseum Frankfurt) for support with segmentation of the μCT scans. Finally, we thank both reviewers who helped to improve the manuscript.

REFERENCES

Asher, R. J., Meng, J., Wible, J. R., McKenna, M. C., Rougier, G. W., Dashzeveg, D., et al. (2005). Stem Lagomorpha and the antiquity of Glires. *Science* 307, 1091–1094. doi: 10.1126/science.1107808

Asher, R. J., Smith, M. R., Rankin, A., and Emry, R. J. (2019). Congruence, fossils and the evolutionary tree of rodents and lagomorphs. *R. Soc. Open Sci.* 6:190387. doi: 10.1098/rsos.190387

Berlin, J. C., Kirk, E. C., and Rowe, T. B. (2013). Functional implications of ubiquitous semicircular canal non-orthogonality in mammals. *PLoS One* 8:e79585. doi: 10.1371/journal.pone.0079585

Billet, G., Hautier, L., Asher, R. J., Schwarz, C., Crumpton, N., Martin, T., et al. (2012). High morphological variation of vestibular system accompanies slow and infrequent locomotion in three-toed sloths. *Proc. R. Soc. B* 279, 3932–3939. doi: 10.1098/rspb.2012.1212

Cockerell, T. D. A., Miller, L. I., and Printz, M. (1914). The auditory ossicles of American rodents. *Bull. Am. Mus. Nat. Hist.* 33, 347–380.

Dawson, M. R. (1958). Later Tertiary Leporidae of North America. *Univ. Kansas Paleontol. Contr. Vertebr.* 6, 1–75.

Dawson, M. R. (2008). "Lagomorpha," in *Evolution of Tertiary Mammals of North America*, eds C. M. Janis, G. F. Gunnell, and M. D. Uhen (Cambridge: Cambridge University Press), 293–310. doi: 10.1206/0003-00902003275<0001:TOORMG<2.0.CO;2

Doran, A. H. G. (1878). Morphology of the mammalian ossicula auditus. *Trans. Linn. Soc. Lond. Zool.* 1, 371–497. doi: 10.1111/j.1096-3642.1878.tb00663.x

Ekdale, E. G. (2013). Comparative anatomy of the bony labyrinth (inner ear) of placental mammals. *PLoS One* 8:e66624. doi: 10.1371/journal.pone.0066624

Ekdale, E. G. (2016). Form and function of the mammalian inner ear. *J. Anat.* 228, 324–337. doi: 10.1111/joa.12308

Fleischer, G. (1973). Studien am Skelett des Gehörorgans der Säugetiere, einschließlich des Menschen. *Säugetierkdl. Mitt.* 21, 131–239.

Fleischer, G. (1978). Evolutionary principles of the mammalian middle ear. *Adv. Anat. Embr. Cell Biol.* 55, 1–70.

Fostowicz-Frelik, Ł (2013). Reassessment of *Chadrolagus* and *Litolagus* (Mammalia: Lagomorpha) and a new genus of North American Eocene lagomorph from Wyoming. *Am. Mus. Novit.* 3773, 1–76. doi: 10.1206/3773.2

Fostowicz-Frelik, Ł (2017). "Convergent and parallel evolution in early Glires (Mammalia)," in *Evolutionary Biology: Self/Nonself Evolution, Species and Complex Traits Evolution, Methods and Concepts*, ed. P. Pontarotti (Berlin: Springer), 199–216. doi: 10.1007/978-3-319-61569-1_11

Fostowicz-Frelik, Ł, and Meng, J. (2013). Comparative morphology of premolar foramen in lagomorphs (Mammalia: Glires) and its functional and phylogenetic implications. *PLoS One* 8:e79794. doi: 10.1371/journal.pone.0079794

Fostowicz-Frelik, Ł, Ruf, I., and Meng, J. (2021). Anatomy of the nasal and auditory regions of the fossil lagomorph *Palaeolagus haydeni*: systematic and evolutionary implications. *Dryad Dataset* doi: 10.5061/dryad.kh189325r

Frick, H., and Heckmann, U. (1955). Ein Beitrag zur Morphogenese des Kaninchenschädels. *Cells Tissues Organs* 24, 268–314. doi: 10.1159/000141047

Hennig, W. (1984). *Taschenbuch der Speziellen Zoologie Teil 1, Wirbellose I, Ausgenommen Gliedertiere*. Frankfurt: Verlag Harri Deutsch.

Hoyte, D. A. N. (1961). The postnatal growth of the ear capsule in the rabbit. *Am. J. Anat.* 108, 1–16. doi: 10.1002/aja.1001080102

King, A. M., Hall, J., Cranfield, F., and Sullivan, M. (2007). Anatomy and ultrasonographic appearance of the tympanic bulla and associated structures in the rabbit. *Vet. J.* 173, 512–521. doi: 10.1016/j.tvjl.2006.09.002

López-Torres, S., Bertrand, O. C., Lang, M. M., Silcox, M. T., and Fostowicz-Frelik, Ł (2020). Cranial endocast of the stem lagomorph *Megalagus* and brain structure of basal Euarchontoglires. *Proc. R. Soc. B* 287:20200665. doi: 10.1098/rspb.2020.0665

Lundeen, I. K., and Kirk, E. C. (2019). Internal nasal morphology of the Eocene primate *Rooneyia viejaensis* and extant Euarchonta: using μCT scan data to understand and infer patterns of nasal fossa evolution in primates. *J. Hum. Evol.* 132, 137–173. doi: 10.1016/j.jhevol.2019.04.009

Maier, W. (1993). Zur evolutiven und funktionellen Morphologie des Gesichtsschädels der Primaten. *Z. Morph. Anthrop.* 79, 279–299.

Maier, W., and Ruf, I. (2014). Morphology of the nasal capsule of Primates – with special reference to *Daubentonia* and *Homo*. *Anat. Rec.* 297, 1985–2006. doi: 10.1002/ar.23023

Maier, W., Tröscher, A., and Ruf, I. (2018). The anterior process of the malleus in extant Lagomorpha (Mammalia). *J. Morphol.* 279, 132–146. doi: 10.1002/jmor.20759

Malinzak, M. D., Kay, R. F., and Hullar, T. E. (2012). Locomotor head movements and semicircular canal morphology in primates. *Proc. Natl. Acad. Sci. U.S.A.* 109, 17914–17919. doi: 10.1073/pnas.1206139109

Martinez, Q., Clavel, J., Esselstyn, J. A., Achmadi, A. S., Grohé, C., Pirot, N., et al. (2020). Convergent evolution of olfactory and thermoregulatory capacities in small amphibious mammals. *Proc. Natl. Acad. Sci. U.S.A.* 117, 8958–8965. doi: 10.1073/pnas.1917836117

Martinez, Q., Lebrun, R., Achmadi, A. S., Esselstyn, J. A., Evans, A. R., Heaney, L. R., et al. (2018). Convergent evolution of an extreme dietary specialisation, the olfactory system of worm-eating rodents. *Sci. Rep.* 8:17806. doi: 10.1038/s41598-018-35827-0

Mason, M. J. (2016). Structure and function of the mammalian middle ear. I: large middle ears in small desert mammals. *J. Anat.* 228, 284–299. doi: 10.1111/joa.12313

Matthee, C. A., Vuuren van, B. J., Bell, D., and Robinson, T. J. (2004). A molecular supermatrix of the rabbits and hares (Leporidae) allows for the identification of five intercontinental exchanges during the Miocene. *Syst. Biol.* 53, 433–447. doi: 10.1080/10635150490445715

Meng, J., Hu, Y., and Li, C. (2003). The osteology of *Rhombomylus* (Mammalia, Glires): implications for phylogeny and evolution of Glires. *Bull. Am. Mus. Nat. Hist.* 275, 1–247. doi: 10.1206/0003-0090(2003)275<0001:toormg>2.0.co;2

Mennecart, B., Rössner, G. E., Métais, G., DeMiguel, D., Schulz, G., Müller, B., et al. (2016). The petrosal bone and bony labyrinth of early to middle Miocene European deer (Mammalia, Cervidae) reveal their phylogeny. *J. Morphol.* 277, 1329–1338. doi: 10.1002/jmor.20579

Novacek, M. J. (1977). Aspects of the problem of variation, origin and evolution of the eutherian auditory bulla. *Mammal Rev.* 7, 131–150. doi: 10.1111/j.1365-2907.1977.tb00366.x

Paulli, S. (1900). Über die Pneumaticität des Schädels bei Den Säugetieren. Eine morphologische Studie. III. Über die Morphologie des Siebbeins und die der Pneumaticität bei den Insectivoren, Hyracoideen, Chiropteren, Carnivoren, Pinnipedien, Edentaten, Rodentiern, Prosimiern und Primaten, nebsteiner zusammenfassenden Übersicht über die Morphologie des Siebbeins und die der Pneumaticität des Schädels bei den Säugethieren. *Morphol. Jb.* 28, 483–564.

Pfaff, C., Martin, T., and Ruf, I. (2015a). Bony labyrinth morphometry indicates locomotor adaptations in the squirrel-related clade (Rodentia, Mammalia). *Proc. R. Soc. B* 282:20150744. doi: 10.1098/rspb.2015.0744

Pfaff, C., Martin, T., and Ruf, I. (2015b). "Septal compass" and "septal formula": a new method for phylogenetic investigations of the middle ear region in the squirrel-related clade (Rodentia: Mammalia). *Org. Divers. Evol.* 15, 721–730. doi: 10.1007/s13127-015-0222-x

Pfaff, C., Nagel, D., Gunnell, G., Weber, G. W., Kriwet, J., Morlo, M., et al. (2017). Palaeobiology of *Hyaenodon exiguus* (Hyaenodonta, Mammalia) based on morphometric analysis of the bony labyrinth. *J. Anat.* 230, 282–289. doi: 10.1111/joa.12545

Reinbach, W. (1952a). Zur Entwicklung des Primordialcraniums von *Dasypus novemcinctus* Linné (*Tatusia novemcincta* Lesson). Teil 1. *Z. Morphol. Anthropol.* 44, 375–444.

Reinbach, W. (1952b). Zur Entwicklung des Primordialcraniums von *Dasypus novemcinctus* Linné (*Tatusia novemcincta* Lesson). Teil 2. *Z. Morphol. Anthropol.* 45, 1–72. doi: 10.1007/978-3-319-23534-9_1

Ruf, I. (2014). Comparative anatomy and systematic implications of the turbinal skeleton in Lagomorpha (Mammalia). *Anat. Rec.* 297, 2031–2046. doi: 10.1002/ar.23027

Ruf, I. (2020). Ontogenetic transformations of the ethmoidal region in Muroidea (Rodentia, Mammalia): new insights from perinatal stages. *Vert. Zool.* 70, 383–415. doi: 10.26049/VZ70-3-2020-10

Ruf, I., Frahnert, S., and Maier, W. (2009). The chorda tympani and its significance for rodent phylogeny. *Mamm. Biol.* 74, 100–113. doi: 10.1016/j.mambio.2008.01.002

Ruf, I., Janßen, S., and Zeller, U. (2015). The ethmoidal region of the skull of *Ptilocercus lowii* (Ptilocercidae, Scandentia, Mammalia) – a contribution to the reconstruction of the cranial morphotype of primates. *Primate Biol.* 2:89. doi: 10.5194/pb-2-89-2015

Ruf, I., Volpato, V., Rose, K. D., Billet, G., de Muizon, C., and Lehmann, T. (2016). Digital reconstruction of the inner ear of *Leptictidium auderiense* (Leptictida, Mammalia) and North American leptictids reveals new insight into leptictidan locomotor agility. *Pal. Z.* 90, 153–171. doi: 10.1007/s12542-015-0276-2

Smith, T. D., Martell, M. C., Rossie, J. B., Bonar, C. J., and Deleon, V. B. (2016). Ontogeny and microanatomy of the nasal turbinals in Lemuriformes. *Anat. Rec.* 299, 1492–1510. doi: 10.1002/ar.23465

Spoor, F., Garland, T., Krovitz, G., Ryan, T. M., Silcox, M. T., and Walker, A. (2007). The primate semicircular canal system and locomotion. *Proc. Natl. Acad. Sci. U.S.A.* 104, 10808–10812. doi: 10.1073/pnas.0704250104

Voit, M. (1909). Das Primordialcranium des Kaninchens. *Anat. Hefte* 38, 425–616. doi: 10.1007/BF02214638

Wagner, F., and Ruf, I. (2019). Who nose the borzoi? Turbinal skeleton in a dolichocephalic dog breed (*Canis lupus familiaris*). *Mamm. Biol.* 94, 106–119. doi: 10.1016/j.mambio.2018.06.005

Wible, J. R. (2007). On the cranial osteology of the Lagomorpha. *Bull. Carnegie Mus. Nat. Hist.* 39, 213–234. doi: 10.2992/0145-9058(2007)39[213:otcoot]2.0.co;2

Wible, J. R. (2009). The ear region of the pen-tailed treeshrew, *Ptilocercus lowii* Gray, 1848 (Placentalia, Scandentia, Ptilocercidae). *J. Mammal. Evol.* 16:199. doi: 10.1007/s10914-009-9116-z

Wible, J. R., Rougier, G. W., Novacek, M. J., and Asher, R. J. (2009). The eutherian mammal *Maelestes gobiensis* from the late Cretaceous of Mongolia and the phylogeny of Cretaceous Eutheria. *Bull. Am. Mus. Nat. Hist.* 327, 1–123. doi: 10.1206/623.1

Wolniewicz, A. S., and Fostowicz-Frelik, Ł (2021). CT-informed skull osteology of *Palaeolagus haydeni* (Mammalia: Lagomorpha) and its bearing on the reconstruction of the early lagomorph body plan. *Front. Ecol. Evol.* 9:56. doi: 10.3389/fevo.2021.634757

Conflict of Interest: The authors declare that the research was conducted in the absence of any commercial or financial relationships that could be construed as a potential conflict of interest.

frontiers in Ecology and Evolution

ORIGINAL RESEARCH
published: 24 June 2021
doi: 10.3389/fevo.2021.638754

Effects of Sex and Breeding Status on Skull Morphology in Cooperatively Breeding Ansell's Mole-Rats and an Appraisal of Sexual Dimorphism in the Bathyergidae

Kai R. Caspar, Jacqueline Müller and Sabine Begall**

Department of General Zoology, Faculty of Biology, University of Duisburg-Essen, Essen, Germany

African mole-rats of the genus *Fukomys* (Northern common mole-rats) combine a monogamous mating system and pronounced sexual size dimorphism; a pattern highly untypical for mammals. At the same time, they live in cooperatively breeding groups composed of reproductive and non-reproductive members of both sexes. How and to which degree sex and breeding status influence morphofunctional characters in eusocial mole-rats is not well characterized but essential to come to a comprehensive understanding of their peculiar social system. Here, we explore patterns of morphological differentiation in skulls of Ansell's mole-rats (*Fukomys anselli*) by means of multivariate analysis of linear skull measurements combined with a 2D shape analysis of cranium and mandible. Compared to females, males display larger skulls relative to body size and show an expansion of the facial portion of the cranium, while reproductive status did not have an effect on any of the traits studied. We also show that species of *Fukomys* mole-rats display a scaling of relative sexual body size dimorphism in compliance to Rensch's rule, which is deemed indicative of intense male intrasexual competition. For the bathyergid family as a whole, results of scaling analyses were more ambiguous, but also indicative of Rensch's rule conformity. In line with genetic field data, our results point to a greater role of male-male conflicts in *Fukomys* than is traditionally assumed and support the notion that reproductive status does not correlate with morphofunctional segregation in these unusual rodents.

Keywords: Bathyergidae, Rensch's rule, shape analysis, osteology, geometric morphometrics

OPEN ACCESS

Edited by:
Lucja A. Fostowicz-Frelik, Institute of Paleobiology, Polish Academy of Sciences, Poland

Reviewed by:
Daniel Frynta, Charles University, Czechia
Wieslaw Bogdanowicz, Museum and Institute of Zoology, Polish Academy of Sciences, Poland

****Correspondence:***
Kai R. Caspar
kai.caspar@uni-due.de
Sabine Begall
sabine.begall@uni-due.de

Specialty section:
This article was submitted to Behavioral and Evolutionary Ecology, a section of the journal Frontiers in Ecology and Evolution

Received: *08 December 2020*
Accepted: *11 May 2021*
Published: *24 June 2021*

Citation:
Caspar KR, Müller J and Begall S (2021) Effects of Sex and Breeding Status on Skull Morphology in Cooperatively Breeding Ansell's Mole-Rats and an Appraisal of Sexual Dimorphism in the Bathyergidae. Front. Ecol. Evol. 9:638754. doi: 10.3389/fevo.2021.638754

INTRODUCTION

African mole-rats (Bathyergidae) are a speciose group of sub-Saharan rodents which are renowned for their superb adaptation to life underground (Gomes Rodrigues et al., 2016). Despite their ecological uniformity and specialization, bathyergids encompass species with strongly contrasting social systems (**Figure 1**). The genera *Bathyergus* (dune mole-rats), *Georychus* (Cape mole-rat), and *Heliophobius* (silvery mole-rat) lead strictly solitary lives, while the sister genera *Cryptomys* (Southern common mole-rats) and *Fukomys* (Northern common mole-rats) as well as the basalmost branching

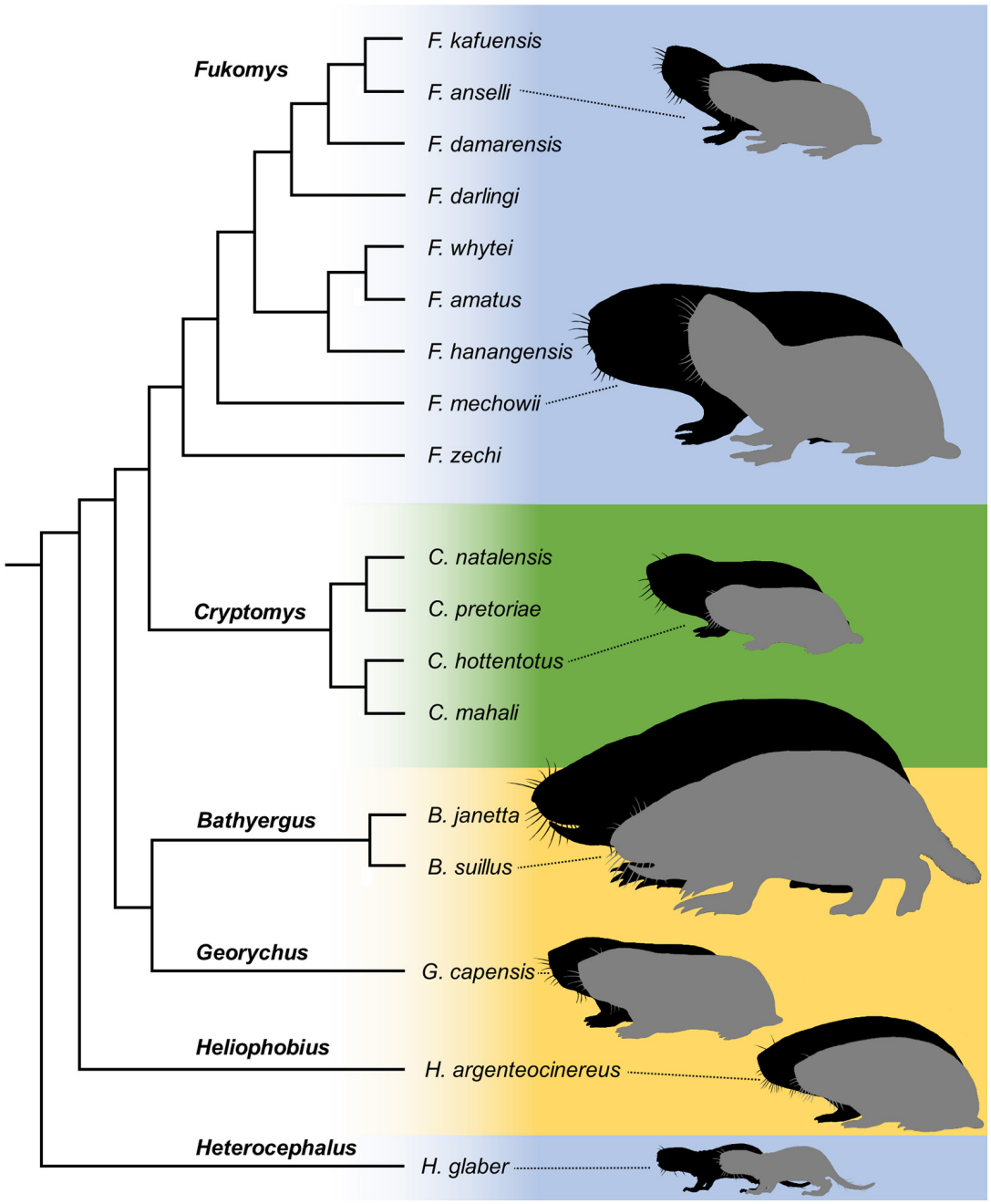

FIGURE 1 | Taxonomy, sexual size dimorphism and social systems of African mole-rats following Visser et al. (2019). Silhouettes indicate variation of body size between species and the degree of dimorphism between the sexes (males = black, females = gray, sexes and species only roughly set to scale for purposes of comprehension). Colors indicate social systems realized in the respective genera: blue – eusocial groups; green – social groups; and yellow – solitary. Silhouettes by Kai R. Caspar.

bathyergid genus *Heterocephalus* (naked mole-rat), live in cooperatively breeding groups. These families typically comprise only a single breeding female in all social genera, while the number of simultaneously active reproductive males varies.

In *Fukomys*, the reproductive female is typically monogamous (Burland et al., 2002; Šumbera et al., 2012; Patzenhauerová et al., 2013). When applying the term monogamy, it is important to differentiate between social monogamy (living and raising offspring with a single partner) and genetic monogamy (exclusively mating and producing offspring with such partner). Many socially monogamous mammals are not genetically monogamous (Cohas and Allainé, 2009). However,

current evidence suggests that *Fukomys* indeed exhibits strict social and predominant sexual monogamy, the latter fluctuating in frequency between populations (Burland et al., 2002; Patzenhauerová et al., 2013). While staying faithful to their current mate for prolonged periods (Bappert et al., 2012; Begall et al., 2021), *Fukomys* may experience serial changes in partners over their lifetime (Burland et al., 2002; Šumbera et al., 2012; Patzenhauerová et al., 2013). Different mating systems are expressed in the other two social bathyergid genera. The breeding female in *Heterocephalus* families may mate with two (seldom more) males at a time (Braude et al., 2020) and in *Cryptomys* it often has multiple partners (Bishop et al., 2004). In *Heterocephalus* as well as in *Fukomys*, more than six generations of pups overlap in average family groups and the majority of offspring remains with their parents and assist in provisioning their siblings instead of reproducing themselves (Burda et al., 2000; Torrents-Ticó et al., 2018). Because of this high degree of philopatry in combination with partitioning of reproductive labor and cooperative breeding, these genera have at times been characterized as eusocial mammals (Burda et al., 2000). In *Cryptomys*, levels of philopatry and male reproductive skew are notably lower than in the other social genera (Bishop et al., 2004; Ingram et al., 2004) so that they are generally not considered to be eusocial. Less is known about the mating systems of solitary genera, but morphological, genetic and behavioral evidence suggests that they are either polygynous or promiscuous (Patzenhauerová et al., 2010; Bray et al., 2012; Visser et al., 2017).

In social mole-rats such as *Fukomys*, non-reproductive individuals are believed to reduce the workload of the breeding female, granting a fitness benefit (Burda et al., 2000). Empirical evidence in support of this assumption has been provided for *Fukomys damarensis*, the Damaraland mole-rat. In captivity, the fecundity of *F. damarensis* breeding females as well as the time they spend resting and feeding correlates positively with the number of non-reproductive helpers (Houslay et al., 2020) and in the wild, breeders spend significantly less time foraging than helpers (Francioli et al., 2020). Although at times stated differently, mole-rat helpers do not show developmentally fixed patterns of task specialization (Lacey and Sherman, 1991; Zöttl et al., 2016; Thorley et al., 2018b; Van Daele et al., 2019), meaning that no helper casts dedicated to specific tasks (e.g., foraging, pup raising, and nest defense) exist, as it is the case in many social insects. Rather than that, an individual's age influences the frequency in which it engages in specific helping behaviors (Zöttl et al., 2016), with differences in the contributions of male and female helpers being negligible (Thorley et al., 2018b).

Due to the differing social and mating systems among bathyergids, it would be predicted that mole-rat genera display varying patterns of sexual size dimorphism (SSD) and sexually selected weaponry directly linked to their mating system (Heske and Ostfeld, 1990; Schulte-Hostedde, 2007). In the solitary genera, one would predict pronounced SSD since access to partners is contested and individual males can gain a reproductive advantage by mating with multiple females via the monopolization of defendable resources. Fitting this assumption, pronounced SSD is found in many solitary subterranean rodents that belong to diverse evolutionary lineages (Daly and Patton, 1986; Mauk et al., 1999; Su et al., 2018). A conjoint prediction would be that males in these species evolve more formidable weapons, in case of mole-rats more powerful and robust jaws and incisors, to solve this task. More subtle or absent sexual dimorphism would be expected in the social genera, particularly so in monogamous *Fukomys*, where physical breeding competition is low for prolonged periods once a pair-bond is established (Patzenhauerová et al., 2013). Among the few non-bathyergid social subterranean rodents, monogamy and a lack of SSD is for instance evident in the Northern mole vole (*Ellobius talpinus*; Moshkin et al., 2001). On the other hand, it might be expected that these social genera display differences in functional morphology that relate to reproductive status, for example more strongly developed weaponry in breeders of both sexes to defend their status against challengers (Young and Bennett, 2013). Such hypotheses appear reasonable, since at least female breeders in *Fukomys* and *Heterocephalus* show marked changes in their postcranial skeletal anatomy when attaining breeding status (Dengler-Crish and Catania, 2007; Thorley et al., 2018a), indicating a notable degree of developmental plasticity. So far, such differences are not evident in the skulls of female mole-rats (Thorley et al., 2018a) but precise methods such as geometric morphometrics have not yet been employed to differentiate between reproductive status groups and male mole-rats were never studied at all in this respect.

Surprisingly, SSD expression does not appear to correlate with social systems or phylogeny among bathyergids (Burda, 1990, **Figure 1**). Although these patterns are inconsistent and counterintuitive, the phenomenon received only little scientific attention and is seldom comparatively assessed: The solitary *Bathyergus* and at least most species of eusocial *Fukomys* are highly sexually dimorphic in body size with adult males being the larger sex with more massive skulls (Hart et al., 2007; Chimimba et al., 2010; Young and Bennett, 2013). Nevertheless, potential dimorphism in skull shape unrelated to size remains essentially unaddressed in these genera (but see Faulkes et al., 2017 for *Fukomys*). Within the remaining groups of African mole-rats, available studies suggest that skulls are not sexually dimorphic (Taylor et al., 1985; van Rensburg et al., 2004; Barčíová et al., 2009) and that differences in body size are variably expressed. Solitary *Heliophobius* are notably dimorphic in mass (Šumbera et al., 2003). For male-biased SSD in social *Cryptomys*, contradictory results have been published, but studies relying on data from multiple family groups agree that it is indeed present to varying degrees (Spinks et al., 2000; van Rensburg et al., 2004). Finally, eusocial *Heterocephalus* as well as solitary *Georychus* are assumed to lack SSD (Brett, 1991; Jarvis and Bennett, 1991; Bennett et al., 2006, see also Thomas et al., 2012).

If no clear relationship with sociality is evident, what factors underly the expression of SSD in African mole-rats? In many animal groups, SSD scales with body mass, a phenomenon most prominently described by Rensch's rule (Abouheif and Fairbairn, 1997). Rensch's rule posits that among closely related species, SSD grows with increasing general body size when males are the larger sex (Rensch, 1950) and *vice versa* when the opposite is the case (Rensch, 1960, but see Webb and Freckleton, 2007). However, it is commonly assumed that Rensch's rule can only be observed

among socially polygynous or polygamous species (Dale et al., 2007; Bidau and Martinez, 2016) so that bathyergids and even more so *Fukomys* species would not be expected to comply to it. In other subterranean rodents studied so far, the polygynous South American tuco-tucos (*Ctenomys*) and Central Asian zokors (*Eospalax* and *Myospalax*), Rensch's rule is not in effect (Martínez and Bidau, 2016; Su et al., 2018), and notable SSD appears to be rare among small-bodied mammals in general (Lu et al., 2014). Finding Rensch's rule among bathyergids would be unexpected and could indicate so far unappreciated social dynamics acting across the boundaries of social systems in this group.

In this exploratory study, we focus on patterns of sexual dimorphism and correlates of breeding status in *Fukomys anselli*, the Ansell's mole-rat. *F. anselli* is a typical representative of its genus in displaying the puzzling combination of pronounced SSD in conjunction with prolonged sexual monogamy and cooperative breeding (Burda and Begall, 1998; Patzenhauerová et al., 2013). Besides employing craniometric methods to assess morphological differentiation, we also quantify differences in relative skull size between the sexes. This phenomenon received little study in mammals (but see Young and Bennett, 2013) but is well investigated in squamate reptiles, where it is prominently discussed as an indicator for intrasexual competition (e.g., Baird, 2013). To place sexual dimorphism in the Ansell's mole-rat into its phylogenetic context, we further compile a dataset on body mass in the sexes of various bathyergid species and test for SSD scaling conforming to Rensch's rule. By combining these different approaches, we aim to arrive at a comprehensive characterization of sexual dimorphism in cooperatively breeding *Fukomys* mole-rats, which is a crucial step to understand the interplay between monogamous mating systems and pronounced SSD found in these animals.

MATERIALS AND METHODS

SSD and the Validity of Rensch's Rule in the Bathyergidae

We conducted a literature search for information on sex-specific body mass in the Bathyergidae and concluded with a dataset spanning 18 species from all six extant genera, which cover almost the complete spectrum of body sizes found in the family, including size extremes (**Table 1**). The genus *Fukomys* is represented by nine species. Species were included when data for at least five specimens per sex and species corresponding to wild adult animals were available. Data from pregnant females were excluded, whenever provided by the respective sources. Following Ingram et al. (2004), we refer to populations of *Cryptomys* (*C. hottentotus*, *C. mahali*, *C. natalensis*, and *C. pretoriae*) as full species, since the age of these lineages as well as their genetic divergence exceeds that of many *Fukomys* populations which are differentiated at the species level.

We tested for the validity of Rensch's rule in both bathyergids in general and in *Fukomys* by employing two established methods to investigate SSD scaling. If both were to yield comparable outcomes, the respective results could be assumed to be robust. First, we employed phylogenetic reduced major axis (pRMA) regression, a widely accepted method to study scaling in SSD (Abouheif and Fairbairn, 1997; Fairbairn, 1997; Bidau and Martinez, 2016; Martínez and Bidau, 2016), by utilizing the *phytools* package in R (Revell, 2012). For such interspecific comparisons, phylogenetic relationship must be accounted for to address the non-independence of species data points due to shared ancestry. Based on the bathyergid phylogeny of Visser et al. (2019; see **Figure 1**), we calculated pRMA regressions of $\log_{10}$(male body mass) on $\log_{10}$(female body mass) to estimate whether SSD in bathyergids scales with body mass in compliance with Rensch's rule. The rule is in effect when the coefficient β of said regressions is significantly greater than the expected value 1 (Abouheif and Fairbairn, 1997; Martínez and Bidau, 2016). Clarke's T statistic with adjusted degrees of freedom was employed to assess the deviation of the slope from the expectation (Bidau and Martinez, 2016).

Second, we calculated phylogenetic linear regression models based on modified Lovich-Gibbons' ratios (two-step LG ratio) on $\log_{10}$(female body mass) as recommended by Smith (1999). The two-step LG ratio is calculated as follows: If the mean body mass of males is higher than that of females: M/F; if the mean body mass of females is higher than that of males: 2-F/M. Smith (1999) recommends the application of the two-step LG ratio for typical mammalian data sets where male-biased SSD is prevalent. Linear regression models were corrected for phylogeny by using phylogenetic independent contrasts. According to this method, Rensch's rule is in effect when the coefficient β of the regression line is significantly greater than 0.

Skull Morphometrics of *Fukomys anselli*

All morphometric data was collected blindly with the researchers taking measurements being unaware of sex and reproductive status of the specimen concerned. All analyses, if not otherwise indicated, were carried out in R Studio for Mac Version 1.3.1093 (RStudio Team, 2020).

Material

Skulls of 40 adult *Fukomys anselli*, representing ten non-breeders and ten breeders of either sex were extracted from ethanol-fixed or frozen animals from the research collection of the Department of General Zoology, University of Duisburg-Essen (**Supplementary Table 1**). Respective individuals were kept and often bred in the laboratories of the University but genealogically derive from animals captured close to the type locality of the species in the Lusaka area of Central Zambia. Relying on captive subjects allowed for an unequivocal determination of an individual's reproductive status, as breeding was closely monitored in the laboratory. Only captive-born individuals that never reproduced where classified as non-breeders, while breeders where required to have produced at least one offspring. All skulls derived from animals that were at least 30 months old at the time of death and therefore fully mature. *F. anselli* is full grown at an age of approximately 12 months (Burda and Begall, 1998). Mean age for breeders was 111.2 months (=9.3 years; SD: 41.4 months), while mean age for helpers was 57.9 months (=4.8 years; SD: 36.3 months). This stark discrepancy is largely explained by the bimodal aging pattern in the genus *Fukomys*,

TABLE 1 | Mean body mass (BM, *g*) and sexual size dimorphism (SSD, male:female) based on BM in African mole-rats.

Species	n_{males}	$n_{females}$	BM_{males}	$BM_{females}$	SSD	References
Bathyergus janetta	100	106	429.4	330.4	1.30	Herbst et al., 2004
Bathyergus suillus	87	100	955.2	778.5	1.23	Bennett et al., 2009
Cryptomys hottentotus	31	19	77	57	1.35	Jarvis and Bennett, 1991
Cryptomys mahali	8	8	131	92.1	1.42	van Jaarsveld et al., 2019
Cryptomys natalensis	106	95	108.8	77.3	1.41	Oosthuizen, 2008
Cryptomys pretoriae	96	184	100.5	90.7	1.11	van Rensburg et al., 2004
Fukomys amatus	9	5	71.6	65.2	1.10	Scharff, 1998
Fukomys anselli	87	86	63	52.9	1.19	Sichilima et al., 2011
Fukomys damarensis	290	281	165	141.5	1.17	Bennett and Jarvis, 2004
Fukomys darlingi	23	20	69.5	63.5	1.10	Bennett et al., 1994; Gabathuler et al., 1996
*Fukomys hanangensis**	12	5	89.7	78.2	1.15	Faulkes et al., 2017
Fukomys kafuensis sensu lato*	5	12	89.8	75.6	1.19	Van Daele et al., 2019, reclassified according to Visser et al., 2019
Fukomys mechowii	79	76	570.7	391.8	1.46	Sichilima et al., 2008
*Fukomys whytei**	11	11	131.1	107.3	1.22	Burda et al., 2005; Faulkes et al., 2017
Fukomys zechi	28	29	234.1	202.2	1.16	Yeboah and Dakwa, 2002
Georychus capensis	189	277	193.1	195.8	0.99	Bennett et al., 2006; Thomas et al., 2012; Visser et al., 2017
Heliophobius argenteocinereus	70	74	190.1	162.1	1.17	Šumbera et al., 2003
Heterocephalus glaber	n_{total} = 651		34.1	36.5	0.93	Brett, 1991

*In case that data were pooled from different studies, weighted means have been calculated. Data presented refer to adult animals measured in the wild (age class assignment followed respective references). *only unequivocally sexed specimens with body masses equal to or above 50 g were considered and, if applicable, those in adult dental age categories as assigned by the respective authors. The two-step Lovich-Gibbons' ratios (Smith, 1999) were identical with SSD values to the second decimal place.*

with breeders reaching on average two times the age of helpers in captivity (Dammann and Burda, 2006). However, mean ages of males (7.8 years; SD: 49.2 months) and females (6.3 years; SD: 44 months) did not differ significantly (Student's *t*-Test, $p > 0.2$). Each specimen derived from a different litter and for the most part from different families. Only two pairs of different aged siblings were sampled, all of the respective individuals being non-breeders.

Multivariate Skull Morphometrics

A set of 24 linear measurements from cranium and mandible (**Table 2**) were collected with digital calipers (fixpoint® model 77001). Measurements were taken by a single observer (KRC) to 0.1 mm from either the sagittal plane or the right side of the skull (see **Table 2** and **Supplementary Table 1**) and are visualized in **Figure 2**. In case relevant structures of the right side of the skull were damaged, measurements were taken from the left one (11 measurements = 1.1% of total measurements). Missing measurements [10 measurements = 1% of total measurements (n = 950), see **Supplementary Table 1**] were estimated using the *LOST* package (Arbour and Brown, 2020). Hindfoot length was chosen as a proxy for body size to assess its influence on cranial measurements. Foot length is a common metric in small mammal research that is insensitive to changes in body condition and was measured to the nearest 0.1 mm excluding claws, following Ansell (1965).

Measurements were log-transformed and analyzed using principal component analysis (PCA). Subsequently, leave-one-out cross-validated linear discriminant function analysis (LDA) was performed on the principal components (PC) generated by the PCA to estimate how well sexes and breeding status groups could be differentiated based on cranial measurements. One-tailed exact binomial tests were used to check whether correct assignment rates differed significantly from chance level. Suitability of PC covariance for LDA was tested with Box's *M* test. The assumption of multivariate normality was tested using the Shapiro–Wilk multivariate normality test. A MANOVA was used to test for the effects of body size, sex, and reproductive status as well as their interaction on skull morphology. Comparisons of each linear measurement between the respective groups of specimens were performed by employing Welch's two sample *t*-test for normally distributed measurements and Wilcoxon rank sum test for non-normally distributed ones, respectively, controlling for alpha error accumulation via Bonferroni correction. This resulted in an adjusted significance level of $\alpha_{adjusted} = 0.002$.

2D Geometric Morphometrics of Cranium and Mandible

Size-independent differences in skull shape were analyzed by employing a 2D landmark approach. Crania were photographed with a Canon EOS 200D reflex digital camera in a standardized fashion from dorsal and ventral perspectives. Mandibles were photographed from a lateral perspective. Specimens were placed on a checkered mat with squares of 1 cm edge length that was used to provide spatial orientation and acted as a size reference. The inclination of the crania was adjusted with a piece of plasticine. The camera focus was adjusted on the molars

TABLE 2 | Summary of linear cranial measurements collected for multivariate morphometric analysis.

Measurement	Abbreviation	Description
Length of diastema	DIAS	Distance between alveoli of the upper incisor and premolar.
Palatilar length	PALA	Distance between staphylion and the alveoli of the upper incisors
Length of upper alveolar row	UPAL	Length of upper tooth row, measured at the alveolar margins.
Width of premolar	PREW	Breadth of upper premolar, measured at the alveolar margin
Length of bulla	BULL	Length of bulla measured from styliform process to the external auditory meatus
Width of bulla	BULW	Width of bulla measured from the jugular foramen to the external auditory meatus
Basilar length	BASI	Distance between the anterior margin of the foramen magnum and the anterior margin of the incisor alveoli
Greatest length of skull	SKUL	Distance between the premaxillary tip and the posteriormost extension of the occipital in the sagittal plane
Interorbital width	IORW	Smallest distance between the outer margins of the frontals at the reduced bony orbits
Width of posterior portion of zygomatic arch	ZYPW	Width of squamosal portion of zygomatic arch measured in parallel to the sagittal plane
Width of zygomatic arches	ZYAW	Maximum width of zygomatic arches measured at the anterior tips of the squamosals
Width of skull base	BASW	Minimal distance between squamosals measured ventrally
Width of skull at paroccipital processes	PAPW	Maximum width of cranium measured at paroccipital processes
Size of infraorbital foramen	FIOL	Maximum extension of the infraorbital foramen
Width of processus zygomaticus maxillaris	PZMW	Width of the processus zygomaticus maxillaris at the infraorbital foramen
Width of incisors	INCW	Width of upper incisors measured at the alveolar margins
Length of rostrum	ROSL	Distance between alveolar margins of incisors and the nasofrontal suture.
Height of cranium	SKUH	Distance between anterior alveolar margin of the premolar and the nasofrontal suture.
Width of condyle	CONW	Greatest width of condyle
Height of occiput	SOCC	Greatest length of the supraoccipital bone (including skull crests, if present)
Mandible length	MANL	Length of the ramus mandibulae measured from condyle to the incisors' alveolar margin
Total height of mandible	MANH	Distance between tip of coronoid process and the ventral margin of the angular process
Height of coronoid process	CONH	Distance between tip of coronoid and ventral margin of the mandibular ramus
Length of angular process	ANGL	Greatest length of angular process

Measurements were adopted and modified from Van Daele et al. (2013).

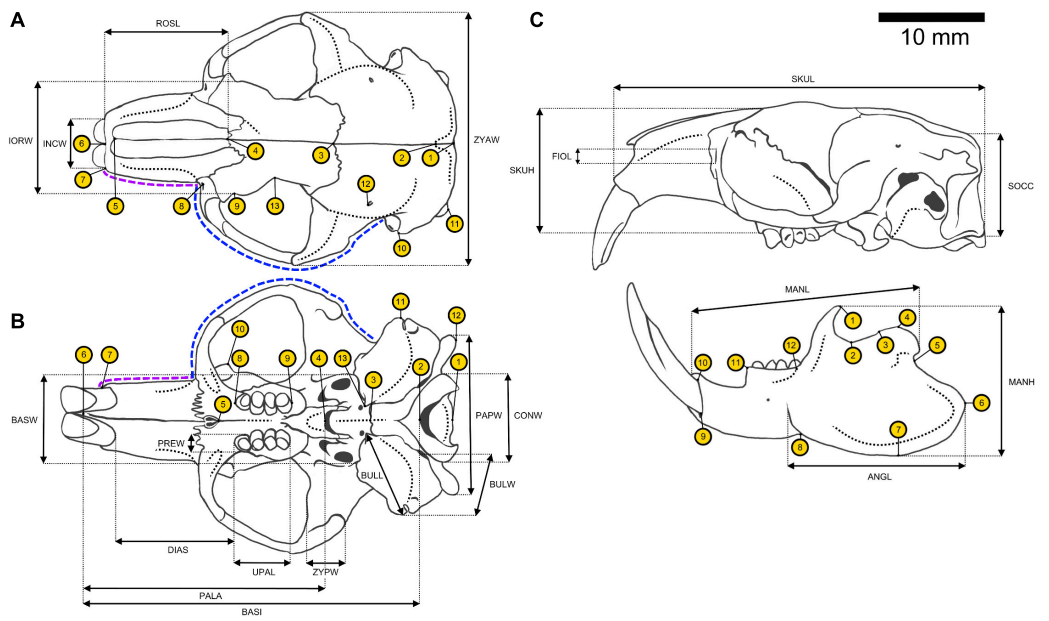

FIGURE 2 | Schematic drawing of a male Ansell's mole-rat skull with annotated linear measurements and landmarks used in this study. Definitions of landmarks and measurements are provided in **Table 2** and **Supplementary Table 2**. Semilandmarks are indicated as dashed lines. Rostral semilandmarks (purple) encompassed 8 landmark points, while zygomatic semilandmarks (blue) comprised 24. **(A)** Dorsal perspective of cranium with dorsal landmark set. **(B)** Ventral perspective of cranium with ventral landmark set. **(C)** Lateral perspective of cranium and mandible with mandibular landmark set.

for both ventral cranium and mandible photos and on the interfrontal suture of the skull roof for pictures taken from the dorsal perspective. Unilateral sets of 13 landmarks for the dorsal and ventral cranium and 12 landmarks for the mandible were selected and analyzed independently from each other (**Figure 2**; definitions are listed in **Supplementary Table 2**). Dorsal and ventral sets were amended by two lateral semilandmarks. The first one consisted of 8 semilandmark points and was set

along the rostrum from the incisor to the zygomatic arch. The second one comprised 24 landmark points and demarcated the zygomatic arch (**Figure 2**). Bending energy was used as criterion to optimize landmark positioning during sliding. Landmarks' digitization and scaling of photographs was achieved in TPSDig2 version 2.31 (Rohlf, 2018) and done by a single researcher for each landmark set (JM: dorsal/ventral; KRC: mandible). The geomorph package (Adams et al., 2020) was employed to analyze shape data. Occasional damage to the coronoid process led to missing landmarks (6 landmark points = 1.25%) in the mandible dataset, which were estimated and replaced by aid of the *LOST* package (Arbour and Brown, 2020). Landmarks were Procrustes superimposed to allow for subsequent analysis. Allometry was assessed by an ANOVA, regressing shape variables against centroid size, which is a measure of overall size in superimposed landmark datasets. PCA and LDA were employed with procedures analogous to those used in the analysis of linear cranial measurements and served the same purpose. However, the mandible dataset was not normally distributed. Therefore, statistical differences in measurements for sexes and reproductive status groups as well as interaction effects were assessed via MANOVA for dorsal and ventral cranial datasets and via a PERMANOVA for the mandibular one, respectively. Since LDA requires normal distribution of data as well, the randomForest method was used as an alternative classification procedure for mandibular landmark data (Liaw and Wiener, 2002).

Sex Differences in Relative Skull Dimensions

The greatest lengths of the skull (SKUL) and zygomatic arch width (ZYAW) were chosen to represent skull length and width, respectively, while hindfoot length was again used as a proxy for body size. Differences in hindfoot length between sexes and reproductive status groups were assessed in a linear regression model with hindfoot length as the dependent variable and sex and breeding status as predictors. Subsequently, the influence of body size and sex on skull size was tested the same way with either skull length or width as the dependent and hindfoot length as well as sex as predictor variables. Based on results from our previous morphometric analyses, the influence of breeding status on these parameters was not tested. Data were inspected visually for biasing outliers, linearity, normality, and homogeneity of variances in diagnostic plots. The latter two aspects were also assessed through Shapiro–Wilk and Levene tests, respectively, and found to be suitable for linear regression. Values for Cohen's d were derived from models' t statistics to provide a measure of effect size.

RESULTS

Occurrence and Scaling of SSD in the Bathyergidae

We found large differences in SSD among bathyergids and within the most speciose genus, *Fukomys* (**Table 1**). Lowest SSD values indicating sexual monomorphism were recovered for *Georychus* and *Heterocephalus*. All other bathyergids show a male-biased SSD which is pronounced in *Fukomys mechowii*, the giant mole-rat, and in the small-bodied genus *Cryptomys*. There was only a modest correlation between $\log_{10}$ female body mass and SSD in the Bathyergidae in general (Pearson correlation: $r = 0.3$; $t = 1.26$; and $p = 0.23$) but a strong one among *Fukomys* species (Pearson correlation: $r = 0.76$; $t = 3.1$; and $p = 0.017$).

Analyses of body mass data via pRMA models (**Table 3** and **Figure 3**) recovered that bathyergids as a whole show a trend to follow Rensch's rule of SSD scaling ($\beta = 1.072$, $p = 0.079$) while *Fukomys* species clearly comply to it ($\beta = 1.102$; $p = 0.021$). For both groups a strong phylogenetic signal associated with SSD was found ($\lambda = 0.999$), indicating a tight correlation between the expression of SSD and phylogenetic affiliation in bathyergids. Results of the regression models on two-step LG ratios did only partially align with the ones of the pRMA models. The former found bathyergids to comply to Rensch's rule ($\beta = 0.2214$; $p = 0.01$) while the data for *Fukomys* is approaching significance ($\beta = 0.2611$; $p = 0.05$).

Multivariate Skull Morphometrics

Male and female *F. anselli* were recovered as almost completely separated in the PCA morphospace based on linear cranial measurements, while reproductive groups were not discernible from each other (**Figure 4** and **Table 4**). Further analyses provided results consistent with this finding. MANOVA indicated a strong influence of sex on cranial morphometrics ($F = 12.13$, $p \ll 0.001$) but none of reproductive status ($F = 0.63$, $p = 0.74$) or the interaction between both ($F = 0.34$, $p = 0.84$). Hindfoot length was a strong general predictor of cranial morphology ($F = 7.33$, $p < 0.001$), but not among individuals of the same sex ($F = 0.40$, $p = 0.8$), and irrespective of their reproductive status ($F = 0.1$, $p = 0.98$). While males (90%) and females (80%) could be reliably classified in the linear measurement LDA ($p < 0.01$), individuals of the same sex were randomly assigned to reproductive status groups ($p > 0.1$, **Table 5**).

For the linear measurements, PCA computed 24 principal components, the first four of which had eigenvalues > 1 and explained 79.9% of total variance in the sample (**Table 4**). The most important measurements for group separation in PC1 were indicators of overall skull size, but particularly of its facial portion: mandibular length (MANL: 6.35%), basilar

TABLE 3 | Results from phylogenetic major reduced axis models investigating the relationship between male and female body mass in African mole-rats.

Group	N	λ	r^2	a	β	p
Bathyergidae	18	0.999	0.979	–0.093	1.072	0.079
Fukomys	9	0.999	0.993	–0.136	1.102	0.021

N gives the number of analyzed species in the respective group. Northern common mole-rats (Fukomys sp.) obey Rensch's rule, while the family in total does not, according to this method. Different from that, the regression models on two-step LG ratios suggest that bathyergids follow Rensch's rule as well (β = 0.2214; p = 0.01).

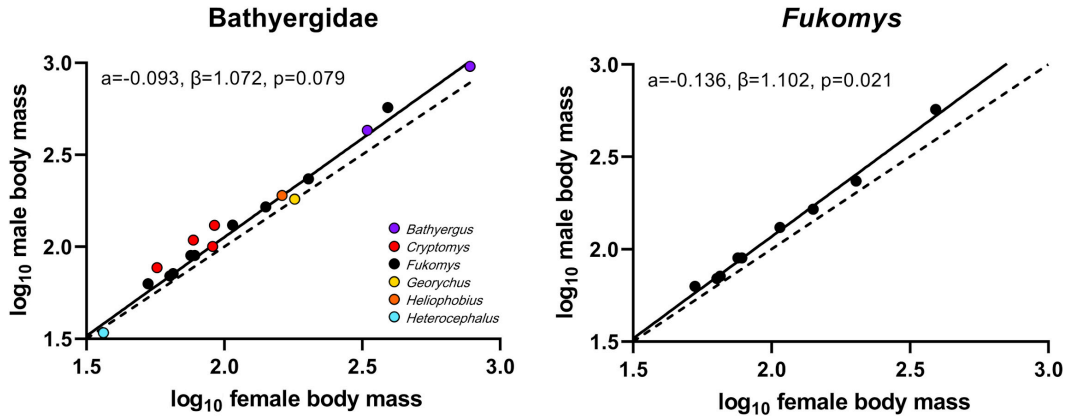

FIGURE 3 | Scaling of sexual size dimorphism in the family Bathyergidae and *Fukomys* species. The broken line indicates a size ratio of 1.0, equating to isometric scaling. *Fukomys* follows Rensch's rule as indicated by a significant deviation of $\beta > 1$. At family level, a similar trend could be recovered using phylogenetic major reduced axis models. However, the regression models on two-step LG ratios found that also bathyergids follow Rensch's rule revealed by a significant deviation of $\beta > 0$.

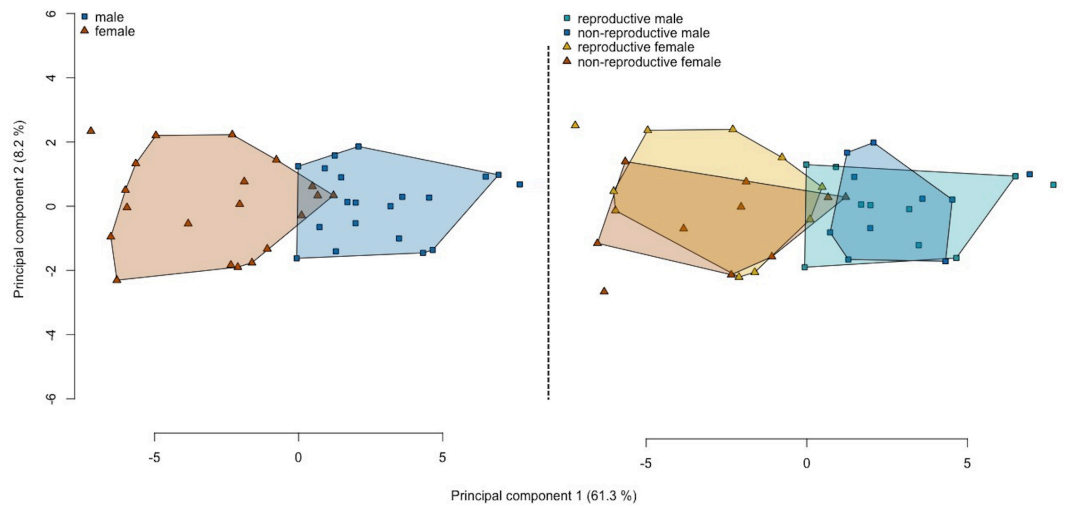

FIGURE 4 | Visualization of PCA results based on linear cranial measurements of *F. anselli*. Specimens are well separated by sex but not reproductive status.

length (BASI: 6.35%), and zygomatic arch width (ZYAW: 6.29%). However, PC1 factor loadings were to a large extent evenly distributed over the measurements, excluding several measurements concerned with dental characters and the skull base, which were of specific relevance to PC2. Width of skull base (BASW: 22.04%), width of premolar (PREW: 21.43%), and upper tooth row length (UPAL: 15.9%) contributed most to PC2 (**Table 4**).

The comparison of individual measurements between sexes and reproductive groups supported results of other analyses in showing distinct sexual dimorphism and the absence of cranial differences between breeders and non-breeders (**Table 5**). All but six variables differed significantly between the sexes ($p_{adjusted} < 0.002$). Non-significant variables primarily encompassed measurements relevant to the dentition and skull base. They related to the upper cheek dentition (PREW, UPAL), condyle (CONW) and paroccipital processes (PAPW), infraorbital foramen size (FIOL) and the width of the tympanic bulla (BULW). Differences between breeders and non-breeders of the same sex were consistently non-significant.

Sex Differences in Relative Skull Dimensions

Hindfoot length, approximating body size, was not found to differ intrasexually within reproductive status groups (t = -0.355, $p > 0.7$, and d = 0.12), but between the sexes (t = 2.626, p = 0.012, and d = 0.88). Skull length as well as width was found to increase proportionally with body size without significant differences among regression slopes between the sexes (skull length: t = 1.543, p = 0.131, and d = 0.51; skull width: t = 1.773, p = 0.085, and d = 0.59; **Figure 5**). However, relative skull length and width was greater in males compared to females as

TABLE 4 | Results of PCA based on linear cranial measurements in *F. anselli*.

Variable	PC1		PC2		PC3		PC4	
	EV: 14.70	Var. expl. 61.3%	EV: 1.95	Var. expl. 8.2%	EV: 1.44	Var. expl. 6.0%	EV: 1.09%	Var. expl. 4.55%
DIAS*	5.44%	0.23	2.82%	0.17	0.12%	–0.04	0.27%	0.05
PALA*	6.26%	0.25	0.16%	0.04	0.12%	0.04	0.11%	–0.03
UPAL	0.54%	0.07	15.90%	–0.40	5.65%	0.24	1.36%	–0.12
PREW	0.10%	0.03	21.53%	–0.46	2.78%	0.17	27.81%	–0.53
BULL*	4.68%	0.22	1.53%	0.12	9.76%	–0.31	0.58%	–0.08
BULW	3.49%	0.19	3.75%	0.19	10.98%	–0.33	0.08%	–0.03
BASI*	6.35%	0.25	0.56%	0.07	0.25%	0.05	0.02%	0.02
SKUL*	6.11%	0.25	0.16%	0.04	0.20%	0.04	0.32%	0.06
IORW*	5.56%	0.24	0.77%	0.09	0.94%	0.10	1.86%	–0.14
ZYPW*	3.86%	0.20	0.92%	–0.10	5.02%	–0.22	3.08%	–0.18
ZYAW*	6.29%	0.25	0.43%	0.07	0.14%	0.04	0.30%	0.05
BASW*	0.12%	0.04	22.04%	–0.47	0.35%	–0.06	37.99%	0.62
PAPW	3.34%	0.18	5.77%	–0.24	0.60%	–0.08	3.05%	0.17
FIOL	0.92%	0.10	9.37%	–0.31	22.05%	–0.47	8.46%	–0.29
PZMW*	3.78%	0.19	2.11%	–0.15	11.14%	0.33	0.15%	0.04
INCW*	5.55%	0.24	0.96%	0.10	2.55%	0.16	1.53%	0.12
ROSL*	5.19%	0.23	0.73%	0.09	0.32%	0.06	5.48%	–0.23
SKUH*	5.44%	0.23	1.21%	0.11	0.02%	0.01	0.05%	0.02
CONW	1.97%	0.14	5.09%	–0.23	11.35%	–0.34	0.05%	0.02
SOCC*	3.00%	0.17	0.41%	0.06	14.21%	0.38	2.59%	–0.16
MANL*	6.35%	0.25	0.36%	0.06	0.32%	–0.06	0.02%	0.01
MANH*	5.42%	0.23	0.37%	–0.06	0.01%	0.01	1.32%	0.11
CONH*	4.69%	0.22	2.91%	–0.17	0.98%	0.10	0.83%	0.09
ANGL*	5.54%	0.24	0.13%	–0.04	0.15%	0.04	2.72%	0.16

indicates measurements that differed significantly ($p_{adjusted} < 0.002$) between the sexes. See **Table 2 for abbreviations of linear measurements; EV, eigenvalue; Var. expl., percentage of explained variance.*

TABLE 5 | Correct assignment rates (%) of *F. anselli* skulls based on sex and reproductive status according to discriminant function analyses (based on LDA or in the case of mandibular landmarks on randomForest).

	Linear measurements				Dorsal landmarks				Ventral landmarks				Mandibular landmarks			
Sex (n = 20)	♂♂		♀♀		♂♂		♀♀		♂♂		♀♀		♂♂		♀♀	
	90		**80**		**90**		**85**		**95**		**85**		70		65	
Breeding status (n = 10)	*R*	NR	*R*	NR	*R*	NR	*R*	NR	*R*	NR	*R*	NR	*R*	NR	*R*	NR
	30	20	60	50	40	50	50	50	40	60	50	50	60	70	50	60

Bold numbers indicate correct assignments significantly different from chance ($p < 0.05$, one-tailed exact binomial test). NR, non-reproductive, R, reproductive.

indicated by significantly different regression constants (skull length: $t = 3.849$, $p < 0.001$, and $d = 1.27$; skull width: $t = 6.665$, $p < 0.001$, and $d = 2.19$). There was a mean sex difference of 1.5 mm (SD: 0.39) in skull length and 2.4 mm (SD: 0.36) in width at equal body size, conforming to 4.4 and 10.1% of mean female skull length and width, respectively.

2D Geometric Morphometrics of Cranium and Mandible

Analyses on the two landmark sets corresponding to dorsal and ventral cranium yielded similar results, while the mandibular dataset deviated from the latter ones in some respects, being less sensitive to influences of sex and skull size. In the dorsal and ventral cranial datasets, the PCA was able to separate specimens well regarding sex but not breeding status. However, the first two principal components encompassed only a fraction of total variance (38.1 and 44.8%, respectively; **Figure 6**), indicating high overall morphological variability. A similar pattern was recovered for the mandibular dataset, although morphospace overlap between the sexes as well as the variance explained by the first two PCs (49.3%) was greater compared to the other ones (**Figure 6**, see below). Accordingly, only sex was recovered to significantly influence the shape of the dorsal ($F = 6.36$, $p = 0.001$) and ventral cranium ($F = 5.32$, $p = 0.001$) as well as mandibular shape ($F = 4.82$, $p = 0.001$). Reproductive status or the combined

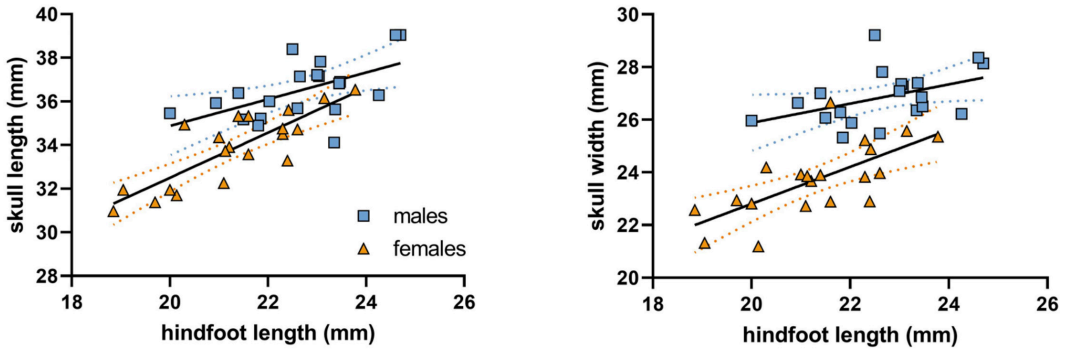

FIGURE 5 | Cranial length and width in Ansell's mole-rat in relation to body size (approximated by hindfoot length). Dotted lines indicate 95% confidence intervals of sex-specific regression lines.

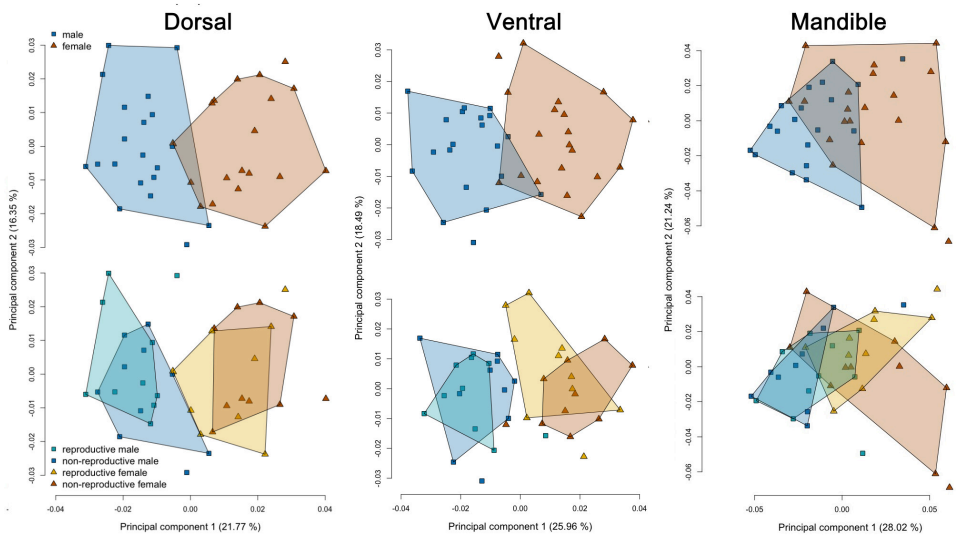

FIGURE 6 | Visualization of PCA-results based on geometric morphometrics of the cranium and mandible in *F. anselli*. Specimens are well separated by sex in plots based of dorsal and ventral landmarks, while overlap between the sexes is large for the mandibular dataset. No separation of reproductive groups was achieved. Polygons indicate the 95% convex hulls.

effect of sex and breeding status had no significant effect on these traits ($p > 0.1$). Shape allometry was detected for the dorsal ($F = 3.80$, $p = 0.001$) and ventral ($F = 3.17$, $p = 0.001$) cranium, but not for the mandible ($F = 1.97$, $p = 0.06$). However, since males had almost consistently larger skulls than females (**Figure 6**), this result is trivial. No pattern of allometry was found among specimens of the same sex in either landmark dataset (dorsal: $F = 0.69$, $p = 0.25$; ventral: $F = -0.44$, $p = 0.66$; and mandible: $F = 1.1$, $p = 0.40$).

Compared to females, the facial portion of the skull in males is enlarged, with longer rostra and widened zygomatic arches, which flare out more anteriorly (**Figure 7**). When scaled to the same size, the braincase and occipital region of male skulls therefore appear notably compressed compared to those of females. **Figure 7** visualizes shape differences between male and female *F. anselli* in a vector plot, highlighting relevant shape differences. Shape variable contributions and eigenvalues of PCs can be derived from **Supplementary Table 3**. Male mandibles were found to display a deeper and slightly more elongated processus angularis (landmark 6: 7.8% of PC1 variance, 16.9% of PC2 variance; landmark 7: 41.2% of PC1 variance, 22.7% of PC 2 variance) thicker lower incisors (landmark 9: 23.2% of PC1 variance, 14% of PC2 variance) and a longer, more sickle shaped coronoid process (landmark 1: 14.4% of PC1 variance, 12% of PC2 variance), when compared to females (**Figure 7**). However, sex differences in the shape of the lower jaw were altogether less pronounced than the ones in cranial shape. This was indicated by a more pronounced morphospace overlap and markedly higher error rates for assignments of individuals to one sex based on mandibular compared to cranial shape (**Table 5**, see below).

Cranial shape was found to be highly diagnostic for the sexes in *F. anselli*, but more so for males than for females mirroring the results from linear measurements (**Table 5**). LDA assigned 90% of males and 85% of females correctly based on dorsal cranial shape, while the ventral dataset allowed to classify 90% of males and 85% of females correctly. In both cases, these proportions

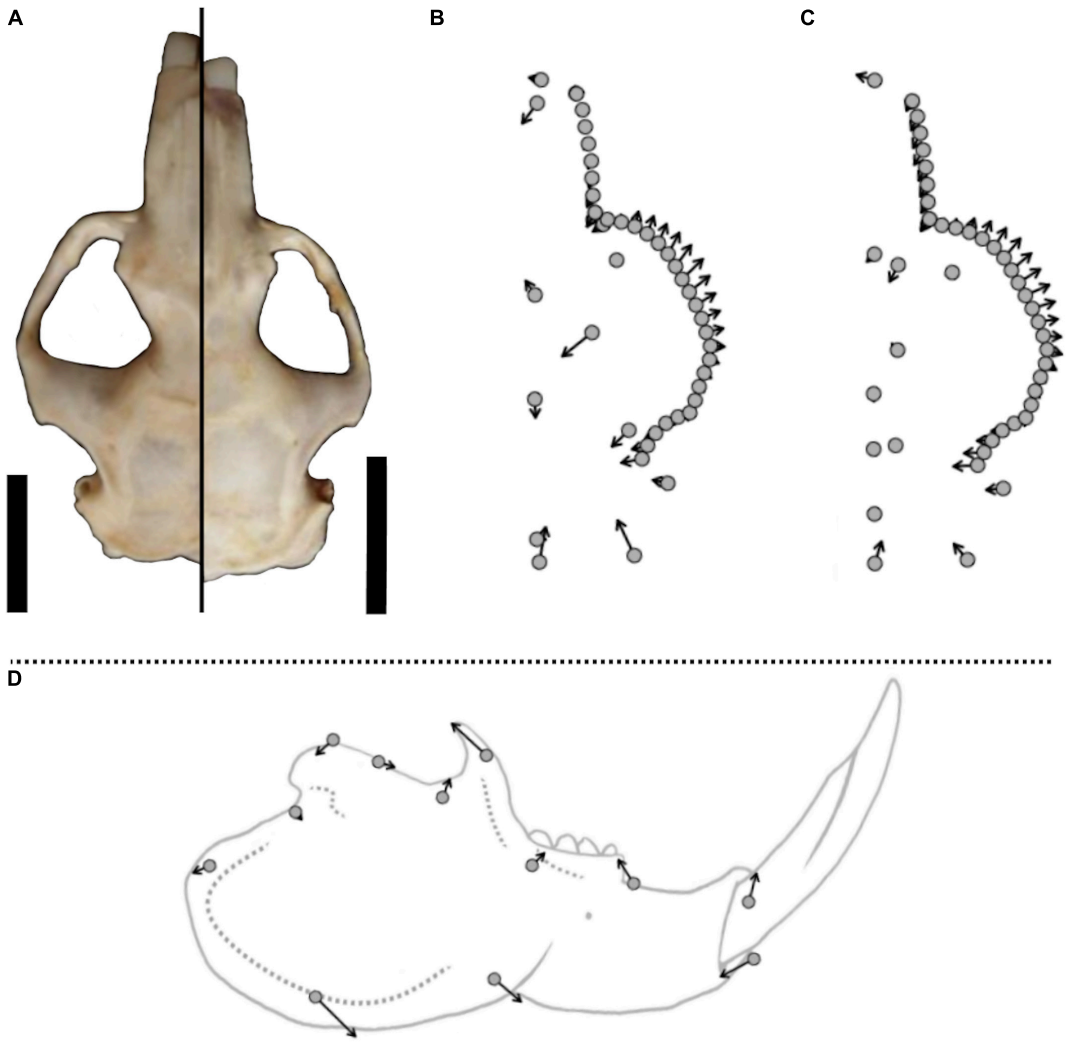

FIGURE 7 | Sex-specific shape differences in the cranium and mandible of *F. anselli*. Vector plots illustrate mean sex differences with vectors 4x magnified. Points indicate landmarks on female crania, arrows indicate landmark replacements in male crania compared to female ones. **(A)** Dorsal perspective of a male (left) and female (right) cranium, scaled to the same size and centered on the level of the orbita. Scale bars equal 10 mm and correspond to the specimen's original size. **(B)** Vector plot of the dorsal cranium. **(C)** Vector plot of the ventral cranium. **(D)** Vector plot of the mandible superimposed on a scheme of a male mandible.

differed significantly from random assignments ($p \leq 0.001$). The mandibular shape yielded less definite results: 70% of males and 65% of females were assigned to the correct categories, rates that did not significantly deviate from chance levels ($p > 0.05$). All intrasexual assignments based on reproductive status were randomized ($p > 0.1$).

DISCUSSION

Occurrence and Scaling of SSD in the Bathyergidae

Regression analyses based on both pRMA and two step LG ratios found Rensch's rule expressed in the monogamous mole-rat genus *Fukomys*, while only the latter did so for the bathyergid clade as a whole. The evidence for *Fukomys* following Rensch's rule is therefore robust, while its validity for bathyergids might still be questioned. However, although the pRMA regression did not reveal bathyergid SSD scaling significantly deviating from an isometric trajectory, a statistical trend ($p < 0.1$) emerged. If this is considered together with the positive results from the LG ratio based regression, one could therefore tentatively assume that Rensch's rule could apply to bathyergids on family level as well. Differences in the clarity of analytical outcomes between the two studied groups (*Fukomys* versus all bathyergids) might result from more uniform intrasexual selection pressures in *Fukomys*, when compared to other genera, which encompass a greater diversity of mating systems (compare Bray et al., 2012; Visser et al., 2017; Braude et al., 2020). Still, with the exception of *Heterocephalus*, aggressive competition between males, deduced either from direct observations (see below for *Fukomys* and, e.g., Jarvis and Bennett, 1991 for *Bathyergus* and Oosthuizen, 2008

for *Georychus*) or from morphological correlates such as sexual dimorphism, is evident throughout the bathyergid radiation. As such, it could underly the prevalence and scaling of SSD in these different taxa.

It is, however, important to point at the limitations of our dataset: Various studies have shown that intraspecific variation in bathyergid SSD (as approximated by body mass) can correlate with geographic provenance (*Cryptomys hottentotus* – Spinks et al., 2000; *Fukomys mechowii* — Scharff, 1998) and season of the year (*Georychus capensis* – Oosthuizen, 2008), factors for which we did not and could not control. Additionally, as we only included adult animals as assigned by the respective studies, we have to expect inconsistencies in the assignment of somatic maturity by the various authors we drew data from (see below). We must therefore consider a certain bias to our dataset. However, since most recovered rates of SSD correspond well to general reporting in the literature, we do not see the validity of our results compromised in that regard. Still, a more comprehensive dataset would have been desirable, especially regarding *Fukomys* species occurring North to the equator and for unambiguously localized populations of the solitary bathyergid genera, which might encompass significantly more species than currently recognized (Visser et al., 2019). However, biometric information on these mole-rats is currently unavailable.

Smaller-bodied species in our dataset (<150 *g*) are more variable regarding the expression of dimorphism than larger ones, where marked male-biased SSD is prevalent (**Table 1**). Among the small species, SSD is particularly pronounced in *Cryptomys*, in which male reproductive competition can be intense since multiple breeding males are regularly cohabiting a burrow and high incidences of extra-group paternity are common (Bishop et al., 2004). Bathyergids with strongly expressed SSD such as *Cryptomys* ssp. and *F. mechowii* are even among the most dimorphic of all rodents (Schulte-Hostedde, 2007), pointing to a crucial biological relevance of SSD in these animals. The latter must be especially emphasized for the genus *Fukomys*, where SSD scaling unambiguously follows Rensch's rule.

It appears that if at all, only modest SSD should be considered the ancestral condition in the Bathyergidae. Notable SSD is predominately found in derived bathyergids and is missing in the most basal genus *Heterocephalus* as well as among the closely allied rodent taxa Thryonomyidae and Petromuridae (Adu et al., 2002; Rathbun and Rathbun, 2006). Still, future studies might try to retrace the evolution of SSD in African hystricognaths in detail to eventually solve this question. Clarifying the matter might be specifically relevant to add to our understanding of the independent evolution of eusociality in *Fukomys* and *Heterocephalus*, which apparently derived from ancestors that strongly differed in SSD. In any case, some bathyergid SSD patterns will remain challenging to explain (compare **Figure 1**). The lack of SSD in *Georychus* appears to be secondarily acquired and is unexpected in an aggressively territorial solitary species. Not only are other non-social bathyergids, including its sister genus *Bathyergus*, dimorphic, but well-developed SSD is found in the majority of solitary subterranean rodents (Ctenomyidae – Martínez and Bidau, 2016; Geomyidae – Daly and Patton, 1986; Mauk et al., 1999; and Spalacidae – Su et al., 2018). On the other hand, the presence of pronounced SSD in at least several of the monogamous *Fukomys* species is surprising: their social system is commonly assumed to result in monomorphic sexes, and compliance to Rensch's rule could not be expected *a priori*. Possible explanations for this trait combination based on male-biased dynamic replacement of breeders will be discussed below.

Effects of Breeding Status on Skull Morphology in *F. anselli*

None of our analyses recovered significant differences between breeding and non-breeding mole-rats of the same sex, while sexual dimorphism was found to be pronounced within both groups. An important caveat to our analysis is the limited sample size of only ten individuals per status group and sex, especially in light of the high morphological variability we recover. However, since none of the different datasets we compared indicated even a trend of morphological segregation, we are reasonably confident that our findings reflect the actual conditions. Additionally, although our study is the first to explicitly address potential differences in skull morphology between mole-rats of different reproductive status, previous publications have already alluded to the lack of status-dependent cranial differentiation in *Fukomys* (Thorley et al., 2018a). Still, there surely is the possibility that future studies relying on more refined methods, such as 3D geometric morphometrics, may show detectable differences between mole-rat status groups. Nevertheless, even if such disparities would eventually be demonstrated, respective traits will be far more subtle than general sex-specific skull characteristics.

The uniformity of cranial characters contrasts with the pronounced differences in postcranial skeletal anatomy of breeding and non-breeding females in this genus (Thorley et al., 2018a) and points to similar functional demands to the skull among reproductive and non-reproductive mole-rats. Although there is evidence that non-reproductive *Fukomys* mole-rats are generally more active (Šklíba et al., 2016; Van Daele et al., 2019; Francioli et al., 2020; Houslay et al., 2020), both breeders and helpers engage in the same set of tasks, resulting in quantitative rather than qualitative differences in behavior, which could explain the lack of cranial divergence between them. Our results suggest that breeders do not develop more formidable weaponry or experience further somatic growth (safe for already documented allometric changes in breeding females' postcranium – Thorley et al., 2018a) after acquiring their status. Still, having more powerful jaws or greater body size might enhance the chances of becoming a breeder in the wild (compare Young and Bennett, 2013).

Field studies reported reproductives (excluding pregnant females) to be significantly heavier than helpers in *F. anselli* (Sichilima et al., 2011). de Bruin et al. (2012) even describe breeders (males: 81.45 ± 13.71 *g*, $n = 18$; females: 63.87 ± 11.39 *g*, $n = 19$) to be on average roughly two times as heavy as helpers (males: 39.80 ± 18.97 *g*, $n = 49$; females: 33.47 ± 11.78 *g*, $n = 64$). However, there are several problems with status assignment

in these studies. First, the authors assume a very early onset of maturity, classifying individuals ≥35 *g* as adults, whereas laboratory results suggest that this species reaches adulthood at approximately two times this body mass (Burda and Begall, 1998). We consider this difference to be too extreme to simply derive from the likely higher growth rates in provisioned captive animals. The assumption of such an early onset of maturity will strongly skew the results toward lower weights in non-reproductive animals. This way, a certain fraction of immature individuals will be counted as adult helpers since diagnostic traits of breeders are missing. Such practices will also bias estimations of SSD (see above). Unfortunately, precise aging of mole-rats in the wild is not possible offhand. Second, typically employed phenotypical criteria to assign breeding status in wild *F. anselli* males (and some congeneric species), such as testes size estimated by palpation or perioral secretions, are ambiguous. The latter frequently occur in non-reproductive males, at least in captivity (pers. obs.) and apart from the difficulty of assessing testes size by touch, contradicting findings have been published on testes volume differences between reproductive groups (de Bruin et al., 2012; Garcia Montero et al., 2016). Therefore, the reliability of available field data on weight distributions, especially for males can be questioned.

In case significant intrasexual differences in both sexes are confirmed, it needs to be clarified whether wild *F. anselli* might attain breeding status because of elevated body mass or develop it after succeeding to do so. Since body size is typically only approximated by mass in field studies, findings of intrasexual size differences might simply result from the allocation of limited resources in combination with lower activity levels of breeders in the wild (compare Francioli et al., 2020). In provisioned captive families, no such deviation in body mass is apparent (pers. obs., see Thorley et al., 2018a for *F. damarensis*) and even the opposite pattern might occur (Schielke et al., 2017). In any case, data on captive animals from this study and others demonstrate that attaining permanent breeding status *per se* does not go along with an isometric increase in body size (which would affect both hindfoot and cranial measurements, see **Figure 5**) or body mass in this species.

On a different note, our findings of uniform skull morphology in *F. anselli* status groups are relevant to *Fukomys* taxonomy, indicating that missing information about a specimen's reproductive history does not bias outcomes of anatomical studies.

Effects of Sex on Skull Morphology in *F. anselli*

In contrast to reproductive status, sex importantly influences both skull size and shape in *F. anselli*. In fact, *F. anselli* was also recovered as one of the more dimorphic small (<200 *g*) *Fukomys* species in regard to body mass, with males being roughly 20% heavier than females in the wild (Sichilima et al., 2011, but see above for problems with this estimate), with data from captive animals indicating even 40% higher body mass in males (Burda and Begall, 1998). Detected cranial difference are profound and not only point to a larger relative skull size in males but also to greater robustness of the male jaw apparatus. In light of this, it is surprising that a previous landmark analysis of the dorsal and ventral skull in sexually dimorphic *F. anselli*, *F. hanangensis* and *F. whytei* (compare **Table 1**) found no sex specific shape patterns (Faulkes et al., 2017). However, this study included immature specimens, which could have led to biased results.

Sex-specific cranial differences in *F. anselli* emerge due to hypertrophy of the facial portion of the skull in males (compare **Figure 7**), while several measurements of the skull base vary little between the sexes (**Table 4**). When scaled to the same size, males display wider as well as thicker zygomatic arches and larger angular processes than females which permit the development of a more voluminous musculus masseter, the most important masticatory muscle (Cox et al., 2020). Shape analysis also revealed a higher coronoid process in male mandibles, which together with more pronounced sagittal crests in males (pers. obs.) indicates a more strongly developed musculus temporalis, another jaw adductor (Cox et al., 2020). We therefore predict higher bite forces in male *F. anselli* compared to females relative to body mass (but see Van Daele et al., 2019 reporting equal bite forces in a small sample of a similar-sized *Fukomys* species). Apart from that, males can be expected to display a wider gape, since their rostra and mandibles are more elongated than the ones of females (**Table 4**). Still, there appears to be no noteworthy sex difference in cheek dentition, indicating that masticatory demands do not drive the sex-specific differentiation in the facial skeleton. The incisors on the other hand, which represent the most important weapons of African mole-rats, are hypertrophied in males, indicating adaptation to combat (Young and Bennett, 2013). This sex-specific trait was not only recovered herein but has already been noticed by Burda (1990) for *F. anselli* and by Young and Bennett (2013) for *F. damarensis*.

Sexual size dimorphism in relative skull size has been seldomly studied in mammals, but its occurrence was reported for *F. damarensis* (Young and Bennett, 2013). Our results agree with the respective study, in which head width (cranium and adhering soft tissues) in anesthetized *F. damarensis* was measured and males were found to have significantly wider heads than females relative to their body size. Unfortunately, head dimensions were only approximated by that single measure and raw data were not communicated, so that no further comparison with our findings on *F. anselli* can be drawn.

Clues to what underlies relative skull size SSD in mole-rats might derive from comparisons with reptiles, since the phenomenon has been intensively researched in lizards, subterranean amphisbaenians, and snakes, where exaggerated relative male head size is a common trait (Shine, 1991; Gienger and Beck, 2007; Martín et al., 2012; Baird, 2013). In fact, squamate reptiles and mole-rats differ little in that jaw and gape dimensions rather than other physical characteristics can decide conflicts with conspecifics. Just as male-biased body mass SSD in general, it is commonly assumed that enlarged heads in reptiles are intrasexually selected traits (Baird, 2013). Alternatively, ecological niche divergence between sexes could underly this anatomical difference (Shine, 1991, but see Baird, 2013), a factor also hypothesized to explain SSD in some monogamous mammals (e.g., Hillis and Mallory, 1996). However, the peculiar

lifestyle and foraging behavior of mole-rats argues against ecological influences on dimorphic head dimensions and again points to males combating competitors. There is also no evidence that male and female *Fukomys* differ in distances or mode of dispersal (above ground or underground) when leaving their natal family (Finn, 2017), so that an influence of this factor can also be ruled out (compare Young and Bennett, 2013). Instead, all the cranial traits discussed beforehand as well as the pattern of SSD scaling in *Fukomys* indicate a pronounced role of male-male combat in the social life of this genus. But how does that comply with the monogamous mating strategy of these mole-rats?

Socioecological Implications of Sexual Dimorphism in *Fukomys* Mole-Rats

Mammals exhibiting social and/or sexual monogamy are not expected to show pronounced SSD (compare Bidau and Martinez, 2016), so that the patterns found in *Fukomys* are surprising. Field studies employing microsatellite data demonstrated that reproductive skew in wild *Fukomys* is indeed extremely high. In *F. anselli*, only a single resident breeder of each sex is present and juveniles are sired almost exclusively by the established breeding male ($n_{families}$ = 13; 96.4% – Patzenhauerová et al., 2013). At the same time, the number of immigrants into established colonies is very small ($n_{non-breeders}$ = 85; 3.5%) but it is yet unclear whether these data are representative for *Fukomys* in general. In *F. damarensis*, a similar field study found the number of immigrants to be higher, at 7.5%, and the rate of extra-pair paternity was increased compared to *F. anselli* [up to 16% (31.9% if two outlier families are included); Patzenhauerová et al., 2013 referring to Burland et al., 2002]. These results do not challenge the assumption that both social and sexual monogamy is predominant in *Fukomys* but suggest that the latter may become compromised under specific circumstances.

However, although mating partners stay mostly faithful to each other and do so over long periods of time, once formed pairs can still be disrupted. This process appears to be mediated by male intrusion into established families. Shorter tenure length in reproductive males compared to females has been demonstrated by several genetic and capture-recapture studies (Young and Bennett, 2013, see below), indicating sex-biased social dynamics compliant with asymmetric reproductive competition and male-male combat. Genetic relatedness levels in males compared to females in wild *F. damarensis* groups also suggest that males do more frequently invade foreign groups and take over a breeding position (Burland et al., 2002). In case a breeder succession happens, or when a foreign male joins a group which lost its male breeder, a "patchwork family" with offspring of mixed descent can be established. Breeding male turnovers by intruders appear not to be rare (but see Torrents-Ticó et al., 2018), as all parentage studies on wild *Fukomys* found evidence for it in at least one family group analyzed (*F. anselli* – Patzenhauerová et al., 2013; *F. damarensis* – Burland et al., 2002; and *F. mechowii* – Šumbera et al., 2012).

Established wild *Fukomys* groups therefore exhibit high reproductive skew, experience at least some degree of immigration pressure and can tolerate the replacement of male breeders. The extreme, cooperatively enacted xenophoby found in laboratory-housed *Fukomys* appears to be an artifact of captivity (compare Bishop et al., 2004 for a similar pattern in *Cryptomys*). We suggest that the increased rate of male compared to female breeder turnover in the wild might be an unappreciated indication for stronger male intrasexual competition in *Fukomys* with major implications for SSD. Given the degree of SSD in *Fukomys* and the cranial adaptations described herein, it is likely that these replacements follow violent attacks. Still, such interactions are not documented so far. The reproductive benefit of securing a reproductive female, a burrow system and even a number of helpers for potentially several years must be extreme and might explain why SSD in *Fukomys* is more strongly expressed than in many polygynous or polygamous rodents, were mating associations are shorter-lived.

But there are several caveats to this hypothesis. First, it must be explained why such reproductive competition would occur in *Fukomys* and not in other cooperatively breeding rodents with slow life histories that occupy self-constructed defendable home ranges, such as mole-voles (*Ellobius* spp.), beavers (*Castor* spp.) and most importantly, *Heterocephalus*. It could also be argued that low documented rates of male group takeovers (Torrents-Ticó et al., 2018) could not create a sufficient selective pressure to explain the observed sexual dimorphism. Besides, faster male turnovers might not be provoked by intrasexual combat but by males facing higher mortality risks, for example increased predation pressure. For this, however, one would expect differences in the activity and ranging patterns of males and females, which is so far not apparent in wild *Fukomys* (*F. damarensis* – Francioli et al., 2020). A final potential caveat is the lack of intraspecific combat adaptations in *Fukomys* that are found in other bathyergids: Even large-bodied *Fukomys* lack defensive dermal shields, a trait found in the dune mole-rats of the genus *Bathyergus* (Jarvis and Bennett, 1991), which might be expected to evolve convergently in both genera in case males commonly experience violent encounters with competitors.

CONCLUSION

Our study provides a comprehensive description of the well-developed sexual dimorphism in the skull of *F. anselli*, which points to a significant role of male competition in the social life of mole-rats belonging to this cooperatively-breeding genus. *Fukomys* might best be characterized as serially monogamous rodent genus, in which males stay faithful to their partners for prolonged time but have to regularly engage in conflicts with same-sex rivals to secure their mate. That assumption is further supported by the recovery of SSD scaling conforming to Rensch's rule among *Fukomys* species, indicating violent monopolization of breeding females by males. At the same time, we show that no morphological differentiation in the cranium of breeders and non-breeders exists, indicating a lack of morpho-functional caste specialization beyond characters relevant to reproduction. The currently available data can only be considered a starting point regarding efforts to understand the evolutionary pressures influencing sexual dimorphism in social mole-rats. Future studies might address the following

questions to characterize the evolutionary pressures behind these morphological findings: How frequent are attempts to take over groups by foreign males in the wild and how do invaded family groups react? Why do helpers accept unrelated male breeders within the "patchwork family" scheme? To which degree do *Fukomys* species differ in respect to this behavior and how do they compare to *Cryptomys* and *Heterocephalus*? What factors underly the varying expression of SSD in the three solitary bathyergid genera?

Solving these questions will importantly contribute to fully unravel the remarkable diversity of social patterns found within the Bathyergidae and the factors that shaped it.

DATA AVAILABILITY STATEMENT

The original contributions presented in the study are included in the article/**Supplementary Material**; further inquiries can be directed to the corresponding author/s.

AUTHOR CONTRIBUTIONS

KRC conceived the study and its methodology with input from SB. KRC and SB prepared the skulls, took linear measurements, and prepared the figures. JM photographed the skulls and compiled landmark datasets of the dorsal and ventral skull. KRC collected landmark data on the mandibles. SB and JM analyzed the data with input from KRC. All authors interpreted the findings. KRC wrote the first draft, which was reviewed by SB and JM. All authors contributed to the article and approved the submitted version.

FUNDING

KRC was supported by a Ph.D. fellowship of the German National Academic Foundation (Studienstiftung des deutschen Volkes e.V.). We acknowledge support by the Open Access Publication Fund of the University of Duisburg-Essen.

ACKNOWLEDGMENTS

We thank Irina Ruf for inviting us to contribute our manuscript to this special issue and two reviewers for their insightful comments on earlier versions of this manuscript. Martin Schnorr is acknowledged for assisting the preparation of the skulls used in this study.

SUPPLEMENTARY MATERIAL

The Supplementary Material for this article can be found online at: https://www.frontiersin.org/articles/10.3389/fevo.2021.638754/full#supplementary-material

Supplementary Table 1 | Linear skull measurements and hindfoot lengths of *Fukomys anselli* specimens used in this study. Yellow mark: Measurement was taken from the left side of the skull. Red mark: Measurement was estimated using the LOST package (Arbour and Brown, 2020).

Supplementary Table 2 | Overview and definitions of point landmarks used to characterize skull traits in *Fukomys anselli*.

Supplementary Table 3 | Variable contributions (%) and eigenvalues of principal components computed for the shape of the dorsal and ventral cranium as well as for the mandible of *Fukomys anselli*.

REFERENCES

Abouheif, E., and Fairbairn, D. J. (1997). A comparative analysis of allometry for sexual size dimorphism: assessing Rensch's rule. *Am. Nat.* 149, 540–562. doi: 10.1086/286004

Adams, D. C., Collyer, M., and Kaliontzopoulou, A. (2020). *Geomorph: Software for Geometric Morphometric Analyses. R package version 3.2.1.*

Adu, E. K., Wallace, P. A., and Ocloo, T. O. (2002). Efficacy of sex determination in the greater cane rat, *Thryonomys swinderianus*, Temminck. *Trop. Anim. Health Product.* 34, 27–33.

Ansell, W. F. H. (1965). Standardisation of field data on mammals. *Zool. Afr.* 1, 97–113. doi: 10.1080/00445096.1965.11447303

Arbour, J., and Brown, C. (2020). *LOST: Missing Morphometric Data Simulation and Estimation. R package version 2.0.2.*

Baird, T. A. (2013). "Lizards and other reptiles as model systems for the study of contest behaviour," in *Animal Contests*, eds C. W. Hardy and M. Briffa (Cambridge: Cambridge University Press), 258–286. doi: 10.1017/cbo9781139051248.014

Bappert, M.-T., Burda, H., and Begall, S. (2012). To mate or not to mate? Mate preference and fidelity in monogamous Ansell's mole-rats, *Fukomys anselli*, Bathyergidae. *Folia Zool.* 61, 71–83. doi: 10.25225/fozo.v61.i1.a11.2012

Barčíová, L., Šumbera, R., and Burda, H. (2009). Variation in the digging apparatus of the subterranean silvery mole-rat, *Heliophobius argenteocinereus* (Rodentia, Bathyergidae): the role of ecology and geography. *Biol. J. Linn. Soc.* 97, 822–831. doi: 10.1111/j.1095-8312.2009.01228.x

Begall, S., Nappe, R., Hohrenk, L., Schmidt, T. C., Burda, H., et al. (2021). Life expectancy, family constellation, and stress in giant mole-rats (*Fukomys mechowii*). *Philos. Trans. R. Soc. B* 376:20200207. doi: 10.1098/rstb.2020.0207

Bennett, N. C., Faulkes, C. G., Hart, L., and Jarvis, J. U. M. (2009). *Bathyergus suillus*. *Mamm. Spec.* 2009, 1–7. doi: 10.1644/828.1

Bennett, N. C., and Jarvis, J. U. M. (2004). *Cryptomys damarensis*. *Mammal. Spec.* 2004, 1–5. doi: 10.1644/756

Bennett, N. C., Jarvis, J. U. M., and Cotterill, F. P. D. (1994). The colony structure and reproductive biology of the afrotropical Mashona mole-rat, *Cryptomys darlingi*. *J. Zool.* 234, 477–487. doi: 10.1111/j.1469-7998.1994.tb04861.x

Bennett, N. C., Maree, S., and Faulkes, C. G. (2006). *Georychus capensis*. *Mamm. Spec.* 2006, 1–4.

Bidau, C. J., and Martinez, P. A. (2016). Sexual size dimorphism and Rensch's rule in Canidae. *Biol. J. Linn. Soc.* 119, 816–830. doi: 10.1111/bij.12848

Bishop, J. M., Jarvis, J. U. M., Spinks, A. C., Bennett, N. C., and O'Ryan, C. (2004). Molecular insight into patterns of colony composition and paternity in the common mole-rat *Cryptomys hottentotus hottentotus*. *Mol. Ecol.* 13, 1217–1229. doi: 10.1111/j.1365-294x.2004.02131.x

Braude, S., Hess, J., and Ingram, C. (2020). Inter-colony invasion between wild naked mole-rat colonies. *J. Zool.* 313:12834.

Bray, T. C., Bloomer, P., O'Riain, M. J., and Bennett, N. C. (2012). How attractive is the girl next door? An assessment of spatial mate acquisition and paternity in the solitary Cape dune mole-rat, *Bathyergus suillus*. *PLoS One* 7:e39866. doi: 10.1371/journal.pone.0039866

Brett, R. A. (1991). "The population structure of naked mole-rat colonies," in *The Biology of the Naked Mole-Rat*, eds P. W. Sherman, J. U. M. Jarvis, and R. D. Alexander (New Jersey: Princeton Univ. Press), 97–136. doi: 10.1515/9781400887132-007

Burda, H. (1990). Constraints of pregnancy and evolution of sociality in mole-rats with special reference to reproductive and social patterns in *Cryptomys*

hottentotus (Bathyergidae, Rodentia). *J. Zool. Syst. Evol. Res.* 28, 26–39. doi: 10.1111/j.1439-0469.1990.tb00362.x

Burda, H., and Begall, S. (1998). Reproductive characteristics and growth in the eusocial Zambian common mole-rat (*Cryptomys* sp., Bathyergidae). *Z. Säugetierkunde* 63, 297–306.

Burda, H., Honeycutt, R. L., Begall, S., Locker-Grütjen, O., and Scharff, A. (2000). Are naked and common mole-rats eusocial and if so, why? *Behav. Ecol. Sociobiol.* 47, 293–303. doi: 10.1007/s002650050669

Burda, H., Šumbera, R., Chitaukali, W. N., and Dryden, G. L. (2005). Taxonomic status and remarks on ecology of the Malawian mole-rat *Cryptomys whytei* (Rodentia, Bathyergidae). *Acta Theriol.* 50, 529–536. doi: 10.1007/bf03192646

Burland, T. M., Bennett, N. C., Jarvis, J. U. M., and Faulkes, C. G. (2002). Eusociality in African mole-rats: new insights from patterns of genetic relatedness in the Damaraland mole-rat (*Cryptomys damarensis*). *Proc. R. Soc. Lond. Ser. B Biol. Sci.* 269, 1025–1030. doi: 10.1098/rspb.2002.1978

Chimimba, C. T., Sichilima, A. M., Faulkes, C. G., and Bennett, N. C. (2010). Ontogenetic variation and craniometric sexual dimorphism in the social giant mole-rat, *Fukomys mechowii* (Rodentia: Bathyergidae), from Zambia. *Afr. Zool.* 45, 160–176. doi: 10.3377/004.045.0218

Cohas, A., and Allainé, D. (2009). Social structure influences extra-pair paternity in socially monogamous mammals. *Biol. Lett.* 5, 313–316. doi: 10.1098/rsbl.2008.0760

Cox, P. G., Faulkes, C. G., and Bennett, N. C. (2020). Masticatory musculature of the African mole-rats (Rodentia: Bathyergidae). *PeerJ* 8:e8847. doi: 10.7717/peerj.8847

Dale, J., Dunn, P. O., Figuerola, J., Lislevand, T., Székely, T., and Whittingham, L. A. (2007). Sexual selection explains Rensch's rule of allometry for sexual size dimorphism. *Proc. R. Soc. B Biol. Sci.* 274, 2971–2979. doi: 10.1098/rspb.2007.1043

Daly, J. C., and Patton, J. L. (1986). Growth, reproduction, and sexual dimorphism in *Thomomys bottae* pocket gophers. *J. Mammal.* 67, 256–265. doi: 10.2307/1380878

Dammann, P., and Burda, H. (2006). Sexual activity and reproduction delay ageing in a mammal. *Curr. Biol.* 16, R117–R118.

de Bruin, P. R., Viljoen, H., Sichilima, A. M., and Bennett, N. C. (2012). Socially induced infertility in Ansell's mole-rat: are there depressed hormone levels in non-reproductive males and females? *J. Zool.* 286, 15–21. doi: 10.1111/j.1469-7998.2011.00841.x

Dengler-Crish, C. M., and Catania, K. C. (2007). Phenotypic plasticity in female naked mole-rats after removal from reproductive suppression. *J. Exp. Biol.* 210:4351. doi: 10.1242/jeb.009399

Fairbairn, D. J. (1997). Allometry for sexual size dimorphism: pattern and process in the coevolution of body size in males and females. *Annu. Rev. Ecol. Syst.* 28, 659–687. doi: 10.1146/annurev.ecolsys.28.1.659

Faulkes, C. G., Mgode, G. F., Archer, E. K., and Bennett, N. C. (2017). Relic populations of *Fukomys* mole-rats in Tanzania: description of two new species *F. livingstoni* sp. nov. and *F. hanangensis* sp. nov. *PeerJ* 5:e3214. doi: 10.7717/peerj.3214

Finn, K. T. (2017). *Density-Dependent Effects on Body Size, Philopatry, and Dispersal in the Damaraland Mole-Rat (Fukomys damarensis)*. M.Sc. thesis. Grahamstown: Rhodes University.

Francioli, Y., Thorley, J., Finn, K., Clutton-Brock, T., and Zöttl, M. (2020). Breeders are less active foragers than non-breeders in wild Damaraland mole-rats. *Biol. Lett.* 16:20200475. doi: 10.1098/rsbl.2020.0475

Gabathuler, U., Bennett, N. C., and Jarvis, J. U. M. (1996). The social structure and dominance hierarchy of the Mashona mole-rat, *Cryptomys darlingi* (Rodentia: Bathyergidae) from Zimbabwe. *J. Zool.* 240, 221–231. doi: 10.1111/j.1469-7998.1996.tb05281.x

Garcia Montero, A., Vole, C., Burda, H., Malkemper, E. P., Holtze, S., Morhart, M., et al. (2016). Non-breeding eusocial mole-rats produce viable sperm—spermiogram and functional testicular morphology of *Fukomys anselli*. *PLoS One* 11:e0150112. doi: 10.1371/journal.pone.0150112

Gienger, C. M., and Beck, D. D. (2007). Heads or tails? Sexual dimorphism in helodermatid lizards. *Can. J. Zool.* 85, 92–98. doi: 10.1139/z06-198

Gomes Rodrigues, H., Šumbera, R., and Hautier, L. (2016). Life in burrows channelled the morphological evolution of the skull in rodents: the case of African mole-Rats (Bathyergidae, Rodentia). *J. Mamm. Evol.* 23, 175–189. doi: 10.1007/s10914-015-9305-x

Hart, L., Chimimba, C. T., Jarvis, J. U. M., O'Riain, J., and Bennett, N. C. (2007). Craniometric sexual dimorphism and age variation in the South African Cape dune mole-rat (*Bathyergus suillus*). *J. Mammal.* 88, 657–666. doi: 10.1644/06-mamm-a-058r1.1

Herbst, M., Jarvis, J. U. M., and Bennett, N. C. (2004). A field assessment of reproductive seasonality in the threatened wild Namaqua dune mole-rat (*Bathyergus janetta*). *J. Zool.* 263, 259–268. doi: 10.1017/s0952836904005114

Heske, E. J., and Ostfeld, R. S. (1990). Sexual dimorphism in size, relative size of testes, and mating systems in North American voles. *J. Mammal.* 71, 510–519. doi: 10.2307/1381789

Hillis, T. L., and Mallory, F. F. (1996). Sexual dimorphism in wolves (*Canis lupus*) of the Keewatin District, Northwest Territories, Canada. *Can. J. Zool.* 74, 721–725. doi: 10.1139/z96-081

Houslay, T. M., Vullioud, P., Zöttl, M., and Clutton-Brock, T. H. (2020). Benefits of cooperation in captive Damaraland mole-rats. *Behav. Ecol.* 31, 711–718. doi: 10.1093/beheco/araa015

Ingram, C. M., Burda, H., and Honeycutt, R. L. (2004). Molecular phylogenetics and taxonomy of the African mole-rats, genus *Cryptomys* and the new genus *Coetomys* Gray, 1864. *Mol. Phylogenet. Evol.* 31, 997–1014. doi: 10.1016/j.ympev.2003.11.004

Jarvis, J. U. M., and Bennett, N. C. (1991). "Ecology and behaviour of the family Bathyergidae," in *The Biology of the Naked Mole-Rat*, eds P. W. Sherman, J. U. M. Jarvis, and R. D. Alexander (New Jersey: Princeton Univ. Press), 66–96. doi: 10.1515/9781400887132-006

Lacey, E. A., and Sherman, P. W. (1991). "Social organization of naked-mole rat colonies: evidence for the division of labor," in *The Biology of the Naked Mole-Rat*, eds P. W. Sherman, J. U. M. Jarvis, and R. D. Alexander (New Jersey: Princeton University Press), 275–336. doi: 10.1515/9781400887132-013

Liaw, A., and Wiener, M. (2002). Classification and Regression by randomForest. *R News* 2, 18–22.

Lu, D., Zhou, C. Q., and Liao, W. B. (2014). Sexual size dimorphism lacking in small mammals. *N. W. J. Zool.* 10, 53–59.

Martín, J., Polo-Cavia, N., Gonzalo, A., López, P., and Civantos, E. (2012). Sexual dimorphism in the North African amphisbaenian *Trogonophis wiegmanni*. *J. Herpetol.* 46, 338–341. doi: 10.1670/10-286

Martínez, P. A., and Bidau, C. J. (2016). A re-assessment of Rensch's rule in tuco-tucos (Rodentia: Ctenomyidae: *Ctenomys*) using a phylogenetic approach. *Mamm. Biol.* 81, 66–72. doi: 10.1016/j.mambio.2014.11.008

Mauk, C. L., Houck, M. A., and Bradley, R. D. (1999). Morphometric analysis of seven species of pocket gophers *(Geomys)*. *J. Mammal.* 80, 499–511. doi: 10.2307/1383296

Moshkin, M. P., Novikov, E. A., and Petrovski, D. V. (2001). Seasonal changes of thermoregulation in the mole vole *Ellobius talpinus*. *Physiol. Biochem. Zool.* 74, 869–875. doi: 10.1086/324750

Oosthuizen, M. K. (2008). *The Reproductive Biology of the Solitary Cape Mole-Rat, Georychus capensis and the Social Natal mole-rat, Cryptomys hottentotus Natalensis (Rodentia : Bathyergidae)*. Ph.D. thesis. Pretoria: University of Pretoria.

Patzenhauerová, H., Bryja, J., and Šumbera, R. (2010). Kinship structure and mating system in a solitary subterranean rodent, the silvery mole-rat. *Behav. Ecol. Sociobiol.* 64, 757–767. doi: 10.1007/s00265-009-0893-4

Patzenhauerová, H., Šklíba, J., Bryja, J., and Šumbera, R. (2013). Parentage analysis of Ansell's mole-rat family groups indicates a high reproductive skew despite relatively relaxed ecological constraints on dispersal. *Mol. Ecol.* 22, 4988–5000. doi: 10.1111/mec.12434

Rathbun, G. B., and Rathbun, C. D. (2006). Social monogamy in the noki or dassie-rat (*Petromus typicus*) in Namibia. *Mamm. Biol.* 71, 203–213. doi: 10.1016/j.mambio.2006.01.008

Rensch, B. (1950). Die Abhängigkeit der relativen Sexualdifferenz von der Körpergröße. *Bonner Zool. Beiträge* 1, 58–69.

Rensch, B. (1960). *Evolution Above the Species Level*. New York, NY: Columbia University Press.

Revell, L. J. (2012). phytools: an R package for phylogenetic comparative biology (and other things). *Methods Ecol. Evol.* 3, 217–223. doi: 10.1111/j.2041-210x.2011.00169.x

Rohlf, F. J. (2018). *tpsDig2, Digitize Landmarks and Outlines, Version 2.31*. New York, NY: Department of Ecology and Evolution, State University of New York.

RStudio Team (2020). *RStudio: Integrated Development for R*. Boston, MA: RStudio, PBC.

Scharff, A. (1998). *Systematik und Verhaltensökologie sambischer Sandgräber (Bathyergidae, Rodentia)*. Ph.D. thesis. Duisburg: University of Essen.

Schielke, C. K. M., Burda, H., Henning, Y., Okrouhlík, J., and Begall, S. (2017). Higher resting metabolic rate in long-lived breeding Ansell's mole-rats (*Fukomys anselli*). *Front. Zool.* 14:45. doi: 10.1186/s12983-017-0229-6

Schulte-Hostedde, A. (2007). "Chapter 10 Sexual size dimorphism in rodents," in *Rodent Societies: An Ecological and Evolutionary Perspective*, eds J. O. Wolff and P. W. Sherman (Chicago, IL: The University of Chicago Press), 115–128.

Shine, R. (1991). Intersexual dietary divergence and the evolution of sexual dimorphism in snakes. *Am. Nat.* 138, 103–122. doi: 10.1086/285207

Sichilima, A. M., Bennett, N. C., and Faulkes, C. G. (2011). Field evidence for colony size and aseasonality of breeding and in Ansell's mole-rat, *Fukomys anselli* (Rodentia: Bathyergidae). *Afr. Zool.* 46, 334–339. doi: 10.1080/15627020.2011.11407506

Sichilima, A. M., Faulkes, C. G., and Bennett, N. C. (2008). Field evidence for aseasonality of reproduction and colony size in the Afrotropical giant mole-rat *Fukomys mechowii* (Rodentia: Bathyergidae). *Afr. Zool.* 43, 144–149. doi: 10.3377/1562-7020-43.2.144

Šklíba, J., Lövy, M., Burda, H., and Šumbera, R. (2016). Variability of space-use patterns in a free living eusocial rodent, Ansell's mole-rat indicates age-based rather than caste polyethism. *Sci. Rep.* 6:37497.

Smith, R. J. (1999). Statistics on sexual size dimorphism. *J. Hum. Evol.* 36, 423–459. doi: 10.1006/jhev.1998.0281

Spinks, A. C., Bennett, N. C., and Jarvis, J. U. M. (2000). A comparison of the ecology of two populations of the common mole-rat, *Cryptomys hottentotus hottentotus*: the effect of aridity on food, foraging and body mass. *Oecologia* 125, 341–349. doi: 10.1007/s004420000460

Su, J., Hegab, I. M., Ji, W., and Nan, Z. (2018). Function-related drivers of skull morphometric variation and sexual size dimorphism in a subterranean rodent, plateau zokor (*Eospalax baileyi*). *Ecol. Evol.* 8, 4631–4643. doi: 10.1002/ece3.3986

Šumbera, R., Burda, H., and Chitaukali, W. N. (2003). Reproductive biology of a solitary subterranean bathyergid rodent, the silvery mole-rat (*Heliophobius argenteocinereus*). *J. Mammal.* 84, 278–287. doi: 10.1644/1545-1542(2003)084<0278:rboass>2.0.co;2

Šumbera, R., Mazoch, V., Patzenhauerová, H., Lövy, M., Šklíba, J., Bryja, J., et al. (2012). Burrow architecture, family composition and habitat characteristics of the largest social African mole-rat: the giant mole-rat constructs really giant burrow systems. *Acta Theriol.* 57, 121–130. doi: 10.1007/s13364-011-0059-4

Taylor, P. J., Jarvis, J. U. M., Crowe, T. M., and Davies, K. C. (1985). Age determination in the Cape molerat *Georychus capensis*. *S. Afr. J. Zool.* 20, 261–267.

Thomas, H. G., Bateman, P. W., Scantlebury, M., and Bennett, N. C. (2012). Season but not sex influences burrow length and complexity in the non-sexually dimorphic solitary Cape mole-rat (Rodentia: Bathyergidae). *J. Zool.* 288, 214–221. doi: 10.1111/j.1469-7998.2012.00944.x

Thorley, J., Katlein, N., Goddard, K., Zöttl, M., and Clutton-Brock, T. (2018a). Reproduction triggers adaptive increases in body size in female mole-rats. *Proc. R. Soc. B Biol. Sci.* 285:20180897. doi: 10.1098/rspb.2018.0897

Thorley, J., Mendonça, R., Vullioud, P., Torrents-Ticó, M., Zöttl, M., Gaynor, D., et al. (2018b). No task specialization among helpers in Damaraland mole-rats. *Anim. Behav.* 143, 9–24. doi: 10.1016/j.anbehav.2018.07.004

Torrents-Ticó, M., Bennett, N. C., Jarvis, J. U. M., and Zöttl, M. (2018). Sex differences in timing and context of dispersal in Damaraland mole-rats (*Fukomys damarensis*). *J. Zool.* 306, 252–257. doi: 10.1111/jzo.12602

Van Daele, P. A., Blonde, P., Stjernstedt, R., and Adriaens, D. (2013). A new species of African mole-rat (*Fukomys*, Bathyergidae, Rodentia) from the Zaire-Zambezi watershed. *Zootaxa* 3636, 171–189. doi: 10.11646/zootaxa.3636.1.7

Van Daele, P. A. A. G., Desmet, N., Šumbera, R., and Adriaens, D. (2019). Work behaviour and biting performance in the cooperative breeding Micklem's mole-rat *Fukomys micklemi* (Bathyergidae, Rodentia). *Mamm. Biol.* 95, 69–76. doi: 10.1016/j.mambio.2019.02.002

van Jaarsveld, B., Bennett, N. C., Hart, D. W., and Oosthuizen, M. K. (2019). Locomotor activity and body temperature rhythms in the Mahali mole-rat (*C. h. mahali*): the effect of light and ambient temperature variations. *J. Therm. Biol.* 79, 24–32. doi: 10.1016/j.jtherbio.2018.11.013

van Rensburg, L. J., Chimimba, C. T., van der Merwe, M., Schoeman, A. S., and Bennett, N. C. (2004). Relative age and reproductive status in *Cryptomys hottentotus pretoriae* (Rodentia: Bathyergidae) from South Africa. *J. Mammal.* 85, 1225–1232. doi: 10.1644/ber-113.1

Visser, J. H., Bennett, N. C., and Jansen van Vuuren, B. (2017). Distributional range, ecology, and mating system of the Cape mole-rat (*Georychus capensis*) family Bathyergidae. *Can. J. Zool.* 95, 713–726. doi: 10.1139/cjz-2017-0016

Visser, J. H., Bennett, N. C., and Jansen van Vuuren, B. (2019). Phylogeny and biogeography of the African Bathyergidae: a review of patterns and processes. *PeerJ* 7:e7730. doi: 10.7717/peerj.7730

Webb, T. J., and Freckleton, R. P. (2007). Only half right: species with female-biased sexual size dimorphism consistently break Rensch's rule. *PLoS One* 2:e897. doi: 10.1371/journal.pone.0000897

Yeboah, S., and Dakwa, K. B. (2002). Colony and social structure of the Ghana mole-rat (*Cryptomys zechi*, Matchie) (Rodentia: Bathyergidae). *J. Zool.* 256, 85–91. doi: 10.1017/s0952836902000110

Young, A. J., and Bennett, N. C. (2013). Intra-sexual selection in cooperative mammals and birds: why are females not bigger and better armed? *Philos. Trans. R. Soc. B Biol. Sci.* 368:20130075. doi: 10.1098/rstb.2013.0075

Zöttl, M., Vullioud, P., Mendonça, R., Torrents Ticó, M., Gaynor, D., Mitchell, A., et al. (2016). Differences in cooperative behavior among Damaraland mole rats are consequences of an age-related polyethism. *Proc. Natl. Acad. Sci. U.S.A.* 113:10382. doi: 10.1073/pnas.1607885113

Conflict of Interest: The authors declare that the research was conducted in the absence of any commercial or financial relationships that could be construed as a potential conflict of interest.

frontiers in Ecology and Evolution

REVIEW
published: 01 July 2021
doi: 10.3389/fevo.2021.636402

Lagomorpha as a Model Morphological System

Brian Kraatz[1], Rafik Belabbas[2], Łucja Fostowicz-Frelik[3,4,5], De-Yan Ge[6], Alexander N. Kuznetsov[7], Madlen M. Lang[8], Sergi López-Torres[5,9,10], Zeinolabedin Mohammadi[11], Rachel A. Racicot[12,13], Matthew J. Ravosa[14], Alana C. Sharp[15], Emma Sherratt[16], Mary T. Silcox[8], Justyna Słowiak[5], Alisa J. Winkler[17,18] and Irina Ruf[13]*

[1] Department of Anatomy, Western University of Health Sciences, Pomona, CA, United States, [2] Laboratory of Biotechnologies Related to Animal Reproduction, Institute of Veterinary Sciences, Blida 1 University, Blida, Algeria, [3] Key Laboratory of Vertebrate Evolution and Human Origins, Institute of Vertebrate Paleontology and Paleoanthropology, Chinese Academy of Sciences, Beijing, China, [4] CAS Center for Excellence in Life and Paleoenvironment, Beijing, China, [5] Institute of Paleobiology, Polish Academy of Sciences, Warsaw, Poland, [6] Key Laboratory of Zoological Systematics and Evolution, Institute of Zoology, Chinese Academy of Sciences, Beijing, China, [7] Borissiak Paleontological Institute, Russian Academy of Sciences, Moscow, Russia, [8] Department of Anthropology, University of Toronto Scarborough, Toronto, ON, Canada, [9] Division of Paleontology, American Museum of Natural History, New York, NY, United States, [10] New York Consortium in Evolutionary Primatology, New York, NY, United States, [11] Department of Biology, Faculty of Science, Gorgan, Golestan, Iran, [12] Department of Biological Sciences, Vanderbilt University, Nashville, TN, United States, [13] Abteilung Messelforschung und Mammalogie, Senckenberg Forschungsinstitut und Naturmuseum Frankfurt, Frankfurt am Main, Germany, [14] Departments of Biological Sciences, Aerospace and Mechanical Engineering, and Anthropology, University of Notre Dame, Notre Dame, IN, United States, [15] Evolutionary Morphology and Biomechanics Group, Institute of Life Course and Medical Sciences, University of Liverpool, Liverpool, United Kingdom, [16] School of Biological Sciences, The University of Adelaide, Adelaide, SA, Australia, [17] Roy M. Huffington Department of Earth Sciences, Southern Methodist University, Dallas, TX, United Stats, [18] Department of Cell Biology, University of Texas Southwestern Medical Center, Dallas, TX, United States*

OPEN ACCESS

Edited by:
Rodney L. Honeycutt, Pepperdine University, United States

Reviewed by:
Conrad Matthee, Stellenbosch University, South Africa
John Wible, Carnegie Museum of Natural History, United States
Thomas Martin, University of Bonn, Germany

***Correspondence:**
Brian Kraatz
bkraatz@westernu.edu

Specialty section:
This article was submitted to Phylogenetics, Phylogenomics, and Systematics, a section of the journal Frontiers in Ecology and Evolution

Received: *04 January 2021*
Accepted: *14 May 2021*
Published: *01 July 2021*

Citation:
Kraatz B, Belabbas R, Fostowicz-Frelik Ł, Ge D-Y, Kuznetsov AN, Lang MM, López-Torres S, Mohammadi Z, Racicot RA, Ravosa MJ, Sharp AC, Sherratt E, Silcox MT, Słowiak J, Winkler AJ and Ruf I (2021) Lagomorpha as a Model Morphological System. Front. Ecol. Evol. 9:636402. doi: 10.3389/fevo.2021.636402

Due to their global distribution, invasive history, and unique characteristics, European rabbits are recognizable almost anywhere on our planet. Although they are members of a much larger group of living and extinct mammals [Mammalia, Lagomorpha (rabbits, hares, and pikas)], the group is often characterized by several well-known genera (e.g., *Oryctolagus*, *Sylvilagus*, *Lepus*, and *Ochotona*). This representation does not capture the extraordinary diversity of behavior and form found throughout the order. Model organisms are commonly used as exemplars for biological research, but there are a limited number of model clades or lineages that have been used to study evolutionary morphology in a more explicitly comparative way. We present this review paper to show that lagomorphs are a strong system in which to study macro- and micro-scale patterns of morphological change within a clade that offers underappreciated levels of diversity. To this end, we offer a summary of the status of relevant aspects of lagomorph biology.

Keywords: Lagomorpha, Leporidae, Ochotonidae, evolution, morphofunction, model organism, morphology, phylogeny

INTRODUCTION

Lagomorpha (rabbits, hares, and pikas) is a globally distributed (barring Antarctica) extant mammalian order within the larger superorder Euarchontoglires (rodents, lagomorphs, treeshrews, colugos, and primates) (Murphy et al., 2001). The order consists of herbivorous species across two extant families, the Ochotonidae (pikas) and the Leporidae (rabbits and hares) (Stock, 1976;

Forsyth et al., 2005; Hoffmann and Smith, 2005; Burgin et al., 2018; Smith et al., 2018; **Figure 1**). There are presently 12 living lagomorph genera recognized, subsuming 108 recognized species (see Burgin et al., 2018 for a recent treatment). These genera are distributed unequally between two families; the Leporidae contains 11 genera, the most well-known being *Lepus* (hares and jackrabbits), *Sylvilagus* (cottontails), and *Oryctolagus* (European rabbit) (Naff and Craig, 2012; Graham, 2015) while Ochotonidae includes only a single living genus, *Ochotona* (pikas) (Hoffmann and Smith, 2005; Ge et al., 2012; Smith et al., 2018; **Figure 2**).

Lagomorphs have featured prominently in the set of non-human model organisms that have driven many advances within the biological sciences over the last century, particularly to understand genetic, genomic, or developmental processes that drive biological change (Leonelli and Ankeny, 2013). Recent research on understanding the genome level architecture of life has included the European rabbit (*Oryctolagus cuniculus*), the mountain hare (*Lepus timidus*), the snowshoe hare (*Lepus americanus*), and the American pika (*Ochotona princeps*) (Marques et al., 2020). *Oryctolagus* and *Ochotona* have often served as the model lagomorphs in larger scale comparative studies of mammals (e.g., Sánchez-Villagra et al., 2017; Hecker et al., 2019). Though such studies have revealed much about broad patterns among mammals, often in an evolutionary context, there has been little comprehensive comparative work done within the lagomorph clade.

Monaghan (2014, p. 1019), through the lens of behavioral ecology, argue that the modern concept of model organisms

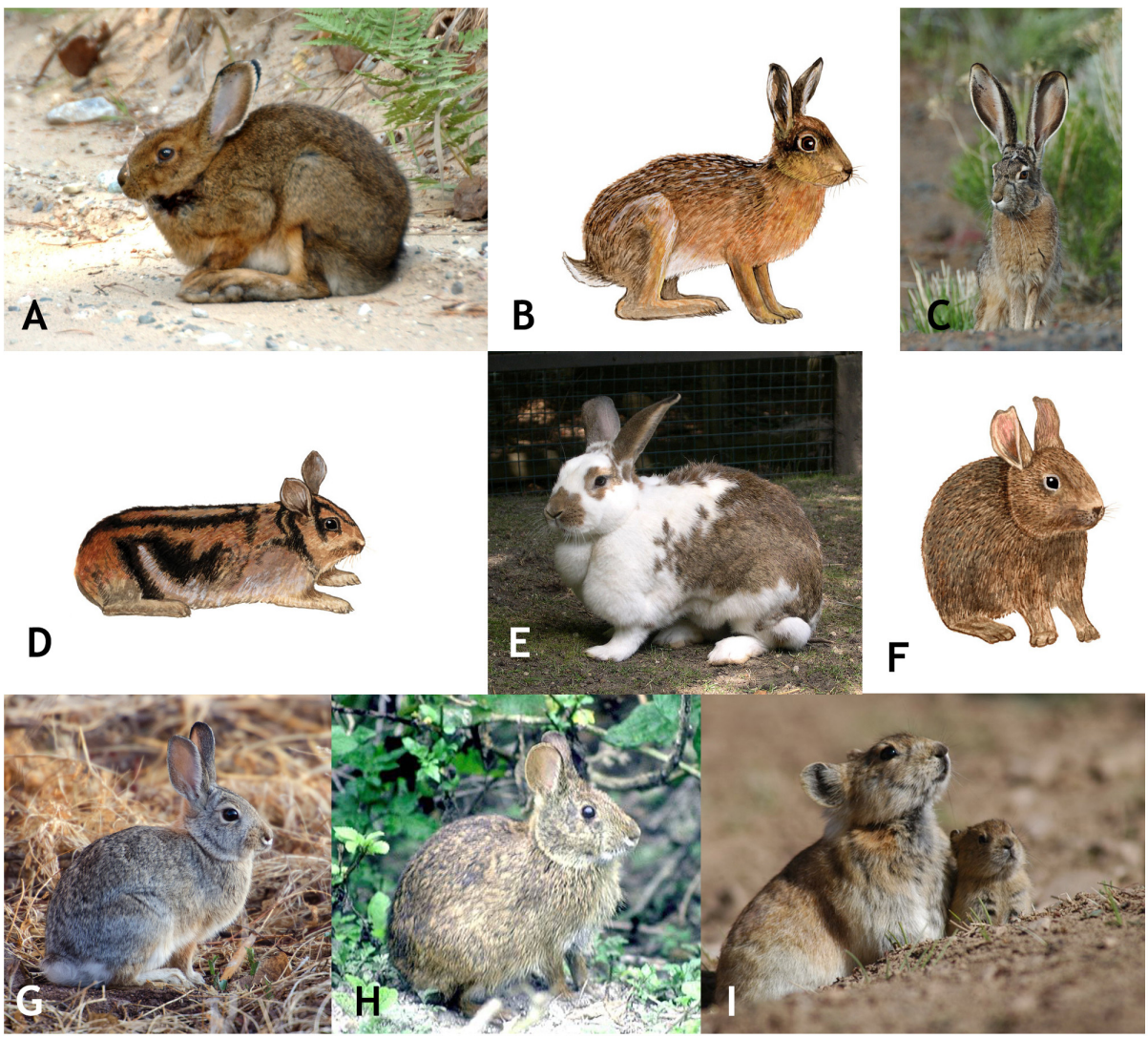

FIGURE 1 | A representative selection of extant lagomorphs, including: **(A)** *Lepus americanus* (snowshoe hare); **(B)** *Lepus europaeus* (European hare); **(C)** *Lepus californicus* (Black-tailed jackrabbit); **(D)** *Nesolagus timminsi* (Annamite striped rabbit); **(E)** *Oryctolagus cuniculus* (European rabbit); **(F)** *Romerolagus diazi* (Volcano rabbit); **(G)** *Sylvilagus audubonii* (Audobon's cottontail); **(H)** *Sylvilagus palustris* (Marsh rabbit); **(I)** *Ochotona curzoniae* (Black-lipped pika). All images from Myers et al. (2020).

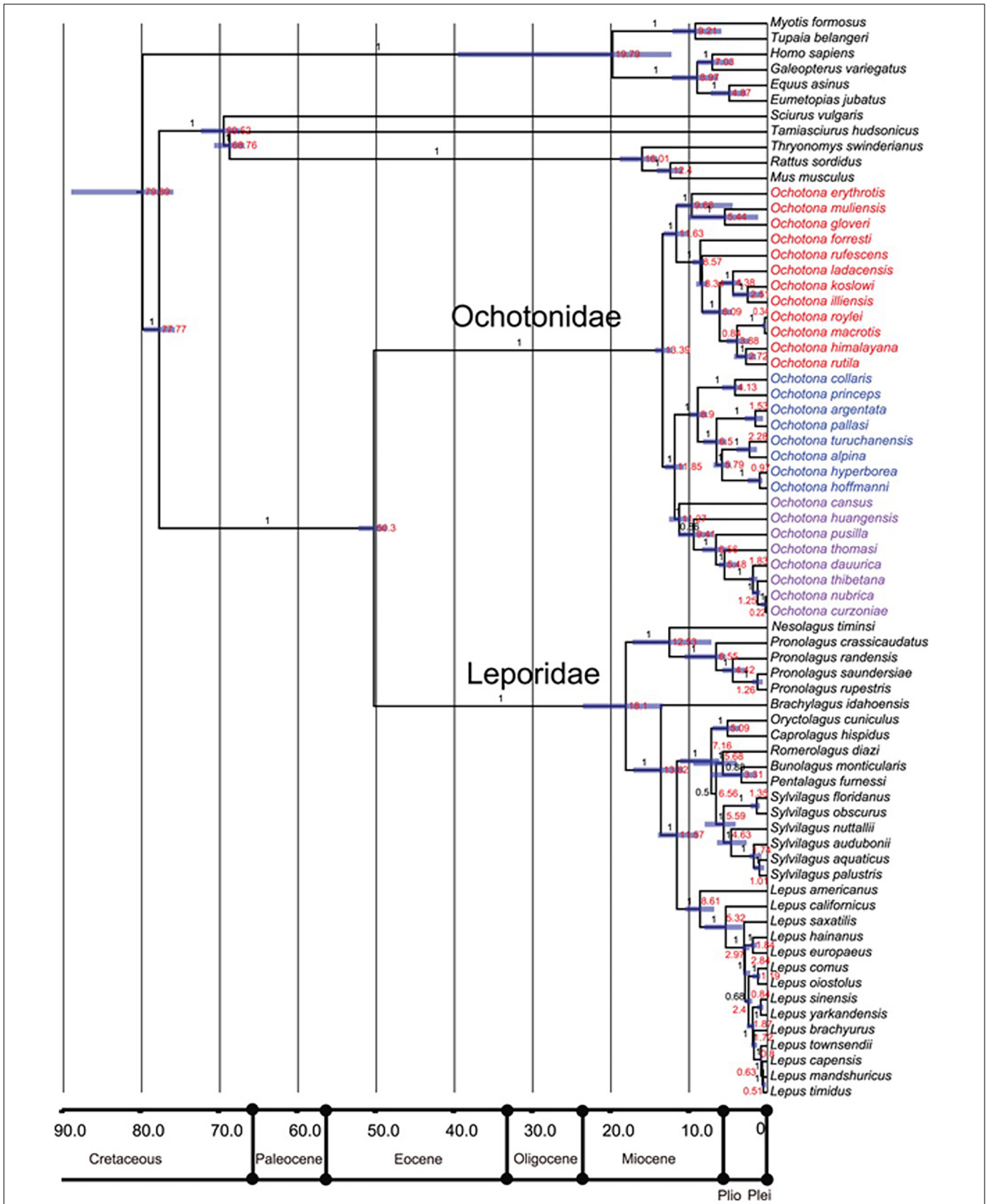

FIGURE 2 | Phylogeny of selected extant lagomorph species by Ge et al. (2013).

has limited some insights within the biological sciences away from a more intentional focus "to understand the processes responsible for the diversity that we see in animal form and function." Because such mechanisms often can be best understood by studying lineages and clades, we argue that Lagomorpha represent an ideal clade with which to explore these processes. Chapman and Flux (1990) have made such an argument for lagomorphs, which we expand here to include current scientific standings.

Among vertebrates, the radiations of anole lizards (*Anolis*) are a strong example of a clade that has served as a model system to study integrative processes in evolution and adaptive radiations (Sanger and Kircher, 2017). Extensive work on *Anolis* has included the historical, genetic, and developmental basis of anole diversity (e.g., Losos, 2011; Sanger et al., 2012; Sherratt et al., 2015; Corbett-Detig et al., 2020; Velasco et al., 2020). Though *Anolis* represents a strong comparative system, it is limited at scales that span longer geological periods. Lagomorpha are anchored by an extensively used model organism, the European rabbit (*O. cuniculus*), but include a rich fossil record that goes back to the Paleocene, a diverse group of living lineages, significant morphological and ecological disparity, and functional variation in multiple key aspects of behavioral biology. The goal of this review is to summarize key biological features of the lagomorph clade to highlight how they represent an ideal group to investigate both macro- and micro-level questions in morphological biology.

LAGOMORPH BIOLOGY

Rabbits and hares are found in forests, in open scrub, or savannah in Eurasia, Africa, and North, Central, and northern South America. Additionally, the European rabbit and hare have been introduced into Australia and South America (Chapman and Flux, 1990; Ge et al., 2013). Lagomorphs are hind-gut fermenters and require cecotrophy as well as at least a 15% crude fiber diet to maintain gastrointestinal health. Leporids are typically crepuscular and most active during the twilight hours at sunrise and sunset. They eat a wide variety of herbaceous material and grasses represent 30% of the plant food species ingested (Ge et al., 2013; Delaney et al., 2018). Pikas require a more specialized environment than hares and rabbits. They are most often found at high elevations in cold semiarid regions (Delaney et al., 2018). Pikas are distributed mainly throughout Asia, Eastern Europe, and western North America (Berkovitz and Shellis, 2018). They consume a wide variety of herbaceous plants, but grasses are a much smaller component of the diet than in that of rabbits and hares (Ge et al., 2013). The eyes of lagomorphs are laterally positioned, providing a circular field of vision (Delaney et al., 2018).

Among lagomorphs, the pikas are generally smaller (12–25 cm long; 100–400 g), with short limbs and small ears compared to their larger rabbit and hare counterparts (Ge et al., 2013; Delaney et al., 2018). Rabbits and hares have a short tail and lack or have minimal sexual dimorphism (e.g., Chapman and Ceballos, 1990; Fa and Bell, 1990; though see Orr, 1940 on sexual dimorphism in *Sylvilagus*); pikas lack an external tail and both sexes have a cloaca-like structure and lack sexual dimorphism (Graham, 2015). Most leporid males have testes located in a scrotum in front of the penis and females possess two to five pairs of mammary glands. Embryonically, the mammary glands develop from the mammary line (ridge), as is typical for placentals. However, it was found that, in the European rabbit, the anterior pair of mammary glands appear separately above the mammary ridge, in the axilla region of the forelimb (Propper, 1976). Gestation is 21–30 days in Ochotonidae and 24–55 days in Leporidae. Ochotonidae are typically altricial, though in some species the neonates are covered with fur. Leporidae show both patterns, altricial (*Brachylagus idahoensis*, *Bunolagus monticularis*, *O. cuniculus*, and *Sylvilagus* spp.) and precocial (*Lepus* spp.) species (Lissovsky, 2016). *Pentalagus furnessi*, *Poelagus marjorita*, *Pronolagus rupestris,* and *Romerolagus diazi* are altricial as well but the young are variable with respect to fur at birth. For some rare species of *Pronolagus*, *Nesolagus* spp., and *Caprolagus hispidus*, almost no information is yet available due to their rarity (Lissovsky, 2016; Schai-Braun and Hackländer, 2016). This is representative of our anatomical knowledge of lagomorphs, while there are comprehensive treaties on *Oryctolagus cuniculus* (Krause, 1884; Bensley, 1921; Barone et al., 1973) other species are much less studied.

SYSTEMATICS

Within the 11 extant leporid genera there are approximately 75 species and 35 species in the single extant ochotonid genus, *Ochotona* (Hoffmann and Smith, 2005; Ge et al., 2012, 2013; Burgin et al., 2018). A summary of the fossil record of the Lagomorpha by Ge et al. (2013) includes about 45 genera and more than 190 species of Leporidae, and about 32 genera and 180 species of Ochotonidae (for both families, these are formally nominated taxa). The following sections highlight key features of these groups and the status of systematic relationships.

Key Craniodental Characters

Lagomorpha have been defined by a broad set of specific characters, most of which are related to mastication and locomotion, due somewhat to the relevant abundance of related osteological regions in the fossil record (e.g., López Martínez, 1985; Asher et al., 2005, 2019; Wible, 2007; Lopez-Martinez, 2008; Koenigswald et al., 2010). The living lagomorph families can be easily distinguished by several morphological characters. Besides obvious external anatomical traits such as size and shape of the outer ear and limb proportions, there exist discrete craniodental differences between the two families: e.g., proportions of the rostrum and absence or presence of fenestration and pitting of the os maxillare and bones of the posterior skull (Wood, 1940; Angermann et al., 1990; Wible, 2007). As in rodents, all lagomorphs have hypselodont (evergrowing) incisors, which are unreplaced deciduous teeth. They differ from rodents in having a second set of small permanent upper incisors. The dental formula in leporids is: I 2/1, C 0/0, P 3/2, M 3/3 with 28 total teeth and in ochotonids is: I 2/1, C 0/0, P 3/2, M 2/3 with 26 teeth (Graham, 2015; Delaney et al., 2018). See Wible (2007),

Fostowicz-Frelik and Meng (2013), and Ruf (2014) for a review of lagomorph cranial literature. Soft tissue structures such as the cephalic arterial system (Bugge, 1974) also can be used for investigation of fossil species because adjacent bony structures (e.g., foramina, sulci) serve as proxies.

In contrast, taxonomy and systematic relationships at the genus and species level, and the phylogenetic position of certain fossil taxa, remain unresolved due to possible homoplastic evolution of certain characters (Robinson and Matthee, 2005; Kraatz et al., 2010; Fostowicz-Frelik and Meng, 2013; Asher et al., 2019). For instance, the premolar foramen was regarded as a synapomorphic character of Ochotonidae although a puzzling pattern among extant Lagomorpha became evident (Corbet, 1983: lateral palatal foramen); however, a study using broad taxon sampling including fossil species clearly revealed its diversity and homoplastic nature among Lagomorpha (Fostowicz-Frelik and Meng, 2013). In his comprehensive comparative description of the external craniomandibular anatomy of *O. princeps*, *R. diazi* and further selected Leporidae, Wible (2007) complemented and refined a character matrix comprising 229 traits including 92 craniomandibular characters (Meng et al., 2003; Asher et al., 2005). To date, intracranial structures are underrepresented in phylogenetic studies of Lagomorpha. Recent studies on the nasal and ear region defined new intracranial characters that can significantly contribute to a deeper understanding of lagomorph systematics, evolution, and morphofunction. For example, extant Ochotonidae and Leporidae differ significantly in the number of turbinals (Ruf, 2014). The former have a reduced number of olfactory turbinals and lack the interturbinal in the frontoturbinal recess. The turbinal pattern in the ethmoturbinal recess of Leporidae shows certain apomorphic character states (number of ethmo- and interturbinals) in several clades that can also be used for systematic purposes at the genus and species level (Ruf, 2014).

The middle ear morphology of extant Lagomorpha reveals unique family-specific patterns of the anterior attachment of the malleus by means of the processus anterior and its processus internus praearticularis; however, the phylogenetic polarization of this character still was pending (Maier et al., 2018). A first attempt to polarize the observed patterns could be achieved by the first high-resolution computed tomography (μCT) study on intracranial structures in a fossil lagomorph; *Palaeolagus haydeni* reveals that early ontogenetic stages of *Ochotona* may represent the plesiomorphic lagomorph pattern (Ruf et al., 2021). This clearly shows the potential of μCT investigations of fossil Leporidae and Ochotonidae for elucidating the evolution of intracranial characters.

Traditionally, dental characters play a major role in lagomorph taxonomy and systematics, especially in fossil species, and there is extensive literature summarizing this important system (e.g., Dawson, 1958; Hibbard, 1963; White, 1991; Averianov and Tesakov, 1997; Patnaik, 2002; Kraatz et al., 2010; Winkler and Tomida, 2011). The occlusal pattern of anterior premolars (particularly p3) is highly diagnostic, even on a lower taxonomic level. However, although most individuals within an extant or fossil population will have the diagnostic pattern, there often are individuals (in particular, younger ones with less occlusal wear) preserving a pattern that would suggest assignment to a different taxon (Hibbard, 1963). The masticatory pattern, also reflected in the occlusal morphology and the number of shearing blades of the cheek teeth, separates most Ochotonidae from all but two genera (*Romerolagus diazi* and *Pronolagus*) of extant Leporidae (Koenigswald et al., 2010). Beside systematic relationships and some species-specific patterns, this character complex provides insight into the evolution of functional adaptations. The lagicone structure, a complex enamel structure on the buccal occlusal surface of stem lagomorphs and certain Ochotonidae (López Martínez, 1985), becomes reduced in fossil European ochotonids; thus, the shearing function in pikas is increased. In most Leporidae the grinding function is enhanced by crenulation of specific enamel bands (Koenigswald et al., 2010). The two living lagomorph families also can be distinguished by the enamel pattern (schmelzmuster) of their incisors, a key character complex in terms of evolution and morphofunction of Glires (Martin, 1999, 2004). Generally, the incisors of Leporidae show a single-layered schmelzmuster in concert with multi-layered Hunter-Schreger bands (HSB). This pattern is derived from a double-layered schmelzmuster as observed in an undetermined leporid from the early Eocene of Kyrgyzstan and in some Mimotonidae. In contrast, Ochotonidae have a multi-layered schmelzmuster with modified HSB and enamel patterns differing in upper and lower incisors (Martin, 1999, 2004).

Key Postcranial Characters

Overall, the body-plan of lagomorphs is relatively uniform throughout their evolutionary history. There are two basic archetypes, which are represented by two extant families: the longer legged rabbits and hares, and shorter legged, rather stocky ochotonids. The ochotonid-like morphotype (or small, relatively short-limbed rabbits) dominated during the Paleogene, which suggests that true cursorial abilities appeared within lagomorphs later in the early Neogene. However, the structure of the lagomorph hindlimb with the closely connected tibia and fibula (fused already in the late Eocene *Palaeolagus*), and a unique direct calcaneo-fibular contact known from the Middle Paleocene duplicidentate of China (Fostowicz-Frelik, 2017) indicate cursorial adaptations since the groups' inception. The calcaneus is known in several Eocene lagomorphs, including the Asian *Dawsonolagus* and *Strenulagus* (Li et al., 2007; Fostowicz-Frelik et al., 2015a) and North American *Palaeolagus* (Wood, 1940). In most Paleogene lagomorphs, calcaneal structure is similar to *Ochotona*; the latter is somewhat stockier (compared to that of leporids) with a proportionally shorter tuber and calcaneal body. The calcaneal canal is a striking synapomorphy of Lagomorpha (Bleefeld and Bock, 2002).

Beginning with the Mio-Pliocene radiation, the postcranial skeleton of Leporidae acquires more cursorial adaptations. Overall, the limb bones become slenderer and the tibiofibula and foot complex (including also tarsal elements) elongate (e.g., Fostowicz-Frelik, 2007). Studies of Neogene leporid postcrania based on large samples and/or complete specimens are relatively uncommon. Most studies focus on cursorial and fossorial adaptations, for example, (1) a partial skeleton of *Trischizolagus* (early Pliocene, Moldova; Averianov, 1995) suggests it was less cursorial than *Hypolagus* and was a strong digger, although not as

fossorial as *Oryctolagus*; and (2) a large sample of *Serengetilagus* (based on forelimb anatomy; hindlimb not yet studied) ally this genus with smaller, relatively less cursorial leporids such as *Oryctolagus* and suggest it may have been semi-fossorial (early Pliocene, Tanzania; Winkler et al., 2016). As an example, from Ochotonidae, Dawson (1969) described the osteology of an abundant, albeit geologically younger (Quaternary, ca. 2.6 Ma to 200 BP) species *Prolagus sardus* from collections primarily from Corsica and Sardinia. Dawson concluded that the species "was probably not suited for speed over any great distance but was probably fairly adept at digging and well adapted for climbing and scrambling. . ." (Dawson, 1969, p. 187).

Phylogenetic Placement of Lagomorpha

The placement of Lagomorpha within the larger mammalian clade had been problematic for over a century (see Kraatz et al., 2010 for a review) due to an incomplete fossil record that did not include important stem lagomorphs. The earliest molecular phylogeny based on the eye lens protein alpha-crystallin revealed a close phylogenetic relationship of rabbits to primates (de Jung et al., 1977). That work also showed that rodents and lagomorphs form a supraordinal group (Glires) based on the interphotoreceptor retinoid binding protein (IRBP) (de Jung et al., 1977; Stanhope et al., 1992, 1996). New fossil discoveries such as the primitive rodent *Tribosphenomys* from strata of transitional Paleocene-Eocene age in Inner Mongolia (China) and Mongolia (Meng et al., 1994; Asher et al., 2005) began to support the close relationship between lagomorphs and rodents as cohort Glires. However, 91 orthologous protein sequences supported Lagomorpha as more closely related to Primates and Scandentia (treeshrews) than they are to rodents (Graur et al., 1996). The monophyly of a Glires clade was supported by complete mitochondrial genomes (Lin et al., 2002) and was consistent with the result of three nuclear studies, which included the von Willebrand Factor, an interphotoreceptor retinoid-binding protein, and an Alpha 2B adrenergic receptor (Huchon et al., 2002). Subsequently, a phylogenetic reconstruction based on 18 homologous gene segments confirmed Glires as a sister taxon to primates, colugos and treeshrews (Douady and Douzery, 2003). Analyses based on eight housekeeping genes further confirmed the monophyly of Glires (Kullberg et al., 2006). This was further evidenced by genome level data, including the monophyly of Glires, their close relationship with Primates, Scandentia and Dermoptera; and that all these taxa together formed the clade of Euarchontoglires (=Supraprimates) (Kumar et al., 2013; Foley et al., 2016; Esselstyn et al., 2017; Upham et al., 2019; Genereux et al., 2020).

Phylogenetic Relationships Within Lagomorpha

Early studies of morphological and ecological traits of extant lagomorphs resulted in different phylogenetic hypotheses (Dawson, 1981; Stoner et al., 2003). Considerable homoplasy in the morphology of leporid species was identified by Corbet (1983) after examining 21 morphological characteristics for 22 leporid species. More recent morphometric studies of lagomorphs have also found a high degree of homoplasy, low phylogenetic signal, and adaptive divergence in skull shape (Ge et al., 2015; Kraatz and Sherratt, 2016; Feijó et al., 2020). These studies highlight the difficulties in reconstructing a robust phylogeny for lagomorphs, particularly at the intergeneric level, by using morphological data. Relationships of extant genera were reconstructed based on the combined matrix of five nuclear and two mitochondrial DNA fragments: *Ochotona* is the earliest diverging taxon, which represents a relict genus of Ochotonidae; *Nesolagus*, *Poelagus,* and *Pronolagus* form an early diverging monophyletic clade within Leporidae. *Romerolagus*, *Lepus*, *Sylvilagus*, *Brachylagus*, *Bunolagus*, *Oryctolagus*, *Caprolagus*, and *Pentalagus* form another clade of Leporidae (Matthee et al., 2004; Robinson and Matthee, 2005). The general phylogenetic structure of the tree was supported by genomic orthologous retroposon insertion sites (Kriegs et al., 2010).

Within Lagomorpha, *Lepus* and *Ochotona* represent the most speciose extant genera. Molecular phylogenies within each of these genera have been extensively studied. The early studies are generally based on a single locus mitochondrial DNA marker, cytochrome b (*CYTB*) (Yu et al., 1996; Halanych et al., 1999; Niu et al., 2004). Five major species groups within *Ochotona* were recognized: the northern group, the surrounding Qinghai-Tibet Plateau group, the Qinghai-Tibet Plateau group, the Huanghe group, and the Central Asia group (Niu et al., 2004; Lanier and Olson, 2009). Subsequently, more genes were included, for example, the dataset of *CYTB* 12S, ND4, and the control region of the mitochondrial genome revealed the Chinese hare (*Lepus sinensis*) is not a monophyletic group, with three species groups recognized within *Lepus*: North America species group, South Africa species group and the Eurasia species group (Wu et al., 2005; Liu et al., 2011). Recent studies based on exome of the whole genome supported five subgenera of extant *Ochotona*: *Alienauroa*, *Conothoa*, *Ochotona*, *Lagotona*, and *Pika*, with divergence time and phylogeographic analyses inferring the last common ancestor of extant pikas first occurred in the middle Miocene, approximately 14 Ma (Wang et al., 2020).

Mito-nuclear discordance was shown in *Lepus* (Kinoshita et al., 2019) and *Ochotona* (Lissovsky et al., 2019), which could be the result of incomplete lineage sorting, sex-biased dispersal, asymmetrical introgression, natural selection, or *Wolbachia*-mediated genetic sweeps. The genome of four lagomorph species (*O. cuniculus*, *L. timidus*, *L. americanus*, and *O. princeps*) has been sequenced and annotated (Marques et al., 2020). These data provide references for more deep level studies in exploring the morphology, behavior, as well as population genetics of lagomorphs. However, more novel sampling is still needed for a complete phylogenomic analyses of Lagomorpha. Moreover, integrating data from fossils with extant species probably will provide a more comprehensive overview on the evolutionary history of lagomorphs.

THE FOSSIL RECORD

Lagomorphs of modern aspect are known in the fossil record since the Early Eocene (ca. 52 Ma) of China (Li et al., 2007;

Wang et al., 2010) and Mongolia (Lopatin and Averianov, 2008). The Asian record of Lagomorpha precedes that of North America by over 10 million years, and that of Europe by almost 20 Ma. Asia is considered the diversification center for the Duplicidentata, treated as a more inclusive group including crown lagomorphs and species more closely related to extant lagomorphs than rodents. Many of these earliest species are characterized by a double set of the upper and lower incisors and are referred to the ancestral Mimotonidae (Meng and Wyss, 2001; Fostowicz-Frelik et al., 2015b; Fostowicz-Frelik, 2017), an extinct fossil group restricted to China, Mongolia, and Kyrgyzstan (Li, 1977; Li and Ting, 1985; Averianov, 1994; Asher et al., 2005; Li C. K. et al., 2016; Fostowicz-Frelik, 2020). The mimotonids are a paraphyletic group with two distinct lineages: the small Paleocene mimotonids (Li, 1977; Li C. K. et al., 2016; Fostowicz-Frelik, 2020) and the large Eocene forms (Bohlin, 1951; Averianov, 1994; Meng et al., 2004; Asher et al., 2005; Fostowicz-Frelik et al., 2015b). One of the large forms, *Mimolagus*, likely survived to the Eocene–Oligocene boundary (Bohlin, 1951; see also Zhang and Wang, 2016) and was the terminal representative of the mimotonids (Fostowicz-Frelik et al., 2015b). Although Lagomorpha and Mimotonidae share many similarities in dental structure, most of these characters are plesiomorphic; thus, none of the mimotonids could be unquestionably named the direct ancestor of lagomorphs. All the Eocene lagomorph taxa and a substantial part of the Oligocene species are regarded as stem lagomorphs, although they frequently show similarities to either of the crown groups (Leporidae and Ochotonidae, see Fostowicz-Frelik and Meng, 2013).

The earliest findings of non-mimotonid stem lagomorphs come from the latest Early Eocene of Asia: *Dawsonolagus* from Inner Mongolia, China (Li et al., 2007), and *Arnebolagus* from Mongolia and Kyrgyzstan (Averianov and Lopatin, 2005; Lopatin and Averianov, 2008, 2020). By the Middle Eocene, China and Kyrgyzstan witnessed the first lagomorph diversification, yielding multiple genera (Li, 1965; Tong, 1997; Averianov and Lopatin, 2005; Meng et al., 2005; Fostowicz-Frelik et al., 2012, 2015a; Fostowicz-Frelik and Li, 2014; Li Q. et al., 2016). By the end of the Eocene, the lagomorph fauna of Asia was enriched, in particular, by *Desmatolagus* (Meng et al., 2005), a key lagomorph genus for the Oligocene in Asia (Erbajeva and Daxner-Höck, 2014).

Asian Eocene lagomorphs were very small, with an estimated body mass under 150 g (Fostowicz-Frelik et al., 2015b). Starting from the Middle Eocene, Asian lagomorphs doubled in size, but even then, most of the Paleogene genera did not exceed the size of a large *Ochotona* (ca. 250 g). With the beginning of the Oligocene, the *Desmatolagus* lineage became diverse, abundant, and widespread throughout Central Asia (Sych, 1975; Huang, 1987; Wang, 2007), surviving until the Miocene, and possibly entering Europe (Early Oligocene, Vianey-Liaud and Lebrun, 2013) and North America (Late Oligocene; Dawson, 2008). Along with *Desmatolagus*, in the late Early/Middle Oligocene, the first plausible representatives of crown lagomorphs appear in Asia: *Sinolagomys* (an early ochotonid from China and Mongolia; see Erbajeva et al., 2017) and *Ordolagus* (probably an early leporid from China; Bohlin, 1942).

In North America, the lagomorph fossil record starts in the late Middle Eocene (ca. 42 Ma; see Dawson, 2008). Two genera, *Mytonolagus* and *Procaprolagus*, are known from this period and likely represent two different immigrations from Asia (Dawson, 2008). There is a significant increase in diversity in the Lagomorpha of North America beginning in the Late Eocene: this includes genera with true hypselodont cheek teeth such as *Chadrolagus* (Gawne, 1978; Fostowicz-Frelik, 2013) and the first representatives of *Palaeolagus* and *Megalagus* (Dawson, 1958, 2008). At the Eocene-Oligocene boundary (EOB), a turnover in the lagomorph fauna is observed, defined by a shift from unilateral hypsodonty (i.e., high-crowned, evergrowing lingual sided and low-crowned buccal sided cheek teeth) toward a hypselodont condition in their cheek teeth ('full' hypsodonty). Among *Megalagus* and *Palaeolagus*, the unilaterally hypsodont species went extinct at the EOB and were replaced by species either with greatly reduced buccal roots, or fully developed hypselodont cheek teeth. *Litolagus*, with its advanced cranial morphology, may represent either crown Leporidae (see Fostowicz-Frelik, 2013) or an advanced stem taxon. Later during the Early Oligocene, other hypselodont species appear, for example, *Palaeolagus burkei* may be closely related to *Litolagus* or it may have convergent traits in dentition and bulla structure, which could be a result of adaptations to more open habitats of the North American plains. All lagomorph lineages that originated during the Eocene-to-Oligocene interval in North America went extinct by the Early Miocene (Dawson, 2008).

In Europe, the earliest lagomorphs are known from the Early Oligocene of France (*Ephemerolagus nievae*; Vianey-Liaud and Lebrun, 2013) and Germany (*Shamolagus franconicus*; Heissig and Schmidt-Kittler, 1975, 1976). The remains are scarce, and their appearance is limited only to the type localities, but these genera clearly represent two distinct lineages. Lagomorph lineages reappearing in Europe by the end of the Oligocene (Tobien, 1974, 1975) are regarded as either primitive ochotonids (McKenna, 1982) or as stem line representatives (Fostowicz-Frelik and Meng, 2013). These lineages persist in Europe from the Late Oligocene (Fostowicz-Frelik, 2016) until the Early Miocene (Tobien, 1974).

The Early to Middle Miocene (beginning ca. 23 Ma) is characterized by the last records of the stem lagomorphs and the worldwide radiation of the Ochotonidae (Dawson, 2008; Ge et al., 2013). The Early Miocene record of stem Lagomorpha consists mostly of derived *Desmatolagus* (Lopatin, 1998; Wang et al., 2009) and Asian representatives of *Amphilagus*, a Late Oligocene-Early Miocene genus from Europe, which has been reported recently also from Mongolia and Siberia (Erbajeva, 2013; Erbajeva et al., 2016). In North America, the earliest Miocene marks the last appearance of taxa such as *Megalagus* and *Palaeolagus* (Dawson, 2008). In Europe a plethora of Ochotonidae appeared in the Early Miocene, for example *Alloptox* and *Prolagus* (Tobien, 1974, 1975; López Martínez, 2001). In the Early and Middle Miocene taxa such as these existed alongside the stem lineages, which went extinct no later than the Middle Miocene (Tobien, 1974; Fostowicz-Frelik et al., 2012). *Prolagus*, first reported from the Early Miocene, was the most speciose and long-lived lineage of the European ochotonids and the last

species, *P. sardus*, survived in the Mediterranean until historic times (Lopez-Martinez, 2008). Simultaneously, starting from the Middle Miocene, a lineage leading to extant *Ochotona*, the only surviving member of the Ochotonidae, arose in Central Asia (Wang et al., 2009; Fostowicz-Frelik and Frelik, 2010): this lineage also flourished in Asia during the Pliocene.

The earliest known ochotonids from North America are from near the Oligocene-Miocene boundary: all these early immigrants went extinct not later than ca. 9 Ma (Dawson, 2008). *Ochotona* was first reported in North America in the Late Miocene: this genus was geographically and taxonomically diverse during the Late Miocene-Pliocene in the Northern Hemisphere (Erbajeva et al., 2015). The genus decreased in diversity and relative abundance beginning in the Pleistocene (ca. 2.6 Ma; Erbajeva et al., 2015).

The earliest lagomorphs to reach Africa were representatives of the Asian sinolagomyine ochotonids, which dispersed into Africa as far as southern Africa in the Early Miocene (Winkler and Avery, 2010). Extinction of the African sinolagomyines by the Middle Miocene was coincident with the global extinction of archaic ochotonids by the end of the Middle Miocene (Erbajeva et al., 2015). The only post Middle Miocene reports of ochotonids from Africa are *Prolagus*, reported from the Late Miocene to Early Pleistocene of northern Africa (López Martínez, 2001; Winkler and Avery, 2010). In contrast to the ochotonids, Ge et al. (2013) noted that the diversity of the Leporidae was relatively modest during much of the Miocene, increasing around the Miocene-Pliocene transition, and with high diversity continuing into the Pliocene and Pleistocene.

The earliest record of leporids in Africa is in the Late Miocene (Winkler and Avery, 2010) as part of a geographically widespread and relatively abrupt dispersal of leporids at ca. 8 Ma that Flynn et al. (2014) called the Leporid Datum. Leporids dispersed from North America to northern Asia, spread throughout Eurasia, and entered Southern Asia (by 7.4 Ma) and Africa (ca. 7 Ma) (Flynn et al., 2014). Ge et al. (2013) correlated the geographic dispersal and increase in diversity of the leporids around the Late Miocene (and the opposite response of the ochotonids) with a period of global cooling and drying, and the expansion and diversification of C4 plants (at the expense of the C3 plants) in tropical and temperate areas.

KEY FUNCTIONAL GENES OF LAGOMORPHS

Wild populations of lagomorphs are greatly affected by two diseases, rabbit hemorrhagic disease and myxomatosis. The genes relating to the immune system and these diseases are well studied. These are, for example, interleukins, chemokines and chemokine receptors, Toll-like receptors, antiviral proteins (RIG-I and Trim5), and the genes encoding fucosyltransferases that are utilized by rabbit hemorrhagic disease virus as a portal for invading host respiratory and gut epithelial cells (Pinheiro et al., 2016). Fourteen IgA (immunoglobulin A) subclasses have been identified in *O. cuniculus*, eleven of which are expressed. In contrast, most other mammals have only one IgA, or in the case of hominoids, two IgA subclasses (Pinheiro et al., 2018). VHn genes are a conserved ancestral polymorphism that has been maintained in the leporid genome and being used for the generation of VDJ rearrangements by both modern *Lepus* and *Oryctolagus* (Pinheiro et al., 2019). Toll-like receptors (TLRs) are one of the first lines of defense against pathogens and are crucial for triggering an appropriate immune response: strong selection of the TLR2 coding region among the Lagomorpha suggests an evolutionary history that differs from other mammals (Neves et al., 2019). A high level of variation in the tripartite motif-containing protein 5 alpha (TRIM5) PRYSPRY domain of Lagomorpha species that belong to the same genus was believed to restrict retroviral infections (Águeda-Pinto et al., 2019). Recent study revealed the winter coat color polymorphism of snowshoe hares was associated to the genomic region of the pigmentation gene Agouti (Giska et al., 2019; Jones et al., 2020). Genetic variation at Agouti clustered by winter coat color occurs across multiple hare and jackrabbit species (Jones et al., 2018).

HYBRIDIZATION IN LAGOMORPHA

Hybridization may accelerate speciation via adaptive introgression or cause near-instantaneous speciation by allopolyploidization (Abbott et al., 2013). There are many articles referring to the hybridization, gene flow or reticulate evolution of lagomorphs (**Table 1**). Previous studies reported hybridization occurred within *Lepus*, *Oryctolagus*, and *Ochotona* usually based on single, multilocus DNA markers, and microsatellite loci (Chapman and Morgan, 1973; Wu et al., 2011; Koju et al., 2017). In some cases, selective advantages of hybrid forms to special climate condition in the contact zone and competitive exclusion of parental forms causes hybrid superiority over parental species (Mohammadi et al., 2020) because enhanced reproductive success may be due to the selective advantages of new combinations of mito-nuclear packages.

In addition, transitional phenotype of hybrids and introgressions also encounter traditional taxonomy with confusion in hybrid zones while reticulate and mosaic evolution of the genome and incomplete lineage sorting especially within nuclear loci also make application of new molecular tools such as DNA barcoding for identification of species useless. Plausible conspecificity have been raised from lack of morphological diagnostic characters and low genetic divergence in phylogenetic reconstructions based on some few nuclear loci (Liu et al., 2011). There are still gaps in sampling from type localities of some taxa (e.g., *Lepus tibetanus pamirensis*; type locality: near Lake Sarui-Kul, Pamir Mountains) and gaps for understanding the intraspecific genetic diversity (e.g., in *Lepus saxatilis* from Africa, in *Lepus melainus* and all other kinds of Manchurian hares). The taxon *przewalskii* is still controversial and the taxonomic status of *centrasiaticus* has not been resolved due to its morphological similarities to *Lepus oiostolus*, and its morphometric (Cheng et al., 2012) and molecular affinity to *L. tolai* (Wu et al., 2011; Smith et al., 2018). Possible paraphyly of some taxa such as *L. timidus* and *Lepus tolai* in China (Wu et al., 2005; Shan et al., 2020); *Lepus capensis s.l.* in Africa

TABLE 1 | Research activities related to hybridization of Lagomorpha.

Species	Data	Major conclusion	References
L. granatensis *L. europaeus* *L. castroviejoi* *L. corsicanus* *L. timidus* *L. capensis* *L. arcticus* *L. othus* *L. americanus* *L. californicus* *L. townsendii*	14 nuclear DNA and 2 mtDNA fragments	Highly incongruent with mtDNA phylogeny using parametric bootstrap. Simulations of mtDNA evolution under the speciation history inferred from nuclear genes did not support the hypothesis of mtDNA introgression from *L. timidus* into the American *L. townsendii* but did suggest introgression from *L. timidus* into four temperate European species.	Melo-Ferreira et al., 2012
L. europaeus *L. granatensis*	Autosomal microsatellite loci and X- and Y-linked diagnostic loci	The lack of mtDNA differentiation across the boundary is mostly due to sharing of mtDNA from a boreal species currently extinct in Iberia (*L. timidus*) whose mitochondria have thus remained in place since the last deglaciation despite successive invasions by two other species.	Melo-Ferreira et al., 2014a
O. cuniculus algirus *O. c. cuniculus*	Transcriptome and the target enrichment datasets	Genes lying within differentiated regions were often associated with transcription and pigenetic activities, including chromatin organization, regulation of transcription, and DNA binding.	Carneiro et al., 2014
L. americanus *L. townsendii* *L. californicus*	Eight nuclear markers and one mitochondrial DNA	The isolation-with-migration model suggested that nuclear gene flow was generally rare or absent among species or major genetic groups, coalescent simulations of mtDNA divergence revealed historical mtDNA introgression from *L. californicus* into the Pacific Northwest populations of *L. americanus*.	Melo-Ferreira et al., 2014b
L. granatensis *L. timidus*	100 nuclear SNPs	The distribution of allele frequencies across populations suggests a northward range expansion, particularly in the region of mtDNA introgression.	Marques et al., 2017
O. spp.	Two mitochondrial (CYT B and COI) and five nuclear gene segments (RAG1, RAG2, TTN, OXAIL and IL1RAPL1)	Conflicting gene trees implied mitochondria introgression from *O. cansus* to *O. curzoniae*.	Koju et al., 2017
L. timidus *L. europaeus*	6833 SNP markers	Introgression is highly asymmetrical in the direction of gene flow from mountain hare to brown hare, and that the levels of nuclear gene introgression are independent of mtDNA introgression.	Levanen et al., 2018
L. americanus	Whole genome sequence	Genetic variation at *Agouti* clustered by winter coat color across multiple hare and jackrabbit species, revealing a history of recurrent interspecific gene flow.	Jones et al., 2018
O. princeps	24 microsatellite loci	Fine-scale population genetic analysis suggests gene flow is limited but not completely obstructed by extreme topography such as glacial valleys, as well as streams including the Colorado River.	Castillo Vardaro et al., 2018
L. timidus *L. granatensis*	Whole genome sequencing	Post-glacial invasive replacement of *L. timidus* by *L. granatensis*. Outliers of elevated introgression include several genes related to immunity, spermatogenesis, and mitochondrial metabolism.	Seixas et al., 2018

(Lado et al., 2016) and *L. timidus* from northern Europe, Siberia, and Fennoscandian regions (Waltari and Cook, 2005) add to the complexity of the taxonomic status of some of the members of the genus *Lepus* and essential need for revision based on complete genome phylogenetic analyses. There are many reports of hybridization between different species like between *L. tolai,* and *L. timidus* with *L. sinensis*, from *L. sinensis* into *L. mandshuricus* (Liu et al., 2011), between *L. tolai* and *L. yarkandensis* (Wu et al., 2011), *L. timidus* into *L. granatensis* and *L. europaeus* (Alves et al., 2003), from *L. europaeus* into *L. tolai* (Mohammadi et al., 2020). Sharing of the same haplotypes between two different species and some cases of hybridization and introgression between sister taxa have been also reported within pikas [e.g., between *Ochotona cansus* and *Ochotona curzoniae* (Koju et al., 2017), *Ochotona dauurica* and *O. cansus* (Lissovsky et al., 2019), *O. curzoniae* and *Ochotona nubrica* (Yu et al., 2000; Niu et al., 2004; Lissovsky, 2014; Lissovsky et al., 2019)]. Moreover, lack of type specimens and the probable presence of hybrid forms even in the type localities, which makes molecular comparisons doubtful (e.g., for *L. tolai*; see Mohammadi et al., 2020) and have raised even further questions concerning the taxonomy and evolutionary relationships between taxa. More comprehensive studies are needed to address taxonomic challenges remaining around the North American white-tailed jackrabbit *Lepus townsendii*, *Lepus corsicanus* from Italy, and *Lepus castroviejoi* from the Iberian Peninsula.

The vast variety of introgression and evidence of hybridization between two species in areas of sympatry and parapatry (e.g., between *L. europaeus* and *L. tolai* in Iran; *L. europaeus* and *L. timidus* in Sweden; *L. tolai* and *L. yarkandensis* in Tarim Basin, China) and the lack of evidence of hybridization in other cases

of geographical sympatry (e.g., between *L. europaeus* and *L. tolai* in Kazakhstan; between *L. tibetanus*, *L. oiostolus*, and *L. tolai* in China; *L. yarkandensis* and *L. timidus* also in China) have suggested the genus *Lepus* as a good natural model for studying and tracing hybridization and the speciation process and also highlights the insufficient taxonomic knowledge to identify many of the taxa indicated as hybridized in scientific literature.

DOMESTICATION OF LEPORIDAE

The domesticated rabbit is derived from *O. cuniculus* and has its history in early European cultures (Clutton-Brock, 1989). While it is hypothesized that the Romans spread wild rabbits out of the native Iberian Peninsula to much of Europe and British Isles, they did not attempt to domesticate it. Several authors recounting the history of rabbit domestication place the origin with French Medieval monks (Clutton-Brock, 1989; Naff and Craig, 2012), where rabbits were kept in hutches or walled gardens to be fattened up for consumption, and thus selectively bred to increase body size. The morphological diversity among the ∼50 breeds of the domesticated rabbit known today is driven by body size (e.g., dwarf and giant forms), thus many differences in morphological features are likely a result of allometry, the associated shape changes with size, and heterochrony, the changes in timing of development (e.g., Fiorello and German, 1997; Sánchez-Villagra et al., 2017). Studies of morphological variation in companion and laboratory rabbits are predominantly focused on pathological and skeletal abnormalities resulting from their continual tooth growth (e.g., Okuda et al., 2007; Böhmer and Böhmer, 2017; Parés-Casanova and Cabello, 2020).

LAGOMORPH DEVELOPMENT

Our knowledge of lagomorph development is based primarily on the common laboratory rabbit, *O. cuniculus*, because this species is easy to keep and breed and therefore early ontogenetic stages are readily available. *O. cuniculus* is an induced ovulator (Boussit, 1989; Delaney et al., 2018). Sexual differentiation is established on the 16th day of embryonic development, and oogenesis continues for about 2 weeks after birth (Mauleon, 1967; Kennelly et al., 1970). Graafian follicles appear in the New Zealand breed at 12 weeks of age. Ovulation occurs between 10 and 12 h after mating and the peak of fecundity is observed between 12 and 15 h *post coitum* (*pc*) (Harper, 1961; Thibault, 1967; Foote and Carney, 2000). Based on the observations of Lopez-Bejar (1995), embryos have completed their first cell cycle at 26 h *pc*, then continue to divide to reach the 4-cell stage at 26–32 h *pc*, followed by 8-cell (32–40 h *pc*), 16-cell (40–47 h *pc*), morula (47–68 h *pc*), and blastocyst (68–76 h *pc*) stages. The embryo begins to implant 7 days after fertilization (DeSesso, 1996). The blastocyst loses its zona pellucida, which is replaced by layers of glycoproteins whose adhesive properties play an important role in implantation (Alliston and Pardee, 1973). The ectoblast covers a deep layer or endoblast. A medium or mesoblast layer is isolated between the two previous layers. The embryo begins to lie down on the 8th day of gestation; then on the 11th day the head becomes dominant in size and the limbs lengthen. From the 19th day (end of organogenesis), the limbs are well formed, and the muzzle lengthens. From 12th day of gestation, development of the bi-discoid and hemochorial placenta will ensure the growth and development of the fetus until parturition (Rodriguez et al., 1985). The weight of the young rabbits does not change much until the 16th day but then increases very quickly: between 24th and 30th day, the rabbit fetus multiplies its weight by six (Bruce and Abdul-Karim, 1973). Gestation is from 30 to 33 days.

Understanding the development of the mammalian cranium requires the investigation from early prenatal to adult stages (Gaupp, 1906; Novacek, 1993; Maier and Ruf, 2014). These data provide the ultimate baseline for character polarization and a deeper understanding of ontogenetic transformations into adult stages and thus, significantly contribute to comparative anatomical, morphofunctional, systematic and evolutionary studies (e.g., Maier and Ruf, 2014; Sánchez-Villagra and Forasiepi, 2017; Ruf, 2020). To date models of cranial development in Lagomorpha are still mainly based on *Oryctolagus cuniculus* (e.g., Voit, 1909; de Beer and Woodger, 1930; Frick and Heckmann, 1955; Hoyte, 1961) because access to ontogenetic series is easy. Only a few other species are known by pre- or perinatal stages, although their cranial development has not been studied in as much detail. These are: *L. capensis* (Eloff, 1950), *Ochotona rufescens* and *Ochotona roylei* (Insom et al., 1990), and *Ochotona* sp. (Frahnert, 1998). However, all these studies comprise single or very few stages that were prepared as histological serial sections. Postnatal ontogeny of the lagomorph cranium has been mainly investigated based on osteological features, for instance, skull size and shape changes in *O. curzoniae*, *L. oiostolus*, and *L. capensis* (Lu, 2003; Zhang and Ge, 2014), growth of the ear capsule in *O. cuniculus* (Hoyte, 1961). Regarding cranial development, Lagomorpha, and especially Leporidae, can be the ideal model organism because they comprise different modes of reproduction (altricial, precocial) that help to elucidate developmental and evolutionary constraints in lagomorph evolution. The ontogenetic transformation of cranial features in altricial versus precocial species provides key features to character polarization and transformation serving as baseline for the understanding of systematics, morphofunction, and evolution of the respective species and clades. This has been attempted recently by the study of perinatal dental eruption in selected Glires (including *O. cuniculus* and *L. europaeus*) or the comparison of chondrocranial transformations in altricial and precocial Muroidea (Ruf, 2020; Ruf et al., 2020).

Comprehensive studies of the cranial development in selected lagomorph species that include ontogenetic series spanning from fetal to adult are still pending, although sufficient material of selected species is certainly available in scientific collections. This approach is essential to understand cranial characters and adult patterns, as demonstrated by a recent study on the auditory ossicles in lagomorphs (Maier et al., 2018). Based on both histological serial sections of perinatal stages and μCT scans of adult skulls of Ochotonidae and Leporidae, Maier et al. (2018) revealed a family-specific pattern of the

processus anterior and processus internus praearticularis of the malleus. The perinatal stages provide insight into the development of the two very different adult patterns that correlate with adaptations in sound transmission and allow for refining previous functional classifications of mammalian auditory ossicles (Maier et al., 2018).

New Methods in Assessing Development

The cranial anatomy and development of prenatal to early postnatal stages in mammals traditionally have been investigated using histological serial sectioning (Hall, 2005). Although this method is destructive and time consuming it allows the detailed study of hard and soft tissue structures and has led to important observations regarding the development of soft tissue (e.g., Maier et al., 2002; Ruf et al., 2009). Advances in modern imaging techniques such as μCT, allow for non-destructive investigation of any ontogenetic stage, as well as rare, collection specimens. Promising new diffusion based methods that increase the radio-opacity (and thus contrast) of soft tissues in specimens prior to μCT scanning are becoming more widespread and represent a frontier in the study of development in a wide variety of taxonomic groups (Metscher, 2009a,b; Gignac et al., 2016). Phosphotungstic acid and inorganic iodine are the two stains that are becoming increasingly common research tools; they are relatively easy to handle and produce high-contrast X-ray images of many soft tissues. Iodine (IKI and I2E) staining followed by μCT scanning works particularly well with mammals, including lagomorphs (Racicot and Ruf, 2020; **Figure 3**) and also is reversible using simple destaining methods. Specimens still may be processed for histological staining and sectioning or other methods after μCT scanning, and thus provide a record of their original internal and external three-dimensional geometries prior to employing subsequent destructive methods.

While μCT scanning has become a standard method for paleontologists, biologists, and museum researchers (e.g., Racicot, 2017), using staining to increase radio-opacity before μCT scanning still is a relatively new approach. Some general guidelines and examples of success with iodine staining and scanning methods are described in the literature (summarized in Metscher, 2009a,b; Gignac et al., 2016). Iodine provides clear contrast between neural and other tissues because its inner shell electron binding energy is similar to lower energy X-rays used in scans and often is used in medical contexts.

The most conservative methodology for rare museum specimens has been exemplified by recent work on cetaceans (Lanzetti et al., 2018) and tested with a prenatal stage of a lagomorph (**Figure 3**). Specimens that are preserved in formalin may be directly placed either in pre-prepared or self-prepared ∼1% Lugol's iodine solution (e.g., **Figure 3**). For specimens preserved in 70% alcohol, metal iodide is mixed first in the highest alcohol concentration possible (96–100%), then diluted to 70% alcohol with iodine before beginning staining. Rotating or moving the specimens either constantly or daily while staining is recommended because the stain can settle.

Other staining methods have been employed but may not work well with larger specimens. Phosphotungstic acid can be used effectively, particularly after fixation with Bouin's solution, but penetration times are slower than iodine methods, and it is unclear whether this method is reversible (Metscher, 2009a,b). It has been suggested that specimens fixed in Bouin's solution and preserved in 70% alcohol can be stained with I2E before μCT scanning (Metscher, 2009b) for effective increase in contrast. After the staining and scanning process is completed, specimens can be destained using 3% sodium thiosulfate dissolved in deionized water (for formalin specimens) or 70% ethanol (for ethanol specimens). The specimen subsequently can be used for future research, including re-staining and/or sectioning as desired. It is recommended to note in the documentation associated with the specimen that the specimen has been stained and μCT scanned previously. Some workers have noted that DNA perhaps should not be extracted from specimens after this procedure (Gignac et al., 2016) because the impact of staining on

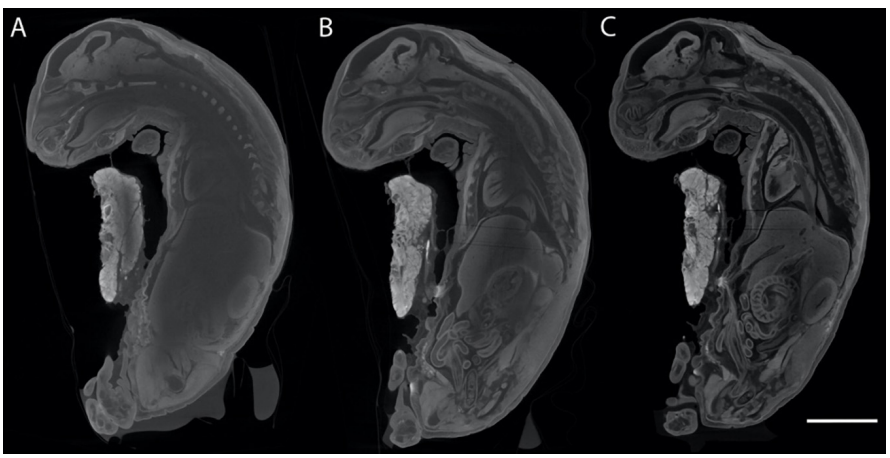

FIGURE 3 | Sagittal μCT slices taken from generally the same area of the same *O. cuniculus* specimen (Racicot and Ruf, 2020), stained for different lengths of time to show increasing contrast imparted by the Lugol's iodine stain. **(A)** Stain penetration after 5 weeks and 2 days, **(B)** penetration after 7 weeks, **(C)** stain penetration after 11 weeks and 2 days. Scale bar of 10 mm applies to all specimens.

DNA analyses has not been explored: experiments along these lines thus may be interesting. μCT scanning in combination with iodine staining represents a promising frontier in studying the development and ontogeny of lagomorphs, particularly in rare species/museum specimens for which destructive methods are unattractive options. Maintaining the 3D geometry of soft tissues, while also 'remotely' observing these tissues with high contrast will increase the natural history value of the specimens by providing a permanent digital record that can also be used in educational contexts.

FUNCTIONAL MORPHOLOGY

Leporids are characterized by increased cursoriality, in general; pikas are the least cursorial and jackrabbits the most cursorial, with rabbits and cottontails (e.g., *Sylvilagus*) occupying an intermediate position (Camp and Borell, 1937; Gambaryan, 1974). A small number of previous studies have discussed the gradation in cursoriality among lagomorphs and sought to identify morphological correlates of this behavioral cline (Camp and Borell, 1937; Gambaryan, 1974; Bramble, 1989; Kraatz and Sherratt, 2016). Among lagomorphs, leporids are perhaps best known for their gait, in which maximum running speeds of some species match the upper limit of racehorses and greyhounds; a speed unknown for any other mammal of leporid size. Leporid speeds vary from 40 km/h (11 m/s) in *Sylvilagus* through 56 km/h (16 m/s) in *O. cuniculus* and up to 72 km/h (20 m/s) in *L. europaeus* and *Lepus alleni* (Garland, 1983). While leaping abilities are common among most leporid lineages, they are also known to be facultatively semiaquatic, scansorial, fossorial, or exhibit a more generalized, non-hopping form of locomotion (Chapman and Flux, 1990). The most comprehensive framework for understanding lagomorph locomotion and locomotor apparatus in an evolutionary perspective was proposed by Gambaryan (1974), who suggested that lagomorphs originated as talus-dwellers and, therefore, regarded ochotonids as living fossils (**Figure 4**). The coupled half-bound action of the hindlimbs in lagomorphs is suggested to be the adaptative remnant of leaping from rock to rock. Among the variety of quadrupedal asymmetrical gaits in mammals, Gambaryan (1974) distinguishes two main categories: (1) true gallops, including the lagomorph half-bound and (2) 'the primitive ricochet.' The latter should not be confused with bipedal ricochet (i.e., proper hopping) of kangaroos and jerboas. According to Gambaryan (1974), the primitive ricochet is retained by many poorly running mammals, including most of the rodents.

The main difference between the true gallop and the primitive ricochet is the pattern of hindlimb motion during the extended suspension. In the primitive ricochet hindlimbs start protraction immediately as they finish their thrust and lose contact with the ground. In contrast, in the true gallop, there is a considerable delay in the hindlimb protraction where hindlimbs are held in retracted position from the end of their contact phase and throughout the extended suspension. The hindlimbs protract in gallop (e.g., lagomorph half-bound) when the forelimbs are landed; the forward swing of the hindquarters is much faster than in the primitive ricochet. According to Gambaryan (1974), the advantage of the hindlimb delay is the ability of an animal to arrive at the landing point more precisely when the hindlimbs are held fixed during a leap. Landing precision is crucial on irregular substrates such as tree branches and rocks, but also, the hindlimb delay would likely be advantageous while covering obstacles

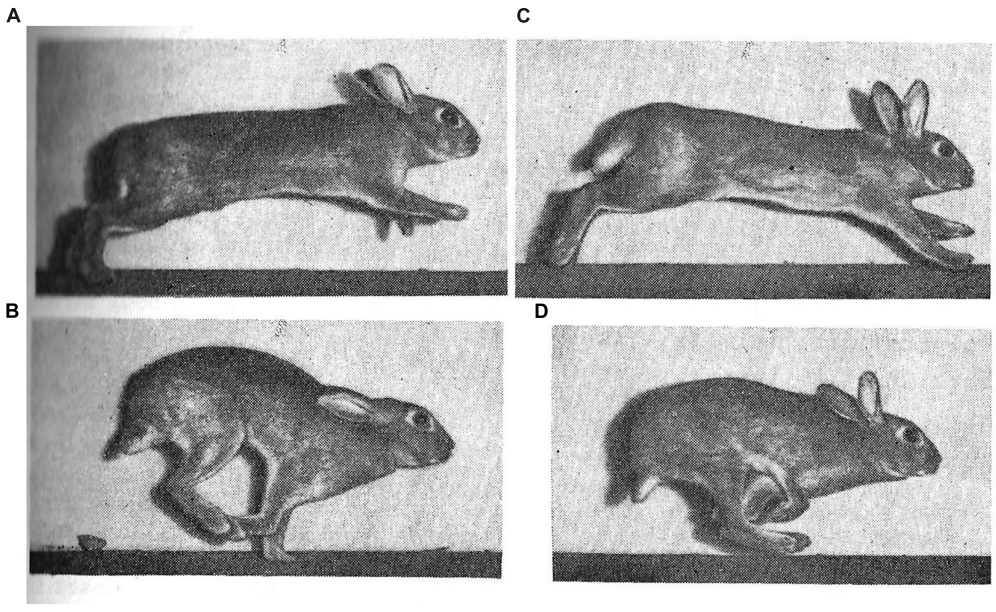

FIGURE 4 | Stages of wild rabbit (*O. cuniculus*) gait as captured and described by Gambaryan (1974), including: **(A)** support on hindlimbs; **(B)** extended flight; **(C)** support on forelimb; and **(D)** crossed flight.

at high speeds. Gambaryan (1974) summarized lagomorph locomotor patterns as a dorsomobile-metalocomotor type. While a metalocomotor type implies the prevalence of the hindlimbs, dorsomobile implies an additional active usage of the spine; more exactly, the use of lumbar region. Lagomorphs not only actively extend their spine with hindlimb thrust, but also flex their spine when the forelimbs are landed, and the hindquarters need to be rapidly protracted.

Recording Lagomorph Gaits

The first image sequences of lagomorph locomotion were recorded as early as in 1893–1894 by Étienne-Jules Marey, which capture a very slow half-bound of the white domestic rabbit (*O. cuniculus*)[1]. However, images from those movies were not included as illustrations in his subsequent publications (Marey, 1894, 1901). This is likely why Pablo Magne de la Croix, an Argentinean Frenchman who was among the first to study the evolution of quadrupedal gaits, had an incorrect impression on the rabbit's gait (Magne de la Croix, 1928, 1933, 1936); he only depicted an extended (centrifugal) suspension, and no gathered (centripetal) suspension stage in the locomotor cycle of the rabbit. The former is characterized by the straightened spine, retracted hindlimbs and protracted forelimbs, while in the latter the spine is flexed, the hindlimbs are protracted and cross the retracted forelimbs. In rabbits, with speed growth, there is at first no suspension in the locomotor cycle, then the gathered suspension appears (missed by Magne de la Croix), and finally the extended suspension is added (not recorded by Marey). Both stages of suspension were recorded by Gambaryan (1974) in the wild European rabbit 80 years after Marey's first observations. Also, Gambaryan's (1974) work was the first publication representing the frames of cinematographic record of the running cycle of the Alpine pika (*Ochotona alpina*). He noted that in pika the gathered suspension is almost absent, but the extended stage is prolonged to ensure leaping from stone to stone in their usual rocky habitat.

After Marey (1894, 1901) and Gambaryan (1974), there appeared in scientific publications a few additional illustrations of running lagomorphs. Dimery (1985) filmed wild rabbits at a high frequency (300 frames per second) but depicted only the outlines of the hindlimb movements. Bramble (1989) depicted the fast-running cycle of *Lepus californicus,* showing both the gathered and the extended suspension and filmed at 200 fps. Simons (1999) depicted the fast-running cycle of the domestic rabbit with both suspension stages filmed at 100 fps in X-ray to visualize viscera movements. Bertram and Gutmann (2009) depicted the slow-running cycle of *L. townsendii* with only one suspension stage. Like in Marey's faster rabbit, it appears after the forelimb thrust and, thus, corresponds to the gathered suspension. However, the forelimbs and hindlimbs are not really gathered under the body but remain parallel to each other like in a pronking (stotting) gait of gazelle or mara (Climaco das Chagas et al., 2019). Kuznetsov et al. (2017) published a video recording image sequence of a cornering maneuver of *L. europaeus* and also represented its gait diagram for maneuver and fast forward running. As to pikas, their half-bound gait was recorded due to successful keeping of a population of *O. rufescens* in Germany and appeared in a series of papers on locomotion of small mammals, with *O. rufescens* as a central object (Witte et al., 2002; Hackert et al., 2006; Schilling and Hackert, 2006). Both suspension stages were brief, so for pictures of faster running pikas one must return to Gambaryan (1974).

[1]https://www.youtube.com/watch?v=cqVlnVEcGwg

Limb Architecture

Camp and Borell (1937) were the first to compare the hindlimb bones and muscles of lagomorphs using a series of increasingly cursorial taxa: *Ochotona*, *Sylvilagus*, and *Lepus*. They note a tendency in this series in which muscle bellies become shorter, and tendons become longer. The first research of the entire postcranial locomotor apparatus of Mongolian species of pikas, aimed at ecological interpretation, was a dissertation subject of Cevegmid (1950), but has never been published. Klebanova et al. (1971) presented a detailed account of postcranial bone dimensions and muscle masses and attachments for six pika and five leporid species. Lammers and German (2002) attempted to find the specific features in the growth of limb bones of the rabbit and chinchilla, both of which use a half-bound gait. Williams et al. (2007a) quantified the hindlimb muscles and tendons of *L. europaeus*. They did not cite the early paper by Camp and Borell (1937) but explained their finding of increased development of tendons in the hare's hindlimb as an adaption for elastic energy storage. The same authors (Williams et al., 2007b) published a similar analysis of the forelimb muscles of *L. europaeus*, showing that the tendons in the forelimb are less developed than in the hindlimb. This implies that the forelimbs have a smaller role in energy saving via elastic storage and recoil. Reese et al. (2013) compared limb bone proportions between the meadow-dwelling and talus-dwelling pikas and found differences that they qualitatively attributed to the different actions of digging in meadows versus leaping in rocks. Young et al. (2014) took the same series of increasing cursoriality represented by *Ochotona*, *Sylvilagus*, and *Lepus*, as was earlier studied by Camp and Borell (1937) and Fostowicz-Frelik (2007) and performed a morphometric analysis of fore- and hindlimb bones, examining relative length and robusticity. Their results suggest that with increasing cursoriality in lagomorphs, the proximal limb bones become more gracile (decrease in robustness), while the distal bones do not. They hypothesize that limb bone morphology of lagomorphs is indicative of a trade-off between locomotor economy (cursors requiring longer, gracile limbs) and the need to be fracture-resistant (i.e., more robust) in the distal regions involved in impact.

Locomotory Adaptations to Cornering

Although lagomorphs exhibit exceptional levels of maneuverability, there is only one scientific publication documenting this phenomenon (Kuznetsov et al., 2017). This study is based on field records of the *L. europaeus* chased by sighthounds. Hares' stereotyped turn begins by a lateral kick of a forelimb against the ground, which initiates the turn to the opposite side of the kicking forelimb. Centripetal forces are produced by the forelimbs, and the braking forces by the hindlimbs. In contrast, the chasing dogs perform braking by the forelimbs and therefore, sometimes somersault overhead.

The anterior and posterior halves of the hares' trunk yaw and roll separately. Separate rolling employs axial rotation in the thoracic region of the spine. The morphological application of this study is the explanation of unique hypertrophy of the musculus subclavius in lagomorphs with its expansion over the whole scapula. This muscle became a specialized pronator of the scapula (there is no other efficient pronator of the scapula in mammals). Contracting together with the musculus serratus ventralis cervicis, it ensures centripetal force production by the forelimb and, first, the lateral kick at the touch-down of the forelimb initiating the maneuver. In leporids, the musculus subclavius comprises 1% of the total muscular mass of the limbs, while in rodents no more than 0.5% (Gambaryan, 1974). In pikas, it comprises 4% of the total muscular mass of the limbs. The musculus serratus ventralis cervicis, which assists the musculus subclavius in the lateral kick, comprises 1.5% of the total muscular mass of the limbs in leporids, and 2.3% in pikas. The greater relative mass of both muscles in pikas may highlight their elevated ability for sharp turning and smaller prevalence of the hindlimbs.

Locomotory Adaptations of the Spine

In the leporid vertebral skeleton, the most prominent structures related to the unique role of axial bending during the half-bound are the ventral spinous processes of the three anterior lumbar vertebrae and the posterior two or three thoracic vertebrae (Klebanova et al., 1971; Gambaryan, 1974). These processes provide an additional attachment site for the major lumbar flexors, which comprise 5–10% of the total muscular mass of the limbs in lagomorphs but never more than 5% in ungulates and carnivorans (Gambaryan, 1974). The antagonists extending the spine are equivalent to 30% of the total muscular mass of the limbs in leporids and 15% in pikas. In addition to the unique ventral spinous processes, leporids also show a set of skeletal features typical to other dorsomobile mammals. These are the elongate and anteriorly inclined transverse processes and short and anteriorly inclined dorsal spinous processes of lumbar vertebrae (Gambaryan, 1974; Jones et al., 2018).

Vertebral range of motion was studied *in vitro* in three lumbar joints (those between vertebrae L4–L7) of the rabbit (Grauer et al., 2000). It was found that each lumbar joint can be flexed ventrally by 12–15°, extended dorsally by 6°, bent laterally by 4–8°, and rotated axially to every side by about 1°. The prevalence of sagittal flexion and extension, as well as reduction of axial twisting of the lumbar region is expected given what is known about overall locomotor behavior in lagomorphs. *In vivo* spine movements in the sagittal plane were studied for pikas based on high-frequency filming in X-ray (Schilling and Hackert, 2006). Simons (1999) filmed rabbit running to study a visceral piston hypothesis according to which the breath in gallop is synchronized with the stages of locomotor cycle and with spine sagittal bending. The inertia of the viscera, and especially of the liver, are said to act as a pump for inhalation and exhalation, while the activity of the diaphragm and rib cage muscles might be virtually unnecessary. Simons (1999) falsified this hypothesis for the rabbit by showing inappropriate mutual phasing of locomotor and breathing cycles. Instead, an idea of pneumatic stabilization of the thorax was suggested.

Cranial Kinesis and Locomotion

Cranial kinesis is the ability of bones of the cranium to move relative to each other (as such, it is opposed to the mobility of visceral skeleton, e.g., jaw opening and movements of the middle ear ossicles). Cranial kinesis within leporids, unknown among other mammals, has been suggested to play an important role in locomotor behavior (Bramble, 1989), though the extent of this kinesis of leporid has not yet been fully characterized. In both ochotonids and leporids, ethmoid-orbital and otic-occipital part parts of the braincase are partially separated laterally by a piriform fenestra that passes subvertically along the posterior border of os alisphenoideum and (in leporids) os squamosum (Wible, 2007). Ventrally, the piriform fenestra comes into a transverse fissure which separates os basisphenoideum from os basioccipitale (in contrast to tight junction or even fusion of those two bones in other mammals). Notably, this is not a fetal, but an adult condition. Thus, the piriform fenestra and basisphenoid/basioccipital fissure serve as an intracranial joint, which Bramble (1989) suggests helps to dampen forces that occur during the locomotor cycle of lagomorphs, especially in high-speed hares. Due to soft tissue attachments across the intracranial joint, the large ears of hares may also act to support and reset the anterior (ethmoid-orbital) part of the cranium (Stott et al., 2010).

Bramble (1989) assumed that in steady quadrupedal running the forelimbs produce a significant braking effect, while the hindlimbs primarily accelerate the body. In fact, this was a common assumption at that time, which was shared by Gambaryan (1974) in his biomechanical considerations of a wide variety of mammals. More recent force-plate recordings, including those for pikas (Witte et al., 2002), show two significant patterns that challenge earlier assumptions. First, the vertical component of the ground reaction force in steady terrestrial walking and running is always several times greater than the horizontal component (longitudinal and transversal). Second, the longitudinal horizontal component is directed posteriorly (braking the body) in the first half of the contact phase, and anteriorly (accelerating the body) in the second half. This is true for both for the forelimb and the hindlimb. Therefore, the rule is not the deceleration by the forelimb and acceleration by the hindlimb, but deceleration in the first part of the contact phase of every limb and acceleration in the second part. It is also of note that large horizontal forces and accelerations take place not in steady running but at the rapid start and stop of the forward motion and in cornering. At the start and stop, longitudinal forces prevail, while in cornering the transverse forces are dominant. Thus, during cornering, the anterior part of the skull may tend to yaw centrifugally. In fact, Bramble (1989) has described the structure that prevents this distortion of the head, although he did not appreciate its adaptive role. In leporids, the os squamosum has a specific process, "the petrosal bar" which protrudes far posteriorly, crosses the piriform fenestra, and is housed by a matching "supratympanic sulcus" in the os petrosum. Therefore, the left and the right petrosal bars brace the basicranial block of the skull from both sides preventing lateral distortions in

the kinetic zone in case of transverse accelerations. In such cases the heavy ears fall aside (Kuznetsov et al., 2017) and cannot help to save skull integrity.

BRAIN EVOLUTION

Rabbits are well-known laboratory mammals for which there is an extensive historical record of the study of their brain morphology starting in the late 19th century (see Lewis, 1882; Mann, 1895; and references therein). Although the brain of the domesticated rabbit (*O. cuniculus*) is well studied, little is known about the evolution of the lagomorph brain. Until recently, data on brain morphology of fossil lagomorphs were derived from the fossil natural endocasts of *Prolagus* (Edinger, 1929), *Hypolagus* (Sych, 1967; Czyżewska, 1985), and *Palaeolagus* (Cope, 1884, but see Wood, 1940). These show similarities with modern lagomorph brains, such as narrow frontal lobes. The growing accessibility of μCT data has transformed the way we understand endocranial anatomy, especially regarding incorporation of quantitative data. The first virtual endocast of a fossil lagomorph, *Megalagus turgidus*, was described by López-Torres et al. (2020). The cranium of *M. turgidus* is the oldest (early Oligocene; Olson, 1942) and most complete lagomorph cranium for which mostly complete endocranial information can be recovered. Historically, *M. turgidus* has been classified as a leporid (Olson, 1942; Dawson, 1958, 2008), but more recently it has been considered to belong to a more primitive lineage outside crown lagomorphs (Lopez-Martinez, 2008). In the most comprehensive relevant phylogenetic analyses, the position of *Megalagus* as a stem lagomorph was supported (Fostowicz-Frelik, 2013; Fostowicz-Frelik and Meng, 2013). The study of the endocast of a stem lagomorph provides us with very valuable information on the brain morphology of lagomorphs before the split between the leporid and ochotonid lineages.

The endocast of *Megalagus turgidus* (**Figure 5A**) shows it had larger olfactory bulbs relative to its endocranial volume than any modern lagomorph. With respect to the cerebrum, the frontal lobes of *Megalagus* are wider than those observed in modern lagomorphs (narrow frontal lobes are a typical modern lagomorph trait), but they also are not as expanded rostrally, exposing much of the circular fissure. In contrast, ochotonids generally exhibit exposure of a portion of the circular fissure, and the circular fissure is covered in leporids (**Figure 5B**). The endocast of *Megalagus* possesses only a lateral sulcus on the neocortex, similar to the condition seen in leporids. The cerebral outline in dorsal view is markedly different among *Megalagus*, modern leporids, and modern ochotonids. The broadest point in the cerebrum of *Megalagus* is approximately midway between the rostral and caudal ends of the cerebrum, making the endocast have a rather ovoid outline. In contrast, leporids and ochotonids both have cerebra that are much broader in their caudal region (**Figure 5**). Therefore, there was likely a shift in lagomorph evolution to expand the caudal area of the cerebrum through time. In the caudal end of the cerebrum, the midbrain is partially exposed in *Megalagus*, similar to midbrain exposure in other

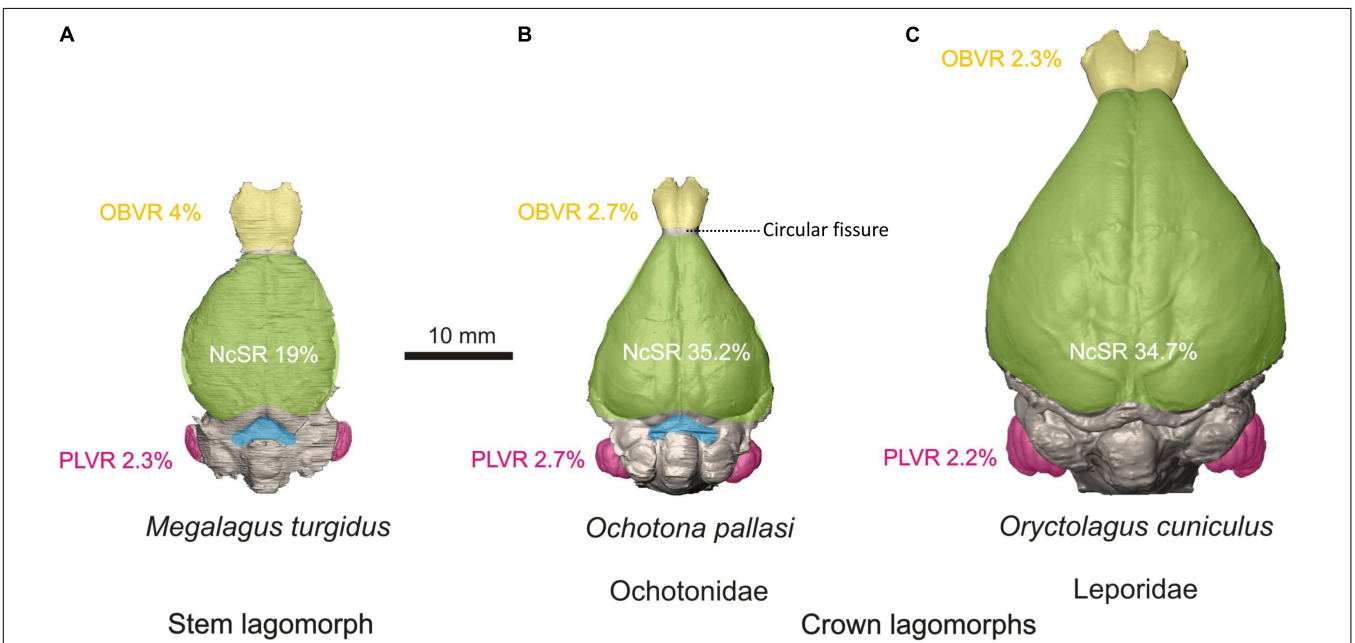

FIGURE 5 | Comparative morphology of the brain endocast in stem lagomorphs. (**A** *Megalagus turgidus*) and crown clades: Ochotonidae (**B** *Ochotona pallasi*) and Leporidae (**C** *Oryctolagus cuniculus*). The colors mark the brain areas of particular interest: yellow, olfactory bulbs; green, neocortical surface; blue, midbrain exposure; pink, petrosal lobules. See the comparative metric data of selected indices: NcSR, neocortical surface ratio (the ratio of the neocortex surface area to total endocast surface area); OBVR, olfactory bulb volume ratio (the ratio of the olfactory bulb volume to the total endocast volume); PLVR, petrosal lobule volume ratio (the ratio of the petrosal lobule volume to the total endocast volume); all indices are percentage values. The images and metrical data are taken from López-Torres et al. (2020).

primitive Euarchontoglires (e.g., most plesiadapiforms; Silcox et al., 2009, 2010; Orliac et al., 2014).

With respect to the modern lagomorph lineages, the range of relative olfactory bulb size of ochotonids is found within the range of leporids (López-Torres et al., 2020). In modern leporids, the midbrain is completely covered, and in modern ochotonids the midbrain is only slightly exposed (**Figure 5C**). The endocasts of ochotonids are completely lissencephalic, contrary to the endocasts of leporids, which only possess a lateral sulcus on the neocortex. The main difference in the cerebral outline between leporids and ochotonids is that the antero-lateral margins of the cerebrum in dorsal view are concave in leporids and either straight or slightly convex in ochotonids. This makes leporids have a rather pear-shaped dorsal outline, whereas in ochotonids it is more triangular (**Figure 5**). Modern lagomorph lineages also differ in that leporids have a proportionally longer (and larger) cerebrum than ochotonids (López-Torres et al., 2020).

Some tentative conclusions can be sketched about trends in the evolution of the lagomorph brain. Leporid and ochotonid lineages differ in many aspects of brain morphology, including the rostral expansion of the frontal lobes in leporids, a higher relative petrosal lobule volume in ochotonids, and the caudal expansion of the occipital region of the cerebrum in leporids. With respect to the latter, Kraatz et al. (2015) and Kraatz and Sherratt (2016) suggested a need for increased visual perception of the substrate in leporids, which might explain the more developed caudal region of the cerebrum in that group. In contrast, *Megalagus* exhibits a more 'primitive' brain, sharing more resemblances to endocasts that have been reconstructed for early fossil rodents (i.e., ischyromyids; Bertrand and Silcox, 2016; Bertrand et al., 2016, 2019) and plesiadapiforms (Silcox et al., 2009, 2010; Orliac et al., 2014). In particular, *Megalagus* has fairly large, pedunculated olfactory bulbs, some extent of midbrain exposure, and low neocorticalization. As in larger plesiadapiforms and rodents, *Megalagus* develops a lateral sulcus, with the brain being otherwise lissencephalic. These similarities with primitive members of Euarchontoglires, such as plesiadapiforms and primitive rodents, may indicate that lagomorphs are an old, relatively basal lineage and that they are conservative in their morphology.

LAGOMORPHS AS BIOMECHANICAL MODELS

Rabbits were one of the first vertebrates for which the *in vivo* range of sarcomere shortening was precisely measured with diffraction techniques (Dimery, 1985). Contrary to the previous expectations, the shortening range in 12 hindlimb muscles appeared to be much less than 30%. The shortening employs the plateau of the well-known force-tension curve, which is the best for force production. Until now, similar data are available for very few other vertebrate species other than humans and rabbits (Burkholder and Lieber, 2001). Additionally, it has been shown that the number of successive sarcomeres in myofibrils directly depends on the excursions experienced by the muscle during an individual's growth. Koh and Herzog (1998) released the musculus tibialis anterior from its retinacular restraint in 4-week-old rabbits. Free of the restraint, the muscle gained increased range for shortening and extension with the unchanged angular amplitude in the ankle joint. Twelve weeks later the operated muscles showed considerable difference from the control; muscle fibers became longer, while the tendons became shorter. As a byproduct, the force of operated muscle decreased. Rabbits have also proven to be a convenient model animal for human orthopedics. They are used in biomechanical modeling of the joints of both the spine (Grauer et al., 2000) and the limbs (Grover et al., 2007).

Cranial Biomechanics

Beyond those detailed by Bramble (1989), other morphological features of the cranium have been associated with locomotion including a pronounced ventral flexion of the facial region and unique fenestrations in the posterior cranial bones and lateral portion of the maxilla (DuBrul, 1950; Moss and Feliciano, 1977; Stott et al., 2010; Kraatz et al., 2015; Kraatz and Sherratt, 2016). The unique rostral vacuity (Ochotonidae) and fenestration (Leporidae) in lagomorphs were noted by Gray (1867), and DuBrul (1950) suggested that the latticing of the maxilla in Leporidae could increase the efficiency of speedy locomotion by reducing weight of the rostrum, and potentially contributing to Bramble's (1989) anterior capital suspensory system hypothesis. However, Moss and Feliciano (1977) argued that these fenestrations are related to the lack of transmission of masticatory forces through the lateral aspect of the rostrum. They proposed that the more vertical orientation of the ramus of the mandible in some leporids redirects incisal forces along the dorsal and ventral aspects of the rostrum, and away from the lateral side. Although this has yet to be tested, methods such as *in vivo* strain-gage analysis coupled with *in silico* finite element analysis could provide more resolution.

Leporids process food through differing modes of mastication within a single bite cycle (Weijs, 1980), including incisor biting, molar crushing and molar shearing, and the potential influence of these modes on bone deposition and skull shape, including the fenestrated rostrum, remains unknown. Biomechanical modeling using multibody dynamics analysis has demonstrated varied muscle lines of action and bite force magnitudes and directions during a bite cycle (Watson et al., 2014). However, it is unknown whether the largest and/or more frequent masticatory strains across the whole cranium are generated through incisor biting, and how these are directed through the rostrum, or by crushing or shearing of food at the molars. What is evident is that the bony form of the circumorbital region, cranial vault and basicranium in lagomorphs is unlikely to be related to stresses experienced during biting and chewing (Jašarević et al., 2010; Franks et al., 2016, 2017). The debate about determinants of skull form, however, continues, as faster, saltatorial species such as hares and jackrabbits of the genus *Lepus*, have more extensive fenestration and a more pronounced ventral facial tilt (Kraatz et al., 2015; Kraatz and Sherratt, 2016). This is in comparison to generalists, including cottontail and pygmy rabbits (e.g., *Sylvilagus* spp. and *B. idahoensis*), suggesting that there

may be a correlation between posture, locomotion, and rostral fenestrations as well as mastication.

Feeding Apparatus

In many ways, the function of the lagomorph oral cavity is especially well known among mammals. This is due largely to *in vivo* studies of jaw-adductor muscle activity, jaw kinematics and mandibular bone strain, and more recent work on diet-induced adaptive plasticity in domestic white rabbits (*O. cuniculus*). Rabbits exhibit a vertically deep facial skull and a jaw joint correspondingly elevated above the toothrow that that allows the jaw both rotational and translational movements (Weijs and Dantuma, 1981; Crompton et al., 2006). Transverse mandibular movements during the chewing cycle in rabbits are similar to primates in being due to delayed activity of the balancing-side deep-masseter muscle, which is in part related to dietary stiffness, i.e., elastic modulus (Weijs and Dantuma, 1981; Hylander et al., 1987, 2000; Weijs et al., 1989; Agrawal et al., 1997, 1998, 2000; Vinyard et al., 2006). Such kinematics are facilitated via a partially fused mandibular symphysis, a midline anteriorly located joint that closely binds the two jaw halves (Weijs and Dantuma, 1981; Ravosa and Hogue, 2004; Ravosa et al., 2016). Rabbits and diverse mammals have similar mandibular peak strains during the mastication of mechanically challenging foods (Weijs and de Jongh, 1977; Ravosa et al., 2010b). Rabbits share feeding patterns with other mammals whereby items with greater toughness and/or higher stiffness require larger and protracted jaw-adductor forces during biting and chewing, which results in greater occlusal forces and masticatory stresses (e.g., Herring and Scapino, 1973; Weijs and de Jongh, 1977; Hylander, 1979; Gorniak and Gans, 1980; Weijs and Dantuma, 1981; Dessem and Druzinsky, 1992; Hylander et al., 1992, 1998, 2000; Ravosa and Hogue, 2004; Vinyard et al., 2008). Rabbits are likewise noteworthy due to extensive ontogenetic data about the *in vivo* links among masticatory function, feeding behavior and food mechanical properties (e.g., Weijs et al., 1987, 1989; Langenbach et al., 1991, 2001; Langenbach and van Eijden, 2001; Martin et al., 2020).

Skeletal adaptations are related to either high-magnitude, singular loads or low-magnitude, cyclical loading. Although high bite forces have long been linked to greater jaw robusticity in mammals (e.g., Hylander, 1979), the dietary underpinnings of repetitive or cyclical loading are still poorly known for masticatory features. Rabbits are but one of two taxa for which mechanically challenging foods are known elevate cyclical loading (Ravosa et al., 2015; Nett et al., in press). Rabbits also resemble mid-to-large sized mammals in exhibiting intracortical remodeling, a skeletal repair mechanism related to microcrack damage in adult bone that does not appear to characterize smaller species (Bouvier and Hylander, 1996a,b; Hirano et al., 2000; Lad et al., 2021).

Rabbits are perhaps the best studied mammals in terms of dietary plasticity in the skull and jaws. A series of experiments have explored the implications of dynamic changes in elevated and cyclical loads on craniomandibular ontogeny and function in rabbits subjected to long-term, naturalistic modifications of dietary properties (Ravosa et al., 2007, 2016). Analyses have explored ontogenetic variation in jaw-loading patterns due to seasonality and fallback foods (Scott et al., 2014a,b); differences in age-related performance of bone and cartilage in jaw joints (Ravosa et al., 2007, 2008; Jašarević et al., 2010; Ravosa and Kane, 2017); reaction norms of bony vs. muscular components (Ravosa et al., 2010a); regional and hierarchical variation in patterns of cranial bone formation (Ravosa et al., 2007; Menegaz et al., 2009; Franks et al., 2016, 2017; Terhune et al., 2020; Lad et al., 2021); and morphological inference in the fossil record (Ravosa et al., 2016). Another finding is that dietary plasticity in rabbit jaws is similar to shorter-term studies of this phenomenon in monkeys, hyraxes, ferrets and rats (Beecher and Corruccini, 1981; Bouvier and Hylander, 1981, 1996a,b; Beecher et al., 1983; Yamada and Kimmel, 1991; He and Kiliaridis, 2003; Lieberman et al., 2004). These integrative analyses have marshaled a suite of histological, imaging and engineering approaches to understand masticatory development and phenotypic diversity in rabbits. Despite the differential focus of such research on the role of long-term plasticity in craniomandibular evolution and diversity, such an ontogenetic perspective to the mechanobiology of lagomorphs invariably lends itself to ongoing revolutions in 'omics' as well as clinical approaches to aging and pathobiology of connective tissues.

CLINICAL MODEL

Understanding of the healthy rabbit masticatory system and cranial morphology is important for diagnosis and treatment of dental disease in rabbits (Harcourt-Brown, 2007; Lennox, 2008; Jekl and Redrobe, 2013). The rabbit is also one of the most used animals in clinical experimental modeling (Neyt et al., 1998; Stübinger and Dard, 2013), often used to investigate the remodeling of bone in response to dental implants (Kim and Shin, 2018; Leventis et al., 2018; Manju et al., 2018) and impaired muscle function (Balanta-Melo et al., 2019; Huang et al., 2019). Rabbits are also a good clinical model for craniosynostosis, a condition that involves the premature closure of cranial sutures in infants. Craniosynostotic rabbits are the only existing colony of any species affected by familial craniosynostosis in the world (Mooney et al., 1998a,b; Cooper et al., 1999; Lyn Chong et al., 2003). Suture defects must be artificially created to investigate this question in any other species of mammal. Therefore, these rabbits are the most similar non-human model to naturally occurring craniosynostosis in other mammals and require less surgical manipulation.

SUMMARY

Though model organisms are critical tools for understanding much of the biology of life, larger systems of organisms can offer a more dynamic and comparative framework to reveal the tempo and mode of evolutionary change. Understanding the adaptative processes that drive these changes is often best accomplished by studying groups of closely related organisms at multiple time scales. We offer the Lagomorpha

(rabbits, hares, pikas, and their ancestors) as an exemplar system in which to study the evolutionary patterns of morphologic change. Anchored by the common laboratory rabbit (*O. cuniculus*), the order offers a rich diversity of extant species within the monogeneric Ochotonidae and the more lineage rich Leporidae. The molecular phylogenetics of these groups have been well studied, and indeed, four species have established genome level architecture. Understanding lagomorph intraordinal relationships has also advanced through a rich, consistent fossil record that dates back nearly 50 million years. The evolutionary trees are already in place to develop phylogenetically constrained models of evolution, but more work is needed combining molecular and morphological data into a comprehensive phylogeny of lagomorphs.

Using existing phylogenetic frameworks and emerging methods, lagomorphs are already an excellent system in which to study a rich array of functional systems. The locomotor behavior of these small mammals has been of long-standing interest, and research within this system has increasingly incorporated evidence from the fossil record, soft tissue systems, and novel connections to the cranium. The expanding research on the lagomorph cranium has shown important patterns of evolution of the brain and auditory systems and new methods have only increased the scope and breadth of research on the lagomorph masticatory system. The European rabbit will continue to remain a seminal research species for the biological sciences. Most importantly, new methods have allowed researchers to expand our knowledge more broadly among rabbit relatives, offering a more explicitly evolutionary context. The emergence of new methods of morphological research, an ever-improving phylogenetic framework, and a growing interest in lagomorphs will only serve to better place rabbits and *all* of their relatives as an essential system in which we can better understand the patterns and processes of evolutionary morphology.

AUTHOR CONTRIBUTIONS

BK and IR designed the idea for the review manuscript. All authors contributed equally to the manuscript.

FUNDING

ES was supported by an Australian Research Council Future Fellowship (ARC FT190100803). RR was funded by the Alexander von Humboldt Foundation, which is sponsored by the Federal Ministry for Education and Research (Germany). Research discussed by MR herein was supported by the following United States National Science Foundation grants (BCS-1749453, BCS-1029149/1214767, and BCS-0924592/1214766).

ACKNOWLEDGMENTS

We dedicate this paper to the late Mary R. Dawson (1931–2020) as a token of gratitude for her tremendous contribution to the morphological and evolutionary exploration on lagomorphs. We would like to thank the World Lagomorph Society and the organizers of the 6th World Lagomorph Conference, which was scheduled to occur in July of 2020 in Montpellier, France, but postponed due to the global pandemic of COVID-19. IR and BK had organized a session for that meeting titled *Lagomorphs as a Model Morphological System.* In lieu of that meeting and session, participants met virtually on July 06, 2020 to outline this review paper. We all look forward to gathering for a similar session in July of 2022 in Montpellier for the rescheduled World Lagomorph Conference. We thank reviewers for their thoughtful and helpful comments.

REFERENCES

Abbott, R., Albach, D., Ansell, S., Arntzen, J. W., Baird, S. J. E., Bierne, N., et al. (2013). Hybridization and speciation. *J. Evol. Biol.* 26, 229–246. doi: 10.1111/j.1420-9101.2012.02599.x

Agrawal, K. R., Lucas, P. W., and Bruce, I. C. (2000). The effects of food fragmentation index on mandibular closing angle in human mastication. *Arch. Oral Biol.* 45, 577–584. doi: 10.1016/S0003-9969(00)00019-4

Agrawal, K. R., Lucas, P. W., Bruce, I. C., and Prinz, J. F. (1998). Food properties that influence neuromuscular activity during human mastication. *J. Dent. Res.* 77, 1931–1938. doi: 10.1177/00220345980770111101

Agrawal, K. R., Lucas, P. W., Prinz, J. F., and Bruce, I. C. (1997). Mechanical properties of foods responsible for resisting food breakdown in the human mouth. *Arch. Oral Biol.* 42, 1–9. doi: 10.1016/S0003-9969(96)00102-1

Águeda-Pinto, A., Lemos, de Matos, A., Abrantes, M., Kraberger, S., Risalde, M. A., et al. (2019). Genetic characterization of a recombinant myxoma virus in the Iberian hare (*Lepus granatensis*). *Viruses* 11:530. doi: 10.3390/v11060530

Alliston, C. W., and Pardee, N. R. (1973). Variability of embryonic development in the rabbit at 19 to 168 hours after mating. *Lab. Anim. Sci.* 23, 665–670.

Alves, P. C., Ferrand, N., Suchentrunk, F., and Harris, D. J. (2003). Ancient introgression of *Lepus timidus* mtDNA into *L. granatensis* and *L. europaeus* in the Iberian Peninsula. *Mol. Phylogenet. Evol.* 27, 70–80. doi: 10.1016/S1055-7903(02)00417-7

Angermann, R., Flux, J. E. C., Chapman, J. A., and Smith, A. T. (1990). "Chapter 2: Lagomorph classification," in *Rabbits, Hares and Pikas. Status Survey and Conservation Action Plan, IUCN/SSC Lagomorph Specialist Group*, eds J. A. Chapman and J. E. C. Flux (Oxford: Information Press), 7–13.

Asher, R. J., Meng, J., Wible, J. R., McKenna, M. C., Rougier, G. W., Dashzeveg, D., et al. (2005). Stem Lagomorpha and the antiquity of Glires. *Science* 307, 1091–1094. doi: 10.1126/science.1107808

Asher, R. J., Smith, M. R., Rankin, A., and Emry, R. J. (2019). Congruence, fossils and the evolutionary tree of rodents and lagomorphs. *R. Soc. Open Sci.* 6:190387. doi: 10.1098/rsos.190387

Averianov, A. O. (1994). Early eocene mimotonids of Kyrgyzstan and the problem of Mixodontia. *Acta Palaeontol. Pol.* 39, 393–411.

Averianov, A. O. (1995). Osteology and adaptations of the early Pliocene rabbit *Trischizolagus dumitrescuae* (Lagomorpha: Leporidae). *J. Vertebr. Paleontol.* 15, 375–386. doi: 10.1080/02724634.1995.10011236

Averianov, A. O., and Lopatin, A. V. (2005). Eocene Lagomorpha of Asia: 1. *Aktashmys* (Strenulagidae fam. nov.). *Paleontol. J.* 39, 308–317.

Averianov, A. O., and Tesakov, A. S. (1997). Evolutionary trends in Mio-Pliocene Leporinae, based on *Trischizolagus* (Mammalia, Lagomorpha). *Paläontol. Z.* 71, 145–153.

Balanta-Melo, J., Toro-Ibacache, V., Kupczik, K., and Buvinic, S. (2019). Mandibular bone loss after masticatory muscles intervention with botulinum toxin: an approach from basic research to clinical findings. *Toxins* 11:84. doi: 10.3390/toxins11020084

Barone, R., Pavaux, C., Blin, P. C., and Cuq, P. (1973). *Atlas of Rabbit Anatomy*. Paris: Masson et Cie.

Beecher, R. M., and Corruccini, R. S. (1981). Effects of dietary consistency on craniofacial and occlusal development in the rat. *Angle Orthod.* 51, 61–69. doi: 10.1043/0003-32191981051<0061:EODCOC<2.0.CO;2

Beecher, R. M., Corruccini, R. S., and Freeman, M. (1983). Craniofacial correlates of dietary consistency in a nonhuman primate. *J. Cranl. Genet. Dev. Biol.* 3, 193–202.

Bensley, B. A. (1921). *Practical Anatomy of the Rabbit: An Elementary Laboratory Text Book in Mammalian Anatomy*. Philadelphia: Blakiston Co.

Berkovitz, B., and Shellis, P. (2018). "Chapter 7 - Lagomorpha and Rodentia," in *The Teeth of Mammalian Vertebrates*, eds B. Berkovitz and P. Shellis (Amsterdam: Elsevier Academic Press), 105–143.

Bertram, J. E., and Gutmann, A. (2009). Motions of the running horse and cheetah revisited: fundamental mechanics of the transverse and rotary gallop. *J. R. Soc. Interface* 6, 549–559. doi: 10.1098/rsif.2008.0328

Bertrand, O. C., Amador-Mughal, F., and Silcox, M. T. (2016). Virtual endocasts of Eocene *Paramys* (Paramyinae): oldest endocranial record for Rodentia and early brain evolution in Euarchontoglires. *Proc. R. Soc. B* 283:20152316. doi: 10.1098/rspb.2015.2316

Bertrand, O. C., Amador-Mughal, F., Lang, M. M., and Silcox, M. T. (2019). New virtual endocasts of Eocene Ischyromyidae and their relevance in evaluating neurological changes occurring through time in Rodentia. *J. Mammal. Evol.* 26, 345–371. doi: 10.1007/s10914-017-9425-6

Bertrand, O. C., and Silcox, M. T. (2016). First virtual endocasts of a fossil rodent: *Ischyromys typus* (Ischyromyidae, Oligocene) and brain evolution in rodents. *J. Vertebr. Paleontol.* 36:e1095762. doi: 10.1080/02724634.2016.1095762

Bleefeld, A. R., and Bock, W. J. (2002). Unique anatomy of lagomorph calcaneus. *Acta Palaeontol. Pol.* 47, 181–183.

Bohlin, B. (1942). The fossil mammals from the tertiary deposits of Taben-Buluk, western Kansu. Part 1. Insectivora and Lagomorpha. *Palaeontol. Sin. C* 8, 1–113.

Bohlin, B. (1951). "Some mammalian remains from Shih-ehr-ma-ch'eng, Hui-hui-p'u area, Western Kansu. Reports from the scientific expeditionto the North-Western Provinces of China under Leadership of Dr Sven Hedin," in *The Sino-Swedish Expedition Publication 35, VI. Vertebrate Paleontology 5*, ed. S. Hedin (Stockholm: Hasse W. Tullberg), 1–48.

Böhmer, C., and Böhmer, E. (2017). Shape variation in the craniomandibular system and prevalence of dental problems in domestic rabbits: a case study in evolutionary veterinary science. *Vet. Sci.* 4:5. doi: 10.3390/vetsci4010005

Boussit, D. (1989). *Reproduction et Insemination Artificielle en Cuniculture. Association Française de Cuniculture*. France: Lempdes.

Bouvier, M., and Hylander, W. L. (1981). Effect of bone strain on cortical bone structure in macaques (*Macaca mulatta*). *J. Morph.* 167, 1–12.

Bouvier, M., and Hylander, W. L. (1996b). The mechanical or metabolic function of secondary osteonal bone in the monkey *Macaca fascicularis*. *Arch. Oral Biol.* 41, 941–950. doi: 10.1016/S0003-9969(96)00047-7

Bouvier, M., and Hylander, W. L. (1996a). "Strain gradients, age, and levels of modeling and remodeling in the facial bones of *Macaca fascicularis*," in *The Biological Mechanisms of Tooth Movement and Craniofacial Adaptation*, eds Z. Davidovitch and L. A. Norton (Boston, MA: Harvard Society for the Advancement of Orthodontics), 407–412.

Bramble, D. M. (1989). Cranial specialization and locomotor habit in the Lagomorpha. *Am. Zool.* 29, 303–317. doi: 10.1093/icb/29.1.303

Bruce, N. W., and Abdul-Karim, R. W. (1973). Relationship between fetal weight, placental weight and maternal placental circulation in the rabbit at different stages of gestation. *J. Reprod. Fertil.* 32, 15–24. doi: 10.1530/jrf.0.0320015

Bugge, J. (1974). The cephalic arterial system in insectivores, primates, rodents and lagomorphs, with special reference to the systematic classification. *Acta Anat.* 87, 1–159.

Burgin, C. J., Colella, J. P., Kahn, P. L., and Upham, N. S. (2018). How many species of mammals are there? *J. Mamm.* 99, 1–14. doi: 10.1093/jmammal/gyx147

Burkholder, T. J., and Lieber, R. L. (2001). Sarcomere length operating range of vertebrate muscles during movement. *J. Exp. Biol.* 204, 1529–1536.

Camp, C. L., and Borell, A. E. (1937). Skeletal and muscular differences in the hind limbs of *Lepus, Sylvilagus*, and *Ochotona*. *J. Mammal.* 18, 315–326. doi: 10.2307/1374205

Carneiro, M., Albert, F. W., Afonso, S., Pereira, R. J., Burbano, H., Campos, R., et al. (2014). The genomic architecture of population divergence between subspecies of the European rabbit. *PLoS Genet.* 10:e1003519. doi: 10.1371/journal.pgen.1003519

Castillo Vardaro, J. A., Epps, C. W., Frable, B. W., and Ray, C. (2018). Identification of a contact zone and hybridization for two subspecies of the American pika (*Ochotona princeps*) within a single protected area. *PLoS One* 13:e0199032. doi: 10.1371/journal.pone.0199032

Cevegmid, D. (1950). *Comparative Ecological-Morphological Analysis of the Organism of Pikas of Mongolia*. Dissertation. Moscow: Moscow State University.

Chapman, J. A., and Ceballos, G. (1990). "The cottontails," in *Rabbits, Hares and Pikas, Status Survey and Conservation Action Plan: IUCN*, eds J. A. Chapman and J. E. C. Flux (Gland: IUCN), 95–110.

Chapman, J. A., and Flux, J. E. C. (1990). "Introduction and overview of the lagomorphs," in *Rabbits, Hares and Pikas, Status Survey and Conservation Action Plan: IUCN*, eds J. A. Chapman and J. E. C. Flux (Gland: IUCN), 1–6.

Chapman, J. A., and Morgan, R. P. (1973). Systematic status of the cottontail complex in western Maryland and nearby West Virginia. *Wildlife Monogr.* 36, 3–54.

Cheng, C., Ge, D. Y., Xia, L., Zhou, C. Q., and Yang, Q. S. (2012). Morphometrics study on the so called 'Cape hare' (Lagomorpha: Leporidae: *Lepus*) in China. *Acta Theriol. Sin.* 32, 275–286.

Climaco das Chagas, K. S., Vassallo, A. I., Becerra, F., Echeverría, A., de Castro Loguercio, M. F., et al. (2019). Locomotion in the fastest rodent, the mara Dolichotis patagonum (Caviomorpha; Caviidae; Dolichotinae). *Mastozool. Neotrop.* 26, 65–79.

Clutton-Brock, J. (1989). Five thousand years of livestock in Britain. *Biol. J. Linn. Soc.* 38, 31–37. doi: 10.1111/j.1095-8312.1989.tb01560.x

Cooper, G. M., Mooney, M. P., Burrows, A. M., Smith, T. D., Dechant, J., Losken, H. W., et al. (1999). Brain growth rates in craniosynostotic rabbits. *Cleft Palate Craniofac. J.* 36, 314–321. doi: 10.1597/1545-1569_1999_036_0314_bgricr_2.3.co_2

Cope, E. D. (1884). The Vertebrata of the tertiary formations of the West. *Rep. United States Geol. Surv. Territ.* 3, 1–35.

Corbet, G. B. (1983). A review of classification in the family Leporidae. *Acta Zool. Fennica* 174, 11–15.

Corbett-Detig, R. B., Russell, S. L., Nielsen, R., and Losos, J. (2020). Phenotypic convergence is not mirrored at the protein level in a lizard adaptive radiation. *Mol. Biol. Evol.* 37, 1604–1614. doi: 10.1093/molbev/msaa028

Crompton, A. W., Lieberman, D. E., and Aboelela, S. (2006). "Tooth orientation during occlusion and the functional significance of condylar translation in primates and herbivores," in *Amniote Paleobiology: Perspectives on the Evolution of Mammals, Birds, and Reptiles*, eds M. T. Carrano, T. J. Gaudin, R. W. Blob, and J. R. Wible (Chicago, IL: University of Chicago Press), 367–388.

Czyżewska, T. (1985). Natural endocranial casts of *Hypolagus brachygnathus* Kormos, 1934 (Leporidae, Lagomorpha) from Węże I near Działoszyn. *Acta Zool. Crac.* 29, 1–12.

Dawson, M. R. (1958). Later Tertiary Leporidae of North America. *Univ. Kansas Paleontol. Contr. Vertebr.* 6, 1–75.

Dawson, M. R. (1969). Osteology of *Prolagus sardus*, a quaternary ochotonid (Mammalia, Lagomorpha). *Palaeovertebrata* 2, 157–191.

Dawson, M. R. (1981). "Evolution of modern leporids," in *Proceedings of the World Lagomorph Conference*, eds K. Myers and C. D. MacInnes (Ontario: University of Guelph Press), 1–8.

Dawson, M. R. (2008). "Lagomorpha," in *Evolution of Tertiary Mammals of North America, Volume 2: Small Mammals, Xenarthrans, and Marine Mammals*, eds C. M. Janis, G. F. Gunnell, and M. D. Uhen (Cambridge: Cambridge University Press), 293–310.

de Beer, G. R., and Woodger, J. H. (1930). The early development of the skull of the rabbit. *Philos. Trans. R. Soc. Lond. B* 218, 373–414. doi: 10.1098/rstb.1930.0009

de Jung, W. W., Gleaves, J. T., and Boulter, D. (1977). Evolutionary changes of alpha-crystallin and the phylogeny of mammalian orders. *J. Mol. Evol.* 10, 123–135. doi: 10.1007/BF01751806

Delaney, M. A., Treuting, P. M., and Rothenburger, J. L. (2018). "Chapter 19 – Lagomorpha," in *Pathology of Wildlife and Zoo Animals*, eds K. A. Terio, D. McAloose, and J. S. Leger (Cambridge, MA: Academic Press), 481–496.

DeSesso, J. M. (1996). "Comparative embryology," in *Handbook of Developmental Toxicology*, ed. R. D. Hood (Boca Raton, FL: CRC Press), 111–174.

Dessem, D., and Druzinsky, R. E. (1992). Jaw-muscle activity in ferrets, *Mustela putorius furo*. *J. Morphol.* 213, 275–286. doi: 10.1002/jmor.1052130211

Dimery, N. J. (1985). Muscle and sarcomere lengths in the hind limb of the rabbit (*Oryctolagus cuniculus*) during a galloping stride. *J. Zool.* 205, 373–383. doi: 10.1111/j.1469-7998.1985.tb05623.x

Douady, C. J., and Douzery, E. J. P. (2003). Molecular estimation of eulipotyphlan divergence times and the evolution of "Insectivora". *Mol. Phylogenet. Evol.* 28, 285–296. doi: 10.1016/S1055-7903(03)00119-2

DuBrul, E. L. (1950). Posture, locomotion and the skull in Lagomorpha. *Am. J. Anat.* 87, 277–313. doi: 10.1002/aja.1000870205

Edinger, T. (1929). Die fossilen Gehirne. *Z. ges. Anat.* 28, 1–221.

Eloff, F. C. (1950). On the nasal region of the chondrocranium of the Cape hare, *Lepus capensis*. *Ann. Transv. Mus.* 21, 222–233.

Erbajeva, M. A. (2013). New species of *Amphilagus* (Lagomorpha, Mammalia) from the Miocene of the Valley of Lakes, central Mongolia. *Paleontol. J.* 47, 311–320. doi: 10.1134/S0031030113030040

Erbajeva, M. A., and Daxner-Höck, G. (2014). The most prominent Lagomorpha from the Oligocene and early Miocene of Mongolia. *Ann. Naturhist. Mus. Wien* 116, 215–245.

Erbajeva, M. A., Baatarjav, B., Daxner-Höck, G., and Flynn, L. J. (2017). Occurrences of *Sinolagomys* (Lagomorpha) from the Valley of Lakes (Mongolia). *Palaeobiol. Palaeoenviron.* 97, 11–24. doi: 10.1007/s12549-016-0262-z

Erbajeva, M., Angelone, C., and Alexeeva, N. (2016). A new species of the genus *Amphilagus* (Lagomorpha, Mammalia) from the Middle Miocene of south-eastern Siberia. *Hist. Biol.* 28, 199–207. doi: 10.1080/08912963.2015.1034119

Erbajeva, M., Flynn, L. J., and Alexeeva, N. (2015). Late cenozoic Asian ochotonidae: taxonomic diversity, chronological distribution and biostratigraphy. *Quat. Int.* 355, 18–23. doi: 10.1016/j.quaint.2014.10.064

Esselstyn, J. A., Oliveros, C. H., Swanson, M. T., and Faircloth, B. C. (2017). Investigating difficult nodes in the placental mammal tree with expanded taxon sampling and thousands of ultraconserved elements. *Genome Biol. Evol.* 9, 2308–2321. doi: 10.1093/gbe/evx168

Fa, J. E., and Bell, D. J. (1990). "The volcano rabbit *Romerolagus diazi*," in *Rabbits, Hares and Pikas, Status Survey and Conservation Action Plan: IUCN*, eds J. A. Chapman and J. E. C. Flux (Gland: IUCN), 143–146.

Feijó, A., Ge, D., Wen, Z., Xia, L., and Yang, Q. (2020). Divergent adaptations in resource-use traits explain how pikas thrive on the roof of the world. *Funct. Ecol.* 34, 1826–1838. doi: 10.1111/1365-2435.13609

Fiorello, C. V., and German, R. Z. (1997). Heterochrony within species: craniofacial growth in giant, standard, and dwarf rabbits. *Evolution* 51, 250–261. doi: 10.1111/j.1558-5646.1997.tb02406.x

Flynn, L. J., Winkler, A. J., Erbaeva, M., Alexeeva, N., Anders, U., Cermák, S., et al. (2014). The Leporid Datum: a late Miocene biotic marker. *Mammal Rev.* 14, 164–176. doi: 10.1111/mam.12016

Foley, N. M., Springer, M. S., and Teeling, E. C. (2016). Mammal madness: is the mammal tree of life not yet resolved? *Philos. Trans. R. Soc. Lond. B Biol. Sci.* 371, 20150140. doi: 10.1098/rstb.2015.0140

Foote, R. H., and Carney, E. W. (2000). The rabbit as a model for reproductive and developmental toxicity studies. *Reprod. Toxicol.* 14, 477-493. doi: 10.1016/S0890-6238(00)00101-5

Forsyth, N. R., Elder, F. F. B., Shay, W. J., and Wright, E. W. (2005). Lagomorphs (rabbits, pikas and hares) do not use telomere-directed replicative aging in vitro. *Mech. Ageing Dev.* 126, 685–691. doi: 10.1016/j.mad.2005.01.003

Fostowicz-Frelik, Ł (2007). The hind limb skeleton and cursorial adaptations of the Plio–Pleistocene rabbit *Hypolagus beremendensis*. *Acta Palaeontol. Pol.* 52, 447–476.

Fostowicz-Frelik, Ł (2013). Reassessment of *Chadrolagus* and *Litolagus* (Mammalia: Lagomorpha) and a new genus of North American Eocene Lagomorpha from Wyoming. *Am. Mus.* 3773, 1–76. doi: 10.1206/3773.2

Fostowicz-Frelik, Ł (2016). A late Oligocene lagomorph (Mammalia) from Herrlingen 9 (Baden- Württemberg, Germany). *Neues Jahrb. Geol. und Pal. Abh.* 280, 143–151. doi: 10.1127/njgpa/2016/0571

Fostowicz-Frelik, Ł (2017). "Convergent and parallel evolution in early Glires (Mammalia)," in *Evolutionary Biology: Self/Nonself Evolution, Species and Complex Traits Evolution, Methods and Concepts*, ed. P. Pontarotti (Berlin: Springer International Publishing), 199–216.

Fostowicz-Frelik, Ł (2020). "Most successful mammals in the making: a review of the Paleocene Glires," in *Evolutionary Biology: A Transdisciplinary Approach*, ed. P. Pontarotti (Cham: Springer Verlag Nature).

Fostowicz-Frelik, Ł, and Frelik, G. J. (2010). The earliest occurrence of the steppe pika (*Ochotona pusilla*) in Europe near the Pliocene/Pleistocene boundary. *Naturwissenschaften* 97, 325–329. doi: 10.1007/s00114-009-0634-6

Fostowicz-Frelik, Ł, and Li, Q. (2014). A new genus of stem lagomorph (Mammalia: Glires) from the Middle Eocene of the Erlian Basin, Nei Mongol, China. *Acta Zool. Crac.* 57, 29–42. doi: 10.3409/azc.57_1-2.29

Fostowicz-Frelik, Ł, and Meng, J. (2013). Comparative morphology of premolar foramen in lagomorphs (Mammalia: Glires) and its functional and phylogenetic implications. *PLoS One* 8:e79794. doi: 10.1371/journal.pone.0079794

Fostowicz-Frelik, Ł, Li, C. K., Li, Q., Meng, J., and Wang, Y. Q. (2015a). *Strenulagus* (Mammalia: Lagomorpha) from the middle Eocene Irdin Manha Formation of the Erlian Basin, Nei Mongol, China. *Acta Geol. Sin.* 89, 12–26. doi: 10.1111/1755-6724.12391

Fostowicz-Frelik, Ł, Li, C. K., Mao, F., Meng, J., and Wang, Y. Q. (2015b). A large mimotonid from the Middle Eocene of China sheds light on the evolution of lagomorphs and their kin. *Sci. Rep.* 5:9394. doi: 10.1038/srep09394

Fostowicz-Frelik, Ł, Li, C. K., Meng, J., and Wang, Y. Q. (2012). New *Gobiolagus* (Mammalia: Lagomorpha) material from the Middle Eocene of Erden Obo (Nei Mongol, China). *Vertebr. PalAsiatica* 50, 219–236.

Frahnert, S. (1998). *Zur Stellung des Bibers (Castoridae*: Castor) - *Eine craniogenetische Studie zur Ethmoidalregion sciurognather Rodentia*. Dissertation. Berlin: Humboldt-Universität Berlin.

Franks, E. M., Holton, N. E., Scott, J. E., McAbee, K. R., Rink, J. T., Pax, K., et al. (2016). Betwixt and between: intracranial perspective on zygomatic arch plasticity and function in mammals. *Anat. Rec.* 299, 1646–1660. doi: 10.1002/ar.23477

Franks, E. M., Scott, J. E., McAbee, K. R., Scollan, J. P., Eastman, M. M., and Ravosa, M. J. (2017). Intracranial and hierarchical perspective on dietary plasticity in mammals. *Zoology* 124, 30–41. doi: 10.1016/j.zool.2017.03.003

Frick, H., and Heckmann, U. (1955). Ein beitrag zur morphogenese des kaninchenschädels. *Acta Anat.* 24, 268–314. doi: 10.1159/000141047

Gambaryan, P. P. (1974). *How Mammals Run. Anatomical Adaptations*. New York, NY: Wiley.

Garland, T. (1983). The relation between maximal running speed and body mass in terrestrial mammals. *J. Zool.* 199, 157–170. doi: 10.1111/j.1469-7998.1983.tb02087.x

Gaupp, E. (1906). "Die Entwickelung des Kopfkelettes," in *Handbuch der vergleichenden und experimentellen Entwickelungslehre der Wirbeltiere*, Vol. 3, ed. O. Hertwig (Jena: Fischer), 573–874.

Gawne, C. E. (1978). Leporids (Lagomorpha, Mammalia) from the Chadronian (Oligocene) deposits of Flagstaff Rim, Wyoming. *J. Paleontol.* 52, 1103–1118.

Ge, D. Y., Lissovsky, A. A., Xia, L., Cheng, C., and Smith, A. T. (2012). Reevaluation of several taxa of Chinese lagomorphs (Mammalia: Lagomorpha) described on the basis of pelage phenotype variation. *Mammal Biol.* 77, 113–123. doi: 10.1016/j.mambio.2011.09.009

Ge, D. Y., Wen, Z. X., Xia, L., Zhang, Z. Q., Erbajeva, M., Hung, C. M., et al. (2013). Evolutionary history of lagomorphs in response to global environmental change. *PLoS One* 8:e59668. doi: 10.1371/journal.pone.0059668

Ge, D. Y., Yao, L., Xia, L., Zhang, Z. Q., and Yang, Q. S. (2015). Geometric morphometric analysis of skull morphology reveals loss of phylogenetic signal at the generic level in extant lagomorphs (Mammalia: Lagomorpha). *Contr. Zool.* 84, 267–284. doi: 10.1163/18759866-08404001

Genereux, D. P., Serres, A., Armstrong, J., Johnson, J., Marinescu, V. D., Murén, E., et al. (2020). A comparative genomics multitool for scientific discovery and conservation. *Nature* 587, 240–245. doi: 10.1038/s41586-020-2876-6

Gignac, P. M., Kley, N. J., Clarke, J. A., Colbert, M. W., Morhardt, A. C., Cerio, D., et al. (2016). Diffusible iodine-based contrast-enhanced computed tomography (diceCT): an emerging tool for rapid, high-resolution, 3-D imaging of metazoan soft tissues. *J. Anat.* 228, 889–909. doi: 10.1111/joa.12449

Giska, I., Farelo, L., Pimenta, J., Seixas, F. A., Ferreira, M. S., Marques, J. P., et al. (2019). Introgression drives repeated evolution of winter coat color polymorphism in hares. *PNAS* 116, 24150–24156. doi: 10.1073/pnas.1910471116

Gorniak, G. C., and Gans, C. (1980). Quantitative assay of electromyograms during mastication in domestic cats (*Felis catus*). *J. Morphol.* 163, 253–281. doi: 10.1002/jmor.1051630304

Graham, J. E. (2015). "Chapter 41 - Lagomorpha (Pikas, Rabbits, and Hares)," in *Fowler's Zoo and Wild Animal Medicine*, Vol. 8, eds R. E. Miller and M. E. Fowler (Amsterdam: Elsevier), 8375–8384.

Grauer, J. N., Erulkar, J. S., Patel, T. C., and Panjabi, M. M. (2000). Biomechanical evaluation of the New Zealand white rabbit lumbar spine: a physiologic characterization. *Eur. Spine J.* 9, 250–255. doi: 10.1007/s005860000141

Graur, D., Duret, L., and Gouy, M. (1996). Phylogenetic position of the order Lagomorpha (rabbits, hares and allies). *Nature* 379, 333–335. doi: 10.1038/379333a0

Gray, J. E. (1867). XXVII.—Notes on the skulls of hares (Leporidæ) and picas (Lagomyidæ) in the British Museum. *Ann. Magaz. Nat. Hist.* 20, 219–225. doi: 10.1080/00222936708694118

Grover, D. M., Chen, A. A., and Hazelwood, S. J. (2007). Biomechanics of the rabbit knee and ankle: muscle, ligament, and joint contact force predictions. *J. Biomech.* 40, 2816–2821. doi: 10.1016/j.jbiomech.2007.01.002

Hackert, R., Witte, H., and Fischer, M. S. (2006). "Interactions between motions of the trunk and the angle of attack of the forelimbs in synchronous gaits of the Pika (*Ochotona rufescens*)," in *Adaptive Motion of Animals and Machines*, eds H. Kimura, K. Tsuchiya, A. Ishiguro, and A. H. Witt (Tokyo: Springer), 69–77.

Halanych, K., Demboski, J., Van Vuuren, B., Klein, D., and Cook, J. (1999). Cytochrome b phylogeny of North American hares and jackrabbits (Lepus, Lagomorpha) and the effects of saturation in outgroup taxa. *Mol. Phylogenet. Evol.* 11, 213–221. doi: 10.1006/mpev.1998.0581

Hall, B. K. (2005). *Bones and Cartilage: Developmental and Evolutionary Skeletal Biology*. Amsterdam: Academic Press.

Harcourt-Brown, F. M. (2007). The progressive syndrome of acquired dental disease in rabbits. *J. Exot. Pet. Med.* 16, 146–157. doi: 10.1053/j.jepm.2007.06.003

Harper, M. J. (1961). The time of ovulation in the rabbit following the injection of luteinizing hormone. *J. Endocrinol.* 22, 147-152. doi: 10.1677/joe.0.0220147

He, T., and Kiliaridis, S. (2003). Effects of masticatory muscle function on craniofacial morphology on growing ferrets (*Mustela putorius furo*). *Eur. J. Oral Sci.* 11, 510–517. doi: 10.1111/j.0909-8836.2003.00080.x

Hecker, N., Sharma, V., and Hiller, M. (2019). Convergent gene losses illuminate metabolic and physiological changes in herbivores and carnivores. *PNAS* 116, 3036–3041. doi: 10.1073/pnas.1818504116

Heissig, K., and Schmidt-Kittler, N. (1975). Ein primitiver Lagomorphe aus dem Mitteloligozän Süddeutschlands. *Mitt. Bayer. Staatsml. Pal. Hist. Geol.* 15, 57–62.

Heissig, K., and Schmidt-Kittler, N. (1976). Neue Lagomorphen-funde aus dem Mitteloligozän. *Mitt. Bayer. Staatsml. Pal. Hist. Geol.* 16, 83–93.

Herring, S. W., and Scapino, R. P. (1973). Physiology of feeding in miniature pigs. *J. Morphol.* 141, 427–460. doi: 10.1002/jmor.1051410405

Hibbard, C. W. (1963). The origin of the p3 pattern of *Sylvilagus, Caprolagus, Oryctolagus* and *Lepus*. *J. Mammal.* 44, 1–15. doi: 10.2307/1377162

Hirano, T., Burr, D. B., Cain, R. L., and Hock, J. M. (2000). Changes in geometry and cortical porosity in adult, ovary-intact rabbits after 5 months treatment with LY333334 (hPTH 1-34). *Calcif. Tissue Int.* 66, 456–460. doi: 10.1007/s002230010091

Hoffmann, R. S., and Smith, A. T. (2005). "Order Lagomorpha," in *The Mammal Species of the World: A Taxonomic and Geographic Reference*, eds D. E. Wilson and D. M. Reeder (London: Johns Hopkins, University Press), 185–211.

Hoyte, D. A. N. (1961). The postnatal growth of the ear capsule in the rabbit. *Am. J. Anat.* 108, 1–16. doi: 10.1002/aja.1001080102

Huang, D., Wu, Q., Zhou, X., and Kang, F. (2019). Activity and morphologic changes in the mandible after mandibular osteotomy. *Am. J. Orthodont. Dentofac. Orthoped.* 155, 40–47. doi: 10.1016/j.ajodo.2018.02.016

Huang, X. S. (1987). Fossil ochotonids from the middle Oligocene of Ulantatal, Nei Mongol. *Vert. PalAsiatica* 25, 260–282.

Huchon, D., Madsen, O., Sibbald, M. J. J. B., Ament, K., Stanhope, M. J., Catzeflis, F., et al. (2002). Rodent phylogeny and a timescale for the evolution of Glires: evidence from an extensive taxon sampling using three nuclear genes. *Mol. Biol. Evol.* 19, 1053–1065. doi: 10.1093/oxfordjournals.molbev.a004164

Hylander, W. L. (1979). The functional significance of primate mandibular form. *J. Morphol.* 160, 223–240. doi: 10.1002/jmor.1051600208

Hylander, W. L., Johnson, K. R., and Crompton, A. W. (1987). Loading patterns and jaw movements during mastication in *Macaca fascicularis*: a bone-strain, electromyographic and cineradiographic analysis. *Am. J. Phys. Anthropol.* 72, 287–314. doi: 10.1002/ajpa.1330720304

Hylander, W. L., Johnson, K. R., and Crompton, A. W. (1992). Muscle force recruitment and biomechanical modeling: an analysis of masseter muscle function during mastication in *Macaca fascicularis*. *Am. J. Phys. Anthropol.* 88, 365–387. doi: 10.1002/ajpa.1330880309

Hylander, W. L., Ravosa, M. J., Ross, C. F., and Johnson, K. R. (1998). Mandibular corpus strain in primates: further evidence for a functional link between symphyseal fusion and jaw-adductor muscle force. *Am. J. Phys. Anthropol.* 107, 257–271. doi: 10.1002/(SICI)1096-8644(199811)107:3<257::AID-AJPA3<3.0.CO;2-6

Hylander, W. L., Ravosa, M. J., Ross, C. F., Wall, C. E., and Johnson, K. R. (2000). Symphyseal fusion and jaw-adductor muscle force: an EMG study. *Am. J. Phys. Anthropol.* 112, 469–492. doi: 10.1002/1096-8644(200008)112:4<469::AID-AJPA5<3.0.CO;2-V

Insom, E., Magnoni, M. L., and Simonetta, A. M. (1990). Etudes sur la morphologie évolutive des Ochotonidés (Mammalia, Lagomorpha). 1. La morphologie crânienne d'*Ochotona rufescens* et d'*Ochotona roylei*. *Mammalia* 54, 633–651. doi: 10.1515/mamm.1990.54.4.633

Jašarević, E., Ning, J., Daniel, A. N., Menegaz, R. A., Johnson, J. J., Stack, M. S., et al. (2010). Masticatory loading, function and plasticity: a microanatomical analysis of mammalian circumorbital soft-tissue structures. *Anat. Rec.* 293, 642–650. doi: 10.1002/ar.21135

Jekl, V., and Redrobe, S. (2013). Rabbit dental disease and calcium metabolism - the science behind divided opinions. *J. Small Anim. Pract.* 54, 481–490. doi: 10.1111/jsap.12124

Jones, M. R., Mills, L. S., Alves, P. C., Callahan, C. M., Alves, J. M., Lafferty, D. J. R., et al. (2018). Adaptive introgression underlies polymorphic seasonal camouflage in snowshoe hares. *Science* 360, 1355–1358. doi: 10.1126/science.aar5273

Jones, M. R., Mills, L. S., Jensen, J. D., and Good, J. M. (2020). Convergent evolution of seasonal camouflage in response to reduced snow cover across the snowshoe hare range. *Evolution* 74, 2033–2045. doi: 10.1111/evo.13976

Kennelly, J. J., Foote, R. H., and Jones, R. C. (1970). Duration of premeiotic deoxyribonucleic acid synthesis and the stages of prophase I in rabbit oocytes. *J. Cell. Biol.* 47, 577–584. doi: 10.1083/jcb.47.3.577

Kim, I.-J., and Shin, S.-Y. (2018). Comparative study of new bone formation capability of zirconia bone graft material in rabbit calvarial. *J. Adv. Prosthodont.* 10, 167–176. doi: 10.4047/jap.2018.10.3.167

Kinoshita, G., Nunome, M., Kryukov, A. P., Kartavtseva, I. V., Han, S. H., Yamada, F., et al. (2019). Contrasting phylogeographic histories between the continent and islands of East Asia: massive mitochondrial introgression and long-term isolation of hares (Lagomorpha: Lepus). *Mol. Phylogenet. Evol.* 136, 65–75. doi: 10.1016/j.ympev.2019.04.003

Klebanova, E. A., Polyakova, R. S., and Sokolov, A. S. (1971). Morpho-functional features of the organs of support and locomotion in lagomorphs. *Trans. Zool. Inst.* 48, 58–120.

Koenigswald, W. V., Anders, U., Engels, S., Schultz, J. A., and Ruf, I. (2010). Tooth morphology in fossil and extant Lagomorpha (Mammalia) reflects different mastication patterns. *J. Mammal. Evol.* 17, 275–299. doi: 10.1007/s10914-010-9140-z

Koh, T. J., and Herzog, W. (1998). Excursion is important in regulating sarcomere number in the growing rabbit tibialis anterior. *J. Physiol.* 508, 267–280. doi: 10.1111/j.1469-7793.1998.267br.x

Koju, N. P., He, K., Chalise, M. K., Ray, C., Chen, Z., Zhang, B., et al. (2017). Multilocus approaches reveal underestimated species diversity and inter-specific gene flow in pikas (*Ochotona*) from southwestern China. *Mol. Phylogenet. Evol.* 107, 239–245. doi: 10.1016/j.ympev.2016.11.005

Kraatz, B. P., and Sherratt, E. (2016). Evolutionary morphology of the rabbit skull. *PeerJ* 4:e2453. doi: 10.7717/peerj.2453

Kraatz, B. P., Meng, J., Weksler, M., and Li, C. (2010). Evolutionary patterns in the dentition of Duplicidentata (Mammalia) and a novel trend in the molarization of premolars. *PLoS One* 5:e12838. doi: 10.1371/journal.pone.0012838

Kraatz, B. P., Sherratt, E., Bumacod, N., and Wedel, M. J. (2015). Ecological correlates to cranial morphology in leporids (Mammalia, Lagomorpha). *PeerJ* 3:e844. doi: 10.7717/peerj.844

Krause, W. (1884). *Die Anatomie des Kaninchens*. Leipzig: Wilhelm Engelmann.

Kriegs, J. O., Zemann, A., Churakov, G., Matzke, A., Ohme, M., Zischler, H., et al. (2010). Retroposon insertions provide insights into deep lagomorph evolution. *Mol. Biol. Evol.* 27, 2678–2681. doi: 10.1093/molbev/msq162

Kullberg, M., Nilsson, M. A., Arnason, U., Harley, E. H., and Janke, A. (2006). Housekeeping genes for phylogenetic analysis of eutherian relationships. *Mol. Biol. Evol.* 23, 1493–1503. doi: 10.1093/molbev/msl027

Kumar, V., Hallstrom, B. M., and Janke, A. (2013). Coalescent-based genome analyses resolve the early branches of the Euarchontoglires. *PLoS One* 8:e60019. doi: 10.1371/journal.pone.0060019

Kuznetsov, A. N., Luchkina, O. S., Panyutina, A. A., and Kryukova, N. V. (2017). Observations on escape runs in wild European hare as a basis for the mechanical concept of extreme cornering with special inference of a role of the peculiar subclavian muscle. *Mamm. Biol.* 84, 61–72. doi: 10.1016/j.mambio.2017.01.003

Lad, S. E., Anderson, R. J., Cortese, S. A., Alvarez, C. E., Danison, A. D., Morris, H. M., et al. (2021). Bone remodeling and cyclical loading in maxillae of New Zealand white rabbits (*Oryctolagus cuniculus*). *Anat. Rec.* [Epub ahead of print] doi: 10.1002/ar.24599

Lado, S., Alves, P. C., Brito, J., et al. (2016). Population history and taxonomy of African hares (genus *Lepus*) inferred from genetic variation. *Mamm. Biol.* 81:12. doi: 10.1016/j.mambio.2016.07.035

Lammers, A. R., and German, R. Z. (2002). Ontogenetic allometry in the locomotor skeleton of specialized half-bounding mammals. *J. Zool.* 258, 485–495. doi: 10.1017/S0952836902001644

Langenbach, G. E. J., and van Eijden, T. M. G. J. (2001). Mammalian feeding motor patterns. *Am. Zool.* 41, 1338–1351. doi: 10.1093/icb/41.6.1338

Langenbach, G. E. J., Weijs, W. A., and Koolstra, J. H. (1991). Biomechanical changes in the rabbit masticatory system during postnatal development. *Anat. Rec.* 230, 406–416. doi: 10.1002/ar.1092300313

Langenbach, G. E. J., Weijs, W. A., Brugman, P., and van Eijden, T. M. G. J. (2001). A longitudinal electromyographic study of the postnatal maturation of mastication in the rabbit. *Arch. Oral Biol.* 46, 11–20. doi: 10.1016/S0003-9969(01)00043-7

Lanier, H. C., and Olson, L. E. (2009). Inferring divergence times within pikas (*Ochotona* spp.) using mtDNA and relaxed molecular dating techniques. *Mol. Phylogenet. Evol.* 53, 1–12. doi: 10.1016/j.ympev.2009.05.035

Lanzetti, A., Berta, A., and Ekdale, E. G. (2018). Prenatal development of the humpback whale: growth rate, tooth loss, and skull shape changes in an evolutionary framework. *Anat. Rec.* 303, 180–204. doi: 10.1002/ar.23990

Lennox, A. M. (2008). Diagnosis and treatment of dental disease in pet rabbits. *J. Exot. Pet. Med.* 17, 107–113. doi: 10.1053/j.jepm.2008.03.008

Leonelli, S., and Ankeny, R. A. (2013). What makes a model organism? *Endeavour* 37, 209–212. doi: 10.1016/j.endeavour.2013.06.001

Levanen, R., Thulin, C. G., Spong, G., and Pohjoismaki, J. L. O. (2018). Widespread introgression of mountain hare genes into Fennoscandian brown hare populations. *PLoS One* 13:e0191790. doi: 10.1371/journal.pone.0191790

Leventis, M., Fairbairn, P., Mangham, C., Galanos, A., Vasiliadis, O., Papavasileiou, D., et al. (2018). Bone healing in rabbit calvaria defects using a synthetic bone substitute: a histological and micro-CT comparative study. *Materials* 11:2004. doi: 10.3390/ma11102004

Lewis, W. B. (1882). On the comparative structure of the brain in rodents. *Philos. Trans. R. Soc. Lond.* 173, 699–746. doi: 10.1098/rspl.1881.0066

Li, C. K. (1965). Eocene leporids of North China. *Vertebr. PalAsiatica* 9, 23–36.

Li, C. K. (1977). Paleocene eurymyloids (Anagalida, Mammalia) of Qianshan, Anhui. *Vertebr. PalAsiatica* 15, 103–118.

Li, C. K., and Ting, S. Y. (1985). "Possible phylogenetic relationships of eurymylids and rodents, with comments on mimotonids," in *Evolutionary Relationships Among Rodents: A Multidisciplinary Analysis*, eds W. P. Luckett and J. L. Hartenberger (New York, NY: Plenum Press), 35–58.

Li, C. K., Meng, J., and Wang, Y. Q. (2007). *Dawsonolagus antiquus*, a primitive lagomorph from the eocenetheeocene arshanto formation, Nei Mongol, China. *Bull. Carnegie Mus.* 39, 97–110. doi: 10.2992/0145-9058200739[97:DAAPLF]2.0.CO;2

Li, C. K., Wang, Y. Q., Zhang, Z. Q., Mao, F. Y., and Meng, J. (2016). A new mimotonidan mammal Mina hui (Mammalia, Glires) from the Middle Paleocene of Qianshan, Anhui Province, China. *Vertebr. PalAsiatica* 54, 121–136.

Li, Q., Wang, Y. Q., and Fostowicz-Frelik, Ł (2016). Small mammal fauna from Wulanhuxiu (Nei Mongol, China) implies the Irdinmanhan–Sharamurunian (Eocene) faunal turnover. *Acta Palaeontol. Pol.* 61, 759–776. doi: 10.4202/app.00292.2016

Lieberman, D. E., Krovitz, G. E., Yates, F., Devlin, M., and St Claire, M. (2004). Effects of food processing on masticatory strain and craniofacial growth in a retrognathic face. *J. Hum. Evol.* 46, 655–677. doi: 10.1016/j.jhevol.2004.03.005

Lin, Y.-H., Waddell, P. J., and Penny, D. (2002). Pika and vole mitochondrial genomes increase support for both rodent monophyly and Glires. *Gene* 294, 119–129. doi: 10.1016/S0378-1119(02)00695-9

Lissovsky, A. (2014). Taxonomic revision of pikas *Ochotona* (Lagomorpha, Mammalia) at the species level. *Mammalia* 78, 199–216. doi: 10.1515/mammalia-2012-0134

Lissovsky, A. A. (2016). "Ochotonidae (pikas)," in *Handbook of the Mammals of the World. Lagomorphs and Rodents I*, Vol. 6, eds D. E. Wilson, T. E. Lacher, and R. A. Mittermeier (Barcelona: Lynx Edicions), 28–60.

Lissovsky, A. A., Yatsentyuk, S. P., and Koju, N. P. (2019). Multilocus phylogeny and taxonomy of pikas of the subgenus Ochotona (Lagomorpha. Ochotonidae). *Zool. Scr.* 48, 1–16. doi: 10.1111/zsc.12325

Liu, J., Yu, L., Arnold, M., Wu, C.-H., Wu, S.-F., Lu, X., et al. (2011). Reticulate evolution: frequent introgressive hybridization among chinese hares (genus *Lepus*) revealed by analyses of multiple mitochondrial and nuclear DNA loci. *BMC Evol. Biol.* 11:223. doi: 10.1186/1471-2148-11-223

Lopatin, A. V. (1998). A revision of the early Miocene Lagomorpha (Mammalia) from the North Aral region. *Paleont. J. C* 32, 291–304.

Lopatin, A. V., and Averianov, A. O. (2008). The earliest lagomorph (Lagomorpha, Mammalia) from the basal Eocene of Mongolia. *Doklady Biol. Sci.* 419, 131–132.

Lopatin, A., and Averianov, A. O. (2020). *Arnebolagus*, the oldest eulagomorph, and phylogenetic relationships within the Eocene Eulagomorpha new clade (Mammalia, Duplicidentata). *J. Paleontol.* 95, 394–405. doi: 10.1017/jpa.2020.94

López Martínez, N. (1985). "Reconstruction of the ancestral cranioskeletal features in the order Lagomorpha," in *Evolutionary Relationships Among Rodents: A Multidisciplinary Analysis*, eds W. P. Luckett and J.-L. Hartenberger (New York, NY: Plenum Press), 151–189.

López Martínez, N. (2001). Paleobiogeographical history of *Prolagus*, a European ochotonid (Lagomorpha). *Lynx* 32, 215–231.

Lopez-Bejar, M. (1995). *Evaluacion de la Viabilidad de Embriones de Conejo de Diversos Estadios Preimplantaciones Crioconservados Mediante Procedimientos de la Congelacion Rapida*. Disseration. Barcelona: Universidad Autònoma de Barcelona.

Lopez-Martinez, N. (2008). "The lagomorph fossil record and the origin of the European rabbit," in *Lagomorph Biology: Evolution, Ecology, and Conservation*, eds P. C. Alves, N. Ferrand, and K. Hackländer (Berlin: Springer-Verlag), 27–46.

López-Torres, S., Bertrand, O. C., Lang, M. M., Silcox, M. T., and Fostowicz-Frelik, Ł (2020). Cranial endocast of the stem lagomorph *Megalagus* and brain structure of basal Euarchontoglires. *Proc. R. Soc. B* 287:20200665. doi: 10.1098/rspb.2020.0665

Losos, J. B. (2011). *Lizards in an Evolutionary Tree: Ecology and Adaptive Radiation of Anoles*. Berkeley: University of California Press.

Lu, X. (2003). Postnatal growth of skull linear measurements of Cape Hare *Lepus capensis* in northern China: an analysis in adaptive context. *Biol. J. Linn. Soc.* 78, 343–353. doi: 10.1046/j.1095-8312.2003.00145.x

Lyn Chong, S., Mitchell, R., Moursi, A. M., Winnard, P., Losken, H. W., Bradley, J., et al. (2003). Rescue of coronal suture fusion using transforming growth factor-beta 3 (Tgf-β3) in rabbits with delayed-onset craniosynostosis. *Anat. Rec. A* 274A, 962–971. doi: 10.1002/ar.a.10113

Magne de la Croix, P. (1928). Sobre la evolución del galope de carrera y la consecutiva de la forma causa de la evolución en perisodáctiles y artiodáctiles. *Anal. Soc. Cient. Argentina* 106, 317–331.

Magne de la Croix, P. (1933). Des retours de l'évolution et la relativité des théories. *Anal. Soc. Cient. Argentina* 116, 225–239.

Magne de la Croix, P. (1936). The evolution of locomotion in mammals. *J. Mammal.* 17, 51–54. doi: 10.2307/1374551

Maier, W., and Ruf, I. (2014). Morphology of the nasal capsule of Primates - with special reference to *Daubentonia* and *Homo*. *Anat. Rec.* 297, 1985–2006. doi: 10.1002/ar.23023

Maier, W., Klingler, P., and Ruf, I. (2002). Ontogeny of the medial masseter muscle, pseudo-myomorphy, and the systematic position of the Gliridae (Rodentia, Mammalia). *J. Mamm. Evol.* 9, 253–269. doi: 10.1023/A:1023979212759

Maier, W., Tröscher, A., and Ruf, I. (2018). The anterior process of the malleus in extant Lagomorpha (Mammalia). *J. Morphol.* 279, 132–146. doi: 10.1002/jmor.20759

Manju, V., Anitha, A., Menon, D., Iyer, S., Nair, S. V., and Nair, M. B. (2018). Nanofibrous yarn reinforced HA-gelatin composite scaffolds promote bone formation in critical sized alveolar defects in rabbit model. *Biomed. Mater.* 13:065011. doi: 10.1088/1748-605X/aadf99

Mann, G. (1895). Homoplasy of the brain of rodents, insectivores, and carnivores. *J. Anat. Physiol.* 30, 1–36.

Marey, ÉJ. (1894). *Le Mouvement*. Paris: G. Masson.

Marey, ÉJ. (1901). La locomotion animale. *Traité Phys. Biol.* 1, 229–287.

Marques, J. P., Farelo, L., Vilela, J., Vanderpool, D., Alves, P. C., Good, J. M., et al. (2017). Range expansion underlies historical introgressive hybridization in the Iberian hare. *Sci. Rep.* 7:40788. doi: 10.1038/srep40788

Marques, J. P., Seixas, F. A., Farelo, L., Callahan, C. M., Good, J. M., Montgomery, W. I., et al. (2020). An annotated draft genome of the mountain hare (*Lepus timidus*). *Genome Biol. Evol.* 12, 3656–3662. doi: 10.1093/gbe/evz273

Martin, L. F., Krause, L., Ulbricht, A., Winkler, D. E., Codrone, D., Kaiser, T. M., et al. (2020). Dental wear at macro- and micoscopic scale in rabbits fed diets of different abrasiveness: a pilot investigation. *Palaeogeogr. Palaeocl.* 556:109886. doi: 10.1016/j.palaeo.2020.109886

Martin, T. (1999). Phylogenetic implications of Glires (Eurymylidae, Mimotonidae, Rodentia, Lagomorpha) incisor enamel microstructure. *Zoosyst. Evol.* 75, 257–273. doi: 10.1002/mmnz.19990750207

Martin, T. (2004). Evolution of incisor enamel microstructure in Lagomorpha. *J. Vertebr. Paleontol.* 24, 411–426.

Matthee, C. A., Van Vuuren, B. J., Bell, D., and Robinson, T. J. (2004). A molecular supermatrix of the rabbits and hares (Leporidae) allows for the identification of five intercontinental exchanges during the Miocene. *Syst. Biol.* 53, 433–447. doi: 10.1080/10635150490445715

Mauleon, P. (1967). Différenciation et évolution des cellules sexuelles. La lignée femelle. *Arch. Anat. Microsc.* 56, 125–150.

McKenna, M. C. (1982). Lagomorph interrelationships. *Geobios* 15, 213–223. doi: 10.1016/S0016-6995(82)80115-0

Melo-Ferreira, J., Boursot, P., Carneiro, M., Esteves, P. J., Farelo, L., and Alves, P. C. (2012). Recurrent introgression of mitochondrial DNA among hares (*Lepus* spp.) revealed by species-tree inference and coalescent simulations. *Syst. Biol.* 61, 367–381. doi: 10.1093/sysbio/syr114

Melo-Ferreira, J., Farelo, L., Freitas, H., Suchentrunk, F., Boursot, P., and Alves, P. C. (2014a). Home-loving boreal hare mitochondria survived several invasions in Iberia: the relative roles of recurrent hybridisation and allele surfing. *Heredity* 112, 265–273. doi: 10.1038/hdy.2013.102

Melo-Ferreira, J., Seixas, F. A., Cheng, E., Mills, L. S., and Alves, P. C. (2014b). The hidden history of the snowshoe hare, *Lepus americanus*: extensive mitochondrial DNA introgression inferred from multilocus genetic variation. *Mol. Ecol.* 23, 4617–4630. doi: 10.1111/mec.12886

Menegaz, R. A., Sublett, S. V., Figueroa, S. D., Hoffman, T. J., and Ravosa, M. J. (2009). Phenotypic plasticity and function of the hard palate in growing rabbits. *Anat. Rec.* 292, 277–284. doi: 10.1002/ar.20840

Meng, J., and Wyss, A. R. (2001). The morpology of *Tribosphenomys* (Rodentiaformes, Mammalia): phylogenetic implications for basal Glires. *J. Mamm. Evol.* 8, 1–71. doi: 10.1023/A:1011328616715

Meng, J., Bowen, G. J., Ye, J., Koch, P. L., Ting, S. Y., Li, Q., et al. (2004). *Gomphos elkema* (Glires, Mammalia) from the erlian basin: evidence for the early tertiary bumbanian land mammal age in Nei-Mongol, China. *Am. Mus. Nov.* 3425, 1–24. doi: 10.1206/0003-00822004425<0001:GEGMFT<2.0.CO;2

Meng, J., Hu, Y., and Li, C. K. (2005). *Gobiolagus* (Lagomorpha, Mammalia) from Eocene Ula Usu, Inner Mongolia, and comments on Eocene lagomorphs of Asia. *Palaeont. Electr.* 8:23.

Meng, J., Hu, Y.-M., and Li, C.-K. (2003). The osteology of *Rhombomylus* (Mammalia, Glires): implications for phylogeny and evolution of Glires. *Bull. Am. Mus. Nat. Hist.* 275, 1–247. doi: 10.1206/0003-00902003275<0001:TOORMG<2.0.CO;2

Meng, J., Wyss, A. R., Dawson, M. R., and Zhai, R. (1994). Primitive fossil rodent from Inner Mongolia and its implications for mammalian phylogeny. *Nature* 370, 134–136. doi: 10.1038/370134a0

Metscher, B. D. (2009a). Micro-CT for comparative morphology: simple staining methods allow high-contrast 3D imaging of diverse non-mineralized animal tissues. *BMC Physiol.* 9:11. doi: 10.1186/1472-6793-9-11

Metscher, B. D. (2009b). Micro-CT for developmental biology: a versatile tool for high-contrast 3-D imaging at histological resolutions. *Dev. Dyn.* 238, 632–640. doi: 10.1002/dvdy.21857

Mohammadi, Z., Aliabadian, M., Ghorbani, F., Moghaddam, F. Y., Lissovsky, A. A., Obst, M., et al. (2020). Unidirectional introgression and evidence of hybrid superiority over parental populations in Eastern Iranian Plateau population of hares (Mammalia: Lepus Linnaeus, 1758). *J. Mamm. Evol.* 27, 723–743. doi: 10.1007/s10914-019-09478-5

Monaghan, P. (2014). Behavioral ecology and the successful integration of function and mechanism. *Behav. Ecol.* 25, 1019–1021. doi: 10.1093/beheco/aru082

Mooney, M. P., Siegel, M. I., Burrows, A. M., Smith, T. D., Losken, H. W., Dechant, J., et al. (1998a). A rabbit model of human familial, nonsyndromic unicoronal suture synostosis I. Synostotic onset, pathology, and sutural growth patterns. *Child's Nerv. Syst.* 14, 236–246.

Mooney, M. P., Siegel, M. I., Burrows, A. M., Smith, T. D., Losken, H. W., Dechant, J., et al. (1998b). A rabbit model of human familial, nonsyndromic unicoronal suture synostosis II. Intracranial contents, intracranial volume, and intracranial pressure. *Child's Nerv. Syst.* 14, 247–255. doi: 10.1007/s003810050220

Moss, M. L., and Feliciano, W. C. (1977). A functional analysis of the fenestrated maxillary bone of the rabbit (*Oryctolagus cuniculus*). *Anat. Histol. Embryol.* 6, 167–187. doi: 10.1111/j.1439-0264.1977.tb00431.x

Murphy, W. J., Eizirik, E., O'Brien, S. J., Madsen, O., Scally, M., Douady, C. J., et al. (2001). Resolution of the early placental mammal radiation using Bayesian phylogenetics. *Science* 294, 2348–2351. doi: 10.1126/science.1067179

Myers, P., Espinosa, R., Parr, C. S., Jones, T., Hammond, G. S., and Dewey, T. A. (2020). *The Animal Diversity Web*. Available online at: https://animaldiversity.org (accessed on 23 November 2020)

Naff, K. A., and Craig, S. (2012). "Chapter 6 - The domestic rabbit, *Oryctolagus cuniculus*: origins and history," in *The Laboratory Rabbit, Guinea Pig, Hamster, and Other Rodents. American College of Laboratory Animal Medicine*, eds M. A. Suckow, K. A. Stevens, and R. P. Wilson (Cambridge, MA: Academic Press), 157–163.

Nett, E. M., Jaglowski, B. A., Ravosa, L. J., Ravosa, D. D., and Ravosa, M. J. (in press). Food mechanical properties and cyclical loading in the feeding apparatus of llamas. *J Mammal.*

Neves, F., Agueda-Pinto, A., Pinheiro, A., Abrantes, J., and Esteves, P. J. (2019). Strong selection of the TLR2 coding region among the Lagomorpha suggests an evolutionary history that differs from other mammals. *Immunogenetics* 71, 437–443. doi: 10.1007/s00251-019-01110-3

Neyt, J. G., Buckwalter, J. A., and Carroll, N. C. (1998). Use of animal models in musculoskeletal research. *Iowa Orthop. J.* 18, 118–123.

Niu, Y., Wie, F., Li, M., Liu, X., and Feng, Z. (2004). Phylogeny of pikas (Lagomorpha, *Ochotona*) inferred from mitochondrial cytochrome b sequences. *Folia Zool.* 53, 141–155.

Novacek, M. J. (1993). "Patterns of diversity in the mammalian skull," in *The Skull*, Vol. II, eds J. Hanken and B. K. Hall (Chicago, IL: University Press), 438–545.

Okuda, A., Hori, Y., Ichihara, N., Asari, M., and Wiggs, R. B. (2007). Comparative observation of skeletal-dental abnormalities in wild, domestic, and laboratory rabbits. *J. Vet. Dent.* 24, 224–229. doi: 10.1177/089875640702400403

Olson, E. C. (1942). The skull of *Megalagus turgidus* (Cope). *Am. J. Sci.* 240, 505–511. doi: 10.2475/ajs.240.7.505

Orliac, M. J., Ladevèze, S., Gingerich, P. D., Lebrun, R., and Smith, T. (2014). Endocranial morphology of Palaeocene *Plesiadapis tricuspidens* and evolution of the early primate brain. *Proc. R. Soc. B* 281:20132792. doi: 10.1098/rspb.2013.2792

Orr, R. T. (1940). The rabbits of California. occasional papers of the California. *Acad. Sci.* 19, 1–227.

Parés-Casanova, P. M., and Cabello, M. (2020). Patterns of mandibular asymmetries in two types of companion rabbits. *Anat. Histol. Embr.* 49, 227–232. doi: 10.1111/ahe.12517

Patnaik, R. (2002). Pliocene Leporidae (Lagomorpha, Mammalia) from the Upper Siwaliks of India: implications for phylogenetic relationships. *J. Vertebr. Paleontol.* 22, 443–452. doi: 10.1671/0272-46342002022[0443:PLLMFT]2.0.CO;2

Pinheiro, A., de Sousa-Pereira, P., Almeida, T., Ferreira, C. C., Otis, J. A., Boudreau, M. R., et al. (2019). Sequencing of VDJ genes in *Lepus americanus* confirms a correlation between VHn expression and the leporid species continent of origin. *Mol. Immunol.* 112, 182–187. doi: 10.1016/j.molimm.2019.05.008

Pinheiro, A., de Sousa-Pereira, P., Strive, T., Knight, K. L., Woof, J. M., Esteves, P. J., et al. (2018). Identification of a new European rabbit IgA with a serine-rich hinge region. *PLoS One* 13:e0201567. doi: 10.1371/journal.pone.0201567

Pinheiro, A., Neves, F., Lemos, de Matos, A., Abrantes, J., van der Loo, W., et al. (2016). An overview of the lagomorph immune system and its genetic diversity. *Immunogenetics* 68, 83–107. doi: 10.1007/s00251-015-0868-8

Propper, A. Y. (1976). Modalités et déterminisme du développement embryonnaire de la glande mammaire. *Senologia* 1, 19–26.

Racicot, R. A. (2017). "Fossil secrets revealed: X-ray CT scanning and applications in paleontology. *Paleontol. Soc. Pap.* 22, 21–38.

Racicot, R., and Ruf, I. (2020). *Data from: MicroCT Scans of an Iodine Stained Prenatal Rabbit. MorphoSource*. Available online at: http://www.morphosource.org/Detail/ProjectDetail/Show/project_id/1184 (accessed November 25, 2020).

Ravosa, M. J., and Hogue, A. S. (2004). "Function and fusion of the mandibular symphysis in mammals: a comparative and experimental perspective," in *Anthropoid Evolution. New Visions*, eds C. F. Ross and R. F. Kay (New York, NY: Springer/Kluwer Academic Publishers), 413–462.

Ravosa, M. J., and Kane, R. J. (2017). Dietary variation and mechanical properties of articular cartilage in the temporomandibular joint: implications for the role of plasticity in mechanobiology and pathobiology. *Zoology* 124, 42–50. doi: 10.1016/j.zool.2017.08.008

Ravosa, M. J., Kunwar, R., Stock, S., and Stack, M. S. (2007). Pushing the limit: masticatory stress and adaptive plasticity in mammalian craniomandibular joints. *J. Exp. Biol.* 210, 628–641. doi: 10.1242/jeb.02683

Ravosa, M. J., López, E. K., Menegaz, R. A., Stock, S. R., Stack, M. S., and Hamrick, M. W. (2008). "Adaptive plasticity in the mammalian masticatory complex: you are what, and how, you eat," in *Primate Craniofacial Biology and Function*, eds C. J. Vinyard, M. J. Ravosa, and C. E. Wall (New York, NY: Springer), 293–328.

Ravosa, M. J., Menegaz, R. A., Scott, J. E., Daegling, D. J., and McAbee, K. R. (2016). Limitations of a morphological criterion of adaptive inference in the fossil record. *Biol. Rev.* 91, 883–898. doi: 10.1111/brv.12199

Ravosa, M. J., Ning, J., Costley, D. B., Daniel, A. N., Stock, S. R., and Stack, M. S. (2010a). Masticatory biomechanics and masseter fiber-type plasticity. *J. Musculoskel. Neuron.* 10, 46–55.

Ravosa, M. J., Ross, C. F., Williams, S. H., and Costley, D. B. (2010b). Allometry of masticatory loading parameters in mammals. *Anat. Rec.* 293, 557–571. doi: 10.1002/ar.21133

Ravosa, M. J., Scott, J. E., McAbee, K. R., Veit, A. J., and Fling, A. L. (2015). Chewed out: An experimental link between food mechanical properties and repetitive loading of the masticatory apparatus in mammals. *PeerJ* 3:e1345. doi: 10.7717/peerj.1345

Reese, A. T., Lanier, H. C., and Sargis, E. J. (2013). Skeletal indicators of ecological specialization in pika (Mammalia, Ochotonidae). *J. Morphol.* 274, 585–602. doi: 10.1002/jmor.20127

Robinson, T., and Matthee, C. (2005). Phylogeny and evolutionary origins of the Leporidae: a review of cytogenetics, molecular analyses and a supermatrix analysis. *Mammal. Rev.* 35, 231–247. doi: 10.1111/j.1365-2907.2005.00073.x

Rodriguez, J. M., Sanz, J., Alonso, F., and Acosta, M. (1985). Factores que influyen en la duracion de la gestacion de la coneja. *Arch. Zootec.* 34, 183–194.

Ruf, I. (2014). Comparative anatomy and systematic implications of the turbinal skeleton in Lagomorpha (Mammalia). *Anat. Rec.* 297, 2031–2046. doi: 10.1002/ar.23027

Ruf, I. (2020). Ontogenetic transformations of the ethmoidal region in Muroidea (Rodentia, Mammalia): new insights from perinatal stages. *Vert. Zool.* 70, 383–415. doi: 10.26049/VZ70-3-2020-10

Ruf, I., Frahnert, S., and Maier, W. (2009). The chorda tympani and its significance for rodent phylogeny. *Mamm. Biol.* 74, 100–113. doi: 10.1016/j.mambio.2008.01.002

Ruf, I., Meng, J., and Fostowicz-Frelik, Ł (2021). Anatomy of the nasal and auditory regions of the fossil lagomorph *Palaeolagus haydeni*: systematic and evolutionary implications. *Front. Ecol. Evol.* 9:636110. doi: 10.3389/fevo.2021.636110

Ruf, I., Schubert, A. M., and Koenigswald, W. V. (2020). "Case studies on functional aspects and constraints in early and late tooth ontogeny," in *Mammal Teeth – Form and Function*, eds T. Martin and W. V. Koenigswald (München: Verlag Dr. Friedrich Pfeil), 102–124.

Sánchez-Villagra, M. R., and Forasiepi, A. M. (2017). On the development of the chondrocranium and the histological anatomy of the head in perinatal stages of marsupial mammals. *Zool. Lett.* 3:1. doi: 10.1186/s40851-017-0062-y

Sánchez-Villagra, M. R., Segura, V., Geiger, M., Heck, L., Veitschegger, K., and Flores, D. (2017). On the lack of a universal pattern associated with mammalian domestication: differences in skull growth trajectories across phylogeny. *R. Soc. Open Sci.* 4:170876. doi: 10.1098/rsos.170876

Sanger, T. J., and Kircher, B. K. (2017). "Model clades versus model species: *Anolis* lizards as an integrative model of anatomical evolution," in *Avian and Reptilian Developmental Biology: Methods and Protocols*, ed. G. Sheng (New York, NY: Humana Press), 285–297.

Sanger, T. J., Revell, L. J., Gibson-Brown, J. J., and Losos, J. B. (2012). Repeated modification of early limb morphogenesis programmes underlies the convergence of relative limb length in *Anolis* lizards. *Proc. R. Soc. B* 279, 739–748. doi: 10.1098/rspb.2011.0840

Schai-Braun, S. C., and Hackländer, K. (2016). "Leporidae (hares and rabbits)," in *Handbook of the Mammals of the World. Vol. 6. Lagomorphs and Rodents I*, eds D. E. Wilson, T. E. Lacher, and R. A. Mittermeier (Barcelona: Lynx Edicions), 62–148.

Schilling, N., and Hackert, R. (2006). Sagittal spine movements of small therian mammals during asymmetrical gaits. *J. Exp. Biol.* 209, 3925–3939. doi: 10.1242/jeb.02400

Scott, J. E., McAbee, K. R., Eastman, M. M., and Ravosa, M. J. (2014a). Experimental perspective on fallback foods and dietary adaptations in early hominins. *Biol. Lett.* 10:20130789. doi: 10.1098/rsbl.2013.0789

Scott, J. E., McAbee, K. R., Eastman, M. M., and Ravosa, M. J. (2014b). Teaching an old jaw new tricks: diet-induced plasticity in a model organism from weaning to adulthood. *J. Exp. Biol.* 217, 4099–4107. doi: 10.1242/jeb.111708

Seixas, F. A., Boursot, P., and Melo-Ferreira, J. (2018). The genomic impact of historical hybridization with massive mitochondrial DNA introgression. *Genome Biol.* 19:91. doi: 10.1186/s13059-018-1471-8

Shan, W., Zhang, Y., Tursun, M., Zhou, S., Dai, H., and Maimaiti, M. (2020). The complete mitochondrial genome sequence of *Lepus tibetanus pamirensis*. *Mitochondr. DNA Part B* 5, 1359–1360. doi: 10.1080/23802359.2020.1736959

Sherratt, E., del Rosario, Castañeda, M., Garwood, R. J., Mahler, D. L., Sanger, T. J., et al. (2015). Amber fossils demonstrate deep-time stability of Caribbean lizard communities. *PNAS* 112, 9961–9966. doi: 10.1073/pnas.1506516112

Silcox, M. T., Benham, A. E., and Bloch, J. I. (2010). Endocasts of *Microsyops* (Microsyopidae, Primates) and the evolution of the brain in primitive primates. *J. Hum. Evol.* 58, 505–521. doi: 10.1016/j.jhevol.2010.03.008

Silcox, M. T., Dalmyn, C. K., and Bloch, J. I. (2009). Virtual endocast of *Ignacius graybullianus* (Paromomyidae, Primates) and brain evolution in early Primates. *PNAS* 106, 10987–10992. doi: 10.1073/pnas.0812140106

Simons, R. S. (1999). Running, breathing and visceral motion in the domestic rabbit (*Oryctolagus cuniculus*): testing visceral displacement hypotheses. *J. Exp. Biol.* 202, 563–577.

Smith, A. T., Johnston, C. H., Alves, P. C., and Hackländer, K. (2018). *Lagomorphs: Pikas, Rabbits, and Hares of the World*. Baltimore: Johns Hopkins University Press.

Stanhope, M. J., Czelusniak, J., Si, J. S., Nickerson, J., and Goodman, M. (1992). A molecular perspective on mammalian evolution from the gene encoding interphotoreceptor retinoid binding protein, with convincing evidence for bat

monophyly. *Mol. Phylogenet. Evol.* 1, 148–160. doi: 10.1016/1055-7903(92)90026-D

Stanhope, M. J., Smith, M. R., Waddell, V. G., Porter, C. A., Shivji, M. S., and Goodman, M. (1996). Mammalian evolution and the interphotoreceptor retinoid binding protein (IRBP) gene: convincing evidence for several superordinal clades. *J. Mol. Evol.* 43, 83–92.

Stock, A. D. (1976). Chromosome banding pattern relationships of hares, rabbits, and pikas (order Lagomorpha). A phyletic interpretation. *Cytogenet. Cell. Genet.* 17, 78–88. doi: 10.1159/000130692

Stoner, C. J., Bininda-Emonds, O. R. P., and Caro, T. (2003). The adaptive significance of coloration in lagomorphs. *Biol. J. Linn. Soc.* 79, 309–328. doi: 10.1046/j.1095-8312.2003.00190.x

Stott, P., Jennings, N., and Harris, S. (2010). Is the large size of the pinna of the ear of the European hare (*Lepus europaeus*) due to its role in thermoregulation or in anterior capital shock absorption? *J. Morphol.* 271, 674–681. doi: 10.1002/jmor.10825

Stübinger, S., and Dard, M. (2013). The rabbit as experimental model for research in implant dentistry and related tissue regeneration. *J. Investig. Surg.* 26, 266–282. doi: 10.3109/08941939.2013.778922

Sych, L. (1967). Fossil endocranial cast of *Hypolagus brachygnathus* Kormos (Leporidae, Mammalia). *Acta Zool. Crac.* 12, 27–30.

Sych, L. (1975). Lagomorpha from the Oligocene of Mongolia. *Palaeont. Pol.* 33, 183–200.

Terhune, C. E., Sylvester, A. D., Scott, J. E., and Ravosa, M. J. (2020). Trabecular architecture of the mandibular condyle of rabbits is related to dietary resistance during growth. *J Exp. Biol.* 223:jeb220988s. doi: 10.1242/jeb.220988

Thibault, C. (1967). Analyse comparée de la fécondation et de ses anomalies chez la brebis, la vache et la lapine. *Ann. Biol. Anim. Bioch. Biophys.* 7, 5–23.

Tobien, H. (1974). Zur Gebißstruktur, Systematik und Evolution der Genera *Amphilagus* und *Titanomys* (Lagomorpha, Mammalia) aus einigen Vorkommen im jüngeren Tertiär Mittel-und Westeuropas. *Mainz. Geowiss. Mitt.* 3, 95–214.

Tobien, H. (1975). Zur Gebißstruktur, Systematik und Evolution der Genera *Piezodus, Prolagus* und *Ptychoprolagus* (Lagomorpha, Mammalia) aus einigen Vorkommen im jüngeren Tertiär Mittel- und Westeuropas. *Notizbl. Hess. Ldsamt. Bodenforsch. Wiesb.* 103, 103–186.

Tong, Y. (1997). Middle Eocene small mammals from Liguanqiao Basin of Henan Province and Yuanqu Basin of Shanxi Province, Central China. *Palaeont. Sin. C* 26, 1–256.

Upham, N. S., Esselstyn, J. A., and Jetz, W. (2019). Inferring the mammal tree: species-level sets of phylogenies for questions in ecology, evolution, and conservation. *PLoS Biol.* 17:e3000494. doi: 10.1371/journal.pbio.3000494

Velasco, J. A., Villalobos, F., Diniz–Filho, J. A. F., Poe, S., and Flores–Villela, O. (2020). Macroecology and macroevolution of body size in *Anolis* lizards. *Ecography* 43, 812–822. doi: 10.1111/ecog.04583

Vianey-Liaud, M., and Lebrun, R. (2013). New data about the oldest European lagomorpha: description of the new genus *Ephemerolagus nievae* gen. nov. et sp. nov. *Span. J. Palaeont.* 28, 3–16.

Vinyard, C. J., Ravosa, M. J., Williams, S. H., Wall, C. E., Johnson, K. R., and Hylander, W. L. (2006). "Jaw muscle function and the origin of primates," in *Primate Origins: Adaptations and Evolution*, eds M. J. Ravosa and M. Dagosto (New York, NY: Springer), 179–231.

Vinyard, C. J., Yamashita, N., and Tan, C. L. (2008). Linking laboratory and field approaches in studying the evolutionary physiology of biting in bamboo lemurs. *Int. J. Primatol.* 29, 1421–1439. doi: 10.1007/s10764-007-9178-9

Voit, M. (1909). Das Primordialcranium des Kaninchens unter Berücksichtigung der Deckknochen. *Anat. Hefte* 38, 425–616.

Waltari, E., and Cook, J. A. (2005). Hares on ice: phylogeography and historical demographics of *Lepus arcticus*, *L. othus*, and *L. timidus* (Mammalia: Lagomorpha). *Mol. Ecol.* 14, 3005–3016. doi: 10.1111/j.1365-294X.2005.02625.x

Wang, B. Y. (2007). Late Eocene lagomorphs from Nei Mongol, China. *Vertebr. PalAsiatica* 45, 43–58.

Wang, X., Liang, D., Jin, W., Tang, M., Shalayiwu, and Liu, S. (2020). Out of Tibet: genomic perspectives on the evolutionary history of extant pikas. *Mol. Biol. Evol.* 37, 1577–1592. doi: 10.1093/molbev/msaa026

Wang, X.-M., Qiu, Z.-D., Li, Q., Tomida, Y., Kimura, Y., Tseng, Z. J., et al. (2009). A new Early to Late Miocene fossiliferous region in central Nei Mongol: lithostratigraphy and biostratigraphy in Aoerban strata. *Vertebr. PalAsiatica* 47, 111–134.

Wang, Y. Q., Meng, J., Beard, K. C., Li, Q., Ni, X. J., Gebo, D. L., et al. (2010). Early Paleogene stratigraphic sequences, mammalian evolution and its response to environmental changes in Erlian Basin, Inner Mongolia, China. *Sci. China Earth Sci.* 53, 1918–1926. doi: 10.1007/s11430-010-4095-8

Watson, P. J., Gröning, F., Curtis, N., Fitton, L. C., Herrel, A., McCormack, S. W., et al. (2014). Masticatory biomechanics in the rabbit: a multi-body dynamics analysis. *J. R. Soc. Interf.* 11:20140564. doi: 10.1098/rsif.2014.0564

Weijs, W. A. (1980). Biomechanical models and the analysis of form: a study of the mammalian masticatory apparatus. *Am. Zool.* 20, 707–719. doi: 10.1093/icb/20.4.707

Weijs, W. A., and Dantuma, R. (1981). Functional anatomy of the masticatory apparatus in the rabbit (*Oryctolagus cuniculus* L.). *Neth. J. Zool.* 31, 99–147. doi: 10.1163/002829680X00212

Weijs, W. A., and de Jongh, H. J. (1977). Strain in mandibular alveolar bone during mastication in the rabbit. *Arch. Oral Biol.* 22, 667–675. doi: 10.1016/0003-9969(77)90096-6

Weijs, W. A., Brugman, P., and Grimbergen, C. A. (1989). Jaw movements and muscle activity during mastication in growing rabbits. *Anat. Rec.* 224, 407–416. doi: 10.1002/ar.1092240309

Weijs, W. A., Brugman, P., and Klok, E. M. (1987). The growth of the skull and jaw muscles and its functional consequences in the New Zealand rabbit *Oryctolagus cuniculus*. *J. Morphol.* 194, 143–161. doi: 10.1002/jmor.1051940204

White, J. A. (1991). North American Leporinae (Mammalia: Lagomorpha) from late Miocene (Clarendonian) to latest Pliocene (Blancan). *J. Vertebr. Paleontol.* 11, 67–89. doi: 10.1080/02724634.1991.10011376

Wible, J. R. (2007). On the cranial osteology of the Lagomorpha. *Bull. Carnegie Mus. Nat. Hist.* 39, 213–234. doi: 10.2992/0145-9058200739[213:OTCOOT]2.0.CO;2

Williams, S. B., Payne, R. C., and Wilson, A. M. (2007a). Functional specialisation of the pelvic limb of the hare (*Lepus europeus*). *J. Anat.* 210, 472–490. doi: 10.1111/j.1469-7580.2007.00704.x

Williams, S. B., Wilson, A. M., and Payne, R. C. (2007b). Functional specialisation of the thoracic limb of the hare (*Lepus europeus*). *J. Anat.* 210, 491–505. doi: 10.1111/j.1469-7580.2007.00703.x

Winkler, A. J., and Avery, D. M. (2010). "Lagomorpha," in *Cenozoic Mammals of Africa*, eds L. Werdelin and W. J. Sanders (New York, NY: University of California Press), 169–317.

Winkler, A. J., and Tomida, Y. (2011). "Chapter 3 The lower third premolar of *Serengetilagus praecapensis* (Mammalia: Lagomorpha: Leporidae) from Laetoli, Tanzania," in *Paleontology and Geology of Laetoli: Human Evolution in Context. Volume 2: Fossil Hominins and the Associated Fauna, Vertebrate Paleobiology and Paleoanthropology*, ed. T. Harrison (Berlin: Springer Science+Business Media B.V.).

Winkler, A. J., Winkler, D. A., and Harrison, T. (2016). Forelimb anatomy of *Serengetilagus praecapensis* (Mammalia: Lagomorpha): a Pliocene leporid from Laetoli, Tanzania. *Hist. Biol.* 28, 252–263. doi: 10.1080/08912963.2015.1023302

Witte, H., Biltzinger, J., Hackert, R., Schilling, N., Schmidt, M., Reich, C., et al. (2002). Torque patterns of the limbs of small therian mammals during locomotion on flat ground. *J. Exp. Biol.* 205, 1339–1353.

Wood, A. E. (1940). The mammalian fauna of the White River Oligocene. Part III. Lagomorpha. *Trans. Am. Phil. Soc.* 28, 271–362. doi: 10.2307/1005524

Wu, C., Wu, J., Bunch, T. D., Li, Q., Wang, Y., and Zhang, Y. P. (2005). Molecular phylogenetics and biogeography of *Lepus* in Eastern Asia based on mitochondrial DNA sequences. *Mol. Phylogenet. Evol.* 37, 45–61. doi: 10.1016/j.ympev.2005.05.006

Wu, Y., Xia, L., Zhang, Q., Yang, Q., and Meng, X. (2011). Bidirectional introgressive hybridization between Lepus capensis and Lepus yarkandensis. *Mol. Phylogenet. Evol.* 59, 545–555. doi: 10.1016/j.ympev.2011.03.027

Yamada, K., and Kimmel, D. B. (1991). The effect of dietary consistency on bone mass and turnover in the growing rat mandible. *Arch. Oral Biol.* 36, 129–138. doi: 10.1016/0003-9969(91)90075-6

Young, J. W., Danczak, R., Russo, G. A., and Fellmann, C. D. (2014). Limb bone morphology, bone strength, and cursoriality in lagomorphs. *J. Anat.* 225, 403–418. doi: 10.1111/joa.12220

Yu, N., Zheng, C., Shi, L., Wang, W., Lan, H., and Zhang, Y. (1996). Phylogenetic relationships of five pika species (genus *Ochotona*) based on mitochondrial DNA restriction maps. *Sci. China C Life Sci.* 39, 113–122. doi: 10.1360/yc1996-39-2-113

Yu, N., Zheng, C. L., Zhang, Y. P., and Li, W. H. (2000). Molecular systematics of pikas (genus *Ochotona*) inferred from mitochondrial DNA sequences. *Mol. Phylogenet. Evol.* 16, 85–95. doi: 10.1006/mpev.2000.0776

Zhang, Z. Q., and Wang, J. (2016). On the geological age of mammalian fossils from Shanmacheng, Gansu Province. *Vertebr. PalAsiatica* 54, 351–357.

Zhang, Z.-G., and Ge, D.-Y. (2014). Postnatal ontogenetic size and shape changes in the craniums of plateau pika and woolly hare (Mammalia: Lagomorpha). *Zool. Res.* 35, 287–293. doi: 10.13918/j.issn.2095-8137.2014.4.287

Conflict of Interest: The authors declare that the research was conducted in the absence of any commercial or financial relationships that could be construed as a potential conflict of interest.

The reviewer TM declared a past co-authorship with one of the authors IR to the handling Editor.

frontiers in Genetics

MINI REVIEW
published: 11 August 2021
doi: 10.3389/fgene.2021.657468

Current Progress in Evolutionary Comparative Genomics of Great Apes

Aisha Yousaf[1,2,3], Junfeng Liu[1,2], Sicheng Ye[1,2,3] and Hua Chen[1,2,3,4]**

[1] CAS Key Laboratory of Genomic and Precision Medicine, Beijing Institute of Genomics, Chinese Academy of Sciences, Beijing, China, [2] China National Center for Bioinformation, Beijing, China, [3] University of Chinese Academy of Sciences, Beijing, China, [4] CAS Center for Excellence in Animal Evolution and Genetics, Chinese Academy of Sciences, Kunming, China

The availability of high-quality genome sequences of great ape species provides unprecedented opportunities for genomic analyses. Herein, we reviewed the recent progress in evolutionary comparative genomic studies of the existing great ape species, including human, chimpanzee, bonobo, gorilla, and orangutan. We elaborate discovery on evolutionary history, natural selection, structural variations, and new genes of these species, which is informative for understanding the origin of human-specific phenotypes.

Keywords: evolutionary comparative genomics, natural selection, structural variations, new genes, great apes

OPEN ACCESS

Edited by:
Irina Ruf,
Senckenberg Research Institute and Natural History Museum Frankfurt, Germany

Reviewed by:
Martin Kuhlwilm,
Pompeu Fabra University, Spain
Deyan Ge,
Institute of Zoology, Chinese Academy of Sciences (CAS), China

***Correspondence:**
Junfeng Liu
liujunfeng@big.ac.cn
Hua Chen
chenh@big.ac.cn

Specialty section:
This article was submitted to Evolutionary and Population Genetics, a section of the journal Frontiers in Genetics

Received: *22 January 2021*
Accepted: *15 July 2021*
Published: *11 August 2021*

Citation:
Yousaf A, Liu J, Ye S and Chen H (2021) Current Progress in Evolutionary Comparative Genomics of Great Apes. Front. Genet. 12:657468. doi: 10.3389/fgene.2021.657468

INTRODUCTION

The pronounced upsurge in modern sequencing technologies during the recent past has led to immense genomic data across a wide range of species. This spearheaded efforts to better understand the divergent species' genome architecture, and unfold the potential adaptation mechanisms. Recently, interest has grown to provide enhanced insights into the genetic diversity of primates using comparative and population genomic data. Being *Homo sapiens*' closely related cousins, non-human primates (NHPs) provide a stepping stone for better understanding the evolutionary origins of human-specific traits. Moreover, they can also serve as models for studying the genetic basis of human disease phenotypes. Humans markedly differ from the closely related NHPs on various grounds, including, but not limited to, brain size, cognitive capacities, social behavior, language, craniofacial features, bipedalism, hairless skin, and advanced tool usage (Gagneux and Varki, 2001; Carroll, 2003). Natural selection is deemed responsible for species' adaptations to changing environments. During recent years, a plethora of studies focused on pinpointing the natural selection signatures in humans and their closely related cousins to understand the genetic basis of modern humans' adaptation and their evolutionary uniqueness. Herein, we briefly review the recently conducted evolutionary comparative genomic studies of great apes regarding their evolutionary history, natural selection, new genes (originated in humans), and structural variation landscape. **Figure 1** illustrates the phylogenetic relationship among great ape species.

GENOME ASSEMBLIES

The first genome sequence of chimpanzee was assembled in 2005, which was compared with the human genome for generating the catalog of genetic differences found among both species (The Chimpanzee Sequencing and Analysis Consortium, 2005). The Sumatran orangutan draft genome

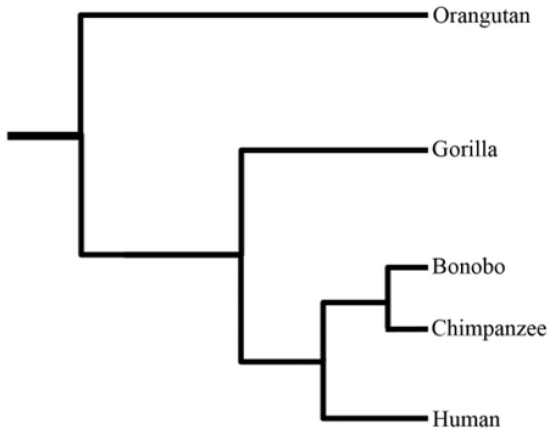

FIGURE 1 | The phylogenetic tree of great ape species (Prado-Martinez et al., 2013).

has been assembled in 2011 and compared to the other primates (Locke et al., 2011). Prüfer et al. (2012) sequenced and assembled the bonobo genome in 2012 for studying the evolutionary relationship with chimpanzee and human genomes. Although the short-read sequencing has been widely used for whole-genome assembly due to the decreasing cost and increasing throughput, the repetitive DNA sequences may make the assembly incomplete (Gordon et al., 2016). Recently developed long-read sequencing technologies, single-molecule real-time (SMRT) sequencing by PacBio sciences, and Oxford Nanopore Technologies' (ONT) nanopore sequencing have proved promising in generating the highly contiguous genomes. Using SMRT sequencing, Gordon et al. (2016) presented the long-read sequence assembly of gorilla genome with a novel assembly algorithm, which can use long (>10 Kbp) sequence reads. Kronenberg et al. (2018) generated the genome assemblies of human, chimpanzee, and orangutan using SMRT long-read sequencing with over 65-fold coverage. Mao et al. (2021) reported a new high-quality bonobo genome assembly using the long-read PacBio platform with 74-fold sequence coverage. The details of recently assembled genomes of great apes can be found in **Table 1**. The availability of high-quality whole-genome sequences of extant great ape species provides an avenue to conduct highly refined comparative genomics research in great ape lineages.

EVOLUTIONARY HISTORY

Genomic Introgression

Previous studies based on molecular data report that humans and chimpanzees diverged ∼5–7 million years ago (Mya) (Chen and Li, 2001; Brunet et al., 2002). However, this estimate is incompatible with the divergence estimates drawn based on fossil data, which is ∼6–7 Mya. The study led by Langergraber indicates that human–chimpanzee split likely occurred at least 7–8 Mya (Langergraber et al., 2012). Recently, Besenbacher et al. (2019) yielded divergence estimates by extrapolating the non-human mutation rates over the great apes' phylogenetic tree and dated humans and chimpanzees split to 10.6 Mya. The difference between the two genomes is ∼1%. By analyzing the divergence among hundreds of DNA sequences between the two genomes, Osada and Wu (2005) inferred that the speciation history between human and chimpanzee could not be the same for coding and intergenic regions. The results suggest that the speciation of human and chimpanzee may not be allopatric speciation. The divergence time between sequences, which belong to two closely related species, shows variation throughout the genome because of the polymorphism and the stochastic fluctuation. The exponential distribution can be used to describe the variation. However, gene flow occurring between the species elicits increased disparity in the divergence time between sequences. By comparing neutral autosomal loci between human and chimpanzee, the data unveiled gene flow in ancestral lineages leading to humans and chimpanzees millions of years ago (Yang, 2010; Liu et al., 2015).

Genetic admixture events among chimpanzee subspecies and bonobos were also investigated based on the genome-wide statistics and site frequency spectrum (SFS)-based modeling (de Manuel et al., 2016). A demographic model based on SFS supports multiple events of genetic admixture between chimpanzees and bonobos. According to this model, gene flow from bonobos into the central and eastern chimpanzees occurred approximately 200,000 and 550,000 years ago. This subsequently spread into Nigeria–Cameroon as a result of admixture between Nigeria–Cameroon and central and eastern chimpanzees. A more recent gene flow event occurred between bonobos and central chimpanzees approximately >200,000 years ago. Furthermore, Kuhlwilm et al. (2019) also detected the signatures of archaic gene flow between bonobos and extinct great ape populations and found the evidence for archaic admixture between bonobos and divergent great ape lineage. They compared the landscapes of introgression in humans and bonobos and showed that *SERPINA11* and *SERPINA9*, which are related to adaptive immunity, are in the longest introgression regions.

Demographic History

Chimpanzees (*Pan troglodytes*) and bonobos (*Pan paniscus*), which together form the *Pan* genus, are the closest extant relatives of the humans, which experienced a bottleneck out of Africa (Li and Durbin, 2011). They have an estimated divergence time of 1–2 Mya (Prüfer et al., 2012). Despite the very short split time, both species markedly differ in terms of their demographic histories and also exhibit lineage-specific differences for several behavioral and phenotypic traits, which make them an interesting subject for comparative genomic studies. Chimpanzees are distributed across Africa ranging from central Africa to eastern and western regions of Africa. Radiation among chimpanzee subspecies began approximately 600,000 years ago (Hoelzel, 2016). Although substantial differences exist in the effective population sizes (*Ne*) of chimpanzee subspecies, all chimpanzee subspecies have greater *Ne* except western chimpanzees and harbor higher genetic diversity than their sister species bonobo (de Manuel et al., 2016). Bonobos are found in the Democratic Republic of the Congo (central Africa); central chimpanzees (*Pan troglodytes troglodytes*)

TABLE 1 | A summary of whole-genome sequencing in great apes.

Species	Platform	Genome coverage	Assembly size (Gbp)	Number of contigs	Contig N50 (Mbp)	Scaffold N50 (Mbp)	References
Chimpanzee	PacBio RSII	>65.0×	2.99	5,037	12.42	53.10	Kronenberg et al., 2018
Bonobo	PacBio RSII	74.0×	3.02	4,975	16,580	68,247	Mao et al., 2021
Gorilla	PacBio RSII	74.8×	3.08	16,073	9.56	23.14	Gordon et al., 2016
Orangutan	PacBio RSII	>65.0×	3.04	5,813	11.07	98.47	Kronenberg et al., 2018

bound their distribution to the west, and the eastern chimpanzee (*Pan troglodytes schweinfurthii*) to the north and south. Bonobos have experienced population bottlenecks and have a smaller long-term *Ne* (11,900–23,800) (Prado-Martinez et al., 2013; de Manuel et al., 2016). The rapid decline in the bonobo population during the recent past has rendered them among the endangered species.

In gorillas, there are four sub-species: eastern gorillas, western gorillas, cross-river gorillas, and mountain gorillas. The four gorilla species have different demographic histories over the past 200,000 years (Prado-Martinez et al., 2013). The western gorillas have the largest historical *Ne* while the historical *Ne* of the eastern gorillas is the smallest. Additionally, the mountain gorillas experienced severe population bottleneck and are a critically endangered subspecies in central Africa (Xue et al., 2015). Orangutans are the most distant relatives of humans among the extant great apes and have two sub-species: Sumatran orangutans and Bornean orangutans, which were designated as distinct species in 2001 (Xu and Arnason, 1996; Groves, 2001). They have an estimated divergence time of 1 Mya and also experienced severe population bottleneck, which makes it urgent to protect these endangered species (Prado-Martinez et al., 2013). However, Nater et al. (2017) show a new orangutan sub-species, which is an isolated population from Batang Toru and is distinct from Sumatran and Bornean populations. Their analyses revealed that the divergence time between Batang Toru populations and the ancestral populations of Sumatran orangutans and Bornean orangutans is ∼3.38 Mya.

NATURAL SELECTION

Many tests designed to detect the natural selection signals identify the genomic loci that show departure from a standard neutral model as probable targets of natural selection. Usually, dN/dS (the non-synonymous/synonymous rate) ratios provide a simplistic measure of selective pressures experienced by a genomic loci, with dN/dS >1 as an indicator of positive selection at the protein level (McDonald and Kreitman, 1991; Yang and Nielsen, 2002, 2008). In comparison, it is difficult to detect the adaptive evolution of non-coding DNA because of the lack of natural benchmark. Siepel et al. introduced methods to test natural selection on non-coding DNA (Gronau et al., 2013; Huang et al., 2017). The method analyzes polymorphism of a single population with sequences of one or several outgroup species, and can distinguish the effects of strong positive, strong negative, and weak negative selection on the basis of their influence on polymorphism and divergence patterns. The aforementioned methods provide an opportunity to detect the natural selection signal across the whole genome.

In earlier studies of *Pan* genus, the effectiveness of purifying selection has been analyzed and the results showed the correlation between past *Ne* and the efficacy of natural selection (Bataillon et al., 2015; Cagan et al., 2016). Cagan et al. (2016) presented the first global map of natural selection in great apes based on genome-wide information by combining several neutrality tests. They found that most signatures of positive selection are species-specific, such as the signature driven by the gene *AMY2B* related to diet. Daub et al. (2017) focused on four branches of the primate tree and identified the biological pathway signals of adaptation in the primate phylogeny. They found that the selection signals in the candidate pathways are elicited by different genes in the different branches during the course of primate evolution. Bertranpetit et al. tested signatures of adaptive introgression in chimpanzees based on SFS (Nye et al., 2018). They found the evidence of subspecies-specific adaptations in introgressed regions, which are involved in processes such as the male reproduction in central chimpanzees, the immune system in eastern chimpanzees, and the nervous system in Nigeria–Cameroon chimpanzees. Han et al. (2019) analyzed the largest available dataset of *Pan* populations and reported the demographic history and purifying selection as the underlying factors for existing genetic variation in *Pan* species. They also found that the small past *Ne* correlates with a larger number of deleterious alleles and the genes enriched with bonobo-specific non-synonymous changes are related to age at menarche in humans. Based on a new bonobo genome assembly, Mao et al. (2021) identified some novel genes and found that most of the novel genes showed selective sweeps in bonobo, such as *DIRC1*, *GULP1*, and *ERC2*.

Recently, Zhao et al. (2019) developed a method, HDMKPRF (aka high-dimensional MKPRF), which is built in the Poisson random field framework developed by Sawyer and Hartl (1992), and is an extension of their MKPRF method from two species to multiple species (Bustamante et al., 2001). They constructed a spatial–temporal landscape of natural selection signatures that occurred across the species' evolutionary history (Zhao et al., 2019). The method pools information over multiple gene loci and gains power over the traditional single-gene-based MK test to

detect positive selection signals (Zhao et al., 2019). Given the high efficiency of the method, genome-wide selection scans across great apes except of bonobos using the HDMKPRF method, which jointly analyzes the within-species polymorphism and cross-species divergence data, provide comprehensive insights into the lineage-specific selection across multiple species. The authors found that the positively selected genes identified in the human lineage are enriched in gene expression regulation pathways, immune system, and metabolic pathways.

STRUCTURAL VARIATIONS

Structural variants (SVs) are an important class of variants that are at least 50 bp in size. SVs have increased capacity to rearrange genomic content than small-scale insertions/deletions (indels; <50 bp) or single-nucleotide variants (SNVs). Owing to their size and abundance, SVs potentially have increased capacity to affect gene expression, shape up genome evolution, and impact phenotypes (Perry et al., 2008; Weischenfeldt et al., 2013). A large number of studies aimed at detecting structural variations in humans and NHPs have contributed a great deal to our understanding of SV abundance and their functional impact. These studies used a wide array of technologies to discover SVs (Gokcumen et al., 2013; Kuderna et al., 2017; Catacchio et al., 2018; Kronenberg et al., 2018).

Catacchio et al. (2018) performed genome-wide comparisons between human, great ape, and macaque genomes and detected 156 putative inversions belonging to 136 human gene loci. These inversions showed considerable variation in their size ranging from 103 Kbp to 91 Mbp. They also found 67 inversions in either one or multiple primates, with 36 inversion breakpoints overlapping with 81 human genes. In addition, they also unveiled the evolutionary history of these genomic inversions to investigate functional differences among primate genomes. The genes impacted by these inversions showed enrichment in several functional categories, including transport proteins, DNA-binding proteins, receptors (G protein-coupled receptors and olfactory receptors), and drug metabolism (cytochrome P450). However, the importance of these genes in bringing about phenotypic differences among humans and other primates remains unknown. Kronenberg et al. (2018) employed long-read sequencing technology to generate high-quality assemblies of human, chimpanzee, and orangutan genomes and identified all SVs >50 bp in size within great ape genomes. They identified a total of 17,789 SVs specifically fixed in human lineage (fhSVs) that impact protein-coding regions as well as regulatory regions with some of these deletions related to human-specific phenotypes. For instance, a large human-specific deletion SV (65 Kbp) was detected in two genes, *FADS1* and *FASD2*, which are also positive selection targets in modern humans and are implicated in fatty-acid biosynthesis (Ameur et al., 2012). This fhSV may have functionally contributed to differential dietary habits of great apes (from herbivores to omnivores) during the course of their evolution (Ye et al., 2017). Notably, two fhSVs were also found in *WEE1* and *CDC25C* genes, which are cell cycle regulators and act as ultrasensitive antagonists. These genes are expressed in radial glia and, as a result of increased cell division therein, are speculated to underlie neocortical expansions in human lineage.

In a recent study, Soto et al. (2020) performed long-range and -read sequencing (using optical nanopore sequencing) of two chimpanzee individuals (belonging to the *Pan. troglodytes verus* subspecies) in order to characterize their SV landscape. A total of 124 novel SVs with size ≥10 kb (including 88 deletions and 36 inversions) were identified in chimpanzees. The study highlighted that 56 genes impacted by putative chimpanzee-specific SVs could lead to chimpanzee-specific phenotypic traits. Deletion SVs showed overrepresentation in "sensory perception of smell" and "G-protein coupled receptor signaling pathway." Furthermore, some of the genes impacted by SVs appeared likely targets of natural selection, which is suggestive of the significance of SVs in impacting the chimpanzee adaptation during the course of evolution. Comparing the bonobo genome to the other great apes' genomes, Mao et al. (2021) identified 22,868 bonobo-specific SVs with size >50 bp (including 7,082 deletions and 15,786 insertions), among which there are 1,965 fixed deletions and 3,604 fixed insertions.

NEW GENES

New genes are often implicated in the emergence of lineage-specific traits and serve as an important resource for evolutionary innovation. For decades, the birth of new genes was attributed to the modification of preexisting genes (Ohno, 1970). In the recent past, studies also reported the birth of new genes from scratch, by DNA- or RNA-mediated mechanisms (Kaessmann, 2010; Betrán, 2015). These mechanisms include gene fusion, horizontal gene transfer, virus domestication, retroduplication, and *de novo* gene origination. *De novo* genes also known as "motherless" or "orphan" genes may constitute a significant proportion (up to 10%) of all new genes (Zhang et al., 2010). Interestingly, *de novo* protein-coding genes have also been found in humans similar to other species (Wu et al., 2011). Wu et al. (2011) identified 60 protein-coding genes of *de novo* origin in human lineage implicating a higher-than-expected rate of *de novo* gene birth. Some of these genes were highly expressed in the cerebral cortex pertaining to their involvement in cognitive capacities.

Cai and Petrov (2010) classified human and chimpanzee orthologous protein-coding genes into distinct age classes (i.e., young and old genes) based on their distribution breadth across the phylogenetic tree. Old genes are broadly distributed compared with young genes, which exhibit restricted phylogenetic distribution and appear in closely related species. Notably, the study unveiled frequent non-synonymous polymorphism experienced by young genes contrary to old genes. These findings suggested that stronger purifying selection acts upon old genes while young genes experience weaker purifying selection and hence evolve faster (Cai and Petrov, 2010). Furthermore, the study also highlighted disparities in the deleterious mutation burden of two gene classes with older genes being abundant in slightly deleterious mutations than younger genes.

Xie et al. (2012) conducted genome-wide identification of *de novo* protein-coding genes that were specific to hominoids and unveiled the precise origin timing of these genes in vertebrate phylogeny. Furthermore, comparative transcriptomic profiling was also performed in human, chimpanzee, and rhesus macaque to address how these *de novo* protein-coding genes came into being. Notably, most of these protein-coding genes were found to be originated from non-coding RNAs (Xie et al., 2012). The study presented a "semi-product" model of *de novo* gene birth and evolution.

Focusing on new genes, Shao et al. (2019) created an integrated online database, named GenTree. GenTree gleans age estimations from multiple gene-dating methods and incorporates the functional genomic data, gathered from Human Protein Atlas, for new genes. By performing genome-wide comparison of the existing age estimation methods, the study unveiled synteny-based pipeline (SBP) as the most suitable method for dating recently duplicated genes. However, for dating ancient genes, protein-family-based methods proved promising. Shao et al. (2019) also curated a list of 254 SBP-dated primate-specific protein-coding genes (PSGs) with different levels of protein evidence. Classifying these PSGs into co-expressing modules spotlighted the functional bias of these PSGs. Notably, PSGs were predominantly involved in male reproduction, defense response, mother–fetus interaction, and brain development. These findings highlighted that PSGs are recruited to processes under strong selection pressure or show biased recruitment in organs with rapidly evolving pathways, for instance, an expanded brain and placenta. Taken together, PSGs were contemplated as a group of genes potentially contributing to primate-specific phenotypic evolution.

CONCLUSION

Over the past years, the successful completion of the human genome project and the release of whole-genome sequences of NHPs led to a plethora of studies highlighting the most conspicuous differences between humans and their closely related phylogenetic cousins. Natural selection is deemed responsible for conferring unique characteristics to a species or within species trait divergence that includes behavioral, cognitive, dietary, and phenotypic differences, among others. Furthermore, the natural selection signatures identified in humans and their closely related cousins help reveal the mechanism of human evolution. In addition, the systematic discovery of SVs by comparing improved great ape genome assemblies provides enhanced insights into the evolution of structural variations and their contribution to lineage-specific phenotypes during the course of great apes' evolution.

Although a large number of fossils of humans have been found, they are mainly used to calibrate the divergence time in the studies of evolutionary comparative genomics of great apes. However, ancient DNA that can be extracted from the fossil has great potential advantages in the evolutionary comparative genomics research (Pickrell and Reich, 2014; Hofreiter et al., 2015). Firstly, ancient DNA can be used to track migration and natural selection directly. Secondly, ancient DNA makes it possible to observe genetic variation patterns of extinct species directly. Finally, ancient DNA allows us to study history interactions between extinct species and modern species. Therefore, ancient DNA from archaic hominins, such as Neanderthals and Denisovans, can serve as more closely related outgroups and provide novel insights into the evolution of humans (Slatkin and Racimo, 2016; Yang and Fu, 2018; Zhang and Fu, 2020). Furthermore, how to take advantage of ancient DNA in the studies of evolutionary comparative genomics of great apes will be a promising direction for future research.

AUTHOR CONTRIBUTIONS

HC designed the manuscript. AY, JL, SY, and HC wrote the manuscript. All authors contributed to the article and approved the submitted version.

FUNDING

This work was supported by the National Key R&D Program of China (2018YFC1406902), the National Natural Science Foundation of China (Grant Nos. 31571370, 91631106, and 91731302), and CAS-TWAS President's fellowship to AY.

REFERENCES

Ameur, A., Enroth, S., Johansson, A., Zaboli, G., Igl, W., Johansson, A. C. V., et al. (2012). Genetic adaptation of fatty-acid metabolism: a human-specific haplotype increasing the biosynthesis of long-chain omega-3 and omega-6 fatty acids. *Am. J. Hum. Genet.* 90, 809–820. doi: 10.1016/j.ajhg.2012.03.014

Bataillon, T., Duan, J., Hvilsom, C., Jin, X., Li, Y., Laurits, S., et al. (2015). Inference of purifying and positive selection in three subspecies of chimpanzees (*Pan troglodytes*) from exome sequencing. *Genome Biol. Evol.* 7, 1122–1132. doi: 10.1093/gbe/evv058

Besenbacher, S., Hvilsom, C., Marques-Bonet, T., Mailund, T., and Schierup, M. H. (2019). Direct estimation of mutations in great apes reconciles phylogenetic dating. *Nat. Ecol. Evol.* 3, 286–292. doi: 10.1038/s41559-018-0778-x

Betrán, E. (2015). The "life histories" of genes. *J. Mol. Evol.* 80, 186–188. doi: 10.1007/s00239-015-9668-x

Brunet, M., Guy, F., Pilbeam, D., Mackaye, H. T., Likius, A., Ahounta, D., et al. (2002). A new hominid from the upper miocene of chad, Central Africa. *Nature* 418, 145–151. doi: 10.1038/nature00879

Bustamante, C. D., Wakeley, J., Sawyer, S., and Hartl, D. L. (2001). Directional selection and the site-frequency spectrum. *Genetics* 159, 1779–1788. doi: 10.1093/genetics/159.4.1779

Cagan, A., Theunert, C., Laayouni, H., Santpere, G., Pybus, M., Casals, F., et al. (2016). Natural selection in the great apes. *Mol. Biol. Evol.* 33, 3268–3283. doi: 10.1093/molbev/msw215

Cai, J. J., and Petrov, D. A. (2010). Relaxed purifying selection and possibly high rate of adaptation in primate lineage-specific genes. *Genome Biol. Evol.* 2, 393–409. doi: 10.1093/gbe/evq019

Carroll, S. B. (2003). Genetics and the making of *Homo sapiens*. *Nature* 422, 849–857. doi: 10.1038/nature01495

Catacchio, C. R., Maggiolini, F. A. M., D'Addabbo, P., Bitonto, M., Capozzi, O., Signorile, M. L., et al. (2018). Inversion variants in human and primate genomes. *Genome Res.* 28, 910–920. doi: 10.1101/gr.234831.118

Chen, F. C., and Li, W. H. (2001). Genomic divergences between humans and other hominoids and the effective population size of the common ancestor of humans and chimpanzees. *Am. J. Hum. Genet.* 68, 444–456. doi: 10.1086/318206

Daub, J. T., Moretti, S., Davydov, I. I., Excoffier, M., and Robinson-Rechavi, M. (2017). Detection of pathways affected by positive selection in primate lineages ancestral to humans. *Mol. Biol. Evol.* 34, 1391–1402. doi: 10.1093/molbev/msx083

de Manuel, M., Kuhlwilm, M., Frandsen, P., Sousa, V. C., Desai, T., Prado-Martinez, J., et al. (2016). Chimpanzee genomic diversity reveals ancient admixture with bonobos. *Science* 354, 477–481. doi: 10.1126/science.aag2602

Gagneux, P., and Varki, A. (2001). Genetic differences between humans and great apes. *Mol. Phylogenet. Evol.* 18, 2–13. doi: 10.1006/mpev.2000.0799

Gokcumen, O., Tischler, V., Tica, J., Zhu, Q., Iskow, R. C., Lee, E., et al. (2013). Primate genome architecture influences structural variation mechanisms and functional consequences. *Proc. Natl. Acad. Sci. U.S.A.* 110, 15764–15769. doi: 10.1073/pnas.1305904110

Gordon, D., Huddleston, J., Chaisson, M. J., Hill, C. M., Kronenberg, Z. N., Munson, K. M., et al. (2016). Long-read sequence assembly of the gorilla genome. *Science* 352:aae0344. doi: 10.1126/science.aae0344

Gronau, I., Arbiza, L., Mohammed, J., and Siepel, A. (2013). Inference of natural selection from interspersed genomic elements based on polymorphism and divergence. *Mol. Biol. Evol.* 30, 1159–1171. doi: 10.1093/molbev/mst019

Groves, C. P. (2001). *Primate Taxonomy*. Washington DC: Smithsonian Institution Press.

Han, S., Andrés, A. M., Marques-Bonet, T., and Kuhlwilm, M. (2019). Genetic variation in pan species is shaped by demographic history and harbors lineage-specific functions. *Genome Biol. Evol.* 11, 1178–1191. doi: 10.1093/gbe/evz047

Hoelzel, A. R. (2016). The road to speciation runs both ways. *Science* 354, 414–415. doi: 10.1126/science.aaj2007

Hofreiter, M., Paijmans, J. L. A., Googchild, H., Speller, C. F., Barlow, A., Fortes, G. G., et al. (2015). The future of ancient DNA: technical advances and conceptual shifts. *Bioessays* 37, 284–293. doi: 10.1002/bies.201400160

Huang, Y.-F., Gulko, B., and Siepel, A. (2017). Fast, scalable prediction of deleterious noncoding variants from functional and population genomic data. *Nat. Genet.* 49, 618–624. doi: 10.1038/ng.3810

Kaessmann, H. (2010). Origins, evolution, and phenotypic impact of new genes. *Genome Res.* 20, 1313–1326. doi: 10.1101/gr.101386.109

Kronenberg, Z. N., Fiddes, I. T., Gordon, D., Murali, S., Cantsilieris, S., Meyerson, O. S., et al. (2018). High-resolution comparative analysis of great ape genomes. *Science* 360:eaar6343. doi: 10.1126/science.aar6343

Kuderna, L. F. K., Tomlinson, C., Hillier, L. W., Tran, A., Fiddes, I. T., Armstrong, J., et al. (2017). A 3-way hybrid approach to generate a new high-quality chimpanzee reference genome (Pan_tro_3.0). *Gigascience* 6, 1–6. doi: 10.1093/gigascience/gix098

Kuhlwilm, M., Han, S., Sousa, V. C., Excoffier, L., and Marues-Bonet, T. (2019). Ancient admixture from an extinct ape lineage into bonobos. *Nat. Ecol. Evol.* 3, 957–965. doi: 10.1038/s41559-019-0881-7

Langergraber, K. E., Prüfer, K., Rowney, C., Boesch, C., Crockford, C., Fawcett, K., et al. (2012). Generation times in wild chimpanzees and gorillas suggest earlier divergence times in great ape and human evolution. *Proc. Natl. Acad. Sci. U.S.A.* 109, 15716–15721. doi: 10.1073/pnas.1211740109

Li, H., and Durbin, R. (2011). Inference of human population history from individual whole-genome sequences. *Nature* 475, 493–U84. doi: 10.1038/nature10231

Liu, J., Zhang, D.-X., and Yang, Z. (2015). A discrete-beta model for testing gene flow after speciation. *Methods Ecol. Evol.* 6, 715–724. doi: 10.1111/2041-210X.12356

Locke, D. P., Hillier, L. W., Warren, W. C., Worley, K. C., Nazareth, L. V., Muzny, D. M., et al. (2011). Comparative and demographic analysis of orang-utan genomes. *Nature* 469, 529–533. doi: 10.1038/nature09687

Mao, Y., Catacchio, C. R., Hillier, L. W., Porubsky, D., Li, R., Sulovari, A., et al. (2021). A high-quality bonobo genome refines the analysis of hominoid evolution. *Nature* 594, 77–81. doi: 10.1038/s41586-021-03519-x

McDonald, J. H., and Kreitman, M. (1991). Adaptive protein evolution at the adh locus in *Drosophila*. *Nature* 351, 652–654. doi: 10.1038/351652a0

Nater, A., Mattle-Greminger, M. P., Nurcahyo, A., Nowak, M. G., de Manuel, M., Desai, T., et al. (2017). Morphometric, behavioral, and genomic evidence for a new orangutan species. *Curr. Biol.* 27, 3487–3498. doi: 10.1016/j.cub.2017.09.047

Nye, J., Laayouni, H., Kuhlwilm, M., Mondal, M., Marques-Bonet, T., and Bertranpetit, J. (2018). Selection in the Introgressed Regions of the Chimpanzee Genome. *Genome Biol. Evol.* 10, 1132–1138. doi: 10.1093/gbe/evy077

Ohno, S. (1970). *Evolution by Gene Duplication*. New York, NY: Springer-Verlag.

Osada, N., and Wu, C. I. (2005). Inferring the mode of speciation from genomic data: a study of the great apes. *Genetics* 169, 259–264. doi: 10.1534/genetics.104.029231

Perry, G. H., Ben-Dor, A., Tsalenko, A., Sampas, N., Rodriguez-Revenga, L., Tran, C. W., et al. (2008). The fine-scale and complex architecture of human copy-number variation. *Am. J. Hum. Genet.* 82, 685–695. doi: 10.1016/j.ajhg.2007.12.010

Pickrell, J. K., and Reich, D. (2014). Toward a new history and geography of human genes informed by ancient DNA. *Trends Genet.* 30, 377–389. doi: 10.1016/j.tig.2014.07.007

Prado-Martinez, J., Sudmant, P., Kidd, J., Li, H., Kelley, J. H., Lorente-Galdos, B., et al. (2013). Great ape genetic diversity and population history. *Nature* 499, 471–475. doi: 10.1038/nature12228

Prüfer, K., Munch, K., Hellmann, I., Akagi, K., Miller, J. R., Walenz, B., et al. (2012). The bonobo genome compared with the chimpanzee and human genomes. *Nature* 486, 527–531. doi: 10.1038/nature11128

Sawyer, S. A., and Hartl, D. L. (1992). Population genetics of polymorphism and divergence. *Genetics* 32, 1161–1176.

Shao, Y., Chen, C., Shen, H., He, B. Z., Yu, D., Jiang, S., et al. (2019). GenTree, an integrated resource for analyzing the evolution and function of primate-specific coding genes. *Genome Res.* 29, 682–696. doi: 10.1101/gr.238733.118

Slatkin, M., and Racimo, F. (2016). Ancient DNA and human history. *Proc. Natl. Acad. Sci. U.S.A.* 113, 6380–6387. doi: 10.1073/pnas.1524306113

Soto, D. C., Shew, C., Mastoras, M., Schmidt, J. M., Sahasrabudhe, R., Kaya, G., et al. (2020). Identification of structural variation in chimpanzees using optical mapping and nanopore sequencing. *Genes* 11:276. doi: 10.3390/genes11030276

The Chimpanzee Sequencing and Analysis Consortium. (2005). Initial sequence of the chimpanzee genome and comparison with the human genome. *Nature* 437, 69–87. doi: 10.1038/nature04072

Weischenfeldt, J., Symmons, O., Spitz, F., and Korbel, J. O. (2013). Phenotypic impact of genomic structural variation: insights from and for human disease. *Nat. Rev. Genet.* 14, 125–138. doi: 10.1038/nrg3373

Wu, D. D., Irwin, D. M., and Zhang, Y. P. (2011). De novo origin of human protein-coding genes. *PLoS Genet.* 8:e1002942. doi: 10.1371/journal.pgen.1002942

Xie, C., Zhang, Y. E., Chen, J. Y., Liu, C. J., Zhou, W. Z., Li, Y., et al. (2012). Hominoid-specific De Novo protein-coding genes originating from long non-coding RNAs. *PLoS Genet.* 8:e1002942.

Xu, X., and Arnason, U. (1996). The mitochondrial DNA molecule of Sumatran orangutan and a molecular proposal for two (Bornean and Sumatran) species of orangutan. *J. Mol. Evol.* 43, 431–437. doi: 10.1007/BF02337514

Xue, Y., Prado-Martinez, J., Sudmant, P. H., Narasimhan, V., Ayub, Q., Szpak, M., et al. (2015). Mountain gorilla genomes reveal the impact of long-term population decline and inbreeding. *Science* 348, 242–245. doi: 10.1126/science.aaa3952

Yang, M. A., and Fu, Q. (2018). Insights into modern human prehistory using ancient genomes. *Trends Genet.* 34, 184–196. doi: 10.1016/j.tig.2017.11.008

Yang, Z. (2010). A likelihood ratio test of speciation with gene flow using genomic sequence data. *Genome Biol. Evol.* 2, 200–211. doi: 10.1093/gbe/evq011

Yang, Z., and Nielsen, R. (2002). Codon-substitution models for detecting molecular adaptation at individual sites along specific lineages. *Mol. Biol. Evol.* 19, 908–917. doi: 10.1093/oxfordjournals.molbev.a004148

Yang, Z., and Nielsen, R. (2008). Mutation-selection models of codon substitution and their use to estimate selective strengths on codon usage. *Mol. Biol. Evol.* 25, 568–579. doi: 10.1093/molbev/msm284

Ye, K., Gao, F., Wang, D., Bar-Yosef, O., and Keinan, A. (2017). Dietary adaptation of FADS genes in Europe varied across time and geography. *Nat. Ecol. Evol.* 1:167. doi: 10.1038/s41559-017-0167

Zhang, M., and Fu, Q. (2020). Human evolutionary history in eastern Eurasia using insights from ancient DNA. *Curr. Opin. Genet. Dev.* 62, 78–84. doi: 10.1016/j.gbe.2020.06.009

Zhang, Y. E., Vibranovski, M. D., Krinsky, B. H., and Long, M. (2010). Age-dependent chromosomal distribution of male-biased genes in *Drosophila*. *Genome Res.* 20, 1526–1533. doi: 10.1101/gr.107334.110

Zhao, S., Zhang, T., Liu, Q., Wu, H., Su, B., Shi, P., et al. (2019). Identifying lineage-specific targets of natural selection by a Bayesian analysis of genomic polymorphisms and divergence from multiple species. *Mol. Biol. Evol.* 36, 1302–1315. doi: 10.1093/molbev/msz046

Conflict of Interest: The authors declare that the research was conducted in the absence of any commercial or financial relationships that could be construed as a potential conflict of interest.

The reviewer DG declared a past co-authorship with one of the authors SY to the handling editor.

Advantages of publishing in Frontiers

OPEN ACCESS
Articles are free to read for greatest visibility and readership

FAST PUBLICATION
Around 90 days from submission to decision

HIGH QUALITY PEER-REVIEW
Rigorous, collaborative, and constructive peer-review

TRANSPARENT PEER-REVIEW
Editors and reviewers acknowledged by name on published articles

Frontiers
Avenue du Tribunal-Fédéral 34
1005 Lausanne | Switzerland

Visit us: www.frontiersin.org
Contact us: frontiersin.org/about/contact

REPRODUCIBILITY OF RESEARCH
Support open data and methods to enhance research reproducibility

DIGITAL PUBLISHING
Articles designed for optimal readership across devices

FOLLOW US
@frontiersin

IMPACT METRICS
Advanced article metrics track visibility across digital media

EXTENSIVE PROMOTION
Marketing and promotion of impactful research

LOOP RESEARCH NETWORK
Our network increases your article's readership